



HAL
open science

Emergence of NLRP1 inflammasome as a sensor of microbial virulence in human epithelium

Miriam Pinilla

► **To cite this version:**

Miriam Pinilla. Emergence of NLRP1 inflammasome as a sensor of microbial virulence in human epithelium. Human health and pathology. Université Paul Sabatier - Toulouse III, 2023. English. NNT : 2023TOU30116 . tel-04266241

HAL Id: tel-04266241

<https://theses.hal.science/tel-04266241>

Submitted on 31 Oct 2023

HAL is a multi-disciplinary open access archive for the deposit and dissemination of scientific research documents, whether they are published or not. The documents may come from teaching and research institutions in France or abroad, or from public or private research centers.

L'archive ouverte pluridisciplinaire **HAL**, est destinée au dépôt et à la diffusion de documents scientifiques de niveau recherche, publiés ou non, émanant des établissements d'enseignement et de recherche français ou étrangers, des laboratoires publics ou privés.

Université Fédérale



Toulouse Midi-Pyrénées

THÈSE

En vue de l'obtention du
DOCTORAT DE L'UNIVERSITÉ DE TOULOUSE
Délivré par l'Université Toulouse 3 - Paul Sabatier

Présentée et soutenue par
Miriam PINILLA

Le 8 juin 2023

Emergence de l'inflammasome NLRP1 en tant que senseur de virulence microbienne dans l'épithélium humain

Ecole doctorale : **BSB - Biologie, Santé, Biotechnologies**

Spécialité : **IMMUNOLOGIE**

Unité de recherche :

IPBS - Institut de Pharmacologie et Biologie Structurale

Thèse dirigée par

Etienne MEUNIER et EMMANUEL RAVET

Jury

M. Fabio MARTINON, Rapporteur
Mme Cécile ARRIEUMERLOU, Rapporteur
M. Pablo PELEGRIN, Examineur
M. Joost VAN-MEERWIJK, Examineur
Mme Rebecca COLL, Examinatrice
M. Etienne MEUNIER, Directeur de thèse
M. Emmanuel RAVET, Co-directeur de thèse

Dedicada a mis padres y a Luis.
Sin vosotros nada de esto sería posible.
Os quiero.

Remerciements

Au jury

Au Professeur Joost van Meerwijk. Aujourd'hui je vous remercie de présider le jury de ma thèse mais mes remerciements commencent un petit peu plus tôt, plus précisément en 2019. Merci de votre confiance, merci de m'avoir acceptée dans le Master Immunologie et surtout de m'avoir accueillie dans votre labo pendant mon stage de M2. Sans vous je ne serai pas en train de soutenir ma thèse aujourd'hui. Merci infiniment.

A mes rapporteurs, Fabio Martinon et Cécile Arrieumerlou. Merci pour votre bienveillance, pour tout le temps que vous avez dédié à la lecture et correction de ma thèse et surtout merci pour vos retours chaleureux. C'est pour moi un réel honneur que vous soyez membres de mon jury.

Rebecca Coll. Thank you for having accepted without hesitation to be part of my jury, thank you for your enthusiasm, for your interest in our work, for wanting to come to Toulouse and especially for wanting to celebrate with us. I am honored that you are part of my jury.

Pablo Pelegrin. Es un honor para mí presentar mi trabajo delante de personas tan importantes que trabajan en la temática inflamatoria. Muchas gracias por aceptar de formar parte de mi tribunal de tesis, por venir a Toulouse y por todo tu tiempo.

A mes directeurs de thèse, Etienne Meunier et Emmanuel Ravet. J'aurai quelques petits mots par la suite, mais merci, merci pour m'avoir fait confiance, merci de m'avoir donné l'opportunité de faire cette thèse incroyable, merci de m'avoir soutenue et merci de m'avoir fait grandir.

A mon comité de thèse

Merci aux membres de mon comité de thèse, Bénédicte Py et Eric Jeziorski pour avoir suivi mon travail au cours de ces 3 années. Merci pour vos retours et votre aide.

A la direction d'Invivogen

Merci à la direction et surtout à Michèle Tiraby de m'avoir donné l'opportunité de faire ma thèse CIFRE en collaboration avec l'IPBS et Invivogen. Grâce à cette collaboration j'ai pu faire une thèse incroyable et enrichissante. Merci de votre confiance et de votre temps consacré au bon déroulement de mes projets.

A Invivogen

Je dois remercier tout d'abord à mon co-directeur de thèse, Emmanuel Ravet. Je me rappellerai toujours de notre première réunion de thèse autour ~~d'un café~~ d'une bière dans un bar. Merci de ces réunions pas comme les autres. Je me rappellerai aussi du premier poster que j'ai dû faire pour un congrès. Tu m'avais fait m'asseoir à côté de toi dans ton bureau, tu m'avais rassuré et tu m'avais donné un café et un cookie. Merci pour ton soutien pendant ces 3 dernières années.

Je remercie tous les employés et personnes que j'ai pu côtoyer au sein d'Invivogen, notamment l'équipe R&D.

A Audrey. Toujours avec un sourire et de bonne humeur. Tu as été mon guide (ou ange gardien si tu préfères) pendant ma première année. Merci infiniment pour ton aide et ta patience. Tu m'as beaucoup manqué depuis que tu es partie.

A Aurore. Je pense que je ne pourrai jamais oublier ton rire en salle de culture. Merci d'être toujours là pour discuter, de ta bonne humeur et ta zénitude.

A Alex, merci de toute ton aide dans tous les projets, tu m'as beaucoup aidé et sauvé pendant ces 3 ans. Merci d'être aussi chaleureux et accueillant, merci pour toutes nos conversations et tous tes conseils.

A ma Perrinette d'amour. Tu es un rayon de soleil, toujours souriante et de bonne humeur. Je ne sais pas si je dois te dire merci ou pardon pour t'avoir posé 1 million de questions/jour... Je ne sais pas comment je pourrai te remercier de toute ton aide. Merci, vraiment. Je t'attends à Murcie !

A Remi. Que ce soit à l'IPBS ou à Invivogen tu m'as tout appris. Tu m'as encadré tout au long de ma thèse, que ce soit en manip, biblio, présentations, tu as toujours été une aide précieuse. Tu gères 1 million de projets en même temps et même comme ça tu as toujours des nouvelles idées et du temps pour aider les autres. Si j'ai une question c'est toujours ton prénom qui me vient en tête. Merci du temps que tu as dédié à toute ma thèse depuis le premier jour jusqu'au dernier jour. Je te souhaite que du bonheur mon petit Remichou.

A ma petite Clémence. Un autre petit rayon de soleil. Merci pour m'avoir toujours aidée et soutenue, notamment pendant la fin de ma thèse, pour tous tes conseils, pour ta bonne humeur et pour tes gâteaux délicieux. Merci !

A ~~Pauline~~, je pense que je t'appellerai toujours par ton faux nom. Tu es incroyablement drôle et c'est toujours un plaisir de discuter avec toi. Merci pour toute ton aide et tous tes conseils, reste aussi courageuse et forte ! Merci

A Marion, merci pour toutes les pauses café et repas. Tu connais Invivogen comme la paume de ta main, merci pour tous tes conseils, c'est toujours un plaisir ! Merci

A Isa. Je dois dire que je crois que tu as un don, tu es la reine de la biomol. Merci pour ton aide, merci pour tous les plasmides que tu as réussi du premier coup alors que je n'avais jamais réussi à faire. Merci aussi de toutes nos conversations et d'être aussi chaleureuse.

A Nathalie. Merci pour tous tes conseils et toutes nos conversations. Et merci pour ton travail, tu fais des revues incroyables, ça fait toujours plaisir de les lire.

A Fernanda. Merci de ta bonne humeur, de ta sympathie, de tes conseils... C'est toujours agréable de discuter avec toi. J'espère qu'après la maison et le mariage tu pourras souffler ahha

A Svetlana. Merci infiniment de tout ton temps, je suis désolée de t'avoir autant harcelé avec tous mes e-mails.

A Dominique et Benjamin. QUOI DIRE DE CES DEUX LA. Partir avec vous en congrès c'est juste incroyable, j'ai passé de très beaux moments à vos côtés. C'est toujours stressant de présenter en congrès mais savoir que vous étiez là ça m'a toujours rassuré. Merci pour tout. Je vous apprécie énormément et j'ai hâte de vous revoir dans un futur congrès.

A l'équipe Inflamm

En 2019, j'ai commencé mon Master et j'ai rencontré ma petite Julie et ma petite Karin. Je me rappellerai toujours quand j'ai commencé à devenir assez proche de Karin et qu'elle m'a dit mon équipe de M2 est incroyable, faut que tu viennes faire la thèse avec moi. Et donc, j'ai passé un entretien avec

Etienne, le chef. Moi, petite étudiante de master qui va passer un entretien de thèse qu'est-ce que je fais ? J'imprime toute la biblio de ce fameux Etienne Meunier et je me prépare à fond. J'arrive le jour de l'entretien et première chose qu'Etienne me dit : Tu veux un café ? Puis ensuite on rentre dans son bureau et il met les pieds sur la table. L'entretien se passe très bien, mais pas une seule question de la biblio que j'avais lu, et il me dit « Je te veux en thèse chez moi ». J'ai commencé à comprendre que ce fameux Etienne Meunier n'était pas un chef comme les autres.

En Octobre 2019 j'ai intégré cette équipe qui, comme le chef, n'est pas une équipe comme les autres. Cette équipe est beaucoup plus qu'une équipe de recherche c'est une ~~petite~~ grande famille qui ne reçoit jamais les allocations familiales. Dans cette famille on retrouve le papa (Etienne) et la maman (Celine), l'oncle un peu beauf mais que tout le monde aime (David), le grand-père qui vieillit jamais (Raoul), la tante stricte mais adorable (Audrey), l'oncle qui sait tout réparer (PJ), l'oncle qu'on voit une fois par mois mais qui ramène toujours des cadeaux (Rémi), la fille adolescente qui enlève jamais ses écouteurs (Sali), le fils gentil et adorable (Stephen), la fille hyperactive (KK), les fils médecins (et oui dans toutes les familles il y a des médecins), Romain et Guigui, le fils qui travaille tout le temps (Ron), la fille en garde alterné (Lea F), la fille qui s'occupe de tout à la maison (Leana), la petite-fille maniaque (Margaux), le fitboy de la famille (Baba, aussi appelé Bibi), la dernière à être arrivée, pleine d'envie et d'énergie (Lea), et le petit général Franco. Comme dans toutes les familles on a les repas de famille, des règles jamais suivies, des engueulades et surtout **le soutien inconditionnel**.

A ceux qui sont partis...

Karin. Je ne réalise toujours pas que tu sois partie. J'ai l'impression que tu es encore là au labo, sauf qu'on j'entend la voix de Margaux et je me dis que non, effectivement tu n'es pas là (je rigole je te taquine). On a vécu tellement de choses ensemble que je ne sais pas même par où commencer. On a passé plus de 3 ans collées h24, au labo, au téléphone, en voyage, en congrès, à la piscine, à la salle de sport... inséparables. Tu es une amie que je pourrai appeler à n'importe quelle heure et elle serait là. J'ai passé 3 ans de thèse incroyables à tes côtés et comme j'ai dit lors de mon discours, après tout ce temps je suis devenue un petit peu Karin et tu es devenue un petit peu Miriam. Merci de ton soutien inconditionnel, tes câlins et ton amour, tu me manques.

Audrey. Tu es une scientifique, une femme, une mère et une amie incroyable. J'ai passé des années inoubliables à tes côtés que ce soit au labo ou en dehors du labo, tu es devenue beaucoup plus qu'une collègue, tu es devenue une amie en majuscules. Merci pour toutes nos conversations, pour ta patience à tout m'expliquer, pour ton aide inconditionnelle...Tu me manques terriblement au labo, ce n'est pas pareil sans toi.

PJ. Ton prénom ressort au moins une fois par semaine : quand PJ était là... Ta bonne humeur, ton initiative, tes questions, ton expertise nous manquent terriblement.

Elif, tu es partie très tôt et on n'a pas pu trop se connaître mais tu es une scientifique incroyable. Merci pour tous tes conseils.

Sali. Ma petite Sali. La première thésarde du labo à avoir soutenue et être partie. C'était le début de tous nos départs... Nos pauses, nos cafés, nos discussions, nos conneries au labo me manquent. Je te souhaite que du bonheur.

Aux étudiants...

Vous êtes les plus grosses AVERSES que je n'ai jamais rencontré de ma vie ! Vous faites du labo un endroit où on peut travailler énormément tout en s'amusant et en rigolant. Merci pour tous ces moments de pétage de câble au labo mais aussi pour tous les restos, les pizzas, les soirées, les weekends. Vous allez terriblement me manquer. Vous savez que vous avez tous une maison à Murcie et que ceci n'est pas une option mais une obligation. Signé, GF.

Stephen. Eres un científico increíble y una de las personas más buenas que he conocido en mi vida. Gracias por ser un amigo que siempre está ahí para escuchar, apoyar y ayudar. Sin ti, esto no hubiera sido igual. Ojalá me pudieras dar un poco de calma y serenidad jajajajaj. Gracias por ser como eres, no cambies nunca. Te deseo todo lo mejor.

Baba. Aka, le chaud lapin. Aka, Bibi. Toujours de bonne humeur, souriant, drôle. C'est un plaisir de t'avoir au labo, surtout parce que tu travailles toujours tard les Vendredi et on peut boire et manger plus lors de l'apéro (je rigooooooooou). J'adore t'embêter et passer du temps avec toi. Je te souhaite une thèse incroyable, aie confiance en toi, tu es le best !

Guigui. Aka, notre médecin préféré. J'adore t'avoir parmi nous au labo, tu es incroyablement intelligent mais en même temps tellement con ! Naaan je rigole. J'adore tous les moments passés avec toi, merci d'être si gentil et si adorable ! Tu vas me manquer.

Léa. Ma petite Lele. Enfin tu formes partie de la famille Inflammé ! Je suis très contente que tu sois parmi nous. On peut toujours compter sur toi, merci d'être toujours là et d'être une amie incroyable. Je te souhaite que du beau pour cette thèse poulette. Je serai toujours là, tu vas me manquer.

Roro. J'espère que tu vas nous revenir vite, ton odeur dans les couloirs nous manquent. Merci pour toute ton aide dans tous les projets, merci d'être toujours présent alors que tu es totalement débordé.

Léa F. Notre thésarde en garde alterné. Tu es une fille adorable, intelligente, toujours de bonne humeur et souriante. Tu ramènes de l'air frais dans cette équipe, ça fait du bien. C'est un plaisir de t'avoir rencontré, ne changes jamais.

Ron. Is a pleasure to have you in the team. Du arbeitest immer noch sehr viel, ich hoffe, dass deine Dissertation perfekt verläuft, ich wünsche dir alles Gute!

AUX SALOPARDES DE PORTIGIRLS. LM²

Léana. Aka, la stagiaire. Aka, la bénévole. Aka, la racaille. Aka, la plus saloparde. Je pense que tu ne te rends pas compte à quel point tu m'as aidé pendant cette période un peu rude, que ce soit au labo ou en tant qu'amie. Merci infiniment pour tout ce que tu as fait pour moi. Tu vas faire une thèse incroyable ma petite LELE. Tu es devenue quelqu'un d'essentiel dans ma vie et je veux que tu saches que je serai toujours là pour toi. Tu vas terriblement me manquer !

Margaux. Aka ma stagiaire d'amour. Aka, l'autre saloparde. Je ne peux dire que Merci. Depuis ton premier stage tu n'as pas été une stagiaire comme les autres, tu es incroyablement organisée, intelligente et bosseuse. Ça été un plaisir de t'avoir au labo ces deux dernières années et j'espère te voir grandir au sein de ce labo comme une fantastique thésarde. Merci pour tout. Merci pour tes corrections, pour ton aide, pour ta chanson, pour ton amitié.

Aux adultes (ou c'est ce qu'ils disent) ...

David. Je ne comprends toujours pas pourquoi tu as voulu changer de bureau alors que tu avais la meilleure place à mes côtés. Merci de tous tes conseils sur la vie, de me dire que je suis mal habillée tous les jours, de tes conneries, de ta bonne humeur. Toi et Isa vous êtes adorables et je vous aime énormément.

Raoul. Notre incroyable Raoul. Bientôt à la retraite et on dirait qu'il n'a même pas 50 ans. Merci pour être comme tu es, tu donnes de la vie au labo, tu es toujours souriant et de bonne humeur. C'est vraiment agréable de t'avoir tous les jours parmi nous.

Céline. Tu es une scientifique incroyable et ambitieuse. Depuis que je suis arrivée au labo je t'ai vu que réussir et grandir comme chercheuse. C'est un plaisir de travailler à tes côtés. Merci beaucoup pour tout ton travail et pour ton soutien ces dernières années.

Etienne. Tu n'es pas un chef comme les autres, tu es proche de tes étudiants, tu t'inquiètes pour nous et tu nous défendrais comme tes propres enfants s'il le fallait. Pendant ce temps tu m'as fait grandir comme personne, comme étudiante et finalement tu m'as fait devenir une scientifique. Quand je suis arrivée au labo j'avais peur de faire un simple labmeeting, puis tu nous as envoyés en congrès, tu nous as inscrit à des présentations un peu partout... finalement j'ai plus peur de faire ces présentations, et ce qui est le plus important, je suis fière de mon travail. Merci. Merci de m'avoir fait confiance et de m'avoir fait croire en moi.

A l'IPBS

A Gilberto. Ton don pour me mettre des chansons dans la tête me rend FOLLE. Tu es compétitif à mourir mais qu'est-ce que tu es drôle. J'ai passé de très beaux moments et beaucoup rigolé à tes côtés. Je te souhaite le meilleur. Merci

Je veux remercier à toutes les personnes avec lesquelles j'ai partagé des beaux moments au sein de l'IPBS : Celia, Greg, Eva, Rim ... et notamment tous les thésards de ma promo avec lesquels on a organisé ce super Symposium.

Je tiens à remercier toutes les équipes de l'IPBS (direction, informatique, logistique, accueil, communication, administration etc) et notamment à Yvane, qui a toujours été très présente au cours de ma thèse, et à Marcelle qui a été indispensable afin que je puisse organiser ma thèse. Merci infiniment.

A mes amis...

Ainoha et Irene. Por mucho que estemos lejos y que nos veamos poco sois de las personas que cuando nos vemos todo es como antes. Os odio mucho cada vez que me dejáis en visto, pero sois de las personas que más quiero en esta vida y por las que daría cualquier cosa. Sois CASA, sois FAMILIA, sois TODO. Gracias por todo.

Carmen. Croquetita. Garbanzito. La charo. La Mami. Eres una amiga increíble, siempre estás ahí para cualquier cosa, dando los mejores consejos y recetas del universo. Eres valiente, fuerte y SIEMPRE consigues lo que te propones porque nunca te rindes. Gracias por todo, te quiero.

Aza. Mi pollito. Hemos vivido un montón de aventuras juntas y siempre has estado a mi lado. Hoy te doy las gracias por ser una amiga increíble y por esas conversaciones con un café que acaban en un futuro

post-doc. GRACIAS. Siempre me acordaré de ese café. Tienes otra casa en Murcia. Estoy deseando vernos por ahí. Te quiero pollito.

Julie. Gatito negro. Depuis qu'on s'est connu j'ai toujours regretté de pas avoir pu te connaître avant. J'ai passé un M2 incroyable à tes côtés, on est devenus proches et inséparables très rapidement, ce genre d'amitié très forte qu'on n'oublie jamais. Je suis très triste que tu ne puisses pas être là mais très contente que tu poursuives ton rêve au Canada. J'espère qu'on se verra vite ma petite Julie. Tu me manques.

Mes puces, Morgane, Elena et Emilie. Toujours là. On se connaît depuis très longtemps maintenant et vous êtes toujours à l'écoute et toujours là, pour boire un verre, faire un restau, un weekend, une soirée, un petit brunch le dimanche ou simplement écouter les peines de l'une ou de l'autre. Merci les filles. Je vous aime. Je vous attends à la playa !

JB et Lucas. Vous avez été mes premiers vrais amis à Toulouse. Merci, merci pour tout. Je n'oublierai jamais toutes les soirées et aventures avec vous. Vous avez une maison à Murcia quand vous voulez !

A Leticia y Sandra. Mis bichotas. Gracias por todos los fines de semana y momentos de locura y juntos. Hacéis que me olvide de todo. Esto no es un adiós, espero seguir viéndoos en vías ferratas y barrancos. Os quiero.

A mis cuarenton@s guaperas, Paola, Isra y Javi y a mi Isabela. Por todos esos fines de semana juntos de risas, cervezas, cenas y barrancos. No necesitamos nada más. Muchísimas gracias por hacer que esto del barranquismo sea tan especial. Sois lo mejor.

Loic et Flo. Depuis la première fois qu'on s'est rencontrés on a vite très bien accroché et délirez ensemble. Je vous adore. Merci pour tous ces bons moments passés ensemble. On va être obligés de se revoir, je sais que tu passes tous les étés à Murcie Flo, muahahahahah vous n'allez pas vous débarrasser de moi

Lucie. Tu es quelqu'un d'extrêmement important pour moi et tu le seras toujours. Tu as toujours eu confiance et cru en moi. De Jefa Pinilla je suis passé au général Franco au labo. Je crois que tu avais raison et j'aime bien donner des ordres. Je te souhaite que du bon. Gros bisous

Samuel. Si pudiera borrar algo de esta vida, borraría aquel día. Ojalá fuera tan sencillo y pudiéramos borrar las cosas injustas que pasan en nuestras vidas. Lo único que puedo hacer es prometerte vivir como si la vida se acabase mañana. Ojalá estuvieras aquí hoy con todos nosotros. Ojalá no te hubieses ido nunca de nuestras vidas. Nunca te olvidare. Eres eterno. Te quiero.

A lo que esta por llegar...

Ana Belén. Nunca pensaba que tomando un café con una amiga podría acabar buscando tu nombre en Google, escribiéndote, conociéndote y queriendo a toda costa hacer un post-doc contigo. Y es que hay cosas que simplemente se sienten. Tengo muchísimas ganas de empezar esta nueva etapa de mi vida trabajando contigo. Gracias por tu apoyo y confianza.

A mi familia...

Mi gato. Gasdermine, Gas para los amigos. Gracias por ser el gato mas suicida y desastroso del mundo, gracias por no dejarme dormir y obligarme a tener que dormir con tapones todos los días de mi vida.

Pero también gracias por darme ese cariño y esa compañía, eres parte de mi familia, Miriam sin su hijo Gas no existe. Te quiero peludín.

Maria José y Daniel. Gracias por tratarme como una más y hacerme sentir como en casa desde el primer día. Me encanta pasar tiempo con vosotros y ojalá pudiéramos vernos más. Estoy deseando que vengáis a disfrutar de la playa.

Papu y Mamu. Mi familia. Las personas que más me quieren en esta vida. Los que darían todo por mí. Nunca os podre agradecer todo el sacrificio y esfuerzo que habéis hecho para que tenga una infancia y una vida increíblemente feliz. Gracias a vosotros he crecido yendo de campamentos, yendo a hacer rutas por la montaña, haciendo escalada, barranquismo y espeleo. Desde pequeña me habéis transmitido el amor por la naturaleza y los animales, me habéis enseñado a ser buena y respetar a los demás. Me habéis enseñado a esforzarme y sacrificarme por lo que quiero, y gracias a vosotros hoy soy DOCTORA. Gracias por haber hecho que sea una mujer fuerte, independiente, con hobbies y ambiciones y sobre todo que sea TAN FELIZ. GRACIAS. Gracias por vuestro apoyo y amor incondicional. Os quiero.

A ti, mi persona favorita. Apareciste en mi vida cuando menos lo esperaba y cuando más lo necesitaba. Es gracioso porque nos conocemos de toda la vida y siempre hemos tenido una relación muy especial pero nunca hubiese imaginado que acabaríamos juntos, queriéndonos como nunca habíamos querido antes. ¿Y qué paso? Que nos besamos, empezamos a hablar sin parar durante un mes, nos volvimos a ver, nos enamoramos perdidamente el uno del otro y ya no nos pudimos soltar. Desde aquel día me siento la persona más afortunada del mundo por tenerte a mi lado. Haces que contigo al lado la vida sea fácil y sencilla, los problemas se esfuman y solo estamos nosotros en un rinconcito del sofá siendo felices y queriéndonos bonito. Hay pocas cosas que tenga claras en mi vida, no sé dónde viviré, ni donde trabajaré, ni si tendré algún día un trabajo fijo (jeje viva la ciencia), lo único que tengo claro es que quiero despertarme todos los días contigo a mi lado. Eres la persona que me da paz, tranquilidad, pero a la vez me vuelve loca, me hace reír, me escucha, me entiende y simplemente me hace feliz. Gracias por haberme ayudado tanto estos últimos 6 meses, han sido duros, pero has estado ahí día tras día apoyándome, escuchándome, creyendo en mí y recordándome lo mucho que me quieres y todo lo bonito que nos espera. No hay cosa que desee más que empezar esta nueva etapa contigo.

PS: No sé cómo define Google una carita perfecta, pero si tuviera que apostar seguro que sale una carita tuya en tamaño gigante. QUE GUAPO ERES.

➤	Figures index	3
➤	Table index	4
➤	Abbreviations	5
➤	Abstract	8
➤	Résumé	10
I.	INTRODUCTION	12
1.	PATTERN RECOGNITION RECEPTORS (PRRs)	12
I.	<i>Toll-Like Receptors (TLRs)</i>	13
II.	<i>RIG-I like receptors (RLR)</i>	14
III.	<i>C-type Lectin Receptors (CLRs)</i>	15
IV.	<i>Nucleotide-binding domain, leucine-rich repeat containing (NLRs)</i>	16
V.	<i>Cytosolic DNA sensors (CDS)</i>	18
➤	AIM2-like receptors (ALRs)	18
➤	cGAS-STING	18
2.	THE IMMUNE SYSTEM	19
I.	<i>Innate immunity</i>	19
➤	Innate immune cells in phagocytosis and inflammation	20
II.	<i>Adaptive immunity</i>	21
III.	<i>Cell-autonomous immunity</i>	22
➤	Antimicrobial peptides	22
➤	Autophagy	23
➤	IFN response	23
➤	Programmed cell death	24
•	Apoptosis.....	25
•	Necrosis	25
▪	Necroptosis	26
▪	Ferroptosis:	27
▪	Pyroptosis.....	27
II.	INFLAMMASOME.....	29
1.	THE CANONICAL INFLAMMASOME.....	31
I.	<i>Receptors of inflammasome</i>	32
➤	The NLRP3 inflammasome	34
•	Activation of NLRP3	35
•	NLRP3 inflammasome-driven diseases.....	37
▪	NLRP3-dependent auto-inflammatory diseases	38
•	Inhibition of NLRP3 activation.....	38
➤	The NLRC4 inflammasome	40
•	NLRC4 inflammatory disorders	43
➤	The AIM2 inflammasome	44
➤	PYRIN inflammasome	45
➤	The NLRP1 and CARD8 inflammasome	47
2.	THE NON-CANONICAL INFLAMMASOME	47
3.	ALTERNATIVE INFLAMMASOME ACTIVATING-PATHWAYS.....	48
4.	GASDERMIN D CLEAVAGE AND PYROPTOSIS.....	49
I.	<i>Gasdermin family as executors of pyroptosis</i>	49
➤	GSDMD	50
➤	GSDMA	53
➤	GSDMB.....	54
➤	GSDMC.....	54
➤	GSDME.....	55
➤	PJVK	55
II.	<i>Fungal gasdermin-like proteins</i>	57
5.	INFLAMMASOME MEDIATED IL-1B AND IL-18 PRODUCTION	57
III.	THE NLRP1 AND CARD8 INFLAMMASOME.....	59

6.	WHY NLRP1 AND CARD8 ARE SO UNIQUE INFLAMMASOMES?.....	59
I.	<i>Difference between species</i>	59
II.	<i>Structure and tissue expression</i>	59
➤	NLRP1	59
➤	CARD8.....	61
III.	<i>Activation by the universal activator: Val-boro-Pro (VbP)</i>	62
7.	MOUSE NLRP1B	65
I.	<i>Activation by lethal factor (LF)</i>	65
8.	HUMAN NLRP1 INFLAMMASOME	67
I.	<i>The emerging functions of epithelial inflammasomes in immunity to infection and diseases</i>	67
II.	<i>Activation of human NLRP1 by cleavage</i>	69
III.	<i>Activation by UVB radiation</i>	71
IV.	<i>Activation of hNLRP1 by double-stranded RNA (dsRNA) and poly (dA:dT)</i>	72
V.	<i>Activation by reductive stress</i>	73
VI.	<i>Proteasome independent activation of NLRP1</i>	75
IV.	WORK CONTEXT AND RESULTS	78
1.	WORK CONTEXT 1: HUMAN NLRP1 IS A SENSOR OF PATHOGENIC CORONAVIRUS 3CL PROTEASES IN LUNG EPITHELIAL CELLS 79	
I.	<i>Study context and objectives</i>	79
II.	<i>Paper</i>	82
2.	WORK CONTEXT 2: EEF2-INACTIVATING TOXINS ENGAGE THE NLRP1 INFLAMMASOME AND PROMOTE EPITHELIAL DAMAGE UPON <i>PSEUDOMONAS AERUGINOSA</i> INFECTION	120
I.	<i>Study context and objectives</i>	120
II.	<i>Paper (Pinilla et al., 2023 under review in JEM)</i>	121
V.	CONCLUSIONS AND PERSPECTIVES	171
VI.	REFERENCES	179
VII.	APPENDIX	200
1.	CASPASE-1 DRIVEN NEUTROPHIL PYROPTOSIS AND ITS ROLE IN HOST SUSCEPTIBILITY TO <i>PSEUDOMONAS AERUGINOSA</i>	200
2.	HOST PHOSPHOLIPID PEROXIDATION FUELS EXO ω -DEPENDENT CELL NECROSIS AND SUPPORTS <i>PSEUDOMONAS AERUGINOSA</i> - DRIVEN PATHOLOGY	229
3.	IRGM2 AND GATE-16 COOPERATIVELY DAMPEN GRAM-NEGATIVE BACTERIA-INDUCED CASPASE-11 RESPONSE.....	259

➤ Figures index

Figure 1: The cellular locations of the mammalian Toll-like receptors

Figure 2: Viral RNA detection by RIG-I and MDA5

Figure 3: Human NOD-like receptors (NLRs)-classification and domain organization

Figure 4: cGAS-STING signalling pathway

Figure 5: Function and differentiation of different CD4 T cell effectors from

Figure 6: The autophagy pathway

Figure 7: Model of IFN response

Figure 8: Apoptotic versus necrotic cell features

Figure 9: Model of necroptosis triggered downstream of different pathways

Figure 10: Mechanisms of inflammasome activation leading to a pyroptotic cell death

Figure 11: Structures of inflammasome-forming receptors in humans

Figure 12: The inflammasome compounds and interactions

Figure 13: Mechanisms of caspase-1 activation

Figure 14: Models of NLRP3 activation

Figure 15: Model of NLRC4 activation

Figure 16: Activation of the AIM2 inflammasome by cytosolic ds DNA

Figure 17: Model of Pyrin inflammasome activation by Rho-modifying toxins

Figure 18: Key events in the history of gasdermins

Figure 19: Signalling pathways of GSDM family members

Figure 20: NLRP1 and CARD8 inflammasomes

Figure 21: The ternary complex structure of the inhibited form of NLRP1

Figure 22: Activation of the hNLRP1 inflammasome by Valbopro

Figure 23: Model of mNLRP1B activation

Figure 24: Mechanism of NLRP1 activation by HRV-3Cpro following HRV infection in human airway epithelium from

Figure 25: Model of hNLRP1 activation by the ribotoxic stress response

Figure 26: NLRP1 activation by dsRNA or the dsDNA mimetic poly(dA:dT) detection

Figure 27: Model of NLRP1 and CARD8 activation by reductive or proteotoxic stress

Figure 28: Two forms of autoinhibited NLRP1 complexes

Figure 29: Proteasome dependent or independent NLRP1 activation

➤ **Table index**

Table 1: Receptors forming inflammasomes.

Table 2: Gasdermin family

Table 3: Current knowledge about hNLRP1 and CARD8 binding to DPP9

Table 4: Implication of hNLRP1 in rare inflammatory skin disorders

➤ Abbreviations

AIADK: autoinflammation with arthritis and dyskeratosis

AIM2: Absence in melanoma 2

ALR: absent in melanoma (AIM)-like receptors

AMD: atrophic macular degeneration

AP: aminopeptidase

BIR: baculoviral inhibitory repeat

CAPS: Cryopyrin-associated periodic syndromes

CARD: caspase activation and recruitment domains

CDS: cytosolic DNA sensors

CGAS: cyclic GMP-AMP synthase

CINCA: chronic infantile neurological cutaneous articular

CLR: C-type Lectin Receptors

CNS: central nervous system

CRD: carbohydrate-recognition domain

CRS: cytokine release syndrome

CTLD: C-type lectin-like domains

CTLs: cytotoxic T lymphocytes

CUL: cullin

CVB3: Coxsackievirus B3

DAMP: damage-associated molecular patterns

DC: dendritic cell

DNA: deoxyribonucleic acid

DPP: dipeptidylpeptidase

dsRNA: double stranded RNA

dTGN: dispersed trans-Golgi network

EAE: experimental autoimmune encephalomyelitis

FCAS: familial cold auto-inflammatory syndrome

FIIND: function-to-find domain

FKLC: familial keratosis lichenoides chronica

FMF: familial Mediterranean fever

GBP: Guanylate-Binding Proteins

GSDM: gasdermin

GSDMD-CT: gasdermin D C-terminal

GSDMD-NT: gasdermin D N-terminal

Gzm: granzyme

hNLRP1: human NLRP1

HRV: human rhinovirus

IBD: inflammatory bowel disease

IFI16: IFN- γ inducible protein 16

IFN: interferon

IMQ: imiquimod

IRF1: Interferon regulatory factor 1

IRF8: interferon regulatory factor 8

KSHV: Kaposi's sarcoma-associated herpesvirus

LF: lethal factor

LGP2: laboratory of genetics and physiology 2

LPS: lipopolysaccharides

LT: Anthrax lethal toxin

MDA5: melanoma differentiation-associated protein 5

MeBs: bestatin methyl ester

MNDA: myeloid cell nuclear differentiation antigen

mNLRP1: murin NLRP1

MSPC: multiple self-healing palmoplantar carcinoma

MSU: monosodium urate

mtDNA: mitochondrial DNA

mtROS: mitochondrial reactive oxygen species

MWS: Muckle–Wells syndrome

NEK7: NIMA-related kinase 7

NF-KB: Nuclear factor kappa-light-chain-enhancer of activated B cells

NINJ1: Nerve Injury-induced Protein 1

NK: natural killer

NLR: NOD-like receptors

NLRP1: nucleotide-binding domain leucine-rich repeat pyrin domain containing 1

NOMID: neonatal-onset multisystem inflammatory disorder

OMV: outer membrane vesicles

PA : protective antigen

PAMP: pathogen-associated molecular patterns

PBMC: peripheral blood mononuclear cell

PRR: pattern recognition receptors

PtdIns4P: phosphatidylinositol-4-phosphate

PYD: pyrin domain

RCD: regulated cell death

RIG-I: retinoic acid-inducible gene

RLR: RIG-I like receptors

RSR: ribotoxic stress response

SCCs: squamous cell carcinomas

SCCs: squamous cell carcinomas

SFV: Semliki Forrest Virus

SINE: short interspersed nuclear element

SLE: systemic lupus erythematosus

SpeB: Streptococcal pyrogenic exotoxin B

SREBP: sterol regulatory element-binding protein-2

T2D: type 2 diabetes

T2SS : type 2 secretion system

T3SS : type 3 secretion system

TEV: tobacco etch virus

TGN: trans-Golgi network

TIR: Toll/Interleukin-1 receptor

TLR: Toll-Like Receptors

TNFR: tumor necrosis receptor

TRX1: thioredoxin-1

TWIK2: two-pore domain weak inwardly rectifying K⁺ channel 2

UPA: conserved in UNC5, PIDD, and Ankyrin domain

Vbp: Valboropro

ZU5: found in ZO-1 and UNC5

➤ **Abstract**

All living organisms are continuously exposed to threatening pathogens that can attack and invade them. For this reason, the host developed a series of defence mechanisms in order to detect and eliminate pathogens. One of these mechanisms is mediated by the assembly of inflammasomes. Inflammasomes are multiprotein complexes that activate the inflammatory caspase-1 in response to microbial components, danger or stress. The active caspase-1 leads to the formation of a gasdermin D pore in the cell membrane allowing the release of inflammatory cytokines IL-1 β and IL-18, therefore resulting in a lytic and highly inflammatory cell death, called pyroptosis. The inflammasomes were shown to play a crucial role in the innate host defense against a broad variety of microbial pathogens, different danger signals, and stress. Therefore, there is a wide variety of inflammasomes (NLRP3, NLRC4, AIM2, PYRIN, NLRP1) and their expression and assembly are tightly regulated.

The role of inflammasomes has been extensively studied in innate immune cells such as macrophages and neutrophils but not in epithelial cells. However, it's important to note that epithelial cells are frequently the initial cells barrier that pathogens meet, and their response determines the start of an infection. Interestingly, the human NLRP1 inflammasome (hNLRP1) is highly expressed in epithelial cells (lung, skin, cornea) and the molecular mechanisms that govern its activation have remained enigmatic until recently. Particularly, NLRP1 has recently gained much attention and is rising as an important epithelial sensor involved in antimicrobial defence as well as in the development of pathologies.

During my PhD, I studied the role of the NLRP1 inflammasome as a sensor of microbial virulence in the human epithelium, in the context of viral infection by the SARS-Cov-2 virus but also in the context of bacterial infection by *Pseudomonas aeruginosa*.

The virus of severe acute respiratory syndrome coronavirus 2 (SARS-Cov-2), that causes the COVID-19 pandemic, primarily infects the respiratory tract (nasal, bronchial and lung epithelial cells). Interestingly, one of the most important cytokines released during severe COVID was IL-18, suggesting a critical role of inflammasomes during a SARS-CoV-2 infection. During my PhD one of my works consisted to study the role of hNLRP1 during a COVID-19 infection. Using alveolar epithelial cell line A549 expressing the receptor of SARS-CoV-2, ACE2 and over-expressing or not human NLRP1, we found that infection with SARS-Cov-2 leads to a pyroptotic form of cell death only in cells expressing NLRP1. Mechanistically, we showed that the NSP5 3CL protease cleaves NLRP1 and induces a pyroptotic cell death by an alternative pyroptosis pathway that involves the activation of gasdermin E. Finally, we showed a higher amount of gasdermine E and IL-18 in patients with Severe COVID, suggesting that an over-activation of the NLRP1 pathway may be pathological during SARS-CoV-2 infection.

In addition, we observed cystic fibrosis patients who are chronically infected with *P. aeruginosa* exhibit enrichment of IL-1 β in the lungs. These observations strongly suggest the involvement of inflammasomes. Thus, our work demonstrated that *P.aeruginosa*'s exotoxin A induces NLRP1 activation via the activation of a ribotoxic stress pathway involving ZAK α and p38 kinases. Finally, we observed that epithelial cells isolated from cystic fibrosis patients exhibit enhanced inflammatory responses leading to increased cell death and IL-18 release in response to *P.aeruginosa*.

Together, our data demonstrated the important role of human NLRP1 in the immune response against microbial pathogens (viruses or bacteria) in the human epithelium and their possible involvement in different associated diseases.

The first project is published (Planes et al., 2022) and the second project is under revisions in Journal Experimental of Medicine (Pinilla et al., 2023).

Keywords: Inflammasome- Pyroptosis – NLRP1 – human epithelium – SARS-CoV-2– *P.aeruginosa*

➤ **Résumé**

Tous les organismes vivants sont continuellement exposés à des agents pathogènes qui peuvent les attaquer et les envahir. Pour cette raison, l'hôte a développé une série de mécanismes de défense afin de détecter et d'éliminer les pathogènes. Un de ces mécanismes est médié par l'assemblage des inflammasomes, des complexes multi-protéiques qui, suite à leur activation, recrutent et activent une protéase inflammatoire, la caspase-1. A son tour, caspase-1, clive une protéine appelée gasdermine D, qui va former un pore dans la membrane cellulaire permettant la libération des cytokines inflammatoires IL-1 β et IL-18 et la rupture membranaire, entraînant ainsi une mort cellulaire lytique et hautement inflammatoire, appelée pyroptose. Il a été démontré que les inflammasomes jouent un rôle crucial dans la défense innée de l'hôte. De ce fait, il existe donc une grande variété d'inflammasomes capables de reconnaître différents stimulus. Le rôle des inflammasomes a été largement étudié dans les cellules de l'immunité innée telles que les macrophages et les neutrophiles, mais pas dans les cellules épithéliales. Cependant, il est important de noter que les cellules épithéliales sont souvent la première barrière cellulaire que les pathogènes rencontrent, et leur réponse est cruciale pour la défense de l'organisme. Il est intéressant de noter que l'inflammasome NLRP1 est fortement exprimé dans les cellules épithéliales (poumon, peau, cornée) et que les mécanismes moléculaires qui régissent son activation sont restés énigmatiques jusqu'à récemment. Au cours de mon doctorat, j'ai étudié le rôle de l'inflammasome NLRP1 en tant que capteur de virulence microbienne dans l'épithélium humain, dans le contexte d'une infection virale par le virus SARS-Cov-2, mais aussi dans le contexte d'une infection bactérienne par *Pseudomonas aeruginosa*.

Le virus du SARS-CoV-2, responsable de la pandémie de COVID-19, infecte principalement les voies respiratoires et il est intéressant de noter que l'une des principales cytokines libérées lors d'un COVID sévère dans les poumons est l'IL-18, ce qui suggère un rôle critique des inflammasomes lors d'une infection par le SARS-CoV-2. En utilisant la lignée cellulaire épithéliale alvéolaire A549 exprimant le récepteur du SARS-CoV-2, ACE2, et surexprimant ou non NLRP1, nous avons découvert que l'infection par le SARS-Cov-2 conduit à une forme pyroptotique de mort cellulaire uniquement dans les cellules exprimant la NLRP1. En détail, nous avons montré que la protéase NSP5 3CL clive NLRP1 et induit une mort cellulaire pyroptotique par une voie alternative qui implique l'activation de la gasdermine E. Enfin, nous avons montré une quantité plus élevée de gasdermine E et d'IL-18 chez les patients atteints de COVID sévère, suggérant qu'une suractivation de la voie NLRP1 pourrait être pathologique pendant l'infection par le SARS-CoV-2.

De plus, nous avons observé que les patients atteints de mucoviscidose qui sont infectés de manière chronique par *P. aeruginosa* présentent un enrichissement en IL-1 β dans les poumons. Ces observations suggèrent fortement l'implication des inflammasomes. Ainsi, nos travaux ont démontré que l'exotoxine

A de *P.aeruginosa* induit l'activation de NLRP1 via l'activation d'une voie de stress ribotoxique impliquant les kinases ZAK α et p38. Enfin, nous avons observé que les cellules épithéliales isolées de patients atteints de mucoviscidose présentent des réponses inflammatoires accrues conduisant à une augmentation de la mort cellulaire et de la libération d'IL-18 en réponse à *P.aeruginosa*.

L'ensemble de nos données ont démontré le rôle important de NLRP1 dans la réponse immunitaire contre les pathogènes microbiens (virus ou bactéries) dans l'épithélium humain et leur implication possible dans différentes maladies associées. Le premier projet a déjà été publié (Planes et al., 2022) et le second est en cours de révision dans le Journal Experimental of Medicine (Pinilla et al., 2023).

Mots clés : Inflammasome- Pyroptose – NLRP1 –épithélium – SARS-CoV-2– *P.aeruginosa*

I. Introduction

“Each species must constantly evolve to avoid extinction in the face of competitors who are also constantly evolving”(Lacey & Miao, 2020). This observation made by the evolutionary biologist Leigh Van Valen in 1973 is illustrated in Lewis Carol’s book *Through the Looking Glass*, in which the protagonist, Alice, engages in a footrace with the Red Queen. The Red Queen hypothesis also applies to host-pathogen interactions. Multicellular organisms, from plants to vertebrates, are continuously exposed to invading pathogens (viruses, bacteria, fungi and parasites) that are capable to attack and to invade. For this reason, all living organisms developed a series of defence mechanisms in order to preserve their integrity, homeostasis and survival. As hosts develop defence mechanisms to protect it selves against infection, pathogens must, in turn, develop virulence factors to thrive. This constant evolutive race by the two competitors ensures that neither the host nor the pathogen disappears. The integrity, homeostasis and survival of organisms from infection depends on the detection and elimination of pathogens while limiting tissue damage. The vital need for this balance in host response has led evolution to develop a powerful array of cellular defences ranging from cell autonomous immunity to innate and adaptive immunity that all together constitutes the human immune system. These defence mechanisms are first initiated by the detection of danger signals through receptors dedicated to this function: the pattern recognition receptors (PRRs).

1. Pattern recognition receptors (PRRs)

All host cells have evolved sophisticated harm detection systems that involve cell receptors binding to molecular motifs broadly conserved across pathogens (pathogen-associated molecular patterns—PAMPs), or indicative of host damage (damage-associated molecular patterns—DAMPs). PAMPs (now also referred to as MAMPs for “microbe-associated molecular patterns”) are components from many microorganisms that have been conserved during evolution, making them excellent targets for recognition. DAMPs were introduced by Polly Matzinger as a “danger theory”, suggesting that the main determinant of immune activation is not the origin of the antigen itself but the extent of the damage it causes. Consequently, DAMPs are endogenous ligands that are usually produced as a result of injury (stress or damage). For example, HMGB1 is one of the classic DAMP, it localizes in the nucleus to promote protein assembly on specific DNA sequences, while in response to pathogenic insults, cells damages or death, it can be released in the extracellular medium. Released HMGB1 mediates the activation of immune cells and induces the inflammation.

The cellular receptors responsible for the recognition of PAMPs or DAMPs were named Pattern Recognition receptors (PRR). The existence of these receptors was predicted by Pr. Charles Janeway in 1989, before the mechanisms of innate recognition were known. PRRs are expressed in a broad set of

immune (monocytes, macrophages, neutrophils, dendritic cells and other myeloid cells) and non-immune cells (especially endothelial and epithelial cells) and exist in various forms. The different PRRs vary according to their location, the specificity of their ligands and their downstream signalling pathway, providing a complete and effective response to various infections or damage. Several families of PRRs have been identified, among them, the membrane-bound receptors that include the Toll-Like Receptors (TLRs), C-type Lectin Receptors (CLRs) and the cytoplasmic receptors including the Nucleotide-binding domain, leucine-rich repeat containing receptors (NLRs) and RIG-I like receptors (RLR). A number of other PRRs including the cytosolic DNA sensors (CDS) cGAS-STING and the family of absent in melanoma (AIM)-like receptors (ALRs). Interestingly, like animals, plants requires, and have evolved a robust innate system to detect and respond to pathogen-derived molecules (Jones et al., 2016). This is mediated by cell surface or intracellular receptors typically encoded by disease resistance (R) genes which share architectural and functional similarities with animals (inflammasomes-like, gasdermins) that I will describe later.

Upon recognition of their cognate-specific ligands, PRRs rapidly induce host immune responses: mobilization of soluble defence molecules, killing of the infected cells or tissues, acquisition of specialized functions by sentinel cells, induction of co-stimulatory molecules by antigen-presenting cells, and many other physiological responses. One of these immune responses is the activation of conserved signalling pathways (NF-KB and IFN) that culminate in the activation of specific genes dedicated to orchestrating the eradication of the pathogen, and the induction of a pro-inflammatory response with the release of cytokines and chemokines. While most of these pathways initiate a robust transcriptional reprogramming of gene expression, a subset of PRRs is implicated in the induction of host defence mechanisms causing cell death. In my manuscript, I will be particularly interested in PRRs that induce cell death, and more specifically, a lytic form of cell death called pyroptosis, induced after the assembling of a multiprotein complex: **the inflammasome** (see later in part II)

I. Toll-Like Receptors (TLRs)

The TLRs were so-called according to their similarity to the protein encoded by the toll gene identified during embryonic development and dorsoventral polarization of the drosophila in 1985 by Christiane Nüsslein-Volhard (Anderson et al., 1985). The role of the Toll receptor in the host's innate immunity against fungal infection in *Drosophila melanogaster* was confirmed by Jules Hoffman in 1996 (Lemaitre et al., 1996). One year later, the first Toll homolog in humans (now called TLR4) was discovered (Medzhitov et al., 1997). The discovery of TLRs was an important event for immunology research and was recognized as such with the awarding of the 2011 Nobel Prize to Jules Hoffman at the French National Center for Scientific Research in Strasbourg and Bruce Beutler at the Scripps Research

Institute in California. TLRs represent an ancient pathogen-recognition system that detects PAMP derived from microorganisms: microbial molecular structures such as proteins, flagellin from bacterial flagella, lipoteichoic acid (LTA) and peptidoglycan (PGN) from Gram-positive bacteria, LPS from Gram-negative bacteria, lipopeptides, double-stranded (ds) RNA of viruses, and DNA) or DAMPs from damaged tissue. To date, 10 humans and 13 murine homologous of TLR have been identified (Fitzgerald & Kagan, 2020). They are expressed in all innate immune cells such as macrophages, neutrophils, dendritic cells (DC), natural killer (NK) cells, mast cells, basophils, and eosinophils. We can divide them into two subfamilies depending on their localization, either on the plasma membrane or in intracellular vesicles membranes, such as endosomes.

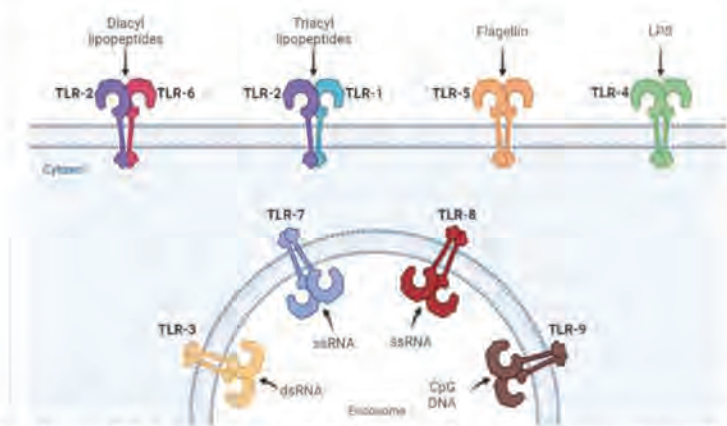


Figure 1: The cellular locations of the mammalian Toll-like receptors. Toll-like receptors (TLRs) are transmembrane receptors localized at the cellular or endosomal membranes. They recognize diverse PAMPs from bacteria, fungi, parasites and viruses, including lipid-based bacterial cell walls components such as lipopolysaccharide (LPS) and lipopeptides, microbial protein components such as flagellin, and nucleic acids such as single-stranded or double-stranded RNA and CpG DNA.

TLRs are transmembrane proteins with extracellular or endosomal leucine-rich repeats (LRR) for the recognition of PAMP/DAMP, transmembrane domain and intracellular toll-interleukin 1 (IL1-R) receptor (TIR) domains required for the activation of downstream signal transduction pathways. TLR signalling includes at least two distinct pathways (Kagan, 2012) : MyD88-dependent pathway utilized by all TLRs, except TLR3, leading to the production of inflammatory cytokines. TRIF dependent pathway is used in TLR3 and 4 and associates with type 1 interferon stimulation. The activation of these pathways induces an antimicrobial activity and the production of inflammatory cytokines essential in the fight against infections.

II. RIG-I like receptors (RLR)

Retinoic acid-inducible gene I-like receptors (RLR) are expressed in most cell types and are primarily located in the cytosol (Rehwinkel & Gack, 2020). This protein family is composed of three members: retinoic acid-inducible gene (RIG-I), melanoma differentiation-associated protein 5 (MDA5) and laboratory of genetics and physiology 2 (LGP2). All RLRs have a central helicase domain and a so-called

carboxy-terminal domain (CTD). These two domains work together to detect viral RNAs. RIG-I and MDA5 additionally have two amino-terminal caspase activation and recruitment domains (CARDs), which mediate downstream signal transduction. LGP2 lacks the CARDs and is widely believed to regulate RIG-I and MDA5. RIG-I discriminates between host and viral RNA by sensing the unmodified 5' triphosphate end of the ssRNA viral genome that is not found in host RNA. MDA-5 senses long double-stranded RNA. (Rehwinkel & Gack, 2020).

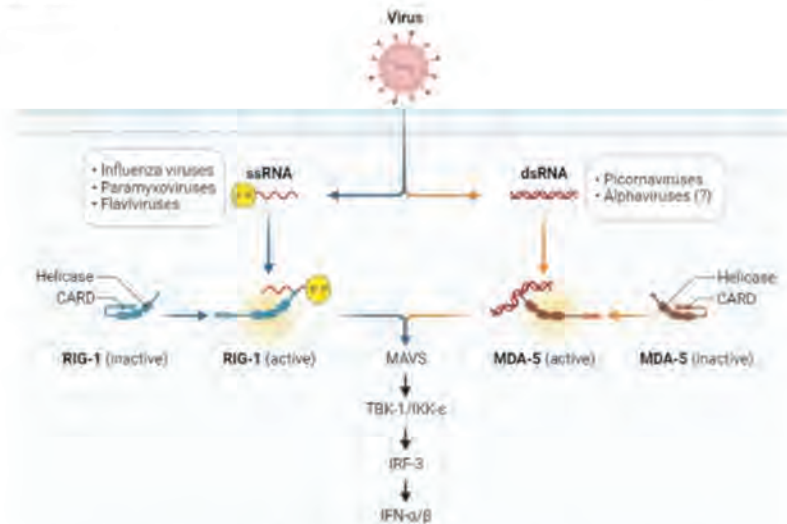


Figure 2: Viral RNA detection by RIG-I and MDA5. RIG-I (retinoic-acid-inducible protein 1) and MDA-5 (melanoma-differentiation-associated gene 5) are cytoplasmic RNA helicases that belong to the RIG-I-like receptors (RLRs) family. RIG-I and MDA-5 are key protein sensors of viral RNA and are critical for host antiviral responses. After the detection of viral RNA, they interact with the mitochondrial antiviral signaling protein MAVS leading to the production of type-I interferons (IFN- α and IFN- β).

III. C-type Lectin Receptors (CLRs)

Cells of the innate and adaptive immune systems, including all myeloid cells and lymphocytes, express various C-type lectins. These molecules were originally named for their ability to bind to carbohydrates in a Ca^{2+} -dependent manner thanks to the carbohydrate-recognition domain (CRD). However, the CRD of many C-type lectins lack the components required for Ca^{2+} -dependent carbohydrate recognition and thus do not bind sugars, which has led to the distinction between the sugar-binding C-type CRDs and the broader family of C-type lectin-like domains (CTLDs) that can recognize a broader repertoire of ligands including glycans, proteins and lipids among others. On the basis of their molecular structure, C-type lectins are found as secreted molecules or as transmembrane proteins, and they have been implicated in a diverse range of physiological functions because of their ability to recognize self (endogenous) and non-self (exogenous) ligands. In fact, many C-type lectins can recognize both classes of ligands and are involved in numerous physiological functions. Soluble C-type lectins can function, for example, as growth factors, opsonins, antimicrobial proteins and components of the extracellular matrix

(ECM), and they regulate many essential processes such as development, respiration, coagulation, angiogenesis and inflammation. Transmembrane C-type lectin receptors (CLRs) can use various intracellular signalling pathways to directly modulate cellular, developmental, homeostatic and immunological responses.

IV. Nucleotide-binding domain, leucine-rich repeat containing (NLRs)

Nucleotide-binding domain, leucine-rich repeat containing (NLRs) are a large family of cytoplasmic innate sensors that detect microbial products or cellular injury and stress. The NLRs are considered a very ancient family of innate immunity receptors because they were first identified in plants where they play a critical role in disease resistance (R genes) that are part of plant defences against microbial and parasite pathogens (Chisholm et al., 2006). Homologues of the NLRs are present in vertebrates and phylogenetically more primitive organisms such as the sea urchin but also in plants that express NB-LRR receptors with remarkable structural and functional similarities. The evolutionary conservation of the NLRs suggests that they play an important function in host defence.

There are 23 NLR family members in humans and at least 34 NLR genes in mice. NLRs are expressed in many cell types including immune cells and epithelial cells. Members of the NLR family of proteins are multidomain proteins that share many common structural features. They all possess the following domains (Lamkanfi & Dixit, 2014):

- C-terminal leucine-rich repeat (**LRR**) domains that usually confer ligand recognition specificity
- a central **NACHT** nucleotide-binding domain (NBD) domain (also referred to as NOD domain) closely related to the oligomerization module found in the AAA+ family of adenosine triphosphatases (ATPases) that is critical for activation. NACHT domain includes a nucleotide-binding domain (NBD), helical domain 1 (HD1), a winged helix domain (WHD), and helical domain 2 (HD2).
- a variable **N-terminal** protein-protein interaction domain required for signal transduction that divided the NLR into a variety of subfamilies.

Based on the different types of N-terminal domains, NLRs are classified into five subfamilies (Inohara et al., 2005): NLRA (acidic transactivation domains), NLRB (baculoviral inhibitory repeat (BIR) domain), NLRC (caspase-associated recruitment domain (CARD)), and NLRP (pyrin (PYD) domain). An additional subfamily, NLRX, characterized by the presence of an N-terminal domain without significant homology to any known domains and by its localization to the mitochondria, has been recognized (Tattoli et al., 2008; Ting et al., 2008).

The NLRA subfamily contains only one member named CIITA which presents an acidic transactivation domain involved in the transcriptional regulation of the MHC class II genes. The other three subfamilies are characterised by the presence of homotypic protein–protein interaction modules that are involved in the recruitment of signal transduction molecules. The NLRB subfamily is distinguished by the presence of the baculovirus inhibitor repeat (BIR) domain. The presence of a CARD is a feature of the NLRC subfamily, while members of the NLRP family contain a pyrin domain (PYD). Finally, NLRX1, a CARD-related X effector domain of unknown function shows no strong homology to the N-terminal domain of any other NLR subfamily member.

The NLRs can be classified functionally in two categories: those inducing innate immune pathways, such as NFκB, and those inducing the assembly of cytosolic signalling complexes known as inflammasomes. In these families of NLR, we find NLRC4 that belongs to the NLRC family, NLRP1-3,-6,-7,-9b,-12 that belong to the NLRP family but also atypical NLR-like proteins: B30.2 containing proteins as PYRIN (in human). Inflammasomes are high molecular weight oligomeric complexes that act as caspase 1-activating platforms in response to microbial components or sterile danger and stress signals leading to the release via a nonclassical secretion pathway depending on gasdermin D pore formation of inflammatory cytokines IL-1β and IL-18. The following chapters will discuss in detail the inflammasomes (see part II).

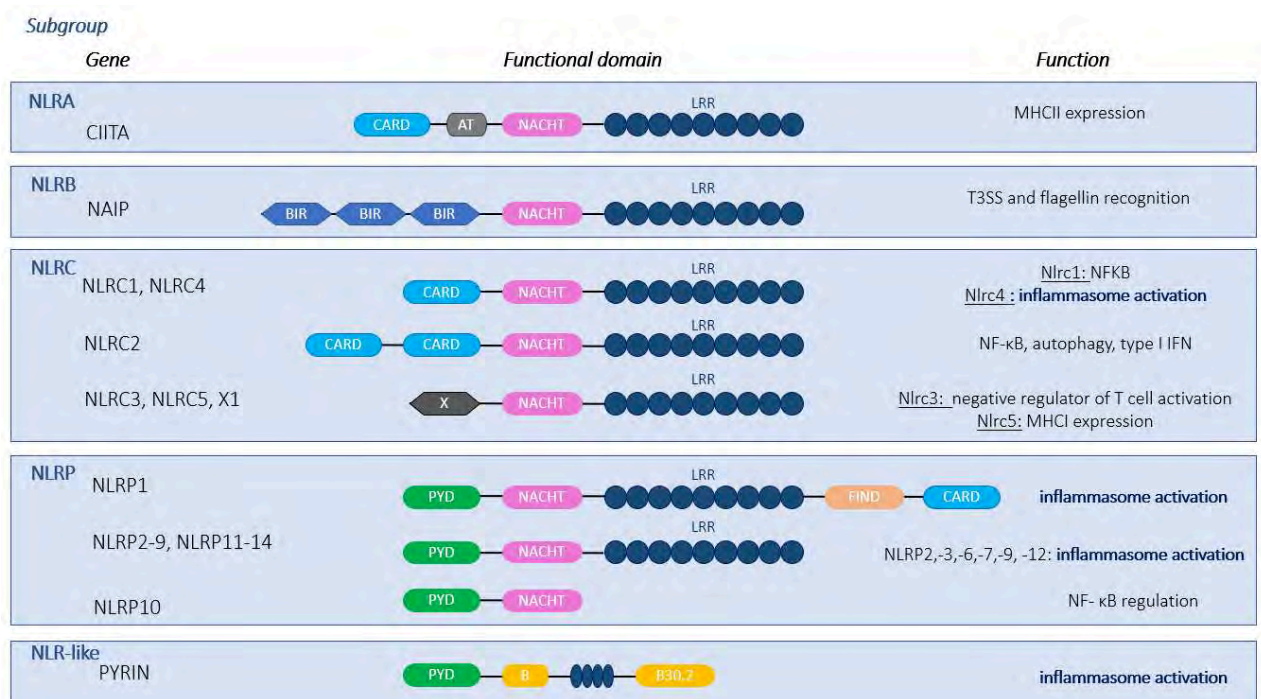


Figure 3: Human NOD-like receptors (NLRs)-classification and domain organization. LRR—leucine-rich repeats; NACHT—NAIP, CIITA, HET-E, and TP1 proteins; CARD—caspase activation and recruitment domain; AD—activation domain; BIR—baculovirus IAP repeat; PYD—pyrin domain. Adapted from: (Meunier & Broz, 2017)

V. Cytosolic DNA sensors (CDS)

➤ AIM2-like receptors (ALRs)

ALRs are DNA sensors activated by pathogens infection and stress conditions such as DNA break. We found 4 family members in humans and six in mice. The four members in human include: Absence in melanoma 2 (AIM2), IFN- γ inducible protein 16 (IFI16), Interferon-inducible protein X (IFIX or pyrin and HIN domain family member1, PYHIN1) and myeloid cell nuclear differentiation antigen (MNDA). While members in mice include AIM2, p202, p203, p204 and p205. Importantly, until now only AIM2 and IFI16 have been reported as PRRs. The fact that ALRs have only been described in mammals suggests that they are a novel family of receptors that appeared later in evolution.

The members of the ALR family are characterised by the presence of a HIN 200 domain that conserved repeats of 200 amino acid residues towards the C-terminus. The HIN domain in the proteins allows them to bind double-stranded DNA (dsDNA). Most members (except p202) also contain a PYRIN domain (PYD) in the N-terminus. Three members of the family in humans (MNDA, PYHIN1 and AIM2) present an N-terminal PYD domain, whereas the fourth member IFI16 harbours two tandem HIN200 domains and one PYD. In addition to DNA sensing and subsequent immune activation, the PYD domain can recruit the adaptor ASC to form an inflammasome, this is the case particularly for AIM2 and IFI16. AIM2 inflammasome can be activated by bacterial pathogens such as *Francisella tularensis*, *Listeria monocytogenes*, *Streptococcus pneumoniae*, *Mycobacterium tuberculosis* etc. IFI16 can also lead to inflammasome activation after dsDNA binding to nuclear IFI16. In addition, dsDNA binding to IFI16 triggers the expression of pro-inflammatory and antiviral cytokines via the STING/TBK1/IRF3 signalling.

➤ cGAS-STING

The cGAS -STING signalling molecules are intracellular PRRs that recognizes the cytosolic dsDNA (of viruses but also host-derived self dsDNA) and comprise a crucial cytosolic innate immune signalling pathway (in innate immune cells, including fibroblasts, macrophages, and DCs) to induce type 1 IFN production. cGAS was discovered in the year 2013 (Sun et al., 2013; J. Wu et al., 2013) and functions as a primary cytosolic DNA sensor that recognizes a broad repertoire of DNA from both foreign and self-origin and engages STING. STING is an adapter protein located on the endoplasmic reticulum (ER) that initiate the induction of type I IFNs and an extensive array of IFN-stimulated genes (ISGs), the output of which represents canonical cGAS-STING signalling. Given the central role of cGAS in detecting DNA of multi-purpose origin, the cGAS-STING pathway exerts remarkably diverse functions in varied cellular processes. Alternatively, cGAS-STING signalling have noncanonical functions and was recently linked with the induction of senescence and autophagy and to immune cell death and the regulation of

proliferation (Chen & Xu, 2022). Additionally cGAS is well conserved in evolution since bacterial form of cGAS were recently discovered (Whiteley et al., 2019)

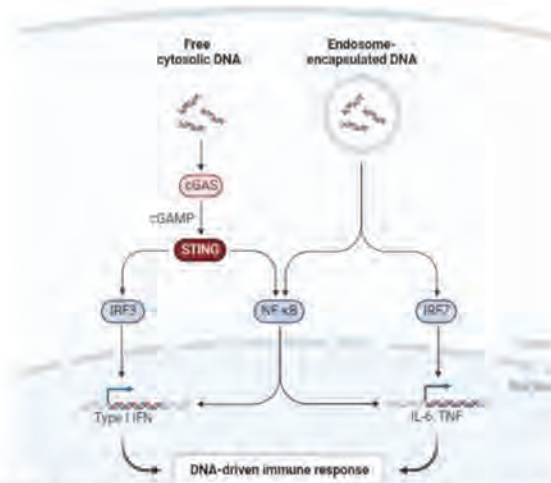


Figure 4: cGAS-STING signaling pathway. The cyclic GMP-AMP synthase (cGAS) stimulator of interferon gene (STING) signaling pathway is a critical immune pathway that functions to detect the presence of cytosolic DNA. This activation triggers an antiviral response leading to type-I IFN (IFN- α and IFN- β) production.

2. The immune system

1. Innate immunity

Innate immunity is the first line of defence against pathogens and provides a rapid nonspecific response to infection pathogenic microorganisms, metabolic perturbations and injury. This is set up in the first hours and involves different cell types. The activation of innate immunity is crucial for the downstream development of adaptive immunity, which is slower to develop and that can recognize and destroy specific pathogens.

Innate immunity is divided into two levels: the chemical and physical barriers (skin, saliva, stomach acid and urine flow) and the innate immune cells. Our body surfaces are defended by the epithelial cells, which impose a physical barrier between the internal environment and the external world to maintain homeostasis, integrity and permeability. We found epithelial cells in the skin but also in the respiratory, urogenital and gastrointestinal tracts. Due to their location, epithelial cells are specialized for their specific functions, such as the lung (gas exchange) and intestine (nutrient uptake) and have unique innate defence strategies against the pathogens they usually encounter. The internal epithelial are known as mucosal epithelia because they secrete a viscous fluid called mucus, which contains many glycoproteins called mucins that represent a key avoidance strategy that prevents pathogens from entering the body. Moreover, our surface epithelia are more than just physical barriers to infection, they also produce a wide range of chemicals that are microbicides or inhibit microbial growth. For example, the acid pH of the stomach and the microbicidal enzymes in the gastrointestinal tract. If these

barriers are crossed other elements of the innate immune system may immediately come into play, the innate immune cells.

Although these mechanisms have been known for many years, they have generally been considered to have only minor roles in the immune system. Consequently, epithelial cells have not received much attention in front-line immunology research. However, during my thesis, I was able to show a crucial role of epithelial cells following a viral (Sars-Cov2) or bacterial (*Pseudomonas aeruginosa*) infection that I will describe later in the results chapter.

➤ **Innate immune cells in phagocytosis and inflammation**

If a microorganism crosses an epithelial barrier and begins to replicate in the host's tissues, in most cases, it is immediately recognized by resident phagocytic cells. In the innate immune system, macrophages and monocytes, granulocytes, and dendritic cells are the primary classes of phagocytic cells. Macrophages are the major phagocyte population resident in most normal tissues at homeostasis. They can arise either from progenitor cells that enter the tissues during embryonic development, and then self-renew at steady state during life, or from circulating monocytes. Macrophages can also develop from monocytes that leave the bloodstream and infiltrate tissues after an infection or inflammation.

Neutrophils, eosinophils, and basophils are members of the granulocytes, which make up the second largest family of phagocytes. Neutrophils, also known as polymorphonuclear neutrophilic leukocytes (PMN) are the cells most directly involved in innate defence against infectious pathogens. These brief-lived cells are common in the blood but absent from healthy tissues. Because they can identify, eat, and eliminate a variety of pathogens without the assistance of an adaptative immune response, macrophages and granulocytes play a significant role in innate immunity.

The third class of phagocytes in the immune system is the immature dendritic cells that reside in lymphoid organs and in peripheral tissues. Conventional (or classical) dendritic cells (cDCs) that are subdivided into cDC1 and cDC2)) and plasmacytoid dendritic cells are the two primary functional varieties of dendritic cells (pDCs). Both types of cells develop from progenitors in the bone marrow, which largely branch from cells with myeloid potential, and they travel through the circulation to peripheral lymphoid organs and tissues throughout the body. Dendritic cells ingest and break down microbes, but, unlike macrophages and neutrophils, their primary role in immune defence is not the front-line, large-scale direct killing of microbes. A major role of cDCs is to process ingested microbes in order to generate peptide antigens that can activate T cells and induce an adaptive immune response. They also produce cytokines in response to microbial recognition that activates other types of cells against infection. cDCs are thus considered to act as a bridge between innate and adaptive immune

responses. pDCs are major producers of a class of cytokines known as type I interferons, or antiviral interferons.

An important effect of the interaction between microbes and innate immune cells is the activation of the inflammation. Inflammation is an important component of the innate immune response. It was originally described by pain, warmth, redness and tissue damage. It is induced following the release of cytokines and chemokines by macrophages and other immune cells. Collectively, these proteins induce a state of inflammation in the tissue, attract monocytes and neutrophils to the infection, and allow plasma proteins to enter the tissue from the blood. It is induced by the recognition of PAMPs and/or DAMPs by Pattern Recognition Receptors (PRRs) leading to the classical inflammatory response described in four steps: recognition of the danger signal, recruitment of cells, elimination of the danger and resolution of the inflammation.

II. Adaptive immunity

Adaptive immunity involves antigen-specific responses which are highly adapted to the specific pathogen and firmly regulated by crosstalk between innate immune cells. Adaptive immunity is composed of lymphocytes T and lymphocytes B.

T cells enter the bloodstream after completing their main development in the thymus. When they get to a secondary lymphoid organ, they leave the blood and move through the lymphoid tissue. They then return via the lymphatics to the bloodstream to circulate back and forth between the blood and secondary lymphoid tissues. Mature recirculating T cells that have not yet encountered their specific antigens are known as naive T cells. A naive T cell needs to encounter its particular antigen, which is delivered to it as a peptide: MHC complex on the surface of an antigen-presenting cell, in order to be stimulated to multiply and develop into effector T cells, which have new activities that help remove antigen. Naive T cells differentiate into numerous functional classes of effector T cells that are specialized for particular functions upon identifying antigens. Naive CD8 T cells differentiate into cytotoxic effector T cells that recognize and destroy infected cells when they recognize pathogen peptides presented by MHC class I molecules. The effector repertoire of CD4 T cells is more flexible. Naive CD4 T cells can develop down diverse pathways that produce effector subsets with different immunological activities against various microorganisms after identifying pathogen peptides presented by MHC class II molecules. The primary regulatory T cells, or Treg cells, which limit the degree of immunological activation, are TH1, TH2, TH17, and TFH, which activate their target cells (see figure 5).

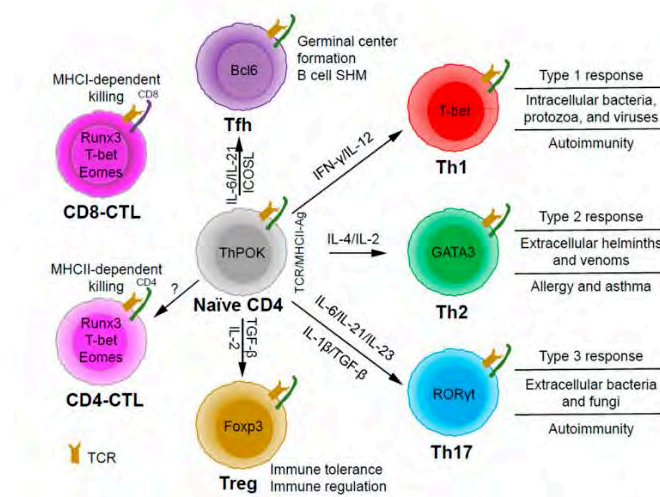


Figure 5: Function and differentiation of different CD4 T cells (X. Zhu & Zhu, 2020). Naïve CD4 T cells can differentiate into Th1, Th2, Th17, Tfh (follicular T helper), and Treg (T regulatory) subsets upon T cell receptor (TCR) activation through the role of different cytokines. T cells may also become cytotoxic CD4 T cells (CD4-CTLs) that kill their target cells in a major histocompatibility complex class II (MHCII)-restricted manner.

B cells perform a variety of critical functions in the immune system, including antigen presentation, cytokine secretion, and setting up the structure of lymphoid organs, but they are most well-known as the adaptive immune system's antibody-producing cells. B cells have the capacity to respond to a range of foreign antigen molecules by making highly specific antibodies.

III. Cell-autonomous immunity

Our prevailing view of vertebrate host defence is strongly shaped by the notion of a specialized set of immune cells as sole guardians of antimicrobial resistance. However, this view seriously underestimates the ability of most cells, the majority of which are not part of the traditional immune system, to defend themselves against infection. This old and pervasive form of host protection is called autonomous cell immunity. Cell-autonomous immunity, which is defined as the ability of a host cell to eliminate an invasive infectious agent is mediated by immune signalling networks that sense microbial pathogens and stimulate downstream pathogen elimination programs. It relies on antimicrobial proteins, specialized degradative compartments, interferon responses and programmed host cell death.

➤ Antimicrobial peptides

Self-defence begins even before pathogens come into contact with the cell surface. Our body surfaces are defended by the epithelial cells, which impose a physical barrier between the internal environment and the external world to maintain homeostasis, integrity and permeability. Epithelial barriers have developed also chemical secretions, such as the anti-microbial peptides (defensins, cathelicidins...) to inhibit microbial growth. For example, specialized gut epithelial Paneth cells secrete the antimicrobial lectin, RegIIIg, into the lumen of the small intestine to maintain a germ-free barrier.

➤ Autophagy

Host cells have evolved methods to link pathogen detection with pathogen disposal. One of the best examples is the recognition of cytosolic pathogens and their subsequent delivery to lysosomes by the process of macroautophagy. A large number of ubiquitin E3 ligases have been identified and are responsible to coat viral and bacterial surfaces with ubiquitin, thus targeting microorganisms for loading into autophagosomes (*de novo* generated membrane-bound compartment) through interaction with the autophagosome-associated protein LC3 (Chang, 2020). During infection, eukaryotic cells co-opt autophagy to defend the cytosol against bacterial invaders, to attack microbe-containing vacuoles, and to remove pathogen-derived inclusion bodies (Randow & Münz, 2012). Selective autophagy relies on cargo receptors that cross-link “eat-me” signals on prospective cargo to ubiquitin-like proteins of the ATG8 family displayed on the phagophore membrane. Antimicrobial autophagy (“xenophagy”) uses many of the same eat-me signals that alert the autophagic machinery to engulf host protein aggregates and damaged organelles. Autophagy efficiently restricts the subpopulation of vesicle-inhabiting bacteria that, by damaging the limiting membrane of their vacuole, become exposed to the cytosol, for example, *Mycobacterium tuberculosis* and *Salmonella Typhimurium*.

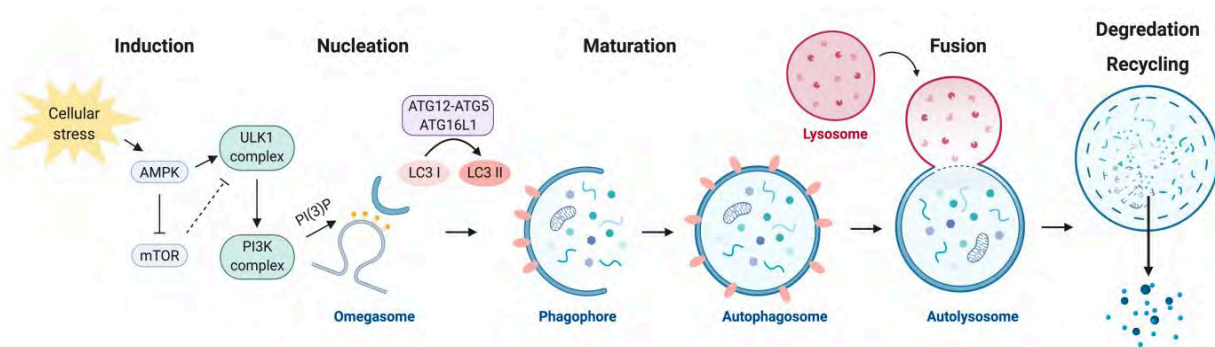


Figure 6: The autophagy pathway from (Chang, 2020). Autophagy is a multi-step process of sequential events that sequester intracellular components (proteins and organelles) in phagosomes to induce degradation and recycling of nutrients. This process depends on the maturation of the autophagosome and the fusion with the lysosome.

➤ IFN response

A variety of specialized pattern recognition receptors, most notably those that sense viral nucleic acids such as cyclic GMP-AMP synthase (cGAS), AIM2, RIG-I, MDA5, OAS1 and several Toll-like receptors (TLRs), are used to detect viral infection (Sun et al., 2013). Typically, these sensors initiate signalling cascades that eventually activate the synthesis of interferons. This response to viruses involves the release of interferons as well as the expression of hundreds of genes known as interferon-stimulated genes (ISGs), which have various antiviral functions within the cell. Antiviral genes encode enzymes such as APOBEC3 that edit and destroy viral nucleic acids¹, SMHD1 (SAM domain and HD domain-containing protein 1) and other enzymes that deplete the cell of nutrients essential for virus replication, viperin proteins that produce antiviral chain terminator molecules, and proteins that interfere with viral entry, uncoating,

assembly and budding (such as IFITM, TRIM proteins, tetherin and GBPs) (Meunier & Broz, 2016; Wein & Sorek, 2022).

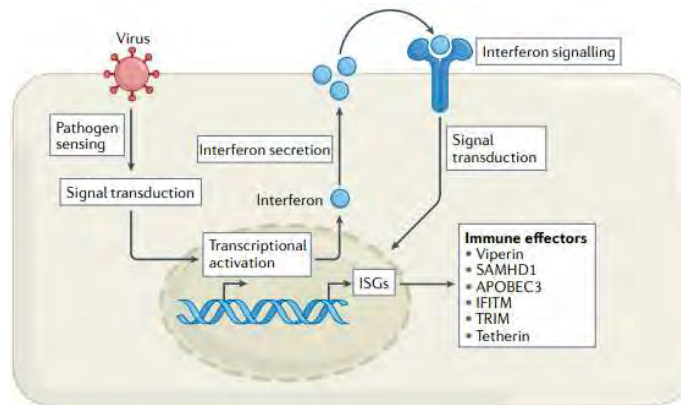


Figure 7: Model of IFN response from (Wein & Sorek, 2022). Type I IFNs are transcriptionally regulated, and are induced following the recognition of pathogens components during infection by various host pattern recognition receptors. Following their production, type I IFNs trigger antiviral responses by binding to a common receptor (IFNAR). IFN α/β binding to IFNAR stimulates the JAK1-STAT pathway leading to the expression of IFN-stimulated genes (ISG) implicated in a large group of genes which play a role in host resistance to viral infections.

➤ **Programmed cell death**

An important host defence mechanism against pathogens is the induction of a regulated cell death. By this strategy, the host can eliminate infected cells in order to kill intracellular pathogens or to eliminates cells that were hijacked for the benefit of the pathogen. The regulated cell death can be categorized into apoptotic cell death or necrotic cell death (including necroptosis, ferroptosis and pyroptosis). Both pyroptosis and necroptosis result in the rupture of the plasma membrane that releases cellular content into the extracellular space, while apoptosis converts a cell into apoptotic bodies that retain cell content within membranes. Regulated cell death can be initiated by a variety of sensors of the innate immune system: direct sensors as PRRs, that can bind microbial ligands but also by “guards” that monitor normal function of cellular proteins and “decoys” that act like lures, tempting virulence factors to attack them.

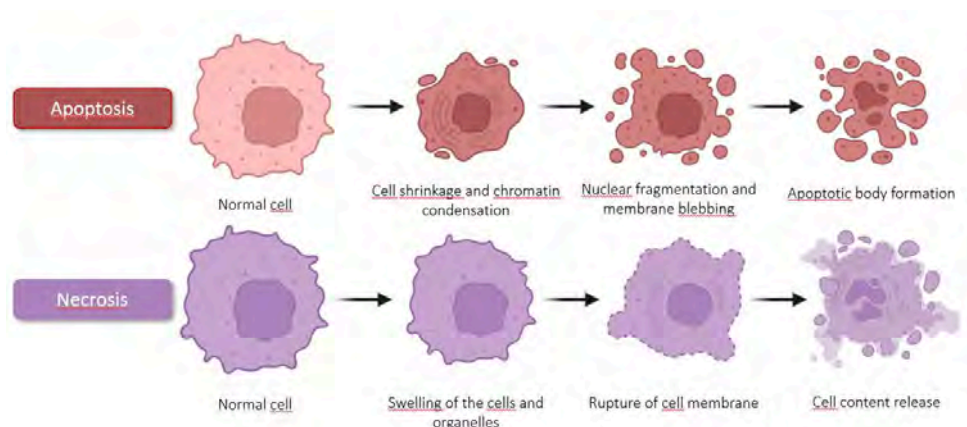


Figure 8: Apoptotic versus necrotic cell features. Regulated cell death can be categorized into apoptotic cell death and regulated cell necrosis, depending on the morphological characteristics and molecular mechanisms. This figure represents the morphological characteristics of these two regulated cell death and shows that apoptosis retains cell membrane integrity compared to cell necrosis that is characterized by membrane rupture and cell content release.

- **Apoptosis**

Apoptosis was the first type of programmed cell death to be described, initially based on morphological features that distinguished it from necrosis. In this regard, John Kerr, Andrew Wyllie, and Alastair Currie described and characterized apoptosis for the first time in 1972 by cell shrinkage, membrane blebbing, and chromatin condensation as well as nuclear fragmentation (Kerr et al., 1972). Importantly, during apoptosis, the plasma integrity is preserved, avoiding the release of intracellular contents to the extracellular milieu, these features contribute to the reputation of apoptosis as an immunologically “silent” process without an inflammatory response. It exists a wide variety of stimuli and conditions (physiological and pathological) that can trigger apoptosis. Apoptosis is physiologically implicated in the normal eukaryotic development and ageing but also in the maintenance of the cell homeostasis that occurs without the cardinal signs of inflammation. However, apoptosis also occurs as a defence mechanism such as in immune reactions or when cells are damaged by disease or stress factors that will generate a change in cell homeostasis. In this case, the apoptotic cells will release a series of so-called “find-me” signals, such as extracellular ATP capable of recruiting phagocytes to the site of apoptotic corpses, therefore, at least one aspect of an inflammatory reaction. Additionally, it has recently been demonstrated that apoptosis triggered by the FAS/CD95 death receptor is linked to the production of chemokines and other immunologically active proteins that regulate phagocyte migration and effective apoptotic cell clearance (Hochreiter-Hufford & Ravichandran, 2013). All things considered, it is acceptable to conclude that although not completely “silent,” apoptosis is a form of cell death that does not trigger an over inflammatory response. The apoptotic cell death is mechanistically dependent on the activation of apoptotic effectors caspase-3/-7 (D. Tang et al., 2019). Caspases are an evolutionarily conserved family of cysteine proteases that, upon activation, induce the cleavage of proteins implicated in the structural integrity of the cell and nucleus.

- **Necrosis**

For two decades, necrosis was mostly thought of as an "accidental" cell death that happened in reaction to physicochemical insults, whereas apoptosis was thought to be the usual cell death form during development, homeostasis, infection, and disease. This viewpoint has been significantly altered by recent genetic findings, as well as the discovery of pharmacological necrosis inhibitors, and the identification of various mechanisms for controlled necrosis. Regulated necrosis is characterized visually by cytoplasmic granulation, organelle and/or cellular enlargement ('oncosis'), and is defined as a genetically controlled cell death process that eventually ends in cellular leakage. These physical characteristics are shared by numerous cell death mechanisms, and it is now necessary to investigate any shared or unique underlying signalling pathways. In an effort to identify and categorize different types of cell death and the underlying pathways that underlie them, numerous neologisms have been

created, including necroptosis, parthanatos, oxytosis, ferroptosis, ETosis, NETosis, pyronecrosis, and pyroptosis. These various forms of cell death were classified as controlled necrosis.

In this section, I will briefly describe some regulated cell necrosis, focusing in particular on Pyroptosis, which is the cell death in which I worked during my thesis.

▪ **Necroptosis**

Necroptosis is a well-characterized programmed necrosis induced by perturbations of the extracellular or intracellular microenvironment. This type of cell death occurs following the activation of the tumor necrosis receptor (TNFR1) by TNF α , 3 even though TNF α has long been considered an inducer of apoptosis. Activation of other cellular receptors can also trigger necroptosis. These receptors include death receptors Fas (also referred to as CD95 or Apo-1), DR3 (also referred to as Apo-3), DR4 (also referred to as Apo-2 or TRAIL-R1), DR5 (also referred to as TRAIL-R2), Toll-like receptors (TLR4 and TLR3) and cytosolic nucleic acid sensors such as RIG-I and STING, which induce type I interferon (IFN-I) and TNF α production and thus promote necroptosis in an autocrine feedback loop.

The majority of these pathways trigger NF κ B dependent proinflammatory and prosurvival signals. The necroptotic pathway is nevertheless activated by further suppression of the proteolytic enzyme Caspase-8 by microorganisms or pharmacological agents. Downstream of the abovementioned receptors, active RIPK1 is recruited within an oligomeric complex that includes FADD, caspase-8 and caspase-10. In the absence of caspase-8 activity, RIPK1 recruits and phosphorylates RIPK3, forming a complex called the ripoptosome. The RIPK1/RIPK3 complex recruits and phosphorylates MLKL, thus forming the necrosome. Phosphorylated MLKL undergoes oligomerization and migrates to the plasma membrane where it induces necroptosis by initiating membrane rupture or regulating ion flux. In the necroptosis process, these proteins are fine-tuned by posttranslational regulation via phosphorylation, ubiquitination, glycosylation, and protein–protein interactions.

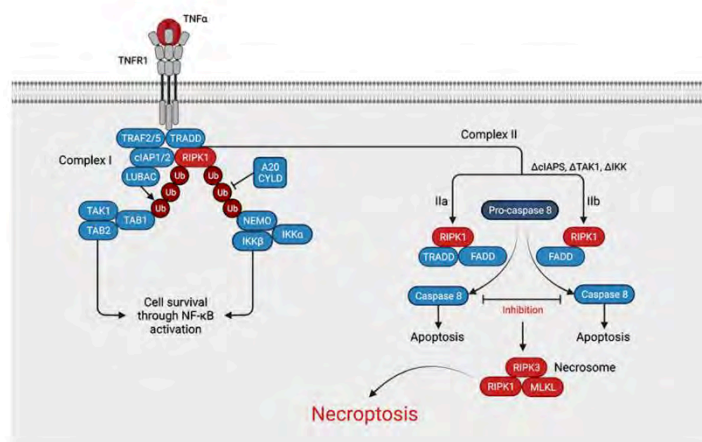


Figure 9: Model of necroptosis pathway adapted from (J. Chen et al., 2019). Necroptosis can be induced by various stimuli such as TNF α . In short, ubiquitination of RIPK1 leads to cell survival through activation of NF- κ B, whereas de-ubiquitination of RIPK1 leads to the formation of the complex II. In the absence of caspase-8 activity, RIPK1 recruits and phosphorylates RIPK3. The RIPK1/RIPK3 complex recruits and phosphorylates

MLKL, thus forming the necrosome. Phosphorylated MLKL undergoes oligomerization and migrates to the plasma membrane where it induces necroptosis by initiating membrane rupture or regulating ion flux.

- **Ferroptosis:**

Ferroptosis is a newly discovered form of regulated cell death (RCD), characterized by excessive iron accumulation and subsequent unbalanced redox states. Although there were several studies on ferroptosis and its mechanisms several years ago, the term "ferroptosis" was first described by the laboratory of Bren R. Stockwell in 2012 and has become a research hotspot in the field of cell death. The molecular mechanisms of ferroptosis depend mainly on the production and elimination of lipid peroxidation. Ferroptosis is triggered when excess iron induces high intracellular production of ROS through the Fenton reaction, disturbing the redox balance and triggering lipid peroxidation. Several antioxidant mechanisms regulate the redox state of the cell, such as glutathione peroxidase 4 (GPX4), which catalyses the reduction reaction of lipid peroxide (LOOH) and maintains the balance of the redox reaction. When cells are unable to remove the excess peroxide, the accumulation of lipid peroxidation leads to ferroptosis. This regulated necrosis is characterized by increased membrane density, shrunken mitochondria, and rupture of the outer mitochondrial membrane. Ferroptosis has been implicated in several diseases, including Parkinson's and Huntington's disease, cancer, ischemia-reperfusion of the kidneys and liver, as well as infectious diseases.

- **Pyroptosis**

Pyroptosis is a type of necrotic cell death culminating in the loss of plasma membrane integrity and release of pro-inflammatory cytokines. To distinguish this novel form of cell death from the other types of necrosis the term pyroptosis was proposed: 'pyro' meaning fire or fever, and 'ptosis' meaning to fall. The pyroptosis is induced by activation of so-called inflammasome sensors. These include the Nod-like receptor (NLR) family, the DNA receptor Absent in Melanoma 2 (AIM2) and the Pyrin receptor. The pyroptotic cell death is induced by the detection of a large variety of PAMPs and DAMPs released by pathogens or cellular stress and damage. Upon detection, the inflammasome sensors will oligomerize and recruit the adaptor protein (ASC) and the procaspase 1, therefore forming the multimolecular inflammasome complex (Martinon et al., 2002). Once assembled, the inflammasome cleaves and activates the caspase-1 that will cleave different substrates in the cell. On one hand, caspase1 will cleave the pro-inflammatory cytokines IL-1 β and IL-18 into their mature form and on the other hand caspase 1 will cleave gasdermin-D protein, generating an N-terminal fragment that binds to the plasma membrane, oligomerizes and induce the pore formation that allows the release of pro-inflammatory cytokines IL-1 β and IL-18 (Rühl & Broz, 2022). Of note, IL-1 family members are cytokines that are released in an ER/Golgi-independent manner. Importantly, gasdermin-D is in most cases still required for the secretion of these cytokines, implying that gasdermin-D pores can act as channels for unconventional protein secretion. A non-canonical pathway (non-caspase1 dependent) inducing

pyroptosis was described in 2011 (Kayagaki et al., 2011a). This pathway depends on the activation of caspase 11 (caspase 4/5 in humans) that will upon recognition of LPS induce the cleavage of gasdermin-D and lead to pyroptosis.

Despite evidence of the role of gasdermin-D in the execution of pyroptotic cell death and the release of IL-1 β and IL-18, the mechanisms leading to plasma membrane rupture and cell death were not clear. Gasdermin-D mediated pore formation collapses the electrochemical gradient across the plasma membrane, depletes ATP levels and disturbs cellular metabolism and homeostasis, which eventually will lead to water influx and increase in osmotic pressure inside the cell that culminates in a plasma membrane rupture (Rühl & Broz, 2022). It was however recently described (Kayagaki et al., 2021) a novel protein known as Nerve Injury-induced Protein 1 (NINJ1) linked to the control of the plasma membrane rupture. Indeed, cells lacking NINJ1 still undergo cell swelling and plasma membrane pore formation- mediated by GSDM-D- but failed to release cytoplasmic content, indicating a role for NINJ1 downstream of Gasdermin-D pore formation. Still, unanswered questions persist, such as how NINJ1 gets activated and how it permeabilizes or disrupts the plasma membrane. Oligomerization of NINJ1 to the plasma membrane is required for plasma membrane rupture but the signals promoting NINJ1 activation are still unknown.

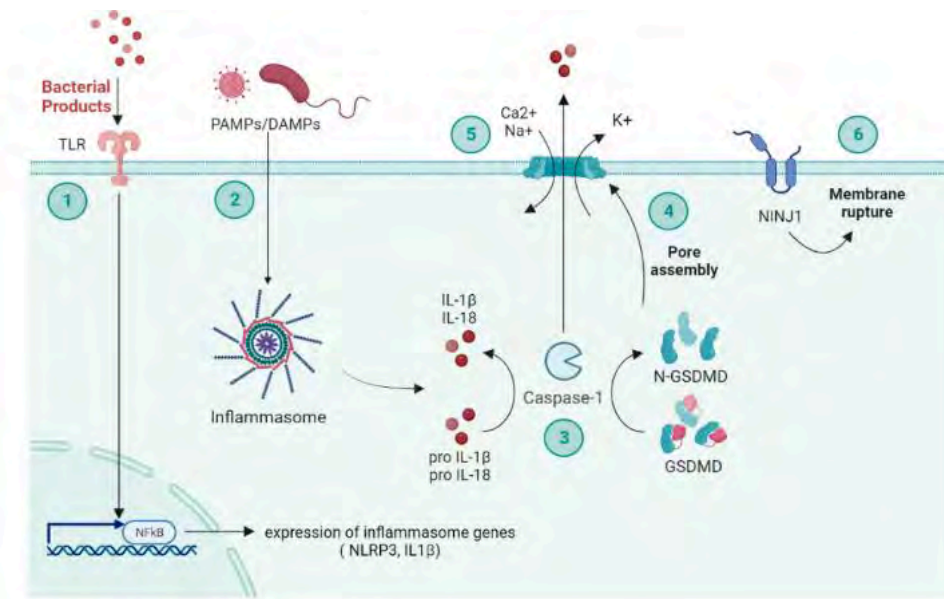


Figure 10: Mechanisms of inflammasome activation leading to a pyroptotic cell death. Pyroptosis is a lytic cell death induced by the detection of a large variety of PAMPs and DAMPs released by pathogens or cellular stress and damage. Upon detection, the inflammasome sensors will oligomerize and recruit the adaptor protein (ASC) and the procaspase 1, therefore forming the multimolecular inflammasome complex. Once assembled, the inflammasome cleaves and activates the caspase-1, which will cleave the pro-inflammatory cytokines IL-1 β and IL-18 into their mature form, and the gasdermin-D protein, generating an N-terminal fragment that binds to the plasma membrane, oligomerizes and induces the assembly of a gasdermin-D pore in the cell membrane. The gasdermin-D pore allows the release of pro-inflammatory cytokines IL-1 β and IL-18. Finally, oligomerization of NINJ1 into the plasma membrane induces the rupture of the cell membrane and the release of the cell content. Abbreviations: DAMPs, damage-associated molecular patterns- PAMPs, pathogen-associated molecular patterns- N-GSDMD: N-terminal gasdermin D, GSDMD: gasdermin D- NINJ1, ninjurin 1.

II. Inflammasome

Recently, in 2002, the term inflammasome was coined by the team of Jurg Tschopp that discovered a huge molecular platform composed of three core proteins: a receptor (in this case an NLR protein named NLRP1), the adaptor protein apoptosis-associated speck-like protein containing a CARD (ASC) and the pro-inflammatory protease caspase-1 (Martinon et al., 2002). Following this, different groups showed that different NLRs can be implicated in the inflammasome formation. Tschopp and colleagues showed in 2004 that NLRP3 also forms an inflammasome complex with ASC, and caspase-1 (Agostini et al., 2004). Dixit and colleagues, in the same year, reported the crucial role of the adaptor protein ASC in the assembly of the inflammasome, supported by the creation of ASC and Nlrp4-deficient mice (Mariathasan et al., 2004). Importantly, macrophages lacking either ASC or Nlrp4 were not able to induce a pyroptosis caspase-1-dependent cell death.

Inflammasomes are signaling platforms crucial to the innate immune response to infectious diseases. Nowadays, a large variety of inflammasomes exist, capable of recognizing molecular patterns unique to pathogens, dangers, stress or homeostatic perturbations. Inflammasomes are platforms leading to the activation of pro-inflammatory caspases, namely caspase-1 for canonical inflammasomes, and human caspase-4-5 (caspase-11 in mouse) for non-canonical inflammasomes (described later) that triggers the induction of pyroptotic cell death and release of proinflammatory cytokines.

Simplistically, inflammasomes are comprised of a sensor, an adapter and an effector. Typically, inflammasome complexes are named after their sensor including NLRP1, NLRP3, NLRC4, AIM2 and PYRIN. The majority of sensors that oligomerize to an inflammasome belong to the family of NLRs composed of a central nucleotide-binding and oligomerization domain (NACHT), a C-terminal leucine-rich repeat (LRRs) and N-terminal caspase recruitment domain (CARD) or pyrin (PYD) domains. However, not all receptors with a NACHT domain have been described as forming an inflammasome and not all receptors forming an inflammasome have a NACHT domain (AIM2, Pyrin, CARD8) (Figure 11). Inflammasomes can signal directly to caspase-1 if they contain a CARD (NLRC4, mouse NLRP1b, CARD8) or indirectly via the ASC adaptor if they signal through a PYD domain (AIM2, PYRIN, NLRP3). In contrast, caspase-11 is a combined direct sensor and protease that activates itself when it binds to LPS, activating a non-canonical inflammasome.

Although these complexes play crucial roles in host defence, aberrant inflammasome activation has been associated with a number of diseases. Cryopyrin-associated periodic syndromes (CAPS) and familial Mediterranean fever (FMF) are two autoinflammatory disorders that are brought on by mutations in the NLRP3 and Pyrin genes. Chronic inflammasome activation has also been linked to the progression of cancer, metabolic disorders, and neurodegenerative diseases (Karki & Kanneganti, 2019;

Voet et al., 2019; H. Wen et al., 2012). Therefore, it is not surprising that the expression of inflammasome components, downstream effector molecules, and the upstream regulatory molecules necessary for effective activation is tightly regulated by a number of transcription factors (Interferon regulatory factor 1 (IRF1)) (Christgen et al., 2020). Furthermore, each sensing molecule-specific mechanism controls how each inflammasome is activated. These activation mechanisms can be broadly categorized into those that depend on direct ligand-binding and indirect activation mechanisms.

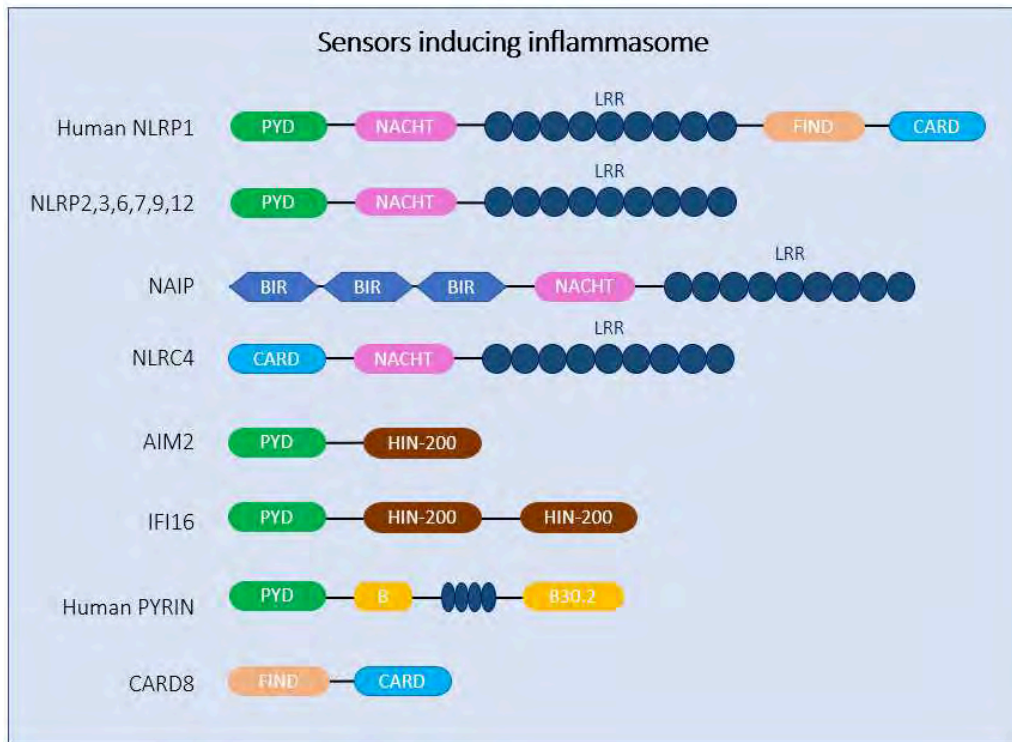


Figure 11: Structures of inflammasome-forming receptors in humans. Abbreviations: LRR (leucine rich repeats), NACHT (NAIP, CIITA, HET-E and TP1 proteins), CARD (caspase activation and recruitment domain), BIR (baculovirus IAP repeat), PYD (Pyrin domain), HIIN-200 (hematopoietic interferon-inducible nuclear proteins with 200 amino-acids), FIIND (function-to-find domain).

Many nucleotide-binding, leucine-rich repeat (NLR) proteins are revealed by analysis of plant genome sequences and are encoded by putative R genes. Although we currently know very little about the mechanism of action, our understanding is increasing. In 2019, it was shown that the *Arabidopsis thaliana* HOPZ-ACTIVATED RESISTANCE 1 (ZAR1) protein, which activates defense in response to several pathogenic bacterial effectors, works similarly to mammalian NLRs inflammasome forming sensors. ZAR1 is a flexible signaling platform that has evolved to monitor the homeostasis of an important immune system, the receptor-like cytoplasmic kinase (RLCK) class VII kinases family. In the presence of bound ADP, ZAR1 is in an autoinhibited resting state associated with several RLCK class XII kinases. However, with ATP, induced by rupture of homeostasis, ZAR1 oligomerize into a large form with a pentameric structure that has the potential to form pores in membranes, they called it the

“resistosome”. Activated ZAR1 relocates to the plasma membrane, and the amino-terminal α -helix is required for this. This result remains to be confirmed but they encourage many interesting future experiments in plants (Dangl & Jones, 2019).

1. The canonical inflammasome

Canonical inflammasomes are composed of a receptor/sensor (NLR, Pysin or PYHIN), the adaptor protein (ASC), when required, and the inflammatory protease, pro-caspase-1. The assembly of inflammasome start with the recognition of DAMPs and/or PAMPs by the sensors. Upon this recognition, sensors will oligomerize and recruit the adaptor ASC, which will finally recruit and activates pro-caspase-1 in its mature and active form.

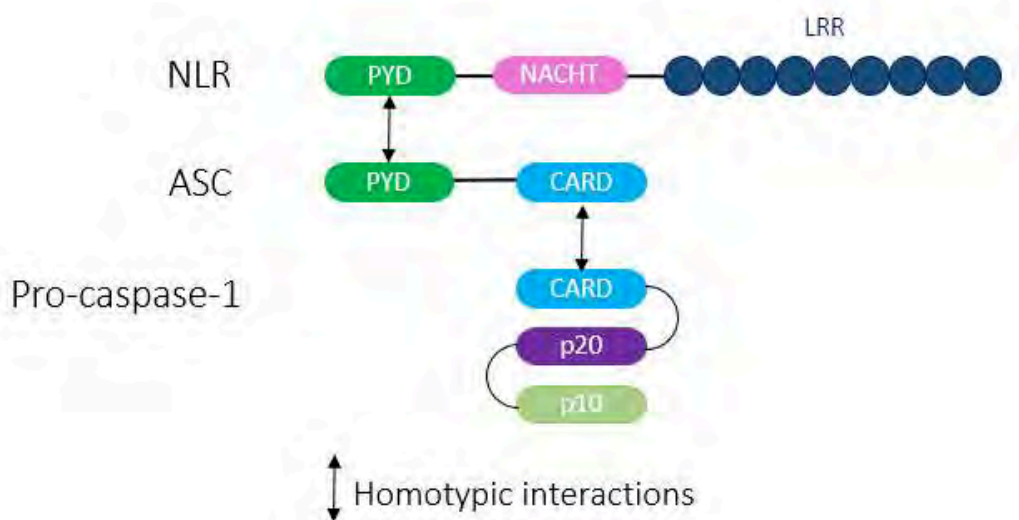


Figure 12: The inflammasome compounds and interactions. The inflammasome complex is composed of a receptor/sensor (NLR, Pysin or PYHIN), the adaptor protein (ASC) and the inflammatory protease, pro-caspase-1. The assembly of the complex depends on homotypic interactions between the PYD and the CARD domains.

ASC is a small molecule (encoded by PYCARD) constitutively expressed in many cells that multiple inflammasomes require to recruit and activate caspase-1. ASC contains a PYD domain in the N-terminal and a CARD (Caspase Recruitment Domain) domain in C-terminal. The PYD domain allows the binding with the sensor through PYD-PYD interactions while the CARD domain allows the binding to pro-caspase-1 through CARD-CARD interactions. ASC is not required for all inflammasome assembly as some receptors already express a CARD domain and are able to interact directly with caspase-1, such as NLRC4 and CARD8 (see figure 11). Given the important role that ASC plays in inflammasome activation, it’s not surprising that the promoter of ASC (containing a large CpG island) is silenced by methylation in some cancers, notably in breast cancer (Stimson & Vertino, 2002). A better understanding of its regulation may provide insights into how cancers and other diseases progress.

Caspase-1 is a cysteine protease that cleaves specific substrates present after aspartic acid residues. Caspase-1 is synthesized as an inactive zymogen form, the pro-caspase-1, composed with a CARD

domain (N-terminal) and two catalytic subunits p20 and p10. Once it's recruited by the adaptor ASC, pro-caspase 1 gets activated by proximity-induced dimerization, leading to self-proteolytic cleavage into the enzymatically active heterodimer p33/p10 (see figure 13). Activation of caspase-1 leads to the maturation of the inflammatory cytokines pro-IL1- β /18 and the cleavage of the cytosolic protein gasdermin-D (GSDM-D). There is little understanding of how caspase-1 transcription is regulated. Caspase-1 is expressed constitutively in murine macrophages, and some research suggests that NF- κ B or IRF1 may activate caspase-1 (caspase-1 promoter contains NF- κ B and IRF1-binding sites). In fact, caspase-1 is increased in chronic inflammatory situations and given the crucial function caspase-1 performs in pyroptosis, it is important to understand how it is regulated (D. J. Lee et al., 2015).

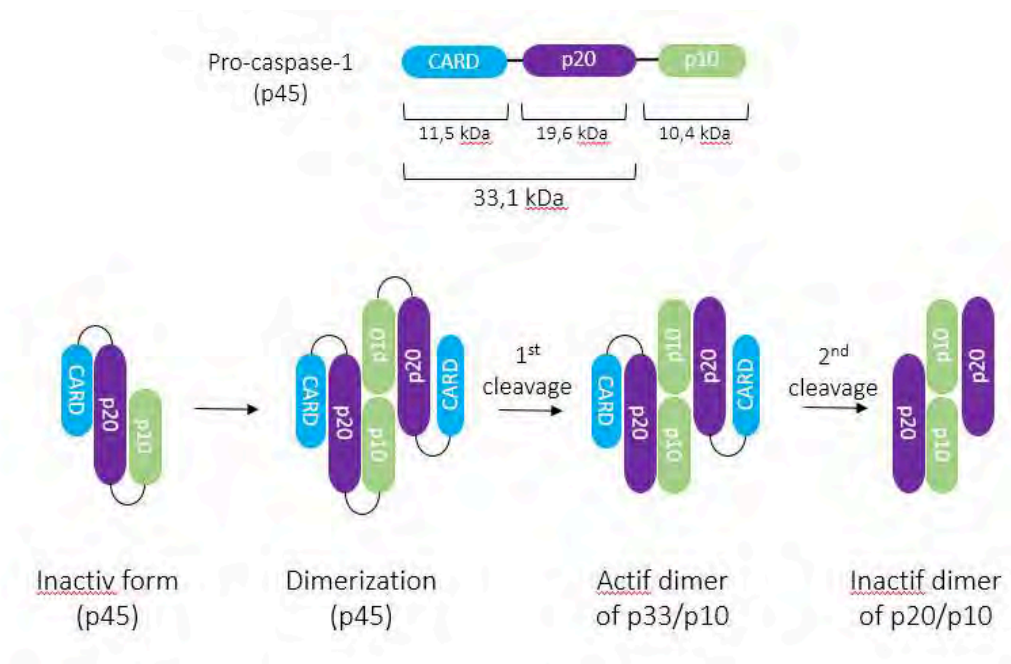


Figure 13: Mechanisms of caspase-1 activation. Pro-caspase-1 is divided into 3 domains: a CARD domain allowing its recruitment to the inflammasome complex and two catalytic subunits p20 and p10. Pro-caspase-1 is expressed in an inactive form in the cytosol, once recruited to the inflammasome, it dimerizes, which weakly activates it and allows the first auto-proteolytic cleavage located between the p20 and p10 domains to give a p33/p10 dimer. This dimer is strongly active and is still located in the inflammasome. The second cleavage takes place, allowing the formation of the p20/p10 dimer, its dissociation from the inflammasome and its quickly inactivation.

I. Receptors of inflammasome

To date several cytosolic sensors have been described to form an inflammasome including PRRs (NLR family, AIM2, IFI16), Pyrin and CARD8 (see table 1).

Inflammasome	Activator	References
Human NLRP1	3C and 3CL protease dsRNA (SFV) ribotoxic stress (UVB, exotoxin A) Valbopropro (Talabostat): DPP8/9 inhibitor Reductive stress	(Bauernfried et al., 2021 ; Jenster et al., 2023a; Planès et al., 2022; Robinson et al., n.d., 2020a)(Q. Wang et al., 2023) Pinilla et al., under review 2023
NLRP2	ATP	(J. Xu & Núñez, 2022)
NLRP3	Diverse stimuli, and multiple molecular and cellular events, including ionic flux (K ⁺ /Ca ²⁺), mitochondrial dysfunction, lysosomal damage...	(Swanson et al., 2019)
NLRP6	Lipoteichoic acid	(Hara et al., 2018)
NLRP9B	Short ds RNA (only in rodents)	(Ngo & Man, 2017)
NLRC4	Flagellin Bacterial T3SS (needle, rod) Retrotransposons RNA	(Kofoed & Vance, 2011a; Shao-bin Wang, 2021)
AIM2	Cytosolic dsDNA (Specific to rodent cells and epithelial human cells but not human monocytes/macrophages)	(Hornung et al., 2009b)
PYRIN	Loss of Rho-GTPases Phosphorylation	(Gao et al., 2016a; Heilig & Broz, 2018; Park et al., 2016a)
CARD8	Valbopropro (Talabostat): DPP8/9 inhibitor Viral proteases (HIV-PR, CVB3) Reductive stress Intracellular peptides accumulation (through inhibition of aminopeptidases including M24B)	(Johnson et al., 2020a; Nadkarni et al., 2022; Rao et al., 2022; Q. Wang et al., 2021, 2023)
Controversial inflammasomes		
NLRP7	Positively and negatively affect inflammasome responses (context dependent)	(Carriere et al., 2021)
NLRP12	Positively and negatively affect inflammasome responses (context dependent)	(Tuladhar & Kanneganti, 2020)
IFI16	KSHV DNA Still discussed	(Kerur et al., 2011)

Table 1: Receptors forming inflammasomes. Abbreviations: CVB3-Coxsackievirus B3, dsRNA-double stranded RNA, HIVPR- HIV protease, KSHV-Kaposi's sarcoma-associated herpesvirus, SFV-Semliki Forest virus, T3SS-type 3 system secretion

➤ The NLRP3 inflammasome

The NLRP3 inflammasome is currently the most fully characterized inflammasome and shares the common three domain structure: a central NACHT domain, a PYD domain in the N-terminal and an LRR in C-terminal (see Figure 11). The NLRP3 inflammasome can be activated through three pathways: canonical, non-canonical, and alternative pathways. In the following paragraphs, I will focus on the canonical activation of NLRP3. Non-canonical activation will be described later in the paragraph on non-canonical inflammasome.

NLRP3 has the particularity to require two signals to be fully activated: the priming and the activation signal. Initially, the necessity of priming had been ascribed to the fact that NLRP3, in murine macrophages, is expressed at a low level in basal conditions, and therefore the priming step was necessary to induce transcriptional upregulation of NLRP3 and it was named transcriptional priming. This priming signal is induced upon recognition of PAMPs/DAMPs by the TLRs leading to the upregulation of NLRP3 and pro-inflammatory cytokines expression through the NF- κ B/MYD88 pathway (Bauernfeind et al., 2009). Lipopolysaccharide (LPS) activating TLR4 is commonly used to provide a priming signal. However, NLRP3 can also be primed non-transcriptionally, for example, by a brief pulse of LPS treatment (Juliana et al., 2012). Several post-translational changes of NLRP3, such as phosphorylation, dephosphorylation, deubiquitination, and de-sumoylation, have been implicated in these forms of priming (Barry et al., 2018; Shim & Lee, 2018). Under steady-state conditions, many cells already express NLRP3 in adequate numbers, which highlights the importance of non-transcriptional priming (McKee & Coll, 2020). Following the priming, the NLRP3 inflammasome can be activated by an array of stimuli.

Different from other inflammasomes, the NLRP3 inflammasome requires a critical cofactor for inflammasome activation in murine macrophage cells. It was shown that the NIMA-related kinase 7 (NEK7), a serine-threonine mitotic kinase is critical for inflammasome activation downstream of K⁺ efflux in mice (He, Hara, et al., 2016; He, Zeng, et al., 2016; Schmid-Burgk et al., 2016; H. Shi et al., 2016). NEK7 specifically interacts with NLRP3, and promotes NLRP3 self-oligomerization and activation. However, NEK7 appears to function in NLRP3 priming, but not NLRP3 activation, in human macrophages. It was recently shown, in human cells that they employ a NEK7-independent signaling cascade instead that drives IKK β -dependent, post-translational priming (Schmacke et al., 2022). Mechanistically, IKK β activity recruited NLRP3 to PI4P, a phospholipid enriched on the trans-Golgi network (TGN). Tethering NLRP3 to PI4P led to inflammasome activation independently of NEK7, confirming that increased PI4P interaction serves to prime NLRP3 for inflammasome formation.

Recent evidences suggest a key role of the trans-Golgi network (TGN) in NLRP3 assembly process. In initial studies, it was shown that NLRP3 forms a ternary complex with the escort activity of sterol regulatory element-binding protein-2 (SREBP) and its partner cleavage-activating protein (SCAP) that transported NLRP3 from the ER to the trans-Golgi network (dTGN) for optimal inflammasome assembly (Guo et al., 2018). It was shown that TGN dispersion is a hallmark of NLRP3 activation, in fact, NLRP3 stimuli lead to the disassembly of the trans-Golgi network (TGN). The recruitment of NLRP3 to the dTGN was dependent on a positively charged polybasic region located between the PYD and the NACHT domain of NLRP3 that interacts with a negatively charged phosphatidylinositol-4-phosphate (PtdIns4P) on the dTGN (J. Chen & Chen, 2018). Chen et al., identified the dispersal of the trans-Golgi network (TGN) as a common denominator of both K⁺ efflux-dependent and -independent NLRP3 triggers.

- **Activation of NLRP3**

NLRP3 can be activated by a large array of stimuli (J. Xu & Núñez, 2022) including: *Candida albicans*, *Saccharomyces cerevisiae* (Gross et al., 2009), pore-forming toxins (Craven et al., 2009; Mariathasan et al., 2006a), viral nucleic acids from viruses (Sendai virus, adenovirus, influenza virus, encephalomyocarditis virus) (Ito et al., 2012; Kanneganti et al., 2006; Muruve et al., 2008). NLRP3 is also known to detect diverse DAMPs inducing plasma membrane change in ion permeability (K⁺ efflux, Cl⁻ efflux, Ca²⁺ cytosolic influx) (Di et al., 2018; Mariathasan et al., 2006c; Pelegrin, 2021), rupture of lysosomes by crystals or particulates, metabolic and mitochondrial stress (Pizzuto et al., 2022; Pizzuto & Pelegrin, 2020; Rajamaki et al., 2010), UVB irradiations (Feldmeyer et al., 2007a) and environmental irritants (Schroder & Tschopp, 2010) (see Table 2). The wide variety of these signals suggests that NLRP3 is a key integration point of cellular stress in cell and that these signals are not directly recognized by NLRP3, but rather that they directly or indirectly create a disruption of the functions and integrity of the cell, which will then be recognized by NLRP3. Actually, K⁺ efflux from the cytosol has been identified as a common denominator of many NLRP3 triggers and in a simplistic manner we can divide the NLRP3 activators into K⁺ efflux dependent or K⁺ efflux independent. I will not detail each activator known for NLRP3 but I will give a brief overview of the main forms to activate NLRP3.

Mechanistically, different signals can induce K⁺ efflux. One of the first NLRP3 activator identified was the bacterial pore-forming toxin, nigericin, a K⁺ ionophore that induces K⁺ efflux. Extracellular adenosine triphosphate (ATP) via the purinergic P2X7 channel induces K⁺ efflux with other ions flux (such as Ca²⁺ and Na⁺). More recently, the two-pore domain weak inwardly rectifying K⁺ channel 2 (TWIK2) was shown to be activated by Ca²⁺ and Na⁺ and to be also implicated in K⁺ efflux (Di et al., 2018). Structural studies showed that low intracellular K⁺ concentration led to a conformational change in inactive NLRP3 (Tapia-Abellán et al., 2021). This structural change was promoted by a unique linker sequence and a short FISNA domain located between the PYD and the NACHT domain of NLRP3 (Tapia-Abellán et al., 2021).

Even though it has been demonstrated that K⁺ efflux plays a direct function in the activation of NLRP3, there is still debate over the roles of Cl⁻ efflux and Ca²⁺ cytosolic influx. It was suggested that K⁺ efflux acts as the upstream of Cl⁻ flux in NLRP3 activation and implies that although intracellular Cl⁻ may help to activate NLRP3, Cl⁻ efflux alone is not sufficient to activate NLRP3.

Several of the NLRP3 activators that have been reported are insoluble particulates, or crystals (endogenous: MSU, cholesterol, Protein aggregates (fibrillar amyloid- β peptide) or exogenous: silica, asbestos, alum, calcium pyrophosphate dehydrates (CPPD)) (Cassel et al., 2008; Dostert et al., n.d.; Hornung et al., 2008a; Martinon et al., 2006; Rajařmaki et al., 2010). Crystals are taken up by phagocytosis and enter macrophages, but once inside endolysosomes, they are resistant to ROS/low pH proteases-mediated destruction and accumulate until they cause the rupture of lysosomes. This rupture of lysosomes causes membrane damage and the release of lysosomal cathepsin in the cytosol (Hornung et al., 2008b). Lysosomal membrane rupture appears to be sufficient for inflammasome activation because the lysosomotropic agent HLLoMe activates NLRP3. Cathepsin inhibitors blocked caspase-1 activation induced by particulate matter. Interestingly, lysosomal damage induces K⁺ efflux, however the mechanism for K⁺ efflux after lysosomal damage remains unclear.

Mitochondria can provide a subcellular site for NLRP3 inflammasome assembly and molecules that can promote NLRP3 activation, including mitochondrial reactive oxygen species (mtROS), cardiolipin and mtDNA. Cardiolipin, a phospholipid that is normally located in the mitochondrial inner membrane and externalized in response to mitochondrial dysfunction, can bind the HD2 and the beginning of the LRR domain of NLRP3 to promote inflammasome activation. Mitochondrial DNA (mtDNA) can be released into the cytosol from damaged mitochondria to promote NLRP3 activation. For example, oxidized mtDNA can bind and activate NLRP3. mtROS, which are generated largely through the electron transport chain (ETC) Complex I and III, have been linked to NLRP3 activation. In line with this, certain imidazoquinolinamines, including imiquimod (IMQ) and CL097, and peptidoglycan were suggested to activate NLRP3 by targeting quinone oxidoreductases (NQO2) and mitochondrial Complex I, which promoted mtROS production. This NLRP3 activation is independent of K⁺ efflux.

In human monocytes, activation of NLRP3 with lipopolysaccharide (LPS) alone via an alternative pathway is K⁺ efflux independent. LPS treatment in human and porcine PBMCs triggers TLR4-TRIF-RIPK1-FADD-Caspase8-dependent NLRP3 activation, which occurs independently of K⁺ efflux. This NLRP3 activation induces IL-1 β secretion but does not cause pyroptosis (Gaidt et al., 2016). Thus, in some cells, there are mechanisms of NLRP3 activation that can bypass K⁺ efflux.

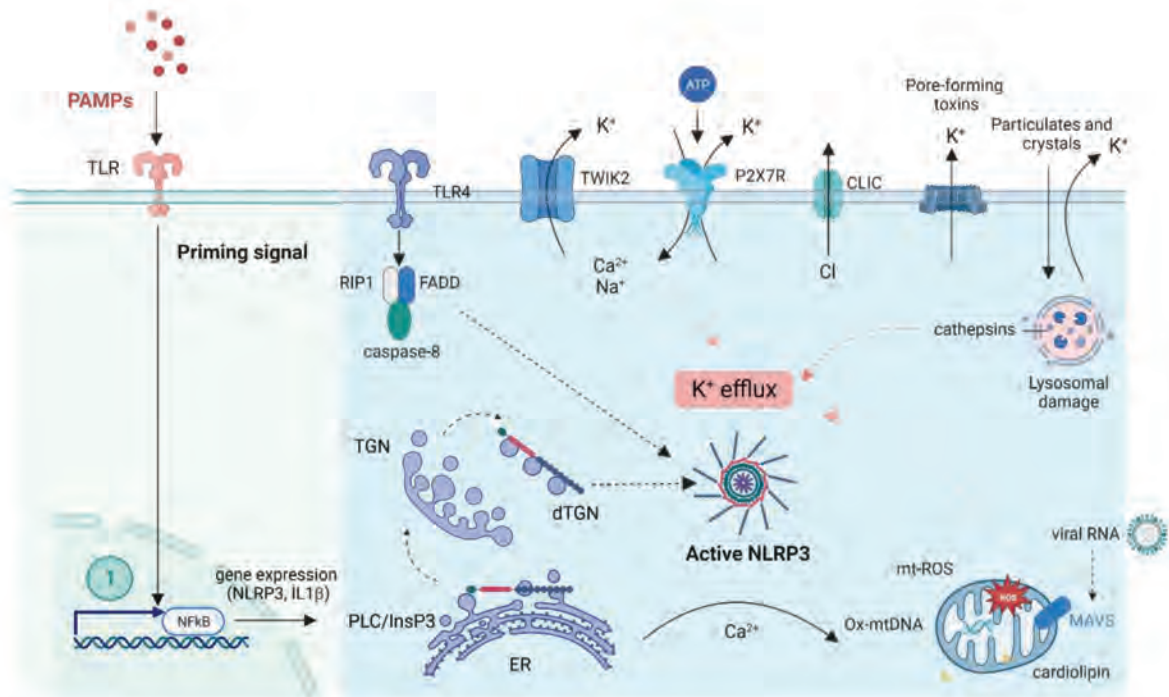


Figure 14: Models of NLRP3 activation. Signal 1 (priming, left) is provided by the activation by cytokines or pathogen-associated molecular patterns (PAMPs), leading to the transcriptional upregulation of NLRP3 inflammasome components. Signal 2 (activation; right) is provided by any of numerous PAMPs or damage-associated molecular patterns (DAMPs), such as particulates, crystals and ATP, that activate multiple upstream signalling events. These include K⁺ efflux, Ca²⁺ flux, lysosomal disruption, mitochondrial reactive oxygen species (mtROS) production, the relocation of cardiolipin to the outer mitochondrial membrane and the release of oxidized mtDNA (Ox-mtDNA), followed by Cl⁻ efflux. RNA viruses activate NLRP3 through mitochondrial antiviral signalling protein (MAVS) on the mitochondrial outer membrane. **Abbreviations:** CLIC, chloride intracellular channel protein; ER, endoplasmic reticulum, NF-κB, nuclear factor-κB; P2X7, P2X purinoceptor 7; ROS, reactive oxygen species; TLR, Toll-like receptor; TWIK2, two-pore domain weak inwardly rectifying K⁺ channel 2; dTGN: disordered trans-Golgi network, Ox-mtDNA: oxidized mitochondrial DNA.

- **NLRP3 inflammasome-driven diseases**

NLRP3 is currently known to be implicated in detecting and combating infections, however, it has now been linked to many diseases and especially diseases that arise in ageing populations. The pathogenesis of many common diseases that present later in life is influenced by chronic inflammation secondary to the presence or accumulation of sterile danger signals in tissues. The main sensor for these kinds of sterile inflammatory signals is NLRP3, which plays a significant role in the initiation of chronic inflammatory tissue reactions in a number of disorders. Based on a mix of studies using animal models and clinical data, NLRP3 has been linked to a wide range of diseases and is a significant factor in inflammatory disease in four categories: genetic NLRP3-dependent auto-inflammatory diseases, diseases driven by metabolic dysfunction (type 2 diabetes, non-alcoholic steatohepatitis (NASH), degenerative aspects of ageing and the development of some cancers), diseases caused by the formation of crystals or aggregates (silicosis, atherosclerosis, gout, kidney dysfunction, Alzheimer) and fibrosis following either acute tissue injury or chronic inflammation (Mangan et al., 2018).

- **NLRP3-dependent auto-inflammatory diseases**

Patients with these rare, inherited, autosomal dominant mutations in NLRP3 develop systemic auto-inflammatory syndromes called cryopyrin-associated periodic syndromes (CAPS). CAPS is a broad definition for a group of auto-inflammatory disorders caused by activating mutations in the NLRP3 gene. These include, in order of severity, familial cold auto-inflammatory syndrome (FCAS), Muckle–Wells syndrome (MWS) and neonatal-onset multisystem inflammatory disorder (NOMID), which is also called chronic infantile neurological cutaneous articular (CINCA) syndrome (Mangan et al., 2018). These three conditions are characterized by blood neutrophilia, fever and tissue-specific inflammation in the skin, joints and conjunctiva. In MWS and NOMID, hearing loss and kidney amyloidosis can also occur. In MWS patients, urticaria and cold-exposure related arthritis are also suffered. In NOMID patients hives, overgrowth of the epiphysis of long bones and inflammation of the central nervous system (CNS) are also suffered. Thus far, more than 200 mutations in the NLRP3 gene associated with CAPS have been documented in the INFEVER database (de Menthière et al., 2003). Among them, 97 mutations are pathogenically associated with CAPS. These mutations result in gain of function proteins, demonstrated by their spontaneous inflammasome formation in the absence of the activating signal when overexpressed, what we called “sterile inflammation”. To gain further understanding of CAPS, mouse lines that express CAPS-associated variants of NLRP3 (FCAS, MWS and NOMID) were generated. These mice display systemic, lethal inflammation that is dependent on ASC, caspase 1 and, partially, on the downstream signalling molecules IL1 β and IL18.

- **Inhibition of NLRP3 activation**

As the deregulation or aberrant activation of NLRP3 inflammasome is linked with many diseases, huge efforts have been made to find an inhibitor of NLRP3 as a therapeutic target. Several NLRP3 inhibitors have been reported from phenotypic screening (see table). These inhibitors target NLRP3 itself or other proteins that indirectly affect the activity of NLRP3 (Coll et al., 2022). A large amount of data has been presented on the ability of these compounds to inhibit inflammasome activity. However, detailed mechanistic information on the mode of inhibition is lacking for many of these molecules; each compound described may be a direct or indirect inhibitor of NLRP3. In addition, activity against other targets for most of the molecules listed below is not well characterized. As such, appropriate caution must be exercised when using these as tool compounds, as any effects observed may be the result of altering pathways not directly related to the NLRP3 inflammasome. Currently, the most well-characterized compound is CP456,773 (MCC950) which specifically inhibits NLRP3 inflammasome activation downstream of K⁺ efflux. MCC950 targets a specific motif in the NLRP3 NACHT domain, blocking ATP hydrolysis and in consequence, NLRP3 activation. MCC950 has no effect on other inflammasomes but inhibits NLRP3 inflammasome *in vivo* and reduces the severity of experimental

autoimmune encephalomyelitis (EAE) mouse model. Other inhibitors targeting other components of the inflammasome, such as IL-1 β , are actually used in clinic to treat patients with autoinflammatory disorders, particularly against CAPS. Three IL-1 inhibitors are available in clinic: Anakinra, an IL-1 receptor antagonist, rilonacept, a decoy receptor of IL-1 α and IL-1 β and finally canakinumab, an IL-1 β neutralizing antibody.

Compound	Inhibition mechanism	Effects in vivo models
Parthenolide (natural)	Reducing ATPase activity. Also inhibits caspase-1 activity downstream AIM2, NLRC4 and NLRP1	-
BAY 11-7082	Forms covalent adducts with cysteine residues of NLRP3 Impairing NLRP3 ATPase activity. Also inhibits NLRC4	-
Glyburide family	Still unidentified.	Effective at blocking multiple NLRP3 dependent pathologies: FCAS in PBMCs, LPS-induced septic shock and bronchopulmonary dysplasia in murine models
CY-09	ATPase inhibitor	Reduces neonatal lethality in CAPS mice, and decreases symptoms in TD2 mouse of HFD.
CP-456,773 (MCC950)	ATPase inhibitor	Effective in a wide range of murine disease models (CAPS and experimental autoimmune encephalitis)
MNS	Suppressing NLRP3 ATPase activity.	-
Fenamate	Blocking VRACs32.	Effective murine model of Alzheimer's disease (3xTgAD mouse), inhibiting microglial activation and IL-1 β production and preventing memory loss
OLT1177	Reduces ATPase activity	Reduces IL1 β release and caspase 1 activity in human blood neutrophils (from patients with CAPS). Preliminary clinical testing with nor any adverse effects : potential inhibitor for NLRP3 patients.
Fc11a-2	Inhibition of caspase 1 activation	<i>In vivo</i> efficacy in the mouse colitis model (reducing body weight loss and pro-inflammatory cytokines, such as TNF, IL1 β and IL18)
INF39	Inhibiting ATP ase activity	Reduce systemic and colonic inflammation in rats
BOT-4-one	Promotes NLRP3 alkylation inducing NLRP3 ubiquitination and impairs NLRP3 assembly. Also decreases NLRP3 ATPase activity. Moderate effects inhibiting NLRC4 inflammasome.	-

Tranilast (TR)	Inhibits NLRP3-ASC complex formation binding to the NACHT domain without affecting ATPase activity.	Potential therapeutic application against CAPS, T2D and gout.
Oridonin (Ori)	Directly bind NLRP3 in a covalent manner in the NACHT domain without affecting ATPase activity.	Therapeutic effects in metabolic disorders in HFD-induced diabetic mice.
BHB	Reducing K ⁺ efflux, leading to reducing oligomerization of ASC	-
Acrylate	INF39 is not cytotoxic and inhibits IL1 β production in macrophages.	Oral administration of INF39 in a rat colitis model attenuated colonic inflammation.

Table 2: NLRP3 inflammasome inhibitors

➤ The NLRC4 inflammasome

NLRC4 (also named IPAF) belongs to the NLR family and has the particularity that its inflammasome activation requires sensing collaboration with another NLR family member, NAIPs. NAIPs and NLRC4 share two common domains, the NACHT domain and the C-terminal LRR. In addition, NAIPs has three BIR domains and NLRC4 contains an N-terminal CARD domain (see Figure 3). Given that NLRC4 has a CARD domain, it was supposed and confirmed that it will directly interact with procaspase-1 (Poyet et al., 2001). Although the function of ASC in the NLRC4 inflammasome is still unknown, it is assumed that these proteins do not directly interact since NLRC4 lacks a PYD domain.

The NLRC4 inflammasome is activated by gram-negative bacteria possessing type III or IV secretion systems, such as *Salmonella typhimurium*, *Shigella flexneri*, *Pseudomonas aeruginosa* and *Legionella pneumophila* (J. Wen et al., 2021). The detection of these pathogens induces caspase-1 activation and pyroptosis through NLRC4 inflammasome activation. The main function of the bacterial secretion system is to mediate the passage of virulence factors (effector proteins), such as flagellin, into the cell cytoplasm by creating holes in the host's membrane. Through the cytoplasmic delivery of flagellin, which results in the activation of the NLRC4 inflammasome, *S. typhimurium*, *L. pneumophila*, and *P. aeruginosa* appear to cause the activation of caspase-1. These results were confirmed by delivering purified flagellin with liposomes in the cytosol or expression systems of flagellin that mimic the inflammatory activation of caspase-1 through NLRC4 in the host's cytosol (Franchi et al., 2006; Miao et al., 2006). Flagellin is not the only activator of NLRC4, indeed *P. aeruginosa* appears to activate NLRC4 through flagellin-dependent and -independent pathways (Miao et al., 2010; Sutterwala & Flavell, 2009) and non-flagellated bacteria such as *S. flexneri* trigger NLRC4 inflammasome activity). Some studies showed that NLRC4 can detect Type 3 system secretion system in a flagellin-independent pathway.

However, no studies have been able to show direct interactions between flagellin or type 3 secretion system (T3SS) and NLRC4. It was supposed that NLRC4 may recruit proteins for ligand recognition. This

hypothesis was confirmed when NAIP5 has been shown to be associated with inflammasome activation and to be required for flagellin-mediated inflammasome activation ((Valeria et al., 2017). Thanks to these results, independent studies by Kofoed and Vance (Kofoed & Vance, 2011b) and by Zhao et al (Zhao et al., 2011) have shown that NAIP proteins can act as upstream sensors for NLRC4-activating ligands (Suzuki et al., 2014). Thus, different NAIP genes in mice encode proteins that confer specific ligand-mediated activation of NLRC4 response to some bacterial ligands confirmed by genetic deletions in mice. The human genomes encode only one functional NAIP protein (hNAIP). Further studies have revealed that hNAIP can mediate NLRC4 activation in response to both T3SS components (rod and needle) and flagellin (Valeria et al., 2017; Yang et al., 2013). In contrast, individual murine NAIPs recognize these different ligands, NAIP1 recognizes the needle, NAIP2 recognizes the inner rod and NAIP5/6 recognizes flagellin.

NLRC4 activation is also influenced by transcriptional regulatory mechanisms. A study found that interferon regulatory factor (IRF8) induces the transcription of NAIPs (-1, -2, -5 and -6) and that IRF8 is required for the optimal activation of NLRC4 inflammasome but dispensable for AIM2, NLRP3 and PYRIN activation. This work provides new insights into the regulation of the NAIP/NLRC4 inflammasome, however, more studies are needed to understand all the transcription regulatory mechanisms. Indeed, a basal expression of NAIPs and NLRC4 inflammasome activity in the absence of IRF8 implies that other factors may also contribute to the transcription of NAIPs and the NLRC4 inflammasome activation in IRF8^{-/-} BMDMs was attenuated but not completely abrogated.

Interestingly, the pathways downstream of NLRC4 appear to be independently regulated by posttranslational modifications, particularly phosphorylation. However, despite two decades of study, several aspects of NLRC4 activation and function remain unclear. In 2012, Qu et al showed that following infection of macrophages with *Salmonella Typhimurium* NLRC4 was phosphorylated in a conserved residue, Ser 533 (Qu et al., 2012). In contrast to those reconstituted with wild-type NLRC4, *Nlrc4*^{-/-} macrophages did not activate caspase-1 and pyroptosis in response to *S. typhimurium*, demonstrating the importance of S533 phosphorylation for NLRC4 inflammasome function. PKC δ was discovered to be a potential NLRC4 kinase using biochemical isolation of the NLRC4-phosphorylating activity and a kinase inhibitor screen. Recombinant PKC δ phosphorylated NLRC4 S533 *in vitro*, immunodepletion of PKC δ from macrophage lysates prevented NLRC4 S533 phosphorylation *in vitro*, and PKC δ ^{-/-} macrophages preferentially responded to *S. typhimurium* with significantly reduced caspase-1 activation and IL-1 β production. However, another paper showed that non-flagellated bacteria such as *S. flexneri* induce NLRC4 inflammasome activation independently of PKC δ (Suzuki et al., 2014). This paper suggested that the role of PKC δ phosphorylation in NLRC4 activation can be different depending on the type of bacterial infection. Later, a different team showed the importance of another kinase named LRRK2 in NLRC4

phosphorylation and activation after an infection with *S. Typhimurium*. The results showed that LRRK2-/- macrophages impaired the caspase-1 activation and IL-1B secretion in response to NLRC4 activators (flagellin, rod, *S. typhimurium* infection). Mechanistically, LRRK2 formed a complex with NLRC4 (LRRK2 interacted with NLRC4 via the WD40 domain) in response to *S. Typhimurium* infection promoting the phosphorylation of NLRC4 at Ser533, a critical modification required for the assembly of NLRC4 inflammasome. However, it is still unclear whether these NLRC4 kinases play a dominant role in NLRC4 activation. In 2014, another paper suggested that NLRC4 activation will require two signals to be activated in which Ser553 phosphorylation prepares NLRC4 for subsequent activation by flagellin sensor Naip5 afterwards. More studies are needed to understand the mechanisms of NLRC4 activation and the role of phosphorylation in NLRC4 priming or direct activation. In 2020, (Tenthorey et al., 2020) in an effort to clarify the role of S533 phosphorylation created three novel lines of NLRC4 mutant mice using CRISPR/Cas9 to better understand the function of S533 phosphorylation in NLRC4 activation: Mice that lack NLRC4 (*Nlrc4*/), orNLRC4S533D/S533D animals with a phosphomimetic mutation, and NLRC4S533A/S533A mice with a non-phosphorylatable mutation, all in the endogenous *Nlrc4* locus. They showed no importance of NLRC4 phosphorylation in serine S533 after NLRC4 activation with flagellin or *S. Typhimurium* infection.

Recently, in 2021, it was reported that endogenous short interspersed nuclear element (SINE) RNAs, (which come from mobile genetic elements known as retrotransposons) induce NLRC4 inflammasome activation independent of NAIPs (Shao-bin Wang et al., 2021). These SINEs are only transcribed into RNAs during times of cellular stress, such as an infection or ageing and are known to promote atrophic macular degeneration (AMD) and systemic lupus erythematosus (SLE). They identify DDX17, a DExD/H box RNA helicase, as the sensor of SINE that licenses the assembly of an inflammasome. In an unexpected manner, they showed that both NLRP3 and NLRC4 proteins were necessary to form an active NLRC4 inflammasome and that the PKC δ is needed to help form the NLRC4 inflammasome. Inhibiting DDX17-mediated NLRC4 inflammasome activation decreased interleukin-18 (IL-18) release in SLE patient peripheral blood mononuclear cells and prevented retinal degeneration in an animal model of AMD.

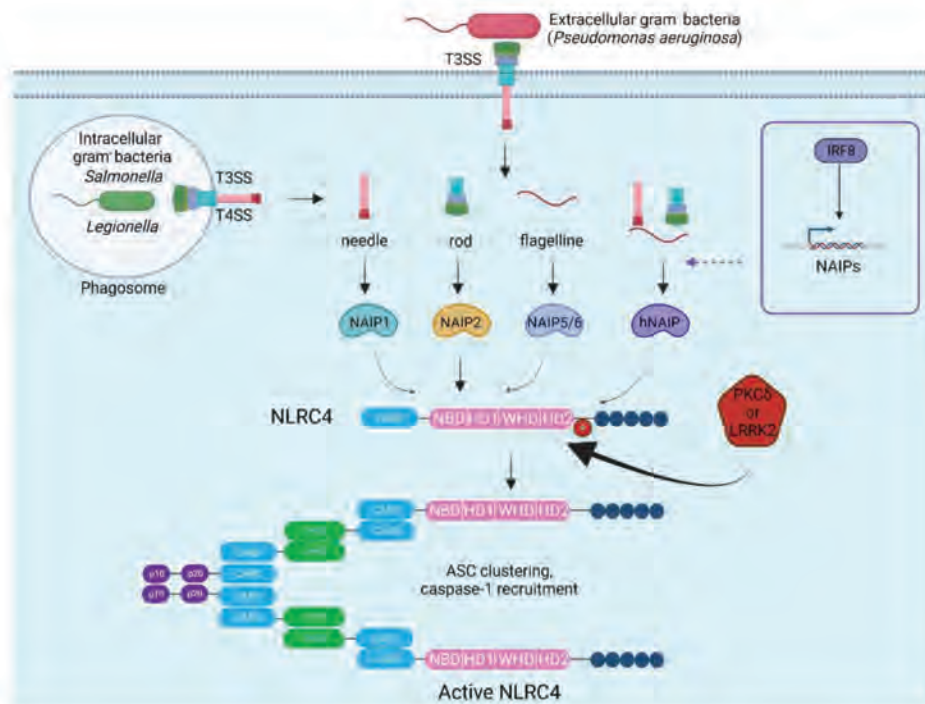


Figure 15: Model of NLRC4 activation. NLRC4 inflammasome is activated by gram-negative bacteria possessing type III or IV secretion. The needle and inner rod components of bacterial type III secretion system (T3SS) are sensed by mouse NAIP1 and NAIP2, whereas flagellin is sensed by murine NAIP5 or NAIP6. The needle and inner rod proteins and flagellin are all sensed by human NAIP. After activation, ligand-bound NAIPs recruit NLRC4 to the same complex to drive activation of the NLRC4 inflammasome that recruits and activates caspase-1. **Abbreviations:** CARD, caspase activation and recruitment domain; hNAIP, human NAIP; HD1, helical domain 1; HD2, helical domain 2; NAIPs, NLR apoptosis inhibitory proteins; NBD, nuclear binding domain; PYD, pyrin domain; WHD, winged helix domain.

- **NLRC4 inflammatory disorders**

The NLRC4 inflammasomopathies are caused by gain-of-function mutations in the gene encoding the inflammasome-forming sensor NLRC4. Mutant NLRC4 promotes the spontaneous formation of the NLRC4 inflammasome, production of inflammatory cytokines (IL-1 β and IL-18) and inflammatory cell death (Romberg et al., 2018). Two distinct molecular mechanisms were reported in NLRC4 inflammasomopathy: mutations within the NACHT (NBD) domain inducing the oligomerization of the inflammasome with an increased response to usual stimuli (Kitamura et al., 2014; L. Wang et al., 2021) or mutations in LRR domain, described as a regulator domain, inducing a constitutively active NLRC4 inflammasome. Despite this molecular dichotomy, phenotypes are extremely varied. The medical presentation most current in patients with mutations in the NBD or LRR domain is the macrophage activation syndrome (MAS) with infantile enterocolitis. Milder phenotypes such as arthritis- or familial cold-induced autoinflammatory syndrome were described in NBD mutations (Bardet et al., 2021; Chear et al., 2020; Moghaddas et al., 2018; Volker-Touw et al., 2017; L. Wang et al., 2021). Key strategies for improving patient outcomes are urgently needed since treatments with Anakinra (targeting IL-1 β) are not effective for the majority of patients. This can be explained by the important role of IL-18 in NLRC4

inflammasomopathy patients. The NLRC4 mutations are associated with chronic elevation of mature IL-18 derived entirely from intestinal epithelia. (Weiss et al., 2018).

➤ **The AIM2 inflammasome**

Recently, four reports identified the HIN-200 family member, AIM2, as a cytosolic double-stranded DNA (dsDNA) sensor that oligomerizes, recruits ASC and induces caspase-1-dependent IL-1 β maturation (Bürckstümmer et al., 2009; Fernandes-Alnemri et al., 2009; Hornung et al., 2009a; Roberts, 2009). This was an important advance in the inflammasome field as it was the first identification of a non-NLR family member forming an inflammasome complex. AIM2 belongs to the family of ALRs structurally defined by two domains: an N-terminal PYD and a C-terminal HIN200 domain. AIM2 is expressed at basal state in the spleen, the small intestine and in peripheral blood (Cridland et al., 2012). However, its expression can be induced by a priming signal that requires the induction of type I IFN, an immune response typical of viral infections. Like NLRP3, the priming signal induces the expression of AIM2, but the full activation of AIM2s requires a signal of activation.

Ligand requirements for AIM2 are quite permissive and the only necessity is that DNA must be double-stranded. Cytosolic dsDNA from viruses, bacteria, or the host itself, synthetic dsDNA can activate the AIM2 inflammasome (Lugrin & Martinon, 2018) and it was found that immunogenicity increases with DNA length. In absence of the typical NACHT domain to oligomerizes, the oligomerization of the complex is suggested to be mediated by clustering upon multiple binding sites in the ligand, dsDNA, to which AIM2 binds via its C-terminal HIN domain. The PYD domain interacts with ASC via homotypic PYD-PYD interactions, allowing the ASC CARD domain to recruit procaspase-1 to the complex. Activated caspase-1 triggers IL-1 β processing and secretion in cells primed by inflammatory stimuli to express pro-IL-1 β . If prolonged, caspase-1 activation eventually leads to pyroptotic cell death. In addition, cytosolic DNA elicits the induction of the anti-viral cytokine IFN β , through pathways that are currently unclear but may involve DAI. Signaling by autocrine/paracrine IFN β can regulate the AIM2 inflammasome, as it induces expression of both AIM2 and the AIM2 inflammasome antagonist p202. AIM2 belongs to the family of HIN200 domain receptors also named ALR (see chapter ALR) and it seems that other HIN200 family members did not appear to be able to trigger inflammasome formation. However, it was reported that the mouse HIN-200 protein p202 (composed of 2 PYD domains) negatively regulates AIM2 inflammasome through the binding of p202 to dsDNA that sequesters dsDNA and by interfering with AIM2-ASC interactions. More studies are needed to understand the relevance and the importance of these mechanisms in humans, as p202 has no ortholog in humans.

Further studies are required to firmly establish the physiological relevance of this pathway, but AIM2 is proposed to function in cytosolic surveillance for DNA viruses and may contribute to autoimmune responses against self-DNA in systemic lupus erythematosus.

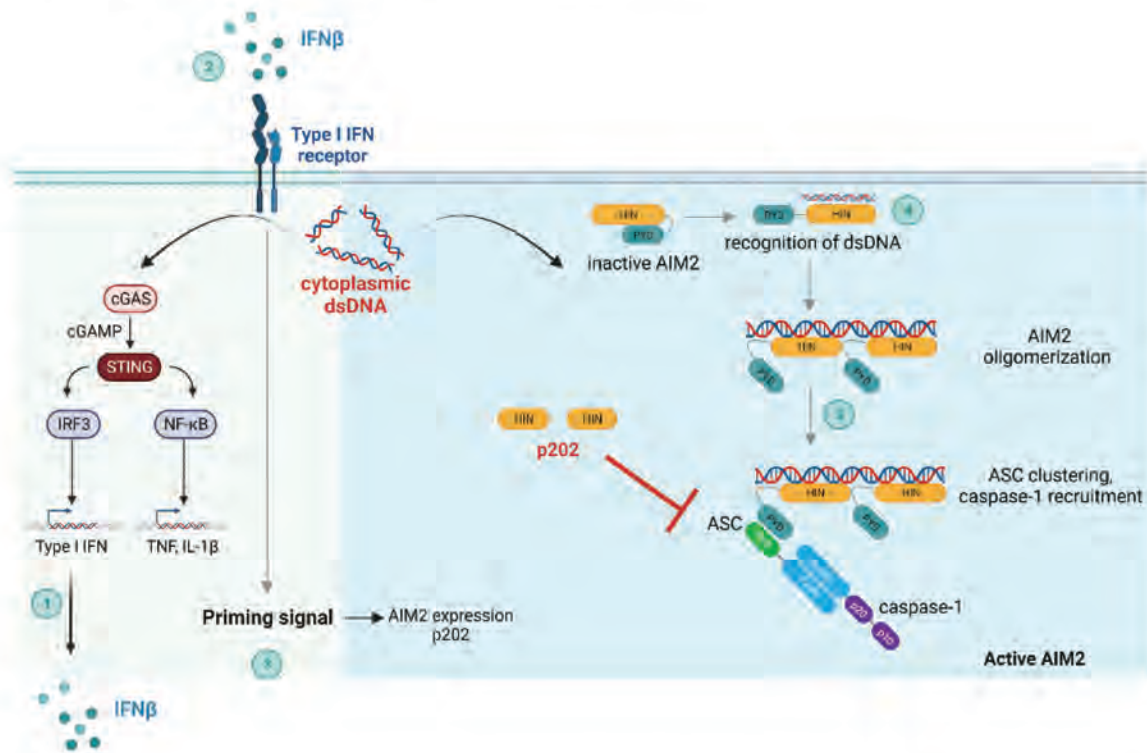


Figure 16: Activation of the AIM2 inflammasome by cytosolic ds DNA. After entry into cells, cytoplasmic DNA is released and recognized by cGAS, followed by activation of STING that induces expression and release of type I IFNs (IFNβ) (1). Released type I IFN binds type I IFN receptor (IFNAR) (2), which induces expression of IFN inducible genes, including AIM2 (AIM2 priming) (3). Upregulated AIM2 protein can sense cytoplasmic DNA (4), oligomerizes (5) and interact with ASC and caspase-1 to form activated AIM2 inflammasome.

➤ PYRIN inflammasome

PYRIN inflammasome (encoded by *Mefv*) highly expressed in granulocytes and monocytes is an atypical NLR-like protein composed with a PYD domain at the N-terminal of the protein and a B30.2 domain (only in humans) in the C-terminal. Via its PYD domain, ASC bind with PYRIN through PYD-PYD homotypic interaction, which induces its oligomerization and subsequently recruitment and activation of pro-caspase-1. MEFV expression increases in response to inflammatory stimuli like interferon-γ (IFN-γ) and tumor necrosis factor-α (TNF-α), (M. Centola et al., 2000) suggesting that pyrin plays a crucial role in the immune response

Prior to 2014, it was unknown which ligands or signals caused PYRIN activation. However, Xu et al researches showed that PYRIN can detect pathogen-induced alteration of host Rho guanosine triphosphatases (Rho GTPases) (H. Xu et al., 2014). This study demonstrated that the *Clostridium difficile*

virulence component TcdB, which is known to glycosylate and therefore inhibit the function of a minor Rho GTPase called RhoA (I. Just et al., 1995), can activate the pyrin inflammasome in mice and humans.

It has also been demonstrated that certain bacterial toxins, including the TecA toxin of *Burkholderia cenocepacia*, VopS (*Vibrio parahaemolyticus*), IbpA (*Histophilus somni*), C3 toxin (*Clostridium botulinum*), pertussis toxin (*Bordetella pertussis*), VopS (*Vibrio parahaemolyticus*), and Vop were able to induce distinct modifications to the Rho GTPase RhoA inducing PYRIN activation. Due to the variety of post-translational modifications detected by PYRIN and the lack of direct interaction between PYRIN and RhoA it was postulated that pyrin essentially monitors for normal biochemical function of the Rho GTPases. PYRIN evolved as a functional guard of RhoGTPases activity, when Rho GTPases are perturbed, PYRIN activates caspase-1. Other studies may suggest that PYRIN might detect alterations in the cytoskeleton organization because Rho GTPases regulate a number of features of the dynamics of the actin cytoskeleton and PYRIN co-localizes with actin (in perinuclear filaments) and microtubules. Studies on WDR1, a regulator of actin-cytoskeleton dynamics, showed that mice and humans lacking the WDR1 gene developed an autoinflammatory phenotype IL-18 dependent suggesting that PYRIN can detect the altered actin polymerization (M. L. Kim et al., 2015). Also, it was shown that treatment with colchicine, a microtubule-disrupting compound, inactivates PYRIN downstream of its dephosphorylation (Gao et al., 2016b).

Current literature elucidated the molecular mechanisms of pyrin regulation downstream of RhoA and demonstrated how changes in host Rho GTPase activity trigger PYRIN inflammasome activation (Gao et al., 2016b; Park et al., 2016b; H. Xu et al., 2014). These publications showed that the RhoA-dependent serine/threonine protein kinases PKN1 and PKN2 directly phosphorylate PYRIN (in two serine residues (S208 and S242) of human PYRIN) which results in an interaction of PYRIN with chaperones proteins 14-3-3. This interaction keeps PYRIN in an inactive state and represses inflammasome assembly. However, RhoA degradation or enzymatic modification causes a decrease in PKN1 and PKN2 activity and results in the lack or reduce levels of phosphorylated PYRIN. By an unclear mechanism, this lack of phosphorylation results in pyrin activation.

PYRIN is associated with inflammatory disorders and the most characterized is Familial Mediterranean fever (FMF)(Park et al., 2016b). FMF is an autosomal recessive disorder induced by a mutation in the Mefv gene characterized by episodes of fever, rash, arthritis and intense inflammation. Massive neutrophil infiltration into the site of inflammation is one of the characteristics of FMF attacks, suggesting that the disease may be the result of enhanced chemotaxis in response to a typically inadequate signal. The microtubule inhibitor colchicine efficiently prevents the inflammatory attacks of FMF in contrast to their resistance to the anti-inflammatory actions of glucocorticoids.

Interestingly, pathogenic *Yersinia* species (*Y. pestis*, *Y. pseudotuberculosis*, and *Y. enterocolitica*) are distinct in possessing an additional virulence factor, YopM, which selectively inhibits the pyrin inflammasome. This makes them different from other pathogenic bacteria that have RhoA-targeting toxins. The numerous, well-documented episodes of the bubonic plague carried on by *Y. pestis* throughout human history may have contributed to the high frequency of FMF mutations found in contemporary Mediterranean populations. It has been demonstrated that FMF-associated pyrin mutations provide resistance to *Y. pestis* infection in humans and in mice models (Park et al., 2020).

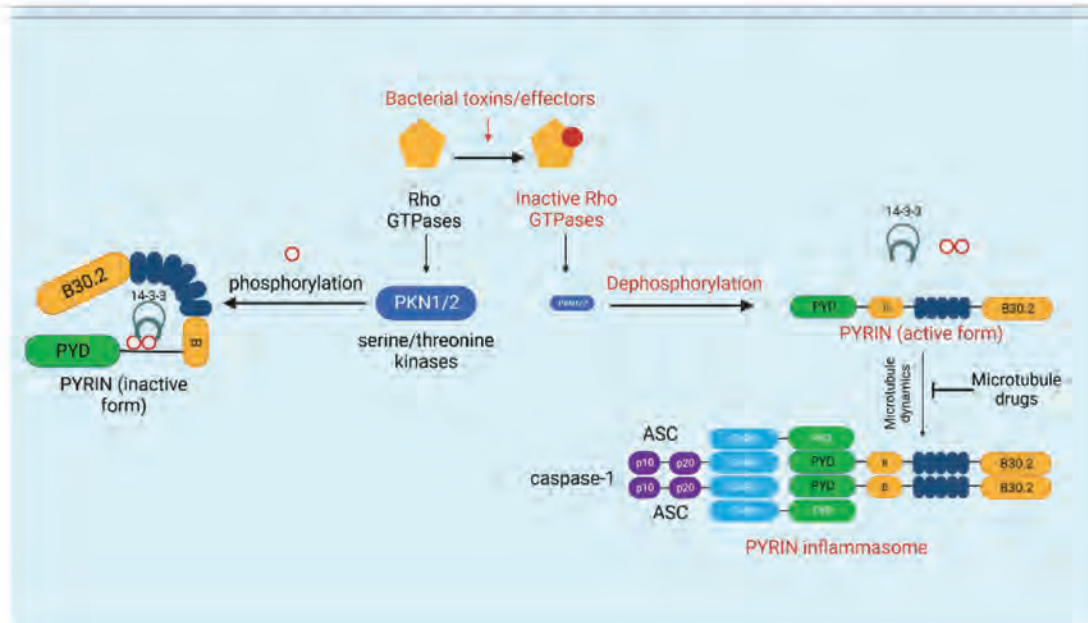


Figure 17: Model of Pyrin inflammasome activation by Rho-modifying toxins. Rho GTPases effector kinases, PKN1 and PKN2 cause phosphorylation of pyrin and binding to inhibitory proteins 14-3-3 that maintains pyrin in an inactive form. Inactive Rho GTPases leads to inactivation of PKN1/4 and decreased phosphorylation of pyrin associated with pyrin inflammasome activation. CARD, caspase activation recruitment domain; PYD, pyrin domain.

➤ The NLRP1 and CARD8 inflammasome

As my main project focus on NLRP1 inflammasome, a detailed description of the NLRP1 inflammasome is proposed in part 3 of my manuscript. And because CARD8 is structurally related to the NLRP1 inflammasome (is the only other human protein with a function-to-find domain (FIIND)) and they have common activation mechanisms as well as differences, I will describe below this inflammasome in parallel to the NLRP1 inflammasome to facilitate the understanding.

2. The non-canonical inflammasome

In addition to the canonical inflammasome which activates caspase-1 after ligand recognition, non-canonical inflammasome activate human caspase-4 and caspase-5 and their homolog mouse caspase-11 upon recognition of lipopolysaccharides (LPS), from gram-negative bacteria, leading to the direct

cleavage of GSDM-D and subsequent pyroptosis (Hagar & Miao, 2014; Kayagaki et al., 2011b; J. Shi et al., 2014; Yang et al., 2015).

In humans, caspase-4 is constitutively expressed in contrary to caspase-11 in mouse that requires its upregulation via a priming step induced by extracellular LPS recognition by TLR4-Myd88. LPS is a potent PAMP which consists of a conserved lipid A, a core oligosaccharide chain and a variable polysaccharide chain known as O-antigen, implicated in sepsis and septic shock. LPS can reach the cytosol upon infection through the CD14/MD2/TLR4 axis or by outer membrane vesicles (OMVs)-mediated entry. To deliver LPS directly in the cytosol, the vacuolar bacterial membrane is disrupted by a superfamily of IFN-induced GTPases named Guanylate-Binding Proteins (GBPs) (Meunier & Broz, 2016). GBPs directly bind to bacterial cell wall inducing bacteriolysis or disrupt outer membrane vesicles allowing LPS release in the cytosol. More recently, GBPs have been described to function as LPS receptors to allow caspase-11/-4/-5 recruitment. Thus, unlike canonical inflammasome activation which requires a multiprotein scaffold for activation, non-canonical inflammasomes directly serve as receptors for intracellular LPS. Non-canonical inflammasomes recognize and bind to the LPS lipid A through its CARD domain inducing its oligomerization but also inducing its catalytic activity. Once activated, it induces the cleavage of GSDM-D, releasing the N-terminal fragment that self-oligomerizes to form a pore through the plasma membrane leading to pyroptosis. By contrast to the caspase-1 dependent canonical inflammasome, caspase-11/-4/-5 are not able to cleave the inflammatory cytokines pro-IL1 β /-18. However, GSDM-D pores formation induces K⁺ efflux that secondary activates the canonical NLRP3 inflammasome resulting in IL-1 β /-18 secretion.

3. Alternative inflammasome activating-pathways

Similar to apoptosis processes that can elicit necroptosis in absence of caspases (Holler et al., 2000), in some contexts, inflammasomes platforms can engage alternative routes to trigger pyroptotic cell death (K. W. Chen et al., 2019; Demarco, Grayczyk, Bjanas, le Roy, et al., 2020; Orning et al., 2018; Sarhan et al., 2018a). Caspase-3 was previously thought to be the executor of apoptosis, but it was suggested that caspase-3 can also induce pyroptosis by cleaving GSDME (Rogers et al., 2017; Y. Wang et al., 2017) and confirmed recently by our group (Planès et al., 2022). More surprisingly, caspase-8 can also directly cleave GSDMD to induce pyroptosis. Caspase-8 is the initiator caspase of extrinsic apoptosis and inhibits necroptosis mediated by RIPK3 and MLKL. Recent studies have revealed that caspase-8, in mice but not in humans, directly cleaves GSDMD (independently of caspase-1 and caspase-11) to trigger pyroptosis under specific conditions such as pharmacological or pathogen-induced inhibition of the kinase TAK1 or the inhibitor of apoptosis (IAP) (Sarhan et al., 2018b). In addition, the activation of caspase-9 is also involved in pyroptosis by cleaving and activating caspase-3, (B. Zhou et al., 2018) and caspase-6 mediates the cleavage of GSDMC. These findings highlight the close coordination between apoptosis, necroptosis,

and pyroptosis and show that there are bridges between the pathways to coordinate cell death if one of them is disrupted.

4. Gasdermin D cleavage and pyroptosis

I. Gasdermin family as executors of pyroptosis

The gasdermin (GSDM) protein family, which was reported in the early 2000s, consists of 6 members with homologous structures: in humans (GSDMA, -B, -C, -D, -E and PJVK) and 10 in mice (GSDMA1, -A2, -A3, -C1, -C2, -C3, -C4, -D, -E and PVJK)(Petr Broz et al., 2019). Every GSDM member has a distinct and restricted pattern of expression in different tissues to detect and respond to various infections (table 1). Their name was based on the expression of murine GSDMA1 in the gastrointestinal tract and dermis. Initially little was known about the function of the gasdermin, but diverse roles in biological processes (cell differentiation, cell proliferation) but also in inflammation and cell death started to emerge shortly after their identification (figure 18).

Most proteins of the GSDM family except for PJVK, have three domains: the GSDM N-terminal (GSDM-NT) domain, a linker region and a GSDM C-terminal (GSDM-CT) domain. Both the N-terminal and C-terminal domains are relatively well conserved in the family whereas the linker region is unique to each group. Due to the high homogeneity among all GSDM-NT, most GSDMs (except for GSDMB and PJVK) may have a common mechanism of autoinhibition and activation to form pores in the membrane. The full-length GSDM protein is thereby kept in an auto-inhibited state through inter-domain interactions between the GSDM-NT and GSDM-CT domains. In response to inflammasome activation signals, GSDMs are cleaved in the central linker region by different inflammatory caspases or granzymes, to generate an active GSDM-NT (N-terminal) fragment and a GSDM-CT (C-terminal fragment). The caspase-1 cleavage site present in GSDMD is not found in the other gasdermins with the exception of a minor splice variant of GSDMB, but other proteases sites might be present. In fact, human and mouse GSDME include a caspase-3 cleavage motif in their linker region and it has been observed that when caspase-3 is activated by apoptotic stimuli, GSDME is cleaved at this location. This result lead to the hypothesis that GSDME promotes pyroptosis after cells had already initiated apoptosis (Rogers et al., 2017; Y. Wang et al., 2017). After cleavage, the active form of GSDM-NT binds to membrane lipids and extensively forms pores, resulting in cytotoxicity and cell death (Aglietti & Dueber, 2017). The conformational changes leading to pore formation are triggered by the binding of the N-terminal domain to membrane phospholipids, such as phosphoinositide and cardiolipin, with a positively charged pocket and negatively charged group, respectively. The surface of this pocket is fully masked by the GSDM-CT domain in the auto-inhibited full-length of GSDMs(Ding et al., 2016). The lipid-binding properties of the other GSDMs-

NT domain are similar to that of GSDMD, suggesting a common membrane targeting mechanism in the pore formation.

We are currently learning about the various physiological and pathological functions (table 3) of GSDMs as pyroptotic executors. Numerous diseases and tissue damage linked to inflammasomes have been linked to GSDMD (Li et al., 2019; Xiao et al., 2018). Additionally, in mice and/or humans, spontaneous mutations of GSDMs result in diseases such as alopecia in mice (GSDMA)(Runkel et al., 2004), asthma (GSDMB)(Das et al., 2016), and hearing impairment (GSDME/PJVK)(Delmaghani et al., 2006; Van Laer et al., 1998). Moreover, the key roles of GSDMs in infection, inflammation and cancer have stimulated investigations of GSDM-targeting therapeutics. Strategies to therapeutically modulate GSDMD activity are beginning to emerge, and several inhibitors of GSDMD have now been reported (Hu et al., 2020; Humphries et al., n.d.-a; Rathkey et al., 2018).

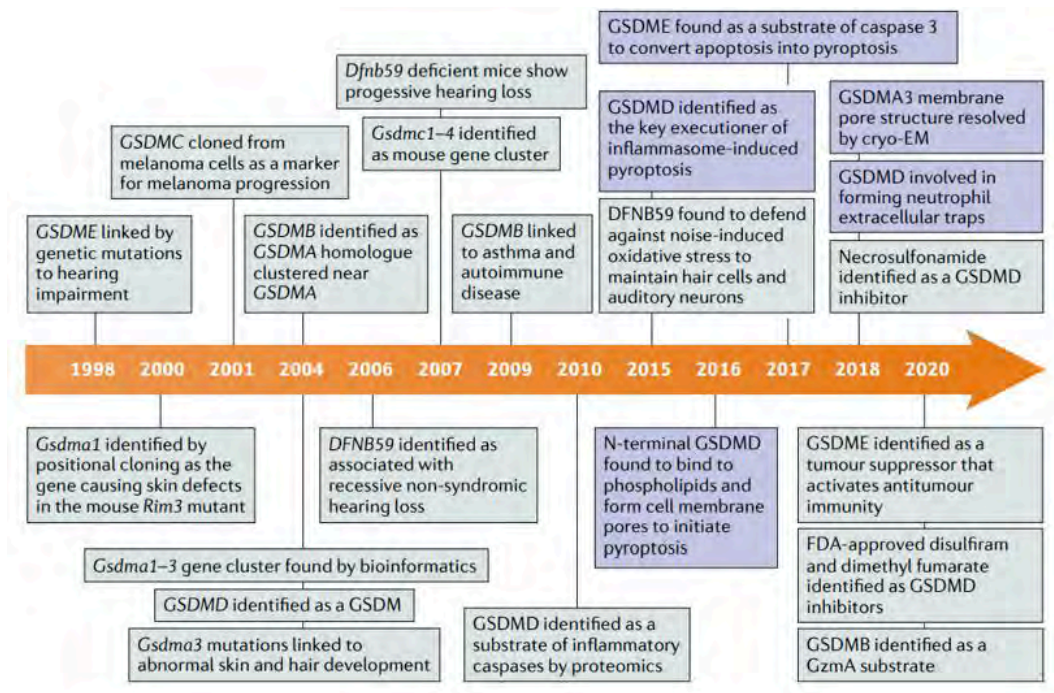


Figure 18: Key events in the history of gasdermin from (X. Liu et al., 2021)

➤ **GSDMD**

GSDMD is the most studied as it is the key executor of inflammasome-induced pyroptosis. Different groups (Kayagaki et al., 2015; J. Shi et al., 2015) demonstrated that GSDMD is a fundamental substrate to caspase 1 and caspase 11 (and caspase -4 and -5 in humans) and the executor of inflammatory cytokine release. The precise mode of execution of cell death by the GSDMD N-terminal has been explored and it was shown that it requires the cleavage of gasdermin D by caspases (-1,-11,-4 and -5) at the position 272FLTD275 in humans and 273LLSD276 in mice, thus generating an active 31-kDa GSDMD-NT fragment and 22-kDa GSDMD-CT fragment(Ding et al., 2016). The active form of GSDMD-NT, which

possesses positively charged motifs binds to negatively charged membrane phospholipids and extensively forms pores, resulting in cytotoxicity and cell death (Aglietti & Dueber, 2017). This pore-forming ability is recapitulated *in vitro* using liposomes, which demonstrated that the cleaved and recombinant GSDMD-NT bind to liposomes, indicating that GSDMD mediates its own recruitment to membranes (Sborgi et al., 2016). GSDMD only lyses cells from the inside and minimizes unneeded cell death and tissue damage since GSDMD-NT is exclusively connected with lipids of the inner wall of the plasma membrane. At the membrane, GSDMD-NT oligomerization is dependent on an active Cys192 (human), Cys191 (mouse), which has to be oxidized to form a 31- to 34-fold symmetric pore. Oligomerization of GSDMD is also influenced by metabolites and by post-translational modification mostly at cysteine residues. For example, in macrophages, GSDMD cleavage was abrogated by the binding of unsaturated dicarboxylic acids at distinct cysteine residues, such as itaconate and fumarate binding (Hoyle et al., 2022). Cysteine modification can be also artificially induced by drugs (e.g., necrosulfonamide, disulfiram) targeting Cys 191 and inhibiting GSDMD formation (Humphries et al., n.d.-b). Interestingly, damage to the plasma membrane does not necessarily result in cell death, since it has been observed that the influx of Ca^{2+} ions from the extracellular milieu triggers repair programs involving the ESCRT-dependent membrane repair that negatively regulates GSDMD. The exact mechanisms of removing GSDMD pores from the membrane remains unknown.

The GSDMD-NT-induced membrane pores function as conduits for IL-1 family cytokine release and other cytosolic contents, including ions, from cells. GSDMD-dependent release of IL-1 cytokines in absence of cell death implies that the pores are large enough to allow the passage of mature IL-1 β , and since they do not allow the passage of larger proteins, such as the caspase1 (60kda), LDH or large DAMPs, that are released after lysis of pyroptotic cells (Heilig et al., 2018). GSDMD pores have a size of 20-25 nm since the mature form of IL-1 β has a diameter of 4-5nm the GSDMD pore should thus easily be large enough to allow the passage of cytokines. Recently, work on the GSDMD structure showed that the pore acts as a negative electrostatic filter, which repels negatively charged amino acids in the IL-1 β precursor molecule and only facilitates the release of positively charged liposome particles. Maturation of IL-1 β by caspase-1 proteolytically removes these negatively charged amino acids in order to facilitate the release of mature IL-1 β . When permeabilized by GSDMD pores, unlysed liposomes release positively charged and neutral cargoes faster than negatively charged cargoes of similar sizes, and the pores favour the passage of IL-1 β and IL-18 over that of their precursors (Xia et al., 2021). Consistently, mutation of these acidic patches on the GSDMD pore also induced more release of pro-IL-1 β . These findings show that GSDMD pores release mature IL-1 cytokines and even other cytosolic proteins before to or even independently of cell lysis, in addition to triggering cell death.

Besides GSDMD, which has now been shown to be cleaved and activated by inflammatory caspases (e.g. caspase-1, -11 [-4, -5 in human cells]) other proteases can also cleave GSDMD. For example, neutrophil elastase can process GSDMD and induce NETosis, and the apoptotic initiator caspase-8, activated by TNF complex IIb, also processes GSDMD at the same site as caspase-1 to drive host defence or TNF-induced inflammation (Demarco, Grayczyk, Bjanes, Le Roy, et al., 2020).

As pyroptosis through the activation of gasdermin D acts as a host defence against invasive pathogen infection, pathogens will develop strategies to counteract the activation of GSDMD. This is the case for one study of the enterovirus 71 (EV71) that shows that EV71 3C protease cleaves GSDMD at the Q193-G194 pair, resulting in a truncated N-terminal fragment disrupted for inducing cell pyroptosis (Lei et al., 2017a). To go further, another study recently showed that EV71 infection induces the cleavage of GSDME (GSDME), an essential step in the switch from caspase-3-mediated apoptosis to pyroptosis (Dong et al., 2022). We showed that this cleavage is independent of the 3C and 2A proteases of EV71. However, caspase-3 activation is essential for this cleavage, as GSDME could not be cleaved in caspase-3-KO cells upon EV71 infection. According to these results, our group recently showed that 3C protease of Sars-Cov2 (NSP5) inactivates GSDMD by cleaving it in its pore-forming domain at Glutamine 193 and triggers a GSDME alternative epithelial pyroptotic cell death upon GSDMD inactivation (Planès et al., 2022) (detailed later in the chapter work and results). It is tempting to speculate that 3C and the closely related 3CL proteases might share conserved targets. Beyond this, two recent studies showed a particular ability of the bacterial pathogen *Shigella flexneri* to ubiquitinate both GSDMD and GSDMB and target them for proteasomal degradation, thereby allowing *Shigella flexneri* to establish a replicative niche in human cells.

In contrast to GSDMD, other members of the GSDM family, such as GSDMA, GSDMB, and GSDMC, are not cleaved by caspase-1 and caspase-11. GSDME is activated during classical apoptosis, by caspase 3 cleavage after Asp270, which converts noninflammatory apoptotic death into inflammatory pyroptotic death in cells that express GSDME. Granzymes (Gzms) A and B, death-inducing proteases in natural killer (NK) cells and cytotoxic T lymphocytes (CTLs), also cleave GSDMB and GSDME, respectively, to activate pyroptosis during killer cell attack, which was previously thought of as noninflammatory. A recent study showed that GSDMC can be cleaved by caspase 8 after TNF-mediated death receptor signalling to trigger pyroptosis. However, the pore-forming function of the GSDMD-NT is not unique to this family member. The N-terminal fragments of all human gasdermin proteins (except PJVK) kill cells upon ectopic expression and possess the ability to form pores in liposomal membranes. Furthermore, the death caused by expression of all gasdermin N-termini is lytic and cells display a morphology similar to that of pyroptotic cells, further confirming that most gasdermin family members can indeed cause pyroptotic cell death.

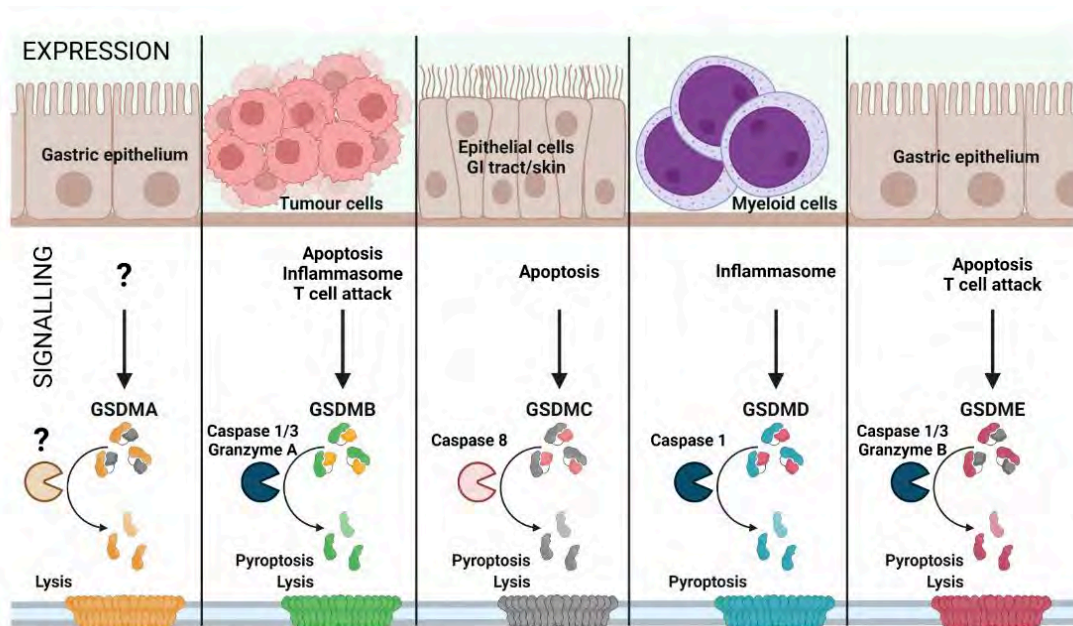


Figure 19: Signalling pathways of GSDM family members (Bittner et al., 2022). The N-terminal domain of GSDMA-E can bind with membrane lipids of the plasma membrane and form pores but each gasdermin is expressed in distinct cell types and are activated by different stimulus and caspases. However, the ability of PJVK to bind membrane lipids or form pores in the plasma membrane is uncertain. GSDMD is involved in pyroptosis via canonical (caspase-1) and non-canonical inflammasome (caspase 4,5,11) mediated pathways following cleavage by inflammatory caspases. The upstream events of GSDMA cleavage are not well characterized. Proliferating tumour cells are recognized by effector T cells that release Granzyme A, which cleaves GSDMB in cancer cells leading to pore formation and tumour cell lysis. Furthermore, GSDMB can also be activated by Caspase 1 or 3 downstream of inflammasome formation or apoptosis, leading to pyroptosis. GSDMC is activated by Caspase 8 downstream of apoptosis, linking apoptosis to pyroptosis. Similar to GSDMC, GSDME links apoptosis to pyroptosis subsequent to cleavage by Caspase 3 in apoptotic cells. Abbreviations: GSDMD-N, Gasdermin N-terminal; GSDMA, Gasdermin A; GSDMB, Gasdermin B; GSDMC, Gasdermin C; GSDMD, Gasdermin D; GSDME, Gasdermin E.

➤ GSDMA

The stomach and skin are the main organs where murine GSDMA3, the closest relative of human GSDMA, is expressed. It has been described that nine GSDMA3 mutations in mice result in alopecia (hair loss) and hyperkeratosis (refers to thickening of the skin's outer layer). All of these mutations act as gain-of-function mutations localized in the Gsdma3-CT domain and unmask the functional NT domain. Human GSDMA is known to be silenced in gastric cancer tissues and cell lines, and it is mostly expressed in epithelial cells of the mammary gland, umbilical cord, upper gastrointestinal tract, and skin. GSDMA mutations have not been reported in human alopecia; however, GSDMA polymorphisms have been linked to systemic sclerosis (an autoimmune fibrotic disease of the skin and visceral organs), inflammatory bowel disease (IBD) and childhood asthma. Similar to other gasdermins, GSDMA3 is able to form pores in membranes, thus this mutation presumably unleashes the pore-forming activity of the GSDMA3-NT. However, protease cleavage in human and mouse GSDMA and their regulatory mechanisms are not well-understood.

Recently, Deng et al showed that GSDMA, the dominant gasdermin in the skin have an important role in the control of microbial pathogens' virulence in the skin. GSDMA can be activated by a major skin pathogen causing morbidity and mortality worldwide: *Streptococcus pyogenes*. They found that *S. pyogenes* thanks to its virulence factor named SpeB (cysteine protease) cleaves GSDMA after Gln246 causing the release of the N-terminal (active) fragment and the following pyroptosis in keratinocytes (Table 3). Gsdma1 genetic deficiency in mice results in uncontrolled bacterial dissemination and death. GSDMA acts as both a sensor and substrate of SpeB and as an effector to trigger pyroptosis. adding a simple one-molecule mechanism for host recognition and control of the virulence of a dangerous microbial pathogen (Deng et al., 2022a).

➤ GSDMB

The human GSDMB is expressed in airway and gastrointestinal epithelia, liver, and neuroendocrine and immune cells. No GSDMB has been identified in rodents. GSDMB was linked to susceptibility to chronic inflammatory diseases including IBD(Rana et al., 2022), asthma(Das et al., 2016) and type I diabetes (Table 3). GSDMB expression is markedly increased in various cancers, including cervical, breast (Hergueta-Redondo et al., 2014), gastrointestinal and hepatic cancers, and its high expression is associated with poor prognosis. Both the full-length and GSDMB-NT can bind to membrane lipids such as phosphoinositide and glycolipid sulfatide, distinguishing them from other GSDMs. GSDMB can be cleaved by caspase-1, -3, -4, -6, and -7 within the pore-forming domain at the 88DNVD91 or D236 sites, which is similar to the cleavage of the pore-forming domain in GSDMD (Q. Chen et al., 2019; Zou et al., 2021). However, GSDMB-NT but not the full GSDMB protein induces pyroptosis-like features in human HEK 293T cells. This suggests that binding by lipids of the full GSDMB protein leads to the production of GSDMB-NT. Also, GSDMB has been found to feature a granzyme A (GrzA) cleavage site between the N-terminal and the C-terminal domain (Z. Zhou et al., 2020).

➤ GSDMC

GSDMC is a protein that is expressed in the trachea, spleen, oesophagus, small intestine, caecum, colon, and skin keratinocytes (table 3), however, their biological functions have not yet been identified. UV radiation significantly increases its expression through calcium-triggered NFATc1 signalling (Kusumaningrum et al., 2018). GSDMC is considered a marker for melanoma progression and is increased in colorectal cancer and promotes cancer cell proliferation which suggests that GSDMC may have an oncogenic role (Miguchi et al., 2016). Hou et al. found that under hypoxia, activated p-Stat3 promoted nuclear PD-L1 translocation. Nuclear PD-L1 and p-Stat3 synergistically promote the expression of GSDMC. GSDMC, has been reported to be cleaved and activated by caspase 8 activated by TNF- α derived from macrophages switching apoptosis into pyroptosis in tumour cells (Hou et al.,

2020) . In this paper, GSDMC was found to be involved in pyroptosis in breast cancer and highly expressed in this disease, which correlates with reduced survival.

➤ GSDME

GSDME was first described as a mutated gene (DFNA5) causing the generation of a cytotoxic truncated protein, itself leading to the activation of GSDME and cell death that results in an autosomal dominant form of hearing impairment, caused by cochlear hair cell loss (van Laer et al., 1998). GSDME is expressed in cochlea, placenta, heart, brain and kidney. GSDME is a physiological substrate of caspase-3 when it is stimulated by apoptotic triggers. GSDME is cleaved and activated by caspase 3 at Asp270 (in humans and in mice) when cells expressing GSDME are triggered to undergo apoptosis. GSDME cleavage generates a necrotic GSDME-NT domain that translocates to the plasma membrane and converts noninflammatory apoptosis into inflammatory pyroptosis.

Consistent with its activation by caspase-3/-7 or granzyme B, recent studies have indicated that GSDME induces tumor cell death by inducing apoptosis and pyroptosis, which may explain that GSDME emerged as a player in anti-tumor immunity (Zhang et al., 2020). GSDME is epigenetically suppressed by methylation in most cancer cells (gastric, colorectal, breast cancers...)(Akino et al., 2007; Croes et al., 2018; M. S. Kim et al., 2008) suggesting that it acts as a tumor suppressor by lowering the threshold of apoptotic signalling. When the expression of GSDME is induced by DNA methyltransferase inhibitors *in vitro*, colony formation in gastric and colorectal cancers and invasiveness in breast cancer are reduced. In contrast, p53, which is inactivated in many cancers, reportedly activates GSDME transcription in DNA-damaged cells, which could promote the removal of cancer cells by inflammatory recruitment and activation of phagocytic macrophages (Masuda et al., 2006). Interestingly, GSDME-driven tumor cell pyroptosis has also been shown to trigger cytokine release syndrome (CRS) during CAR T cell therapy in mice, highlighting a potential role as a target to reduce CRS in patients.

In addition to its anti-tumor role, our team has shown the involvement of GSDME activation after a Sars-Cov2 infection. We recently showed that 3CL proteases inactivate the pyroptosis executioner Gasdermin D (GSDMD) and subsequently, caspase-3 and GSDME promote alternative cell pyroptosis in epithelial cells (Planès et al., 2022).

➤ PJVK

PJVK (DFNB59 gene) is a more distantly related GSDM family member with a truncated non-homologous CT domain. PJVK is expressed in the brain, eye, inner ear, heart, lung, kidney, liver, intestine and testis. Similar to GSDME, PJVK is associated with hearing loss in humans through familial genetic mutations, although these mutations are recessive rather than dominant. Patients with DFNB59 mutations either have auditory neuropathy or defective outer hair cells in the cochlea, which affects the neuronal

transmission of the auditory signal. Interestingly, it has been suggested that PJVK localizes to the membrane of peroxisomes in inner hair cells. Reactive oxygen species (ROS) caused by noise overexposure are detected by PJVK, which then activates the autophagy apparatus to destroy damaged peroxisomes (pexophagy). PJVK-driven pexophagy is followed by peroxisome proliferation, which protects auditory hair cells from oxidative damage. Given that the CT domain of DFN59 is so short, it is unknown if it is a protein that forms pores or whether it is constitutively active. It is worth exploring whether DFN59 forms pores in peroxisome membranes and whether other interacting proteins inhibit or activate it. Two proteins, rho-associated coiled-coil containing protein kinase 2 and the scaffold protein IQGAP1, were shown to bind the C-terminal region of PJVK in a cochlear cDNA library. Whether PJVK can be cleaved by a protease and form membrane pores requires further investigation.

	GSDMA	GSDMB	GSDMC	GSDMD	GSDME	PJVK
Tissue/cell specific expression in human	skin, tongue, oesophagus, stomach, mammary glands, bladder, umbilical cord and	airway epithelium, gastrointestinal tract, brain, endocrine tissue, bone marrow tissue, lung, liver, kidney, testis and lymphocytes	cerebral cortex, endocrine tissues, skin, trachea, spleen, oesophagus, stomach, intestines, vagina and bladder	almost all human organs and tissue and immune cells	brain, endocrine tissue, muscle tissue, gastrointestinal tract, heart, kidney, endometrium, placenta and IgE primed mast cells	inner ear, neurons of the auditory system and testis
Activator	Streptococcal pyrogenic exotoxin B (SpeB)	Human: caspase 1 granzyme A	Caspase-8 Caspase-6	Mouse caspase 1/11 Human: caspase 1/4/5 caspase 8 cathepsin G Neutrophil elastase?	caspase 3 caspase-8, caspase-7 granzyme B,	not known
Inhibitors		Shigella ipah7.8		3C protease of EV71 3C protease of SarsCov2 virus (NSP5) Shigella ipah7.8		
Biological functions	Pyroptosis (skin)	Pyroptosis, anti-tumor immunity	not known	inflammation, pyroptosis, cytokine release, NETosis, bacteria killing	pyroptosis, anti-tumor immunity	not known
Associated disease	Alopecia in mice, asthma, systemic sclerosis in humans,	inflammatory bowel disease, breast cancer, type I diabetes and asthma	cancer	Sepsis, EAE, neonatal onset, atherosclerosis, type 2 diabetes Inflammatory disease	deafness, cancer	deafness

Table 3: Gasdermin family. GSDM family genes currently consist of GSDMA, GSDMB, GSDMC, GSDMD, GSDME and PJVK. Each GSDM member exhibits a unique and restricted pattern of expression in various tissues, which results in a variety of diseases.

II. Fungal gasdermin-like proteins

Gasdermin-like proteins have been identified in fungi and characterized as cell death-inducing toxins. Although there are functional similarities between mammalian and fungal gasdermins, little is known about the molecular systems that control gasdermin activity in fungi. Recently, Clav et al, showed that the fungal gasdermin HET-Q1 can be activated by proteolytic cleavage but also that the majority of fungal gasdermins are genomically grouped with genes encoding proteases (Clav et al., 2022). Some of these genes code for proteins with caspase-related domains or are immunological receptors found in plants and animals, respectively. This study has led to a better understand of how gasdermin-dependent cell death evolved by pointing out several evolutionary similarities between the signaling pathways seen in fungi and mammals.

5. Inflammasome mediated IL-1 β and IL-18 production

Both IL-1 β and IL-18 are potent pro-inflammatory cytokines with an important role during the first steps of inflammation and their deregulation is extremely detrimental to health. Therefore, these are tightly regulated proteins, not only at the transcriptional level but also post-transcriptionally by due to their inflammasome-dependent activation. Both cytokines are synthesized as precursors and need to be processed into their biologically active form by caspase 1, after an inflammasome activation, that removes the N-terminal amino acids, creating mature, signalling-competent cytokines. In addition, other studies have shown that caspase-8 can also directly cleave IL1 β (Gurung & Kanneganti, 2015). Once active cytokines are secreted, they can bind to their cognate cell surface receptors and initiate signalling. IL-1 cytokines bind to and act through specific receptors, which are characterized by intracellular Toll/Interleukin-1 receptor (TIR) domains and an extracellular immunoglobulin-like binding domain (Dinarello, 2009). At the receptor level, signalling can be regulated by antagonistic cytokines. These bind to the primary receptor yet do not allow the accessory receptor to form the trimeric complex, thus prohibiting IL-1 signalling. This can also be achieved by decoy receptors. These receptors bind the cytokine but lack the intracellular TIR domain necessary for signalling, thereby neutralizing agonist cytokines.

IL-1 β is a pleiotropic cytokine that acts on multiple cell types to drive inflammatory responses (Dinarello, 2009), for example, IL-1 β recruits neutrophils to the site of infection, controls the induction of IL-8 by epithelial cells and the release of IL-17 from T cells. IL-1 β expression is never constitutive, IL-1 β is induced in blood mononuclear cells, macrophages, keratinocytes and dendritic cells during stimulation with Toll-like receptor (TLR) ligands and other cytokines (e.g., tumor necrosis factor) (Q. Zhu & Kanneganti, 2017). IL-1 β is mostly produced by cells of the innate immune system and will trigger the production of inflammatory mediators. As a result, there is a fever, lowered pain threshold,

vasodilatation, and hypotension. These effects are mediated by acting directly on the hypothalamic temperature regulation center, and the activation of NF- κ B and the resulting expression of COX-2, an enzyme involved in the synthesis of prostaglandins which increases the expression of adhesion molecules on endothelial cells and promotes the infiltration of inflammatory and immunocompetent cells from the circulation into the extravascular space. IL-1 β is also an angiogenic factor and plays a role in tumor metastasis and blood vessel formation (Dinarello, 2009).

Conversely, IL-18 is constitutively expressed in different cell types, including blood monocytes, macrophages, dendritic cells, keratinocytes and epithelial cells in humans. Despite being constitutively expressed, IL-18 can also be induced, in response to signalling from various TLRs and type I interferon. In contrast to the strong pyrogenic activity of IL-1 α and IL-1 β , IL-18 is only able to induce fever at higher concentrations. IL-18 activates primarily p38 MAPK and AP-1 but fails to activate NF- κ B. IL-18 is best known for its capacity to induce IFN- γ and is expressed by macrophages, epithelial cells, such as keratinocytes, and dendritic cells (J.-K. Lee et al., 2004).

III. The NLRP1 and CARD8 inflammasome

Even though the first inflammasome-forming sensor, nucleotide-binding domain leucine-rich repeat pyrin domain containing 1 (NLRP1), was identified and described 20 years ago (Martinon et al., 2002), the molecular mechanisms underlying its activation have remained enigmatic and poorly understood until recently. This is due to several factors, including its unique structure in comparison to other inflammasomes, its uncommon epithelial expression, its significant structural divergence from rodent NLRP1, and the fact that the majority of human cancer cell lines utilized as research models no longer express NLRP1. Interestingly, CARD8 was identified as an inflammasome-forming PRR for the first time in 2018 (Johnson et al., 2018a) and it was described to be structurally related to the NLRP1 inflammasome and to have common activation mechanisms as well as differences. For this reason, in this part of my manuscript, I will discuss recent discoveries surrounding the NLRP1 inflammasome (human NLRP1 and rodent NLRP1) and its mode of action and I will compare it with the CARD8 inflammasome.

6. Why NLRP1 and CARD8 are so unique inflammasomes?

I. Difference between species

One of the reasons that explain why the hNLRP1 inflammasome has been mysterious and enigmatic until recently is that most of the studies on NLRP1 were done in mice. However, the hNLRP1 and mNLRP1 inflammasomes are highly divergent. Investigating the gene loci coding for NLRP1 reveals a clear distinction between humans and rodents. In the human system, NLRP1 is encoded by a single gene on chromosome 17. However, the mouse genome contains three paralogs (Sastalla et al., 2013), mouse *Nlrp1a* (mNlrp1a), *Nlrp1b* (mNlrp1b) and *Nlrp1c* (mNlrp1c) presents at the same location in tandem on the chromosome 11. mNlrp1c is considered a pseudogene and mNlrp1b is extraordinarily polymorphic, with at least five different alleles present in common inbred mouse strains. Rodent expresses homologs of NLRP1 but not CARD8.

II. Structure and tissue expression

The human and rodent NLRP1 or CARD8 inflammasome sensors are unique because they are the only inflammasome-forming sensors that contain a FIIND domain. However, hNLRP1, mNLRP1 and CARD8 structure remain different.

➤ NLRP1

Human NLRP1 (hNLRP1) contains five different domains: an amino-terminal PYD, followed by a NACHT domain, six leucine-rich repeat (LRR) domains, a function-to-find domain (FIIND), and a carboxyterminal

CARD (Figure 13). It was suggested that the PYD does not act as an effector domain but is required for self-inhibition of NLRP1, an activity that is reduced by GOF mutations (Zhong et al., 2016). hNLRP1 possesses a particular structure : hNLRP1 is the only NLR that contains both PYD and a CARD domain. Indeed, its structure is unusual because the CARD domain is present in the C-terminal and not in the N-terminal like in most NLRs. Furthermore, hNLRP1 contains a function-to-find domain (FIIND) that it can be subdivided into ZU5 (found in ZO-1 and UNC5) and UPA (conserved in UNC5, PIDD, and Ankyrin domain) subdomains. This unusual domain FIIND presents a self-cleavage domain which undergoes constitutive autoproteolysis after its ZU5 subdomain, generating two polypeptides: an N-terminal (PYD-NACHT-ZU5) and a C-terminal (UPA-CARD) fragments that remain non-covalently associated (D’Osualdo et al., 2011). The cleavage in FIIND is not fully processed, and only a fraction of the total NLRP1 protein undergoes autoproteolysis. FIIND autoproteolysis is required for NLRP1 inflammasome activation because, after hNLRP1 activation, the FIIND autoproteolysis allows the release of the C-terminal fragment containing a CARD domain. Each C-terminal fragment (UPA-CARD) is then sequestered in a ternary complex (see figure 20) with one copy of the full-length NLRP1 and one copy of the host protease dipeptidylpeptidase 8 or 9 (DPP8/9), likely to prevent inflammasome formation during homeostatic protein turnover. NLRP1 inflammasome-activating stimuli accelerate the rate of N-terminal degradation (by direct cleavage for example) and/or destabilize the DPP8/9 ternary complex (by Valboropro), thereby releasing a sufficient level of free C-terminal fragments to self-oligomerize, recruits the adaptor ASC and caspase-1 and form an inflammasome-complex. Interestingly, the C-terminal CARD induces ASC recruitment and caspase-1 activation. Although some CARD domains can directly recruit pro-caspase-1 the hNLRP1 fully requires ASC to recruit and oligomerize with pro-caspase-1. hNLRP1 and mNLRP1B share a similar structure but only hNLRP1 contains an N-terminal PYD domain. However, while hNLRP1 critically requires the adapter protein ASC, mNLRP1B can recruit pro-caspase-1 either with or without ASC.

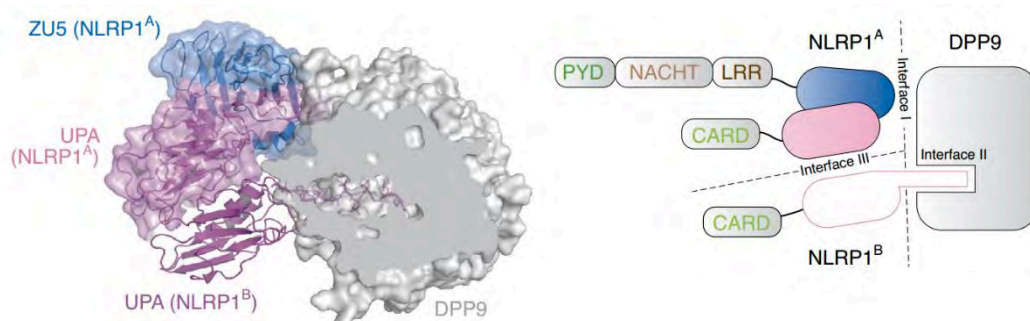


Figure 20: The ternary complex structure of the inhibited form of NLRP1 from (Stefan Bauernfried & Veit Hornung, 2021). NLRP1 is maintained in an inhibitory form that is composed of the full length of NLRP1, a C-terminal fragment (UPA-CARD), and the host protease DPP8/9 that inhibits the release of the C-terminal forms, maintaining the structure of this ternary complex.

In order to bind and hydrolyse ATP and allow the oligomerization of inflammasome platforms, the NACHT domains of NLRs proteins are crucial. Recently, a group showed that NLRP1 (mNLRP1 and hNLRP1) NACHT-LRR region directly interacts with oxidized thioredoxin-1 (TRX1). NLRP1 requires the ATPase activity of its NACHT domain to associate with TRX1 that represses inflammasome activation (Ball et al., 2022). TRX1 is a ubiquitous, highly conserved oxidoreductase that maintains redox balance in the cytosol and protects proteins from oxidative damage and aggregation. This suggests that oxidative stress represses the activation of the NLRP1 inflammasome whereas reductive stress acts as a danger signal. Therefore, they discovered several patient-derived missense mutations in the NACHT-LRR region of NLRP1 that weaken TRX1 binding, leading to inflammasome hyperactivation and autoinflammatory disease. Again, the N-terminal domain of NLRP1 seems to have many inhibitory mechanisms, unlike the rest of the inflammasomes.

➤ **CARD8**

The organized N-terminal domains present in hNLRP1 (PYD-NACHT-LRR) or mNLRP1 (NACHT-LRR) are absent in CARD8. CARD8 is the only other human protein with a FIIND, its structure consists of a FIIND and a CARD domain. Similar to hNLRP1, CARD8 must go through FIIND autoproteolysis in order to be activated, which allows the C-terminal CARD domain to oligomerize. The CARD8 CARD, in contrast to hNLRP1, interacts directly with the CARD of pro-CASP1 and does not require the adapter ASC.

Another important difference between the human and rodent homologs is their expression in different tissues (Figure 13). Rodent NLRP1 activation was induced in cells of the myeloid lineage (classical immune cells). However, hNLRP1 is largely confined to epithelial barrier tissues such as keratinocytes in the skin, bronchial epithelial cells in the lung and corneal epithelial cells from the eyes (Burian & Yazdi, 2018; Griswold et al., 2022). Furthermore, granulocytes, monocytes (very weakly), dendritic cells, Langerhans cells, and B and T cells all express NLRP1 (Kummer et al., 2007). All in all, because of these differences between rodents and humans, the results on mice studies could only partially contribute to deciphering the role of human NLRP1. In contrast, the activation of CARD8 inflammasome has been shown in bone marrow-derived cells (Johnson et al., 2018a, 2020b; Linder et al., 2020) or cancer cell lines (human myeloid cells).

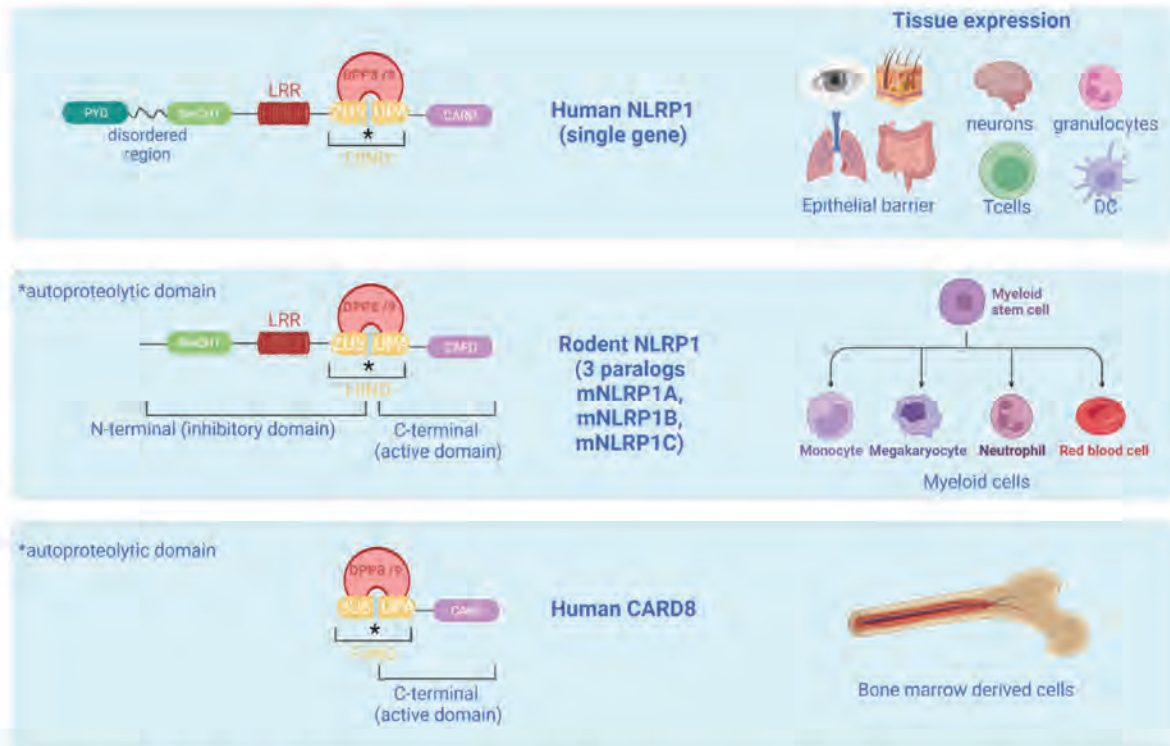


Figure 21: NLRP1 and CARD8 inflammasomes. NLRP1 and CARD8 proteins have FIIND and CARD domains and undergo autoproteolysis between the ZU5 and UPA subdomains that comprise the FIIND. NLRP1 proteins have NACHT and LRR domains preceding the FIIND, and human NLRP1 also has an N-terminal PYD. Human NLRP1 is encoded by a single gene, and the mouse genome contains three paralogs (mNLRP1A, mNLRP1B, and mNLRP1C). Rodent NLRP1 is expressed in cells of the myeloid lineage; however, human NLRP1 is expressed in epithelial barrier tissues (skin, cornea, lungs, and intestine) but also in granulocytes, dendritic cells, Langerhans cells, and B and T cells. In contrast, CARD8 is expressed in bone marrow-derived cells and human cancer cell lines.

III. Activation by the universal activator: Val-boro-Pro (VbP)

Interestingly, although these 3 inflammasomes (hNLRP1, mNLRP1, and CARD8) are different they all possess a “non-conventional” domain FIIND. After numerous studies (Huang et al., 2021a; Johnson et al., 2018b; Sharif et al., 2021; Zhong et al., 2018) it was shown that intracellular proteases called DPP8/9 (notably DPP9) under steady-state conditions directly interacts with hNLRP1 and CARD8 via the FIIND domain (Figure 14). In a poorly understood manner, this interaction with DPP8/9 keeps NLRP1 in an inhibited state. DPP8/9 are intracellular serine proteases that cleave N-terminal dipeptides, and in particular, cleave dipeptide substrates with proline in the second position (NH₂-Xaa-Pro). In 2018, it was shown that dipeptidylpeptidase (DPP) inhibition by the small molecule Val-boroPro (VbP), a broad DPP4/7/8/9 inhibitor, results in its dissociation with the FIIND domain and activates the NLRP1B inflammasome (Johnson et al., 2018b). Subsequently, it was shown that the binding of the DPP9 protease with hNLRP1 as well as its catalytic activity are required for inhibiting the activation of the

human NLRP1 inflammasome (Zhong et al., 2018) (Table 4). Interestingly, Vbp-mediated inflammasome activation is not dependent on the N-end rule pathway suggesting that Vbp-mediated activation of NLRP1 is distinct from N-terminal cleavage.

A large number of groups are working on the mechanisms underlying how DPP8/9 inhibition activates NLRP1 and CARD8. Because DPP9 (as well as DPP8) interacts directly with NLRP1 and CARD8 but also has a catalytic (protease) activity both means have been studied to try to understand the mechanisms of NLRP1 and CARD8 inhibition by DPP8/9. Surprisingly, DPP8/9 was found to inhibit NLRP1 (murine and human) and CARD8 in different ways (table 4). In fact, binding of DPP9 with hNLRP1 as well as DPP9 catalytic activity are required for inhibiting the activation of hNLRP1. However, in the case of CARD8, DPP9 inhibition seems to be independent of its binding and only require its catalytic activity (Bauernfried & Hornung, 2021). The understanding of these mechanisms is still very recent and not well comprehended. In the following paragraphs, I will summarize the current knowledge and differences in the activation of these inflammasomes by DPP8/9 inhibition (table 4).

Different studies showed that DPP9 binding restrains hNLRP1 inflammasome formation by both inhibiting DPP8/9 activity and disrupting the DPP9-hNLRP1 interaction. In fact, Zhong et al, showed that the expression of hNLRP1 and ASC in DPP8/9^{-/-}, but not wild-type, HEK 293T cells caused the formation of spontaneous ASC specks (Zhong et al., 2018). In this system, stable expression of wild-type DPP9, which both binds to hNLRP1 and has catalytic activity, completely abrogated speck formation. Notably, the stable expression of DPP9 S759A, which binds to hNLRP1 but is catalytically inactive, partially rescued speck formation. Consistent with these data, a hNLRP1 P1214R mutant (mutation located immediately after the autoproteolysis site) protein that is unable to bind to DPP9 spontaneously assembles into an inflammasome. Moreover, the autoproteolysis-deficient mutant NLRP1 F1212A protein exhibited impaired binding to DPP9, suggesting that autoproteolysis was required to create the binding interface. Recently, two authors (Hollingsworth et al., 2021; Huang et al., 2021b) have provided a better understanding of the interaction of DPP9 with NLRP1. Both groups revealed an auto-inhibited complex of NLRP1 that consists in a ternary complex that comprises DPP9, full-length NLRP1, and two-auto cleaved NLRP1 C-terminal (UPA-CARD) (Figure 14). The binding of the NLRP1 C-terminal (UPA-CARD) to DPP9 requires full-length NLRP1, which suggests that NLRP1 activation is regulated by the ratio of NLRP1 C-terminal to full-length NLRP1. Co-expression of autoproteolysis-deficient full-length NLRP1 consistently prevents activation of the inflammasome caused by ectopic expression of the NLRP1 C-terminal. VbP prevents the N terminus of the NLRP1 C-terminal from interacting with the S730 residue in the DPP9 active site, which mimics a substrate-bound condition. In order to cause inflammasome activation, VbP impairs the NLRP1-DPP9 interaction and accelerates the degradation of the N-terminal fragment (Hollingsworth et al., 2021). Overall, these findings show that DPP9 acts as a checkpoint for

the activation of the NLRP1 inflammasome by decreasing levels of NLRP1 C-terminal. This can be explained by the fact that NLRP1's activation results from its degradation, and NLRP1's constitutive turnover may release enough active C-terminal (UPA-CARD) to cause caspase-1 activation. All these results suggest that the activation necessitates the accumulation of the UPA-CARD following its sporadic and spontaneous release from the N-terminal domains of NLRP1. This is consistent with the delayed kinetics of VbP-induced inflammasome activation (18 hours). The quick response observed with other NLRP1 activators suggest that the DPP8/9 blockade must be bypassed by 'active' pathogen-induced NLRP1 inflammasome activation.

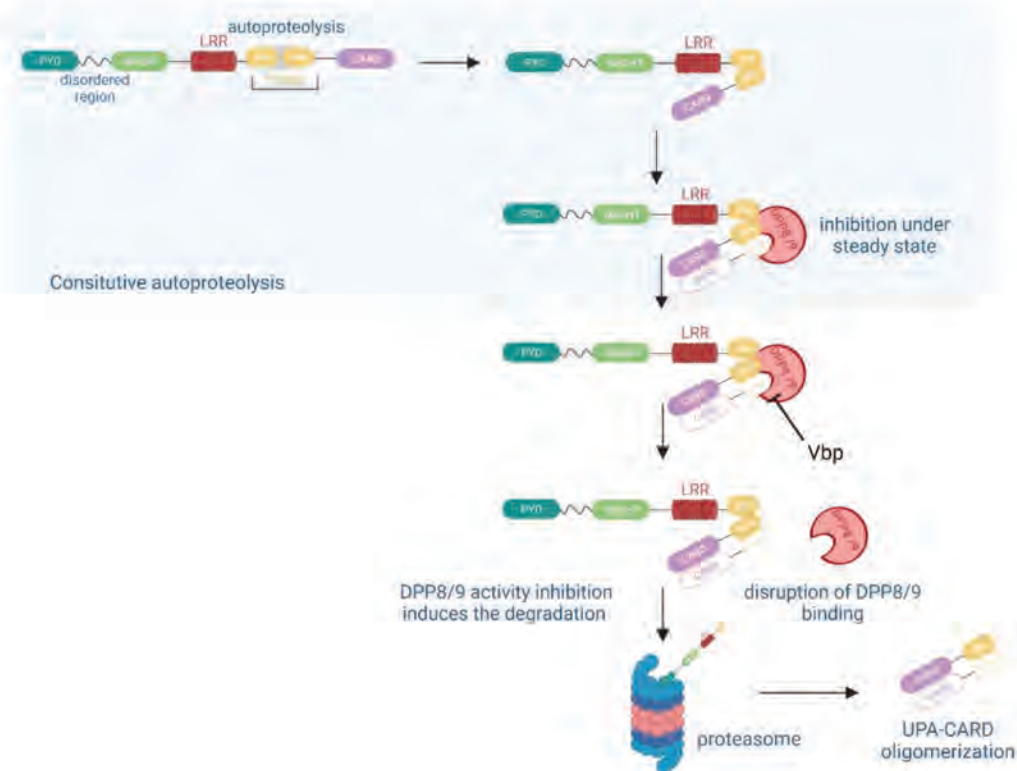


Figure 22: Activation of the hNLRP1 inflammasome by ValboroPro. VbP (ValboroPro) directly disrupts DPP9 binding from the ternary complex, thereby inhibiting DPP8/9 catalytic activity destabilizing hNLRP1, releasing its C-terminus from autoinhibition and initiating the formation of the UPA-CARD oligomerization.

Recent data suggest that VbP didn't activate CARD8 (and mNLRP1) by disrupting the binding with DPP8-9/. It was suggested that VbP didn't disrupt the DPP9-CARD8 interaction but that it activate CARD8 inflammasome exclusively by blocking DPP9 enzymatic activity (Griswold et al., 2019). According to Griswold et al., DPP9^{-/-} HEK293T cells spontaneously died when they expressed CASP1 and CARD8, and VbP did not cause any more cell death (Taabazuig et al., 2020). Stable expression of wild-type DPP9 in this system prevented cell death and restored the cells' sensitivity to VbP. Cell death was not prevented by the expression of DPP9 S759A, which preserves CARD8 binding but is catalytically inactive. Griswold et al., also showed that, unlike hNLRP1, CARD8 autoproteolysis is not required for DPP9 binding. In fact, only full-length CARD8, and not the isolated N- or C-terminal fragments, binds to DPP9.

Future research will be required to understand how and why hNLRP1 and CARD8 interact differently with DPP9. However, the data strongly indicate that the hNLRP1 binding interface involves at least one surface that is close to the DPP9 active site, whereas the CARD8 binding interface appears to be completely spatially remote from the DPP9 active site, so VbP does not detach from the complex but still leads to its activation, probably via the accumulation of peptides not degraded by DPP9 (Q. Wang et al., 2023). Surprisingly, the mNLRP1B-DPP9 contact, which did not require FIIND autoproteolysis and was not affected by VbP, resembled the CARD8-DPP9 interaction more than the hNLRP1-DPP9 relationship.

	hNLRP1-DPP9	CARD8 -DPP9
Binding interaction	Yes	Yes
Catalytic activity of DPP9 is required for binding	Yes	No
DPP9 binds to autoproteolysis deficient mutant	Minimal binding	Yes
Vbp reduces the binding of DPP9?	Yes	No

Table 4: Current knowledge about hNLRP1 and CARD8 binding to DPP9

7. Mouse NLRP1B

I. Activation by lethal factor (LF)

Bacillus anthracis is a Gram-positive bacterium that causes anthrax, a deadly disease to livestock and, occasionally, to humans (zoonosis). Among the virulence factors causing its pathogenicity, one of the most virulent is the anthrax lethal toxin (LT). Anthrax lethal toxin (LT) is a two-component toxin consisting of the zinc metalloprotease lethal factor (LF) and the pore-forming protein protective antigen (PA). Through endocytosis, PA transports LF into the host cell cytosol, where it cleaves a number of host proteins (such as MAPK). In the 1990s it was shown that direct LT injection can cause a quick inflammatory response in mice that results in systemic shock and mortality. This reaction is dependent on macrophages and IL-1 signaling. It was only in 2006, that rodent NLRP1 was identified to be implicated in this response (Boyden & Dietrich, 2006). However, LF induces the activation of only some alleles of mNLRP1B (mNLRP1B1 and mNLRP1B5) and not hNLRP1. Later, in 2012, it was shown that LF cleaves mNLRP1B after Lys44, inducing its activation, and that the use of proteasome inhibitors could block LF-induced NLRP1B activation. These results reveal the importance of the cleavage for mNLRP1B activation but also the implication of the proteasome pathway (Levinsohn et al., 2012; Squires et al., 2007). The concept that an inflammasome is triggered after cleavage was not well understood at the time and it wasn't until 2013 that this concept was validated. In 2013, Chavarria-Smith and Vance confirmed that NLRP1 can be directly activated by cleavage using an engineered system in which

NLRP1B was modified with an N-terminal GFP followed by a synthetically added TEV (tobacco etch virus) cleavage site (Chavarría-Smith & Vance, 2013). Although LF only cleaves a subset of NLRP1 proteins, N-terminal proteolysis by the proteasome is a common mechanism for NLRP1 activation that was confirmed by several studies in 2019 and named the “functional degradation” pathway (Sandstrom et al., 2019a). Based on this concept, it was shown that the cleavage of mNLRP1B on its N-terminal exposes a destabilizing N-terminal residues, which is recognized by a member of the N-end rule pathway, the E3 ligase named Ubr2 (Chui et al., 2019). The N-end rule pathway is complex, but in a simplistic manner, the N-end rule pathway thanks to N-recognins recognizes proteins with destabilizing N-terminal residue (thanks to the identity of its N-terminal amino acid), ubiquitinates and degrades proteins by leading them to the proteasome (Tasaki et al., 2012; Varshavsky, 2011; Varshavsky & Hartl, 2018). After recognition by Ubr2, the N-terminal fragment of NLRP1B is subsequently destroyed by the proteasome. The break in the polypeptide chain within the FIIND prevents the proteasome from degrading the C-terminal NLRP1 domains and instead results in the release of the active C-terminal UPA-CARD fragment. The C-terminal then assembles and oligomerizes directly with caspase-1 leading to pyroptotic cell death. In this case, both, the N-end rule pathway and proteasome pathway were implicated in the mNLRP1B activation.

This "functional degradation" based activation pathway strongly suggests that NLRP1 could operate as a "decoy" to sense pathogenic protease activity. To be more specific, pathogens may have developed a several of strategies, including but not limited to lethal factor (LF), to degrade mammalian NLR proteins and avoid being recognized by the innate immune system. However, the inflammasome is activated and an immunological response is induced when the NLRP1 N-terminus is accidentally destroyed. In line with this “decoy” hypothesis, it was shown that the IpaH7.8 E3 ubiquitin ligase secreted by *Shigella flexneri* bacterium directly ubiquitinates and activates mouse NLRP1B (Sandstrom et al., 2019b). Interestingly, pyroptosis induced by IpaH7.8 also occurs in Ubr2^{-/-} cells, likely because IpaH7.8 itself can directly ubiquitylate NLRP1B and therefore bypasses the requirement for N-end rule E3 ligases, indicating that mNLRP1B activation was independent of the N-end rule pathway but proteasome-dependent.

Toxoplasma gondii has also been reported to activate mNLRP1 in macrophages (from rats and rodents). However, the molecular mechanism of *T. gondii*-induced NLRP1 activation is unknown. Ewald et al reported that *T. gondii* infection does not cleave the NLRP1 N-terminus like LF protease suggesting that the key pathogenic effector of this parasite is not a protease (Ewald et al., 2014). An alternative possibility is that a *T. gondii* activity manipulates the host cell in some way, and NLRP1 senses this perturbation in the host cell's state. It was suggested that NLRP1 could sense pathogen-associated activities by an indirect mechanism such as cellular perturbations (ATP depletion).

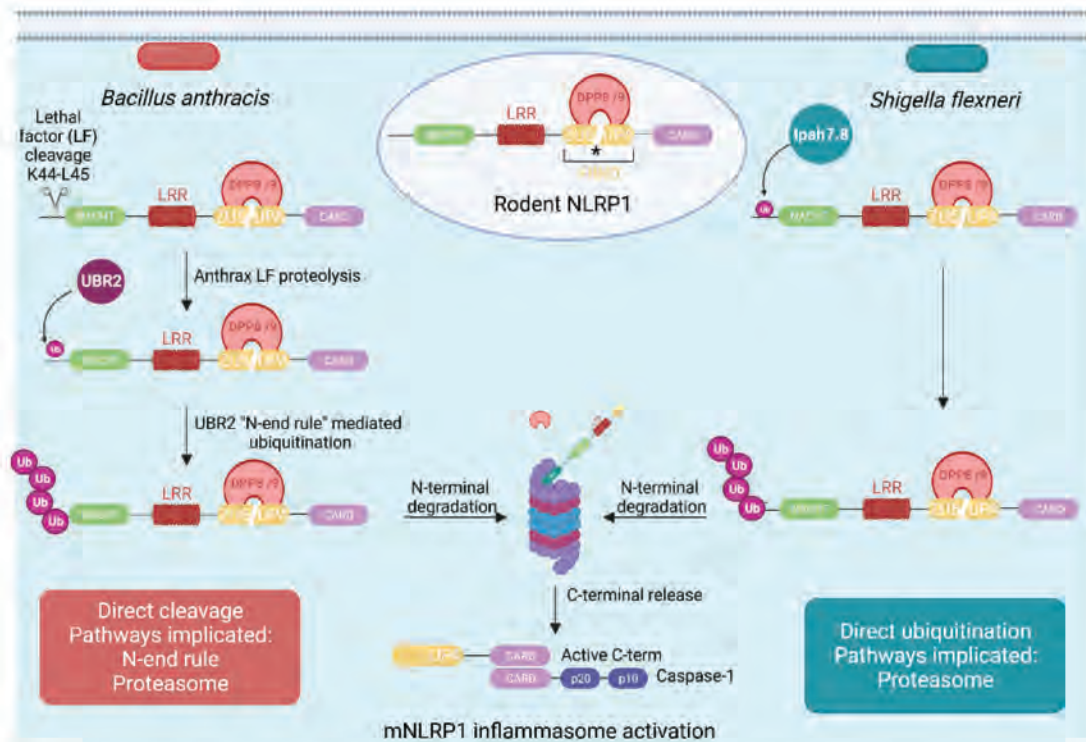


Figure 23: Model of mNLRP1B activation. Anthrax lethal factor (LF) released by *Bacillus anthracis* activates the mNLRP1B inflammasome by protease cleavage (left). LF cleaves between residues K44 and L45 in the N-terminal fragment, generating a destabilized N-terminal residue. The N-end rule E3 ligase UBR2 recognizes and ubiquitinates this neo-N-terminus, inducing its proteasome-mediated degradation. The C-terminal is then released and used to recruit and activate caspase-1, inducing mNLRP1B inflammasome activation. *Shigella flexneri* activates the mNLRP1B inflammasome, thanks to the secretion of Ipah7.8 E3 ubiquitin ligase that directly ubiquitinates and induces the N-terminal degradation by the proteasome that induces the C-terminal release.

8. Human NLRP1 inflammasome

I. The emerging functions of epithelial inflammasomes in immunity to infection and diseases

The epithelium (epidermis, gastrointestinal, and respiratory tract) is constantly exposed to a wide range of pathogens and danger signs as a result of its advantageous placement. Traditionally, the epithelium has been thought of as a protective but passive barrier. However, epithelial surfaces are physical, chemical, and biological barriers. According to the most recent studies of interactions between host epithelium and microorganism. It is now clear that the epithelium senses and actively responds to these signals in order to maintain barrier homeostasis and contributes to the inflammatory response (Palazon-Riquelme & Lopez-Castejon, 2018). Epithelial cells are armed with intrinsic immune defence mechanisms collectively called cell-autonomous immunity that cover a broad set of anti-microbial mechanisms including autophagy, the interferon system, and inflammasome sensors. Particularly, NLRP1 has recently gained much attention since the early 2020s and is rising as an important epithelial sensor involved in antimicrobial defence as well as in the development of pathologies (Bauernfried & Hornung, 2021).

Human NLRP1 polymorphisms have been linked to an elevated risk for numerous autoimmune and autoinflammatory disorders of the skin or respiratory tract, with keratinocytes and respiratory epithelial cells primarily affected (Drutman et al., 2019; Zhong et al., 2016). This suggests that human NLRP1 plays an important tissue-specific role in epithelial cells of barrier tissues rather than within the myeloid compartment.

Three distinct monogenic skin diseases, including familial keratosis lichenoides chronica (FKLC), multiple self-healing palmoplantar carcinoma (MSPC), and autoinflammation with arthritis and dyskeratosis (AIADK), are linked to gain-of-function mutations in the human NLRP1. Interestingly, these mutations are mainly located in three distinct regions (Table 4): PYD domain, between NACHT and LRR domain and the FIIND domain. Individuals with MSPC had missense mutations in the PYD domain of NLRP1 (A54T, A66V M77T), individuals with FKLC had an in-frame deletion (F787-R843) that removed the first LRR domain and part of the preceding linker region and individuals with AIADK had missense mutations located in the FIIND domain. Reconstitution of inflammasome components in 293T cells or immortalized keratinocytes demonstrated that the disease-associated NLRP1 PYD variants A54T, A66V, and M77T were auto-active, spontaneously inducing NLRP1 oligomerization, caspase-1 activation, and IL-1 β release (Zhong et al., 2016).

	MSPC	FKLC	AIADK
Skin auto-inflammatory disease hNLRP1-dependent	Multiple self-healing palmoplantar carcinoma (MSPC)	Familial keratosis lichenoides chronica (FKLC)	Autoinflammation with arthritis and dyskeratosis (AIADK)
GOF mutation	MSPC, A54T, A66V, and M77T are found within the N-terminal PYD	In-frame deletion (F787-R843) that removed the first LRR domain and part of the pre-ceding linker region (Conserved between men and rodents)	R726W and P1214R

Table 4: Implication of hNLRP1 in rare inflammatory skin disorders

The NLRP1 mutations linked to the diseases shed some light on the PYD's mechanism. The PYD of other NLRs serves to recruit ASC. Although it was once thought that the NLRP1 PYD also served this purpose, more recent data suggest that it was not the case. In fact, the MSPC mutations seemed to impair or destabilize PYD folding. Although the authors argued that instability of the PYD eliminates a PYD-

mediated auto-inhibitory interaction, it was also proposed that misfolding of the PYD causes NLRP1 activation. Thus, the misfolding of PYD would be detected by the protein quality control system inducing proteasome 'functional degradation' of NLRP1. The loss of the NLRP1 PYD in numerous species, including mouse-like rodents, raises the intriguing possibility that the adaptive advantages of the NLRP1 PYD may also come at a cost of adaptation (e.g., a lower threshold for undergoing spontaneous activation), which may become unbalanced in the extended absence of PYD-sensed pathogens.

It's interesting to note that GOF mutations of NLRP1 predispose individuals to the growth of squamous cell carcinomas (SCCs), a type of nonmelanoma skin cancer derived from keratinocytes, demonstrating the pro-tumorigenic nature of chronic NLRP1-dependent inflammasome activation and skin inflammation (Zhong et al., 2016). Although the NLRP1 pathway aids in the development of SCCs in human skin, SCC cell lines and tumor biopsies show a strong downregulation of NLRP1 inflammasome proteins and pro-inflammatory cytokines (pro-IL1 β) (Sand et al., 2019). Although NLRP1 activation aids in the early growth of skin tumors, inflammasome pathway activation in established SCC may adversely affect tumor cells by, for instance, inducing pyroptosis or/and antitumor immunity. Thus, NLRP1 plays an important role in human skin. Similarly, poor prognosis is linked to low expression of NLRP1 in lung cancer (Edward Shen et al., 2021).

Furthermore, environmental air pollution is an emerging global issue that significantly impacts lung homeostasis and inflammatory responses. Very recently, a group showed that BaP, a toxic and carcinogenic polycyclic aromatic hydrocarbon in the air, causes DNA damage and lung inflammation that induces inflammatory cytokines in human lung epithelial cells (Kohno et al., 2023). Finally, they demonstrated that Bap enhances NLRP1 expression, activates the NLRP1 inflammasome, and triggers pulmonary inflammation. Interestingly, they show that ROS production signaling increases p53 (a key transcription factor that regulates the expression of genes involved in apoptosis and cell cycle arrest) levels and might be involved in NLRP1 expression (Krześniak et al., 2020).

II. Activation of human NLRP1 by cleavage

Anthrax lethal factor (LF) is the most well-characterized trigger for mNLRP1B, however LF failed to activate hNLRP1 caused by the absence of consensus LF cleavage site in human NLRP1. Despite structural differences detailed above, hNLRP1 and mNLRP1 are both activated by the small molecule Vbp. In 2016, activation of human NLRP1 by cleavage was described with the engineering of an hNLRP1 molecule with an N-terminal GFP and TEV cleavage site. hNLRP1 was activated by a TEV cleavage event suggesting that hNLRP1 activation might be triggered after a direct cleavage (Chavarría-Smith et al., 2016). However, remained unclear if virulence factors from pathogens can activate hNLRP1 until pioneer studies demonstrating that 3C proteases (3Cpros) of several enteroviruses, such as human

rhinovirus (HRV) activates NLRP1 (Robinson et al., 2020b; Tsu et al., 2021). HRV (Human rhinovirus) infection of primary human bronchial epithelial cells was shown to induce caspase-1 activation and IL-1 β and IL-18 release suggesting the activation of an inflammasome platform (Piper et al., 2013). However, the sensing mechanisms were unclear. HRV is the major cause of the common cold and is a member of the Picornaviridae family of single-stranded RNA viruses. All picornavirus, translate their genome as a single polyprotein, which is then cleaved into mature proteins in at least six sites in a sequence-specific manner by a virally encoded 3C protease, termed 3Cpro and 2Apro. Additionally, these proteases can cleave host proteins and facilitate immune evasion. Robinson et al, demonstrated for the first time that a viral protease, HRV-3C protease, cleaves NLRP1 between Gln130 and Gly131, which lies in a poorly conserved region flanked by PYD and NACHT domains, causing the generation of a neo-N terminus recognized by an N-end rule pathway and subsequently degraded by the proteasome. The mode of activation is well in line with the model of “functional degradation” (Figure 16). After cleavage by a protease, the N-terminal fragment is degraded, and the C-terminal UPA-CARD can form an inflammasome. However, unlike for mNLRP1B, the UBR2 ligase was not implicated. The N-terminal glycine produced by HRV-3Cpro cleavage of human NLRP1 is not a conventional type II N-terminal that is recognized by homologous UBR proteins. Recent research (Varshavsky & Hartl, 2023), has identified a glycine-specific N-degron pathway implicating the receptors ZER1 and ZYG11B and their associated cullins CUL2 and CUL5. The proteasome is used by the cullinZER1/ZYG11B mechanism to ubiquitinate substrate proteins having N-terminal glycine residues.

Similarly, we showed, that Human NLRP1 is a sensor of pathogenic 3CL proteases in lung epithelial cells. We showed that *NSP5* 3C-like proteases from coronaviruses, including SARS-CoV-2, directly cleave human NLRP1, promoting functional degradation (Planès et al., 2022). In parallel, Nsp5 cleaves the executor of pyroptosis gasdermin D and makes it non-functional, triggering a GSDME alternative epithelial cell death. This work will be detailed later in the manuscript.

Interestingly, a proteolytic event induced by HIV protease can also activate CARD8. It has been shown that an HIV protease (HIV-1), which is usually only activated after the budding of the virus from the cell, can be activated intracellularly by nonnucleoside reverse-transcriptase inhibitors inducing the cleavage of CARD8 and its following activation in HIV-1 infected CD4+ T cells and macrophages (Wang et al., 2021).

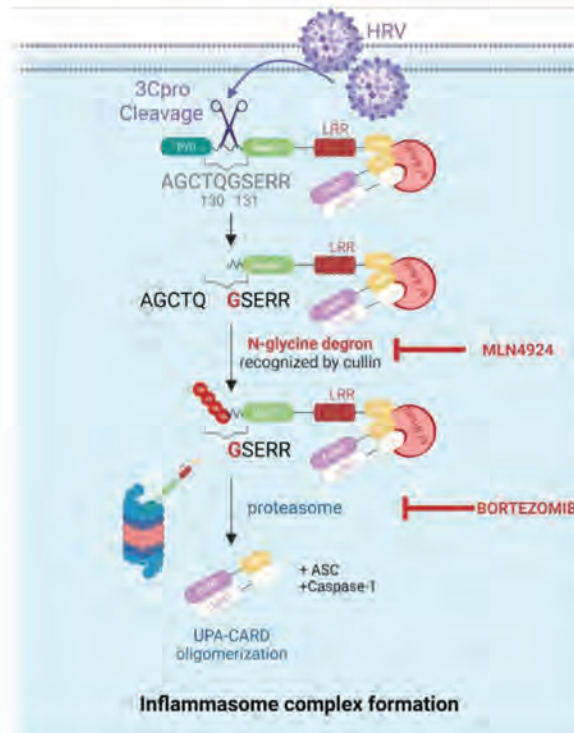


Figure 24: Mechanism of NLRP1 activation by HRV-3Cpro following HRV infection in human airway epithelium adapted from (Robinson et al., 2020b). HRV-3C protease cleaves NLRP1 between Gln130 and Gly131, causing the generation of a neo-N terminus recognized by an N-end rule pathway and subsequently degraded by the proteasome. The degradation of the N-terminus induces C-terminus release, oligomerization, and inflammasome activation.

III. Activation by UVB radiation

The prominent role of NLRP1 in the skin is underlined by strong pathological manifestations in the skin observed in patients bearing gain-of-function mutants of NLRP1 (Zhong et al., 2016). Finally, several reports have suggested that UVB radiation can induce activation of NLRP1 in human keratinocytes, but the mechanism by which NLRP1 could sense UVB remained unclear (Benjamin Faustin & John C. Reed, 2008; Feldmeyer et al., 2007b). Two recent reports revealed new mechanisms to explain how NLRP1 could sense UVB radiation in human keratinocytes (Jenster, Lange, Normann, vom Hemdt, et al., 2023b; Robinson et al., 2022). UVB-induced RNA damage promotes the ribotoxic stress response (RSR) mediated by the MAP kinase kinase kinase ZAK α (Vind et al., 2020; C. C. C. Wu et al., 2020a). Following this lead, the authors found that the activation of NLRP1 upon UVB exposure requires the activity of ZAK α and the downstream p38 kinases. Biochemically, RSR leads to the direct hyperphosphorylation of a human-specific disordered linker region of NLRP1 (between PYD and NACHT domain) by ZAK α kinase and its downstream effector, p38 (Robinson et al., 2022). Indeed, ribotoxic stress is sufficient to drive NLRP1 activation; keratinocytes treated with antibiotics (anisomycin, lactimidomycin, deoxynivalenol, hygromycin, blasticidin) that promote ribosome stalling and MAPKKK ZAK α phosphorylation rapidly induce NLRP1 dependent inflammasome activation. Consistent with the mechanism through which cleavage drives NLRP1 activation, activation of NLRP1 downstream of MAPK signaling also requires

proteasomal activity. These results clearly indicate that NLRP1 can act as a central signaling platform for immune surveillance of cellular homeostasis.

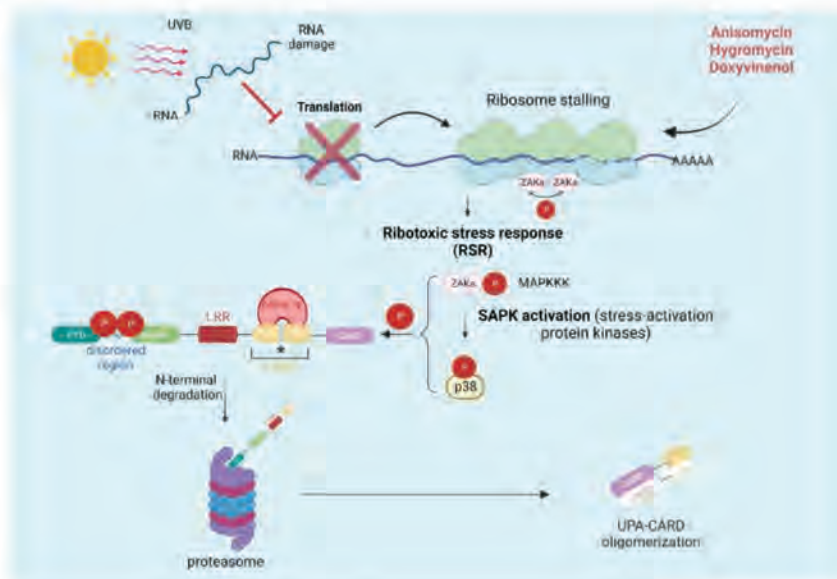


Figure 25: Model of hNLRP1 activation by the ribotoxic stress response. UVB radiation induced RNA damage that promoted ribosome stalling and activated the ribotoxic stress response (RSR), mediated by the phosphorylation and activation of the MAP kinase kinase ZAK α and the downstream p38 kinase. Both kinases lead to the direct hyperphosphorylation of the human disordered region of NLRP1 that induces N-terminal degradation and the C-terminal release, oligomerization, and NLRP1 activation. This model of activation is also conserved for antibiotics like anisomycin, hygromycin, and doxyvinenol.

IV. Activation of hNLRP1 by double-stranded RNA (dsRNA) and poly (dA:dT)

Recently, novel intriguing work by Bauernfried et al. demonstrated that Semliki Forrest Virus (SFV), a positive-sense single-stranded RNA alphavirus that forms long dsRNA during infection, activates hNLRP1 in keratinocytes but not CARD8 or mNLRP1B. Mechanistically, they found that long dsRNA (>500 bp) bound directly to the hNLRP1 (NACHT-LRR domain) through electrostatic interactions. This interaction activates the ATPase NACHT domain of NLRP1 inducing a conformation change that leads to its subsequent activation following proteasome-dependent degradation of the N-terminal domain of NLRP1 and C-terminal fragment release (Bauernfried, Scherr et al. 2021). Recently, this work was confirmed by Jenster et al and other four alphaviruses, namely Sindbis virus, Chikungunya virus, Mayaro virus, and Ross River virus, have been shown to activate NLRP1 (Jenster, Lange, Normann, vom Hemdt, et al., 2023c). Similar to UVB, they showed that these viruses' activation of NLRP1 needs p38 activity and is partially dependent on ZAK α , indicating that MAPK signaling pathways are also involved in the viral activation of NLRP1. Furthermore, pharmacological suppression of either ZAK α or p38 prevents NLRP1 activation by transfected dsRNA. It is important to note that activation of NLRP1 by protease activity or inhibition of DPP9 does not necessitate p38 activity, illustrating independent processes of

activation by these several stimuli. However, further studies are needed to determine the exact mechanism by which dsRNA will activate the ZAK α and p38 pathway.

Very recently, Zhou et al showed that poly(dA:dT), a synthetic dsDNA is unique in its ability to activate NLRP1 in human primary keratinocytes (J. Y. Zhou et al., 2023). Like other activators, activation of NLRP1 by poly(dA:dT) also required functional degradation, as inhibitors of the proteasome abrogated downstream activation. Unlike dsRNA which requires ATP activity, poly (dA:dT) did not induce NLRP1 ATPase activity. Instead, poly (dA:dT) results in oxidative nucleic acid damage and cellular stress, events which activate MAP3kinase including ZAK α , that converge on p38 to activate NLRP1. Interestingly, the poly(dA:dT)-induced NLRP1 response was only partially dependent on ZAK α , indicating that more kinases could be implicated in this pathway.

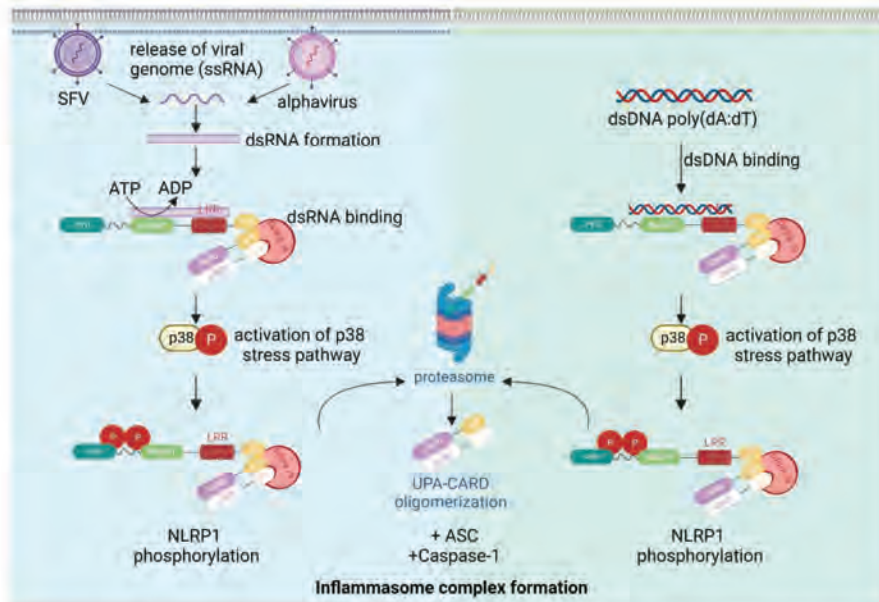


Figure 26: NLRP1 activation by dsRNA or the dsDNA mimetic poly(dA:dT) detection. hNLRP1 detects the long dsRNA from Semliki Forest Virus (SFV) and alphavirus that are generated during its life cycle and triggers inflammasome activation in human primary keratinocytes. Bauernfried et al. showed that dsRNA binds to the NACHT-LRR domain, followed by ATP hydrolysis by the NACHT domain, which is necessary for NLRP1 activation. Very recently, Jenster et al. showed that the cellular stress p38 pathway is activated and implicated in NLRP1 phosphorylation and activation. Furthermore, Zhou et al showed that the dsDNA mimetic poly(dA:dT) induce inflammasome activation via the same p38 cellular stress pathway.

V. Activation by reductive stress

The non-selective metallo-aminopeptidase (AP) inhibitor bestatin methyl ester (MeBs), which induces the accumulation of many peptides and thereby interferes with protein folding, accelerates the rate of NT degradation and synergizes with VbP to induce substantially more pyroptosis. This work indicated that proteotoxic stress potentiates NLRP1 and CARD8 activation (Orth-He et al., 2023) .

Recently, it was shown that the oxidized form of TRX1 binds to NLRP1 and represses inflammasome activation and that genetic deletion of TRX1 sensitizes cells to VbP-induced pyroptosis (Ball et al., 2022). TRX1 is a ubiquitous, highly conserved oxidoreductase that maintains redox balance in the cytosol and protects proteins from oxidative damage and aggregation. These findings suggested that substances that decrease ROS and enhance TRX1 would work together with VbP to increase the amount of NLRP1-dependent pyroptosis. These reductive stress inducers, however, have not yet been recognized and defined until now. Very recently, it was discovered that a panel of related radical-trapping antioxidants, and in particular JSH-23, that induce reductive stress, accelerate N-terminal degradation of both NLRP1 and CARD8, and synergize with VbP to induce more pyroptosis (Q. Wang et al., 2023). Moreover, they found that reductive stress and peptide accumulation together activate both NLRP1 and CARD8 in the absence of VbP. Overall, this work not only establishes chemical probes that induce intracellular reductive stress but also reveals that both NLRP1 and CARD8 detect reductive stress. It should be highlighted that CARD8 lacks NT NACHT-LRR domains, and therefore is unable to bind oxidized TRX1. This suggests that the regulator mechanism of inhibition by TRX1 is only present in hNLRP1 but that both inflammasomes, NLRP1 and CARD8 can detect reductive stress or peptide accumulation.

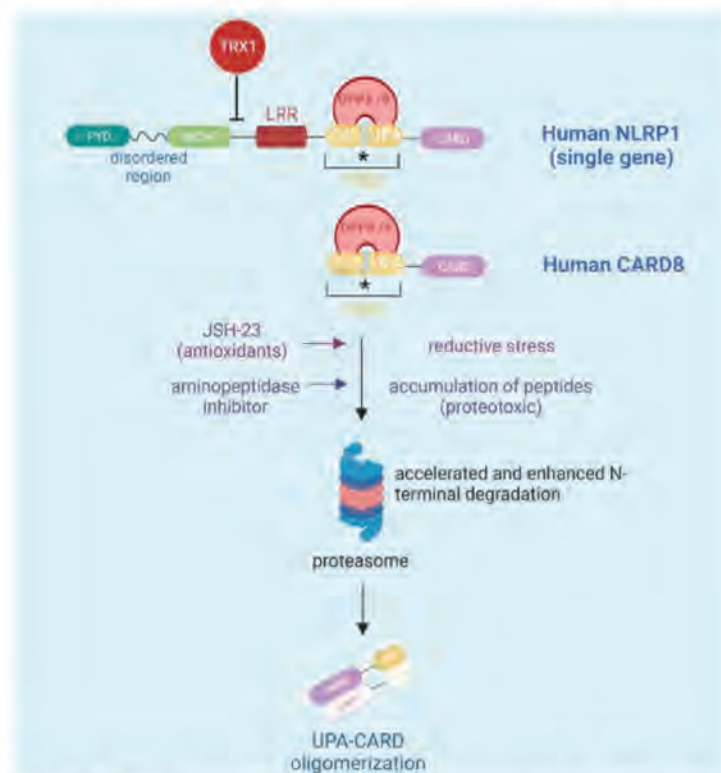


Figure 27: Model of NLRP1 and CARD8 activation by reductive or proteotoxic stress. TRX1 is a ubiquitous, highly conserved oxidoreductase that maintains redox balance in the cytosol and protects proteins from oxidative damage and aggregation. The oxidized form of TRX1 binds to NLRP1 and represses inflammasome activation, and genetic deletion of TRX1 sensitizes cells to VbP-induced pyroptosis. Furthermore, they found that reductive stress (induced by antioxidants) and peptide accumulation (induced by aminopeptidase inhibitors) together activate both NLRP1 and CARD8 in the absence of VbP (ValboroPro). Abbreviations: TRX1, thioredoxin-1.

VI. Proteasome independent activation of NLRP1

Very recently, Yang et al. describe the first viral protein that activates the NLRP1 inflammasome through direct binding that is independent of proteasome activity. The authors found that the protein ORF45 of the virus Kaposi's sarcoma associated herpesvirus (KHSV), also known as human herpesvirus 8, induced inflammasome activation in human epithelial in an NLRP1-dependent manner but in a proteasome-independent manner. Because ORF45 is not a protease but a tegument structural gene, Yang et al. explored how it triggers NLRP1 activation. Using a yeast two-hybrid screen and co-immunoprecipitation, the authors found that ORF45 directly binds to the disordered region of NLRP1 (between the PYD and the NACHT domain), suggesting that ORF45 serves as a direct ligand for NLRP1. The authors try to determine how binding of ORF45 activates NLRP1 and using an elegant biochemical approach, in an unexpected manner they found that NLRP1 forms two inhibitory complexes following FIIND autoproteolysis (Fig 28). They found the previously reported ternary complex form by the NLRP1 full length, the NLRP1-Cterminal and DPP9 and they found a new complex never reported formed by NLRP1N-terminal and NLRP1C-terminal independently of DPP9 and stabilized by an interaction between the disordered region of NLRP1N-terminal and the UPA region of NLRP1C-terminal. This new autoinhibited complex of NLRP1 led the authors to hypothesize that ORF45 could act as a competitor with NLRP1C-terminal to bind to the NLRP1N-terminal disordered region, which would release NLRP1C-terminal for inflammasome activation. Supporting this hypothesis, expressing increasing amounts of ORF45 resulted in progressively higher levels of inflammasome activation and reduced association between NLRP1CT and NLRP1NT. While ORF45 also activated the NLRP1FL–DPP9–NLRP1CT complex by binding to Linker 1 of NLRP1FL, it did not affect the DPP9–FIIND interaction (Fig 29). Finally, they showed that hNLRP1CT inflammasome assembly in the cytoplasm and that hNLRP1NT is translocated to the nucleus with ORF45 and did not undergo degradation. As ORF45-induced NLRP1 activation was not blocked by proteasomal inhibitors, these findings not only characterize the complex interactions by which autoprocessed NLRP1 is kept inactive in cells but also represent the first direct binding activation and proteasome independent mechanism for NLRP1 activation. It's tempting to speculate that other ligands may also bind the disordered region and trigger NLRP1 activation and that disrupting the interaction through post-translational modifications could also trigger NLRP1 activation. Further

investigations are needed to better understand the mechanisms of autoinhibition and activation of NLRP1.

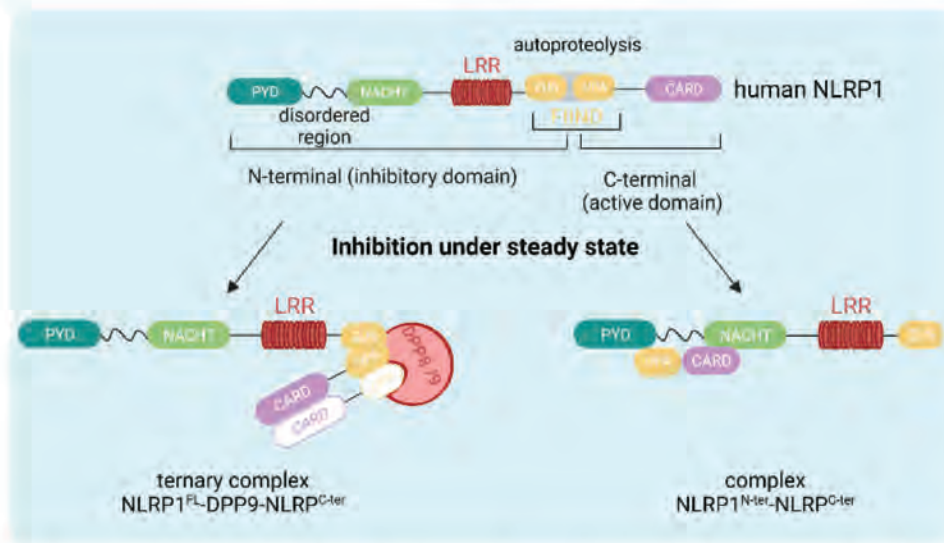
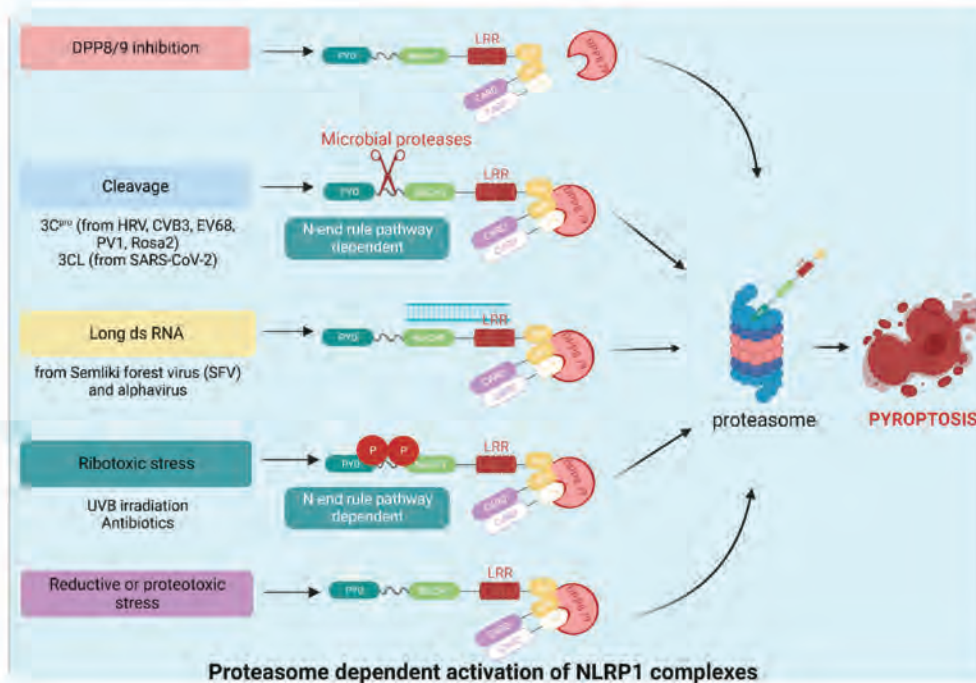
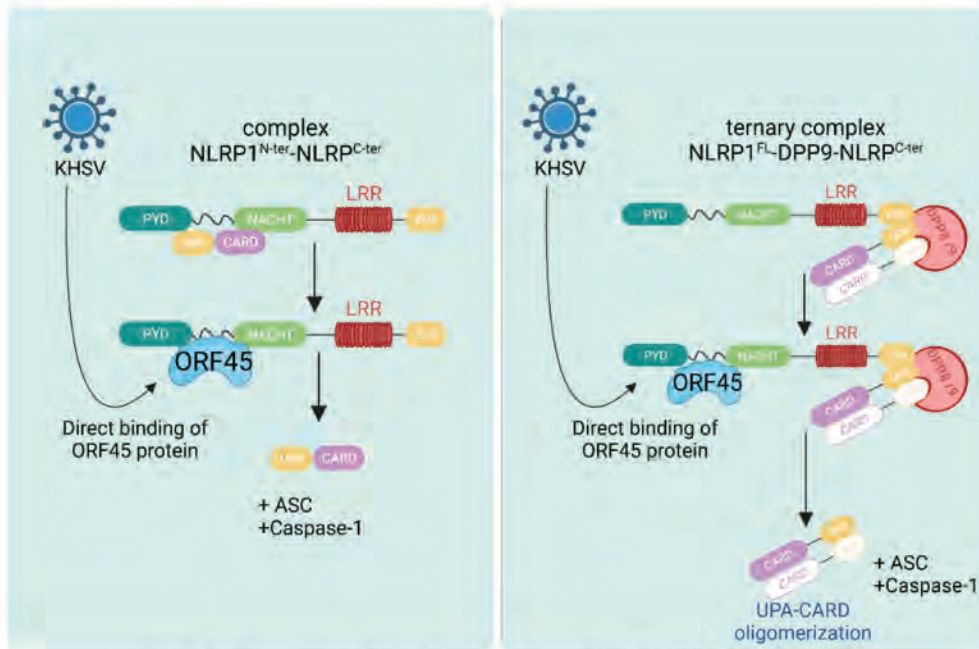


Figure 28: Two forms of autoinhibited NLRP1 complexes. NLRP1 forms two inhibitory complexes following FIIND autoproteolysis. It was previously reported that a ternary complex is formed by the NLRP1 full length, the NLRP1-C terminal, and DPP9. The new complex, which has never been reported before, is formed by NLRP1N- and NLRP1C-terminals independently of DPP9 and is stabilized by an interaction between the disordered region of the NLRP1N-terminal and the UPA region of the NLRP1C-terminal.





Proteasome independent activation of NLRP1 complexes

Figure 29: Proteasome-dependent or independent NLRP1 activation. The classic pathways for activating NLRP1 are totally proteasome-dependent (top figure). However, a new proteasome-independent pathway that activates NLRP1 was recently discovered (lower figure). This pathway implicates the ORF45 protein of the virus Kaposi's sarcoma-associated herpesvirus (KHSV), which directly binds to the disordered region of NLRP1 (between the PYD and the NACHT) and induces activation of the NLRP1 inflammasome.

IV. Work context and results

The role of inflammasomes has been extensively studied in innate immune cells such as macrophages and neutrophils. Despite the fact that this research greatly improved our knowledge of host-pathogen interactions, the *in vivo* scenario is clearly more complex. It's important to note that epithelial cells are frequently the initial cell barrier that pathogens meet, and their response determines the start of an infection. Accordingly, anti-microbial strategies of epithelial cells have gained much attention over the last decades and appeared to be crucial for maintaining a first line of defense against invading pathogens. Interestingly, the human NLRP1 inflammasome (hNLRP1), which was the first inflammasome to be described 20 years ago, is highly expressed in epithelial cells (lung, skin, cornea), and the molecular mechanisms that govern its activation have remained enigmatic until recently. Particularly, NLRP1 has recently gained much attention and is rising as an important epithelial sensor as well as in the development of pathologies. However, its role in host pathogens interactions is not fully elucidated. During my PhD, I observed an enrichment of pro-inflammatory cytokines IL-1 β and IL-18 and cell damage associated in the lung epithelium of severe Covid-19 patients, infected with Sars-Cov2 and cystic fibrosis patients, infected with *Pseudomonas aeruginosa*. These two observations made me think that the inflammasome hNLRP1 could be involved in the inflammatory response. So, during my 3 years of PhD, I studied the role of the NLRP1 inflammasome as a sensor of microbial virulence in the lung epithelium, in the context of viral infection by the SARS-Cov-2 virus but also in the context of bacterial infection by *Pseudomonas aeruginosa*.

The objectives of my PhD were:

- Study if NLRP1-dependent pyroptosis plays an important role during Sars-CoV-2 and *Pseudomonas aeruginosa* infection in the lung epithelium.
- What are the mechanisms implicated in the NLRP1 activation?
- Study the protective or detrimental role of the NLRP1 inflammatory response.

Recently, the COVID-19 pandemic, caused by the severe acute respiratory syndrome coronavirus 2 (SARS-Cov-2), caused the deaths of more than 4 million people worldwide. The virus primarily infects the respiratory tract and it is associated with 2 distinct clinical pictures. In the majority of cases the infection is asymptomatic or associated with minor cold or flu-like symptoms. However, in a minority of cases the infection is pathological and can lead to severe acute respiratory syndrome (ARDS) associated with high mortality. The immune response is crucial in explaining this dichotomy. A deregulated and excessive response correlates with severe forms of the disease. It was shown that an inappropriate hyperinflammatory response, caused by excessive release of inflammatory cytokines is linked many

severe cases of COVID-19 (Paludan & Mogensen, 2022). Interestingly, high levels of IL-18 and IL-1 β were detected in the serum of severe COVID-19 patients and in the bronchiolar lavage fluid (BAL), respectively (Kyriazopoulou et al., 2021) (Rodrigues et al., 2020a). Numerous studies shown the involvement of NLRP3 inflammasome in IL-1B secretion by recruited-monocytes in the lung (Ferreira et al., 2021; Junqueira et al., 2022). However, the virus primarily infects the lung epithelial cells, suggesting a critical role for the hNLRP1 inflammasome during a SARS-CoV-2 infection. To investigate this hypothesis, we were interested in determining if SARS-Cov-2 infection can activate NLRP1. Because SARS-CoV-2 codes for 2 proteases involved in the maturation of viral polyproteins, the NSP3 or PL-pro, a papain-like protease, and the NSP5 or Mpro, a 3C-like cysteine protease, we hypothesized that one of these proteases could be implicated in the protease cleavage of NLRP1 and the following activation. To investigate that, during my PhD, one of my works consisted of deciphering the mechanisms implicated in the NLRP1 activation after a SARS-CoV-2 infection in the lung epithelium. This project is already published (Planes et al., 2022) and presented in the following pages.

Furthermore, different works demonstrated that the human NLRP1 inflammasome can be activated downstream to ribotoxic stress response (RSR)(Andrew Sandstrom, 2023) . While those original reports identified environmental (UVB) and viral stresses that could induce this pathway, it was unclear whether microbial effectors would also induce NLRP1 activation via RSR. In order to investigate the role of hNLRP1 as a sensor of microbial virulence in human epithelium, we focused on the cystic fibrosis (CF) context. Interestingly, we observed cystic fibrosis patients who are chronically infected with *P. aeruginosa* exhibit enrichment of IL-1 in the BALF and strong damage as well as cell death in lung epithelial cells (Palomo et al., 2014; A. Tang et al., 2012) . These observations strongly suggest the involvement of epithelial inflammasomes. During my PhD, I was interested in deciphering the molecular mechanisms implicated in the cellular damage observed in the lung epithelium of CF patients chronically infected by *P. aeruginosa*. This work is under revision in the Journal Experimental Medicine (Pinilla et al., 2023).

1. Work context 1: Human NLPRP1 is a sensor of pathogenic coronavirus 3CL proteases in lung epithelial cells

I. Study context and objectives

Since the early 2020s, NLRP1 has become an important topic of research as is now rising as an important epithelial sensor involved in antimicrobial defence as well as in the development of pathologies. Pioneer studies demonstrated that 3C proteases of several *Picornaviridae* viruses, such as human rhinovirus (HRV), cleaves and activates NLRP1 (Robinson et al., 2020c). Interestingly, NLRP1 is acting as a central decoy receptor aiming to counteract microbial virulence factors. These results suggests that other viruses or microbial pathogens containing 3C proteases could also activate the NLRP1 inflammasome.

During my PhD, one of my works consisted in deciphering the molecular and cellular mechanisms of the immune response to the COVID-19 infection. To do so, we screened the different inflammasome receptors expressed in lung epithelial cells and confirmed, as previously described, that they mainly express the NLRP1 inflammasome. We therefore hypothesized that NLRP1 might act as a SARS-Cov-2 sensor. Because NLRP1 is expressed in primary airway epithelial cells, but its expression is lost in several human tumor cell lines, we over-expressed or deleted hNLRP1 in the alveolar epithelial cell line A549 ACE2: A549^{ACE2/NLRP1+} or A549^{ACE2/NLRP1-}. We found that infection with SARS-Cov-2 leads to a pyroptotic form of cell death in cells expressing NLRP1 but not in NLRP1 deficient cells. Conversely, complementing NLRP1 in NLRP1 deficient cells restored infection-induced cell death. Recent work has shown that NLRP1 can be activated following its cleavage by viral proteases of type 3C of enteroviruses. We investigated the role of SARS-Cov-2 proteases in the NLRP1 activation in lung epithelial cells. SARS-Cov-2 codes for 2 proteases involved in the maturation of viral polyproteins: NSP3 or PL-pro, a papain-like protease, and NSP5 or Mpro, a 3C-like cysteine protease. Consequently, our results demonstrated that the NSP5 3CL protease is able to cleave NLRP1 in its N-terminal domain after glutamine 333, leading to NLRP1 activation. Our work has therefore shown that NLRP1 was activated after a SARS-Cov-2 infection, which leads to cell death by pyroptosis. In the classical pathway of pyroptosis, cell death is triggered by the cleavage of gasdermin-D protein which forms pores on the cell surface. We therefore investigated whether infection leads to the formation of these active forms of gasdermin-D. Surprisingly, we could not observe gasdermin-D active forms but the infection was associated with the appearance of gasdermin D cleavage bands. We tested the effect of the SARS protease NSP5 on these gasdermin D cleavages and observed that the SARS protease NSP5 cleaves Gasdermin D, after Q193, to generate an inactive fragment. This allowed us to demonstrate a new mechanism of SARS virulence that inactivates gasdermin D by cleaving it via its protease NSP5. To decipher what mechanism triggers cell death after SARS-Cov-2 infection we generated knock-out (by CrisprCas9 method) of gasdermin-D, gasdermin-B and gasdermin-E. We demonstrate that the infection by Sars-Cov-2 activates NLRP1 but inactivates the gasdermin-D inducing the engagement of an alternative pyroptosis pathway that involves the activation of gasdermin-E. To understand the effect of the virus detection by NLRP1 on viral replication we measured the production of infectious viruses particles in A549^{ACE2/NLRP1+} or A549^{ACE2/NLRP1-} cells using the TCID50 titration technique (dose of virus that infects 50% of the culture). The results showed that NLRP1 restricts the production of infectious viruses by 5X. This demonstrates that the NLRP1 pathway induces an anti-viral response, at least *in vitro*. Finally, to return to a physiological context, we studied patients to see if we could measure markers of the activation of this NLRP1 pathway. To do this, we were lucky enough to obtain plasma samples from patients with COVID-19, in collaboration with the IMAGINE Institute in Paris and the Toulouse Hospitals. Our results showed a higher amount of

Gasdermine E and IL-18 in patients with Severe COVID, suggesting that the over-activation of the NLRP1 pathway may be pathological during SARS-CoV-2 infection.

To conclude, our work has shown that NLRP1 is an important sensor of SARS-CoV-2 infection in lung epithelial cells. Mechanistically, NLRP1 activation is dependent on the SARS-CoV-2 protease NSP5 3CL. This protease is a virulence factor that is able to inactivate gasdermin D in an attempt to escape pyroptosis but this protease activity is detected by NLRP1 which acts as a decoy receptor and induce a pyroptotic cell death by an alternative pyroptosis pathway that involves the activation of GE. Collectively, the detection of SARS-CoV-2 by the NLRP1 inflammasome leads to cell death by pyroptosis, which limits the production of infectious virus particles. Although this response is protective *in vitro* and limits the production of infectious virus particles, our data suggest that overactivation may be associated with severe disease.

Contribution

In this article, in which I am sharing the first author position with Remi Planes, Karin Santoni, Audrey Hessel, and Charlotte Passemar, I was involved in the development of the entire project and the design of the experiments. Below is a more detailed description of the experiments I performed.

To show that the NSP5 protease was able to cleave NLRP1 and gasdermin D, I performed all the NLRP1 and gasdermin D cleavage experiments *in vitro* and the western blots.

To show that SARS-CoV-2 NSP5 cleaves NLRP1 at the Q333 site, I generated the different mutations in NLRP1 plasmids and transfected A549 cells with NLRP1 wild-type or NLRP1 mutated genes. To examine the ability of NSP5 to cleave wild-type or mutated NLRP1, I performed the *in vitro* cleavage assays.

To show that NSP5 cleaves Gasdermin D in its pore-forming domain and generates an inactive form of Gasdermin D, we performed top-down mass spectrometry (in collaboration with Julien Marcoux at the IPBS). Following this experiment, we showed that SARS-CoV-2 protease Nsp5 generates two different fragments. To study the activity of the fragments, I generated plasmids expressing the full-length of gasdermin D, the active domain N-terminal of gasdermin D (1-275), and the different fragments of gasdermin D generated after the cleavage by SARS-CoV-2 3CL proteases, 1-193 and 194-484. To study their activity to active or not cell death, I expressed these plasmids in A549 cells Gasdermin D deficient, and I measured the induction of cell death thanks to the measure of LDH release.

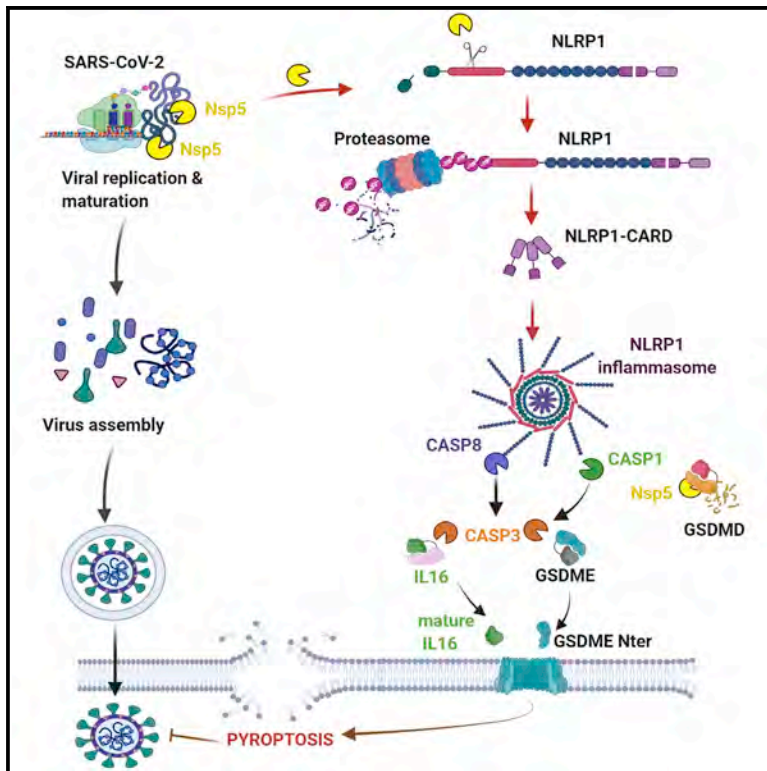
To demonstrate what sites were implicated in the gasdermin D cleavage by NSP5, I generated cells stably expressing the GsdmD gene mutated for protease cleavage sites (GSDMDQ193A and GSDMDQ335A). I performed *in vitro* cleavage assays with lysates of cells expressing GSDMD full length, GSDMDQ193A, and GSDMDQ335A that I incubated with NSP5 or caspase 1.

Remi Planes and I measured the inflammatory mediators (cytokines and caspase activities) in plasmas from hospitalized patients presenting COVID-19 diseases.

II. Paper

Human NLRP1 is a sensor of pathogenic coronavirus 3CL proteases in lung epithelial cells

Graphical abstract



Authors

Rémi Planès, Miriam Pinilla, Karin Santoni, ..., Julien Marcoux, Emmanuel Ravet, Etienne Meunier

Correspondence

remi.planes@ipbs.fr (R.P.), etienne.meunier@ipbs.fr (E.M.)

In brief

Planès et al. identify human NLRP1 as an immune sensor of SARS-CoV2 3CL protease.

Highlights

- SARS-CoV-2 infection activates human NLRP1 inflammasome in epithelial cells
- NSP5 protease cleaves NLRP1 at Glutamine 333 and promotes functional degradation
- NSP5 inactivates GSDMD by cleaving in its pore-forming domain at Glutamine 193
- GSDME triggers alternative epithelial cell death upon GSDMD inactivation



Article

Human NLRP1 is a sensor of pathogenic coronavirus 3CL proteases in lung epithelial cells

Rémi Planès,^{1,2,3,23,24,*} Miriam Pinilla,^{1,2,24} Karin Santoni,^{1,24} Audrey Hessel,^{1,24} Charlotte Passemar,^{4,24} Kenneth Lay,^{5,6} Perrine Paillette,² Ana-Luiza Chaves Valadão,³ Kim Samirah Robinson,⁷ Paul Bastard,^{8,9,10} Nathaniel Lam,^{11,12} Ricardo Fadrique,¹³ Ida Rossi,¹ David Pericat,¹ Salimata Bagayoko,¹ Stephen Adonai Leon-Icaza,¹ Yoann Rombouts,¹ Eric Perouzel,² Michèle Tiraby,² COVID Human Genetic Effort,²⁶ Qian Zhang,⁹ Pietro Cicuta,¹³

(Author list continued on next page)

¹Institute of Pharmacology and Structural Biology (IPBS), University of Toulouse, CNRS, Toulouse, France

²In vivoGen, Toulouse, France

³IRIM, University of Montpellier, CNRS, Montpellier, France

⁴Molecular Immunity Unit, University of Cambridge Department of Medicine, MRC-Laboratory of Molecular Biology, Cambridge, UK

⁵Institute of Medical Biology, Agency of Science, Technology and Research, 8A Biomedical Grove, #06-06 Immunos, 138648 Singapore, Singapore

⁶Laboratory of Human Genetics and Therapeutics, Genome Institute of Singapore (GIS), A*STAR, Singapore, Singapore

⁷A*STAR Skin Research Laboratories, 11 Mandalay Road, 308232 Singapore, Singapore

⁸Laboratory of Human Genetics of Infectious Diseases, Necker Branch, Institut National de la Santé et de la Recherche Médicale U1163, Necker Hospital for Sick Children, Paris, France

⁹University of Paris, Imagine Institute, Paris, France

¹⁰St. Giles Laboratory of Human Genetics of Infectious Diseases, Rockefeller Branch, The Rockefeller University, New York, NY, USA

¹¹University of Cambridge, Department of Veterinary Medicine, Cambridge CB30ES, UK

¹²University of Cambridge, School of Clinical Medicine, Box 111, Cambridge Biomedical Campus, Cambridge CB2 0SP, UK

¹³Biological and Soft Systems, Cavendish Laboratory, University of Cambridge, JJ Thomson Avenue, Cambridge CB3 0HE, UK

(Affiliations continued on next page)

SUMMARY

Inflammation observed in SARS-CoV-2-infected patients suggests that inflammasomes, proinflammatory intracellular complexes, regulate various steps of infection. Lung epithelial cells express inflammasome-forming sensors and constitute the primary entry door of SARS-CoV-2. Here, we describe that the NLRP1 inflammasome detects SARS-CoV-2 infection in human lung epithelial cells. Specifically, human NLRP1 is cleaved at the Q333 site by multiple coronavirus 3CL proteases, which triggers inflammasome assembly and cell death and limits the production of infectious viral particles. Analysis of NLRP1-associated pathways unveils that 3CL proteases also inactivate the pyroptosis executioner Gasdermin D (GSDMD). Subsequently, caspase-3 and GSDME promote alternative cell pyroptosis. Finally, analysis of pyroptosis markers in plasma from COVID-19 patients with characterized severe pneumonia due to autoantibodies against, or inborn errors of, type I interferons (IFNs) highlights GSDME/caspase-3 as potential markers of disease severity. Overall, our findings identify NLRP1 as a sensor of SARS-CoV-2 infection in lung epithelia.

INTRODUCTION

Severe acute respiratory syndrome coronavirus 2 (SARS-CoV-2), responsible for coronavirus disease 2019 (COVID-19), has infected more than 219 million people worldwide. SARS-CoV-2 infection can induce multiorgan failure-associated sepsis with an increased risk in immune-deficient individuals and patients with particular pre-existing comorbidities (Al-Samkari et al., 2020; Cao, 2020; Carvalho et al., 2021; Berlin et al., 2020; Zheng et al., 2020). Given SARS-CoV-2 initially infects nasal, bronchial,

and lung epithelial cells, the host response in these cells can potentially control infection or may result in a response to SARS-CoV-2 that leads to excessive inflammation (Liu et al., 2021; Peng et al., 2021).

Inflammasomes comprise an important response to viral infection. These cytosolic multiprotein complexes are composed of a receptor/sensor, the adaptor protein ASC (at the noticeable exception of the CARD8 inflammasome), and the proinflammatory protease caspase-1 (Broz and Dixit, 2016). Upon inflammasome assembly, caspase-1 autoactivates and processes



Emmanuelle Jouanguy,^{8,9,10} Olivier Neyrolles,¹ Clare E. Bryant,^{11,12} Andres R. Floto,⁴ Caroline Goujon,³ Franklin Zhong Lei,^{7,14,15} Guillaume Martin-Blondel,^{16,17} Stein Silva,¹⁸ Jean-Laurent Casanova,^{8,9,10,19} Céline Cougoule,¹ Bruno Reversade,^{5,6,20,21,22} Julien Marcoux,¹ Emmanuel Ravet,^{2,25} and Etienne Meunier^{1,23,25,27,*}

¹⁴Lee Kong Chian School of Medicine, Nanyang Technological University, 11 Mandalay Road, 308232 Singapore, Singapore

¹⁵Skin Research Institute of Singapore (SRIS), 11 Mandalay Road, 308232 Singapore, Singapore

¹⁶Service des Maladies Infectieuses et Tropicales, CHU de Toulouse, Toulouse, France

¹⁷Institut Toulousain des Maladies Infectieuses et Inflammatoires (Infinity), INSERM UMR1291 - CNRS UMR5051 - Université Toulouse III, Toulouse, France

¹⁸Critical Care Unit, University Hospital of Purpan, Toulouse, France

¹⁹Howard Hughes Medical Institute, New York, NY, USA

²⁰Institute of Molecular and Cell Biology, 61 Biopolis Drive, 138673 Singapore, Singapore

²¹Department of Paediatrics, Yong Loo Lin School of Medicine, National University Health System, National University of Singapore, 10 Medical Drive, 117597 Singapore, Singapore

²²The Medical Genetics Department, Koç University School of Medicine, 34010 Istanbul, Turkey

²³Present address: Institute of Pharmacology and Structural Biology (IPBS), University of Toulouse, CNRS, Toulouse, France

²⁴These authors contributed equally

²⁵These authors contributed equally

²⁶Further details can be found in the supplemental information

²⁷Lead contact

*Correspondence: remi.planes@ipbs.fr (R.P.), etienne.meunier@ipbs.fr (E.M.)

<https://doi.org/10.1016/j.molcel.2022.04.033>

proinflammatory cytokines of the interleukin (IL)-1 family, IL-1 β and IL-18, as well as Gasdermin D (GSDMD) (Broz and Dixit, 2016). GSDMD cleavage activates a type of lytic cell death, pyroptosis, that also triggers the release of the cellular content (Broz and Dixit, 2016; Kayagaki et al., 2021). Although pyroptosis and IL-1-related cytokines are important defenses against a range of microbial infections, dysregulation of the inflammasome promotes excessive inflammation (Kayagaki et al., 2015; Shi et al., 2015; Yu et al., 2021). Specifically, IL-1-related cytokines are detected in SARS-CoV-2-infected patients and are suspected to directly and indirectly contribute to severe COVID-19-linked sepsis (Cauchois et al., 2020; Cavalli and Dagna, 2021; Junqueira et al., 2021; Lucas et al., 2020; Pan et al., 2021; Rodrigues et al., 2021; Yap et al., 2020).

As previously described, immunoblotting analysis of the expression of inflammasome-forming sensors in human primary epithelial and cell lines highlights that primary bronchial and alveolar epithelial cells specifically express the inflammasome-forming sensor NLRP1 (Figures 1A and S1A) (Bauernfried et al., 2021; Lee et al., 2019; Robinson et al., 2020).

NLRP1, a NOD-like receptor (NLR), exhibits a domain FIIND (function-to-find domain) that autocleaves NLRP1 into two proteins noncovalently connected (Chavarría-Smith et al., 2016; Chui et al., 2019; Johnson et al., 2018; Mitchell et al., 2019; Okondo et al., 2018; Sandstrom et al., 2019; Zhong et al., 2018). In this process, the proteases DPP8/DPP9 keep the C-Term CARD in an inactive conformation.

Pathogen-driven activation of the NLRP1 inflammasome can occur in the following different ways. First, cleavage of NLRP1 close to the N-terminal PYRIN domain can send N-terminal NLRP1 to the proteasome, thus allowing the C-terminal CARD domain to oligomerize and activate caspase-1 (Mitchell et al., 2019). This mechanism occurs when murine NLRP1B is exposed to the anthrax lethal factor (LF) protease (Chavarría-Smith et al., 2016; Chui et al., 2019; Sandstrom et al., 2019) and also in humans in response to enterovirus 3C cysteine proteases (Robinson et al., 2020; Tsu et al., 2021). Another mech-

anism that activates NLRP1 is binding of long double-stranded RNA detection to its NACHT- (NAIP [neuronal apoptosis inhibitor protein], C2TA [MHC class 2 transcription activator], HET-E [incompatibility locus protein from *Podospora anserina*] and TP1 [telomerase-associated protein]) LRR (Leucine-Rich Repeats) domain. This mechanism also promotes inflammasome signaling in keratinocytes and bronchial epithelial cells infected with the RNA-positive (+RNA) strand Semliki Forest Virus (Bauernfried et al., 2021). SARS-CoV-2 is a +strand RNA virus that expresses two proteases, a 3CL-(3C-like) protease, namely NSP5, and a chymotrypsin protease, NSP3. Thus, here, we evaluate the ability of NLRP1 to detect SARS-CoV-2 infection.

RESULTS

NLRP1 triggers an inflammasome response upon SARS-CoV-2 infection of epithelial cells

NLRP1 is expressed in primary airway epithelial cells, but its expression is lost in various human tumor cell lines (Figures 1A, S1A, and S1B), limiting the ability to use these cells to analyze the innate immune response to viral infection. Therefore, we expressed hNLRP1 in the alveolar epithelial cell line A549^{ACE2}. This cell line expresses endogenous ASC, caspase-1, and GSDMD (Figure S1A). Fluorescent (GFP)-tagged ASC was coexpressed in some experiments, allowing us to monitor inflammasome assembly upon NLRP1 activation and ASC polymerization (Figure S1B; Dick et al., 2016; Franklin et al., 2014; Lu et al., 2014). We activated NLRP1 using poly(I:C) or the pharmacological agent Val-boroPro (Val-boro) to evaluate the efficacy of our cell lines (Figures S1C–S1F; Johnson et al., 2018; Okondo et al., 2018). Transfection of poly(I:C) or treatment with various doses of Val-boro only triggered cell lysis in NLRP1-expressing cells (Figures S1C–S1E). In addition, only NLRP1-expressing cells contained ASC-GFP specks upon Val-boro treatment, indicating that this fusion protein can be used to monitor inflammasome assembly (Figure S1F).

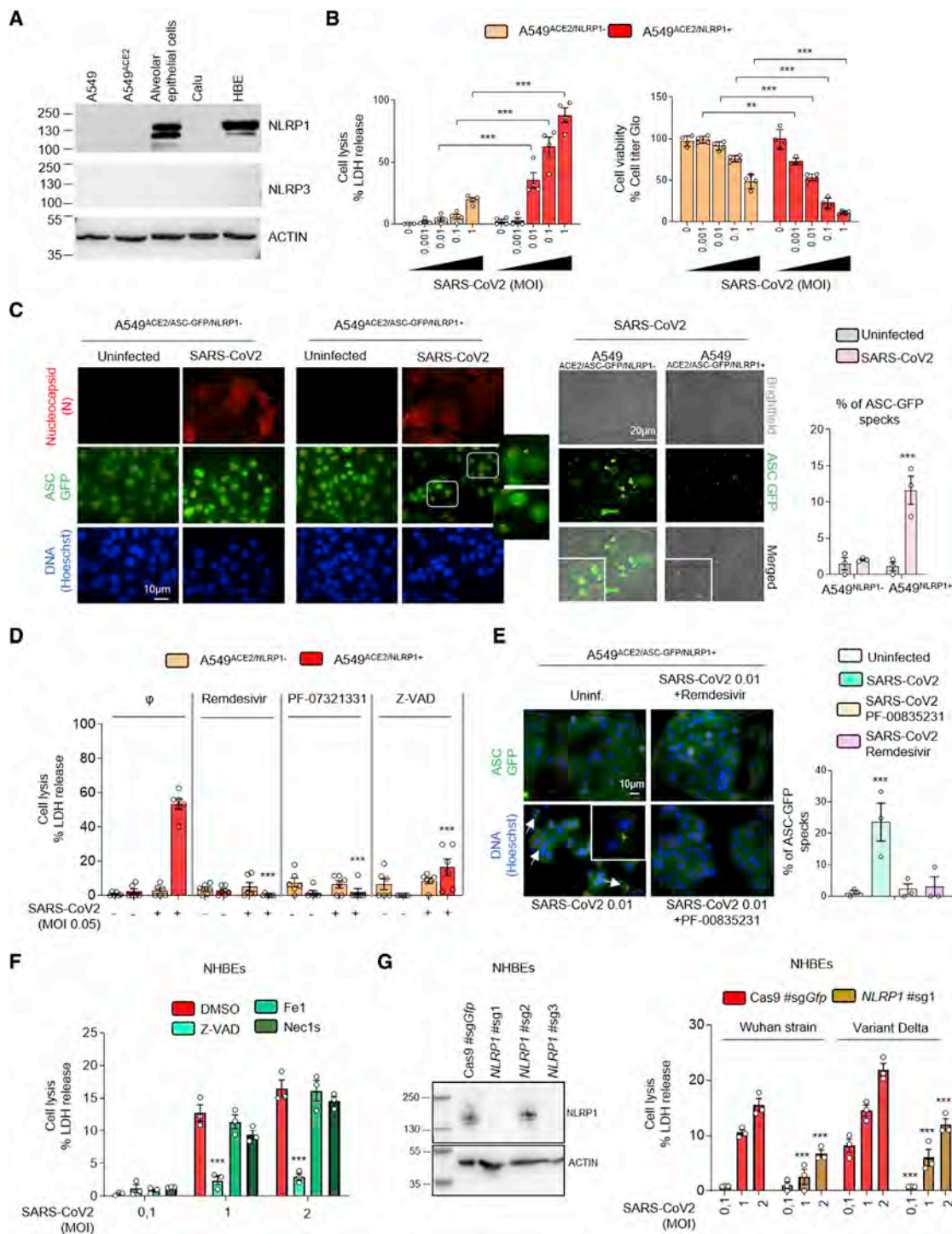


Figure 1. NLRP1 is an innate immune sensor of SARS-CoV-2 infection

(A) Western blot examination of NLRP1, NLRP3, and ACTIN in various human epithelial cells and cell lines.

(B) Cell death (LDH) and viability (ATP Glo) evaluation in A549^{ACE2/NLRP1+} and A549^{ACE2/NLRP1-} airway epithelial cell lines infected with various multiplicity of infection (MOI) of SARS-CoV-2 for 24 h.

(C) Fluorescence microscopy and associated quantifications of ASC-GFP specks in A549^{ACE2/NLRP1+/ASC-GFP} and A549^{ACE2/NLRP1-/ASC-GFP} airway epithelial cell lines infected with SARS-CoV-2 (MOI 0.05) for 24 h. Nucleus was stained with Hoechst (blue), and nucleocapsid (N) was stained in red after fixation. Brightfield/ASC-GFP pictures were taken in dish during cell infection. Images shown are from one experiment and are representative of n = 3 independent

(legend continued on next page)

Next, we infected A549^{ACE2/NLRP1+} or A549^{ACE2/NLRP1-} cells with various multiplicity of infection (MOI) of SARS-CoV-2 and monitored for cell lysis (LDH release), cell viability (ATP levels), and inflammasome activation (ASC-speck formation) over time (Figures 1B–1D). We observed that SARS-CoV-2 infection triggered a dose-dependent cell death of epithelial cells, a process that was dependent on the NLRP1 expression (Figures 1B and 1C). In addition, only cells expressing NLRP1 exhibited active inflammasome complexes upon SARS-CoV-2 infection, hence suggesting that NLRP1 is an innate immune sensor of SARS-CoV-2 infection (Figure 1C). In addition, we observed that such process occurred in the presence of various SARS-CoV-2 variants, suggesting that NLRP1-driven response is not directly impacted by the appearance of those viral mutations (Figure S1G). Although primary bronchial epithelial cells and A549^{ACE2/NLRP1+} cells do not express detectable levels of NLRP3, we controlled that NLRP3 was not involved in triggering this process by treating NHBEs and A549^{ACE2/NLRP1+} cells with an inhibitor of the NLRP3 inflammasome, namely MCC950 (Figures S1H and S1I). We observed no impact of MCC950 in the ability of SARS-CoV-2 to promote cell death or ASC-speck formation in either NLRP1⁺ or NLRP1⁻ cells (Figure S1H). The efficacy of MCC950 was also tested in THP1 human monocyte cell line, which express detectable levels of NLRP3 and inhibited the activation of NLRP3 inflammasome upon exposure with the well-known toxin nigericin (Figure S1I).

Next, we explored the viral steps that were required for efficient NLRP1 inflammasome activation upon SARS-CoV-2 infection. We used two inhibitors of SARS-CoV-2 replication, namely remdesivir that targets SARS-CoV-2 RNA polymerase and PF-00835231 that inhibits the activity of the 3CL NSP5 protease. Both inhibitors efficiently inhibited SARS-CoV-2 replication in A549^{ACE2/NLRP1+} cells as measured by the lack of appearance of the nucleocapsid (N) protein (Figure S1J). When we addressed the ability of both compounds to modulate SARS-CoV-2-dependent NLRP1 activation, we found that cell lysis (LDH release) levels as well as ASC-specks did not appear in presence of those inhibitors (Figures 1D and 1E). As control, those inhibitors did not show any effect in inhibiting NLRP1 inflammasome activation when cells were exposed to Val-boro (Figure S1K). Furthermore, the use of the pan-caspase inhibitor Z-VAD potently inhibited

SARS-CoV-2-induced NLRP1-dependent cell death both in primary and in A549^{ACE2/NLRP1+} cells, suggesting that caspases are important regulators of this process (Figures 1D and S1J).

Finally, we aimed at determining the reproducibility of our observations in primary human epithelial cells. Hence, we used normal human bronchial epithelial cells (NHBEs) and evaluated the importance of NLRP1 in SARS-CoV-2-driven epithelial cell death. Infection of NHBE with various SARS-CoV-2 strains led to the induction of cell death, a process that was strongly impaired in presence of the pan-caspase inhibitor Z-VAD but not in presence of Necroptosis inhibitor Nec1s or the ferroptosis inhibitor Fe1 (Figures 1F and S1L), suggesting a critical function of caspases in SARS-CoV-2-driven epithelial cell death. Next, we generated genetic inactivation of *NLRP1* gene expression using CRISPR-Cas9 in NHBE cells (Figure 1G). Infection of NHBE^{WT} and NHBE^{NLRP1-/-} epithelial cells with SARS-CoV-2 showed a significant involvement of NLRP1 expression in NHBE cell lysis after 36 h of infection (Figure 1G), hence confirming that NLRP1-dependent cell death occurs both in cell lines and in primary epithelial cells.

Altogether, our results suggest that in airway epithelial cells, NLRP1 behaves as a sensor of SARS-CoV-2, a process that requires viral replication.

SARS-CoV-2 3CL protease-cleaved NLRP1 triggers inflammasome assembly

Next, we wondered about the viral effectors able to drive NLRP1 activation. Both dsRNA and HRV 3C proteases promote NLRP1 degradation by the proteasome system that induces an efficient inflammasome response, a process we also observed upon SARS-CoV-2 infection (Figure S2A) (Bauernfried et al., 2021; Hollingsworth et al., 2021; Robinson et al., 2020; Sandstrom et al., 2019). However, 3C protease cleaves NLRP1 between Glutamine Q¹³⁰ and Glycine G¹³¹ sites, which generates a free Nter¹³¹ Glycine. This allows the recruitment of the Ubiquitin-processing complex Cullin ZER1/ZYG11B and the targeting of ubiquitinated-NLRP1 for proteasome degradation and subsequent release and activation of the Cter UPA-CARD domain (Robinson et al., 2020). Consequently, we infected A549^{ACE2/NLRP1+} cells with SARS-CoV-2 in the presence or absence of MLN4924, an inhibitor of the Cullin ZER1/ZYG11B complex, and evaluated the ability of cells to undergo cell lysis (Figure 2A; Eldeeb et al.,

experiments. For quantifications, the percentage of cells with ASC complexes was determined by determining the ratios of cells positives for ASC speckles on the total nuclei. At least 10 fields from $n = 3$ independent experiments were analyzed. Values are expressed as mean \pm SEM.

(D) Cell death (LDH) evaluation in A549^{NLRP1+} and A549^{NLRP1-} airway epithelial cell lines infected with SARS-CoV-2 (MOI 0.05) for 24 h in the presence/absence of the pan-caspase inhibitor Z-VAD (25 μ M), NSP5 protease inhibitor PF-00835231 (10 μ M), or the RNA-dependent RNA polymerase (RdRp) inhibitor remdesivir (5 μ M).

(E) Fluorescence microscopy and associated quantifications of ASC-GFP specks in A549^{ACE2/NLRP1+/ASC-GFP} and A549^{ACE2/NLRP1-/ASC-GFP} airway epithelial cell lines infected with SARS-CoV-2 (MOI 0.05) for 24 h. Nucleus was stained with Hoechst (blue). Brightfield/ASC-GFP pictures were taken in dish during cell infection. Images shown are from one experiment and are representative of $n = 3$ independent experiments; scale bars, 10 μ m. For quantifications, the percentage of cells with ASC complexes was determined by determining the ratios of cells positives for ASC speckles on the total nuclei. At least 10 fields from $n = 3$ independent experiments were analyzed. Values are expressed as mean \pm SEM.

(F) Cell death (LDH) evaluation in NHBE airway epithelial cells infected with various multiplicity of infection (MOI) of SARS-CoV-2 for 36 h in the presence/absence of the pan-caspase inhibitor Z-VAD (25 μ M), Necroptosis inhibitor Necrostatin-1s (Nec1s, 30 μ M), or the Ferroptosis inhibitor Ferrostatin-1 (Fe1, 10 μ M).

(G) Western blot characterization of genetic inactivation of *NLRP1* in NHBE population using CRISPR-Cas9 and measure of cell lysis (LDH release) in NHBE^{WT} and NHBE^{NLRP1-/-} airway epithelial cells infected with various multiplicity of infection (MOI) of Wuhan or Delta variant SARS-CoV-2 for 36 h. Efficiency of genetic inactivation by single-guide RNAs (sgRNAs) were evaluated at the whole cell population.

Data information: western blot (A and G) images are from one experiment performed 3 times. Graphs (B), (D), (F), and (G) show data presented as means \pm SEM from $n = 3$ (F and G), $n = 4$ (B) and $n = 6$ (D) independent pooled experiments; *** $p \leq 0.001$ for the indicated comparisons with t test. Images (C and E) are representative of one experiment performed 3 times.

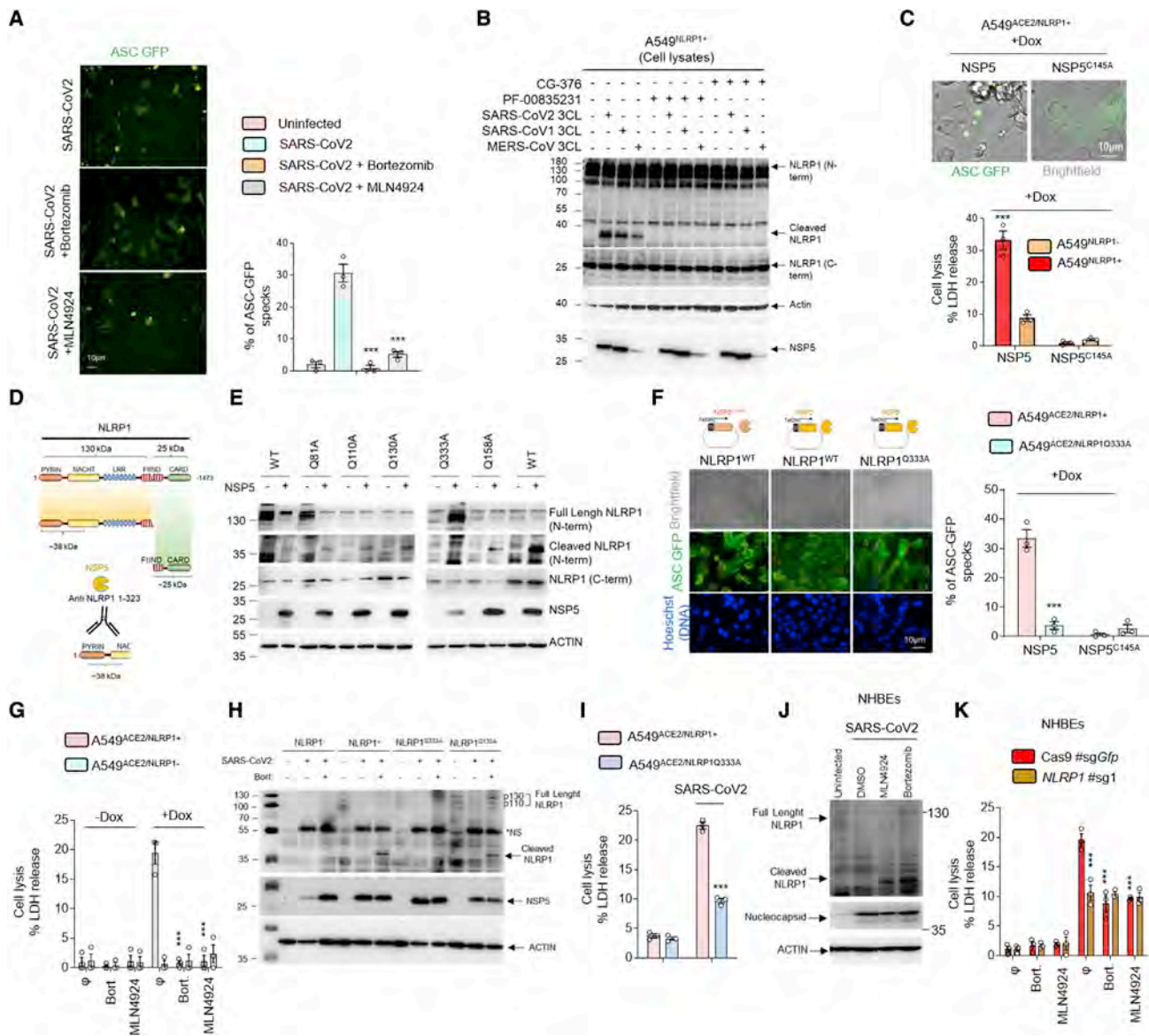


Figure 2. SARS-CoV-2 NSP5 protease-cleaved NLRP1 at the Q333 site nucleates NLRP1 inflammasome

(A) Fluorescence microscopy and associated quantifications of ASC-GFP specks in A549^{NLRP1+/ASC-GFP} and A549^{NLRP1-/ASC-GFP} airway epithelial cell lines infected with SARS-CoV-2 (MOI 0.05) for 24 h in the presence or absence of proteasome inhibitor bortezomib (0.1 μM) or inhibitor of the glycine N-degron pathway MLN4924 (1 μM). Images shown are from one experiment and are representative of n = 3 independent experiments; scale bars 10 μm. For quantifications, the percentage of cells with ASC complexes was determined by determining the ratios of cells positives for ASC speckles on the total cells presents in the wells. At least 10 fields from n = 3 independent experiments were analyzed. Values are expressed as mean ± SEM.

(B) Western blot examination of NLRP1 cleavage using an anti-NLRP1 N-terminal antibody (aa 1–323) upon coinubation of SARS-CoV-2, SARS-CoV-1, or MERS-CoV 3CL (NSP5) proteases (5 μM) with A549^{NLRP1+} airway epithelial cell lysates in presence or absence of the 3CL inhibitors GC-376 (10 μM) or PF-00835231 (10 μM). NLRP1 N-terminal, NLRP1 C-terminal, NSP5, and ACTIN were immunoblotted.

(C) Fluorescence microscopy and associated quantifications of ASC-GFP specks in A549^{NLRP1+/ASC-GFP} airway epithelial cell lines transduced with a doxycycline (dox)-inducible plasmid encoding NSP5 or its catalytically inactive mutant NSP5^{C145A}. Images shown are from one experiment and are representative of n = 3 independent experiments; scale bars, 10 μm. For quantifications, the percentage of cells with ASC complexes was determined by determining the ratios of cells positives for ASC speckles on the total cells presents in the wells. At least 10 fields from n = 3 independent experiments were analyzed. Values are expressed as mean ± SEM.

(D) Schematic representation of the approximate NLRP1 N-terminal fragment generated by NSP5 protease cut.

(E) Western blot examinations of the ability of NSP5 to cleave various NLRP1 constructs mutated in glutamine (Q) at various sites. Immunoblots show anti-N-terminal NLRP1, ACTIN, and NSP5.

(F) Fluorescence microscopy and associated quantifications of ASC-GFP specks in A549^{NLRP1+/ASC-GFP} or A549^{NLRP1Q333A/ASC-GFP} airway epithelial cell lines transduced with a doxycycline (dox)-inducible plasmid encoding NSP5 or its catalytically inactive mutant NSP5^{C145A}. Images shown are from one experiment

(legend continued on next page)

2019). The use of MLN4924 markedly inhibited SARS-CoV-2-induced NLRP1-dependent ASC-speck formation (Figure 2A). This suggested us that a SARS-CoV-2-dependent proteolytic cleavage of NLRP1 might be of importance in triggering inflammasome response in epithelial cells. As SARS-CoV-2 expresses both a 3CL protease NSP5 and a chymotrypsin protease NSP3, we hypothesized that one of those two proteases might cleave NLRP1 and generates a Glycine fragment accessible for Ubiquitination-driven NLRP1 degradation. Hence, we incubated NLRP1⁺ and NLRP1⁻ cell lysates with recombinant NSP3 or NSP5 proteases and analyzed by immunoblotting their ability to process NLRP1 by using an anti-NLRP1 N-terminal antibody (generated with the NLRP1 N-term peptide 1–323 aa) (Figures 2B and S2B–S2E). We observed that NSP5 protease cleaved NLRP1 and generated a 38 kDa Nterm-sized peptide, a process that was inhibited by the 3CL protease inhibitor PF-00835231 (Figures 2B, and S2B–S2D). As other coronaviruses also express 3CL proteases, we also incubated lysates of NLRP1-expressing cells with the MERS-CoV and SARS-CoV-1 3CL proteases. As for NSP5, both proteases also cleaved NLRP1 and generated an Nter fragment of similar sizes, suggesting a conserved ability of coronaviruses 3CL proteases to cleave NLRP1 (Figure 2B). Such process was also seen using recombinant NLRP1 protein in the presence of recombinant NSP5 proteases from pathogenic coronaviruses, hence suggesting that NSP5 alone is sufficient to mediate this process (Figures S2B and S2C). To further determine if NSP5 catalytic activity accounts at activating the NLRP1 inflammasome, we expressed doxycycline-inducible NSP5 or its catalytically inactive mutant (NSP5^{C145A}) in NLRP1⁺ and NLRP1⁻ cells. Monitoring for cell death and ASC-speck formation, we observed a strong ability of the WT NSP5 protease, but not its catalytically dead mutant, to promote both NLRP1-dependent cell death (LDH release) and GFP-ASC-speck formation, suggesting that NSP5 protease activity is required to nucleate an active NLRP1 inflammasome complex (Figure 2C).

Next, we determined where NSP5 cleaves NLRP1. The 3CL protease NSP5 is predicted to cleave after Glutamine (Q) in the amino acid triad LQA, LQS, LQN, or LQG (Anand et al., 2003; Kiemer et al., 2004). In addition, our observation that the anti-NLRP1 Nter antibody (aa 1–323) detected a fragment of approximately 38 kDa allowed us to map cleavage to a region in the

NLRP1 NACHT domain that contains the sequence ³³²LQG³³⁴ (Figures 2B–2D and S2D). Interestingly, protein alignments showed that this sequence is not conserved in murine Nlrp1B isoforms, suggesting that the NSP5-cleavage site in NLRP1 might be species specific (Figure S2D).

Therefore, we generated NLRP1-expressing constructs where Q333 is mutated to an Alanine (NLRP1^{Q333A}). We also used previously generated NLRP1 constructs that carry various mutations in Glutamine (Q) at different positions in the Nter domain (Robinson et al., 2020). Lysates from cells expressing the different NLRP1 mutants were incubated with NSP5. The SARS-CoV-2 protease cleaved NLRP1 and generated 38 kDa fragments from all constructs with the exception of NLRP1^{Q333A} (Figure 2E). To determine if the NLRP1^{Q333} site is important for NSP5-mediated NLRP1 inflammasome nucleation, we transduced ASC-GFP expressing cells with the NLRP1^{WT} or the NLRP1^{Q333A} construct and monitored for NSP5-induced ASC-speck formation and cell death. Cells expressing NLRP1^{WT} exhibited ASC-GFP specks, cell death induction, and proteasome/Cullin ligase-dependency upon NSP5 expression (Figures 2F and 2G). In contrast, NLRP1^{Q333A}-expressing cells did not show ASC-GFP specks or robust cell death upon NSP5 induction. We verified that the NLRP1^{Q333A} construct was still functional using nonprotease activators of NLRP1. Hence, Val-boro treatment induced NLRP1^{WT}- and NLRP1^{Q333A}-dependent cell lysis, suggesting that the NLRP1^{Q333} site is specifically required for efficient NLRP1-dependent cell death upon NSP5 exposure (Figure S2E).

Then, we aimed at determining if SARS-CoV-2-infected epithelial cells also engage NSP5-dependent NLRP1 cleavage. We infected A549^{ACE2/NLRP1+} cells with SARS-CoV-2 in the presence of bortezomib. Indeed, as NLRP1 cleavage leads to proteasomal degradation of the cleaved fragments, the used proteasome or Cullin ligase inhibitors allows cleaved fragment of NLRP1 accumulation and their putative observation by immunoblotting approaches. Thus, immunoblotting experiments against NLRP1 showed that SARS-CoV-2 infection in the absence of bortezomib did not allow detecting NLRP1 cleaved fragments (Figure 2H). However, treatment with bortezomib led to the detection of a cleaved NLRP1 fragment in A549^{ACE2/NLRP1+} and A549^{ACE2/NLRP1Q130A} cells, which was not seen in A549^{ACE2/NLRP1Q333A} cells, hence suggesting that the

and are representative of $n = 3$ independent experiments; scale bars, 10 μm . For quantifications, the percentage of cells with ASC complexes was determined by determining the ratios of cells positives for ASC speckles on the total nuclei (Blue). At least 10 fields from $n = 3$ independent experiments were analyzed. Values are expressed as mean \pm SEM.

(G) Cell death (LDH) evaluation in A549^{NLRP1+} and A549^{NLRP1-} airway epithelial cell lines expressing a doxycycline (dox)-inducible plasmid encoding NSP5 in the presence or absence of the proteasome inhibitor bortezomib (0.1 μM) or inhibitor of the glycine N-degron pathway MLN4924 (1 μM).

(H) Western blot examination of NLRP1 cleavage using an anti-NLRP1 N-terminal antibody (aa 1–323) after infection of A549^{NLRP1-}, A549^{NLRP1+}, A549^{NLRP1Q333A}, or A549^{NLRP1Q130A} airway epithelial cells with SARS-CoV-2 (MOI 0.05) for 24 h in the presence/absence of the proteasome inhibitor bortezomib (0.1 μM , Bort.). NLRP1 N-terminal, NSP5, and ACTIN were immunoblotted. *NS: prominent nonspecific bands, not specific.

(I) Cell death (LDH) evaluation in A549^{NLRP1+} and A549^{NLRP1Q333A} airway epithelial cell lines infected with SARS-CoV-2 (MOI 0.05) for 24 h.

(J) Western blot examination of NLRP1 cleavage using an anti-NLRP1 N-terminal antibody (aa 1–323) after infection of NHBE^{WT} airway epithelial cells with SARS-CoV-2 (MOI 1) for 36 h in the presence/absence of the proteasome inhibitor bortezomib (0.1 μM) or inhibitor of the glycine N-degron pathway MLN4924 (1 μM). NLRP1 N-terminal, nucleocapsid, and ACTIN were immunoblotted.

(K) Measure of cell lysis (LDH release) in NHBE^{WT} and NHBE^{NLRP1-/-} airway epithelial cells infected with SARS-CoV-2 (MOI 1) for 36 h in the presence/absence of the proteasome inhibitor bortezomib (0.1 μM) or inhibitor of the glycine N-degron pathway MLN4924 (1 μM).

Data information: images (A, C, and F) show one experiment performed 3 times. Western blot (B, E, H, and J) images are from one experiment performed 3 times. Graphs (C, G, I, and K) show data presented as means \pm SEM from $n = 3$ independent pooled experiments; *** $p \leq 0.001$ for the indicated comparisons with t test.

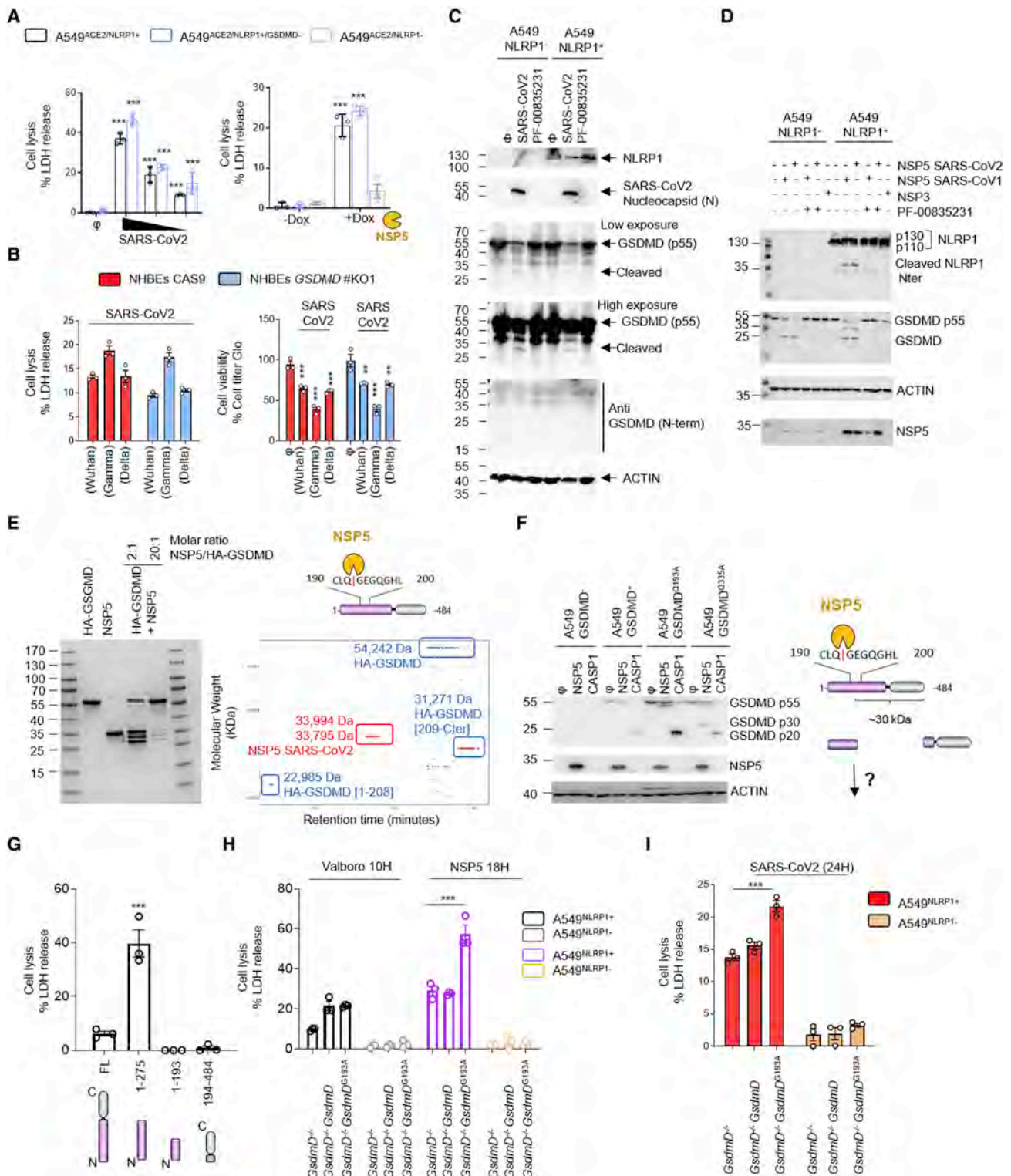


Figure 3. NSP5 protease cleaves Gasdermin D in its pore-forming domain

(A) Cell death (LDH) evaluation in A549^{NLRP1+}, A549^{NLRP1-}, or A549^{NLRP1+/GSDMD-} airway epithelial cell lines infected for 24 h with SARS-CoV-2 (MOIs 0.1, 0.01, and 0.001) or stimulated with doxycycline (dox)-induced NSP5 expression.

(B) Measure of cell lysis (LDH release) and cell viability (Cell titer Glo) in NHBE^{WT} and NHBE^{GSDMD-/-} airway epithelial cells infected with various SARS-CoV-2 viral strains (MOI 1) for 36 h.

(legend continued on next page)

NLRP1^{Q333} site is important for cleavage upon SARS-CoV-2 infection and can be significantly revealed when inhibiting proteasome-driven degradation (Figure 2H). Furthermore, A549^{ACE2/NLRP1Q333A} cells showed greater resistance to cell death than A549^{ACE2/NLRP1+} cells upon SARS-CoV2 infection, arguing that the Q333 site is important for efficient NLRP1 activation during viral infection (Figure 2I).

Finally, we performed NLRP1 immunoblotting in NHBE-infected cells with SARS-CoV-2 and also observed the accumulation of cleaved NLRP1 fragments in the presence of bortezomib or MLN4924 inhibitors (Figure 2J). Both bortezomib and MLN4924 inhibited SARS-CoV-2-dependent cell death in NHBE^{WT} (Figure 2K). Altogether, our results suggest that the SARS-CoV-2 protease NSP5 activates the NLRP1 inflammasome by cleavage at the NLRP1^{Q333} site, a process that depends on a functional degradation pathway (Figure S2F).

SARS-CoV-2 3CL protease dampens inflammasome signaling by inactivating Gasdermin D

In order to further understand the mechanism by which SARS-CoV-2 infection impacts cells, we next examined NLRP1 downstream effectors that promote cell death. Once an inflammasome is nucleated, it licenses caspase-1 autoactivation. Subsequent cleavage of the pyroptosis executioner GSDMD activates this pathway. Using CRISPR-Cas9 editing, we generated GSDMD KO lines in NHBE and A549^{ACE2/NLRP1+} cells and infected them with SARS-CoV-2 (Figures 3A, 3B, and S3A). However, we failed to detect a reliable involvement of GSDMD at regulating NLRP1-dependent cell death upon SARS-CoV-2 infection or NSP5 induction (Figures 3A and 3B). Similarly, immunoblots of infected cell samples (combined supernatants and cell extracts) showed a decrease in the proform of GSDMD (antibody anti-GSDMD-Cter) but also intermediate cleavage bands of GSDMD (25–30 kDa) that do not correspond to the size of active GSDMD (N.B. When using the anti-GSDMD Cter antibody, the expected size of caspase-1-processed GSDMD is around 20 kDa) (Figure 3C). In addition, the use of an antibody that specifically recognizes the active Nter GSDMD fragment failed to detect any active GSDMD (Figure 3B). This result was consistent in A549^{ACE2/NLRP1+} and A549^{ACE2/NLRP1-} cells, suggesting that

some protease-based, but inflammasome-independent, mechanism mediates this distinct processing of GSDMD (Figure 3B).

In order to determine whether SARS-CoV-2-encoded enzymes influence GSDMD activation independently of NLRP1, we tested the hypothesis that the GSDMD intermediate bands are generated by a viral protease. Therefore, we checked whether NSP3 and NSP5 directly or indirectly cleave GSDMD. Coincubation of NSP3 and NSP5 proteases with cell lysates led to GSDMD cleavage at distinct sites from caspase-1, suggesting that the SARS-CoV-2 NSP5 protease can cleave GSDMD (Figures 3D and S3B). We also analyzed the ability of NSP5 to cleave other Gasdermins, including GSDME and GSDMB, both expressed in epithelial cells. However, although NSP5 can cleave GSDMD, the viral protease was unable to cleave GSDMB or GSDME (Figure S3B). Next, we checked whether NSP5-cleaved GSDMD is active. GSDMD was incubated with NSP5, and the resulting mixture was subjected to proteomic analysis. This approach detected GSDMD fragments corresponding to the Nter of GSDMD 1-Q¹⁹³ (Figure 3E). In order to determine if NSP5 effectively cleaves at the Q¹⁹³ site of GSDMD, we expressed GSDMD^{WT}, GSDMD^{193A}, or GSDMD^{335A} encoding constructs in A549^{GSDMD} cells. This approach was previously used to detect enterovirus EV71 3C protease-mediated cleavage at this site (Lei et al., 2017). Incubation of cell lysates with either NSP5 or recombinant human caspase-1 (CASP1) showed that CASP1 efficiently cleaved all GSDMD constructs (Figures 3F and S3C). However, we observed that NSP5 was unable to process GSDMD^{Q193A}, suggesting that NSP5 cleaves GSDMD at the Q¹⁹³ site (Figures 3F and S3C).

Next, we transfected plasmids encoding for NSP5-generated GSDMD fragments (1–193, 194–484) in A549 cells and monitored for their pore-forming activity by measuring cell lysis induction. Although caspase-1-generated GSDMD^{1–275} fragment showed strong lytic activity in A549 cells, none of the NSP5-generated fragments showed pore-forming activity, suggesting that NSP5-cleaved Nterm GSDMD inhibits GSDMD-mediated pyroptosis (Figure 3G). To test our hypothesis, we generated cell expressing GSDMD mutated in the NSP5 cleavage site. Expression of NSP5 protease in cells expressing

(C) Western blot examination of Gasdermin D (GSDMD) processing in A549^{NLRP1+} cells infected with SARS-CoV-2 at MOI of 0.1 for 24 h. GSDMD was immunoblotted using an anti-C-terminal antibody (recognizes full-length and C-terminal cleaved forms of GSDMD) or with an anti-GSDMD active N-terminal fragment (30 kDa) specific antibody. NLRP1, ACTIN, and SARS-CoV-2 nucleocapsid were also evaluated.

(D) Western blot examination of GSDMD and NLRP1 cleavages upon coincubation of SARS-CoV-2 NSP3 protease or SARS-CoV-2/SARS-CoV1 3CL (NSP5) proteases (5 μM) with A549^{NLRP1+} or A549^{NLRP1-} cell lysates in the presence or absence of the 3CL inhibitor PF-00835231 (10 μM). GSDMD (anti C-terminal), NLRP1 N-terminal, NSP5, and ACTIN were immunoblotted.

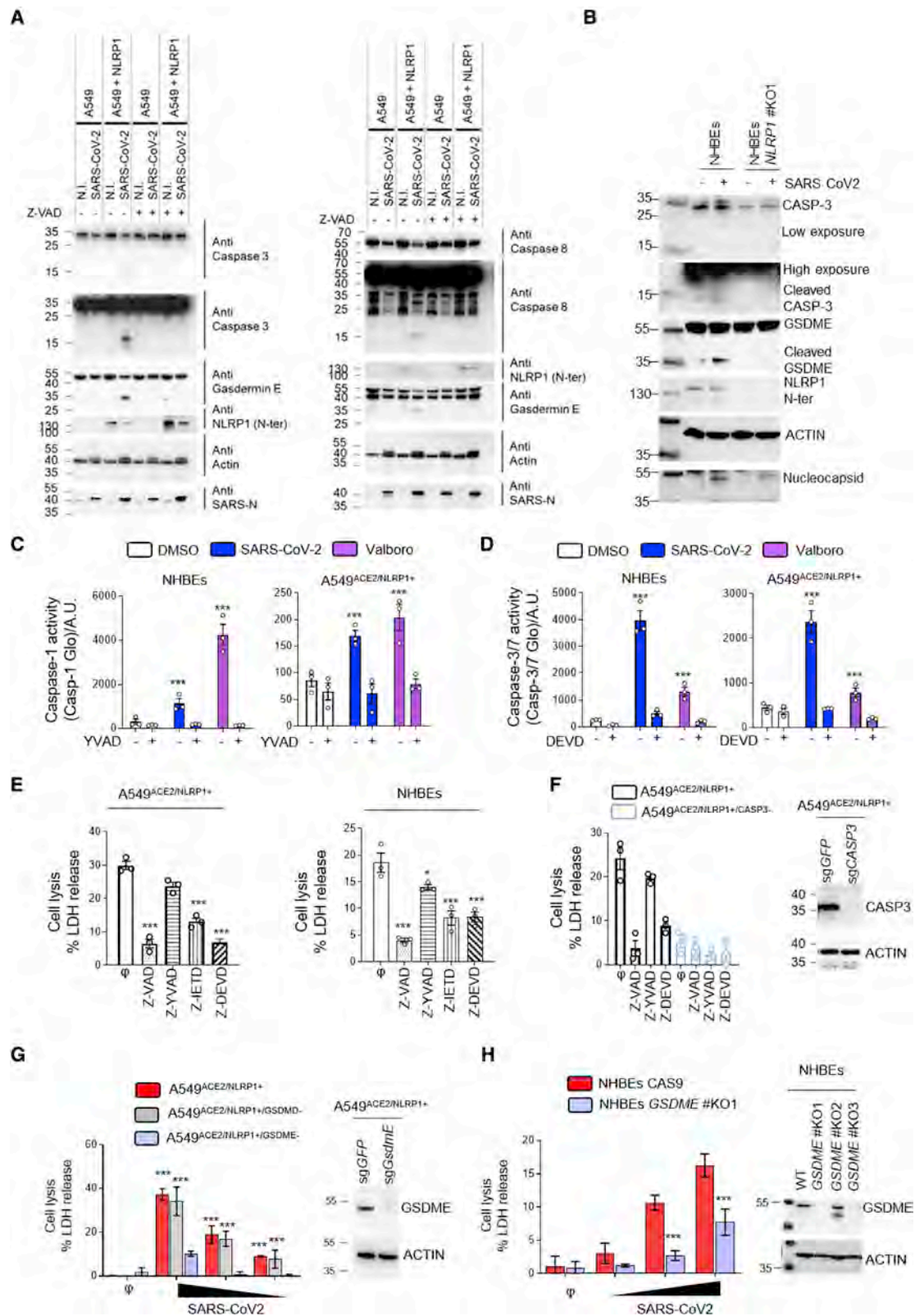
(E) Coomassie observation of recombinant GSDMD cleavage by various amounts of SARS-CoV-2 NSP5 protease and top-down mass-spectrometry identification of GSDMD-cleaved fragments. In blue are represented the various GSDMD fragments identified upon NSP5 coincubation. In red is the NSP5 protease detected by mass spectrometry.

(F) Western blot examination and schematic representation of GSDMD cleavage by SARS-CoV-2 3CL (NSP5) or recombinant human caspase-1 (CASP1) proteases in cell lysates from A549 expressing WT GSDMD or GSDMD^{193A} constructs. GSDMD (anti-C-terminal), NSP5, and ACTIN were immunoblotted.

(G) Cell death (LDH) evaluation in A549 cells expressing doxycycline-inducible GSDMD fragments, including GSDMD full-length (FL), caspase-1-generated active GSDMD (1–275), or NSP5-generated 1–193 and 194–484 GSDMD fragments. Cell lysis was determined 18 h after doxycycline (dox) addition in the culture medium.

(H and I) Cell death (LDH) evaluation in A549^{NLRP1+/GSDMD-} cells complemented or not with constructs coding for WT GSDMD or GSDMD^{193A}. Cells were transfected with dox-inducible NSP5 plasmids, treated with the NLRP1 activator Val-boro (10 μM) or infected (I) with SARS-CoV-2 (MOI 0.01). Cell lysis was determined 18 h after doxycycline (dox) addition, 10 h after Val-boro addition in the culture medium, or 24 h after infection.

Data information: graphs (A, B, G, H, and I) show data presented as means ± SEM from n = 3 independent pooled experiments; ***p ≤ 0.001 for the indicated comparisons with t test. Western blot (C, D, and F) images are from one experiment performed 3 times. Images (E) show one experiment performed 3 times.



(legend on next page)

NSP5-uncleavable GSDMD (GSDMD^{193A}) exhibited enhanced cell death, a process that was lowered in cells expressing WT GSDMD (Figure 3H). To the contrary, Val-boro-induced cell lysis was not altered by the presence of GSDMD^{193A} (Figure 3H). Finally, SARS-CoV-2 infection also induced higher cell death levels in GSDMD^{193A}-expressing cells than that in parental cells, suggesting that GSDMD cleavage by NSP5 might lower the efficiency of GSDMD-dependent pyroptosis upon inflammasome activation in epithelial cells (Figure 3I). Those results suggest that NSP5 can also counteract the inflammasome signaling by directly targeting and inactivating GSDMD.

NLRP1-driven caspase-3 activation promotes Gasdermin E-dependent pyroptosis of airway epithelial cells

The ability of epithelial cells to undergo NLRP1-dependent cell death, even in the absence of GSDMD activation, suggests that additional cell death effectors might be activated by SARS-CoV-2 infection. Previous studies revealed that caspase-1 and/or caspase-8 are important for activating caspase-3 (CASP3)/Gasdermin E (GSDME)-dependent cell death in the absence of GSDMD expression (Heilig et al., 2020; Orzalli et al., 2021; Taabazuig et al., 2017; Tsuchiya et al., 2019; Zhou and Abbott, 2021). Depending on the cell type, CASP3/GSDME activation can trigger apoptosis, lytic apoptosis, or pyroptosis. We hypothesized that NLRP1 uses a distinct pathway involving caspase-3 and GSDMD to promote cell death upon SARS-CoV-2 infection. We tested for the presence of active caspase-8, active caspase-3, and cleaved GSDME in SARS-CoV-2-infected cells using immunoblotting. We observed the appearance of caspase-8 and caspase-3 active fragments as well as processed GSDME fragment in A549^{ACE2/NLRP1+} and HBE^{WT} but not in A549^{ACE2/NLRP1-} or NHE^{NLRP1-/-} cells (Figures 4A and 4B). In addition, the pan-caspase inhibitor Z-VAD strongly impaired GSDME cleavage, suggesting that

NLRP1-dependent caspase-8 and caspase-3 activation licenses GSDME cleavage (Figure 4A). Furthermore, quantitation of caspase-1 or caspase-3/7 activities in SARS-CoV-2-infected A549^{ACE2/NLRP1+} and NHE^{WT} cells revealed that the activity of both caspases is increased (Figures 4C and 4D). However, we noticed that the levels of caspase-1 activity in A549^{ACE2/NLRP1+} cells were extremely low (10 times lower) compared with those observed in NHE^{WT} cells (Figures 4C and 4D). Thus, to definitively determine if caspase-1 plays a role in SARS-CoV-2-driven epithelial cell death, we used specific inhibitors of caspase-8, caspase-1, and caspase-3 and monitored their ability to block NLRP1-dependent cell death upon SARS-CoV-2 infection both in A549^{ACE2/NLRP1+} and in HBE^{WT} cells. Although caspase-1 inhibition showed a negligible reduction in cell death both in A549^{ACE2/NLRP1+} and in NHE^{WT} cells, the most striking inhibition was observed in the presence of Z-VAD as well as the caspases-8 (Z-IETD)-specific and caspases-3 (Z-DEVD)-specific inhibitors (Figures 4E and 4F). These data suggest that in the absence of efficient GSDMD activation, NLRP1 triggers a compensatory pathway involving caspase-8 and caspase-3 in epithelial cells. As caspase-3 can cleave and activate GSDME, which generates pyroptosis in human keratinocytes (Orzalli et al., 2021), but not in macrophages or monocytes (Taabazuig et al., 2017), we explored whether the cell death we observed was caspase-3 and/or GSDME dependent. Hence, we generated A549^{ACE2/NLRP1+} cells deficient for either caspase-3 or GSDME and infected them with SARS-CoV-2 (Figure 4G). Analysis of cell death levels (LDH release) showed that both genetic removal caspase-3 and GSDME improved cell survival upon SARS-CoV-2 infection (Figures 4G and 4H). Finally, SARS-CoV-2 infection of primary NHE cells in which GSDME was knocked out supported the hypothesis that GSDME is involved in NHE lysis upon SARS-CoV-2 infection. In short, our data argue that both caspase-3 and GSDME initiate lytic

Figure 4. NLRP1 engages a caspase-3/Gasdermin E-dependent pyroptosis pathway upon SARS-CoV-2 infection

(A) Western blot examination of Gasdermin E, caspases-3, and caspases-8 processing in A549^{NLRP1+} and A549^{NLRP1-} cells after 24 h of infection with SARS-CoV-2 (MOI 0.05) in the presence or absence of the pan-caspase inhibitor Z-VAD (25 μ M). Immunoblots were performed against full-length and processed forms of Gasdermin E (p55 and p30), caspase-8 (p54 and p15), caspase-3 (p35 and p17/19), SARS-CoV-2 nucleocapsid (p40), NLRP1 N-terminal (p130/110), and ACTIN (p40).

(B) Western blot examination of Gasdermin E and caspases-3 processing in NHE^{WT} and NHE^{NLRP1-/-} cells after 36 h of infection with SARS-CoV-2 (MOI 1). Immunoblots were performed against full-length and processed forms of Gasdermin E (p55 and p30), caspase-3 (p35 and p17/19), SARS-CoV-2 nucleocapsid (p40), NLRP1 N-terminal (p130/110), and ACTIN (p40).

(C and D) Measure of caspase-1 (C) and caspase-3/-7 (D) activities in SARS-CoV-2-infected (MOI 0.5) NHE^{WT} or A549^{NLRP1+} cells for 36 h in the presence or absence of inhibitors of caspase-1 (Z-YVAD, 40 μ M) or caspase-3/-7 (Z-DEVD, 30 μ M). Val-boro (5 μ M) was used as a positive control of NLRP1-driven caspase activity for 10 h.

(E) Measure of cell lysis (LDH release) in A549^{NLRP1+} or NHE-infected cells with SARS-CoV-2 (MOI 0.05 and 1, respectively) for 24 h in the presence/absence of the pan-caspase inhibitor Z-VAD (25 μ M), the caspase-1 inhibitor Z-YVAD (40 μ M), the caspase-8 inhibitor Z-IETD (40 μ M), or the caspase-3 inhibitor Z-DEVD (30 μ M).

(F) Western blot characterization of genetic invalidation of CASP3 in A549 population cells using CRISPR-Cas9 approaches and measure of cell lysis (LDH release) in A549^{NLRP1+} or A549^{NLRP1+/CASP3-}-infected cells with SARS-CoV-2 (MOI 0.05) for 24 h in the presence/absence of the pan-caspase inhibitor Z-VAD (25 μ M), the caspase-1 inhibitor Z-YVAD (40 μ M), or the caspase-3 inhibitor Z-DEVD (30 μ M). Efficiency of genetic invalidation by single-guide RNAs (sgRNAs) targeting GFP or caspase-3 was evaluated at the whole cell population.

(G) Western blot characterization of genetic invalidation of GSDME in A549 population cells using CRISPR-Cas9 approaches and measure of cell lysis (LDH release) in A549^{NLRP1+}, A549^{NLRP1+/GSDMD-}, or A549^{NLRP1+/GSDME-}-infected cells with SARS-CoV-2 (MOIs 0.001, 0.01, and 0.1) for 24 h. Efficiency of genetic invalidation by single-guide RNAs (sgRNAs) targeting GFP or GSDME was evaluated at the whole cell population.

(H) Western blot characterization of genetic invalidation of GSDME in NHE population cells using CRISPR-Cas9 approaches and measure of cell lysis (LDH release) in NHE^{WT} or NHE^{GSDME-/-}-infected cells with SARS-CoV-2 (MOIs 0.1, 0.5, and 1) for 36 h. Efficiency of genetic invalidation by single-guide RNAs (sgRNAs) targeting GFP or GSDME was evaluated at the whole cell population.

Data information: western blot (A, B, and E–G) images are from one experiment performed 3 times. Graphs (C–G) show data presented as means \pm SEM from $n = 3$ independent pooled experiments; *** $p \leq 0.001$ for the indicated comparisons with t test.

cell death in airway epithelial cells upon SARS-CoV-2 infection (Figure 4I).

Altogether, our results underline the crucial function of apoptotic caspase-3 and pyroptotic GSDME as sentinels that trigger efficient epithelial cell death induction during SARS-CoV-2 infection if the canonical pyroptosis executioner GSDMD is inactive.

NLRP1-dependent pyroptosis restricts the generation of viral infectious particles and promotes the release of alarmins/DAMPs

Next, we wondered about the immunological and microbicidal importance of SARS-CoV-2-induced NLRP1 inflammasome activation in epithelial cells. We monitored the viral titers in A549^{ACE2/NLRP1+}, A549^{ACE2/NLRP1-}, or NHBE^{WT}/NHBE^{NLRP1-/-} cells. Measuring the production of infectious particles by the TCID50 method, we observed that NLRP1-deficient cells were significantly more prone at generating SARS-CoV-2 viral particles (Figures S4A and S4B). However, we failed to see a robust involvement of NLRP1 at controlling SARS-CoV-2 replication as measured by the appearance of genes encoding SARS-CoV-2 RNA polymerase (Figure S4C). This suggested to us that pyroptosis might be a good mean to restrict the generation of mature and infectious viral particles but does not account as a direct replication inhibitory mechanism.

As pyroptosis is a very well-known process able to promote the release of specific caspase-associated inflammatory cytokines (e.g., IL-1B/IL-18) but also various alarmins and DAMPs (damage-associated molecular patterns), we next aimed at determining the importance of NLRP1 at regulating alarmins/DAMPs release upon SARS-CoV-2 infection. We specifically dedicated our analysis on already known alarmins and pyroptosis markers such as HMGB1, IL-18, and IL-1B, but also the caspase-3-derived alarmin interleukin-16 (IL-16). IL-16 is not an inflammasome-derived alarmin; however, its cleavage by caspase-3 allows its maturation and release. Hence, given the strong involvement of the caspase-3/GSDME axis in SARS-CoV2-dependent cell death, we also included IL-16 in our analysis as a read out of caspase-3-driven cytokine maturation and release. At the exception of IL-1B, all other alarmins/cytokines tested showed an NLRP1-dependent enrichment in the supernatant of infected A549^{ACE2/NLRP1+} and NHBE^{WT} cells, hence confirming that NLRP1-dependent pyroptosis in epithelial cells generates robust alarmin and DAMP responses (Figures S4D and S4E).

Plasmatic levels of caspase-3/IL-16 and Gasdermin E are associated with COVID-19 severity

Intriguingly, a recent report unveiled that IL-18 and IL-16 are enriched in plasma from severe COVID-19 pneumonia patients, suggesting that the inflammasome route might contribute to the development of the pathology in sensitive patients (Lucas et al., 2020). However, our results suggest that at least in 2D epithelial cell cultures, NLRP1 exhibits some protective function against SARS-CoV-2 infection (Figure S4A). Regarding this, about 20% of patients with critical COVID-19 pneumonia exhibit strong defect either in IFN response or in IFN production, suggesting that the IFN/inflammasome balance might be key in the regulation of COVID-19 severity (Asano

et al., 2021; Bastard et al., 2020, 2021a, 2021b; Koning et al., 2021; Zhang et al., 2020). Therefore, to test this hypothesis, we expressed NLRP1 in A549^{ACE2} cells deficient for the expression of MAVS, a central modulator of interferon production upon SARS-CoV-2 infection (Figures S5A–S5C). We next infected A549^{ACE2/NLRP1-/MAVS+}, A549^{ACE2/NLRP1+/MAVS+}, A549^{ACE2/NLRP1-/MAVS-}, and A549^{ACE2/NLRP1+/MAVS-} cells with SARS-CoV-2 and monitored for cell death. We observed a very strong induction of NLRP1-dependent cell lysis in MAVS-deficient cells, when compared with MAVS-expressing cells after 24 h of infection, suggesting that in absence of a proper IFN response, SARS-CoV-2 hyper replication triggers NLRP1 over activation (Figure S5A). As consequence, the release of the caspase-3-derived alarmin IL-16 as well as IL-18 in the supernatant of MAVS-deficient cells was strongly increased in response to SARS-CoV-2 (Figure S5B). Relying on those observations, we hypothesized that in healthy patients, where the IFN and inflammasome responses are well balanced, NLRP1 might actually be protective, a process completely lost in absence of a proper IFN response.

We obtained plasma samples from SARS-CoV-2 patients admitted at the hospital who exhibited three different profiles (WHO Working Group on the Clinical Characterization and Management of COVID-19, 2020). First, patients with moderate (non-hypoxemic) COVID-19 pneumonia on admission and throughout their stay at the hospital (group “Moderate” with a WHO score of 5); second, patients with moderate COVID-19 on admission with subsequent clinical worsening and severe COVID-19 (WHO score >5) requiring intensive care unit (ICU) admission (group “Moderate → Severe”); and third, patients with severe disease requiring ICU already on admission (group “Severe”) (Figures 5A and S5D).

We sampled 10–15 patients from each category, and already in this small cohort, we were able to distinguish significant trends in the levels of various pyroptosis markers, including a strong correlation between increased levels of plasma caspase-3 (CASP3), cleaved caspase-3, IL-18, IL-16, GSDMD, and GSDME with the severity status of patients (Figure 5A). IL-6 also showed deep correlation with COVID-19 severity as previously described; however, we failed to detect significant differences in IL-1B levels among the different type of patients we assayed (Figure 5A). As genetic or acquired alterations in IFN signaling pathways account for patient sensitivity to SARS-CoV-2 infection, we also analyzed plasma from patients with critical disease due to either genetic inactivating mutations of type I IFN signaling (TBK1, IFNAR1, and IRF7) or developing high titers of autoantibodies against type IFNs (Bastard et al., 2020; Zhang et al., 2020). As control, plasma from low/mid/severe patients were used to determine the relative differences of pyroptosis markers between those patients. All patients with IFN alterations showed a strong enrichment of IL-16, IL-18, CASP3, cleaved CASP3, GSDMD, and GSDME as previously seen with patients exhibiting severe COVID-19 (Figure 5A; Lopez et al., 2021; Wijst et al., 2021). Should NLRP1 specifically be involved will however require the development of more complex models such as humanized mouse for NLRP1. Nevertheless, our findings support a model between pyroptosis-associated markers and COVID-19 severity either in severe COVID-19 or in IFN-altered patients.

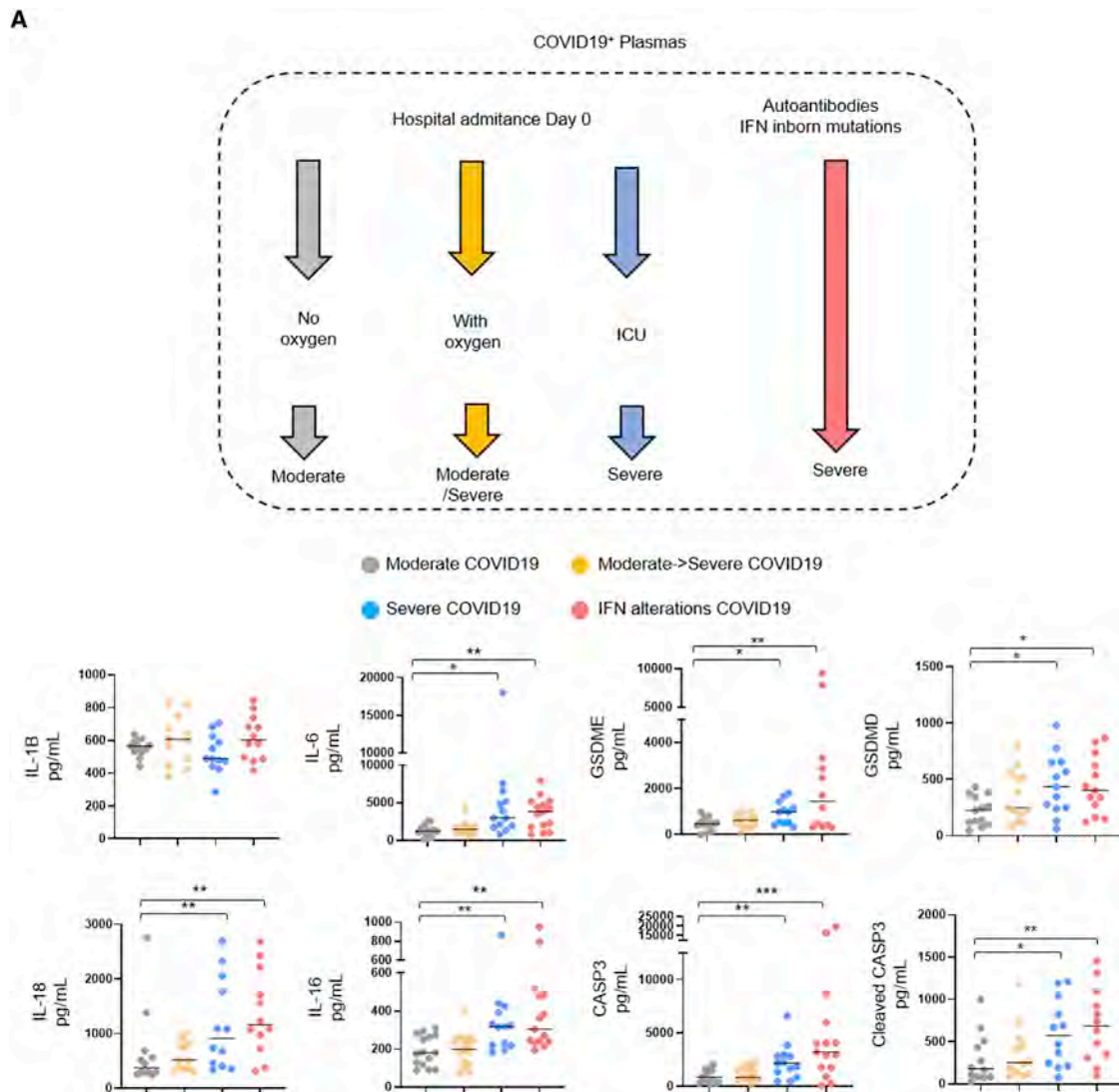


Figure 5. Caspase-3/IL-16 and GSDME as potential markers of COVID-19 severity

(A) Measure of the presence of various inflammatory mediators in plasmas from hospitalized patients presenting COVID-19 disease and analyzed according to their disease severity degree ($n = 60$ patients, including 15 with moderate COVID-19, 15 with moderate COVID-19 on admission, 15 with severe COVID-19 on admission, and 15 IFN alterations with severe COVID-19). Samples were prepared at day 0 posthospitalization.

Data information: data shown as means from $n = 12$ different donors per category (moderate/moderate \rightarrow severe/severe/IFN alterations); each category is represented with a colored circle; * $p \leq 0.05$, ** $p \leq 0.01$, *** $p \leq 0.001$ for the indicated comparisons using t test with Bonferroni correction.

DISCUSSION

Our study identifies NLRP1 as a central sensor of SARS-CoV-2 3CL protease NSP5 but also highlights NSP5 as a virulence factor against GSDMD-mediated pyroptosis. In line with pioneering studies on the ability of picornavirus 3C proteases to cleave human NLRP1 at a different site (Q¹³⁰-G¹³¹) and promote its activation, our study suggests that human NLRP1 is a broad protease sensor that carries evolutionary conserved decoy capabilities (Robinson et al., 2020; Tsu et al., 2021). Since human exposure to pathogenic coronavirus is relatively recent, how NLRP1 and GSDMD are so specifically targeted by viral proteases remains puzzling. Answers may come from future studies that test

whether NLRP1 and GSDMD are targets of viral proteases from nonpathogenic coronaviruses. Regarding this, the 3C protease from EV71 enterovirus was shown to cleave and inactivate GSDMD at the 193Q site (Lei et al., 2017). It is tempting to speculate that 3C and the closely related 3CL proteases might share conserved targets. Beyond this, two recent studies showed a particular ability of the bacterial pathogen *Shigella flexneri* to ubiquitinate both GSDMD and GSDMB and target them for proteasomal degradation, thereby allowing *Shigella* to establish a replicative niche in human cells (Hansen et al., 2021; Luchetti et al., 2021).

Beyond epithelial detection of pathogenic coronavirus proteases by NLRP1, the cytokine storm observed in SARS-CoV-2

associates with a NLRP3 inflammasome signature mostly driven by myeloid cells. Whether exaggerated NLRP1 inflammasome activation or a lack of NLRP1 response directly or indirectly promotes an NLRP3-dependent response in patient myeloid cells is an important future question to pursue. Similarly, recent findings from Bhaduri-McIntosh lab identified SARS-CoV-2 Orf3a as a trigger of the NLRP3 inflammasome in epithelial cells (Xu et al., 2022). In our epithelial cell models, we failed to detect robust NLRP3 expression; however, we always worked in the absence of priming. Whether, priming with various PRR ligands might promote NLRP3 expression in epithelial cells warrants further investigations.

Induction of a well-balanced innate immune response is central to controlling microbial infections, including those triggered by pathogenic coronaviruses (Broggi et al., 2019; Schultze and Aschenbrenner, 2021; Tay et al., 2020; Zheng et al., 2020). Consequently, any delay in a robust type I interferon production/response exposes the host to robust viral replication and exacerbated inflammation, leading to heavy organ damage (Asano et al., 2021; Bastard et al., 2020, 2021a, 2021b, 2021c; Galani et al., 2020; Hadjadj et al., 2020; Koning et al., 2021; Zanoni, 2021; Zhang et al., 2020). Our insights into NLRP1 inflammasome activation upon SARS-CoV-2 infection of epithelial cells *in vitro* suggest that NLRP1-driven inflammation might be both beneficial and detrimental in COVID-19 patients.

Overall, our results place the NLRP1 inflammasome as an innate immune sensor of the SARS-CoV-2 3CL protease but also highlight the virulence mechanisms by which this devastating virus counteracts cell intrinsic immunity.

Limitations of the study

The lack of conservation of the NLRP1 proteins between mice and humans strongly limits the physiopathological translation of our results into a broader and more complex model such as mice. The generation of humanized models in the future should help to determine the importance of the NLRP1 inflammasome in pathogenic coronavirus infections. Finally, although NLRP1 might be of importance to generate proinflammatory mediators at the epithelial barrier level, its role in the development of a cytokine storm observed in patients exhibiting severe COVID-19 has not been formally demonstrated in our study, which will require further investigations.

STAR★METHODS

Detailed methods are provided in the online version of this paper and include the following:

- **KEY RESOURCES TABLE**
- **RESOURCE AVAILABILITY**
 - Lead contact
 - Materials availability
 - Data and code availability
- **EXPERIMENTAL MODEL AND SUBJECT DETAILS**
 - Safety procedures
 - Ethical approvals of human studies
 - Cell culture
- **METHOD DETAILS**

- Cell engineering
- Generation of mutations in Gasdermin D gene
- Generation of mutations in NLRP1 gene
- Generation of doxycycline-inducible plasmids
- Cell transfection/transduction
- SARS-CoV-2 production and infection
- Virus titration by TCID₅₀ calculation
- Viral replication determination by qRT-PCR
- Cell death
- Cell viability
- Cytokins/Alarmins quantification
- Caspase activities
- Top-down LC-MSMS
- Human recombinant Gasdermin D production and purification
- Immunoblot
- *In vitro* cleavage assays
- Cell imaging
- Sample preparation for immunoblot
- Generation of knock-out cells by CRISPR/Cas9
- **QUANTIFICATION AND STATISTICAL ANALYSIS**

SUPPLEMENTAL INFORMATION

Supplemental information can be found online at <https://doi.org/10.1016/j.molcel.2022.04.033>.

CONSORTIA

The members of the COVID Human Genetic Effort are Tayfun Ozcelik, Nevin Hapitoglu, Filomeen Haerynck, Sevgi Keles, Ahmed A. Bousfiha, and Rafael Leon Lopez. For affiliation information, see the supplemental information.

ACKNOWLEDGMENTS

This project was funded by grants from the Fondation pour la Recherche Médicale (F.R.M.) and the ERC StG (INFLAME) to E.M., the ERC StG (ANTIVIR) to C.G., and the French Ministry of Health with the participation of the Groupement Interrégional de Recherche Clinique et d'Innovation Sud-Ouest Outre-Mer (PHRCI 2020 IMMUNOMARK-COV) to G.-M.B. The ASB3 structure is supported by LABEX, Investissement d'Avenir and foundation Bettencourt grants to O.N. M.P. and R.P. were, respectively, funded by a CIFRE PhD fellowship and a research grant from InvivoGen. S.B. is supported by a PhD fellowship from Mali Ministry of Education and from the FRM (FDT 12794). S.A.L.-I. is supported by a Vaincre La Mucoviscidose (VLM) PhD fellowship. We thank the following organizations for the highly valuable contribution of the COVID-BioToul biobank: the CRB TBR, the Clinical Research Center 1436, and the Delegation for clinical research and innovation of the Toulouse University Hospital. The authors acknowledge Celine Beronne and Flavie Moreau of the IPBS Institute Animal Facility Level 3 (ASB3) members for their help regarding the operating and technical procedures. The authors acknowledge BEI for SARS-CoV-2 material transfer, including SARS-CoV-2 variants, NSP5- and NSP5^{C145A}-expressing plasmids, and antibodies.

The authors deeply acknowledge all patients for their willingness and support in contributing and sharing samples for academic research. [Biorender.com](https://biorender.com) was used to generate some graphical figures. Life Science Editors performed language editing. Funders had no influence on how the project was conducted.

AUTHOR CONTRIBUTIONS

E.M. and R.P. conceptualized the study. E.M., R.P., E.R., M.P., K.S., A.H., and C.P. designed the methodology. R.P., M.P., K.S., A.H., C.P., P.P., A.-L.C.V., I.R., N.L., R.F., D.P., S.-A.L.-I., Y.R., C.G., C.C., and J.M. performed the

experiments. E.M., R.P., C.C., G.M.-B., and E.R. conducted the analysis. K.L., K.S.R., E.P., M.T., O.N., F.Z.L., G.M.-B., C.E.B., A.R.F., P.C., J.-L.C., B.R., E.R., E.P., C.G., and M.T. provided critical reagents and essential medical, technological, and infrastructure access and support. E.M., R.P., and E.R. wrote the manuscript with input from all authors. E.M., O.N., E.P., and M.T. acquired and provided funding.

DECLARATION OF INTERESTS

The authors declare no competing interests.

Received: October 19, 2021

Revised: February 16, 2022

Accepted: April 25, 2022

Published: May 16, 2022

REFERENCES

- Akama-Garren, E.H., Joshi, N.S., Tammela, T., Chang, G.P., Wagner, B.L., Lee, D.Y., Rideout, W.M., Papagiannakopoulos, T., Xue, W., and Jacks, T. (2016). A modular assembly platform for rapid generation of DNA constructs. *Sci. Rep.* **6**, 16836.
- Al-Samkari, H., Karp Leaf, R.S.K., Dzik, W.H., Carlson, J.C.T., Fogerty, A.E., Waheed, A., Goodarzi, K., Bendapudi, P.K., Bornikova, L., Gupta, S., et al. (2020). COVID-19 and coagulation: bleeding and thrombotic manifestations of SARS-CoV-2 infection. *Blood* **136**, 489–500.
- Anand, K., Ziebuhr, J., Wadhvani, P., Mesters, J.R., and Hilgenfeld, R. (2003). Coronavirus main proteinase (3CLpro) structure: basis for design of anti-SARS drugs. *Science* **300**, 1763–1767.
- Asano, T., Boisson, B., Onodi, F., Matuozzo, D., Moncada-Velez, M., Maglorius Renkilaraj, M.R.L.M., Zhang, P., Meertens, L., Bolze, A., Materna, M., et al. (2021). X-linked recessive TLR7 deficiency in ~1% of men under 60 years old with life-threatening COVID-19. *Sci. Immunol.* **6**, 65.
- Barger, C.J., Chee, L., Albahrani, M., Munoz-Trujillo, C., Boghean, L., Branick, C., Odunsi, K., Drapkin, R., Zou, L., and Karpf, A.R. (2021). Coregulation and function of FOXM1/ RHNO1 bidirectional genes in cancer. *eLife* **10**, e55070.
- Bastard, P., Gervais, A., Le Voyer, T., Rosain, J., Philippot, Q., Manry, J., Michailidis, E., Hoffmann, H.H., Eto, S., Garcia-Prat, M., et al. (2021a). Autoantibodies neutralizing type I IFNs are present in ~4% of uninfected individuals over 70 years old and account for ~20% of COVID-19 deaths. *Sci. Immunol.* **6**, eab14340.
- Bastard, P., Orlova, E., Sozaeva, L., Lévy, R., James, A., Schmitt, M.M., Ochoa, S., Kareva, M., Rodina, Y., Gervais, A., et al. (2021b). Preexisting autoantibodies to type I IFNs underlie critical COVID-19 pneumonia in patients with APS-1. *J. Exp. Med.* **218**, 29.
- Bastard, P., Rosen, L.B., Zhang, Q., Michailidis, E., Hoffmann, H.H., Zhang, Y., Dorgham, K., Philippot, Q., Rosain, J., Béziat, V., et al. (2020). Autoantibodies against type I IFNs in patients with life-threatening COVID-19. *Science* **370**, eabd4585.
- Bastard, P., Zhang, Q., Cobat, A., Jouanguy, E., Zhang, S.Y., Abel, L., and Casanova, J.L. (2021c). Insufficient type I IFN immunity underlies life-threatening COVID-19 pneumonia. *C. R. Biol.* **344**, 19–25.
- Bauernfried, S., Scherr, M.J., Pichlmair, A., Duderstadt, K.E., and Hornung, V. (2021). Human NLRP1 is a sensor for double-stranded RNA. *Science* **371**, eabd0811.
- Berlin, D.A., Gulick, R.M., and Martinez, F.J. (2020). Severe Covid-19. *N. Engl. J. Med.* **383**, 2451–2460.
- Broggi, A., Granucci, F., and Zanoni, I. (2019). Cytokines Focus Type III interferons: balancing tissue tolerance and resistance to pathogen invasion. *J. Exp. Med.* **217**, e20190295.
- Broz, P., and Dixit, V.M. (2016). Inflammasomes: mechanism of assembly, regulation and signalling. *Nat. Rev. Immunol.* **16**, 407–420.
- Cao, X. (2020). COVID-19: immunopathology and its implications for therapy. *Nat. Rev. Immunol.* **20**, 269–270.
- Carvalho, T., Krammer, F., and Iwasaki, A. (2021). The first 12 months of COVID-19: a timeline of immunological insights. *Nat. Rev. Immunol.* **21**, 245–256.
- Cauchois, R., Koubi, M., Delarbre, D., Manet, C., Carvelli, J., Blasco, V.B., Jean, R., Fouche, L., Bomet, C., Pauly, V., et al. (2020). Early IL-1 receptor blockade in severe inflammatory respiratory failure complicating COVID-19. *Proc. Natl. Acad. Sci. USA* **117**, 18951–18953.
- Cavalli, G., and Dagna, L. (2021). The right place for IL-1 inhibition in COVID-19. *Lancet Respir. Med.* **9**, 223–224.
- Chavarría-Smith, J., Mitchell, P.S., Ho, A.M., Daugherty, M.D., and Vance, R.E. (2016). Functional and evolutionary analyses identify proteolysis as a general mechanism for NLRP1 inflammasome activation. *PLoS Pathog.* **12**, e1006052.
- Chui, A.J., Okondo, M.C., Rao, S.D., Gai, K., Griswold, A.R., Johnson, D.C., Ball, D.P., Taabazuig, C.Y., Orth, E.L., Vittimberga, B.A., et al. (2019). N-terminal degradation activates the NLRP1B inflammasome. *Science* **364**, 82–85.
- Corman, V.M., Landt, O., Kaiser, M., Molenkamp, R., Meijer, A., Chu, D.K., Bleicker, T., Brünink, S., Schneider, J., Schmidt, M.L., et al. (2020). Detection of 2019 novel coronavirus (2019-nCoV) by real-time RT-PCR. *Eurosurveillance* **25**, 2000045.
- Dick, M.S., Sborgi, L., Rühl, S., Hiller, S., and Broz, P. (2016). ASC filament formation serves as a signal amplification mechanism for inflammasomes. *Nat. Commun.* **7**, 1–13.
- Eldeeb, M., Esmaili, M., and Fahlman, R. (2019). Degradation of proteins with N-terminal glycine. *Nat. Struct. Mol. Biol.* **26**, 761–763.
- Eren, E., Planès, R., Bagayoko, S., Bordignon, P.J., Chaoui, K., Hessel, A., Santoni, K., Pinilla, M., Lagrange, B., Burlet-Schiltz, O., et al. (2020). Irgm2 and Gate-16 cooperatively dampen Gram-negative bacteria-induced caspase-11 response. *EMBO Rep.* **21**, e50829.
- Everman, J.L., Rios, C., and Seibold, M.A. (2018). Primary airway epithelial cell gene editing using CRISPR-Cas9. *Methods Mol. Biol.* **1706**, 267–292.
- Franklin, B.S., Bossaller, L., Nardo, D. De, Ratter, J.M., Stutz, A., Engels, G., Brenker, C., Nordhoff, M., Mirandola, S.R., Al-Amoudi, A., et al. (2014). ASC has extracellular and prionoid activities that propagate inflammation. *Nat. Immunol.* **15**, 727–737.
- Galani, I.-E., Rovina, N., Lampropoulou, V., Triantafyllia, V., Manioudaki, M., Pavlos, E., Koukaki, E., Fragkou, P.C., Panou, V., Rapti, V., et al. (2020). Untuned antiviral immunity in COVID-19 revealed by temporal type I/III interferon patterns and flu comparison. *Nat. Immunol.* **22**, 32–40.
- Hadjadji, J., Yatim, N., Barnabei, L., Comeau, A., Boussier, J., Smith, N., Péré, H., Charbit, B., Bondet, V., Chenevier-Gobeaux, C., et al. (2020). Impaired type I interferon activity and inflammatory responses in severe COVID-19 patients. *Science* **369**, 718–724.
- Hansen, J.M., de Jong, M.F., Wu, Q., Zhang, L.S., Heisler, D.B., Alto, L.T., and Alto, N.M. (2021). Pathogenic ubiquitination of GSDMB inhibits NK cell bactericidal functions. *Cell* **184**, 3178–3191.e18.
- Heilig, R., Dilucca, M., Boucher, D., Chen, K.W., Hancz, D., Demarco, B., Shkarina, K., and Broz, P. (2020). Caspase-1 cleaves Bid to release mitochondrial SMAC and drive secondary necrosis in the absence of GSDMD. *Life Sci. Alliance* **3**, e202000735.
- Hollingsworth, L.R., Sharif, H., Griswold, A.R., Fontana, P., Mintseris, J., Dagbay, K.B., Paulo, J.A., Gygi, S.P., Bachovchin, D.A., and Wu, H. (2021). DPP9 sequesters the C terminus of NLRP1 to repress inflammasome activation. *Nature* **592**, 778–783.
- Johnson, D.C., Taabazuig, C.Y., Okondo, M.C., Chui, A.J., Rao, S.D., Brown, F.C., Reed, C., Peguero, E., de Stanchina, E., Kentsis, A., et al. (2018). DPP8/DPP9 inhibitor-induced pyroptosis for treatment of acute myeloid leukemia. *Nat. Med.* **24**, 1151–1156.
- Junqueira, C., Crespo, A., Ranjbar, S., Ingber, J., Parry, B., Ravid, S., de Lacerda, L.B., Lewandrowski, M., Clark, S., Ho, F., et al. (2021).

SARS-CoV-2 infects blood monocytes to activate NLRP3 and AIM2 inflammasomes, pyroptosis and cytokine release. *Res. Sq.* <https://doi.org/10.21203/rs.3.rs-153628/v1>.

Kayagaki, N., Kornfeld, O.S., Lee, B.L., Stowe, I.B., O'Rourke, K., Li, Q., Sandoval, W., Yan, D., Kang, J., Xu, M., et al. (2021). NINJ1 mediates plasma membrane rupture during lytic cell death. *Nature* 591, 131–136.

Kayagaki, N., Stowe, I.B., Lee, B.L., O'Rourke, K., Anderson, K., Warming, S., Cuellar, T., Haley, B., Roose-Girma, M., Phung, Q.T., et al. (2015). Caspase-1 cleaves gasdermin D for non-canonical inflammasome signalling. *Nature* 526, 666–671.

Kiemer, L., Lund, O., Brunak, S., and Blom, N. (2004). Coronavirus 3CLpro protease cleavage sites: possible relevance to SARS virus pathology. *BMC Bioinformatics* 5, 72.

Koning, R., Bastard, P., Casanova, J.L., Brouwer, M.C., van de Beek, D., van Aghmael, M., Algera, A.G., Appelman, B., van Baarle, F., and Bax, D. (2021). Autoantibodies against type I interferons are associated with multi-organ failure in COVID-19 patients. *Intensive Care Med.* 47, 704–706.

Lee, S., Ishitsuka, A., Noguchi, M., Hirohama, M., Fujiyasu, Y., Petric, P.P., Schwemmler, M., Staeheli, P., Nagata, K., and Kawaguchi, A. (2019). Influenza restriction factor MxA functions as inflammasome sensor in the respiratory epithelium. *Sci. Immunol.* 4, eaau4643.

Lei, X., Zhang, Z., Xiao, X., Qi, J., He, B., and Wang, J. (2017). Enterovirus 71 inhibits pyroptosis through cleavage of gasdermin D. *J. Virol.* 91, e01069–e01017.

Liu, J., Li, Y., Liu, Q., Yao, Q., Wang, X., Zhang, H., Chen, R., Ren, L., Min, J., Deng, F., et al. (2021). SARS-CoV-2 cell tropism and multiorgan infection. *Cell Discov.* 7, 1–4.

Lopez, J., Mommert, M., Mouton, W., Pizzorno, A., Brengel-Pesce, K., Mezidi, M., Villard, M., Lina, B., Richard, J.C., Fassier, J.B., et al. (2021). Early nasal type I IFN immunity against SARS-CoV-2 is compromised in patients with autoantibodies against type I IFNs. *J. Exp. Med.* 218, jem.2021121108132021c.

Lu, A., Magupalli, V.G., Ruan, J., Yin, Q., Atianand, M.K., Vos, M.R., Schröder, G.F., Fitzgerald, K.A., Wu, H., and Egelman, E.H. (2014). Unified polymerization mechanism for the assembly of ASC-dependent Inflammasomes. *Cell* 156, 1193–1206.

Lucas, C., Wong, P., Klein, J., Castro, T.B.R., Silva, J., Sundaram, M., Ellingson, M.K., Mao, T., Oh, J.E., Israelow, B., et al. (2020). Longitudinal analyses reveal immunological misfiring in severe COVID-19. *Nature* 584, 463–469.

Luchetti, G., Roncaioli, J.L., Chavez, R.A., Schubert, A.F., Kofoed, E.M., Reja, R., Cheung, T.K., Liang, Y., Webster, J.D., Lehoux, I., et al. (2021). Shigella ubiquitin ligase IpaH7.8 targets gasdermin D for degradation to prevent pyroptosis and enable infection. *Cell Host Microbe* 29, 1521–1530.e10.

Mitchell, P.S., Sandstrom, A., and Vance, R.E. (2019). The NLRP1 inflammasome: new mechanistic insights and unresolved mysteries. *Curr. Opin. Immunol.* 60, 37–45.

Okondo, M.C., Rao, S.D., Taabazuing, C.Y., Chui, A.J., Poplawski, S.E., Johnson, D.C., and Bachovchin, D.A. (2018). Inhibition of Dpp8/9 activates the Nlrp1b inflammasome. *Cell Chem. Biol.* 25, 262–267.e5.

Orzalli, M.H., Prochera, A., Payne, L., Smith, A., Garlick, J.A., and Kagan, J.C. (2021). Virus-mediated inactivation of anti-apoptotic Bcl-2 family members promotes gasdermin-E-dependent pyroptosis in barrier epithelial cells. *Immunity* 54, 1447–1462.e5.

Pan, P., Shen, M., Yu, Z., Ge, W., Chen, K., Tian, M., Xiao, F., Wang, Z., Wang, J., Jia, Y., et al. (2021). SARS-CoV-2 N protein promotes NLRP3 inflammasome activation to induce hyperinflammation. *Nat. Commun.* 12, 1–17.

Peng, R., Wu, L.A., Wang, Q., Qi, J., and Gao, G.F. (2021). Cell entry by SARS-CoV-2. *Trends Biochem. Sci.* 46, 848–860.

Rebendene, A., Valadão, A.L.C., Tauziet, M., Maarifi, G., Bonaventure, B., McKellar, J., Planès, R., Nisole, S., Arnaud-Arnould, M., Moncorgé, O., et al. (2021). SARS-CoV-2 triggers an MDA-5-Dependent interferon response which

is unable to control replication in lung epithelial cells. *J. Virol.* 95, e02415–e02420.

Reed, L.J., and Muench, H. (1938). A simple method of estimating fifty per cent endpoints. *Am. J. Epidemiol.* 27, 493–497.

Resnick, S.J., Iketani, S., Hong, S.J., Zask, A., Liu, H., Kim, S., Melore, S., Lin, F.Y., Nair, M.S., Huang, Y., et al. (2021). Inhibitors of coronavirus 3CL proteases protect cells from protease-mediated cytotoxicity. *J. Virol.* 95, e0237420.

Robinson, K.S., Teo, D.E.T., Tan, K.S., Toh, G.A., Ong, H.H., Lim, C.K., Lay, K., Au, B.V., Lew, T.S., Chu, J.J.H., et al. (2020). Enteroviral 3C protease activates the human NLRP1 inflammasome in airway epithelia. *Science* 370, eaay2002.

Rodrigues, T.S., de Sá, K.S.G., Ishimoto, A.Y., Becerra, A., Oliveira, S., Almeida, L., Gonçalves, A.V., Perucello, D.B., Andrade, W.A., Castro, R., et al. (2021). Inflammasomes are activated in response to SARS-CoV-2 infection and are associated with COVID-19 severity in patients. *J. Exp. Med.* 218, e20201707.

Sandstrom, A., Mitchell, P.S., Goers, L., Mu, E.W., Lesser, C.F., and Vance, R.E. (2019). Functional degradation: A mechanism of NLRP1 inflammasome activation by diverse pathogen enzymes. *Science* 364, eaau1330.

Sanjana, N.E., Shalem, O., and Zhang, F. (2014). Improved vectors and genome-wide libraries for CRISPR screening. *Nat. Methods* 11, 783–784.

Schultze, J.L., and Aschenbrenner, A.C. (2021). COVID-19 and the human innate immune system. *Cell* 184, 1671–1692.

Shi, J., Zhao, Y., Wang, K., Shi, X., Wang, Y., Huang, H., Zhuang, Y., Cai, T., Wang, F., and Shao, F. (2015). Cleavage of GSDMD by inflammatory caspases determines pyroptotic cell death. *Nature* 526, 660–665.

Taabazuing, C.Y., Okondo, M.C., and Bachovchin, D.A. (2017). Pyroptosis and apoptosis pathways engage in bidirectional crosstalk in monocytes and macrophages. *Cell Chem. Biol.* 24, 507–514.e4.

Tay, M.Z., Poh, C.M., Rénia, L., MacAry, P.A., and Ng, L.F.P. (2020). The trinity of COVID-19: immunity, inflammation and intervention. *Nat. Rev. Immunol.* 20, 363–374.

Tsu, B.V., Beierschmitt, C., Ryan, A.P., Agarwal, R., Mitchell, P.S., and Daugherty, M.D. (2021). Diverse viral proteases activate the nlrp1 inflammasome. *eLife* 10, 1–76.

Tsuchiya, K., Nakajima, S., Hosojima, S., Thi Nguyen, D., Hattori, T., Manh Le, T., Hori, O., Mahib, M.R., Yamaguchi, Y., Miura, M., et al. (2019). Caspase-1 initiates apoptosis in the absence of gasdermin D. *Nat. Commun.* 10, 1–19.

WHO Working Group on the Clinical Characterisation and Management of COVID-19 Infection (2020). A minimal common outcome measure set for COVID-19 clinical research. *Lancet Infect. Dis.* 20, e192–e197.

Wijst, M.G.P. van der, Vazquez, S.E., Hartoularos, G.C., Bastard, P., Grant, T., Bueno, R., Lee, D.S., Greenland, J.R., Sun, Y., Perez, R., et al. (2021). Type I interferon autoantibodies are associated with systemic immune alterations in patients with COVID-19. *Sci. Transl. Med.* 13, eab2624.

Xie, X., Muruato, A., Lokugamage, K.G., Narayanan, K., Zhang, X., Zou, J., Liu, J., Schindewolf, C., Bopp, N.E., Aguilar, P.V., et al. (2020). An infectious cDNA clone of SARS-CoV-2. *Cell Host Microbe* 27, 841–848.e3.

Xu, H., Akinyemi, I.A., Chitre, S.A., Loeb, J.C., Lednický, J.A., McIntosh, M.T., and Bhaduri-McIntosh, S. (2022). SARS-CoV-2 viroporin encoded by ORF3a triggers the NLRP3 inflammatory pathway. *Virology* 568, 13–22.

Yap, J.K.Y., Moriyama, M., and Iwasaki, A. (2020). Inflammasomes and pyroptosis as therapeutic targets for COVID-19. *J. Immunol.* 205, 307–312.

Yu, P., Zhang, X., Liu, N., Tang, L., Peng, C., and Chen, X. (2021). Pyroptosis: mechanisms and diseases. *Signal Transduct. Target. Ther.* 6, 1–21.

Zanoni, I. (2021). Interfering with SARS-CoV-2: are interferons friends or foes in COVID-19? *Curr. Opin. Virol.* 50, 119–127.

Zhang, Q., Bastard, P., Liu, Z., Le Pen, J., Moncada-Velez, M., Chen, J., Ogishi, M., Sabli, I.K.D., Hodeib, S., Korol, C., et al. (2020). Inborn errors of type I IFN immunity in patients with life-threatening COVID-19. *Science* 370, eabd4570.

Zheng, Z., Peng, F., Xu, X., Zhao, J., Liu, H., Peng, J., Li, Q., Jiang, Q., Zhou, Y., Liu, S., et al. (2020). Risk factors of critical & mortal COVID-19 cases: A systematic literature review and meta-analysis. *J. Infectol.* *81*, e16–e25.

Zhong, F.L., Robinson, K.S., Teo, D.E.T., Tan, K.Y., Lim, C., Harapas, C.R., Yu, C.H., Xie, W.H., Sobota, R.M., Au, V.B., et al. (2018). Human DPP9 represses

NLRP1 inflammasome and protects against autoinflammatory diseases via both peptidase activity and FIIND domain binding. *J. Biol. Chem.* *293*, 18864–18878.

Zhou, B., and Abbott, D.W. (2021). Gasdermin E permits interleukin-1beta release in distinct sublytic and pyroptotic phases. *Cell Rep.* *35*, 108998.

STAR★METHODS

KEY RESOURCES TABLE

REAGENT or RESOURCE	SOURCE	IDENTIFIER
Antibodies		
Anti- Gasdermin D (N-terminal), 1: 1000	ab215203;RRID: AB_2916166	Abcam
Anti- Gasdermin D (C-terminal), 1: 1000	ab210070;RRID: AB_2893325	Abcam
Anti- NLRP1 (N-terminal), 1: 1000	AF6788-SP;RRID: AB_2916167	R&D system
Anti- NLRP1 (C-terminal), 1: 1000	ab36852;RRID: AB_776633	Abcam
Anti -ACE2, 1: 1000	ab108252;RRID: AB_10864415	Abcam
Anti -TMPRSS2, 1: 1000	ab92323;RRID: AB_10585592	Abcam
Anti-actin 1: 5000	A1978;RRID: AB_476692	Sigma-Aldrich
anti-Sheep igG HRP (1/4000)	HAF016;RRID: AB_562591	R&D
Goat anti-mouse HRP (1/4000)	1034-05;RRID: AB_2794340	SouthernBiotech
Goat-anti-rabbit IgG (H+L), HRP conjugate (1/4000)	R-05072-500;RRID: AB_10719218	Advansta
Rabbit anti-Goat IgG (H+L) Secondary Antibody, HRP (1/4000)	81-1620;RRID: AB_2534006	Invitrogen
Donkey anti-Rabbit IgG (H&L) - Affinity Pure, DyLight®550 Conjugate (1/1000 IF)	DkxRb-003-D550NHSX;RRID: AB_2916168	ImmunoReagents
Anti Caspase 8 (1: 1000)	ALX-804-242-C100;RRID: AB_2050949	Enzo Life
Anti Caspase 1 (1: 1000)	AG-20B-0048-C100;RRID: AB_2916169	Adipogen
Anti Caspase 3 (1: 1000)	9662S;RRID: AB_331439	Cell Signaling
Anti gasdermin E (1: 1000)	Ab215191;RRID: AB_2737000	Abcam
Anti SARS NSP5 (1: 1000)	NBP3-07061;RRID: AB_2916170	Novusbio
Anti SARS Nucleocapsid (1: 1000)	NB100 56683;RRID: AB_838841	Novusbio
Bacterial and virus strains		
BetaCoV/France/IDF0372/2020	Sylvie van der Werf and the National Reference Centre for Respiratory Viruses	Institut Pasteur (Paris, France)
hCoV-19/USA/MD-HP05647/2021 (Delta Variant)		BEI
hCoV-19/USA/OR-OHSU-PHL00037/2021 (Alpha Variant)		BEI
hCoV-19/Japan/TY7-503/2021 (Gamma Variant)		BEI
Biological samples		
Plasma from Covid patients	Covid Biotoul cohort/Toulouse, France	Hospital of Toulouse
Plasma from patients with inborn mutations or autoantibodies	Institut Imagine/Covid genetic effort	Institut Imagine, Paris/France
Chemicals, peptides, and recombinant proteins		
Z-VAD: 40 μ M	tlrl-vad	Invivogen
Y-VAD: 40 μ M	inh-yvad	Invivogen
Z-DEVD: 40 μ M	S7312	Selleck Chemicals
Z-IETD: 40 μ M	inh-ietd	Invivogen
MCC950: 10 μ M	inh-mcc	Invivogen
VX765: 10 μ M	inh-vx765i-1	Invivogen
DMF: 10 μ M	S2586	Selleck Chemicals
MLN4924: 1 μ M	6499	Tocris
Remdesivir: 5 μ M	282T7766	Tebubio
Bortezomib: 0,1 μ M	S1013	Selleck Chemicals
PF-00835231: 10 μ M	S9731	Selleck Chemicals

(Continued on next page)

Continued

REAGENT or RESOURCE	SOURCE	IDENTIFIER
CG-376	SE-S0475	Euromedex
Nigericin	tlrl-nig-5	Invivogen
Hoescht	62249	Invitrogen
Poly(I:C) HMW	tlrl-pic	Invivogen
Nate	lyec-nate	Invivogen
Lipofectamine 2000	11668030	Invitrogen
Lipofectamine LTX	15338030	Invitrogen
Doxycycline	S5159	Selleck chemicals
Recombinant human IL-18	(rcyec-hil18)	Invivogen
Critical commercial assays		
IL-1B	88-7261-77	Fisher Scientific
IL-6	555220	BD
IL-16	DY316	R&D
Caspase 3	BMS2012INST	Invitrogen
Gasdermin E	AG-45B-0024-K101	Adipogen
HMGB1	NBP2-62766	Novusbio
Deposited data		
Original blots and microscopy images	https://doi.org/10.17632/nwhd3w9w5x.1	Mendeley dataset
Experimental models: Cell lines		
THP1 KO NLRP3	Thp-konlrp3z	Invivogen
THP1	Thp-null	Invivogen
A549	A549d-nfis	Invivogen
A549-Dual™ ACE2 & TMPRSS2	a549d-cov2r	Invivogen
A549-Dual™ KO-MAVS Cells	a549d-komavs	Invivogen
A549 ACE2 & TMPRSS2 Cells	a549-hace2tpsa	Invivogen
IL-18 Reporter HEK 293 Cells	(hkb-hmil18)	Invivogen
Lonza, B-ALI kit 00193514	00193514	Lonza
Corning HTS Transwell-24 well permeable supports	CLS3379	Corning
Recombinant DNA		
LentiCas9-Blast	addgen ref 52962	(Sanjana et al., 2014)
p8.91	Didier Trono lab	Didier Trono lab
pMD.2G	addgene ref 12259	Didier Trono lab
LentiGuide-Puro	addgen ref 52963	(Sanjana et al., 2014)
Vector pLVX-EF1 α -IRES-Puro Containing the SARS-CoV-2, USA-WA1/2020 3C-Like Protease Gene, C145A Mutant	BEI NR-52953	BEI
pLEX307-SARS-CoV-2-3CL (NSP5)	addgene #160278	(Resnick et al., 2021)
pSC2+ NLRP1 constructs		(Robinson et al., 2020)
pLV-72-Cas9-GFP	N/A	Invivogen
pLVB-Tet ON	N/A	Invivogen
pLVB-TetR	N/A	Invivogen
pBRGEN	N/A	Invivogen
pMSCV-puro	Addgene plasmid # 68469	(Akama-Garren et al., 2016)
pMSCV-GsdmB	GeneScript	N/A

(Continued on next page)

Continued

REAGENT or RESOURCE	SOURCE	IDENTIFIER
pMSCV-GsdmE	GeneScript	N/A
pMSCV-GsdmD	GeneScript	N/A
pCW57-RFP- P2A-MCS	Addgene #89182	(Barger et al., 2021)
LENTI V2 plasmid	Addgene 52961	N/A
Oligonucleotides		
sgRNA targeting Gasdermin E (Exon 2)	CAGTTTTTATCCCTCACCT	Sigma-Aldrich
sgRNA targeting Gasdermin E (Exon 2)	TAAGTTACAGCTTCTAAGTC	Sigma-Aldrich
sgRNA targeting Gasdermin E (Exon 3)	GTCGGACTTTGTGAAATACG	Sigma-Aldrich
sgRNA targeting Casp1 (Exon 2)	TTGTGAAGAAGACAGTTACC	Sigma-Aldrich
sgRNA targeting Casp1 (Exon 4)	AAGGATATGGAAACAAAAGT	Sigma-Aldrich
sgRNA targeting Gasdermin D (Exon 5)	TTAGGAAGCCCTCAAGCTCA	Sigma-Aldrich
sgRNA targeting Gasdermin D (Exon 6)	GAATGTGTACTCGCTGAGTG	Sigma-Aldrich
sgRNA targeting Gasdermin D (Exon 5)	AGGTTGACACACTTATAACG	Sigma-Aldrich
sgRNA targeting Caspase 3 (Exon 4)	CATACATGGAAGCGAATCAA	Sigma-Aldrich
sgRNA targeting Caspase 3 (Exon 5)	TGTCGATGCAGCAAACCTCA	Sigma-Aldrich
sgRNA targeting MAVS	ACCTCAGCAGATGATAGGCTCGGCC	Sigma-Aldrich
sgRNA targeting MAVS	ACCTCGCCCATCAACTCAACCCGTGC	Sigma-Aldrich
sgRNA targeting NLRP1 (Exon 2)	GCTCAGCCAGAGAAGACGAG	Sigma-Aldrich
sgRNA targeting NLRP1	GATAGCCCGAGTGACATCGG	Sigma-Aldrich
sgRNA targeting NLRP1	AGCCCGAGTGACATCGGTGG	Sigma-Aldrich
sgRNA targeting GFP	GGAGCGCACCATCTTCTCA	Sigma-Aldrich
Fwd Q333A	GAACCTCGCATAGTCATACT GGCGGGGGCTGCTGGAATTGGGAAG	Sigma-Aldrich
Rev Q333A	CTTCCCAATTCCAGCAGCCCCGCCA GTATGACTATGCGAGGTTC	Sigma-Aldrich
HA-GsdmD Q335A fwd2	GGCGCTGGAGgccGGCCAGAGCCTT GGGCC	Sigma-Aldrich
HA-GsdmD Q335 rev2	cgcaacccaaccccgatccCTAGTGGGG CTCCTGGCTC	Sigma-Aldrich
HA-GsdmD Q193 fwd	cagatcgctggagaattggctagcATGTACCCA TACGATGTTCCA	Sigma-Aldrich
HA-GsdmD Q193 rev	cgcaacccaaccccgatcctcaCTGCAAGC ACGTGGCTC	Sigma-Aldrich
HA-GsdmD N-ter fwd	cagatcgctggagaattggctagcATGTACCC ATACGATGTTCC	Sigma-Aldrich
HA-GsdmD N-ter rev	cgcaacccaaccccgatcctcaATCTGTCA GGAAGTTGTGG	Sigma-Aldrich
GsdmD Q193 fwd1	aggcgccggaattagatctctcgagatggactaca aagacgatgacgacaagGGTGGAGGTGGA GGTGA	Sigma-Aldrich
GsdmD Q193A rev1	GGCCCTCACCGgcCAAGCACGTGGC TCCGG	Sigma-Aldrich
HA-GsdmD Q193A fwd2	CACGTGCTTGgccGGTGGAGGCCAG GGCCAT	Sigma-Aldrich
GsdmD Q193 rev2 pMSCV	ctcccctacccgtagaattcCTAGTGGGGC TCCTGGCTC	Sigma-Aldrich
GsdmD Q335 fwd1	aggcgccggaattagatctctcgagatggactaca caaagacgatgacgacaagGGTGGAGG TGGAGGTGGAG	Sigma-Aldrich
GsdmD Q335A rev1	GGCTCTGGCCggcCTCCAGCGCC TCCTCCAA	Sigma-Aldrich

(Continued on next page)

Continued

REAGENT or RESOURCE	SOURCE	IDENTIFIER
HA-GsdmD Q335A fwd2	GGCGCTGGAGgccGGCCAGAGC CTTGGGCC	Sigma-Aldrich
GsdmD Q335 rev2 pMSCV	ctcccctaccggtagaattcCTAGT GGGGCTCCTGGCTC	Sigma-Aldrich

Recombinant proteins

Recombinant SARS-COV 3CL	E-718-050	Novusbio
Recombinant SARS-CoV-2 3CL	E-720-050	Novusbio
Recombinant MERS-CoV 3CL	E-719-050	Novusbio
Recombinant human caspase-1 protein (active)	Ab39901	Abcam
Nsp3, peptidase C16 of PLpro	PX-COV-P004	proteogenix
HRV3C Protease	SAE0045	Sigma-Aldrich

Software and algorithms

Snappgene	GSL Biotech LLC, Chicago, U.S.A.	N/A
Fiji (Image J)		N/A
Benchling Software		N/A
Image Lab 6.1 (Biorad)		N/A
Biorender.com		N/A
Graphpad 8.0a		N/A
Uniprot database		N/A

RESOURCE AVAILABILITY**Lead contact**

Further information and requests for resources and reagents listed in [method details](#) and [key resources table](#) sections should be directed to and will be fulfilled by the lead contact, Etienne Meunier, Etienne.meunier@ipbs or Emmanuel Ravet, e.ravet@invivogen.com

Regarding the [experimental model and subject details](#) that relate to medical aspects of this study, request of information must be sent to jean-laurent.casanova@inserm.fr and Guillaume-martin.blondel@chu-tlse.fr

Materials availability

Plasmids generated in this study are freely accessible upon request.

Cell lines generated in this study are freely accessible upon request and a completed Material Transfer Agreement (MTA).

Data and code availability

All data reported in this paper will be shared by the [lead contact](#) upon request.

Original blots and microscopy images are freely accessible in the following Mendeley data set: <https://doi.org/10.17632/nwhd3w9w5x.1>

Any additional information required to reanalyze the data reported in this paper is available from the [lead contact](#) upon request.

EXPERIMENTAL MODEL AND SUBJECT DETAILS**Safety procedures**

All described experiments involving SARS-CoV-2 infections (Microscopy of infected cells, Cell death assays, ELISA, sample preparation for Immunoblotting, virus production, TCDI50, RNA extraction) have been entirely performed and processed in a Biosafety Level 3 facility.

Ethical approvals of human studies**COVID-BioToul**

Clinical data and blood samples for plasma isolation and cryopreservation were collected at the Toulouse University Hospital, France, in the frame of the COVID-BioToul biobank (ClinicalTrials.gov Identifier: NCT04385108). All donors had given written informed consent and the study was approved by the ethical review board "Comité de Protection des Personnes Est-III" (ID-RCB 2020-A01292-37). Plasma samples were collected on admission to the hospital for COVID-19 proven by a positive PCR performed

on respiratory samples. COVID-19 patients were graded according to the severity on admission and on maximum severity during their hospitalization based on The World Health Organization's (WHO) ordinal scale (WHO Working Group on the Clinical Characterisation and Management of COVID-19, 2020). Patients were considered as having moderate disease when they required oxygen by mask or nasal prongs (WHO grade 5), and severe disease when they required high flow oxygen therapy, non-invasive ventilation, invasive ventilation, or extra-corporeal membrane oxygenation (WHO grade >5). Three groups of non-immunocompromised patients were identified for the purpose of this study: patients with moderate COVID-19 on admission and throughout their stay at the hospital (group "Moderate"); patients with moderate COVID-19 on admission with subsequent clinical worsening and severe COVID-19 requiring ICU admission (group "Moderate/Severe"); and patients with severe disease requiring ICU already on admission (group "Severe"). Mean age of COVID-19 patients was 60.8 ± 12 years, the percentage of females was 24.4.

Plasma from patients with interferon alterations

15 plasmas from patients with life-threatening COVID-19 pneumonia who developed critical disease (Bastard et al., 2020; Zhang et al., 2020) were obtained. Specifically, 3 patients exhibited inborn autosomic recessive (AR) or autosomic dominant (AD) mutation in genes encoding for interferon production/response, including AD TBK1 (MB019430), AR IRF7 (MB019096) and AR IFNAR1 (MB019091) (Zhang et al., 2020). The 12 other plasma samples came from COVID-19 patients with proven auto-antibodies to IFN α 2/IFN ω (Figure S5D; Bastard et al., 2020).

All donors had given written informed consent and the study was approved by local Institutional Review Boards (IRBs).

COVID-19 disease severity was assessed in accordance with the Diagnosis and Treatment Protocol for Novel Coronavirus Pneumonia. The term life-threatening COVID-19 pneumonia describes pneumonia in patients with critical disease, whether pulmonary, with mechanical ventilation [continuous positive airway pressure (CPAP), bilevel positive airway pressure (BIPAP), intubation, or high-flow oxygen], septic shock, or damage to any other organ requiring admission in the intensive care unit (ICU) (Bastard et al., 2020; Zhang et al., 2020).

Plasma and serum samples from the patients were frozen at -20°C immediately after collection.

Cell culture

Vero E6, Calu, THP1, HEK 293FT, THP1^{Nlrp3^{-/-}} and A549 cells were maintained in Dulbecco's modified Eagle's medium (DMEM, Gibco) supplemented with 10% heat-inactivated fetal bovine serum (FBS), 1% penicillin-streptomycin, and 1% L-glutamine.

Primary airway epithelial cells were from Epithelix and NHBE cells were from Lonza (CC-2540 and CC-2541).

Normal Human Bronchial Epithelial (NHBE) cell Air-Liquid interface (ALI) culture

NHBE cell culture was performed as suggested by the manufacturer (Lonza, B-ALI kit 00193514). Briefly, cells were seeded onto collagen-coated (0.03mg/mL) HTS Transwell-24 well permeable supports (Corning, CLS3379) at a density of $5 \cdot 10^4$ cells per insert for three days in B-ALI Growth Medium (Lonza, B-ALI kit 00193514). Cells were then cultured at the air-liquid interface in B-ALI Differentiating Medium (Lonza, B-ALI kit 00193514) at $37^{\circ}\text{C}/5\%\text{CO}_2$ for 20 days, with a medium change every two days.

For SARS infections, $100\mu\text{L}$ of $5 \cdot 10^4$ (MOI 0.5), $1 \cdot 10^5$ (MOI 1) or $2 \cdot 10^5$ (MOI 2) viral inoculum were added on cells for 3 hours. After washing two times the cells, medium was then replaced by B-ALI Differentiating Medium and cells were incubated for 24-36 hours before cell processing for further experiments.

For histological experiments, primary NHBEs were fixed for 30 minutes then processed using a Tissue-Tek VIP 6 and embedded using a Tissue-Tek TEC 5 (Sakura). Transwells were bisected and embedded vertically before sectioning. Serial paraffin sections ($4\mu\text{m}$) were prepared using a RM2135 rotary microtome (Leica), then deparaffinised with xylene and rehydrated with graded ethanols and water. For immunohistochemical staining, sections were heated for 15 minutes at 98°C in a citrate acid-based antigen unmasking solution (Vector Laboratories), then endogenous peroxidase activity blocked with 3% hydrogen peroxide for 15 minutes. Slides were stained in goat serum (1:5; G9023, Sigma) containing mouse monoclonal anti-SARS-CoV-2 spike (1:1000; GTX632604, GeneTex) for 90 minutes at 37°C . Following washing with TBS, sections were incubated with goat anti-mouse immunoglobulins/HRP (1:100; Dako) for 30 minutes at room temperature. Staining was visualised by application of diaminobenzidine for five minutes. For Alcian blue/periodic acid – Schiff (AB-PAS) staining, slides were stained in 1% Alcian blue in 3% acetic acid (Pioneer Research Chemicals) for five minutes, washed with water, then oxidised in 1% aqueous periodic acid (Acros Organics) for five minutes. Following another washing step, sections were stained in Schiff reagent (Thermo Fisher) for 10 minutes. All slides were counter-stained with haematoxylin to stain the nuclei and mounted in DPX Mountant (Sigma-Aldrich) using a CV5030 fully automated glass coverslipper (Leica), then digitally scanned using a Nanozoomer 2.0HT at 40x objective (Hamamatsu).

METHOD DETAILS

Cell engineering

To reconstitute the NLRP1 inflammasome pathway in A549, cells were transduced with VSV-G pseudotyped lentiviral vector carrying the *NLRP1* gene (NCBI accession NP001028225.1) and/or *asc* (NCBI accession NP037390.2) fused to *gfp*. To render cells permissive to SARS-CoV-2 infections cells were transduced with VSV-G pseudotyped lentiviral vector carrying the *ace2* (NCBI accession NP068576.1) and *tmprss2* (NCBI accession NP001128571.1) genes. Engineered A549 cell lines were characterized for NLRP1, ASC-GFP, ACE-2 and TMPRSS2 expression by q-RT-PCR, immunoblot and flow cytometry.

To generate cells stably expressing *GSDMD* gene mutated for protease cleavage sites (*GSDMD*^{Q193A} and *GSDMD*^{Q335A}) we reconstituted *GSDMD* deficient cells with full length or mutated *GSDMD* constructs (*GSDMD*^{Q193A} and *GSDMD*^{Q335A}). Cells were transduced with VSV-G pseudotyped lentiviral vector carrying different *GSDMD* constructs in presence of 8 μg/ml polybrene and centrifugated for 2h at 2900 rpm at 32°C. 48 h later, medium was replaced and Puromycin selection (1 μg/mL) was applied to select positive clones for two weeks.

Generation of mutations in Gasdermin D gene

To express the N-terminal and C-terminal fragments of *GSDMD* generated following cleavage by Sars-CoV-2 3CL protease we used the following strategy: 1) nucleotide sequence coding for the N-terminal and C-terminal domains of *GSDMD* peptides were generated following proteases cleavage by using SnapGene software; 2) N-terminal and C-terminal *GSDMD* coding sequence were generated by PCR with the addition of a 5' Start codon ATG and 3' Stop codon TGA; 3) Amplified PCR fragments were cloned into pCW57-RFP-P2A-MCS lentiviral vector plasmid between BamHI and EcoRI restriction sites. This system allows ectopic expression of the N-terminal and C-terminal domains of *GSDMD* in order to study their activity.

To generate cells stably expressing *Gsdmd* gene mutated for protease cleavage sites (mutations *GSDMD*^{Q193A} and *GSDMD*^{Q335A}) we introduced point mutations in the *GSDMD* coding sequence by overlapping PCR and cloned mutated *GSDMD* in pMSCV-puro vector between BamHI and NotI restriction sites. Restriction enzymes were all from New England BioLabs. All the construct generated were verified by DNA sequencing (Eurofins genomics). Primers of the different constructions are listed in [key resources table](#).

Generation of mutations in NLRP1 gene

The transient expression plasmid of NLRP1Q333A was cloned into the pCS2+ vector using standard restriction cloning using ClaI and XhoI flanking the open reading frames. Site-directed mutagenesis was carried out with QuickChangeXL II (Agilent #200522) according to the manufacturer's instructions. Primers:

Rev Q333A: CTTCCCAATTCCAGCAGCCCCCGCCAGTATGACTATGCGAGGTTC
Fwd Q333A: GAACCTCGCATAGTCATACTGGCGGGGGCTGCTGGAATTGGGAAG

Generation of doxycycline-inducible plasmids

To generate doxycycline-inducible SARS-CoV-2 3-CL protease (NSP5) constructs, WT NSP5 or NSP5C145A were amplified by PCR from pLEX307-SARS-CoV-2-3-CL and pLVX-EF1α-IRES-Puro 3CL^{C145A} template respectively. PCR products were digested with AgeI and NheI restriction enzymes and digested insert were ligated in pLVB-TetON vector between AgeI and NheI restriction sites. To generate cell lines nsp5-inducible A549 cell lines, cells were transduced with both pLVB-nlr-TetR and pLVB-TetON-NSP5.

Primer1 (44-mer): ATTTATATTAACCGGTATGAGTGGTTTTAGAAAAATGGCATTCC
Primer2(45-mer): AATTATAATGCTAGCTTATTGGAAAGTAACACCTGAGCATTGTC

Cell transfection/transduction

A549 transfected with NLRP1 mutated plasmids

The day prior to the transfection, 2 x 10⁵ A549 cells were plated in 6 well plate in 10% FBS DMEM (Gibco) supplemented with 1% penicillin-streptomycin (Gibco). The day after, cells were treated with Nate 1X (Invivogen) for 30 min. DNA-lipids complexes were prepared with 1 μg of pCS2+ NLRP1 mutated plasmids ([Robinson et al., 2020](#)) or pCS2+ NLRP1^{Q333A}, lipofectamine LTX and PLUS reagent diluted in Opti-MEM and incubated for 30 min at room temperature according to the manufacturer's instructions (Invitrogen). DNA-lipid complexes were added to cells and incubated O/N at 37°C in 10% FBS DMEM.

A549 transfected with Gasdermin d plasmids

The day prior to the transfection, 2 x 10⁵ A549 dual cells were plated in 6 well plate in 10% FBS DMEM (Gibco) supplemented with 1% penicillin-streptomycin (Gibco). The day after, DNA-lipids complexes were prepared with 1 μg of *GSDMD*NT pcW57 plasmids and polyethylenimine (PEI) diluted in Opti-MEM. DNA-lipid complexes were added to cells and incubated for 48h at 37°C in Opti-MEM (Fischer Scientific).

SARS-CoV-2 production and infection

Experiments using SARS-CoV-2 virus were performed in BSL-3 environment. The BetaCoV/France/IDF0372/2020 isolate was supplied by Sylvie van der Werf and the National Reference Centre for Respiratory Viruses hosted by Institut Pasteur (Paris, France). The patient sample from which strain BetaCoV/France/IDF0372/2020 was isolated was provided by X. Lescure and PY. Yazdanpanah from the Bichat Hospital, Paris, France. The mNeonGreen (mNG) ([Xie et al., 2020](#)) reporter SARS-CoV-2 were based on 2019-nCoV/USA_WA1/2020 isolated from the first reported SARS-CoV-2 case in the USA, and provided through World Reference Center for Emerging Viruses and Arboviruses (WRCEVA), and UTMB investigator, Dr. Pei Yong Shi. SARS-CoV-2. Isolate hCoV-19/USA/MD-HP05647/2021 (Delta Variant), SARS-CoV-2, Isolate hCoV-19/USA/OR-OHSU-PHL00037/2021 (Alpha Variant) and SARS-CoV-2, Isolate hCoV-19/Japan/TY7-503/2021 (Gamma Variant) were obtained from BEI.

SARS-CoV-2 isolates were amplified by infecting Vero E6 cells (MOI 0.005) in DMEM (Gibco) supplemented with 10mM HEPES and 1% penicillin-streptomycin (Gibco). The supernatant was harvested at 48 h post-infection when cytopathic effects were observed,

cell debris were removed by centrifugation, and aliquots were frozen at -80°C . Viral stocks were titrated by plaque assays in Vero E6 cells. Typical titers were 5 to 10×10^6 PFU/ml.

The day prior to infection, 50,000 or 250,000 A549-ACE2-TMPRSS2, expressing or not NLRP1, cells were seeded in 96-well or 24-well tissue culture plates respectively in 10% FBS DMEM supplemented with 10mM HEPES (Gibco) and 1% penicillin-streptomycin (Gibco), and then incubated overnight at 37°C in a humidified, 5% CO_2 atmosphere-enriched chamber. The day after, cells were infected with mNeonGreen SARS-CoV-2 or the BetaCoV/France/IDF0372/2020 strains at indicated MOI in 50 μL DMEM supplemented with 10mM Hepes, 1% penicillin-streptomycin and 1% L-Glutamine for 1h at 37°C . Then, culture medium was completed up to 200 μL with DMEM or Opti-MEM.

Virus titration by TCID₅₀ calculation

The day prior to infection, 50,000 VeroE6 cells per well were seeded in 96-well tissue culture plates using 10% FBS DMEM, and then incubated overnight at 37°C in a humidified, 5% CO_2 atmosphere-enriched chamber. On the day of infection, serial 2.5-fold dilutions (from 10^{-1} to $10^{-6.5}$) of the A549 cell culture supernatant were prepared in DMEM and used to infect Vero E6 cells; each dilution was tested in four replicates. The plates were incubated for at least 96 h and observed to monitor the development of cytopathic effect (CPE) using an EVOS Fluid microscope (Invitrogen). Viral titers, expressed as TCID₅₀/mL, were calculated according to both Reed and Muench and Karber methods based on three or four replicates for dilution (Reed and Muench, 1938).

Viral replication determination by qRT-PCR

The day prior to infection, 100,000 NHBE, A549-ACE2-NLRP1- or A549-ACE2-NLRP1+ cells per well were seeded in 48-well plates. As previously described (Rebendenne et al., 2021), cells were infected or not with SARS-CoV-2 at the indicated MOI and harvested 24 h and 48 h later, and total RNA was extracted using the RNeasy kit (Qiagen) employing on-column DNase treatment, according to the manufacturer's instructions. 125 ng of total RNAs were used to generate cDNAs. To quantify SARS-CoV-2 RNAs, the cDNAs were analyzed by qPCR using published RdRp primers and probe (Corman et al., 2020), as follow: RdRp_for 5'-GTGARATGGT CATGTGTGGCGG-3', RdRp_rev 5'-CAAATGTAAAACTATTAGCATA-3', and RdRp_probe 5'-FAM-CAGGTGGAACCTCAT CAGGAGATGC-TAMRA-3'. A standard curve was used in parallel to calculate relative cDNA copy numbers and confirm the assay linearity. qPCR reactions were performed in triplicate, in universal PCR master mix using 900 nM of each primer and 250 nM probe or the indicated Taqmans. After 10 min at 95°C , reactions were cycled through 15 s at 95°C followed by 1 min at 60°C for 40 repeats. Triplicate reactions were run according to the manufacturer's instructions using a ViiA7 Real Time PCR system (ThermoFisher Scientific).

Cell death

Cell death was measured by quantification of the lactate dehydrogenase (LDH) release into the cell supernatant using LDH Cytotoxicity Detection Kit (Takara). Briefly, 50 μL cell supernatant were incubated with 50 μL LDH substrate and incubated for 15 min. The enzymatic reaction was stopped by adding 50 μL of stop solution. Maximal cell death was determined with whole cell lysates from unstimulated cells incubated with 1% Triton X-100.

Cell viability

Cell viability was measured by quantification of intracellular ATP using CellTiter-Glo® One Solution Assay (Promega) according to manufacturer's instructions.

Cytokines/Alarmins quantification

Human cytokines secretion were quantified by ELISA kits, according to the manufacturer's instructions, IL-1B (Thermo Fisher Scientific, (88-7261-77), IL-6 (BD, 555220), IL-16 (R&D, DY316), Caspase 3 (Invitrogen, BMS2012INST), Gasdermin E (AG-45B-0024-KI01), Gasdermin D (Abcam, ab272463), Cleaved Caspase-3/caspase-3 (Abcam, ab220655). Before use, the samples were diluted 1/3 to 1/5 with their respective assay diluents. IL-18 was quantified using IL-18 Reporter HEK 293 Cells according to the manufacturer's instructions (InvivoGen). HMGB1 was quantified by ELISA according to the manufacturer's instructions (Novus Biologicals).

Caspase activities

Caspase (G8090, G9951, Promega) activity were addressed in cells after 24 hours treatment or infection according to the manufacturer instructions.

Top-down LC-MSMS

Nano-LC-MSMS analyses of Gasdermin-D were performed on a nanoRS UHPLC system (Dionex) coupled to an LTQ-Orbitrap Fusion Tribrid mass spectrometer (Thermo Fisher Scientific). Briefly, a total of 5 μL of sample at ~ 1 -5 μM was loaded onto a reverse-phase C4-precolum (300 μm i.d. \times 5 mm; Thermo Fisher Scientific) at 20 $\mu\text{L}/\text{min}$ in 2% acetonitrile (ACN) and 0.2% formic acid (FA). After 5 minutes of desalting, the precolum was switched online with an analytical C4 nanocolum (75 μm i.d. \times 15 cm; in-house packed with C4 Reprosil) equilibrated in 95% solvent A (5% ACN, 0.2% FA) and 5% solvent B (0.2% FA in ACN). Proteins were eluted using a binary gradient ranging from 5% to 40% (5 minutes) and then 40% to 99% (33 minutes) of solvent B at a flow rate of 300 nL/min.

The Fusion Tribrid (Thermo Fisher Scientific) was operated in positive mode with the Xcalibur software (Thermo Fisher Scientific). The spray voltage was set to 1900 V, the ion transfer tube temperature to 350°C, the RF lens to 60%, and no in-source dissociation was applied.

MS scans were acquired in the 1000–2000 m/z range, in the Orbitrap at 7500 resolution with the following parameters: 10 μ scans for averaging, AGC target set to 3e5 and maximum injection time to 50 ms. 3 second MSMS cycles were used, with the following parameters: HCD activation was done with 25% activation energy, MSMS spectra were acquired in the Orbitrap at 60000 resolution. The AGC target was set to 1e6 and the maximum injection time to 400 ms. Dynamic exclusion for 60 s was used within 30 s to prevent repetitive selection of the same precursor (selection tolerance: \pm 20ppm) and improve the number of identified proteins. LC-MSMS.raw files were automatically deconvoluted with the rolling window deconvolution software RoWinPro and the proteoform footprints were visualized with VisioProt-MS v2.0. Spectra identification was done in Proteome Discoverer (Thermo Fisher Scientific) v.2.3, using a three Tier search including an Absolute Mass Search (precursor mass tolerance - 100 Da, fragment mass tolerance - 10ppm) followed by a Biomarker Search (no enzyme precursor tolerance - 100 ppm, fragment mass tolerance - 50 ppm) and a last Absolute Mass Search (precursor mass tolerance - 1000 Da, fragment mass tolerance - 10 ppm). The identified truncated proteoforms were then manually validated. The search database was generated using a custom made.fasta file containing the sequences of GSDMD and the 3CL protease.

Human recombinant Gasdermin D production and purification

Human recombinant Gasdermin D fused with an N-terminus hexahistidine-MBP-tag was expressed in BL21 (DE3) E coli strain and purified according to Shiyu Xia et al. (Monitoring Gasdermin pore formation in vitro, *Methods Enzymol.* 2019; 625: 95–107.) with slight modifications. Briefly, after cell harvest, bacteria were lysed by sonication under ice and recombinant human Gasdermin D was purified by a first nickel metal affinity chromatography (Takara). The 6His-MBP tag was removed by O/N TEV digestion at 4°C and a second nickel metal affinity chromatography was performed to separate the Gasdermin D (unbound fraction) from the 6His-MBP tag. After sample concentration, a Superdex 200 size exclusion column (GE Healthcare) was done as a final purification step.

Immunoblot

Cells lysates were homogenized by pipetting up and down ten times and supplemented with laemli buffer (1X final) before boiling sample for 10 min at 95°C. Cell lysates were then separated by denaturing SDS-PAGE and transferred on PVDF membrane. After transfer, the membrane is saturated 1h at room temperature in TBS-T (Tris 10 mM pH 8, NaCl 150 mM, Tween 20 0.05%) containing 5% nonfat milk. Then, the membrane is incubated overnight at 4°C with the different primary antibodies, under agitation. After 3 washes with TBS-T, the membrane is further incubated with the secondary antibodies coupled with the peroxidase enzyme HRP (horseradish peroxidase) for 1 hour at room temperature and under agitation. Then membranes are washed 3 times with TBS-T. The blots are revealed with the ECL revelation kit (Advansta) and images are acquired using ChemiDoc Imaging System (BioRad). The primary antibodies and secondary antibody used are listed in Reagent [key resources table](#).

In vitro cleavage assays

Recombinant proteins

The human purified recombinant gasdermin D (6 μ M final concentration), produced and purified in the lab or the human recombinant NLRP1 (0.7 μ M final concentration), from Origen (CAT#: TP316481) was incubated in 20 mM Tris at pH7.5 150 mM NaCl 1 mM DTT with recombinant SARS-CoV-2 3CL protease (Sigma-Aldrich SAE0172, R&D Systems, Novus Biologicals), recombinant SARS-CoV-2 PL^{pro} recombinant (Sigma-Aldrich) SARS-CoV-1 or MERS-CoV 3CL (Novus Biologicals) at molar ratio of 3:1 otherwise as indicated in figure legends, for O/N at 4°C, in presence or absence of protease inhibitor (PF-00835231, 10 μ M - Selleck Chemicals S9731). Human recombinant caspase 1 (Abcam 39901) was used as a positive control of the gasdermin D cleavage. Then, to detect gasdermin and NLRP1 cleavage(s), samples were analyzed on a SDS-PAGE follow by Coomassie blue staining or by immunoblot following transfer to PVDF membrane. When a cleavage occurred, fragments identification was done by IPBS mass spectrometry platform.

Cell lysate

Cell lysate of A549 and A549-NLRP1 cells was prepared as following: one day before lysis, 2,5 x 10⁵ cells were plated in 24 well plate. The day of lysis, medium was removed and cells were washed once with ice cold PBS 1X (Phosphate Buffered Saline) and incubated for 30 min on ice in 60 μ L of protease assay lysis buffer (20 mM Tris-HCl pH 7.4, 135 mM NaCl, 1% Triton X-100, 10% glycerol). Cell lysate was then collected, and clarified from insoluble fraction by centrifugation at 14,000 rpm for 30 min at 4°C before being stored at -80°C for further assays.

Cell imaging

Cells were imaged in BSL-3 facility under EVOS Floid (Invitrogen) fluorescent microscope with 20 X objective.

Sample preparation for immunoblot

At the end of the experiment, cell' supernatant was collected and soluble proteins from cell supernatant fraction were precipitated using trichloroacetic acid (TCA) as described previously (Eren et al., 2020). Precipitated pellet was then resuspended in 50 μ L of RIPA buffer plus laemli supplemented with protease inhibitor cocktail (Roche). Adherent cells were lysed in 50 μ L of RIPA buffer (150 mM

NaCl, 50 mM Tris-HCl, 1% Triton X-100, 0.5% Na-deoxycholate) supplemented with protease inhibitor cocktail (Roche). Collected cell lysate was homogenized by pipetting up and down ten times and supplemented with laemli buffer (1X final). Cells and supernatant fractions were heat for 20 min at 80°C in BSL-3 facility. Sample were then taken out of BSL-3, and boiled for 15 min at 95°C. Cell lysate and cell supernatant fraction were then analyzed by immunoblot either individually or in pooled sample of lysate plus supernatant (equal vol/vol).

Generation of knock-out cells by CRISPR/Cas9

A549 cells were transfected using lipofectamine LTX transfection reagent, in presence of NATE 1X (Invivogen) with (pCas9-GFP) to allow transient expression of Cas9-GFP and sgRNA targeting Gasdermin D (TTAGGAAGCCCTCAAGCTCA and GAATGTGTAAGCTCGCTGAGTG), Gasdermin E (CAGTTTTTATCCCTCACCT and TAAGTTACAGCTTCTAAGTC), MAVS (ACCTC GCCCATCAACTCAACCCGTGC and ACCTCAGCAGATGATAGGCTCGGCC) and Caspase 3 (CATACATGGAAGCGAATCAA and TGTCGATGCAGCAAACCTCA). 48h after transfection, GFP-expressing cells were isolated by fluorescence associated cell sorting, diluted in single clones and knock-out clones were screened by PCR, and western blot. Alternatively, A549 cells were transduced with lentiviral vectors coding for Cas9 and blasticidin resistance cassette, and lentiviral vectors coding for sgRNA and puromycin resistance cassette. 48h after transduction, cells were selected during 2 weeks and blasticidin/puromycin double resistant cells were used in functional assays.

NHBE deficient cells were obtained by using Ribonucleoprotein (RNP) technic (Everman et al., 2018). Briefly, RNP mixes containing Cas9 protein (90pmoles, 1081059, IDT), gRNA (450pmoles) and electroporation enhancer (1μL/Mix, 1075916, IDT) were electroporated using the Neon transfection system (Life Technologies) in T Buffer (Life Technologies). Settings were the following: 1900 V Voltage, 10 Width, 1 Pulse, 20ms.

The following sgRNA targeting *NLRP1* (GCTCAGCCAGAGAAGACGAG/**KO1**, GATAGCCCGAGTGACATCGG/**KO2**, AGCCC GAGTGACATCGGTGG/**KO3**) *GSDMD* (TTAGGAAGCCCTCAAGCTCA/**KO1/2**, GAATGTGTAAGCTCGCTGAGTG**KO3/4**, AGGTTGA CACACTTATAACG/**KO5**) or *GSDME* (GTCGGACTTTGTGAAATACG/**KO1**, CAGTTTTTATCCCTCACCT/**KO2** and TAAGTTA CAGCTTCTAAGTC/**KO3**) were used for the purpose of this study. Genetic invalidation efficiency was tested by immunoblotting after 21-28 days of cell differentiation onto Transwell.

QUANTIFICATION AND STATISTICAL ANALYSIS

Statistical data analysis was performed using Prism 8.0a (GraphPad Software, Inc.). Comparison of two groups was performed using T-test with Bonferroni correction. Otherwise specified, data are plotted as mean with SEM. P values are given in figures. Significance is defined as *p ≤ 0.05; **p ≤ 0.01, ***p ≤ 0.001.

Supplemental information

**Human NLRP1 is a sensor of pathogenic
coronavirus 3CL proteases in lung
epithelial cells**

Rémi Planès, Miriam Pinilla, Karin Santoni, Audrey Hessel, Charlotte Passemar, Kenneth Lay, Perrine Paillette, Ana-Luiza Chaves Valadão, Kim Samirah Robinson, Paul Bastard, Nathaniel Lam, Ricardo Fadrique, Ida Rossi, David Pericat, Salimata Bagayoko, Stephen Adonai Leon-Icaza, Yoann Rombouts, Eric Perouzel, Michèle Tiraby, COVID Human Genetic Effort, Qian Zhang, Pietro Cicuta, Emmanuelle Jouanguy, Olivier Neyrolles, Clare E. Bryant, Andres R. Floto, Caroline Goujon, Franklin Zhong Lei, Guillaume Martin-Blondel, Stein Silva, Jean-Laurent Casanova, Céline Cougoule, Bruno Reversade, Julien Marcoux, Emmanuel Ravet, and Etienne Meunier

SUPPLEMENTAL INFORMATIONS

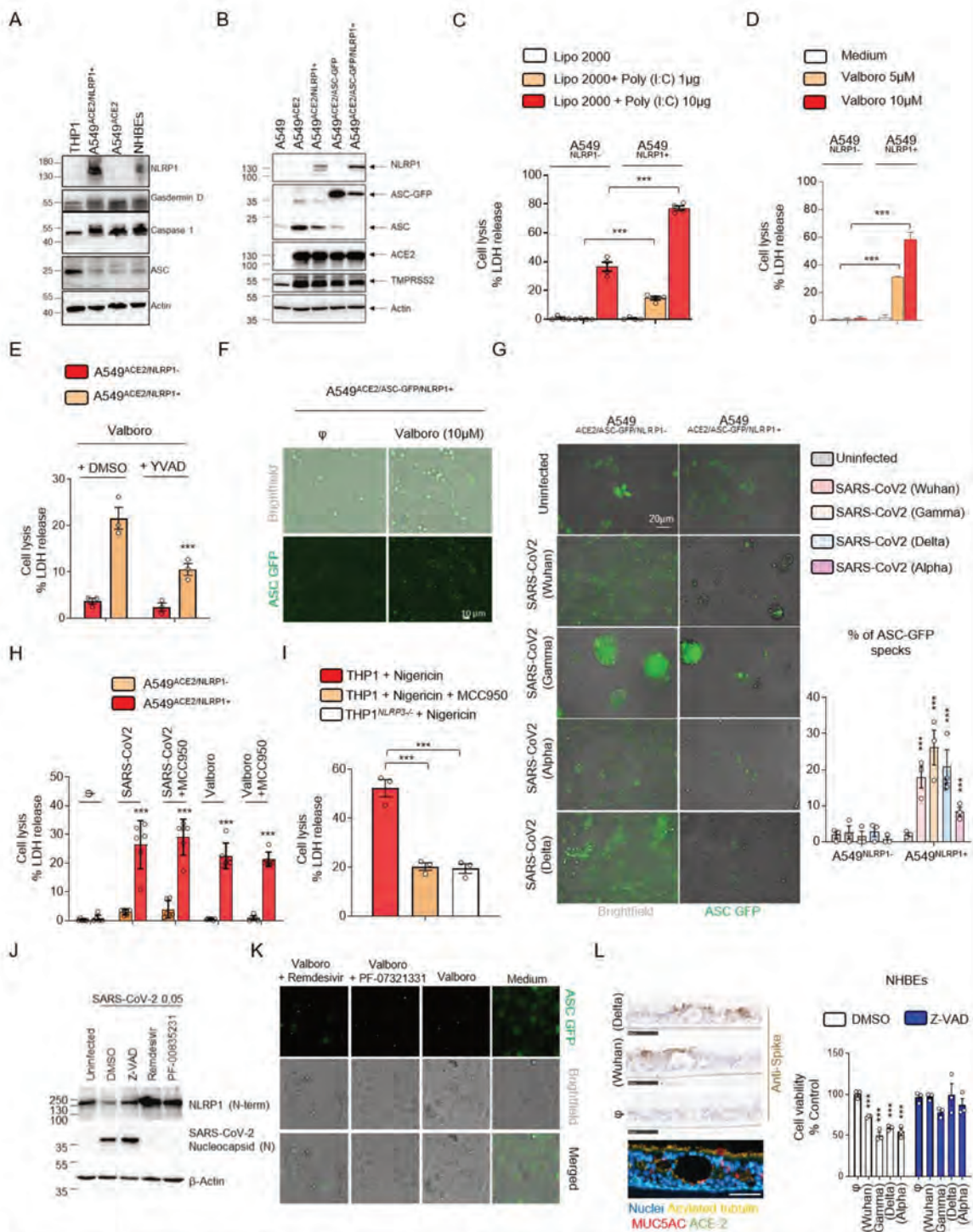


Figure S1 (Related to Figure 1). NLRP1 detects SARS-CoV-2 infection in epithelial cells

(A) Western Blot examination of the expression of NLRP1, ASC, Gasdermin-D (GSDMD), Caspase-1 (CASP1) and ACTIN in THP-1 (monocytes), NHBE (bronchial epithelial cells) or A549 cells engineered for the purpose of this study. Immunoblots

were performed against full-length NLRP1 Nter (p130/110), ASC (p22), GSDMD (p55), CASP1 (p50) and ACTIN (p40).

(B) Western Blot examination of the expression of NLRP1, ASC, ASC-GFP, ACE2, TMRSS2 and ACTIN in A549 cells engineered for the purpose of this study. Immunoblots were performed against full-length NLRP1 Nter (p130/110), ASC (p22), ASC-GFP (p50), TMRSS2 (p54), ACE2 (p130) and ACTIN (p40).

(C-E) Measure of cell lysis (LDH release) in A549^{NLRP1+} or A549^{NLRP1-} transfected with polyI:C (0.1µg or 1µg) (B) or treated with Valboro (5 and 10µM) (C) in presence/absence of the Caspase-1 inhibitor Z-YVAD (25µM) for 10 hours.

(F) Florescence microscopy of ASC-GFP specks in A549^{ACE2/NLRP1+/ASC-GFP} and A549^{ACE2/NLRP1-/ASC-GFP} airway epithelial cell lines treated with 5µM of Valboro for 10 hours. Images shown are from one experiment and are representative of n=3 independent experiments; scale bars 10 µm.

(G) Florescence microscopy and associated quantifications of ASC-GFP specks in A549^{ACE2/NLRP1+/ASC-GFP} airway epithelial cell lines infected for 24 hours with various strains of SARS-CoV-2 (MOI 0.01).

(H) Measure of cell lysis (LDH release) in A549^{NLRP1+} or A549^{NLRP1-} treated with Valboro (5 µM) for 10 hours or infected with SARS-CoV-2 (MOI 0.05) for 24 hours in presence/absence of the NLRP3 inhibitor MCC950 (10µM).

(I) Measure of cell lysis (LDH release) in PMA (100ng/mL)-primed THP1 myeloid cells treated with Nigericin (20µM) for 2 hours in presence/absence of the NLRP3 inhibitor MCC950 (10µM).

(J) Western blot examination of NLRP1 and SARS-CoV-2 Nucleocapsid (N) in A549^{ACE2/NLRP1+} and A549^{ACE2/NLRP1-} airway epithelial cell lines infected with SARS-CoV-2 for 24 hours multiplicity of infection (MOI) of 0.05 in presence /absence of the NSP5 protease inhibitor PF-00835231 (10µM), Remdesivir (5µM), or Z-VAD (25 µM).

(K) Florescence microscopy of ASC-GFP specks in A549^{ACE2/NLRP1+/ASC-GFP} airway epithelial cell lines treated with 5µM of Valboro for 10 hours in presence/absence of the 3CL inhibitor PF-00835231 (10µM) or Remdesivir (5 µM). Images shown are from one experiment and are representative of n=3 independent experiments; scale bars 10 µm.

(L) Microscopy characterization of Air-Liquid Interface-differentiated and infected epithelial cells (ACE2, Mucin 5AC, Acylated tubulin, Nuclei, SARS-CoV-2) and measure of cell lysis (LDH release) in NHBE epithelial cells infected for 36 hours with various strains of SARS-CoV-2 (MOI 1) in presence/absence of the pan Caspase inhibitor Z-VAD (40 μ M). Images shown are from one experiment and are representative of n=2 independent experiments; scale bars 50 μ m.

Data information:

Western Blot (A, B, J) images are from one experiment performed three times. Graphs C, D, E, H, I, L show data presented as means \pm SEM from n=6 (G) or n=3 independent pooled experiments; ***p \leq 0.001 for the indicated comparisons with t-test. Images (F, G, K) show one experiment performed three times.

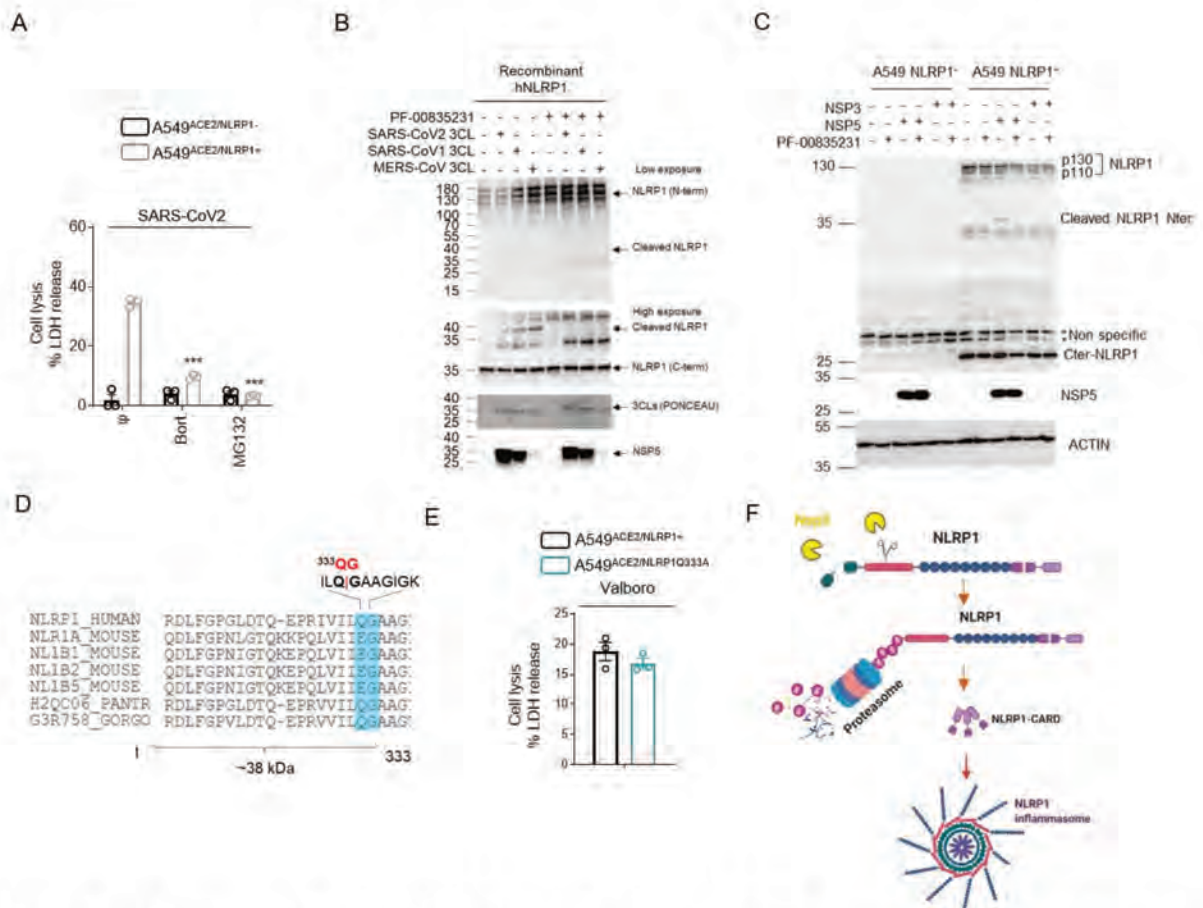


Figure S2 (Related to Figure 2). NSP5-cleaved NLRP1 nucleates inflammasome activation

(A) Measure of cell lysis (LDH release) in A549^{NLRP1+} or A549^{NLRP1-} infected with SARS-CoV-2 (MOI 0.05) for 24 hours in presence/absence of the proteasome inhibitors bortezomib (0.1 μ M) or MG-132 (0.1 μ M).

(B) Western blot examination of NLRP1 cleavage using an anti NLRP1 Nter antibody (aa1-323) upon co incubation of SARS-CoV-2, SARS-CoV1 or MERS-CoV 3CL (NSP5) proteases with recombinant human NLRP1 in presence or absence of the 3CL inhibitor PF-00835231 (10 μ M). NLRP1 N-terminal, NLRP1 C-terminal, NSP5 and ACTIN were immunoblotted.

(C) Western blot examination of NLRP1 cleavage using an anti NLRP1 N-terminal antibody (aa1-323) upon co incubation of SARS-CoV-2 NSP5 or SARS-CoV-2 NSP3 proteases with A549^{NLRP1+} cell lysates in presence or absence of the 3CL inhibitor PF-00835231 (10 μ M). NLRP1 Nter, NLRP1Cetr, NSP5 and ACTIN were immunoblotted.

(D) Sequence alignment of the NSP5-targeted human NLRP1^{Q333} site with mouse and primate NLRP1.

(E) Measure of cell lysis (LDH release) in A549^{NLRP1+} or A549^{NLRP1Q33A} treated with Valboro (10 μ M) for 10 hours.

(F) Proposed mechanism of human NLRP1 activation by NSP5 protease.

Data informations:

Western Blot (A-C) images are from one experiment performed three times. Graph E show data presented as means \pm SEM from n=3 independent pooled experiments; ***p \leq 0.001 for the indicated comparisons with t-test. G was created using biorender.com

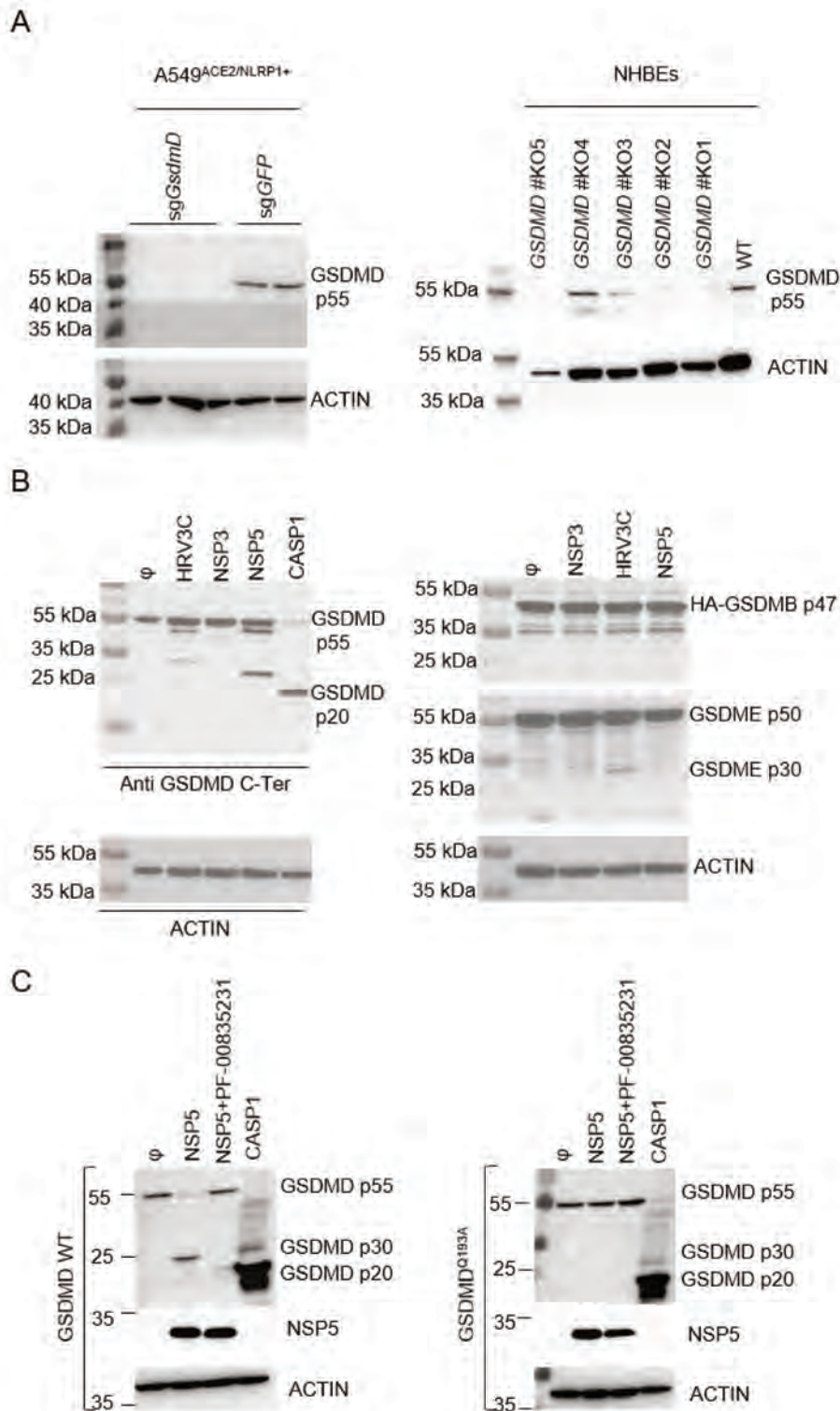


Figure S3 (Related to Figure 3). NSP5 cleaves and inactivates GSDMD

(A) Western Blot examination of genetic invalidation of GSDMD in A549^{NLRP1+} or NHBE cells using CRISPR Cas9 technic.

(B) Western blot examination of Gasdermin cleavages by SARS-CoV-2 NSP5 or NSP3, HRV3C or recombinant human Caspase-1 (CASP1) proteases in cell lysates from A549 expressing GSDMD, GSDMB or GSDME. GSDMD (anti Cter), GSDME, GSDMB, NSP5 and ACTIN were immunoblotted.

(C) Western blot examination of GSDMD cleavage by SARS-CoV-2 3CL (NSP5) or recombinant human Caspase-1 (CASP1) proteases in cell lysates from A549 expressing WT GSDMD or GSDMD^{193A} constructs in presence/absence of the 3CL inhibitor PF-00835231 (10 μ M). GSDMD (anti Cter), NSP5 and ACTIN were immunoblotted.

Data information:

Western Blot (A-C) images are from one experiment performed three times.

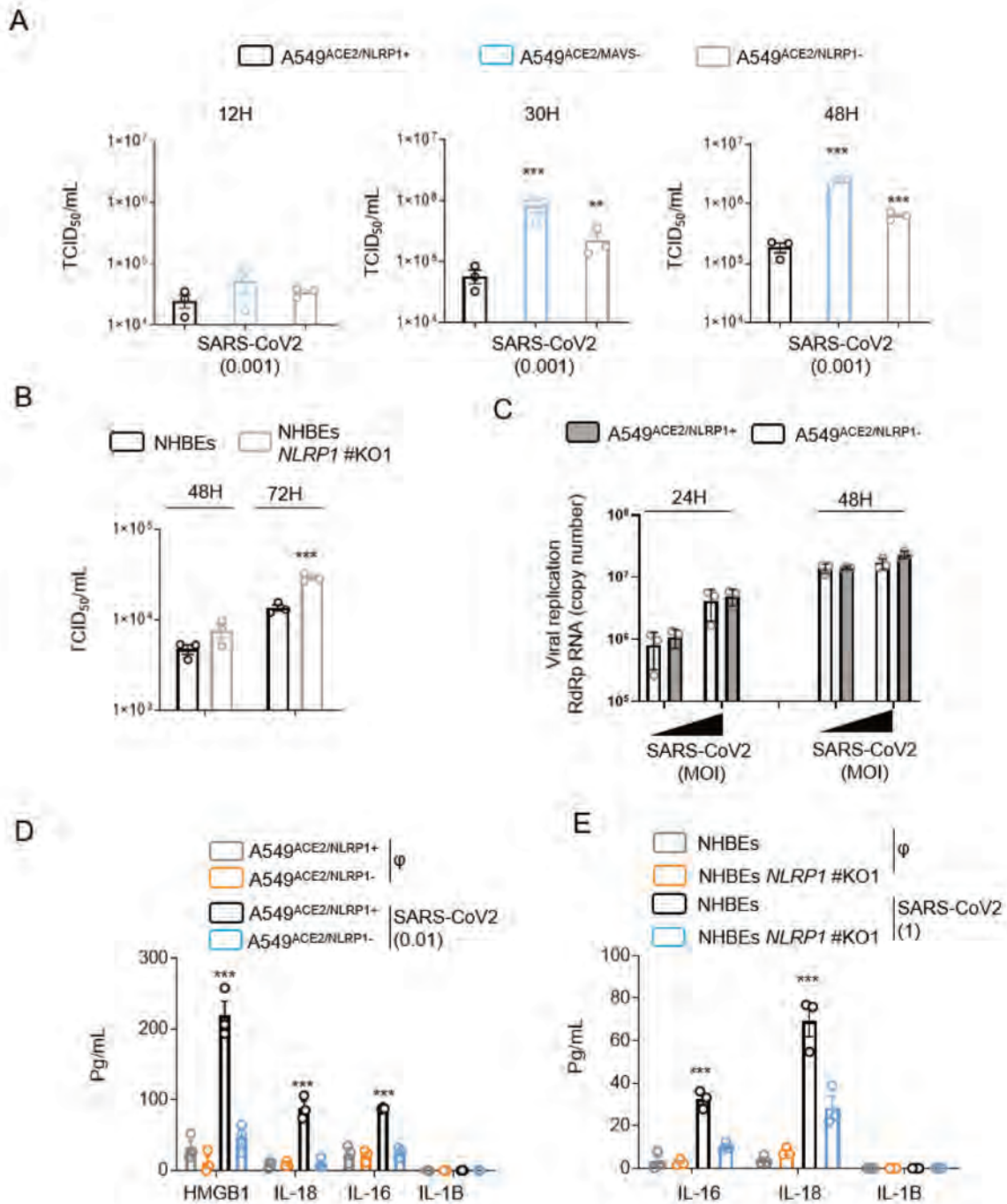


Figure S4 (Related to Figures 1-4). NLRP1-dependent pyroptosis both limits the production of infectious particles and promotes alarmin/DAMP release

(A) TCID₅₀ measure of production of infectious viral particles in A549^{ACE2/NLRP1+}, A549^{ACE2/NLRP1-} and A549^{ACE2/MAVS-} cells infected for various times with SARS-CoV-2.

(B) TCID₅₀ measure of production of infectious viral particles in NHBE^{WT} and NHBE^{*NLRP1*-/-} cells infected for various times with SARS-CoV-2 (MOI 0.5).

(C) Q-RT PCR evaluation of SARS-CoV-2 RdRp mRNA levels in A549^{ACE2/NLRP1+} or A549^{ACE2/NLRP1-} cells after 24 and 48 hours of SARS-CoV-2 infection (MOIs 0.05 and 0.005).

(D, E) Measure of the release of various Alarmins/Cytokines after 24 (D) or 36 (E) hours of infection with SARS-CoV-2 (MOI 0.05 and 1 respectively) by A549^{ACE2/NLRP1+}, A549^{ACE2/NLRP1-}, NHBE^{WT} and NHBE^{NLRP1-/-} cells.

Data informations:

Graphs A-E show data presented as means \pm SEM from n=3 independent pooled experiments; **p \leq 0.01, ***p \leq 0.001 for the indicated comparisons with t-test.

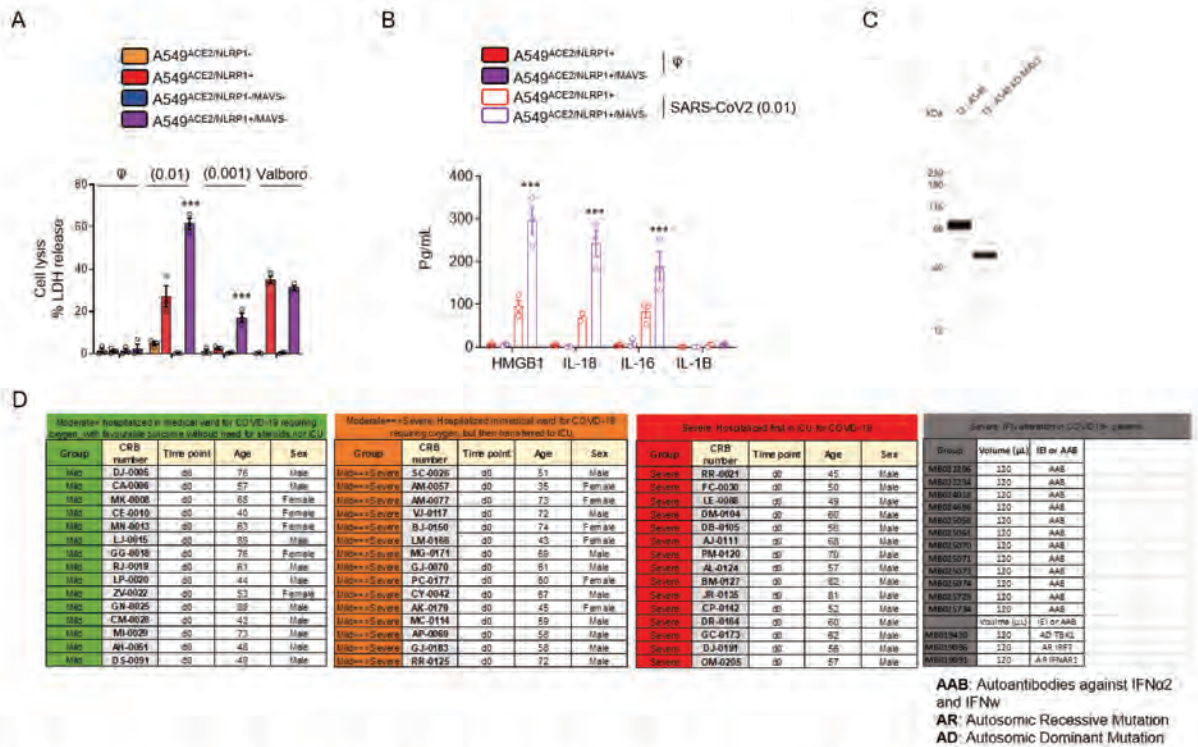


Figure S5 (Related to Figure 4). Plasmas from COVID19 patients show enrichments in (IL)-16/-18/GSDME and CASP3.

(A) Measure of cell lysis (LDH release) in A549^{NLRP1+}, A549^{NLRP1-}, A549^{NLRP1+/MAVS-} and A549^{NLRP1+/MAVS+} upon SARS-CoV-2 infection or Valboro (5 μ M) treatment for 24 hours.

(B) Measure of cytokine/alarmin release in A549^{NLRP1+} or A549^{NLRP1+/MAVS-} upon SARS-CoV-2 infection for 24 hours.

(C) Western Blot examination of genetic invalidation of MAVS in A549 cells. MAVS appears at the 66kDa.

(D) Information on COVID-19+ patients hospitalized and COVID-19+ patients exhibiting Interferon alterations used in this study

Data information:

Graphs A, B show data presented as means \pm SEM from n=3 independent pooled experiments; ***p \leq 0.001 for the indicated comparisons with t-test. Western Blot (C) image is from one experiment.

COVID Human Genetic Effort members and affiliations

The affiliations of the members of the COVID Human Genetic Effort are as follows.

Tayfun Ozcelik: Department of Molecular Biology and Genetics, Bilkent University, Bilkent - Ankara, Turkey

Nevin Hapitoglu: Pediatric Infectious Diseases Unit, Bakirkoy Dr. Sadi Konuk Training and Research Hospital, University of Health Sciences, Istanbul, Turkey

Filomeen Haerynck: Department of Pediatric Immunology and Pulmonology, Center for Primary Immunodeficiency Ghent, Jeffrey Model Diagnosis and Research Center, PID research lab, Ghent University Hospital, Ghent, Belgium

Sevgi Keles: Meram Medical Faculty, Necmettin Erbakan University, Meram Medical Faculty, Konya, Turkey

Ahmed A. Bousfiha: Clinical Immunology Unit, Department of Pediatric Infectious Disease, CHU Ibn Rushd and LICIA, Laboratoire d'Immunologie Clinique, Inflammation et Allergie, Faculty of Medicine and Pharmacy, Hassan II University, Casablanca, Morocco

Rafael Leon Lopez: Hospital Universitario Reina Sofía, Cordoba, Spain

2. Work context 2: EEF2-inactivating toxins engage the NLRP1 inflammasome and promote epithelial damage upon *Pseudomonas aeruginosa* infection

I. Study context and objectives

Pseudomonas aeruginosa is a gram-negative bacterium found ubiquitously in nature that infects most tissues in humans (cornea, lungs...) and exhibits a multi-drug resistance implicated in many economical and health repercussions. In humans, *P. aeruginosa* is known to lead to nosocomial infections but also to be an opportunistic pathogen causing acute or chronic infections, notably, in the lungs of cystic fibrosis (CF) patients. Cystic fibrosis (CF) is a recessive genetic disorder caused by mutations in the CFTR gene leading to inactivation, misfolding, or absence of the CFTR anion channel. This causes the build-up of thick mucus in the lungs, which represents a thriving environment for bacterial pathogens, especially *P. aeruginosa* which is the leading cause of death in cystic fibrosis patients. In CF patients, *P. aeruginosa* infection is often associated with chronic infection and biofilm formation. Interestingly, CF patients chronically infected with *P. aeruginosa* showed enrichment of IL-1 β in the bronchoalveolar lavage fluid (BALF) and strong damage and cell death in lung epithelial cells. These observations strongly suggested the implication of inflammasomes. During my PhD I was interested in deciphering the molecular mechanisms implicated in the cellular damage observed in the lung epithelium of CF patients chronically infected by *P. aeruginosa*.

To investigate that we used a model of human nasal epithelial cells that we infected with PAO1, a strain of *P. aeruginosa*. To mimic *P. aeruginosa* biofilm-like behaviour *in vitro*, we relied on a transwell-adapted method that allowed bacteria to grow on top of a 0.4 μ m porous membrane while epithelial cells were seeded on the bottom of the wells. We demonstrated that PAO1 is able to induce a pyroptotic form of cell death characterized by LDH, IL-1 β , and IL-18 release. We failed to detect NLRP3 expression and due to the important role of hNLRP1 in epithelia, we hypothesized that NLRP1 might be a sensor of extracellular *P. aeruginosa* in the airway epithelium. To address this question, we used our previously described epithelial lung A549-ASC-GFP reporter cell lines in which the hNLRP1 construct was stably introduced to investigate the molecular mechanism inducing hNLRP1 activation. Using different PAO1 strains (deleted for different types of secretion system) we demonstrate that the T2SS was implicated in the hNLRP1 activation and more precisely, that this activation was induced by Exotoxin A, a virulence factor secreted by the T2SS.

Recently, different works demonstrated that the human NLRP1 inflammasome can be activated downstream to ribotoxic stress response (RSR) initiated by the MAPKKK ZAK α and followed by p38 activation. While those original reports identified environmental (UVB) and viral stresses that could induce this pathway it was unclear whether microbial effectors would also induce NLRP1 activation via

RSR. Here, we demonstrated that *P.aeruginosa* (PAO1) induces NLRP1 activation through the Type 2 System Secretion (T2SS) effector Exotoxin A (ExoA) targeting and inhibiting the elongation factor EEF2 that therefore induces a ribosomal stress response (RSR). ExoA is sufficient to induce NLRP1 activation through the ribosomal stress response via ZAK α and p38 in human nasal and corneal primary epithelial cells. We finally observed that epithelial cells isolated from Cystic fibrosis patients show heightened inflammatory responses leading to increased cell death and IL18 release in response to RSR stimuli including ExoA. Interestingly, this increase is not observed during VBP-induced NLRP1 activation.

Altogether, our results show the importance of *P.aeruginosa* virulence factor ExoA in promoting NLRP1-dependent epithelial damage and identify ZAK α as a critical sensor of virulence-inactivated EEF2 suggesting the potential role of its inhibitors in treatment for CF patients chronically infected with *P.aeruginosa*.

Contribution

In this article, of which I am the first author. I performed and/or was involved in all the experiments.

II. Paper (Pinilla et al., 2023 under review in JEM)

1 **EEF2-inactivating toxins engage the NLRP1 inflammasome and**
2 **promote epithelial barrier disruption upon *Pseudomonas* infection**

3
4 Miriam Pinilla¹, Raoul Mazars¹, Romain Vergé¹, Leana Gorse¹, Karin Santoni¹, Kim
5 Samirah Robinson^{2,3}, Gee Ann TOH ^{2,3}, Laure Prouvensier⁴, Stephen Adonai Leon-
6 Icaza¹, Audrey Hessel¹, David Péricat¹, Marlène Murriss^{5,6}, Anthony Henras⁷, Julien
7 Buyck⁴, Céline Cougoule¹, Emmanuel Ravet⁸, Franklin L. Zhong^{2,3}, Rémi Planès^{1,8,*,#,¶},
8 Etienne Meunier^{1,*,#,¶}

9
10
11 ¹ Institute of Pharmacology and Structural Biology (IPBS), University of Toulouse, CNRS,
12 Toulouse, France.

13 ² Lee Kong Chian School of Medicine, Nanyang Technological University, 11 Mandalay
14 Road, 308232 Singapore, Singapore;

15 ³ Skin Research Institute of Singapore (SRIS), 11 Mandalay Road, 308232 Singapore,
16 Singapore.

17 ⁴ UFR Medicine and Pharmacy, INSERM U1070, University of Poitiers, Poitiers, France

18 ⁵ Department of pneumology, Hospital Larrey, Toulouse, France.

19 ⁶ University Hospital of Toulouse, France

20 ⁷ Center of Integrative Biology (CBI), University of Toulouse, CNRS, Toulouse, France.

21 ⁸ Invivogen, Toulouse, France

22
23 * r.planes@invivogen.com (RP), * etienne.meunier@ipbs.fr (EM)

24 # Current Address: Institute of Pharmacology and Structural Biology (IPBS), University of
25 Toulouse, CNRS, Toulouse, France

26
27 ¶ These authors equally supervised this work.

32 **KEY POINTS**

- 33 • *P. aeruginosa* induces NLRP1-dependent pyroptosis in human corneal and nasal
34 epithelial cells
- 35 • *P. aeruginosa* Exotoxin A (EXOA) and other EEF2-inactivating bacterial exotoxins
36 activate the human NLRP1 inflammasome
- 37 • EEF2 inactivation promotes ribotoxic stress response and ZAK α kinase-dependent
38 NLRP1 inflammasome activation.
- 39 • Bronchial epithelial cells from Cystic Fibrosis patients show extreme sensitivity to
40 ribotoxic stress-dependent NLRP1 inflammasome activation in response to
41 Exotoxin A
- 42 • P38 and ZAK α inhibition protects Cystic Fibrosis epithelial cell from EXOA-induced
43 pyroptosis

44
45 **ABSTRACT**

46 The intracellular inflammasome complex have been implicated in the maladaptive tissue
47 damage and inflammation observed in chronic *Pseudomonas aeruginosa* infection.
48 Human airway and corneal epithelial cells, which are critically altered during chronic
49 infections mediated by *P. aeruginosa*, specifically express the inflammasome sensor
50 NLRP1. Here, together with a companion study, we report that the NLRP1 inflammasome
51 detects Exotoxin A (EXOA), a ribotoxin released by *P. aeruginosa* Type 2 Secretion
52 System (T2SS) during chronic infection. Mechanistically, EXOA-driven Eukaryotic
53 Elongation Factor 2 (EEF2) ribosylation and covalent inactivation promotes ribotoxic
54 stress and subsequent NLRP1 inflammasome activation, a process shared with other
55 EEF2-inactivating toxins, Diphtheria Toxin and Cholix Toxin. Biochemically, irreversible
56 EEF2 inactivation triggers ribosome stress-associated kinases ZAK α - and P38-
57 dependent NLRP1 phosphorylation and subsequent proteasome-driven functional
58 degradation. Finally, Cystic Fibrosis cells from patients exhibit exacerbated P38 activity
59 and hypersensitivity to EXOA-induced ribotoxic stress-dependent NLRP1 inflammasome
60 activation, a process inhibited by the use of ZAK α inhibitors. Altogether, our results show
61 the importance of *P. aeruginosa* virulence factor EXOA at promoting NLRP1-dependent
62 epithelial damage and identify ZAK α as a critical sensor of virulence-inactivated EEF2.

63 INTRODUCTION

64 *Pseudomonas aeruginosa* is an opportunistic bacterial pathogen that can cause acute
65 and chronic life threatening infections (Qin et al., 2022; Maurice et al., 2018). Due to
66 widespread antibiotic resistance and its adaptation to the airway, skin and cornea of
67 immune-compromised patients (e.g. ciliated dyskinesia, chronic granulomatous diseases,
68 cystic fibrosis), *Pseudomonas aeruginosa* is listed as an important ESKAPE pathogen in
69 the WHO list of microbes of concerns (De Oliveira et al., 2020). *P. aeruginosa* can trigger
70 acute infections thanks to the expression of a Type 3 secretion system (T3SS), which
71 leads to a robust inflammatory reaction mostly mediated by monocytes/macrophages and
72 neutrophils (Qin et al., 2022). However, during chronic infections *P. aeruginosa* switches
73 into a metabolically different state that represses T3SS expression and allows the
74 expression and secretion of a different arsenal of effectors involved in the
75 formation/maintenance of biofilm-like structures, which are extremely resistant to
76 antibiotic treatments (Qin et al., 2022). In addition, the secretion of numerous matrix
77 remodeling factors such as (phospho)lipases, proteases, siderophores, oxidative and
78 toxic molecules strongly contribute to immune response deviation as well as to tissue
79 damages, including epithelial barrier disruption (Qin et al., 2022). In this context,
80 inflammatory mediator analysis from Cystic Fibrosis (CF) patients chronically infected
81 with *P. aeruginosa* highlights an enrichment in inflammasome-derived cytokine IL-1 β ,
82 suggesting that during the chronic step of *P. aeruginosa* infection one or many
83 inflammasomes might be activated (Bonfield et al., 2012). Given the prominent epithelial
84 cell damage observed in *P. aeruginosa* infected patients, and the poorly addressed
85 function of the epithelial barrier in antibacterial defense, we hypothesized that some
86 epithelial inflammasomes might respond to one or various factors released by *P.*
87 *aeruginosa* during chronic infections.

88 Inflammasomes, which mostly belong to the Nod-Like Receptor (NLR) and AIM2-Like
89 Receptor (ALRs) families, are a subset of germline-encoded innate immune sensors that
90 detect and respond to various signs of infections and environmental stresses (Lacey and
91 Miao, 2020). Upon activation, inflammasome-forming sensors assemble a cytosolic
92 supramolecular structure composed of the sensor/receptor, the adaptor protein ASC and
93 the protease Caspase-1. Inflammasome assembly leads to caspase-1-dependent

94 maturation and release of inflammatory cytokines IL-1 β and IL-18 as well as to pyroptosis,
95 a pro-inflammatory form of cell death characterized by gasdermin (D)-driven pore
96 formation and Ninjurin-1-dependent membrane disassembly (Kayagaki et al., 2021; Broz
97 and Dixit, 2016; Lacey and Miao, 2020).

98 The human NLRP1 inflammasome is notable among other inflammasome sensors
99 because of 1) its epithelia-restricted expression, 2) its divergence from rodent
100 counterparts and 3) its uncommon domain organization. Rare germline mutations and
101 single-nucleotide polymorphisms in NLRP1 are associated with infection sensitivity, skin,
102 corneal and intestinal inflammatory disorders as well as with asthma susceptibility in
103 humans, hence underlying an important function of NLRP1 at triggering an innate immune
104 response in various epithelia (Zhong et al., 2016; Griswold et al., 2022).

105 A conserved mechanism of NLRP1 inflammasome activation relies on proteasome-driven
106 degradation of the NLRP1 N-terminal autoinhibitory fragment (NT) and the subsequent
107 oligomerization of the released C-terminal fragment (CT), which nucleates the NLRP1
108 inflammasome assembly. To this regard, recent studies identified human-specific
109 mechanism of NLRP1 inflammasome activation, including the recognition of viral double-
110 stranded RNA, cleavage by 3C and 3CL proteases from rhinovirus and SARS-CoV-2
111 viruses as well as ZAK α and P38 stress kinase-driven phosphorylation upon exposure to
112 ribosome stressors (UV-B irradiation, anisomycin) (Tsu et al., 2021; Robinson et al., 2020;
113 Griswold et al., 2022; Bauernfried et al., 2021; Robinson et al., 2022; Jenster et al., 2023;
114 Fenini et al., 2018; Planès et al., 2022).

115 In this study, we discover that in human corneal and nasal epithelial cells, *P. aeruginosa*
116 contributes to barrier disruption by secreting the Eukaryotic Elongation Factor 2 (EEF2)-
117 inactivating toxin Exotoxin A (EXOA), which subsequently triggers assembly of the
118 NLRP1 inflammasome and release of associated IL-1 cytokine as well as pyroptotic cell
119 death. In this process, EXOA-inactivated EEF2 promotes ribotoxic stress response (RSR)
120 and subsequent activation of the stress kinases ZAK α and P38 (Wu et al., 2020; Vind et
121 al., 2020). Subsequently, activated ZAK α and P38 stimulate NLRP1 phosphorylation in
122 its disordered region, functional degradation and activation. Finally, Cystic Fibrosis cells
123 from patients show exacerbated P38 activity and hypersensitivity to EXOA-induced
124 ribotoxic stress-dependent NLRP1 inflammasome activation, a process reverted by the

125 use of ZAK α inhibitors. Altogether, our results describe the ability of *P. aeruginosa*
126 virulence factor EXOA at promoting NLRP1-dependent tissue damage and identify ZAK α
127 as a critical sensor of bacterial pathogen-driven ribosome inactivation.

128

129

130

131

132

133

134

135

136

137

138

139

140

141

142

143

144

145

146

147

148

149

150

151

152

153

154

155

156 RESULTS

157

158 *P. aeruginosa* infection activates the NLRP1 inflammasome in human corneal and 159 airways epithelial cells

160 Chronic infections mediated by *P. aeruginosa* can target various sites, including skin
161 (Spernovasilis et al., 2021), cornea (Hazlett, 2005) and airways/lung (Qin et al., 2022)
162 tissues. In certain contexts, *P. aeruginosa* metabolically transitions into a mucoid form
163 that enables biofilm formation. As chronically infected patients exhibit both epithelial
164 alterations and robust IL-1 β cytokine levels, we wondered about the contribution of
165 inflammasome response from epithelial compartments during *P. aeruginosa* infection. To
166 mimic *P. aeruginosa* biofilm-like behavior, we relied on a transwell-adapted method that
167 allowed bacteria to grow on top of a 0.4 μ m porous membrane and where epithelial cells
168 were seeded on the bottom of the wells (**Fig. 1A**). In this context, we analyzed the
169 inflammasome response (IL-1 β /IL-18 and cell death) of primary human corneal (pHCECs)
170 and nasal epithelial cells (pHNECs) co-cultured with *P. aeruginosa*. We observed that *P.*
171 *aeruginosa* triggered robust cell death and IL-1 β /IL-18 release both in pHNECs and
172 pHCECs (**Fig. 1A**). Importantly, the use of Z-YVAD, an inhibitor of Caspase-1 activity,
173 underscored that IL-1 β /IL-18 release fully depended on Caspase-1 activity while cell
174 death was partly dependent on Caspase-1, Caspase-3 and Caspase-8 (**Fig. 1A**). This
175 suggests that the inflammasome in pHNECs and pHCECs could contribute to IL-1 β /IL-18
176 and cell death in response to extracellular *P. aeruginosa*. In order to determine which
177 inflammasome is involved, we immunoblotted for various inflammasome-forming sensors
178 in those epithelial cells (**Fig. 1B**). Although we failed at detecting NLRP3 expression, we
179 could detect expression of the NLRP1 sensor in addition to the complete inflammasome
180 machinery (ASC, Caspase-1, GSDMD) both in nasal and corneal epithelial cells (**Fig. 1B**)
181 (Robinson et al., 2020; Griswold et al., 2022). Hence, we hypothesized that NLRP1 might
182 be a sensor of extracellular *P. aeruginosa* in the airway and corneal compartments. To
183 address this question, we used our previously described epithelial lung A549-ASC-GFP
184 reporter cell lines in which hNLRP1 construct was stably introduced (Planès et al., 2022).
185 Fluorescence microscopy and quantification of active inflammasome complexes (ASC-
186 GFP⁺ puncta/Specks) in co-cultured reporter cells unveiled that *P. aeruginosa* exposure

187 promoted the formation of inflammasome complexes as well as induced significant cell
188 death specifically in NLRP1-expressing cells (**Fig. 1C**). This suggested that NLRP1 could
189 be a sensor of a yet unknown secreted product by *P. aeruginosa*. To further determine
190 the involvement of NLRP1 in primary cells at responding to extracellular *P. aeruginosa*,
191 we invalidated NLRP1 expression in nasal and corneal epithelial cells by using CRISPR-
192 Cas9 method (**Fig. 1D**). Co-culture of WT and NLRP1-deficient cells with *P. aeruginosa*
193 showed that *NLRP1*^{-/-} cells exhibited a defect in cell death (measured by propidium iodide
194 incorporation and LDH release) as well as at releasing IL-1 β /IL-18 cytokines (**Fig. 1D, E**).
195 As hNLRP1 inflammasome activation requires ubiquitination and subsequent
196 proteasome-driven functional degradation, which releases the active NLRP1 C-Ter
197 fragment, we next incubated pHCECs with PAO1 or with Val-boro-pro (Vbp), a known
198 chemical activator of the NLRP1 inflammasome, in presence or absence of the
199 proteasome inhibitor bortezomib (**Fig S1A-C**). Measure of the pyroptosis pore forming
200 protein Gasdermin-D processing, hNLRP1 degradation, cell death and IL-1 β release in
201 pHCECs showed that proteasome inhibition strongly impaired those processes, hence
202 suggesting that the hNLRP1 inflammasome activation by *P. aeruginosa* occurs in a
203 proteasome-dependent manner in corneal and airway epithelial cells (**Fig S1A-C**).

204

205 **EEF2-inactivating Exotoxin A promotes NLRP1 inflammasome response**

206 As the NLRP1 inflammasome responds to a yet to be determined secreted product of *P.*
207 *aeruginosa*, we next wondered about the identity of this factor. *P. aeruginosa* expresses
208 various secretion systems (T1SS to T6SS) that allows either secreting or injecting various
209 elements (Filloux, 2011, 2022). Using co-cultures of A549-ASC-GFP/NLRP1 reporter
210 cells lines with PAO1 transposon mutants for different secretion systems, we observed
211 that Type-2 Secretion System (T2SS)-deficient PAO1 specifically failed at inducing
212 NLRP1 inflammasome complex assembly (**Fig. 2A**). Among other factors released by
213 PAO1 T2SS are phospholipases (PLCN, PLCH), elastase protease LASB and the
214 Exotoxin A (EXOA) (Liao et al., 2022). Using PAO1 transposon mutants for each of those
215 factors, we observed that only the PAO1 strain that is deficient for Exotoxin A (EXOA) lost
216 the ability of promoting the formation of the NLRP1 inflammasome in our reporter cell

217 lines (**Fig. 2B**). This suggests that T2SS-secreted EXOA is the major factor with which
218 extracellular *P. aeruginosa* activates the NLRP1 inflammasome in epithelial cells.

219 EXOA is a ribotoxin that irreversibly ribosylates the elongation factor EEF2, which leads
220 to ribosome inactivation (Jørgensen et al., 2005; Armstrong and Merrill, 2004), a process
221 we also observed by determining ribosome polysomes accumulation (marker of
222 alterations in translation machinery) and translation inhibition (puromycin incorporation as
223 a marker of translation efficiency) (**Fig. 2C, D**). In this context, to determine if EXOA
224 ribosylating activity was required for NLRP1 inflammasome response, we exposed
225 reporter cells to recombinant EXOA and the catalytically dead mutant EXOA^{H426A}, which
226 is unable to promote EEF2 ribosylation (Roberts and Merrill, 2002) (**Fig. 2E, S2A**).

227 Microscopy observation and quantifications of NLRP1 inflammasome complexes in
228 reporter cells showed that EXOA but not its mutant triggered robust inflammasome
229 formation (**Fig. 2E**). EEF2 ribosylation by EXOA requires the presence of a specific
230 modified form of Histidine 715 on human EEF2, namely Diphthamide (Liu et al., 2004;
231 Ivankovic et al., 2006) (**Fig. S2B**). This unique amino acid arises from the enzymatic
232 modification of Histidine by the so-called Diphthamide enzymes (DPHs) (Liu et al., 2004;
233 Ivankovic et al., 2006). Hence, using our reporter cells, we genetically deleted *DPH1*,
234 which is critical to initiate diphthamide synthesis (**Fig. S2C**). Analysis of NLRP1
235 inflammasome complexes in response to EXOA showed that *DPH1*-deficient cells failed
236 to assemble an active NLRP1 inflammasome complex (**Fig. S2D**). As control, activation
237 of the NLRP1 inflammasome by the Val-boro-pro (Vbp) molecule was not affected by the
238 removal of *DPH1*, suggesting that EXOA specifically activates the NLRP1 inflammasome
239 by promoting EEF2-ribosylation on the Diphthamide 715 amino acid (**Fig. S2D**). In
240 addition to EXOA, two other bacterial toxins, namely Diphtheria Toxin (*Corynebacterium*
241 *diphtheriae*) and Cholix toxin (*Vibrio cholera*) (Jørgensen et al., 2008) also promote
242 irreversible ribosylation of human EEF2 on Diphtamide 715 (Liu et al., 2004; Ivankovic et
243 al., 2006; Jørgensen et al., 2005). Hence, to determine if those toxins could also induce
244 NLRP1 inflammasome formation in a similar way than observed with EXOA, we exposed
245 NLRP1 reporter cell lines to those toxins. As for EXOA, we observed that Cholix Toxin
246 and Diphteria Toxin both triggered robust NLRP1 inflammasome complex assembly in
247 those reporter cells (**Fig. S2D**). Furthermore, NLRP1 inflammasome formation was

248 abrogated in *DPH1*-deficient A549 in response to Cholix Toxin and Diphtheria Toxin,
249 hence confirming the existence of a shared pathway for EEF2 inactivation by those toxins
250 **(Fig. S2D)**.

251 Finally, exposure of primary WT and NLRP1-deficient corneal epithelial cells to EXOA
252 highlighted an increased protection of *NLRP1*^{-/-} cells to cell pyroptosis, suggesting that
253 extracellular *P.aeruginosa*-induced NLRP1 inflammasome response in epithelial cells
254 requires T2SS-secreted EXOA and subsequent EEF2 inactivation **(Fig. 2F)**.

255

256 **EEF2 inactivation drives Ribotoxic Stress Response (RSR)-dependent ZAK α and** 257 **P38 MAPkinase activation and subsequent NLRP1 inflammasome nucleation**

258 Recent studies unveiled that ribosome inactivation by UV-B as well as the antibiotic
259 anisomycin also promote NLRP1 inflammasome activation in human keratinocytes
260 (Robinson et al., 2022; Jenster et al., 2023; Fenini et al., 2018). Furthermore, this mode
261 of activation engages the MAP3K ZAK α and the effector P38 α/β kinases (Robinson et al.,
262 2022; Jenster et al., 2023; Fenini et al., 2018). Thus we wondered if EXOA-driven EEF2a
263 irreversible inactivation and subsequent NLRP1 inflammasome formation might also
264 engages a similar pathway. We generated ZAK α -deficient reporter cell lines and
265 measured their ability to promote activation of the MAPK stress kinases in response to
266 EXOA exposure **(Fig. 3A, S3A)**. We observed that EXOA, but not its inactive mutant
267 EXOA^{H426A}, strongly induced P38 and JNK stress kinase phosphorylation, a process that
268 disappeared in absence of ZAK α **(Fig. 3A, S3A)**. Further analysis of NLRP1
269 inflammasome formation using fluorescence microscopy highlighted that ZAK α deficiency
270 completely abrogated assembly of the NLRP1 inflammasome and cell death in response
271 to EXOA **(Fig. 3B)**. To further analyze if ZAK α and its downstream effectors P38 were
272 important for NLRP1 inflammasome formation, we genetically deleted P38 α , P38 β or both
273 P38 α/β in reporter cells and quantified inflammasome assembly in response to EXOA
274 **(Fig. 3C, S3B)**. We observed that single deletion for P38 α or P38 β did not strongly modify
275 inflammasome assembly whereas combined deficiency for P38 α/β led to a robust defect
276 in NLRP1 inflammasome formation upon EXOA exposure **(Fig. 3C)**. This suggests that
277 ZAK α - and ZAK α -activated P38 kinases contribute to NLRP1 inflammasome response to
278 EXOA.

279 ZAK α and P38-driven phosphorylation of Serine and Threonines in the NLRP1 disordered
280 region has been recently shown to promote NLRP1 inflammasome activation upon UV-
281 B-driven ribosome collision (Robinson et al., 2022). Here, using NLRP1 constructs
282 mutated for either phosphorylation site 1 (¹¹⁰TST¹¹²) or site 2 (¹⁷⁸TST¹⁸⁰), we observed
283 that EXOA was unable to trigger assembly of the NLRP1 inflammasome in reporter cells
284 (**Fig. 3D, E**). To the contrary, Vbp- and SARS-CoV-2-induced NLRP1 inflammasome
285 assembly was fully efficient in cells complemented with either construct or in ZAK α -
286 deficient cells (**Fig. 3D, E, S3C**). All in one, those results suggest that ZAK α - and P38-
287 targeted NLRP1 site 1 and 2 is required for efficient inflammasome assembly in response
288 to EXOA but not during Vbp or SARS-CoV-2 exposure.

289

290 **Cystic fibrosis airway epithelial cells show exacerbated sensitivity to EXOA-driven** 291 **cell death, which is reversed by ZAK α inhibition**

292 Next we investigated the role of EXOA-driven pyroptosis in a patho-physiological model
293 of *P. aeruginosa* infection. In addition to causing corneal infections, *P. aeruginosa* is well
294 known to establish life-threatening infection in airways and lungs of Cystic Fibrosis (CF)
295 patients. Due to defective mucus production and clearance (Veit et al., 2016), the airway
296 of CF patients favor chronic *P. aeruginosa* infections. Collaborating with the Hospital of
297 Toulouse, we obtained nasal brushes from healthy and Cystic fibrosis patients carrying
298 the Δ F508 mutation in the CFTR (Δ F508 / 4005+1G>A and Δ F508 / N1303K, respectively
299 referred in the text and figure legends as CF donors 1 and 2) (**Fig. S4A**). CF patients
300 have been described to express very high basal and inducible P38 kinase activation (Raia
301 et al., 2005; Bérubé et al., 2010), a phenotype we could confirm by exposing or not those
302 cells to EXOA (**Fig. 4A**). Given the importance of P38 kinases at promoting EXOA-
303 dependent NLRP1 inflammasome response, we next measured the ability of healthy and
304 CF nasal cells to undergo EXOA-dependent cell death. Propidium incorporation measure
305 in healthy and CF nasal cells showed that EXOA-driven cell death was exacerbated in
306 CF nasal cells, a process that was reduced by the use of P38 inhibitor SB203580 (**Fig.**
307 **4B**). Further experiments also showed that ZAK α inhibition (PLX4720) even further
308 inhibited EXOA-driven cell death, Gasdermin D cleavage and IL-18 release both in
309 healthy and CF nasal cells (**Fig. 4C-F, S4B**). Such process was conserved with the

310 ribotoxic antibiotic anisomycin but not in response to Vbp where nasal cells from healthy
311 and CF patients responded similarly, hence suggesting that P38 pre-activation in CF
312 patients specifically sensitive them to ribotoxic stress-driven NLRP1 response, a process
313 that may contribute to *P. aeruginosa*-driven epithelial barrier disruption (**Fig. 4D-F, S4B**).
314 Altogether, our results suggest that the ZAK α /NLRP1 axis contributes to exacerbated
315 epithelial barrier destabilization upon EXOA-inactivated EEF2 exposure.

316

317 **DISCUSSION**

318 Chronic infections of multiple organs mediated by *P. aeruginosa* are a major source of
319 epithelium damage and inflammatory exacerbations. Due to the lack of robust and
320 relevant models of study as well as its remarkable adaptation to specific environments,
321 the impact of chronic infections mediated by *P. aeruginosa* on host epithelial integrity has
322 long been hard to address. Here, our findings and those from the Zhong group
323 (companion manuscript) that the T2SS-released Exotoxin A, and its relatives Cholix and
324 Diphtheria Toxins, trigger activation of the human NLRP1 inflammasome in skin
325 keratinocytes, corneal and airway epithelial cells, three important sites of *P. aeruginosa*
326 chronic infections. This process exemplifies a novel biochemical pathway by which
327 epithelial organs detect bacterial virulence factors.

328 Although major research studies unveiled that upon acute infection, *P. aeruginosa* T3SS
329 allows both activation of the NLRC4 and NLRP3 inflammasomes in rodent as well as in
330 human macrophage and neutrophil models (Sutterwala et al., 2007; Faure et al., 2014;
331 Franchi et al., 2007; Miao et al., 2008; Deng et al., 2015; Balakrishnan et al., 2018;
332 Santoni et al., 2022a; Ryu et al., 2016), chronic infections mediated by this pathogen is
333 associated with a downregulation of T3SS in favor a biofilm phenotype, where EXOA is
334 strongly produced and released. To this regard, our observation that EXOA-driven
335 ribotoxic stress contributes to exacerbated tissue damage and inflammation strongly
336 correlate with earlier studies which showed that EXOA-deficient bacteria triggered lower
337 tissue damages during infections of human and mice (Michalska and Wolf, 2015; Pillar
338 and Hobden, 2002). Even though the RSR-driven NLRP1 inflammasome path is not
339 conserved among rodents and humans, ZAK α -driven RSR constitutes a shared process
340 between both species, which suggests that evolution selected ZAK α as a versatile stress

341 sensor. To the contrary, for yet to be determined reasons, human-specific evolution has
342 linked RSR to NLRP1 inflammasome response in epithelia, which suggests a specific
343 importance for such selection.

344 A caveat of this work mostly relies on the yet to be determined identification of Ubiquitin
345 ligases that promote NLRP1 functional degradation upon ZAK α -driven phosphorylation,
346 which is currently under investigations. The sensitivity of NLRP1 activation to the Nedd8
347 inhibitor MLN4924 suggests that Nedd8-driven Cullin ligase activation is of major
348 importance in this process (Jenster et al., 2023; Robinson et al., 2022). Among the broad
349 family of Cullin ligases, Cull1 and 2 were found to target phosphorylated proteins for
350 Ubiquitination and subsequent degradation (Chen et al., 2021). Should one of those
351 Ubiquitin ligase complex be involved constitutes an attractive hypothesis to pursue.

352 In addition to UVB, Chikungunya virus, the antibiotic anisomycin and the fungal toxin DON
353 (Fenini et al., 2018; Jenster et al., 2023; Robinson et al., 2022), our work, along the one
354 from Zhong lab, unveils the critical involvement of the NLRP1 inflammasome upon
355 infections mediated by various bacterial pathogens, including *C. diphtheria* and *P.*
356 *aeruginosa*. To this regard, patients developing Cystic fibrosis (CF) show exacerbated
357 inflammation and tissues damages upon chronic infection with *P. aeruginosa*. Specific
358 studies highlighted that stress-activated kinases P38 and JNK were over activated in CF-
359 derived cells from patients (Bérubé et al., 2010; Raia et al., 2005). Although various
360 hypothesis were developed to explain such dysregulation in CF patients, no study,
361 including ours, could unveil the critical molecular and biochemical mechanisms engaged,
362 which warrants for further investigations. However, our findings that in this context,
363 EXOA- but also other RSR inducers specifically triggered an exacerbated cell death
364 response suggest that targeting ZAK α and/or P38 kinases in *P. aeruginosa*-infected
365 patients might constitute a good host-targeted approach in order to limit epithelial
366 damages complementary to the current antibiotic and CFTR modulator strategy used
367 (Kaftrio | European Medicines Agency).

368 Finally, it is long been noted that host EEF2 (and EEF1) is targeted by a variety of
369 exotoxins from different unrelated bacterial species. Indeed, EEF2 is highly conserved in
370 all eukaryotic species, all expressing a specific diphtamide amino acid. In this context,
371 yeasts as well as mammals are similarly targeted by EXOA and relative toxins, which

372 underlines the outstanding adaptation of *P. aeruginosa* to its environment but also raises
373 the question of the specific species where EXOA holds the most prevalent/potent role for
374 bacterial development/survival. Another key question lies on the recent identification
375 DPH1 and 2 deficient patients (Urreizti et al., 2020; Nakajima et al., 2018; Hawer et al.,
376 2020). If those deficiencies might actually confer a selective advantage or not to *C.*
377 *diphtheria*, *V. cholera* or *P. aeruginosa* infections will constitute an exciting field of
378 investigations, as previously observed for HIV- or-malaria-resisting patients (Samson et
379 al., 1996; Allison, 1954) or recently highlighted for *Yersinia pestis*-shaped
380 selection/evolution of the inflammasome-forming sensor PYRIN (Park et al., 2020).
381 All in one, our results describe the critical role of ZAK α -driven NLRP1 inflammasome
382 response and epithelial disruption in response to the pathogen *P. aeruginosa*, and
383 exemplify its deleterious potential in CF pathogenesis.

384

385 **ACKNOWLEDGMENTS**

386 We are extremely grateful to patients and their families for their willingness of participating
387 to this study. Authors also warmly acknowledge Y. Rombouts, L. Boyer, T. Henry, M.
388 Tiraby and all lab members for their outstanding advices and support on this project.

389 This project was supported by the ATIP-Avenir program (to EM), FRM “Amorçage Jeunes
390 Equipes” (AJE20151034460 to EM), the Agence Nationale de la Recherche (ANR
391 Psicopak to EM), the ANRS-MIE (to EM), the ERC (StG INFLAME 804249 to EM), the
392 European Society of Clinical Microbiology and Infectious Diseases (ESCMID, to RP),
393 Invivogen-CIFRE PhD grant (to MP), Vaincre La Mucoviscidose (VLM) and Region
394 Occitanie (GRAINE) grants to CC.

395 The funders had no role in study design, data collection and analysis, decision to publish,
396 or preparation of the manuscript.

397

398

399

400

401

402

403 **MATERIAL AND METHODS**

404

405 **Ethic statements:** Patient data and tissue collection was performed in agreement with
 406 European Network of Research Ethics Committees and French ethic law. The ethical
 407 committee, according to the Medical Research Involving Human Subjects Act, reviewed
 408 and approved the study. Human tissue was provided by the University Hospital of
 409 Toulouse (France) and CNRS (agreements CHU 19 244 C and CNRS 205782). All
 410 patients involved in this study declared to consent to scientific use of the material; patients
 411 can withdraw their consent at any time, leading to the prompt disposal of their tissue and
 412 any derived material.

413

414 **Reagent used in the study**

Antibody	Catalog Reference	Provider
Rabbit anti-ZAK antibody 1: 1000	A301-993A	Bethyl Laboratories
P38 MAPK antibody 1: 1000	9212S	Cell signaling
Phospho-P38 MAPK (Thr180/Tyr182) (D3F9) XPRabbit mAb 1: 1000	4511S	Cell signaling
JNK1 Rabbit anti-Human Polyclonal 1: 1000	44690G	Invitrogen
Phospho-SAPK/JNK (Thr183/Tyr185) (81E11) Rabbit mAb 1: 1000	4668S	Cell signaling
Anti NLRP1 1:200	679802	Biolegend
Anti NLRP1 (N-terminal) 1: 1000	AF6788-SP;RRID: AB_2916167	R&D systems
Anti- NLRP1 (C-terminal), 1: 1000	ab36852;RRID: AB_776633	abcam
anti-Sheep igG HRP (1/4000)	HAF016;RRID: AB_562591	R&D

Goat-anti-rabbit IgG (H+L), HRP conjugate (1/5000)	R-05072-500;RRID: AB_10719218	Advansta
GSDMDC1 antibody 1: 1000	NBP2-33422	biotechne
Anti-Puromycin Antibody, clone 12D10	MABE343	Sigma
EEF2 antibody (1:1000)	2332S	Cell signaling
DPH1 antibody (1:1000)	# H00001801-M02	ThermoFisher scientific
Anti-alpha Tubulin antibody 1: 1000	ab4074	Abcam
Streptavidin - HRP	434323	ThermoFisher scientific
Reagents	Catalog Reference	Provider
Transwell	140620	ThermoFisher scientific
NAD+, Biotin-Labeled	80610	BPSBioscience
Pseudomonas exotoxin A 0.5 mg	P0184-.5MG	sigma
Inactive Exotoxin A	N.A.	Creative Diagnostics
Diphtheria Toxin	D0564-1MG	Sigma
Cholix toxin	This study	This study
Anisomycin	SE-S7409-10MG	selleck
Talabostat (Vbp)	tlrl-vbp-10	invivoGen
PhoSTOP	4906845001	sigma/Roche
cOmplete, Mini, EDTA-free Protease Inhibitor Cocktail	4693159001	Sigma/roche
Lipofectamine LTX	15338030	Invitrogen
Puromycin Dihydrochloride	A1113803	gibco

Molecular Probes SYTOX Green Nucleic Acid Stain	S7020	Thermofisher
Propidium iodide	P1304MP	Thermofisher
Nate	lyec-nate	Invivogen
Critical commercial assays	Catalog Reference	Provider
Human total IL-18 duo set	DY318-05	R&D
Cyquant LDH	C20301	Thermofisher
Human IL-1beta	88-7261-77	Thermofisher
Q5 Site-Directed Mutagenesis Kit Protocol	E0554	NEB
Chemicals	Catalog Reference	Provider
ZAK inhibitor (PLX-4720) 10µM	HY-51424	Med Chem Express
P38 inhibitor SB 203580 10µM	HY-10256	Med Chem Express
Caspase-1 inhibitor - Ac-YVAD-cmk 20µM	inh-yvad	invivogen
Z-VAD-FMK 20µM	vad-tlrl:	invivogen
Caspase-3/7 inhibitor ZDEVD-FMK 20µM	S7312	Selleck
Caspase-8 inhibitor - Z-IETD-FMK	inh-ietd	invivogen
Bortezomib 1µM	S1013	selleck
Cycloheximide (CHX)	C4859-1ML	Sigma
Human Primary Nasal Epithelial cells	Catalog Reference	Provider

Tryple Express Enzyme (1X), no phenol red	10718463	Fisher Scientific
Nutrigen Type I Collagen Solution, 6 mg/ml (Bovine)	5010-50ML	Advanced Biomatrix
Sputolysin	560000-1SET	Sigma
PneumaCult-Ex Plus Medium	05040	Stem cell
Costar 6.5 mm Transwell, 0.4 µm Pore Polyester Membrane Inserts	38024	Stem cell
Human Primary Corneal epithelial cells	Catalog Reference	Provider
Human Corneal Epithelial Cell Growth Medium	221-500	Tebu-bio
Human corneal epithelial cells	630-05a	Tebu-bio
Cell lines	Catalog Reference	Provider
A549 ASC GFP NLRP1	a549-ascg-nlrp1	Invivogen
A549 ASC GFP	a549-ascg	Invivogen
A549 ASC GFP NLRP1/ACE2	a549-ascov2-nlrp1	Invivogen
A549 ASC GFP ACE2	a549-ascov2	Invivogen
Recombinant DNA	Catalog Reference	Provider
hNLRP1 gene	puno1-hnalp1a	Invivogen

415

416 **Cell culture**

417 A549 cells were maintained in Dulbecco's modified Eagle's medium (DMEM, Gibco)
418 supplemented with 10% heat-inactivated fetal bovine serum (FBS), 1% penicillin-
419 streptomycin, and 1% L-glutamine at 37°C 5% CO₂. Primary Human Corneal epithelial
420 cells were maintained in Human Corneal Epithelial Cell Growth Medium (Tebu-bio) at
421 37°C 5% CO₂.

422 Regarding primary Human Nasal Epithelial Cells (pHNECs), patients' pHNECs were
423 collected on superior turbinates using smear brushes at the Hospital of Toulouse, France.

424 After brushing back cells in collection medium, centrifugation was performed for 5 min
425 400g at 4°C. Pellet was resuspended in 4 ml TrypLE express (GIBCO) + 20µl Sputolysin
426 (200X) and incubated at 37°C for 5 minutes to disrupt mucus. TrypLE was diluted with 4
427 ml of Advanced DMEM F12- .

428 Pellet was recovered after centrifugation and culture was continued in the expansion
429 medium Pneumacult). After a week of proliferation, basal cells were counted and seeded
430 onto collagen-coated (0.03mg/mL) and maintained in Pneumacult Ex Plus Medium
431 (StemCell) at 37°C 5% CO₂.

432

433 **Cell Stimulations**

434 Otherwise specified, cells were plated one day before stimulation in 12-well plates at 200
435 000 cells per well in 1mL of DMEM, 10% FCS, 1% PS.

436 Medium was changed to OPTIMEM and cells were preincubated or not with the indicated
437 inhibitors during 1 hour.

438 The pHNE cells were seeded the day before the stimulation in 12-well plates at 200 000
439 cells per well in 1mL of pneumacult medium. Cell's medium was changed to OPTIMEM
440 and cells were treated or not with the indicated inhibitors during 1 hour.

441 The pHCE cells were seeded the day before the stimulation in 12-well plates at 10 000
442 cells per well in 1 mL of corneal epithelial cell growth medium. Medium of the cells was
443 changed to OPTIMEM and cells were treated or not with the indicated inhibitors during 1
444 hour.

445 All cells were treated with the indicated concentration of Exotoxin A (EXOA, 10 ng/mL to
446 1µg/mL), anisomycin (1µM) or with Val-boroPro (15µM) for indicated times.

447 SARS-CoV-2 (BetaCoV/France/IDF0372/2020 isolate) experiments were performed in
448 BSL-3 environment as described in (Planès et al., 2022).

449 Briefly, 250,000 A549^{ASC-GFP/NLRP1/ACE2}, genetically invalidated or not for ZAKα, were
450 infected for 24 hours with BetaCoV/France/IDF0372/2020 strain at indicated MOI in
451 DMEM supplemented with 10mM HEPES, 1% penicillin-streptomycin and 1% L-Glutamine
452 for 1h at 37°C.

453

454

455 **Transwell infections**

456 A549 cells, expressing or not NLRP1, along with the ASC-GFP reporter, were plated in
457 24 well plates at $2, 5 \cdot 10^5$ cells per well one day before experiment. The following day, cell
458 culture media was replaced by 600 μ L of OPTI MEM per wells. Cells were placed in co-
459 culture with Pao1 bacteria WT or mutant (as indicated) at MOI of 10, in 100 μ L of OPTI
460 MEM separated by a semi-permeable transwell insert (0,3 μ m). After 18 hrs of co-culture,
461 transwell inserts containing bacteria were removed and ASC-speck formation in A549 cell
462 was analyzed. Images were acquired using EVOS M700 microscope.

463

464 **Bacterial growth and mutants**

465 *P. aeruginosa* strains (PAO1) and their isogenic mutants were grown in Luria Broth (LB)
466 medium overnight at 37°C with constant agitation. The following day, bacteria were sub-
467 cultured by diluting overnight culture 1:25 and grew until reaching an optical density (OD)
468 O.D.600 of 0.6 – 0.8.

469 PAO1 and its transposon mutants were obtained from two-allele transposon library
470 (Jacobs et al., 2003).

471

Name	Exact	Location	ORF	Gene Abbrev.
PW3079	+	phoAwp05q1C05	PA1148	toxA (EXOA)
PW2538	+	phoAwp03q1H07	PA0844	plcH (PLCH)
PW6586	+	phoAwp08q2E01	PA3319	plcN (PLCN)
PW6221	+	lacZwp03q2D06	PA3105	xcpQ (T2SS)
PW7302	+	phoAbp02q4F10	PA3724	LasB (LASB)
PW4017	+	lacZbp02q3F02	PA1706	pcrV (T3SS)
PW10311	+	lacZbp02q1B09	PA5503	ABC transporter (T1SS)

472

473 Specific deletion of xcpQ (T2SS) and toxA (EXOA) genes was achieved as described
474 previously in (Santoni et al., 2022b). Briefly, pEXG2 suicide vector containing 700-bp
475 sequences of the flanking regions of the selected gene was directly inserted into
476 competent SM10 λ pir (Mix&Go competent cells, Zymo Research Corporation) and

477 subsequently selected on LB-Agar supplemented with 50 µg/mL kanamycin /15 µg/mL
 478 gentamicin. After sequencing resulting clones were mated with PAO1 strains, 4H/37°C.
 479 Mated bacteria were plated on 15 µg/mL gentamicin and 20 µg/mL Irgasan LB-Agar
 480 plates in order to selectively remove E.coli SM10 strains. Next day, 5-10 clones were
 481 grown for 4h in LB and streaked on 5% sucrose LB plates overnight at 30°C. PAO1 clones
 482 were then checked by PCR for mutations.
 483

Name	Sequence	Targeted Gene
607_JB_PA_m _toxA_R1 Fw	CCCAGTCTCGAGGTTCGACGGTATCGATAAGCTTGAT ATCGAATTCggccgacggcggc	toxA
608_JB_PA_m _toxA_R1 Rv	tcgcgatgcacctgacacccgaggacctgaagtaactgccgc	toxA
609_JB_PA_m _toxA_R2 Fw	ggcagttacttcaggtcctcgggtgtcaggtgcatcgc	toxA
610_JB_PA_m _toxA_R2 Rv	CTGGAGCTCCACCGCGGTGGCGGCCGCTCTAGAAC TAGTGGATCCagccattgttcgacgaataaagccacc	toxA
611_JB_PA_m _toxA_Check R1	gaagtactcaacgggttgatcccc	toxA
612_JB_PA_m _toxA_Check R2	cgttccgcaacgcttgaagt	toxA
EM019-xcpQ R1 Fw	ttccacacattatacgagccggaagcataaatgtaaagcaagcttACGAT AAAGACCAGGAGTGATGTATTGCC	XcpQ
EM020-xcpQ R1 Rv	CGCCGTTATTCCGTCATCAGCAAAGGCTGGGACATC GG	XcpQ
EM021-xcpQ R3 Fw	ACCCGATGTCCCAGCCTTTGCTGATGACGGAATAAC GGCGCC	XcpQ
EM022-xcpQ R3 Rv	ggaaattaattaaggtaccgaattcgagctcgagccggggatccACGC CTGGTTCGTGGC	XcpQ

EM023-xcpQ R1 check	CCCGGCCAGTCACACCTATTGAT	XcpQ
EM024-xcpQ R3 check	AGTGCTTGCCGACAACGACC	XcpQ

484

485 **Cell death assays**

486 Cell lysis was measured by quantification of the lactate dehydrogenase (LDH) release
 487 into the cell supernatant using LDH CyQUANT kit (Thermofisher). Briefly, 50 µL cell's
 488 supernatants were incubated with 50 µL LDH substrate and incubated for 30 min at room
 489 temperature protected from light.. The enzymatic reaction was stopped by adding 50 µL
 490 of stop solution. Maximal cell death was determined with whole cell lysates from
 491 unstimulated cells incubated with 1% Triton X-100

492

493 **Plasma membrane permeabilization assays were performed using propidium**
 494 **iodide incorporation.** Cells were plated at density of 1×10^5 per well in Black/Clear 96-
 495 well Plates in OPTI-MEM culture medium supplemented with Propidium Iodide dye
 496 (1µg/mL) and infected/treated as mentioned in figure legends. Red fluorescence is
 497 measured in real-time using a Clariostar plate reader equipped with a 37°C cell incubator
 498 or using an EVOS Flouid microscope (Invitrogen). Maximal cell death was determined with
 499 whole cell lysates from unstimulated cells incubated with 1% Triton X-100.

500

501 **Cytokine quantification**

502 Cytokines secretions was quantified by ELISA kits, according to the manufacturer's
 503 instructions, IL-1B (Thermo Fisher Scientific, (88-7261-77), IL-18 (Biotechne, DY318-05).

504

505 **Sample preparation for immunoblot**

506 At the end of the experiment, cell' supernatant was collected and soluble proteins were
 507 precipitated using trichloroacetic acid (TCA) as described previously (Santoni et al.,
 508 2022b). Precipitated pellet was then resuspended in 50 uL of RIPA buffer (150 mM NaCl,
 509 50 mM Tris-HCl, 1% Triton X-100, 0.5% Na-deoxycholate) supplemented with protease
 510 inhibitor cocktail (Roche). Adherent cells were lysed in 50 uL of RIPA buffer supplemented

511 with protease inhibitor cocktail (Roche). Cell lysate and cell supernatant were
512 homogenized by pipetting up and down ten times and supplemented with laemli buffer
513 (1X final) before boiling sample for 10 min at 95°C.

514

515 **Immunoblot**

516 Cell lysates were separated by denaturing SDS-PAGE and transferred on PVDF
517 membrane. After transfer, the membrane is saturated 1h at room temperature in TBS-T
518 (Tris 10 mM pH 8, NaCl 150 mM, Tween 20 0.05%) containing 5% BSA. Then, the
519 membrane is incubated overnight at 4°C with the different primary antibodies, under
520 agitation. After 3 washes with TBS-T, the membrane is further incubated with the
521 secondary antibodies coupled with the peroxidase enzyme HRP (horseradish
522 peroxidase) for 1 hour at room temperature and under agitation. Then membranes are
523 washed 3 times with TBS-T. ECL revelation kit (Advansta) was used as a substrate to
524 reveal HRP activity and membranes are imaged using ChemiDoc Imaging System
525 (BioRad). The primary antibodies and secondary antibody used are listed in Reagent
526 table.

527

528 **Phosphoblots**

529 At the end of the experiment, cell' supernatant was discarded and adherent cells were
530 lysed in 50 uL of RIPA buffer (150 mM NaCl, 50 mM Tris-HCl, 1% Triton X-100, 0.5% Na-
531 deoxycholate) supplemented with protease inhibitor cocktail (Roche) and phosphatase
532 inhibitors cocktails (Roche). Collected cell lysate was homogenized by pipetting up and
533 down ten times and supplemented with laemli buffer before boiling for 10 min at 95°C.
534 Cell lysates were then separated by SDS-PAGE and handled as described in the
535 immunoblot section.

536

537 **Puromycin incorporation**

538 The day before the stimulation A549 ASC-GFP expressing or not NLRP1 were seeded in
539 12-well plates at 200 000 cells in 1mL of DMEM 10% FCS 1% PS. Cells were treated with
540 exotoxin A (10 ng/mL) for indicated times. 30 min before the end of the treatment
541 puromycin antibiotic was added in cell medium at 1ug/mL final. Following puromycin

542 incubation, supernatant was discarded and adherent cells were prepared for immunoblot
543 as described in the immunoblot section. Puromycin incorporation was revealed using the
544 following antibody Anti-Puromycin Antibody (clone 12D10 MABE343).

545

546 **Polysomes Profiling.** Sucrose gradient preparation. Five sucrose solutions containing
547 10 %, 20 %, 30 %, 40 % and 50 % sucrose (w/v) were prepared in TMK buffer (20 mM
548 Tris-HCl pH 7.4, 10 mM MgCl₂, 50 mM KCl). Layers of 2.1 mL of each solution were
549 successively poured into 12.5 mL polyallomer tubes (Beckman-Coulter, Cat. # 331372),
550 starting from the most concentrated solution (50 %) at the bottom of the tubes to the least
551 concentrated solution (10 %) at the top. Each layer was frozen in liquid nitrogen before
552 pouring the following one. Frozen gradients were stored at - 80 °C and slowly thawed
553 overnight at 4°C before use. Extract preparation. A549 cells were grown to 70%
554 confluency and then treated or not with exotoxin A (10 ng/mL) for indicated times.
555 Following this treatment, cells were incubated with Cycloheximide (CHX, 100 ug/mL) for
556 15 min at 37°C. Following treatment, cells were rinsed twice with PBS and treated with
557 1mL of trypsin (0,25%) for 5 min at 37°C. Trypsin was diluted with DMEM medium
558 containing 100 ug/mL of CHX. Cells were mixed up and down and counted to adjust the
559 final resuspension volume in each condition. Cells were centrifuged at 1200 rpm (300g)
560 for 5 min at 4°C. The cell pellet was washed with ice-cold PBS containing 100ug/mL of
561 CHX. Cells were centrifuged at 1200 rpm (300g) for 5 min at 4°C. Supernatants were
562 aspirated and gently lysed in lysis buffer (20 mM Tris-Cl [pH 8], 150 mM KCl, 15 mM
563 MgCl₂, 1% Triton X-100, 1mM DTT, 100ug/mL CHX, EDTA-free and Protease inhibitor
564 cocktail. Samples were incubated on ice for 20 min and centrifuge at 1000 g for 5 min at
565 4 °C min and supernatant corresponding to the cytosolic fraction of the cells were
566 collected into a 1.5 mL tube. Samples were further centrifugated at 10 000 g for 5 min at
567 4°C to clarify the cytoplasmic extract. Extracts were quantified by measuring absorbance
568 at 260 nm using Nanodrop.

569

570 **Extracts loading, gradient centrifugation and collection.** Normalized amounts of
571 extracts were loaded on 10–50% sucrose gradients, and then centrifuged at 260,800 x
572 g for 2.5 h at 4°C in an Optima L-100XP ultracentrifuge (Beckman–Coulter) using the

573 SW41Ti rotor with brake. Following centrifugation, fractions were collected using a Foxy
574 R1 gradient collector (Teledyne Isco) driven by PeakTrak software (Version 1.10, Isco
575 Inc.). The A_{254} was measured during collection with a UA-6 UV/VIS DETECTOR
576 (Teledyne Isco). The final polysome profiles were generated in Excel from .txt files
577 extracted from PeakTrak software.

578

579 **EEF2 ribosylation assays**

580 Cell lysates from A549 were prepared by suspending one pellet of $1 \cdot 10^6$ A549 cells in 100
581 μ L of RIPA buffer. For in-vitro ADP-ribosylation assays, reactions were performed in
582 Eppendorf tube by mixing 50 μ L of whole cell lysate with 100 μ L of ADP-ribosylation buffer
583 [20 mM Tris-HCl (pH 7.4), 150 mM NaCl and 1 mM DTT] supplemented with NAD⁺ Biotin-
584 Labeled (BPSBioscience) at 50 μ M final, in presence or absence of recombinant EXOA
585 protein (100 ng). Reaction was left for 1h at 25°C. 20 μ L of the reaction was analyzed by
586 SDS-PAGE followed by Western blotting as described in the immunoblot section.
587 Membranes were first subjected to EEF2 detection (using anti-EEF2 followed by HRP-
588 conjugated secondary antibody), then membranes were stripped, and ADP-ribosylation
589 was detected by monitoring the incorporation of the NAD⁺ Biotin-Labeled probe using
590 streptavidin-HRP-conjugate.

591

592 **Generation of mutations in NLRP1 gene**

593 To generate NLRP1 gene mutated for each phosphorylation sites (site 1 (¹¹⁰TST¹¹²) or
594 site 2 (¹⁷⁸TST¹⁸⁰)) Threonines and Serines were substituted with Alanine in the human
595 NLRP1 gene (isoform 1) by site-directed mutagenesis using Q5 site-directed
596 mutagenesis Kit Protocol (E0554) according to the manufacturer's instructions. Following
597 primers were used:

598

Primer FWD site 1 (3406-3414)	cgccGCAGTGCTAATGCCCTGG	68°C
Primer RV site 1	gcggcGGGTTGGCTGGGAGACCC	68°C
Primer FWD site 2 (3604-3612)	cgcaGCAGTGCTGGGGAGCTGG	72°C

Primer RV site 2	gctgcGGGGGCGTTGGGTGACTC	72°C
------------------	-------------------------	------

599

600 **Cell transfection**

601 The day prior to the transfection, A549 cells were plated in 6 well plate at 2×10^5 cells per
602 well in 1ml of DMEM complete medium. The following day, cells were incubated with Nate
603 1X (Invivogen) for 30 min. 1 μ g of NLRP1 plasmids (pLvB72 hNLRP1, pLvB72
604 hNLRP1(3604-3612), pLvB72 hNLRP1 (3406-3414) were transfected using lipofectamine
605 LTX and PLUS reagent according to the manufacturer's instructions (Invitrogen).
606 Transfected cells were incubated for 48 h before further treatments.

607

608 **Cholix toxin production**

609 Recombinant cholix toxin (ChxA) was produced using an adapted methodology from
610 (Ogura et al., 2011). Briefly, BL21 (DE3) *E. coli* expressing chxA with a N-terminus
611 hexahistidine-MBP-tag were harvested and bacteria were lysed by sonication on ice.
612 Recombinant cholix toxin was first purified on nickel metal affinity chromatography
613 (Takara) and subsequent TEV protease-mediated 6His-MBP tag removal at 4°C/Over
614 Night (ON). Then, a second nickel metal affinity chromatography allowed harvesting
615 Cholix toxin in the flow-through fraction.

616

617 **Genetic invalidations**

618 Genetic invalidation of NLRP1 in primary Human Nasal Epithelial Cells (pHNEs) and
619 primary Human Corneal Epithelial Cells (pHCECs) was achieved by using
620 Ribonucleoprotein (RNP) technic and nucleofection as described previously (Planès et
621 al., 2022). RNP mixes containing Cas9 protein (90pmoles, 1081059, IDT), gRNA
622 (450pmoles) and electroporation enhancer (1 μ L/Mix, 1075916, IDT) were electroporated
623 using the Neon transfection system (Life Technologies) in T Buffer (Life Technologies).
624 Settings were the following: 1900 V Voltage, 10 Width, 1 Pulse, 20ms.

625 Efficient NLRP1 targeting sgRNA sequence was provided by FL. Zhong (5'
626 GATAGCCCGAGTGCATCGG 3') (Robinson et al., 2022).

627 Regarding genetic invalidation of P38 isoforms and ZAK α , A549 cells were transduced
628 with LentiCRISPR-V2 vectors containing sgRNA guides against DPH1, P38 isoforms and

629 ZAK α . 48h after transduction, cells were selected during 2 weeks and puromycin double
630 resistant cells were used in functional assays. A second round of lentiviral infection with
631 lenti-Blasticidin-sgP38 β in single KO cells for P38 α achieved generation of double KO
632 cells for P38 α and P38 β . Cells were subsequently selected in blasticidin antibiotic before
633 checking genetic invalidation by immunoblotting.

634

635 Guides used to generate genetic invalidation

P38 alpha (MAPK14)	5' AGGAGAGGCCACGTTCTAC 3'	FWD
P38 beta (MAPK11)	5' GCCCTCGCGCCGGCTTCTAC 3'	FWD
ZAKalpha (MAP3K20)	5' TGTATGGTTATGGAACCGAG 3'	FWD
Dph1	5' GTTCACGGAGGCCGAAGTGA 3'	FWD
CD8	5' TCGTGGCTCTTCCAGCCGCG 3'	FWD

636

637 **Analysis**

638 Prism 8.0a (GraphPad Software, Inc) was used to perform statistical analysis. All relevant
639 information is included directly in figure legends. Otherwise written, data are reported
640 as mean with SEM. Regarding comparison between two groups, T-test with Bonferroni
641 correction was chosen and multiple group comparisons were analyzed by using Two-way
642 Anova with multiple comparisons test. P values are shown in figures and are linked to the
643 following meaning; NS non-significant and Significance is specified as * $p \leq 0.05$; ** $p \leq$
644 0.01 , *** $p \leq 0.001$.

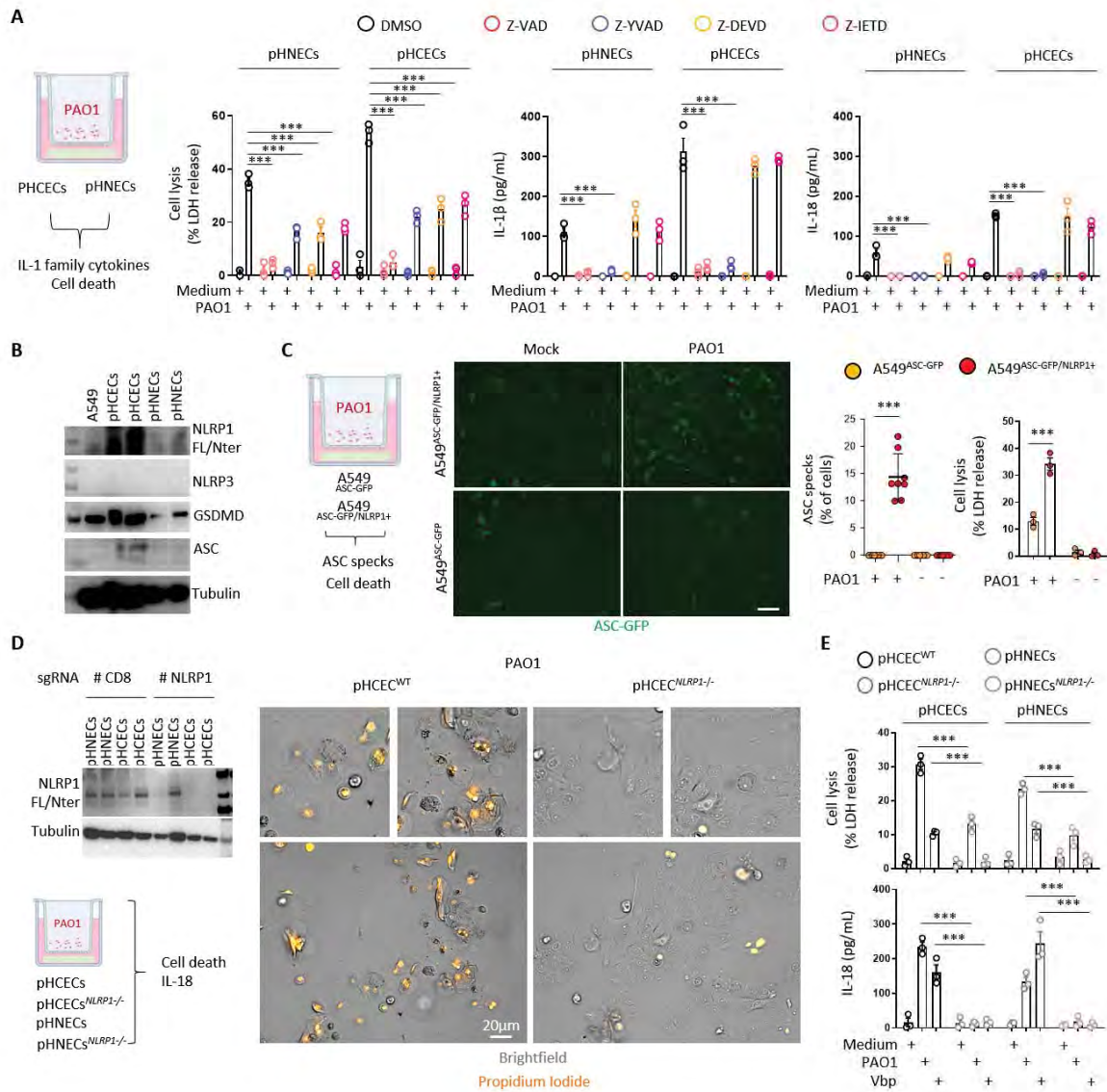
645

646

647

648

649 **FIGURE LEGENDS**



650
 651 **Figure 1. *P. aeruginosa* triggers human NLRP1 inflammasome activation in corneal**
 652 **and nasal epithelial cells.**

653 A. Cell lysis (LDH) and IL-1 β /IL-18 release evaluation in primary Human Corneal and
 654 Nasal Epithelial Cells, respectively pHCECs and pHNECs, upon *P. aeruginosa* (PAO1,
 655 1.10⁵ bacteria) co-culture for 24 hours. ***p \leq 0.001, Two-Way Anova with multiple
 656 comparisons. Values are expressed as mean \pm SEM.

657 B. Immunoblotting examination of NLRP1, NLRP3, GSDMD, ASC and Tubulin in pHCECs
 658 and pHNECs. Immunoblots show lysates from one experiment performed three times.

659 C. Florescence microscopy and associated quantifications of ASC-GFP specks in
660 A549^{NLRP1+/ASC-GFP} and A549^{NLRP1-/ASC-GFP} reporter cell lines exposed to *P. aeruginosa*
661 (PAO1, 1.10⁵ bacteria) for 24 hours. ASC-GFP (Green) pictures were taken in dish during
662 after infection. Images shown are from one experiment and are representative of n = 8
663 independent experiments; scale bars, 50 μm. ASC complex percentage was performed
664 by determining the ratios of cells positives for ASC speckles on the total cells (brightfield).
665 At least 10 fields from each experiment were analyzed. Values are expressed as mean ±
666 SEM. ***p ≤ 0.001, One-Way Anova.

667 D. Immunoblotting characterization of genetic invalidation of *NLRP1* in pHCECs and
668 pHNECs population using CRISPR-Cas9 and microscopy visualization of plasma
669 membrane permeabilization (Propidium Iodide incorporation, orange) in pHCECs co-
670 cultured with PAO1 (1.10⁵ bacteria) for 24 hours. Images shown are from one experiment
671 and are representative of n = 3 independent experiments; scale bars, 20 μm.

672 E. Cell lysis (LDH) and IL-18 release evaluation in WT or *NLRP1*-deficient pHCECs and
673 pHNECs, upon Valbororo pro, Vbp 15μM) treatment or *P. aeruginosa* (PAO1, 1.10⁵
674 bacteria) co-culture for 24 hours. ***p ≤ 0.001, Two-Way Anova with multiple
675 comparisons. Values are expressed as mean ± SEM.

676

677

678

679

680

681

682

683

684

685

686

687

688

689

695 associated isogenic mutants for various Secretion Systems (PAO1^{ΔT3SS}, PAO1^{ΔT2SS},
696 PAO1^{ΔT1SS}) for 24 hours. ASC-GFP (Green) pictures were taken in dish during after
697 infection. Images shown are from one experiment and are representative of n = 3
698 independent experiments; scale bars, 20 μm. ASC complex percentage was performed
699 by determining the ratios of cells positives for ASC speckles on the total cells (brightfield).
700 At least 10 fields from n = 3 independent experiments were analyzed. Values are
701 expressed as mean ± SEM. One-Way Anova.

702 B. Florescence microscopy and associated quantifications of ASC-GFP specks in
703 A549^{NLRP1+/ASC-GFP} reporter cell lines exposed to 1.10⁵ *P. aeruginosa* (PAO1) and
704 associated isogenic mutants for various Type-2 Secretion System virulence effectors
705 (PAO1^{ΔPLCN}, PAO1^{ΔPLCH}, PAO1^{ΔLASB}, PAO1^{ΔEXOA}) for 24 hours. ASC-GFP (Green)
706 pictures were taken in dish during after infection. Images shown are from one experiment
707 and are representative of n = 3 independent experiments; scale bars, 20 μm. ASC
708 complex percentage was performed by determining the ratios of cells positives for ASC
709 speckles on the total cells (brightfield). At least 10 fields from n = 3 independent
710 experiments were analyzed. Values are expressed as mean ± SEM. ***p ≤ 0.001, One-
711 Way Anova.

712 C. Schematic mechanism of *P. aeruginosa* Exotoxin A (EXOA) and related toxins at
713 mediating EEF2 ribosylation and inactivation and subsequent ribosome inactivation.

714 D. Determination of ribosome inactivation in A549^{NLRP1+/ASC-GFP} and A549^{NLRP1-/ASC-GFP}
715 reporter cell lines exposed to Exotoxin A (EXOA, 10ng/mL) for 2 and 6 hours by
716 measuring ribosome polysome accumulation and puromycin incorporation.

717 E. Florescence microscopy and associated quantifications of ASC-GFP specks in
718 A549^{NLRP1+/ASC-GFP} reporter cell lines exposed to EXOA (10ng/mL) or its catalytically dead
719 mutant EXOA^{H426A} (500ng/mL) for 10 hours. ASC-GFP (Green) pictures were taken in
720 dish during after toxin exposure. Images shown are from one experiment and are
721 representative of n = 3 independent experiments; scale bars, 20 μm. ASC complex
722 percentage was performed by determining the ratios of cells positives for ASC speckles
723 (Green, GFP) on the total nuclei (Blue, Hoechst). At least 10 fields from n = 3 independent
724 experiments were analyzed. Values are expressed as mean ± SEM. ***p ≤ 0.001, One-
725 Way Anova.

726 F. Plasma membrane permeabilization determination over time using Propidium Iodide
727 (PI) incorporation in WT or NLRP1-deficient pHCECs exposed to Valboro (Vbp, 15 μ M),
728 EXOA (10ng/mL) or EXOA^{H426A} (10ng/mL) for indicated times. ***p \leq 0.001, T-test. Values
729 are expressed as mean \pm SEM from one experiment (in triplicate) performed at least three
730 times.

731

732

733

734

735

736

737

738

739

740

741

742

743

744

745

746

747

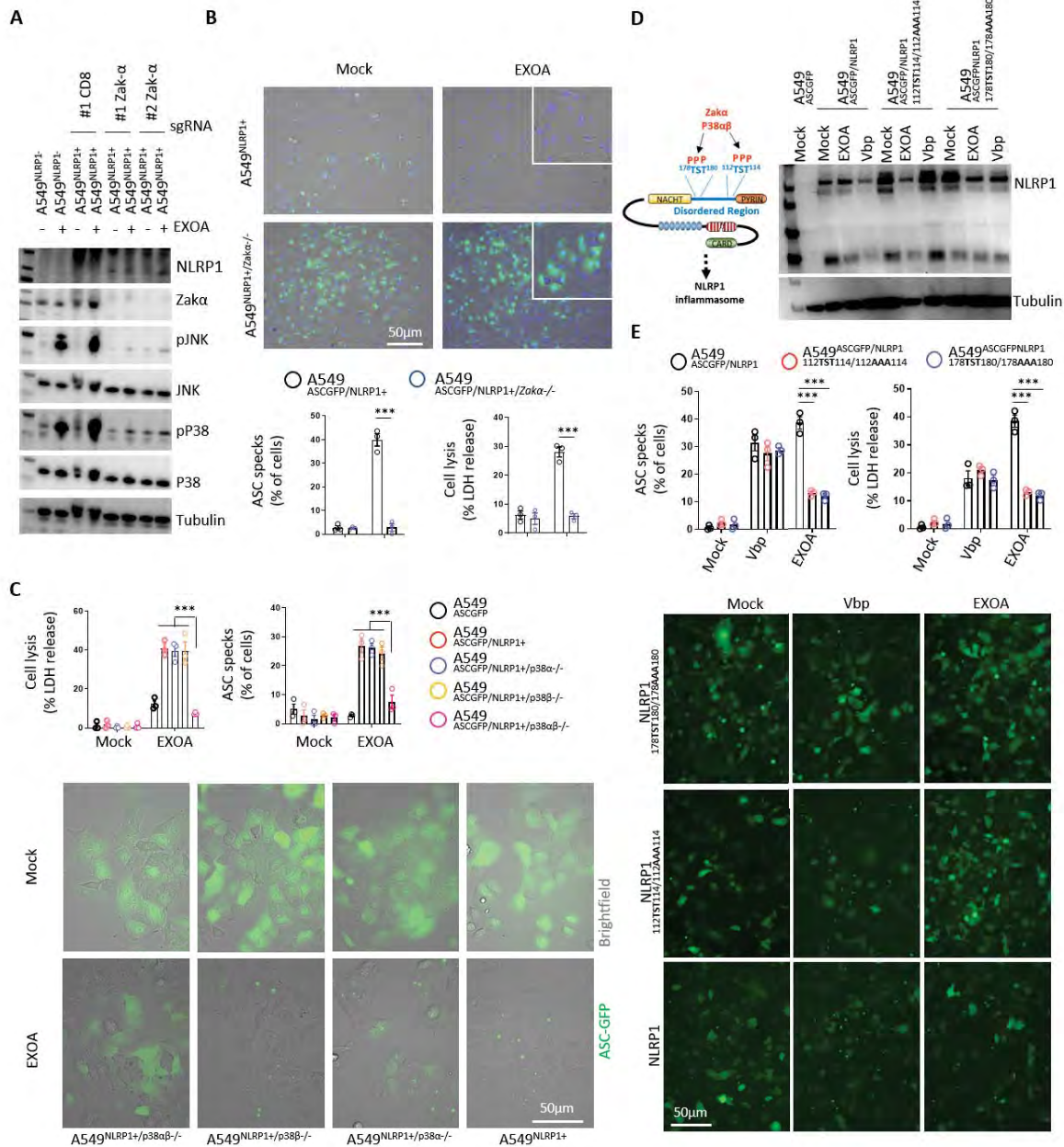
748

749

750

751

752



753

754 **Figure 3. EEF2 inactivation drives ZAK α and P38 MAPKinase activation and**
 755 **subsequent NLRP1 inflammasome nucleation.**

756 A. Immunoblotting of P38, JNK, ZAK α , NLRP1, Tubulin and phosphorylated P38 and JNK
 757 in A549^{NLRP1+} and A549^{NLRP1+/ZAK α -} reporter cell lines exposed or not to EXOA (10ng/mL)
 758 for 3 hours. Immunoblots show lysates from one experiment performed at least three
 759 times.

760 B. Cell lysis (LDH release), fluorescence microscopy and associated quantifications of
761 ASC-GFP specks in A549^{NLRP1+/ASC-GFP} and A549^{NLRP1+/ASC-GFP/ZAK α -} reporter cell lines
762 exposed to EXOA (10ng/mL) for 10 hours. ASC-GFP (Green) pictures were taken in dish
763 during after toxin exposure. Images shown are from one experiment and are
764 representative of n = 3 independent experiments; scale bars, 50 μ m. ASC complex
765 percentage was performed by determining the ratios of cells positives for ASC speckles
766 (Green, GFP) on the total nuclei (Blue, Hoechst). At least 10 fields from n = 3
767 independent experiments were analyzed. Values are expressed as mean \pm SEM. ***p \leq
768 0.001, One-Way Anova.

769 C. Cell lysis (LDH release), fluorescence microscopy and associated quantifications of
770 ASC-GFP specks in A549^{NLRP1+/ASC-GFP} and A549^{NLRP1+/ASC-GFP/P38 α / β -} reporter cell lines
771 exposed to EXOA (10ng/mL) for 10 hours. ASC-GFP (Green) pictures were taken in dish
772 during after toxin exposure. Images shown are from one experiment and are
773 representative of n = 3 independent experiments; scale bars, 50 μ m. ASC complex
774 percentage was performed by determining the ratios of cells positives for ASC speckles
775 (Green, GFP) on the total cells (brightfield). At least 10 fields from n = 3 independent
776 experiments were analyzed. Values are expressed as mean \pm SEM. ***p \leq 0.001, One-
777 Way Anova.

778 D. Western blot examination of NLRP1 using an anti-NLRP1 N-terminal antibody (aa 1–
779 323) in A549^{ASC-GFP} reporter cells reconstituted with hNLRP1 or hNLRP1 plasmid
780 constructs mutated for ¹¹²TST^{114/112}AAA¹¹⁴ or ¹⁷⁸TST^{180/178}AAA¹⁸⁰ after 10 hours
781 exposure to EXOA (10ng/mL) or Vbp (15 μ M).

782 E. Cell lysis (LDH release), fluorescence microscopy and associated quantifications of
783 ASC-GFP specks in A549^{ASC-GFP} reporter cells reconstituted with hNLRP1 or hNLRP1
784 plasmid constructs mutated for ¹¹²TST^{114/112}AAA¹¹⁴ or ¹⁷⁸TST^{180/178}AAA¹⁸⁰ after 10 hours
785 exposure to EXOA (10ng/mL) or Vbp (15 μ M). ASC-GFP (Green) pictures were taken in
786 dish during after toxin exposure. Images shown are from one experiment and are
787 representative of n = 3 independent experiments; scale bars, 50 μ m. ASC complex
788 percentage was performed by determining the ratios of cells positives for ASC speckles
789 (Green, GFP) on the total cells (brightfield). At least 10 fields from n = 3 independent

790 experiments were analyzed. Values are expressed as mean \pm SEM. *** $p \leq 0.001$, Two-
791 Way Anova with multiple comparisons.

792

793

794

795

796

797

798

799

800

801

802

803

804

805

806

807

808

809

810

811

812

813

814

815

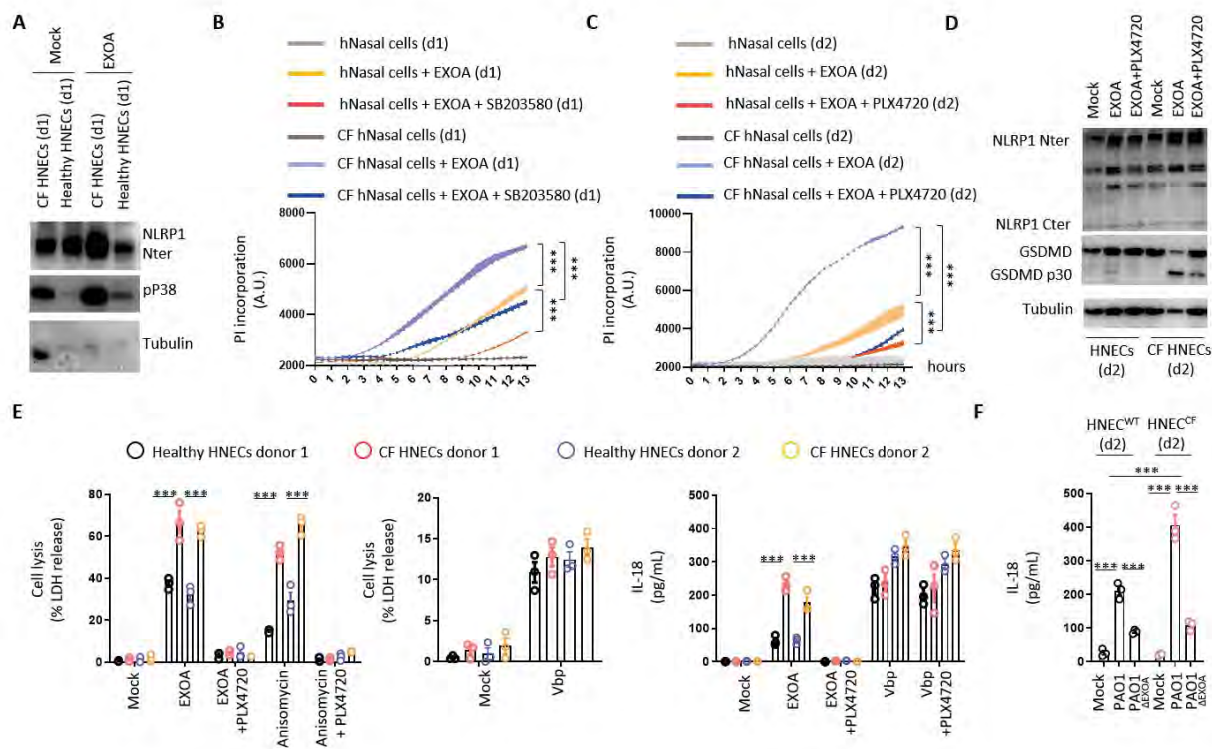
816

817

818

819

820



821
 822 **Figure 4. Cystic fibrosis airway epithelial cells show exacerbated sensitivity to**
 823 **EXOA-driven pyroptosis, which is reversed by ZAKα inhibition.**
 824 A. Immunoblotting of NLRP1, Tubulin and phosphorylated P38 in pHNECs^{WT} and
 825 pHNECs^{CF} from healthy (WT) and Cystic Fibrosis (CF) patients exposed to EXOA
 826 (10ng/mL) or not for 12 hours. Immunoblots show lysates from one experiment performed
 827 at least three times. (d1) stands for “donor 1” from Cystic fibrosis (CF) or healthy (WT)
 828 patients.
 829 B, C. Plasma membrane permeabilization determination over time using Propidium Iodide
 830 (PI) incorporation in pHNECs^{WT} or pHNECs^{CF} exposed to EXOA (10ng/mL) for indicated
 831 times. When specified, SB203580, inhibitor of P38 activity (10μM) or PLX420 (bRaf, ZAKα
 832 inhibitor, 10μM) were used. (d1) and (d2) stand for respective donors 1 or 2. ***p ≤ 0.001,
 833 T-test. Values are expressed as mean ± SEM from one experiment (in triplicate) from one
 834 independent donor (d1/d2, CFd1/CFd2) performed at least three times.
 835 D. Immunoblotting of NLRP1, Gasdermin D (GSDMD) and Tubulin in pHNECs^{WT} and
 836 pHNECs^{CF} from healthy (WT) and Cystic Fibrosis (CF) patients exposed to EXOA

837 (10ng/mL) or not for 12 hours in presence or absence of PLX420 (ZAK α inhibitor, 10 μ M).
838 Immunoblots show combined supernatants and lysates from one experiment performed
839 at least three times. (d2) stands for “donor 2” from Cystic fibrosis (CF) or healthy (WT)
840 patients.

841 E. Cell lysis (LDH) and IL-18 release evaluation in pHNECs^{WT} and pHNECs^{CF} upon EXOA
842 (10ng/mL), Anisomycin (1 μ g/mL) or Vbp (15 μ M) treatment for 18 hours in
843 presence/absence of PLX420 (ZAK inhibitor, 10 μ M). ***p \leq 0.001, T-test. Values are
844 expressed as mean \pm SEM from one experiment (in triplicate) from one independent
845 donor (d1/d2, CFd1/CFd2) performed at least three times.

846 F. IL-18 release in pHNECs^{WT} and pHNECs^{CF} co-cultured with PAO1 or PAO1 Δ EXOA (1.10⁵
847 bacteria) for 24 hours. ***p \leq 0.001, T-test. Values are expressed as mean \pm SEM from
848 one experiment (in triplicate) from one independent donor (d2, CFd2) performed at least
849 three times.

850

851

852

853

854

855

856

857

858

859

860

861

862

863

864

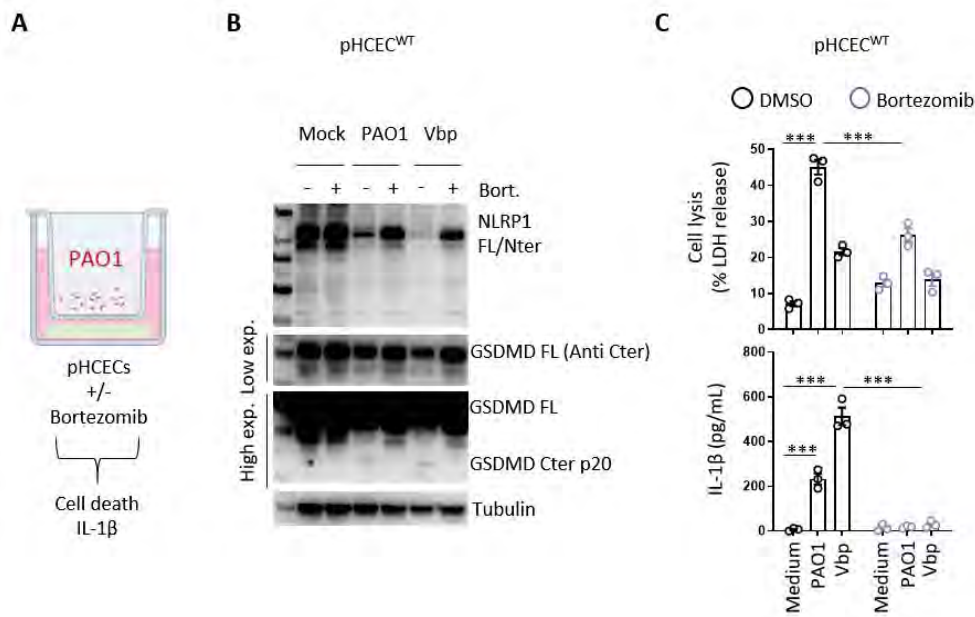
865

866

867

868 SUPPLEMENTAL FIGURE LEGENDS

869



870

871 **Figure S1. *P. aeruginosa*-activated human NLRP1 inflammasome requires**
 872 **proteasome activity.**

873 A. Schematic drawing of *P. aeruginosa* co-culture experiments performed with human
 874 corneal epithelial cells.

875 B. Immunoblotting of NLRP1, Gasdermin-D and Tubulin in pHCECs upon Valbororo pro,
 876 Vbp 15 μ M) treatment or *P. aeruginosa* (PAO1, 1.10⁵ bacteria) co-culture for 24 hours in
 877 presence/absence of proteasome inhibitor bortezomib. Immunoblots show lysates from
 878 one experiment performed at least three times.

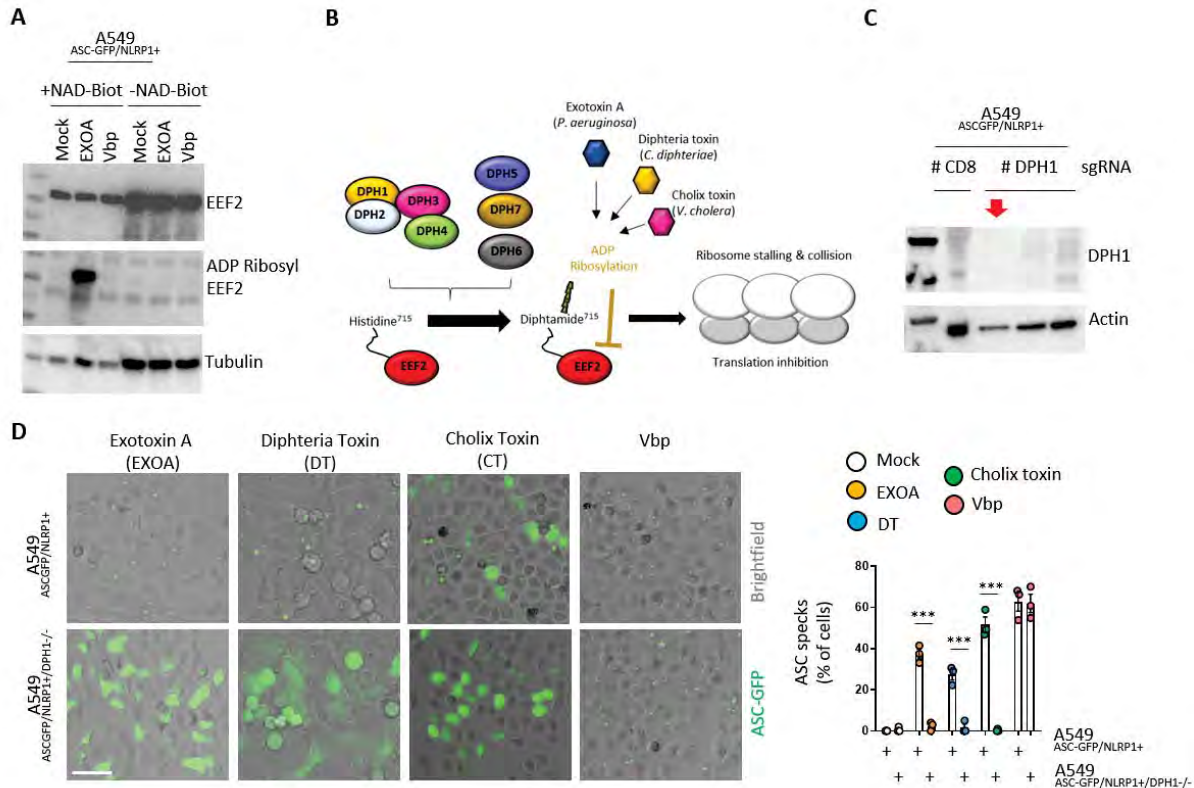
879 C. Cell lysis (LDH) and IL-1 β release evaluation in pHCECs and pHNECs, upon
 880 Valbororo pro, Vbp 15 μ M) treatment or *P. aeruginosa* (PAO1, 1.10⁵ bacteria) co-culture
 881 for 24 hours in presence/absence of proteasome inhibitor bortezomib. ***p \leq 0.001, Two-
 882 Way Anova with multiple comparisons. Values are expressed as mean \pm SEM.

883

884

885

886



887
888 **Figure S2. Multiple EEF2-targeting toxins activate the human NLRP1**
889 **inflammasome.**

890 B. Immunoblotting of ADP-Ribosylated proteins, EEF2 and Tubulin in A549^{NLRP1+/ASC-GFP}
891 cell lysates treated or not with Vbp (15µM) or EXOA (10ng/mL) in presence of NAD-Biot.
892 Immunoblots show lysates from one experiment performed at least three times.

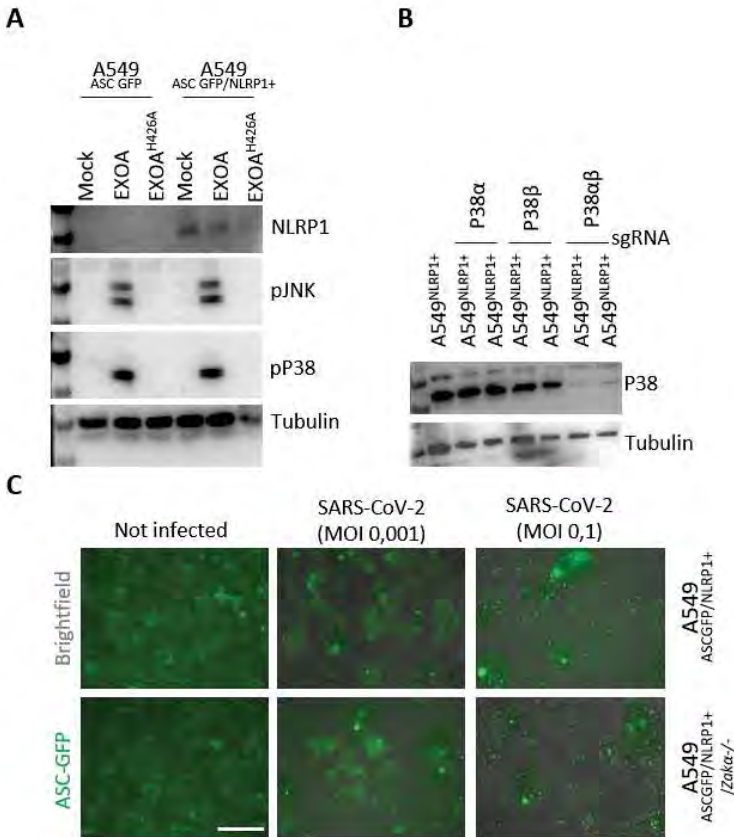
893 B. Schematic mechanism of DPH enzymes at promoting the formation of the Diphtamide
894 aminoacid on EEF2.

895 C. Immunoblotting characterization of genetic invalidation of *DPH1* in A549^{NLRP1+/ASC-GFP}
896 cells using CRISPR-Cas9.

897 D. Fluorescence microscopy and associated quantifications of ASC-GFP specks in
898 A549^{NLRP1+/ASC-GFP} and A549^{NLRP1+/ASC-GFP/DPH1-/-} reporter cell lines exposed to Vbp (15µM),
899 EXOA (10ng/mL), Cholix Toxin (CT, 10ng/mL) and Diphtheria Toxin (DT, 20ng/mL) for 10
900 hours. ASC-GFP (Green) pictures were taken in dish during after toxin exposure. Images
901 shown are from one experiment and are representative of n = 3 independent experiments;
902 scale bars, 50 µm. ASC complex percentage was performed by determining the ratios of
903 cells positives for ASC speckles (Green, GFP) on the total cells (Brightfield). At least 10

904 fields from n = 3 independent experiments were analyzed. Values are expressed as mean
905 ± SEM. ***p ≤ 0.001, One-Way Anova.

906
907
908
909
910
911
912
913
914
915
916
917
918
919
920
921
922
923
924
925
926
927
928
929
930
931
932
933
934



935

936 **Figure S3. Stress kinase ZAK α regulates EXOA-, but not SARS-CoV-2-driven**
 937 **NLRP1 inflammasome activation.**

938 A. Immunoblotting of NLRP1, Tubulin and phosphorylated P38 and JNK in A549^{NLRP1+} and
 939 A549^{NLRP1-} reporter cell lines exposed or not to EXOA (10ng/mL) or its inactive mutant
 940 EXOA^{H426A} for 3 hours. Immunoblots show lysates from one experiment performed at
 941 least three times.

942 B. Immunoblotting characterization of genetic invalidation of *P38 α* and *P38 β* in
 943 A549^{NLRP1+}/ASC-GFP cells using CRISPR-Cas9.

944 C. Fluorescence microscopy and associated quantifications of ASC-GFP specks in
 945 A549^{NLRP1+}/ASC-GFP and A549^{NLRP1+}/ASC-GFP/*ZAK α -/-* reporter cell lines expressing hACE2
 946 infected for 24 hours with various SARS-CoV-2 MOI (Multiplicity of infection). ASC-GFP
 947 (Green) pictures were taken in dish during after toxin exposure. Images shown are from
 948 one experiment and are representative of n = 3 independent experiments; scale bars, 50
 949 μ m. ASC complex percentage was performed by determining the ratios of cells positives
 950 for ASC speckles (Green, GFP) on the total cells (Brightfield).

A

CF03 (donor 1)

Sex: Male
Age: 28
Disease: Cystic Fibrosis
Mutation: $\Delta F508 / 4005+1G>A$
Date of Nasal swab: 09/05/2022

CF06 (donor 2)

Sex: Male
Age: 34
Disease: Cystic Fibrosis
Mutation: $\Delta F508 / N1303K$
Date of Nasal swab: 21/06/2022

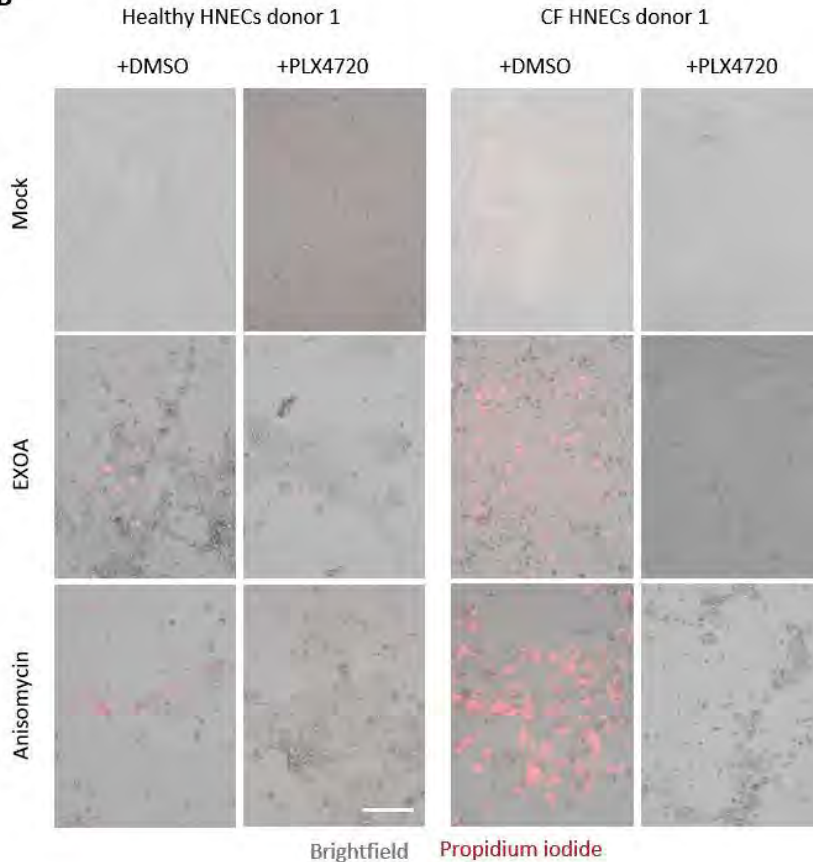
H1 (donor 1)

Sex: Male
Age: 29
Disease: None
Mutation: None
Date of Nasal swab: 09/05/2022

H2 (donor 2)

Sex: Female
Age: 23
Disease: None
Mutation: None
Date of Nasal swab: 20/06/2022

B



951

952 **Figure S4. Cystic fibrosis (CF) cells show exacerbated sensitivity to undergo cell**
953 **death upon ribotoxic stress.**

954 A. Information regarding Healthy and CF patient samples used in this study.

955 B. Fluorescence microscopy of Propidium Iodide (PI, red) incorporation into pHNEC^{WT}

956 (donor 2, d2) and pHNEC^{CF} (donor 1, d1) after exposure to Anisomycin or EXOA for 16

957 hours in presence or not of the ZAK alpha inhibitor PLX4720 (10 μ M). Images shown are
958 from one experiment and are representative of n = 3 independent experiments; scale
959 bars, 50 μ m.

960

961

962

963

964

965

966

967

968

969

970

971

972

973

974

975

976

977

978

979

980

981

982

983

984

985

986

987

988 **REFERENCES**

- 989 Allison, A.C. 1954. Protection Afforded by Sickle-cell Trait Against Subtertian Malarial
990 Infection. *Br. Med. J.* 1:290. doi:10.1136/BMJ.1.4857.290.
- 991 Armstrong, S., and A.R. Merrill. 2004. Toward the Elucidation of the Catalytic
992 Mechanism of the Mono-ADP-Ribosyltransferase Activity of *Pseudomonas*
993 *aeruginosa* Exotoxin A. *Biochemistry.* 43:183–194. doi:10.1021/bi034772u.
- 994 Balakrishnan, A., R. Karki, B. Berwin, M. Yamamoto, and T.D. Kanneganti. 2018.
995 Guanylate binding proteins facilitate caspase-11-dependent pyroptosis in response
996 to type 3 secretion system-negative *Pseudomonas aeruginosa*. *Cell Death Discov.*
997 4:1–12. doi:10.1038/S41420-018-0068-Z.
- 998 Bauernfried, S., M.J. Scherr, A. Pichlmair, K.E. Duderstadt, and V. Hornung. 2021.
999 Human NLRP1 is a sensor for double-stranded RNA. *Science.* 371.
1000 doi:10.1126/SCIENCE.ABD0811.
- 1001 Bérubé, J., L. Roussel, L. Nattagh, and S. Rousseau. 2010. Loss of Cystic Fibrosis
1002 Transmembrane Conductance Regulator Function Enhances Activation of P38 and
1003 ERK MAPKs, Increasing Interleukin-6 Synthesis in Airway Epithelial Cells Exposed
1004 to *Pseudomonas aeruginosa*. *J. Biol. Chem.* 285:22299–22307.
1005 doi:10.1074/JBC.M109.098566.
- 1006 Bonfield, T.L., J.R. Panuska, M.W. Konstan, K.A. Hilliard, J.B. Hilliard, H. Ghnaim, and
1007 M. Berger. 2012. Inflammatory cytokines in cystic fibrosis lungs.
1008 <https://doi.org/10.1164/ajrccm.152.6.8520783>. 152:2111–2118.
1009 doi:10.1164/AJRCCM.152.6.8520783.
- 1010 Broz, P., and V.M. Dixit. 2016. Inflammasomes: mechanism of assembly, regulation and
1011 signalling. *Nat. Rev. Immunol.* 2016 167. 16:407–420. doi:10.1038/nri.2016.58.
- 1012 Chen, Y., X. Shao, J. Cao, H. Zhu, B. Yang, Q. He, and M. Ying. 2021. Phosphorylation
1013 regulates cullin-based ubiquitination in tumorigenesis. *Acta Pharm. Sin. B.* 11:309.
1014 doi:10.1016/J.APSB.2020.09.007.
- 1015 Deng, Q., Y. Wang, Y. Zhang, M. Li, D. Li, X. Huang, Y. Wu, J. Pu, and M. Wu. 2015.
1016 *Pseudomonas aeruginosa* Triggers Macrophage Autophagy To Escape Intracellular
1017 Killing by Activation of the NLRP3 Inflammasome. *Infect. Immun.* 84:56–66.
1018 doi:10.1128/IAI.00945-15.

1019 Faure, E., J.B. Mear, K. Faure, S. Normand, A. Couturier-Maillard, T. Grandjean, V.
1020 Balloy, B. Ryffel, R. Dessein, M. Chignard, C. Uyttenhove, B. Guery, P. Gosset, M.
1021 Chamailard, and E. Kipnis. 2014. *Pseudomonas aeruginosa* type-3 secretion
1022 system dampens host defense by exploiting the NLRC4-coupled inflammasome.
1023 *Am. J. Respir. Crit. Care Med.* 189:799–811. doi:10.1164/RCCM.201307-1358OC.

1024 Fenini, G., S. Grossi, E. Contassot, T. Biedermann, E. Reichmann, L.E. French, and
1025 H.D. Beer. 2018. Genome Editing of Human Primary Keratinocytes by
1026 CRISPR/Cas9 Reveals an Essential Role of the NLRP1 Inflammasome in UVB
1027 Sensing. *J. Invest. Dermatol.* 138:2644–2652. doi:10.1016/J.JID.2018.07.016.

1028 Filloux, A. 2011. Protein Secretion Systems in *Pseudomonas aeruginosa*: An Essay on
1029 Diversity, Evolution, and Function. *Front. Microbiol.* 2.
1030 doi:10.3389/FMICB.2011.00155.

1031 Filloux, A. 2022. Bacterial protein secretion systems: Game of types. *Microbiol. (United*
1032 *Kingdom)*. 168:001193. doi:10.1099/MIC.0.001193/CITE/REFWORKS.

1033 Franchi, L., J. Stoolman, T.D. Kanneganti, A. Verma, R. Ramphal, and G. Núñez. 2007.
1034 Critical role for Ipaf in *Pseudomonas aeruginosa*-induced caspase-1 activation. *Eur.*
1035 *J. Immunol.* 37:3030–3039. doi:10.1002/EJI.200737532.

1036 Griswold, A.R., H.C. Huang, and D.A. Bachovchin. 2022. The NLRP1 Inflammasome
1037 Induces Pyroptosis in Human Corneal Epithelial Cells. *Invest. Ophthalmol. Vis. Sci.*
1038 63. doi:10.1167/IOVS.63.3.2.

1039 Hawer, H., B.A. Mendelsohn, K. Mayer, A. Kung, A. Malhotra, S. Tuupainen, J. Schleit,
1040 U. Brinkmann, and R. Schaffrath. 2020. Diphthamide-deficiency syndrome: a novel
1041 human developmental disorder and ribosomopathy. *Eur. J. Hum. Genet.* 2020
1042 2811. 28:1497–1508. doi:10.1038/s41431-020-0668-y.

1043 Hazlett, L.D. 2005. Inflammatory Response to *Pseudomonas aeruginosa* Keratitis. *Ocul.*
1044 *Surf.* 3:S-139. doi:10.1016/S1542-0124(12)70239-2.

1045 Ivankovic, M., I. Rubelj, M. Matulic, E. Reich, and B. Brdar. 2006. Site-specific
1046 mutagenesis of the histidine precursor of diphthamide in the human elongation
1047 factor-2 gene confers resistance to diphtheria toxin. *Mutat. Res. Toxicol. Environ.*
1048 *Mutagen.* 609:34–42. doi:10.1016/J.MRGENTOX.2006.06.027.

1049 Jacobs, M.A., A. Alwood, I. Thaipisuttikul, D. Spencer, E. Haugen, S. Ernst, O. Will, R.

1050 Kaul, C. Raymond, R. Levy, L. Chun-Rong, D. Guenther, D. Bovee, M. V. Olson,
1051 and C. Manoil. 2003. Comprehensive transposon mutant library of *Pseudomonas*
1052 *aeruginosa*. *Proc. Natl. Acad. Sci. U. S. A.* 100:14339–14344.
1053 doi:10.1073/PNAS.2036282100/SUPPL_FILE/6282TABLE6.HTML.

1054 Jenster, L.-M., K.-E. Lange, S. Normann, A. vom Hemdt, J.D. Wuerth, L.D.J. Schiffelers,
1055 Y.M. Tesfamariam, F.N. Gohr, L. Klein, I.H. Kaltheuner, S. Ebner, D.J. Lapp, J.
1056 Mayer, J. Moecking, H.L. Ploegh, E. Latz, F. Meissner, M. Geyer, B.M. Kümmerer,
1057 and F.I. Schmidt. 2023. P38 kinases mediate NLRP1 inflammasome activation after
1058 ribotoxic stress response and virus infection. *J. Exp. Med.* 220.
1059 doi:10.1084/JEM.20220837.

1060 Jørgensen, R., A.R. Merrill, S.P. Yates, V.E. Marquez, A.L. Schwan, T. Boesen, and
1061 G.R. Andersen. 2005. Exotoxin A-eEF2 complex structure indicates ADP
1062 ribosylation by ribosome mimicry. *Nature.* 436:979–984.
1063 doi:10.1038/NATURE03871.

1064 Jørgensen, R., A.E. Purdy, R.J. Fieldhouse, M.S. Kimber, D.H. Bartlett, and A.R. Merrill.
1065 2008. Cholix toxin, a novel ADP-ribosylating factor from *Vibrio cholerae*. *J. Biol.*
1066 *Chem.* 283:10671–10678. doi:10.1074/JBC.M710008200.

1067 Kaftrio | European Medicines Agency.

1068 Kayagaki, N., O.S. Kornfeld, B.L. Lee, I.B. Stowe, K. O’Rourke, Q. Li, W. Sandoval, D.
1069 Yan, J. Kang, M. Xu, J. Zhang, W.P. Lee, B.S. McKenzie, G. Ulas, J. Payandeh, M.
1070 Roose-Girma, Z. Modrusan, R. Reja, M. Sagolla, J.D. Webster, V. Cho, T.D.
1071 Andrews, L.X. Morris, L.A. Miosge, C.C. Goodnow, E.M. Bertram, and V.M. Dixit.
1072 2021. NINJ1 mediates plasma membrane rupture during lytic cell death. *Nature.*
1073 591:131–136. doi:10.1038/S41586-021-03218-7.

1074 Lacey, C.A., and E.A. Miao. 2020. Programmed Cell Death in the Evolutionary Race
1075 against Bacterial Virulence Factors. *Cold Spring Harb. Perspect. Biol.* 12.
1076 doi:10.1101/CSHPERSPECT.A036459.

1077 Liao, C., X. Huang, Q. Wang, D. Yao, and W. Lu. 2022. Virulence Factors of
1078 *Pseudomonas Aeruginosa* and Antivirulence Strategies to Combat Its Drug
1079 Resistance. *Front. Cell. Infect. Microbiol.* 12:918.
1080 doi:10.3389/FCIMB.2022.926758/BIBTEX.

1081 Liu, S., G.T. Milne, J.G. Kuremsky, G.R. Fink, and S.H. Leppla. 2004. Identification of
1082 the Proteins Required for Biosynthesis of Diphthamide, the Target of Bacterial
1083 ADP-Ribosylating Toxins on Translation Elongation Factor 2. *Mol. Cell. Biol.*
1084 24:9487. doi:10.1128/MCB.24.21.9487-9497.2004.

1085 Maurice, N.M., B. Bedi, and R.T. Sadikot. 2018. *Pseudomonas aeruginosa* biofilms:
1086 Host response and clinical implications in lung infections. *Am. J. Respir. Cell Mol.*
1087 *Biol.* 58:428–439. doi:10.1165/RCMB.2017-
1088 0321TR/SUPPL_FILE/DISCLOSURES.PDF.

1089 Miao, E.A., R.K. Ernst, M. Dors, D.P. Mao, and A. Aderem. 2008. *Pseudomonas*
1090 *aeruginosa* activates caspase 1 through IpaF. *Proc. Natl. Acad. Sci. U. S. A.*
1091 105:2562–2567. doi:10.1073/PNAS.0712183105/ASSET/BDFA0AA1-5368-45F0-
1092 B680-77545D4B3F8B/ASSETS/GRAPHIC/ZPQ0050893430006.JPEG.

1093 Michalska, M., and P. Wolf. 2015. *Pseudomonas* Exotoxin A: Optimized by evolution for
1094 effective killing. *Front. Microbiol.* 6:963. doi:10.3389/FMICB.2015.00963/BIBTEX.

1095 Nakajima, J., S. Oana, T. Sakaguchi, M. Nakashima, H. Numabe, H. Kawashima, N.
1096 Matsumoto, and N. Miyake. 2018. Novel compound heterozygous DPH1 mutations
1097 in a patient with the unique clinical features of airway obstruction and external
1098 genital abnormalities. *J. Hum. Genet.* 63:529–532. doi:10.1038/S10038-017-0399-
1099 2.

1100 Ogura, K., K. Yahiro, H. Tsutsuki, S. Nagasawa, S. Yamasaki, J. Moss, and M. Noda.
1101 2011. Characterization of Cholix toxin-induced apoptosis in HeLa cells. *J. Biol.*
1102 *Chem.* 286:37207–37215. doi:10.1074/JBC.M111.246504.

1103 De Oliveira, D.M.P., B.M. Forde, T.J. Kidd, P.N.A. Harris, M.A. Schembri, S.A. Beatson,
1104 D.L. Paterson, and M.J. Walker. 2020. Antimicrobial resistance in ESKAPE
1105 pathogens. *Clin. Microbiol. Rev.* 33. doi:10.1128/CMR.00181-
1106 19/ASSET/CBA1C1D1-CF90-43DE-A9DF-
1107 32D24A4334AC/ASSETS/GRAPHIC/CMR.00181-19-F0001.JPEG.

1108 Park, Y.H., E.F. Remmers, W. Lee, A.K. Ombrello, L.K. Chung, Z. Shilei, D.L. Stone,
1109 M.I. Ivanov, N.A. Loeven, K.S. Barron, P. Hoffmann, M. Nehrebecky, Y.Z. Akkaya-
1110 Ulum, E. Sag, B. Balci-Peynircioglu, I. Aksentijevich, A. Gül, C.N. Rotimi, H. Chen,
1111 J.B. Bliska, S. Ozen, D.L. Kastner, D. Shriner, and J.J. Chae. 2020. Ancient familial

1112 Mediterranean fever mutations in human pyrin and resistance to *Yersinia pestis*.
1113 *Nat. Immunol.* 21:857–867. doi:10.1038/S41590-020-0705-6.

1114 Pillar, C.M., and J.A. Hobden. 2002. *Pseudomonas aeruginosa* exotoxin A and keratitis
1115 in mice. *Invest. Ophthalmol. Vis. Sci.* 43:1437–1444.

1116 Planès, R., M. Pinilla, K. Santoni, A. Hessel, C. Passemar, K. Lay, P. Paillette, A.L.C.
1117 Valadão, K.S. Robinson, P. Bastard, N. Lam, R. Fadrique, I. Rossi, D. Pericat, S.
1118 Bagayoko, S.A. Leon-Icaza, Y. Rombouts, E. Perouzel, M. Tiraby, Q. Zhang, P.
1119 Cicuti, E. Jouanguy, O. Neyrolles, C.E. Bryant, A.R. Floto, C. Goujon, F.Z. Lei, G.
1120 Martin-Blondel, S. Silva, J.L. Casanova, C. Cougoule, B. Reversade, J. Marcoux,
1121 E. Ravet, and E. Meunier. 2022. Human NLRP1 is a sensor of pathogenic
1122 coronavirus 3CL proteases in lung epithelial cells. *Mol. Cell.* 82:2385-2400.e9.
1123 doi:10.1016/J.MOLCEL.2022.04.033.

1124 Qin, S., W. Xiao, C. Zhou, Q. Pu, X. Deng, L. Lan, H. Liang, X. Song, and M. Wu. 2022.
1125 *Pseudomonas aeruginosa*: pathogenesis, virulence factors, antibiotic resistance,
1126 interaction with host, technology advances and emerging therapeutics. *Signal*
1127 *Transduct. Target. Ther.* 2022 71. 7:1–27. doi:10.1038/s41392-022-01056-1.

1128 Raia, V., L. Maiuri, C. Ciacci, I. Ricciardelli, L. Vacca, S. Auricchio, M. Cimmino, M.
1129 Cavaliere, M. Nardone, A. Cesaro, J. Malcolm, S. Quaratino, and M. Londei. 2005.
1130 Inhibition of P38 mitogen activated protein kinase controls airway inflammation in
1131 cystic fibrosis. *Thorax.* 60:773–780. doi:10.1136/THX.2005.042564.

1132 Roberts, T.M., and A.R. Merrill. 2002. A re-evaluation of the role of histidine-426 within
1133 *Pseudomonas aeruginosa* exotoxin A. *Biochem. J.* 367:601–608.
1134 doi:10.1042/BJ20020768.

1135 Robinson, K.S., D.E.T. Teo, K. Sen Tan, G.A. Toh, H.H. Ong, C.K. Lim, K. Lay, B.V. Au,
1136 T.S. Lew, J.J.H. Chu, V.T.K. Chow, D.Y. Wang, F.L. Zhong, and B. Reversade.
1137 2020. Enteroviral 3C protease activates the human NLRP1 inflammasome in
1138 airway epithelia. *Science.* 370. doi:10.1126/SCIENCE.AAY2002.

1139 Robinson, K.S., G.A. Toh, P. Rozario, R. Chua, S. Bauernfried, Z. Sun, M.J. Firdaus, S.
1140 Bayat, R. Nadkarni, Z.S. Poh, K.C. Tham, C.R. Harapas, C.K. Lim, W. Chu, C.W.S.
1141 Tay, K.Y. Tan, T. Zhao, C. Bonnard, R. Sobota, J.E. Connolly, J. Common, S.L.
1142 Masters, K.W. Chen, L. Ho, B. Wu, V. Hornung, and F.L. Zhong. 2022. ZAK α -

1143 driven ribotoxic stress response activates the human NLRP1 inflammasome.
1144 *Science*. 377:328–335. doi:10.1126/SCIENCE.ABL6324.

1145 Ryu, J.C., M.J. Kim, Y. Kwon, J.H. Oh, S.S. Yoon, S.J. Shin, J.H. Yoon, and J.H. Ryu.
1146 2016. Neutrophil pyroptosis mediates pathology of *P. aeruginosa* lung infection in
1147 the absence of the NADPH oxidase NOX2. *Mucosal Immunol.* 2017 103. 10:757–
1148 774. doi:10.1038/mi.2016.73.

1149 Samson, M., F. Libert, B.J. Doranz, J. Rucker, C. Liesnard, M. Farber, S. Saragosti, C.
1150 Lapoumeroulie, J. Cognaux, C. Forceille, G. Muyldermans, C. Verhofstede, G.
1151 Burtonboy, M. Georges, T. Imai, S. Rana, Y. Yi, R.J. Smyth, M. Parmentier, and al
1152 et. 1996. Resistance to HIV-1 infection in caucasian individuals bearing mutant
1153 alleles of the CCR-5 chemokine receptor gene. *Nature*. 382:722–726.
1154 doi:10.1038/382722A0.

1155 Santoni, K., D. Pericat, L. Gorse, J. Buyck, M. Pinilla, L. Prouvensier, S. Bagayoko, A.
1156 Hessel, S.A. Leon-Icaza, E. Bellard, S. Mazères, E. Doz-Deblauw, N. Winter, C.
1157 Paget, J.P. Girard, C.T.N. Pham, C. Cougoule, R. Poincloux, M. Lamkanfi, E.
1158 Lefrançais, E. Meunier, and R. Planès. 2022a. Caspase-1-driven neutrophil
1159 pyroptosis and its role in host susceptibility to *Pseudomonas aeruginosa*. *PLOS*
1160 *Pathog.* 18:e1010305. doi:10.1371/JOURNAL.PPAT.1010305.

1161 Santoni, K., D. Pericat, L. Gorse, J. Buyck, M. Pinilla, L. Prouvensier, S. Bagayoko, A.
1162 Hessel, S.A. Leon-Icaza, E. Bellard, S. Mazères, E. Doz-Deblauw, N. Winter, C.
1163 Paget, J.P. Girard, C.T.N. Pham, C. Cougoule, R. Poincloux, M. Lamkanfi, E.
1164 Lefrançais, E. Meunier, and R. Planès. 2022b. Caspase-1-driven neutrophil
1165 pyroptosis and its role in host susceptibility to *Pseudomonas aeruginosa*. *PLOS*
1166 *Pathog.* 18:e1010305. doi:10.1371/JOURNAL.PPAT.1010305.

1167 Spornovasilis, N., M. Psychogiou, and G. Poulakou. 2021. Skin manifestations of
1168 *Pseudomonas aeruginosa* infections. *Curr. Opin. Infect. Dis.* 34:72–79.
1169 doi:10.1097/QCO.0000000000000717.

1170 Sutterwala, F.S., L.A. Mijares, L. Li, Y. Ogura, B.I. Kazmierczak, and R.A. Flavell. 2007.
1171 Immune recognition of *Pseudomonas aeruginosa* mediated by the IPAF/NLRC4
1172 inflammasome. *J. Exp. Med.* 204:3235. doi:10.1084/JEM.20071239.

1173 Tsu, B. V., C. Beierschmitt, A.P. Ryan, R. Agarwal, P.S. Mitchell, and M.D. Daugherty.

1174 2021. Diverse viral proteases activate the NLRP1 inflammasome. *Elife*. 10:1–76.
1175 doi:10.7554/ELIFE.60609.

1176 Urreizti, R., K. Mayer, G.D. Evrony, E. Said, L. Castilla-Vallmanya, N.A.L. Cody, G.
1177 Plasencia, B.D. Gelb, D. Grinberg, U. Brinkmann, B.D. Webb, and S. Balcells.
1178 2020. DPH1 syndrome: two novel variants and structural and functional analyses of
1179 seven missense variants identified in syndromic patients. *Eur. J. Hum. Genet.*
1180 28:64–75. doi:10.1038/S41431-019-0374-9.

1181 Veit, G., R.G. Avramescu, A.N. Chiang, S.A. Houck, Z. Cai, K.W. Peters, J.S. Hong,
1182 H.B. Pollard, W.B. Guggino, W.E. Balch, W.R. Skach, G.R. Cutting, R.A. Frizzell,
1183 D.N. Sheppard, D.M. Cyr, E.J. Sorscher, J.L. Brodsky, and G.L. Lukacs. 2016.
1184 From CFTR biology toward combinatorial pharmacotherapy: expanded
1185 classification of cystic fibrosis mutations. *Mol. Biol. Cell*. 27:424.
1186 doi:10.1091/MBC.E14-04-0935.

1187 Vind, A.C., G. Snieckute, M. Blasius, C. Tiedje, N. Krogh, D.B. Bekker-Jensen, K.L.
1188 Andersen, C. Nordgaard, M.A.X. Tollenaere, A.H. Lund, J.V. Olsen, H. Nielsen, and
1189 S. Bekker-Jensen. 2020. ZAK α Recognizes Stalled Ribosomes through Partially
1190 Redundant Sensor Domains. *Mol. Cell*. 78:700–713.
1191 doi:10.1016/J.MOLCEL.2020.03.021.

1192 Wu, C.C.C., A. Peterson, B. Zinshteyn, S. Regot, and R. Green. 2020. Ribosome
1193 Collisions Trigger General Stress Responses to Regulate Cell Fate. *Cell*. 182:404-
1194 416.e14. doi:10.1016/J.CELL.2020.06.006.

1195 Zhong, F.L., O. Mamaï, L. Sborgi, L. Boussofara, R. Hopkins, K. Robinson, I.
1196 Szeverényi, T. Takeichi, R. Balaji, A. Lau, H. Tye, K. Roy, C. Bonnard, P.J. Ahl,
1197 L.A. Jones, P. Baker, L. Lacina, A. Otsuka, P.R. Fournie, F. Malecaze, E.B. Lane,
1198 M. Akiyama, K. Kabashima, J.E. Connolly, S.L. Masters, V.J. Soler, S.S. Omar,
1199 J.A. McGrath, R. Nedelcu, M. Gribaa, M. Denguezli, A. Saad, S. Hiller, and B.
1200 Reversade. 2016. Germline NLRP1 Mutations Cause Skin Inflammatory and
1201 Cancer Susceptibility Syndromes via Inflammasome Activation. *Cell*. 167:187-
1202 202.e17. doi:10.1016/J.CELL.2016.09.001.

1203
1204

V. Conclusions and Perspectives

Human NLRP1 was the first inflammasome-forming sensor discovered and described 20 years ago by Tschopp and colleagues. However, the molecular mechanisms of activation of NLRP1 remained a mystery for a very long time. This might be explained by 3 major reasons: most human cancer cell lines used as a model in research have lost NLRP1 expression, NLRP1 is expressed in the human epithelium (Sand et al., 2018), contrary to NLRP3 and murine NLRP1, which are mainly found in myeloid cells and finally, the majority of data on NLRP1 was obtained in rodents and it is not transposable in humans because of major structural differences. While recent advances in the field are placing NLRP1 as a central epithelial sensor able to integrate a broad range of signals, its role in host-pathogen interaction is not fully elucidated.

The current knowledge about NLRP1 unveils different molecular mechanism of activation: DPP8/9 inhibition, protease cleavage, detection of long dsRNA, redox and ribotoxic stress (Bachovchin, 2021; Bauernfried & Hornung, 2021). These different mechanisms of activation suggest that NLRP1 can act as a sensor for various types of perturbations and place NLRP1 as a central sensor in the human epithelium. However, the mechanisms by which NLRP1 recognizes these perturbations are more complicated than a simple ligand-binding domain. The NLRP1 inflammasome forming sensor possesses two domains (N-terminal and C-terminal) linked in a non-covalent manner with a FIIND-death fold domain. Thanks to this specific structure, NLRP1 is engaged in a pathogen's arms race acting as a decoy for 3C and 3CL microbial proteases. Pioneer studies showed that 3C proteases from several picornaviruses can cleave and activate NLRP1 (Robinson et al., 2020b; Tsu et al., 2021). These results were confirmed by our work, which showed 3CL proteases from SARS-CoV-2, SARS-CoV-1 and MERS cleave and activate NLRP1 (Planès et al., 2022). Interestingly, multiple proteins in the human system exhibit the fusing of a FIIND-death fold domain extension to the C terminus (Liao et al., 2014), showing the importance of this FIIND domain for decoy capabilities. Indeed, human NLRP1 possesses a conserved disordered region between the PYD and the NACHT that can be phosphorylated by cellular kinases (ZAK α and p38) to induce the activation of NLRP1. Recently, it was described that UVB irradiations are implicated in the phosphorylation of NLRP1 (Robinson et al., 2022). However, it was poorly understood if some microbial pathogens can be implicated in this NLRP1 phosphorylation and activation process. It is important to note that the motifs needed for the protease degradation and phosphorylation are not conserved in mice suggesting that these motifs are conserved in humans to preserve an important defence mechanism against pathogens' attacks.

In order to better understand the mechanisms of NLRP1 activation and its role in the pathogen arms race, during my PhD I focused on two different microbial pathogens: SARS-CoV-2 and *P.aeruginosa*.

Thanks to our works, we identified NLRP1 as a sensor of SARS-CoV-2 3CL protease (NSP5) in airway epithelial cells and we described the critical role of ZAK α driven NLRP1 inflammasome response and epithelial damage in response to *P.aeruginosa*.

During COVID-19 pandemic an early sign that inflammasomes were involved in COVID-19 appeared when LDH levels in the lungs and the kidney were correlated with the severity of the disease (Yi Han et al., n.d.). Rodrigues and colleagues then provided evidence for the role of NLRP3 in COVID-19 by demonstrating its activation in PBMCs (peripheral blood mononuclear cells) from COVID-19 patients (Rodrigues et al., 2020b). Similarly, we recently showed that NLRP1 acts as a central sensor of SARS-CoV-2 3CL protease NSP5 in airway epithelial cells and we were unable to find substantial NLRP3 expression in our epithelial cell models. These complementary results show the important role of inflammasomes in the severity of COVID-19 and confirm the different roles and tissue expression of NLRP1 and NLRP3. Mechanistically, we demonstrated that SARS-CoV-2 infection activates human NLRP1 inflammasome in epithelial cells. This mechanism of activation is based on the NSP5 3CL protease that cleaves NLRP1 and promotes functional degradation (Figure 30). Interestingly, NLRP1 act as a decoy of the NSP5 virulence factor. NSP5 cleaves the executor of pyroptosis gasdermin D, in its pore-forming domain in order to inactivate it, but also cleaves NLRP1 promoting its degradation and activation. Similarly, 3C proteases from Enterovirus 71 cleave, and inactivate gasdermin D (Lei et al., 2017b). Interestingly, SpeB, a cysteine protease virulence factor from *S. pyogenes*, triggers keratinocyte pyroptosis by cleaving GSDMA and releasing an active N-terminal fragment (Deng et al., 2022b). All these results showed that non-host ligands (microbial pathogens) might directly cleave and process GSDMs, leading to pyroptosis regulation (activation or inhibition). In fact, GSDM cleavage requires aspartyl proteases (e.g, caspase-1, caspase-11, caspase-3, caspase-8...) and microbial proteases including aspartyl proteases are known virulence factors in various pathogens. For example, both fungal *C. albicans* Sap and viral HIV-1 PR are aspartyl proteases required for efficient infection. Importantly, all mentioned proteases were reported to trigger cell death in cells from various origins (Blanco et al., 2003; Cassone et al., 2016). Following that, our group is interested in studying gasdermins as immune platforms for microbial proteases sensing.

Finally, we showed the importance of the caspase-3/-8 – GSDME cell death pathway induced after a SARS-CoV-2 infection in airway epithelial cells. Interestingly, we found that we have a strong correlation between increased levels of plasma caspase-3, cleaved caspase-3, IL-18, IL-16, IL-6, GSDMD and GSDME with the severity status of patients (IFN-altered patients or not) suggesting that an overactivation of NLRP1 will be deleterious for the patients. Future research should focus on whether excessive NLRP1 inflammasome activation or a lack of NLRP1 response directly or indirectly promotes an NLRP3-dependent response in patient myeloid cells.

In addition, it is also conceivable to think that microbial proteases might cleave directly into the active domain of NLRP1 (CARD domain) in order to block it, just as they can cleave the N-terminus of NLRP1 to cause its activation. It is also tempting to speculate that the proteases DPP8/9 substrates regulate NLRP1 and CARD8 activity and that microbial pathogens could hijack and disrupt the activity of DPP8/9. Identifying substrates of DPP8/9 will be a big advance in the field. Some results identified a few potential substrates and indicates that DPP8/9 cleaves after proline residues in unstructured peptides (Geiss-Friedlander et al., 2009). Consistent with this, DPP9 has been reported to be implicated in the catabolism of proline-containing peptides generated by the proteasome. Based on these data, it is tempting to speculate that inhibition of DPP8/9-mediated peptide cleavage induces a cellular perturbation that is indirectly sensed by NLRP1 and CARD8, as in the PYRIN inflammasome. These hypotheses open novel questions to address for better understanding of the NLRP1 inflammasome and its functions.

In the second study, we showed that in human corneal and nasal epithelial cells, *P. aeruginosa* by secreting the Eukaryotic Elongation Factor 2 (eEF-2) inactivating toxin Exotoxin A (ExoA) triggers the assembly of the NLRP1 inflammasome and induces the release of associated IL-1 cytokine (IL-1 β and IL-18) (Figure 30).

Mechanistically, ExoA inactivates eEF-2 by ribosylating a specific amino acid called diphthamide. Diphthamide is a unique post-translationally modified histidine residue found only in translation elongation factor 2 (eEF-2) (Jørgensen et al., 2005). Interestingly, all eukaryotic organisms and archaeobacteria have been found to contain diphthamide in the elongation factor eEF-2, while eubacteria do not, indicating that this is a specific mechanism for targeting eukaryotic protein-synthetic machinery without inactivating the protein-synthetic machinery of bacterial pathogens. Diphthamide's biosynthesis is one of the most complex posttranslational modifications, but in a simplistic manner, the biosynthesis is accomplished by stepwise additions to the His715 (His699 in yeast) residue of eEF-2. This process needs different genes named DPH (DPH-1, -2, -3, -4 and -5) (S. Liu et al., 2004) that mediate the first step of the posttranslational diphthamide modification. Our results demonstrated that, in response to ExoA, DPH1-deficient cells failed to assemble an active NLRP1 inflammasome. In addition to exoA, the diphthamide serves as the target for other bacterial toxins, namely Diphtheria Toxin (*Corynebacterium diphtheriae*) and Cholix toxin (*Vibrio cholerae*) (Jørgensen et al., 2008). Interestingly, in parallel to our results, the Zhong group in Singapore showed that the Diphtheria Toxin (DT) triggers the activation of human NLRP1 inflammasome in skin keratinocytes. Despite the fact that this modification in histidine, named diphthamide, was discovered for the first time almost 23 years ago, diphthamide has not been clearly implicated in the normal physiology of the eukaryotic cell (Van Ness et al., 1980). To go further, it will be interesting to make efforts to understand the physiological role of diphthamide in eukaryotic cells. Interestingly, very recently a novel ribosomopathy associated with a

“diphthamide-deficiency syndrome” was described (Hawer et al., 2020). Different patients were identified with DPH1 and DPH2 deficiencies (loss of function mutations) linked with a reduction in the functionality of components of the cellular machinery for eEF2-diphthamide synthesis. This syndrome is associated with developmental delay, abnormal head circumference (microcephaly or macrocephaly), short stature, and congenital heart disease. To go further, it could be interesting to test the response to the different ribotoxins in these patients to study if the deficiency of DPH1/2 could induce resistance to different microbial infections or not. Indeed, some deficiencies conferring selective advantage were previously observed for HIV- or-malaria-resisting patients (A.C. Allison & Phill B.M, 1954; Michel Samson et al., 1996) or recently highlighted for *Yersinia pestis*-shaped selection/evolution of the inflammasome-forming sensor PYRIN (Park et al., 2016b).

In addition, we showed that ExoA-inactivated-eEF-2 promotes ribotoxic stress response (RSR) and subsequent activation of the stress kinases ZAK α and p38 (C. C. 38C. Wu et al., 2020b). Subsequently, activated ZAK α and p38 stimulate NLRP1 phosphorylation in its disordered region, functional degradation and activation. Our results showed that ZAK α deletion by Crispr-Cas9, as well as the use of the ZAK α inhibitor (PLX) completely abrogated the assembly of NLRP1 inflammasome and cell death in response to ExoA. These results showed the crucial role of ZAK α kinase in the phosphorylation and activation of NLRP1. P38 is a kinase that can be activated by many different signalling pathways. However, in this context, following a ribotoxic stress, our results suggest that p38 is activated and phosphorylated only after phosphorylation by ZAK α . In fact, no p38 phosphorylation in response to ExoA is shown when ZAK α is genetically deleted. Interestingly, the genetic deletion of p38 inhibits the assembly of NLRP1 inflammasome in an early time point, as well as the p38 inhibitor which partially inhibits NLRP1-dependent cell death, suggesting a potential role of other kinases to phosphorylate NLRP1 downstream to ZAK α . Further investigations are required to identify if other kinases could be implicated in the NLRP1 phosphorylation. It is important to note that the ribotoxic stress response (RSR) and the activation of ZAK are still present in mice. Indeed, it exists ZAK deficient mouse that showed a defective ribotoxic stress response (Jandhyala et al., 2016). However, due to the structural differences between hNLRP1 and mNLRP1, the NLRP1 pathway is not activated.

Furthermore, we demonstrated that ZAK α and p38 phosphorylate NLRP1 in positions ¹¹⁰TST¹¹² and ¹⁷⁸TST¹⁸⁰ and that these sites are required for efficient inflammasome assembly to ExoA but not during Vbp exposure. However, many questions are still unanswered. How can phosphorylation of NLRP1 increase the degradation and activation of NLRP1? Is phosphorylation sufficient to destabilize NLRP1 or is it the endogenous E3 ligases that recognize the phosphorylated NLRP1 to promote ubiquitination and degradation of NLRP1? Using the proteasome inhibitor (bortezomib) and the NEDD8-cullin ligase inhibitor (MLN4924), we showed that the NLRP1 activation following the Exotoxin A exposure is

proteasome and E3 cullin-ligase dependent, suggesting that NEDD8-driven cullin ligase activation is required for NLRP1 degradation and subsequent inflammasome activation. So far, eight E3 cullin ligases have been described, with two of them (Cullin 1 and Cullin 2) recognizing phosphorylated substrates (Y. Chen et al., 2021) Thus, we are currently performing siRNA approaches to understand the role of Cullin 1/2 in promoting NLRP1 functional degradation.

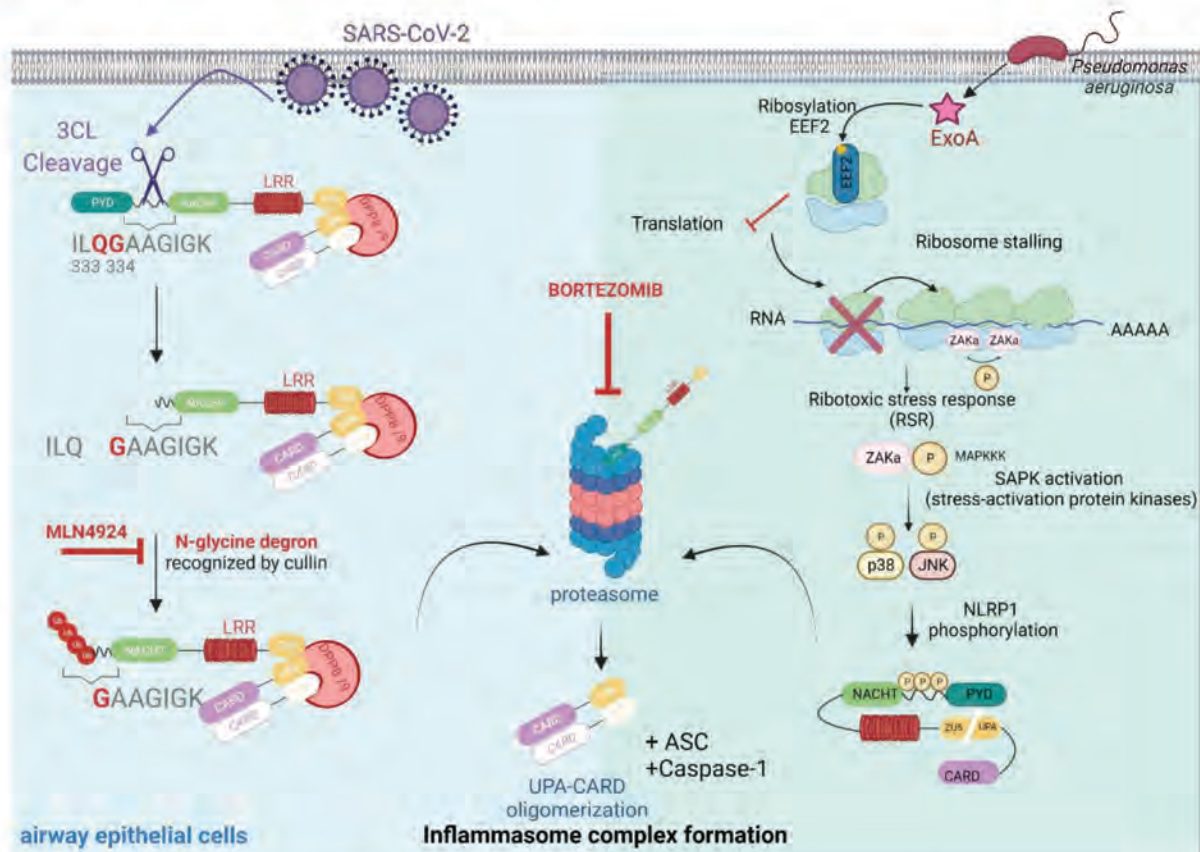


Figure S1: Human NLRP1 as a central sensor of microbial virulence in airway epithelium.

Finally, thanks to our models, we studied the effect of ExoA in cystic fibrosis patients. Cystic fibrosis (CF), which affects over 48,000 people in Europe and 30,000 people in the USA, is one of the most prevalent life-threatening autosomal recessive genetic diseases in Caucasians. CF is a multisystem disease characterized by recurrent lung infections, pancreatic insufficiency, gastrointestinal issues, CF-related diabetes, malnutrition, arthropathies, and male infertility (Q. Chen et al., 2021). Mutations on the transmembrane ion channel cystic fibrosis transmembrane conductance regulator (CFTR) result in the alteration of the physiological function of CFTR production and maturation and are the cause of the disease. The most common mutation is homozygous or heterozygous $\Delta F508$ (Q. Chen et al., 2021). The CFTR is an anion channel implicated in transport of chloride (Cl^-) and bicarbonate (HCO_3^-) ions and a regulator of the epithelial sodium channel (ENaC). The CFTR protein is highly expressed in the respiratory, digestive, and male urogenital tracts. An absence or reduction in functional CFTR leads to

defective CFTR-mediated anion transport and upregulation of ENaC. These changes in normal homeostasis result in fluid hyperabsorption, abnormally thick viscous mucus and defective mucociliary clearance. In our study, we demonstrated that primary nasal epithelial cells derived from cystic fibrosis (CF) patients showed hypersensitivity to ExoA-induced ribotoxic stress-dependent NLRP1 inflammasome activation, a process reverted by the use of ZAK inhibitor (PLX-4720). Interestingly, we showed that ExoA but also other ribotoxic stress inducers (anisomycin) specifically triggered an exacerbated IL-18 cytokines release and cell death response. Besides, a previous study (Scambler et al., 2019), showed an exaggerated pro-inflammatory response in CF cells when challenged with NLRP3-inflammasome activators LPS and ATP, leading to increased IL-18 secretion in CF HBECs (human bronchiolar epithelial cell lines), and IL-1 β and IL-18 in CF monocytes. This exaggerated inflammatory response was reduced when cells were pre-treated with small molecule inhibitors of NLRP3. These controversial results can be explained by the different models of cell lines that we used. In our study, we used primary nasal epithelial cells from CF patients (Δ F508 mutations) or healthy individuals that strongly express NLRP1. Furthermore, we failed to induce the expression of NLRP3 after priming conditions (LPS-EK or IFN γ) and we failed to inhibit cell death with the use of the NLRP3 inhibitor (MCC950) after ExoA or anisomycin exposure. These results confirm the important role of NLRP1 in airway epithelial cells. To this regard, it is currently known that patients developing Cystic fibrosis (CF) show exacerbated inflammation associated with pro-inflammatory cytokine transcription and tissues damages upon chronic infection with *P. aeruginosa*. Other studies showed that when CFTR-deficient airway epithelial cells are exposed to *Pseudomonas aeruginosa*, there is an activation of nuclear factor- κ B (NF- κ B), which drives the expression of IL-8, a potent neutrophil chemoattractant (Venkatakrishnan et al., 2000). Additionally, specific studies highlighted that stress-activated kinase P38 was over-activated in CF-derived cells from patients (Bérubé et al., 2010; Raia et al., 2005). Interestingly, Jenster et al showed that ectopic activation of p38 by co-expression of its upstream kinases MKK3 or MKK6 is sufficient to initiate NLRP1 inflammasome assembly (Jenster, Lange, Normann, Vom Hemdt, et al., 2023). Although several hypotheses were made to explain such dysregulation in CF patients, no study, including ours, could unveil the critical molecular and biochemical mechanisms engaged, which warrants further investigations.

The recent approval of the triple-drug combination therapy, Ivacaftor/Tezacaftor/Elexacaftor (Trikafta) improves CFTR expression and function, and heralds a paradigm shift in the treatment of CF, as this combination is highly efficacious for both patients who are homozygous and heterozygous for the Δ F508 mutation (Zaher et al., 2021). In our study, we pre-treated primary nasal cells from CF patients (heterozygous or homozygous for Δ F508 mutations) with Trikafta therapy and we combined it with ZAK α inhibitor (PLX) before ExoA or anisomycin exposure. This experiment reveals that the combination of

Trikafta treatment with the ZAK α inhibitor synergizes to completely inhibit cell death compared to Trikafta treatment alone. These results suggest that targeting ZAK α in *P.aeruginosa*-infected patients might constitute a good host-targeted approach in order to limit epithelial damages complementary to the current Trikafta treatment. An important aspect to be taken into account is that the PLX-4720 is an inhibitor of B-raf, a gene that encodes a protein belonging to the RAF family of serine/threonine protein kinases including ZAK kinase. We are currently working on the screening of selective inhibitors of ZAK α to test the efficacy of these selective inhibitors in combination with the Trikafta therapy.

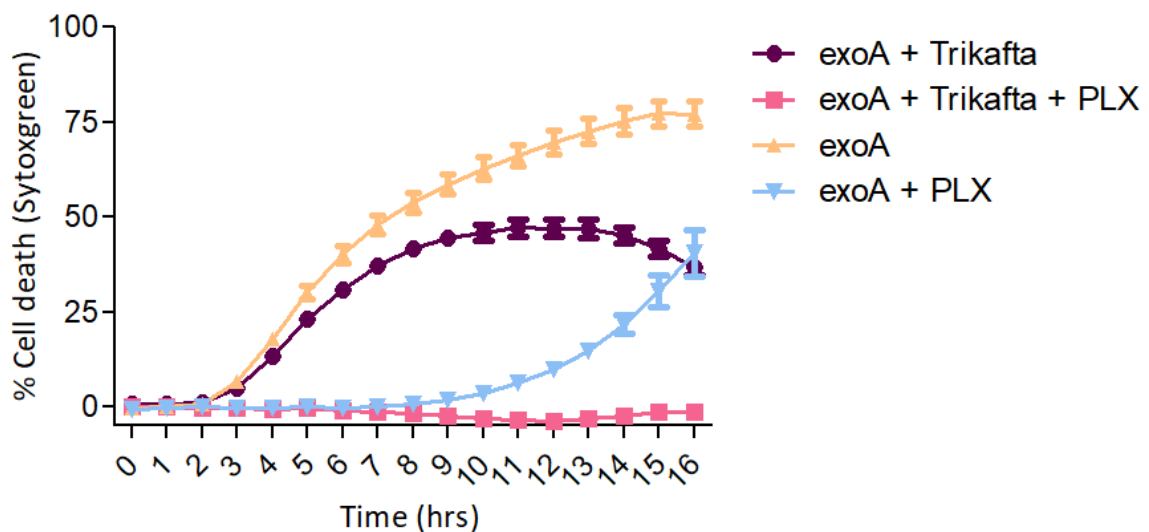


Figure S2: Cell death of primary nasal cells from cystic fibrosis (CF) patients induced by ExoA exposure.

Legend: Primary human nasal cells (pHNECs) derived from Cystic Fibrosis patients were plated at a density of 7000 cells per well in black/clear 96-well plates in Pneumacult medium containing the trikafta therapy: Ivacaftor (VX-770) (10uM), Tezacaftor (VX-661) (10uM), Elexacaftor (VX-445) (5uM). Following 48h of treatment, medium was changed and replaced by Pneumacult medium that contains the Trikafta therapy +/- ZAK inhibitor PLX4720 (10uM) After 1hour of treatment, the cells were stimulated with Exotoxin A and supplemented with SYTOX-Green dye (100ng/mL). Green fluorescence is measured in real-time using Clariostar plate reader equipped with a 37°C cell incubator. Maximal cell death was determined with whole cell lysates from unstimulated cells incubated with 1% Triton X-100.

This study also leaves many unanswered concerns and invites further research, including whether the NF-KB overactivation observed in CF patients could be related to this increased response by the NLRP1 inflammasome? Could overactivation of NF-KB prime and over-activate NLRP1? We failed to show an increase in NLRP1 expression in CF patients but we didn't investigate a possible overactivation of NLRP1. Interestingly, this hypothesis provides the opportunity to investigate new diseases. In this context, I am interested in the study of ubiquitinopathies, a new group of auto-inflammatory diseases. Recently, deregulation in the ubiquitin pathway has been reported in patients with auto-inflammatory diseases. In this context, the A20/TNFAIP3 (HA20) haploinsufficiency relies on the stimulation of the NFkB pro-inflammatory pathway related to decreased recruitment of A20 to the NFkB signaling complex and

decreased deubiquitination by A20. As a result, children (7 months to 16 years of age) may develop a clinical Behçet-like phenotype, which includes bipolar aphtosis, skin lesions, and ophthalmologic involvement (Q. Zhou et al., 2015). All of these data suggest a potential role for NLRP1 in skin and ophthalmic damage. It would be interesting to investigate if this overactivation of the NF-KB pathway (as shown in CF patients) can be connected with a susceptibility to respond to NLRP1 in these tissues.

In the last few years, significant progress has been made in understanding the molecular mechanisms driving the activation of the inflammasome sensor NLRP1 by pathogens and by perturbation of cellular homeostasis. NLRP1 activation is extremely complex and different from the others inflammasome sensors which makes studying it a real challenge. NLRP1 (and CARD8) are the unique inflammasome sensors with an intrinsic autoproteolytic activity that is required but insufficient for activation that needs the release of the effector C-terminal domain. This precise and unique structure gives a chance for specific pharmacological targeting of NLRP1 activation and to develop a treatment for patients with skin cancer and other autoinflammatory skin diseases.

Altogether, we certainly show the importance of the human models to study the NLRP1 inflammasome and we show the importance and the emergence of human NLRP1 inflammasome as a sensor of microbial virulence in airway human epithelium. Our results strongly encourage to develop human models of the lung, skin, cornea and others to really understand all the complexity of the NLRP1 inflammasome.

VI. REFERENCES

- A.C. Allison, & Phill B.M. (1954). *Protection Afforded by Sickle-cell trait against subtertian malarial infection*. <https://doi.org/10.1136/bmj.1.4857.290>
- Aglietti, R. A., & Dueber, E. C. (2017). Recent Insights into the Molecular Mechanisms Underlying Pyroptosis and Gasdermin Family Functions. In *Trends in Immunology* (Vol. 38, Issue 4, pp. 261–271). Elsevier Ltd. <https://doi.org/10.1016/j.it.2017.01.003>
- Agostini, L., Martinon, F., Burns, K., Mcdermott, M. F., Hawkins, P. N., & Jürg Tschopp. (2004). NALP3 Forms an IL-1-Processing Inflammasome with Increased Activity in Muckle-Wells Autoinflammatory Disorder containing protein called ASC binds and activates pro-caspase-1. In *Immunity* (Vol. 20). [https://doi.org/10.1016/s1074-7613\(04\)00046-9](https://doi.org/10.1016/s1074-7613(04)00046-9)
- Akino, K., Toyota, M., Suzuki, H., Imai, T., Maruyama, R., Kusano, M., Nishikawa, N., Watanabe, Y., Sasaki, Y., Abe, T., Yamamoto, E., Tarasawa, I., Sonoda, T., Mori, M., Imai, K., Shinomura, Y., & Tokino, T. (2007). Identification of DFNA5 as a target of epigenetic inactivation in gastric cancer. *Cancer Science*, *98*(1), 88–95. <https://doi.org/10.1111/j.1349-7006.2006.00351.x>
- Anderson, K. V, Bokla, L., & Niisslein-Volhard, C. (1985). Establishment of Dorsal-Ventral Polarity in the Drosophila Embryo: The Induction of Polarity by the Toll Gene Product. In *Cell* (Vol. 42). [https://doi.org/10.1016/0092-8674\(85\)90275-2](https://doi.org/10.1016/0092-8674(85)90275-2)
- Andrew Sandstrom. (2023). NLRP1 activation by UVB: Shedding light on an enigmatic inflammasome. *Journal of Experimental Medicine*, *220*(1). <https://doi.org/10.1084/jem.20220837>
- Bachovchin, D. A. (2021). NLRP1: a jack of all trades, or a master of one? *Molecular Cell*, *81*(3), 423–425. <https://doi.org/10.1016/j.molcel.2021.01.001>
- Ball, D. P., Wang, A. E., Warren, C. D., Wang, Q., Griswold, A. R., Rao, S. D., & Bachovchin, D. A. (2022). Oxidized thioredoxin-1 restrains the NLRP1 inflammasome Short Title: Thioredoxin restrains NLRP1. *Science*. <https://doi.org/10.1101/2021.09.20.461118>
- Bardet, J., Laverdure, N., Fusaro, M., Picard, C., Garnier, L., Viel, S., Collardeau-frachon, S., de Guillebon, J. M., Durieu, I., Casari-thery, C., Mortamet, G., Laurent, A., & Belot, A. (2021). Nlr4 gof mutations, a challenging diagnosis from neonatal age to adulthood. *Journal of Clinical Medicine*, *10*(19). <https://doi.org/10.3390/jcm10194369>
- Barry, R., John, S. W., Liccardi, G., Tenev, T., Jaco, I., Chen, C. H., Choi, J., Kasperkiewicz, P., Fernandes-Alnemri, T., Alnemri, E., Drag, M., Chen, Y., & Meier, P. (2018). SUMO-mediated regulation of NLRP3 modulates inflammasome activity. *Nature Communications*, *9*(1). <https://doi.org/10.1038/s41467-018-05321-2>
- Bauernfeind, F. G., Horvath, G., Stutz, A., Alnemri, E. S., MacDonald, K., Speert, D., Fernandes-Alnemri, T., Wu, J., Monks, B. G., Fitzgerald, K. A., Hornung, V., & Latz, E. (2009). Cutting Edge: NF-κB Activating Pattern Recognition and Cytokine Receptors License NLRP3 Inflammasome Activation by Regulating NLRP3 Expression. *The Journal of Immunology*, *183*(2), 787–791. <https://doi.org/10.4049/jimmunol.0901363>
- Bauernfried, S., & Hornung, V. (2021). Human NLRP1: From the shadows to center stage. *Journal of Experimental Medicine*, *219*(1). <https://doi.org/10.1084/jem.20211405>

- Bauernfried, S., Scherr, M. J., Pichlmair, A., Duderstadt, K. E., & Hornung, V. (2021). Human NLRP1 is a sensor for double-stranded RNA. *Science*, *371*(6528). <https://doi.org/10.1126/science.abd0811>
- Benjamin Faustin, & John C. Reed. (2008). Sunburned skin activates inflammasomes. In *Trends in Cell Biology* (Vol. 18, Issue 1, pp. 1–4). <https://doi.org/10.1016/j.tcb.2007.11.003>
- Bérubé, J., Roussel, L., Nattagh, L., & Rousseau, S. (2010). Loss of cystic fibrosis transmembrane conductance regulator function enhances activation of p38 and erk mapks, increasing interleukin-6 synthesis in airway epithelial cells exposed to *Pseudomonas aeruginosa*. *Journal of Biological Chemistry*, *285*(29), 22299–22307. <https://doi.org/10.1074/jbc.M109.098566>
- Bittner, Z. A., Schrader, M., George, S. E., & Amann, R. (2022). Pyroptosis and Its Role in SARS-CoV-2 Infection. In *Cells* (Vol. 11, Issue 10). MDPI. <https://doi.org/10.3390/cells11101717>
- Blanco, R., Carrasco, L., & Ventoso, I. (2003). Cell killing by HIV-1 protease. *Journal of Biological Chemistry*, *278*(2), 1086–1093. <https://doi.org/10.1074/jbc.M205636200>
- Boyden, E. D., & Dietrich, W. F. (2006). Nalp1b controls mouse macrophage susceptibility to anthrax lethal toxin. *Nature Genetics*, *38*(2), 240–244. <https://doi.org/10.1038/ng1724>
- Bürckstümmer, T., Baumann, C., Blüml, S., Dixit, E., Dürnberger, G., Jahn, H., Planyavsky, M., Bilban, M., Colinge, J., Bennett, K. L., & Superti-Furga, G. (2009). An orthogonal proteomic-genomic screen identifies AIM2 as a cytoplasmic DNA sensor for the inflammasome. *Nature Immunology*, *10*(3), 266–272. <https://doi.org/10.1038/ni.1702>
- Burian, M., & Yazdi, A. S. (2018). NLRP1 Is the Key Inflammasome in Primary Human Keratinocytes. In *Journal of Investigative Dermatology* (Vol. 138, Issue 12, pp. 2507–2510). Elsevier B.V. <https://doi.org/10.1016/j.jid.2018.08.004>
- Carriere, J., Dorfleutner, A., & Stehlik, C. (2021). NLRP7: From inflammasome regulation to human disease. In *Immunology* (Vol. 163, Issue 4, pp. 363–376). John Wiley and Sons Inc. <https://doi.org/10.1111/imm.13372>
- Cassel, S. L., Eisenbarth, S. C., Iyer, S. S., Sadler, J. J., Colegio, O. R., Tephly, L. A., Carter, A. B., Rothman, P. B., Flavell, R. A., & Sutterwala, F. S. (2008). *The Nalp3 inflammasome is essential for the development of silicosis*. <https://doi.org/10.1073/pnas.0803933105>
- Cassone, A., Vecchiarelli, A., & Hube, B. (2016). Aspartyl Proteinases of Eukaryotic Microbial Pathogens: From Eating to Heating. In *PLoS Pathogens* (Vol. 12, Issue 12). Public Library of Science. <https://doi.org/10.1371/journal.ppat.1005992>
- Cauchois, R., Koubi, M., Delarbre, D., Manet, C., Carvelli, J., Benjamin Blasco, V., Jean, R., Fouche, L., Bornet, C., Pauly, V., Mazodier, K., Pestre, V., Jarrot, P.-A., Dinarello, C. A., & Kaplanski, G. (n.d.). *Early IL-1 receptor blockade in severe inflammatory respiratory failure complicating COVID-19*. <https://doi.org/10.1073/pnas.2009017117/-/DCSupplemental>
- Chang, N. C. (2020). Autophagy and Stem Cells: Self-Eating for Self-Renewal. In *Frontiers in Cell and Developmental Biology* (Vol. 8). Frontiers Media S.A. <https://doi.org/10.3389/fcell.2020.00138>
- Chavarría-Smith, J., Mitchell, P. S., Ho, A. M., Daugherty, M. D., & Vance, R. E. (2016). Functional and Evolutionary Analyses Identify Proteolysis as a General Mechanism for NLRP1 Inflammasome Activation. *PLoS Pathogens*, *12*(12). <https://doi.org/10.1371/journal.ppat.1006052>

- Chavarría-Smith, J., & Vance, R. E. (2013). Direct Proteolytic Cleavage of NLRP1B Is Necessary and Sufficient for Inflammasome Activation by Anthrax Lethal Factor. *PLoS Pathogens*, 9(6). <https://doi.org/10.1371/journal.ppat.1003452>
- Chear, C. T., Nallusamy, R., Canna, S. W., Chan, K. C., Baharin, M. F., Hishamshah, M., Ghani, H., Ripen, A. M., & Mohamad, S. bin. (2020). A novel de novo NLRC4 mutation reinforces the likely pathogenicity of specific LRR domain mutation. *Clinical Immunology*, 211. <https://doi.org/10.1016/j.clim.2019.108328>
- Chen, C., & Xu, P. (2022). Cellular functions of cGAS-STING signaling. In *Trends in Cell Biology*. Elsevier Ltd. <https://doi.org/10.1016/j.tcb.2022.11.001>
- Chen, J., & Chen, Z. J. (2018). PtdIns4P on dispersed trans-Golgi network mediates NLRP3 inflammasome activation. *Nature*, 564(7734), 71–76. <https://doi.org/10.1038/s41586-018-0761-3>
- Chen, J., Kos, R., Garssen, J., & Redegeld, F. (2019). Molecular insights into the mechanism of necroptosis: The necrosome as a potential therapeutic target. In *Cells* (Vol. 8, Issue 12). MDPI. <https://doi.org/10.3390/cells8121486>
- Chen, K. W., Demarco, B., Heilig, R., Shkarina, K., Boettcher, A., Farady, C. J., Pelczar, P., & Broz, P. (2019). Extrinsic and intrinsic apoptosis activate pannexin-1 to drive NLRP 3 inflammasome assembly. *The EMBO Journal*, 38(10). <https://doi.org/10.15252/embj.2019101638>
- Chen, Q., Shen, Y., & Zheng, J. (2021). A review of cystic fibrosis: Basic and clinical aspects. In *Animal Models and Experimental Medicine* (Vol. 4, Issue 3, pp. 220–232). John Wiley and Sons Inc. <https://doi.org/10.1002/ame2.12180>
- Chen, Q., Shi, P., Wang, Y., Zou, D., Wu, X., Wang, D., Hu, Q., Zou, Y., Huang, Z., Ren, J., Lin, Z., & Gao, X. (2019). GSDMB promotes non-canonical pyroptosis by enhancing caspase-4 activity. *Journal of Molecular Cell Biology*, 11(6), 496–508. <https://doi.org/10.1093/jmcb/mjy056>
- Chen, Y., Shao, X., Cao, J., Zhu, H., Yang, B., He, Q., & Ying, M. (2021). Phosphorylation regulates cullin-based ubiquitination in tumorigenesis. In *Acta Pharmaceutica Sinica B* (Vol. 11, Issue 2, pp. 309–321). Chinese Academy of Medical Sciences. <https://doi.org/10.1016/j.apsb.2020.09.007>
- Chisholm, S. T., Coaker, G., Day, B., & Staskawicz, B. J. (2006). Host-microbe interactions: Shaping the evolution of the plant immune response. In *Cell* (Vol. 124, Issue 4, pp. 803–814). Elsevier B.V. <https://doi.org/10.1016/j.cell.2006.02.008>
- Christgen, S., Place, D. E., & Kanneganti, T. D. (2020). Toward targeting inflammasomes: insights into their regulation and activation. In *Cell Research* (Vol. 30, Issue 4, pp. 315–327). Springer Nature. <https://doi.org/10.1038/s41422-020-0295-8>
- Chui, A. J., Okondo, M. C., Rao, S. D., Gai, K., Griswold, A. R., Johnson, D. C., Ball, D. P., Taabazuing, C. Y., Orth, E. L., Vittimberga, B. A., & Bachovchin, D. A. (2019). N-terminal degradation activates the NLRP1B inflammasome. In *Science* (Vol. 364).
- Clav, C., Dyrka, W., Turcotte, E. A., Granger-Farbos, A., ea Ibarlosa, L., Pinson, it, Vance, R. E., Saupe, S. J., & Daskalov, A. (2022). Fungal gasdermin-like proteins are controlled by proteolytic cleavage. *PNAS*. <https://doi.org/10.1073/pnas.2109418119/-/DCSupplemental>
- Coll, R. C., Schroder, K., & Pelegrín, P. (2022). NLRP3 and pyroptosis blockers for treating inflammatory diseases. In *Trends in Pharmacological Sciences* (Vol. 43, Issue 8, pp. 653–668). Elsevier Ltd. <https://doi.org/10.1016/j.tips.2022.04.003>

- Craven, R. R., Gao, X., Allen, I. C., Gris, D., Wardenburg, J. B., McElvania-TeKippe, E., Ting, J. P., & Duncan, J. A. (2009). Staphylococcus aureus α -hemolysin activates the NLRP3-inflammasome in human and mouse monocytic cells. *PLoS ONE*, 4(10). <https://doi.org/10.1371/journal.pone.0007446>
- Cridland, J. A., Curley, E. Z., Wykes, M. N., Schroder, K., Sweet, M. J., Roberts, T. L., Ragan, M. A., Kassahn, K. S., & Stacey, K. J. (2012). The mammalian PYHIN gene family: Phylogeny, evolution and expression. *BMC Evolutionary Biology*, 12(1). <https://doi.org/10.1186/1471-2148-12-140>
- Croes, L., Beyens, M., Fransen, E., Ibrahim, J., vanden Berghe, W., Suls, A., Peeters, M., Pauwels, P., van Camp, G., & op de Beeck, K. (2018). Large-scale analysis of DFNA5 methylation reveals its potential as biomarker for breast cancer. *Clinical Epigenetics*, 10(1). <https://doi.org/10.1186/s13148-018-0479-y>
- Dangl, J. L., & Jones, J. D. G. (2019). A pentangular plant inflammasome. In *Science* (Vol. 364, Issue 6435, pp. 31–32). American Association for the Advancement of Science. <https://doi.org/10.1126/science.aax0174>
- Das, S., Miller, M., Beppu, A. K., Mueller, J., McGeough, M. D., Vuong, C., Karta, M. R., Rosenthal, P., Chouiali, F., Doherty, T. A., Kurten, R. C., Hamid, Q., Hoffman, H. M., & Broide, D. H. (2016). GSDMB induces an asthma phenotype characterized by increased airway responsiveness and remodeling without lung inflammation. *Proceedings of the National Academy of Sciences of the United States of America*, 113(46), 13132–13137. <https://doi.org/10.1073/pnas.1610433113>
- de Menthière, C. S., Terrière, S., Pugnère, D., Ruiz, M., Demaille, J., & Touitou, I. (2003). INFEVERS: The registry for FMF and hereditary inflammatory disorders mutations. In *Nucleic Acids Research* (Vol. 31, Issue 1, pp. 282–285). <https://doi.org/10.1093/nar/gkg031>
- Delmaghani, S., del Castillo, F. J., Michel, V., Leibovici, M., Aghaie, A., Ron, U., van Laer, L., Ben-Tal, N., van Camp, G., Weil, D., Langa, F., Lathrop, M., Avan, P., & Petit, C. (2006). Mutations in the gene encoding pejvakain, a newly identified protein of the afferent auditory pathway, cause DFNB59 auditory neuropathy. *Nature Genetics*, 38(7), 770–778. <https://doi.org/10.1038/ng1829>
- Demarco, B., Grayczyk, J. P., Bjanec, E., le Roy, D., Tonnus, W., Assenmacher, C.-A., Radaelli, E., Fettlelet, T., Mack, V., Linkermann, A., Roger, T., Brodsky, I. E., Chen, K. W., & Broz, P. (2020). Caspase-8-dependent gasdermin D cleavage promotes antimicrobial defense but confers susceptibility to TNF-induced lethality. In *Sci. Adv* (Vol. 6).
- Deng, W., Bai, Y., Deng, F., Pan, Y., Mei, S., Zheng, Z., Min, R., Wu, Z., Li, W., Miao, R., Zhang, Z., Kupper, T. S., Lieberman, J., & Liu, X. (2022a). Streptococcal pyrogenic exotoxin B cleaves GSDMA and triggers pyroptosis. *Nature*, 602(7897), 496–502. <https://doi.org/10.1038/s41586-021-04384-4>
- Di, A., Xiong, S., Ye, Z., Malireddi, R. K. S., Kometani, S., Zhong, M., Mittal, M., Hong, Z., Kanneganti, T. D., Rehman, J., & Malik, A. B. (2018). The TWIK2 Potassium Efflux Channel in Macrophages Mediates NLRP3 Inflammasome-Induced Inflammation. *Immunity*, 49(1), 56–65.e4. <https://doi.org/10.1016/j.immuni.2018.04.032>
- Dinareello, C. A. (2009). Immunological and inflammatory functions of the interleukin-1 family. In *Annual Review of Immunology* (Vol. 27, pp. 519–550). <https://doi.org/10.1146/annurev.immunol.021908.132612>
- Ding, J., Wang, K., Liu, W., She, Y., Sun, Q., Shi, J., Sun, H., Wang, D. C., & Shao, F. (2016). Pore-forming activity and structural autoinhibition of the gasdermin family. *Nature*, 535(7610), 111–116. <https://doi.org/10.1038/nature18590>

- Dong, S., Shi, Y., Dong, X., Xiao, X., Qi, J., Ren, L., Xiang, Z., Zhou, Z., Wang, J., & Lei, X. (2022). Gasdermin E is required for induction of pyroptosis and severe disease during enterovirus 71 infection. *Journal of Biological Chemistry*, 298(5). <https://doi.org/10.1016/j.jbc.2022.101850>
- Dostert, C., Pétrilli, V., Bruggen, R. Van, Steele, C., Mossman, B. T., & Tschopp, J. (n.d.). *Innate Immune Activation Through Nalp3 Inflammasome Sensing of Asbestos and Silica*. <https://doi.org/10.1126/science.1156995>
- D’Oswaldo, A., Weichenberger, C. X., Wagner, R. N., Godzik, A., Wooley, J., & Reed, J. C. (2011). CARD8 and NLRP1 undergo autoproteolytic processing through a ZU5-like domain. *PLoS ONE*, 6(11). <https://doi.org/10.1371/journal.pone.0027396>
- Drutman, S. B., Haerynck, F., Zhong, F. L., Hum, D., Hernandez, N. J., Belkaya, S., Rapaport, F., de Jong, S. J., Creytens, D., Tavernier, S. J., Bonte, K., De Schepper, S., der Werff ten Bosch, J. van, Lorenzo-Diaz, L., Wullaert, A., Bossuyt, X., Orth, G., Bonagura, V. R., Béziat, V., ... Laurent-Casanova, J. (2019). Homozygous NLRP1 gain-of-function mutation in siblings with a syndromic form of recurrent respiratory papillomatosis. *Proceedings of the National Academy of Sciences of the United States of America*, 116(38), 19055–19063. <https://doi.org/10.1073/pnas.1906184116>
- Edward Shen, Ying Han, & Min He. (2021). Low expression of NLRP1 is associated with a poor prognosis and immune infiltration in lung adenocarcinoma patients. *Aging*. <https://doi.org/10.18632/aging.202620>
- Ewald, S. E., Chavarria-Smith, J., & Boothroyd, J. C. (2014). NLRP1 is an inflammasome sensor for *Toxoplasma gondii*. *Infection and Immunity*, 82(1), 460–468. <https://doi.org/10.1128/IAI.01170-13>
- Feldmeyer, L., Keller, M., Niklaus, G., Hohl, D., Werner, S., & Beer, H. D. (2007a). The Inflammasome Mediates UVB-Induced Activation and Secretion of Interleukin-1 β by Keratinocytes. *Current Biology*, 17(13), 1140–1145. <https://doi.org/10.1016/j.cub.2007.05.074>
- Fernandes-Alnemri, T., Yu, J. W., Datta, P., Wu, J., & Alnemri, E. S. (2009). AIM2 activates the inflammasome and cell death in response to cytoplasmic DNA. *Nature*, 458(7237), 509–513. <https://doi.org/10.1038/nature07710>
- Ferreira, A. C., Soares, V. C., de Azevedo-Quintanilha, I. G., Dias, S. da S. G., Fintelman-Rodrigues, N., Sacramento, C. Q., Mattos, M., de Freitas, C. S., Temerozo, J. R., Teixeira, L., Damaceno Hottz, E., Barreto, E. A., Pão, C. R. R., Palhinha, L., Miranda, M., Bou-Habib, D. C., Bozza, F. A., Bozza, P. T., & Souza, T. M. L. (2021). SARS-CoV-2 engages inflammasome and pyroptosis in human primary monocytes. *Cell Death Discovery*, 7(1). <https://doi.org/10.1038/s41420-021-00428-w>
- Fitzgerald, K. A., & Kagan, J. C. (2020). Toll-like Receptors and the Control of Immunity. In *Cell* (Vol. 180, Issue 6, pp. 1044–1066). Cell Press. <https://doi.org/10.1016/j.cell.2020.02.041>
- Franchi, L., Amer, A., Body-Malapel, M., Kanneganti, T. D., Özören, N., Jagirdar, R., Inohara, N., Vandenabeele, P., Bertin, J., Coyle, A., Grant, E. P., & Núñez, G. (2006). Cytosolic flagellin requires Ipaf for activation of caspase-1 and interleukin 1 β in salmonella-infected macrophages. *Nature Immunology*, 7(6), 576–582. <https://doi.org/10.1038/ni1346>
- Gaidt, M. M., Ebert, T. S., Chauhan, D., Schmidt, T., Schmid-Burgk, J. L., Rapino, F., Robertson, A. A. B., Cooper, M. A., Graf, T., & Hornung, V. (2016). Human Monocytes Engage an Alternative Inflammasome Pathway. *Immunity*, 44(4), 833–846. <https://doi.org/10.1016/j.immuni.2016.01.012>

- Gao, W., Yang, J., Liu, W., Wang, Y., & Shao, F. (2016a). Site-specific phosphorylation and microtubule dynamics control Pyrin inflammasome activation. *Proceedings of the National Academy of Sciences of the United States of America*, *113*(33), E4857–E4866. <https://doi.org/10.1073/pnas.1601700113>
- Geiss-Friedlander, R., Parmentier, N., Möller, U., Urlaub, H., Van den Eynde, B. J., & Melchoir, F. (2009). The cytoplasmic peptidase DPP9 is rate-limiting for degradation of proline-containing peptides. *Journal of Biological Chemistry*, *284*(40), 27211–27219. <https://doi.org/10.1074/jbc.M109.041871>
- Griswold, A. R., Ball, D. P., Bhattacharjee, A., Chui, A. J., Rao, S. D., Taabazuing, C. Y., & Bachovchin, D. A. (2019). DPP9's Enzymatic Activity and Not Its Binding to CARD8 Inhibits Inflammasome Activation. *ACS Chemical Biology*, *14*(11), 2424–2429. <https://doi.org/10.1021/acschembio.9b00462>
- Griswold, A. R., Huang, H. C., & Bachovchin, D. A. (2022). The NLRP1 Inflammasome Induces Pyroptosis in Human Corneal Epithelial Cells. *Investigative Ophthalmology and Visual Science*, *63*(3). <https://doi.org/10.1167/iovs.63.3.2>
- Gross, O., Poeck, H., Bscheider, M., Dostert, C., Hanneschläger, N., Endres, S., Hartmann, G., Tardivel, A., Schweighoffer, E., Tybulewicz, V., Mocsai, A., Tschopp, J., & Ruland, J. (2009). Syk kinase signalling couples to the Nlrp3 inflammasome for anti-fungal host defence. *Nature*, *459*(7245), 433–436. <https://doi.org/10.1038/nature07965>
- Guo, C., Chi, Z., Jiang, D., Xu, T., Yu, W., Wang, Z., Chen, S., Zhang, L., Liu, Q., Guo, X., Zhang, X., Li, W., Lu, L., Wu, Y., Song, B. L., & Wang, D. (2018). Cholesterol Homeostatic Regulator SCAP-SREBP2 Integrates NLRP3 Inflammasome Activation and Cholesterol Biosynthetic Signaling in Macrophages. *Immunity*, *49*(5), 842–856.e7. <https://doi.org/10.1016/j.immuni.2018.08.021>
- Gurung, P., & Kanneganti, T. D. (2015). Novel Roles for Caspase-8 in IL-1 β and Inflammasome Regulation. In *American Journal of Pathology* (Vol. 185, Issue 1, pp. 17–25). Elsevier Inc. <https://doi.org/10.1016/j.ajpath.2014.08.025>
- Hagar, J. A., & Miao, E. A. (2014). Detection of cytosolic bacteria by inflammatory caspases. In *Current Opinion in Microbiology* (Vol. 17, Issue 1, pp. 61–66). <https://doi.org/10.1016/j.mib.2013.11.008>
- Hara, H., Seregin, S. S., Yang, D., Fukase, K., Chamaillard, M., Alnemri, E. S., Inohara, N., Chen, G. Y., & Núñez, G. (2018). The NLRP6 Inflammasome Recognizes Lipoteichoic Acid and Regulates Gram-Positive Pathogen Infection. *Cell*, *175*(6), 1651–1664.e14. <https://doi.org/10.1016/j.cell.2018.09.047>
- Hawer, H., Mendelsohn, B. A., Mayer, K., Kung, A., Malhotra, A., Tuupainen, S., Schleit, J., Brinkmann, U., & Schaffrath, R. (2020). Diphthamide-deficiency syndrome: a novel human developmental disorder and ribosomopathy. *European Journal of Human Genetics*, *28*(11), 1497–1508. <https://doi.org/10.1038/s41431-020-0668-y>
- He, Y., Hara, H., & Núñez, G. (2016). Mechanism and Regulation of NLRP3 Inflammasome Activation. In *Trends in Biochemical Sciences* (Vol. 41, Issue 12, pp. 1012–1021). Elsevier Ltd. <https://doi.org/10.1016/j.tibs.2016.09.002>
- He, Y., Zeng, M. Y., Yang, D., Motro, B., & Núñez, G. (2016). NEK7 is an essential mediator of NLRP3 activation downstream of potassium efflux. *Nature*, *530*(7590), 354–357. <https://doi.org/10.1038/nature16959>

- Heilig, R., & Broz, P. (2018). Function and mechanism of the pyrin inflammasome. In *European Journal of Immunology* (Vol. 48, Issue 2, pp. 230–238). Wiley-VCH Verlag. <https://doi.org/10.1002/eji.201746947>
- Heilig, R., Dick, M. S., Sborgi, L., Meunier, E., Hiller, S., & Broz, P. (2018). The Gasdermin-D pore acts as a conduit for IL-1 β secretion in mice. *European Journal of Immunology*, 48(4), 584–592. <https://doi.org/10.1002/eji.201747404>
- Hergueta-Redondo, M., Sarrió, D., Molina-Crespo, Á., Megias, D., Mota, A., Rojo-Sebastian, A., García-Sanz, P., Morales, S., Abril, S., Cano, A., Peinado, H., & Moreno-Bueno, G. (2014). Gasdermin-B promotes invasion and metastasis in breast cancer cells. *PLoS ONE*, 9(3). <https://doi.org/10.1371/journal.pone.0090099>
- Hochreiter-Hufford, A., & Ravichandran, K. S. (2013). Clearing the dead: Apoptotic cell sensing, recognition, engulfment, and digestion. *Cold Spring Harbor Perspectives in Biology*, 5(1). <https://doi.org/10.1101/cshperspect.a008748>
- Holler, N., Zaru, R., Micheau, O., Thome, M., Attinger, A., Valitutti, S., Bodmer, J.-L., Schneider, P., Seed, B., & Tschopp, J. (2000). *Fas triggers an alternative, caspase-8-independent cell death pathway using the kinase RIP as effector molecule*. <http://immunol.nature.com>
- Hollingsworth, L. R., Sharif, H., Griswold, A. R., Fontana, P., Mintseris, J., Dagbay, K. B., Paulo, J. A., Gygi, S. P., Bachovchin, D. A., & Wu, H. (2021). DPP9 sequesters the C terminus of NLRP1 to repress inflammasome activation. *Nature*, 592(7856), 778–783. <https://doi.org/10.1038/s41586-021-03350-4>
- Hornung, V., Ablasser, A., Charrel-Dennis, M., Bauernfeind, F., Horvath, G., Caffrey, D. R., Latz, E., & Fitzgerald, K. A. (2009a). AIM2 recognizes cytosolic dsDNA and forms a caspase-1-activating inflammasome with ASC. *Nature*, 458(7237), 514–518. <https://doi.org/10.1038/nature07725>
- Hornung, V., Bauernfeind, F., Halle, A., Samstad, E. O., Kono, H., Rock, K. L., Fitzgerald, K. A., & Latz, E. (2008a). Silica crystals and aluminum salts activate the NALP3 inflammasome through phagosomal destabilization. *Nature Immunology*, 9(8), 847–856. <https://doi.org/10.1038/ni.1631>
- Hou, J., Zhao, R., Xia, W., Chang, C. W., You, Y., Hsu, J. M., Nie, L., Chen, Y., Wang, Y. C., Liu, C., Wang, W. J., Wu, Y., Ke, B., Hsu, J. L., Huang, K., Ye, Z., Yang, Y., Xia, X., Li, Y., ... Hung, M. C. (2020). PD-L1-mediated gasdermin C expression switches apoptosis to pyroptosis in cancer cells and facilitates tumour necrosis. *Nature Cell Biology*, 22(10), 1264–1275. <https://doi.org/10.1038/s41556-020-0575-z>
- Hoyle, C., Green, J. P., Allan, S. M., Brough, D., & Lemarchand, E. (2022). Itaconate and fumarate derivatives inhibit priming and activation of the canonical NLRP3 inflammasome in macrophages. *Immunology*, 165(4), 460–480. <https://doi.org/10.1111/imm.13454>
- Hu, J. J., Liu, X., Xia, S., Zhang, Z., Zhang, Y., Zhao, J., Ruan, J., Luo, X., Lou, X., Bai, Y., Wang, J., Hollingsworth, L. R., Magupalli, V. G., Zhao, L., Luo, H. R., Kim, J., Lieberman, J., & Wu, H. (2020). FDA-approved disulfiram inhibits pyroptosis by blocking gasdermin D pore formation. *Nature Immunology*, 21(7), 736–745. <https://doi.org/10.1038/s41590-020-0669-6>
- Huang, M., Zhang, X., Toh, G. A., Gong, Q., Wang, J., Han, Z., Wu, B., Zhong, F., & Chai, J. (2021a). Structural and biochemical mechanisms of NLRP1 inhibition by DPP9. *Nature*, 592(7856), 773–777. <https://doi.org/10.1038/s41586-021-03320-w>

- Humphries, F., Shmuel-Galia, L., Ketelut-Carneiro, N., Li, S., Wang, B., Nemmara, V. V., Wilson, R., Jiang, Z., Khalighinejad, F., Muneeruddin, K., Shaffer, S. A., Dutta, R., Ionete, C., Pesiridis, S., Yang, S., Thompson, P. R., & Fitzgerald, K. A. (n.d.-a). *Succination inactivates gasdermin D and blocks pyroptosis*. <https://doi.org/10.1126/science.abb9818>
- I. Just, J. Selzer, M. Wilm, C. von Eichel-Streiber, M. Mann, & K. Aktories. (1995). *Glucosylation of Rho proteins by Clostridium difficile toxin B*.
- Inohara, N., Chamailard, M., McDonald, C., & Nuñez, G. (2005). NOD-LRR proteins: Role in host-microbial interactions and inflammatory disease. In *Annual Review of Biochemistry* (Vol. 74, pp. 355–383). <https://doi.org/10.1146/annurev.biochem.74.082803.133347>
- Ito, M., Yanagi, Y., & Ichinohe, T. (2012). Encephalomyocarditis Virus Viroporin 2B Activates NLRP3 Inflammasome. *PLoS Pathogens*, 8(8). <https://doi.org/10.1371/journal.ppat.1002857>
- Jandhyala, D. M., Wong, J., Mantis, N. J., Magun, B. E., Leong, J. M., & Thorpe, C. M. (2016). A novel Zak knockout mouse with a defective ribotoxic stress response. *Toxins*, 8(9). <https://doi.org/10.3390/toxins8090259>
- Jenster, L. M., Lange, K. E., Normann, S., vom Hemdt, A., Wuerth, J. D., Schiffelers, L. D. J., Tesfamariam, Y. M., Gohr, F. N., Klein, L., Kaltheuner, I. H., Ebner, S., Lapp, D. J., Mayer, J., Moecking, J., Ploegh, H. L., Latz, E., Meissner, F., Geyer, M., Kümmerer, B. M., & Schmidt, F. I. (2023a). P38 kinases mediate NLRP1 inflammasome activation after ribotoxic stress response and virus infection. *The Journal of Experimental Medicine*, 220(1). <https://doi.org/10.1084/jem.20220837>
- Johnson, D. C., Okondo, M. C., Orth, E. L., Rao, S. D., Huang, H. C., Ball, D. P., & Bachovchin, D. A. (2020b). DPP8/9 inhibitors activate the CARD8 inflammasome in resting lymphocytes. *Cell Death and Disease*, 11(8). <https://doi.org/10.1038/s41419-020-02865-4>
- Johnson, D. C., Taabazuing, C. Y., Okondo, M. C., Chui, A. J., Rao, S. D., Brown, F. C., Reed, C., Peguero, E., de Stanchina, E., Kentsis, A., & Bachovchin, D. A. (2018b). DPP8/DPP9 inhibitor-induced pyroptosis for treatment of acute myeloid leukemia. *Nature Medicine*, 24(8), 1151–1156. <https://doi.org/10.1038/s41591-018-0082-y>
- Jones, J. D. G., Vance, R. E., & Dangl, J. L. (2016). Intracellular innate immune surveillance devices in plants and animals. In *Science* (Vol. 354, Issue 6316). American Association for the Advancement of Science. <https://doi.org/10.1126/science.aaf6395>
- Jørgensen, R., Merrill, A. R., Yates, S. P., Marquez, V. E., Schwan, A. L., Boesen, T., & Andersen, G. R. (2005). Exotoxin A-eEF2 complex structure indicates ADP-ribosylation by ribosome mimicry. *Nature*, 436(7053), 979–984. <https://doi.org/10.1038/nature03871>
- Jørgensen, R., Purdy, A. E., Fieldhouse, R. J., Kimber, M. S., Bartlett, D. H., & Merrill, A. R. (2008). Cholix toxin, a novel ADP-ribosylating factor from *Vibrio cholerae*. *Journal of Biological Chemistry*, 283(16), 10671–10678. <https://doi.org/10.1074/jbc.M710008200>
- Juliana, C., Fernandes-Alnemri, T., Kang, S., Farias, A., Qin, F., & Alnemri, E. S. (2012). Non-transcriptional priming and deubiquitination regulate NLRP3 inflammasome activation. *Journal of Biological Chemistry*, 287(43), 36617–36622. <https://doi.org/10.1074/jbc.M112.407130>
- Junqueira, C., Crespo, Â., Ranjbar, S., de Lacerda, L. B., Lewandrowski, M., Ingber, J., Parry, B., Ravid, S., Clark, S., Schrimpf, M. R., Ho, F., Beakes, C., Margolin, J., Russell, N., Kays, K., Boucau, J., Das Adhikari, U., Vora, S. M., Leger, V., ... Lieberman, J. (2022). FcγR-mediated SARS-CoV-2 infection of

- monocytes activates inflammation. *Nature*, 606(7914), 576–584. <https://doi.org/10.1038/s41586-022-04702-4>
- Kagan, J. C. (2012). Signaling organelles of the innate immune system. In *Cell* (Vol. 151, Issue 6, pp. 1168–1178). Elsevier B.V. <https://doi.org/10.1016/j.cell.2012.11.011>
- Kanneganti, T. D., Body-Malapel, M., Amer, A., Park, J. H., Whitfield, J., Franchi, L., Taraporewala, Z. F., Miller, D., Patton, J. T., Inohara, N., & Núñez, G. (2006). Critical role for Cryopyrin/Nalp3 in activation of caspase-1 in response to viral infection and double-stranded RNA. *Journal of Biological Chemistry*, 281(48), 36560–36568. <https://doi.org/10.1074/jbc.M607594200>
- Karki, R., & Kanneganti, T. D. (2019). Diverging inflammasome signals in tumorigenesis and potential targeting. In *Nature Reviews Cancer* (Vol. 19, Issue 4, pp. 197–214). Nature Publishing Group. <https://doi.org/10.1038/s41568-019-0123-y>
- Kayagaki, N., Kornfeld, O., Lee, B., Stowe Genentech Karen, I. O., Li Genentech Wendy Sandoval, Q., Modrusan, Z., Reja Genentech Meredith Sagolla, R., Webster, J., & Cho, V. (n.d.). *NINJ1 mediates plasma membrane rupture during lytic cell death*. <https://doi.org/10.21203/rs.3.rs-62714/v1>
- Kayagaki, N., Stowe, I. B., Lee, B. L., O'Rourke, K., Anderson, K., Warming, S., Cuellar, T., Haley, B., Roose-Girma, M., Phung, Q. T., Liu, P. S., Lill, J. R., Li, H., Wu, J., Kummerfeld, S., Zhang, J., Lee, W. P., Snipas, S. J., Salvesen, G. S., ... Dixit, V. M. (2015). Caspase-11 cleaves gasdermin D for non-canonical inflammasome signalling. *Nature*, 526(7575), 666–671. <https://doi.org/10.1038/nature15541>
- Kayagaki, N., Warming, S., Lamkanfi, M., Walle, L. vande, Louie, S., Dong, J., Newton, K., Qu, Y., Liu, J., Heldens, S., Zhang, J., Lee, W. P., Roose-Girma, M., & Dixit, V. M. (2011a). Non-canonical inflammasome activation targets caspase-11. *Nature*, 479(7371), 117–121. <https://doi.org/10.1038/nature10558>
- Kerr, J. F. R., Wyllie, A. H., & Curriet, A. R. (1972). Apoptosis: A basic biological phenomenon with wide-ranging implications in tissue kinetics. In *Br. J. Cancer* (Vol. 26). <https://doi.org/10.1038/bjc.1972.33>
- Kerur, N., Veetil, M. V., Sharma-Walia, N., Bottero, V., Sadagopan, S., Otageri, P., & Chandran, B. (2011). IFI16 acts as a nuclear pathogen sensor to induce the inflammasome in response to Kaposi Sarcoma-associated herpesvirus infection. *Cell Host and Microbe*, 9(5), 363–375. <https://doi.org/10.1016/j.chom.2011.04.008>
- Kim, M. L., Chae, J. J., Park, Y. H., de Nardo, D., Stirzaker, R. A., Ko, H. J., Tye, H., Cengia, L., DiRago, L., Metcalf, D., Roberts, A. W., Kastner, D. L., Lew, A. M., Lyras, D., Kile, B. T., Croker, B. A., & Masters, S. L. (2015). Aberrant actin depolymerization triggers the pyrin inflammasome and autoinflammatory disease that is dependent on IL-18, not IL-1 β . *Journal of Experimental Medicine*, 212(6), 927–938. <https://doi.org/10.1084/jem.20142384>
- Kim, M. S., Chang, X., Yamashita, K., Nagpal, J. K., Baek, J. H., Wu, G., Trink, B., Ratovitski, E. A., Mori, M., & Sidransky, D. (2008). Aberrant promoter methylation and tumor suppressive activity of the DFNA5 gene in colorectal carcinoma. *Oncogene*, 27(25), 3624–3634. <https://doi.org/10.1038/sj.onc.1211021>
- Kitamura, A., Sasaki, Y., Abe, T., Kano, H., & Yasutomo, K. (2014). An inherited mutation in NLRC4 causes autoinflammation in human and mice. *Journal of Experimental Medicine*, 211(12), 2385–2396. <https://doi.org/10.1084/jem.20141091>

- Kofoed, E. M., & Vance, R. E. (2011a). Innate immune recognition of bacterial ligands by NAIPs determines inflammasome specificity. *Nature*, 477(7366), 592–597. <https://doi.org/10.1038/nature10394>
- Kohno, R., Nagata, Y., Ishihara, T., Amma, C., Inomata, Y., Seto, T., & Suzuki, R. (2023). Benzo[a]pyrene induces NLRP1 expression and promotes prolonged inflammasome signaling. *Frontiers in Immunology*, 14. <https://doi.org/10.3389/fimmu.2023.1154857>
- Krześniak, M., Zajkovicz, A., Gdowicz-Kłosok, A., Głowala-Kosińska, M., Łasut-Szyska, B., & Rusin, M. (2020). Synergistic activation of p53 by actinomycin D and nutlin-3a is associated with the upregulation of crucial regulators and effectors of innate immunity. *Cellular Signalling*, 69. <https://doi.org/10.1016/j.cellsig.2020.109552>
- Kummer, J. A., Broekhuizen, R., Everett, H., Agostini, L., Kuijk, L., Martinon, F., Van Bruggen, R., & Tschopp, J. (2007). Inflammasome components NALP 1 and 3 show distinct but separate expression profiles in human tissues suggesting a site-specific role in the inflammatory response. *Journal of Histochemistry and Cytochemistry*, 55(5), 443–452. <https://doi.org/10.1369/jhc.6A7101.2006>
- Kusumaningrum, N., Lee, D. H., Yoon, H. S., Park, C. H., & Chung, J. H. (2018). Ultraviolet light-induced Gasdermin C expression is mediated via TRPV1/calcium/calcineurin/NFATc1 signaling. *International Journal of Molecular Medicine*, 42(5), 2859–2866. <https://doi.org/10.3892/ijmm.2018.3839>
- Kyriazopoulou, E., Poulakou, G., Millionis, H., Metallidis, S., Adamis, G., Tsiakos, K., Fragkou, A., Rapti, A., Damoulari, C., Fantoni, M., Kalomenidis, I., Chrysos, G., Angheben, A., Kainis, I., Alexiou, Z., Castelli, F., Serino, F. S., Tsilika, M., Bakakos, P., ... Giamarellos-Bourboulis, E. J. (2021). Early treatment of COVID-19 with anakinra guided by soluble urokinase plasminogen receptor plasma levels: a double-blind, randomized controlled phase 3 trial. *Nature Medicine*, 27(10), 1752–1760. <https://doi.org/10.1038/s41591-021-01499-z>
- Lacey, C. A., & Miao, E. A. (2020). Programmed cell death in the evolutionary race against bacterial virulence factors. *Cold Spring Harbor Perspectives in Medicine*, 10(2). <https://doi.org/10.1101/cshperspect.a036459>
- Lamkanfi, M., & Dixit, V. M. (2014). Mechanisms and functions of inflammasomes. In *Cell* (Vol. 157, Issue 5, pp. 1013–1022). Elsevier B.V. <https://doi.org/10.1016/j.cell.2014.04.007>
- Lee, D. J., Du, F., Chen, S. W., Nakasaki, M., Rana, I., Shih, V. F. S., Hoffmann, A., & Jamora, C. (2015). Regulation and Function of the Caspase-1 in an Inflammatory Microenvironment. *Journal of Investigative Dermatology*, 135(8), 2012–2020. <https://doi.org/10.1038/jid.2015.119>
- Lee, J.-K., Kim, S.-H., Lewis, E. C., Azam, T., Reznikov, L. L., & Dinarello, C. A. (2004). Differences in signaling pathways by IL-1 and IL-18. <https://www.pnas.org>
- Lei, X., Zhang, Z., Xiao, X., Qi, J., He, B., & Wang, J. (2017a). Enterovirus 71 Inhibits Pyroptosis through Cleavage of Gasdermin D. *Journal of Virology*, 91(18). <https://doi.org/10.1128/jvi.01069-17>
- Lemaitre, B., Nicolas, E., & Michaut, L. (1996). The Dorsoventral Regulatory Gene Cassette *spätzle/Toll/cactus* Controls the Potent Antifungal Response in *Drosophila* Adults. In *Cell* (Vol. 86).

- Levinsohn, J. L., Newman, Z. L., Hellmich, K. A., Fattah, R., Getz, M. A., Liu, S., Sastalla, I., Leppla, S. H., & Moayeri, M. (2012). Anthrax lethal factor cleavage of Nlrp1 is required for activation of the inflammasome. *PLoS Pathogens*, *8*(3). <https://doi.org/10.1371/journal.ppat.1002638>
- Li, S., Wu, Y., Yang, D., Wu, C., Ma, C., Liu, X., Moynagh, P. N., Wang, B., Hu, G., & Yang, S. (2019). Gasdermin D in peripheral myeloid cells drives neuroinflammation in experimental autoimmune encephalomyelitis. *Journal of Experimental Medicine*, *216*(11), 2562–2581. <https://doi.org/10.1084/jem.20190377>
- Liao, Y., Pei, J., Cheng, H., & Grishin, N. V. (2014). An ancient autoproteolytic domain found in GAIN, ZU5 and Nucleoporin98. *Journal of Molecular Biology*, *426*(24), 3935–3945. <https://doi.org/10.1016/j.jmb.2014.10.011>
- Linder, A., Bauernfried, S., Cheng, Y., Albanese, M., Jung, C., Keppler, O. T., & Hornung, V. (2020). CARD8 inflammasome activation triggers pyroptosis in human T cells. *The EMBO Journal*, *39*(19). <https://doi.org/10.15252/embj.2020105071>
- Liu, S., Milne, G. T., Kuremsky, J. G., Fink, G. R., & Leppla, S. H. (2004). Identification of the Proteins Required for Biosynthesis of Diphthamide, the Target of Bacterial ADP-Ribosylating Toxins on Translation Elongation Factor 2. *Molecular and Cellular Biology*, *24*(21), 9487–9497. <https://doi.org/10.1128/mcb.24.21.9487-9497.2004>
- Liu, X., Xia, S., Zhang, Z., Wu, H., & Lieberman, J. (2021). Channelling inflammation: gasdermins in physiology and disease. In *Nature Reviews Drug Discovery* (Vol. 20, Issue 5, pp. 384–405). Nature Research. <https://doi.org/10.1038/s41573-021-00154-z>
- Lugrin, J., & Martinon, F. (2018). *The AIM2 Inflammasome: sensor of pathogens and cellular perturbations*.
- Mangan, M. S. J., Olhava, E. J., Roush, W. R., Seidel, H. M., Glick, G. D., & Latz, E. (2018). Targeting the NLRP3 inflammasome in inflammatory diseases. In *Nature Reviews Drug Discovery* (Vol. 17, Issue 8, pp. 588–606). Nature Publishing Group. <https://doi.org/10.1038/nrd.2018.97>
- Mariathasan, S., Newton, K., Monack, D. M., Vucic, D., French, D. M., Lee, W. P., Roose-Girma, M., Erickson, S., & Dixit, V. M. (2004). *Differential activation of the inflammasome by caspase-1 adaptors ASC and Ipaf*. www.nature.com/nature
- Mariathasan, S., Weiss, D. S., Newton, K., McBride, J., O'Rourke, K., Roose-Girma, M., Lee, W. P., Weinrauch, Y., Monack, D. M., & Dixit, V. M. (2006a). Cryopyrin activates the inflammasome in response to toxins and ATP. *Nature*, *440*(7081), 228–232. <https://doi.org/10.1038/nature04515>
- Martinon, F., Burns, K., & Rg Tschopp, J. (2002). The Inflammasome: A Molecular Platform Triggering Activation of Inflammatory Caspases and Processing of proIL-1 β . In *Molecular Cell* (Vol. 10). [https://doi.org/https://doi.org/10.1016/S1097-2765\(02\)00599-3](https://doi.org/https://doi.org/10.1016/S1097-2765(02)00599-3)
- Martinon, F., Pétrilli, V., Mayor, A., Tardivel, A., & Tschopp, J. (2006). Gout-associated uric acid crystals activate the NALP3 inflammasome. *Nature*, *440*(7081), 237–241. <https://doi.org/10.1038/nature04516>
- Masuda, Y., Futamura, M., Kamino, H., Nakamura, Y., Kitamura, N., Ohnishi, S., Miyamoto, Y., Ichikawa, H., Ohta, T., Ohki, M., Kiyono, T., Egami, H., Baba, H., & Arakawa, H. (2006). The potential role of DFNA5, a hearing impairment gene, in p53-mediated cellular response to DNA damage. *Journal of Human Genetics*, *51*(8), 652–664. <https://doi.org/10.1007/s10038-006-0004-6>

- M.Centola, G.Wood, D.M Frucht, J.Galon, & D.L Kastner. (2000). The gene for familial Mediterranean fever, MEFV, is expressed in early leukocyte development and is regulated in response to inflammatory mediators. *Blood*, 95(10), 3223–3231.
- McKee, C. M., & Coll, R. C. (2020). NLRP3 inflammasome priming: A riddle wrapped in a mystery inside an enigma. In *Journal of Leukocyte Biology* (Vol. 108, Issue 3, pp. 937–952). John Wiley and Sons Inc. <https://doi.org/10.1002/JLB.3MR0720-513R>
- Medzhitov, R., Preston-Hurlburt, P., & Janeway, C. A. (1997). *A human homologue of the Drosophila Toll protein signals activation of adaptive immunity.*
- Meunier, E., & Broz, P. (2016). Interferon-inducible GTPases in cell autonomous and innate immunity. In *Cellular Microbiology* (Vol. 18, Issue 2, pp. 168–180). Blackwell Publishing Ltd. <https://doi.org/10.1111/cmi.12546>
- Meunier, E., & Broz, P. (2017). Evolutionary Convergence and Divergence in NLR Function and Structure. In *Trends in Immunology* (Vol. 38, Issue 10, pp. 744–757). Elsevier Ltd. <https://doi.org/10.1016/j.it.2017.04.005>
- Miao, E. A., Alpuche-Aranda, C. M., Dors, M., Clark, A. E., Bader, M. W., Miller, S. I., & Aderem, A. (2006). Cytoplasmic flagellin activates caspase-1 and secretion of interleukin 1 β via Ipaf. *Nature Immunology*, 7(6), 569–575. <https://doi.org/10.1038/ni1344>
- Miao, E. A., Mao, D. P., Yudkovsky, N., Bonneau, R., Lorang, C. G., Warren, S. E., Leaf, I. A., & Aderem, A. (2010). Innate immune detection of the type III secretion apparatus through the NLRC4 inflammasome. *Proceedings of the National Academy of Sciences of the United States of America*, 107(7), 3076–3080. <https://doi.org/10.1073/pnas.0913087107>
- Michel Samson, Frederick Libert, Benjamin J.Doranz, Gilbert Vassart, & Marc Parmentier. (1996). *Resistance to HIV-1 infection in caucasian individuals bearing mutant alleles of the CCR-5 chemokine receptor gene.* <https://doi.org/10.1038/382722a0>
- Miguchi, M., Hinoi, T., Shimomura, M., Adachi, T., Saito, Y., Niitsu, H., Kochi, M., Sada, H., Sotomaru, Y., Ikenoue, T., Shigeyasu, K., Tanakaya, K., Kitadai, Y., Sentani, K., Oue, N., Yasui, W., & Ohdan, H. (2016). Gasdermin C is upregulated by inactivation of transforming growth factor β receptor type II in the presence of mutated Apc, promoting colorectal cancer proliferation. *PLoS ONE*, 11(11). <https://doi.org/10.1371/journal.pone.0166422>
- Moghaddas, F., Zeng, P., Zhang, Y., Schützle, H., Brenner, S., Hofmann, S. R., Berner, R., Zhao, Y., Lu, B., Chen, X., Zhang, L., Cheng, S., Winkler, S., Lehmborg, K., Canna, S. W., Czabotar, P. E., Wicks, I. P., de Nardo, D., Hedrich, C. M., ... Masters, S. L. (2018). Autoinflammatory mutation in NLRC4 reveals a leucine-rich repeat (LRR)–LRR oligomerization interface. *Journal of Allergy and Clinical Immunology*, 142(6), 1956-1967.e6. <https://doi.org/10.1016/j.jaci.2018.04.033>
- Muruve, D. A., Pétrilli, V., Zaiss, A. K., White, L. R., Clark, S. A., Ross, P. J., Parks, R. J., & Tschopp, J. (2008). The inflammasome recognizes cytosolic microbial and host DNA and triggers an innate immune response. *Nature*, 452(7183), 103–107. <https://doi.org/10.1038/nature06664>
- Nadkarni, R., Chu, W. C., Lee, C. Q. E., Mohamud, Y., Yap, L., Toh, G. A., Beh, S., Lim, R., Fan, Y. M., Zhang, Y. L., Robinson, K., Tryggvason, K., Luo, H., Zhong, F., & Ho, L. (2022). Viral proteases activate the CARD8 inflammasome in the human cardiovascular system. *Journal of Experimental Medicine*, 219(10). <https://doi.org/10.1084/jem.20212117>

- Ngo, C., & Man, S. M. (2017). NLRP9b: A novel RNA-sensing inflammasome complex. In *Cell Research* (Vol. 27, Issue 11, pp. 1302–1303). Nature Publishing Group. <https://doi.org/10.1038/cr.2017.93>
- Orning, P., Weng, D., Starheim, K., Ratner, D., Best, Z., Lee, B., Brooks, A., Xia, S., Wu, H., Kelliher, M. A., Berger, S. B., Gough, P. J., Bertin, J., Proulx, M. M., Goguen, J. D., Kayagaki, N., Fitzgerald, K. A., & Lien, E. (2018). Pathogen blockade of TAK1 triggers caspase-8–dependent cleavage of gasdermin D and cell death. *Science*, *362*(6418), 1064–1069. <https://doi.org/10.1126/science.aau2818>
- Orth-He, E. L., Huang, H. C., Rao, S. D., Wang, Q., Chen, Q., O'Mara, C. M., Chui, A. J., Saoi, M., Griswold, A. R., Bhattacharjee, A., Ball, D. P., Cross, J. R., & Bachovchin, D. A. (2023). Protein folding stress potentiates NLRP1 and CARD8 inflammasome activation. *Cell Reports*, *42*(1). <https://doi.org/10.1016/j.celrep.2022.111965>
- Palazon-Riquelme, P., & Lopez-Castejon, G. (2018). The inflammasomes, immune guardians at defence barriers. In *Immunology* (Vol. 155, Issue 3, pp. 320–330). Blackwell Publishing Ltd. <https://doi.org/10.1111/imm.12989>
- Palomo, J., Marchiol, T., Piotet, J., Fauconnier, L., Robinet, M., Reverchon, F., Bert, M. Le, Togbe, D., Buijs-Offerman, R., Stolarczyk, M., Quesniaux, V. R. F. J., Scholte, B. J., & Ryffel, B. (2014). Role of IL-1 β in experimental cystic fibrosis upon *P. aeruginosa* Infection. *PLoS ONE*, *9*(12). <https://doi.org/10.1371/journal.pone.0114884>
- Paludan, S. R., & Mogensen, T. H. (2022). Innate immunological pathways in COVID-19 pathogenesis. In *Sci. Immunol* (Vol. 7). <https://www.science.org>
- Park, Y. H., Remmers, E. F., Lee, W., Ombrello, A. K., Chung, L. K., Shilei, Z., Stone, D. L., Ivanov, M. I., Loeven, N. A., Barron, K. S., Hoffmann, P., Nehrebecky, M., Akkaya-Ulum, Y. Z., Sag, E., Balci-Peynircioglu, B., Aksentijevich, I., Gül, A., Rotimi, C. N., Chen, H., ... Chae, J. J. (2020). Ancient familial Mediterranean fever mutations in human pyrin and resistance to *Yersinia pestis*. *Nature Immunology*, *21*(8), 857–867. <https://doi.org/10.1038/s41590-020-0705-6>
- Park, Y. H., Wood, G., Kastner, D. L., & Chae, J. J. (2016a). Pyrin inflammasome activation and RhoA signaling in the autoinflammatory diseases FMF and HIDS. *Nature Immunology*, *17*(8), 914–921. <https://doi.org/10.1038/ni.3457>
- Pelegrin, P. (2021). P2X7 receptor and the NLRP3 inflammasome: Partners in crime. In *Biochemical Pharmacology* (Vol. 187). Elsevier Inc. <https://doi.org/10.1016/j.bcp.2020.114385>
- Petr Broz, Pablo Pelegrin, & Feng Shao. (2019). The gasdermins, a protein family executing cell death and inflammation. *Nature Reviews*. <https://doi.org/10.1038/s41577-019-0228-2>
- Piper, S. C., Ferguson, J., Kay, L., Parker, L. C., Sabroe, I., Sleeman, M. A., Briend, E., & Finch, D. K. (2013). The Role of Interleukin-1 and Interleukin-18 in Pro-Inflammatory and Anti-Viral Responses to Rhinovirus in Primary Bronchial Epithelial Cells. *PLoS ONE*, *8*(5). <https://doi.org/10.1371/journal.pone.0063365>
- Pizzuto, M., & Pelegrin, P. (2020). Cardiolipin in Immune Signaling and Cell Death. In *Trends in Cell Biology* (Vol. 30, Issue 11, pp. 892–903). Elsevier Ltd. <https://doi.org/10.1016/j.tcb.2020.09.004>
- Pizzuto, M., Pelegrin, P., & Ruyschaert, J. M. (2022). Lipid-protein interactions regulating the canonical and the non-canonical NLRP3 inflammasome. In *Progress in Lipid Research* (Vol. 87). Elsevier Ltd. <https://doi.org/10.1016/j.plipres.2022.101182>

- Planès, R., Pinilla, M., Santoni, K., Hessel, A., Passemar, C., Lay, K., Paillette, P., Valadão, A. L. C., Robinson, K. S., Bastard, P., Lam, N., Fadrique, R., Rossi, I., Pericat, D., Bagayoko, S., Leon-Icaza, S. A., Rombouts, Y., Perouzel, E., Tiraby, M., ... Meunier, E. (2022). Human NLRP1 is a sensor of pathogenic coronavirus 3CL proteases in lung epithelial cells. *Molecular Cell*, *82*(13), 2385–2400.e9. <https://doi.org/10.1016/j.molcel.2022.04.033>
- Poyet, J. L., Srinivasula, S. M., Tnani, M., Razmara, M., Fernandes-Alnemri, T., & Alnemri, E. S. (2001). Identification of Ipaf, a Human Caspase-1-activating Protein Related to Apaf-1. *Journal of Biological Chemistry*, *276*(30), 28309–28313. <https://doi.org/10.1074/jbc.C100250200>
- Qu, Y., Misaghi, S., Izrael-Tomasevic, A., Newton, K., Gilmour, L. L., Lamkanfi, M., Louie, S., Kayagaki, N., Liu, J., Kömüves, L., Cupp, J. E., Arnott, D., Monack, D., & Dixit, V. M. (2012). Phosphorylation of NLRC4 is critical for inflammasome activation. *Nature*, *490*(7421), 539–542. <https://doi.org/10.1038/nature11429>
- Raia, V., Maiuri, L., Ciacci, C., Ricciardelli, I., Vacca, L., Auricchio, S., Cimmino, M., Cavaliere, M., Nardone, M., Cesaro, A., Malcolm, J., Quarantino, S., & Londei, M. (2005). Inhibition of p38 mitogen activated protein kinase controls airway inflammation in cystic fibrosis. *Thorax*, *60*(9), 773–780. <https://doi.org/10.1136/thx.2005.042564>
- Rajamäki, K., Lappalainen, J., Öörni, K., Välimäki, E., Matikainen, S., Kovanen, P. T., & Kari, E. K. (2010). Cholesterol crystals activate the NLRP3 inflammasome in human macrophages: A novel link between cholesterol metabolism and inflammation. *PLoS ONE*, *5*(7). <https://doi.org/10.1371/journal.pone.0011765>
- Rana, N., Privitera, G., Kondolf, H. C., Bulek, K., Lechuga, S., de Salvo, C., Corridoni, D., Antanaviciute, A., Maywald, R. L., Hurtado, A. M., Zhao, J., Huang, E. H., Li, X., Chan, E. R., Simmons, A., Bamias, G., Abbott, D. W., Heaney, J. D., Ivanov, A. I., & Pizarro, T. T. (2022). GSDMB is increased in IBD and regulates epithelial restitution/repair independent of pyroptosis. *Cell*, *185*(2), 283–298.e17. <https://doi.org/10.1016/j.cell.2021.12.024>
- Randow, F., & Münz, C. (2012). Autophagy in the regulation of pathogen replication and adaptive immunity. In *Trends in Immunology* (Vol. 33, Issue 10, pp. 475–487). <https://doi.org/10.1016/j.it.2012.06.003>
- Rao, S. D., Chen, Q., Wang, Q., Orth-He, E. L., Saoi, M., Griswold, A. R., Bhattacharjee, A., Ball, D. P., Huang, H. C., Chui, A. J., Covelli, D. J., You, S., Cross, J. R., & Bachovchin, D. A. (2022). M24B aminopeptidase inhibitors selectively activate the CARD8 inflammasome. *Nature Chemical Biology*, *18*(5), 565–574. <https://doi.org/10.1038/s41589-021-00964-7>
- Rathkey, J. K., Zhao, J., Liu, Z., Chen, Y., Yang, J., Kondolf, H. C., Benson, B. L., Chirieleison, S. M., Huang, A. Y., Dubyak, G. R., Xiao, T. S., Li, X., & Abbott, D. W. (2018). Chemical disruption of the pyroptotic pore-forming protein gasdermin D inhibits inflammatory cell death and sepsis. *Science Immunology*, *3*(26). <https://doi.org/10.1126/sciimmunol.aat2738>
- Rehwinkel, J., & Gack, M. U. (2020). RIG-I-like receptors: their regulation and roles in RNA sensing. In *Nature Reviews Immunology* (Vol. 20, Issue 9, pp. 537–551). Nature Research. <https://doi.org/10.1038/s41577-020-0288-3>
- Roberts, T. L. et al. (2009). HIN-200 Proteins Regulate Caspase Activation in Response To Foreign Cytoplasmic DNA. *Science*, *323*(5917), 1053–1057. <https://doi.org/10.1126/science.1166386>

- Robinson, K. S., Ann Toh, G., Rozario, P., Chua, R., Bauernfried, S., Sun, Z., Jasrie Firdaus, M., Bayat, S., Nadkarni, R., Sheng Poh, Z., Chian Tham, K., Harapas, C. R., Lim, C. K., Chu, W., S Tay, C. W., Yi Tan, K., Zhao, T., Bonnard, C., Sobota, R., ... Zhong, F. L. (n.d.). *ZAKα-driven ribotoxic stress response activates the human NLRP1 inflammasome*.
- Robinson, K. S., Teo, D. E. T., Tan, K. sen, Toh, G. A., Ong, H. H., Lim, C. K., Lay, K., Au, B. V., Lew, T. S., Chu, J. J. H., Chow, V. T. K., Wang, D. Y., Zhong, F. L., & Reversade, B. (2020a). Enteroviral 3C protease activates the human NLRP1 inflammasome in airway epithelia. *Science*, *370*(6521). <https://doi.org/10.1126/science.aay2002>
- Rodrigues, T. S., de Sá, K. S. G., Ishimoto, A. Y., Becerra, A., Oliveira, S., Almeida, L., Gonçalves, A. V., Perucello, D. B., Andrade, W. A., Castro, R., Veras, F. P., Toller-Kawahisa, J. E., Nascimento, D. C., de Lima, M. H. F., Silva, C. M. S., Caetite, D. B., Martins, R. B., Castro, I. A., Pontelli, M. C., ... Zamboni, D. S. (2020a). Inflammasomes are activated in response to SARS-cov-2 infection and are associated with COVID-19 severity in patients. *Journal of Experimental Medicine*, *218*(3). <https://doi.org/10.1084/JEM.20201707>
- Rogers, C., Fernandes-Alnemri, T., Mayes, L., Alnemri, D., Cingolani, G., & Alnemri, E. S. (2017). Cleavage of DFNA5 by caspase-3 during apoptosis mediates progression to secondary necrotic/pyroptotic cell death. *Nature Communications*, *8*. <https://doi.org/10.1038/ncomms14128>
- Romberg, N., Vogel, T. P., & Canna, S. W. (2018). Author manuscript; available in PMC. *Curr Opin Allergy Clin Immunol*, *17*(6), 398–404. <https://doi.org/10.1097/ACI>
- Rühl, S., & Broz, P. (2022). Regulation of Lytic and Non-Lytic Functions of Gasdermin Pores. In *Journal of Molecular Biology* (Vol. 434, Issue 4). Academic Press. <https://doi.org/10.1016/j.jmb.2021.167246>
- Runkel, F., Marquardt, A., Stoeger, C., Kochmann, E., Simon, D., Kohnke, B., Korthaus, D., Wattler, F., Fuchs, H., Hrabé De Angelis, M., Stumm, G., Nehls, M., Wattler, S., Franz, T., & Augustin, M. (2004). The dominant alopecia phenotypes Bareskin, Rex-denuded, and Reduced Coat 2 are caused by mutations in gasdermin 3. *Genomics*, *84*(5), 824–835. <https://doi.org/10.1016/j.ygeno.2004.07.003>
- Sand, J., Fenini, G., Grossi, S., Hennig, P., di Filippo, M., Levesque, M., Werner, S., French, L. E., & Beer, H. D. (2019). The NLRP1 Inflammasome Pathway Is Silenced in Cutaneous Squamous Cell Carcinoma. *Journal of Investigative Dermatology*, *139*(8), 1788-1797.e6. <https://doi.org/10.1016/j.jid.2019.01.025>
- Sandstrom, A., Mitchell, P. S., Goers, L., Mu, E. W., Lesser, C. F., & Vance, R. E. (2019a). Functional degradation: A mechanism of NLRP1 inflammasome activation by diverse pathogen enzymes. *Science*, *364*(6435). <https://doi.org/10.1126/science.aau1330>
- Sarhan, J., Liu, B. C., Muendlein, H. I., Li, P., Nilson, R., Tang, A. Y., Rongvaux, A., Bunnell, S. C., Shao, F., Green, D. R., & Poltorak, A. (2018a). Caspase-8 induces cleavage of gasdermin D to elicit pyroptosis during Yersinia infection. *Proceedings of the National Academy of Sciences of the United States of America*, *115*(46), E10888–E10897. <https://doi.org/10.1073/pnas.1809548115>
- Sastalla, I., Crown, D., Masters, S. L., McKenzie, A., Leppla, S. H., & Moayeri, M. (2013). Transcriptional analysis of the three Nlrp1 paralogs in mice. *BMC Genomics*, *14*(1). <https://doi.org/10.1186/1471-2164-14-188>

- Sborgi, L., Rühl, S., Mulvihill, E., Pipercevic, J., Heilig, R., Stahlberg, H., Farady, C. J., Müller, D. J., Broz, P., & Hiller, S. (2016). GSDMD membrane pore formation constitutes the mechanism of pyroptotic cell death. *The EMBO Journal*, *35*(16), 1766–1778. <https://doi.org/10.15252/embj.201694696>
- Scambler, T., Jarosz-Griffiths, H. H., Lara-Reyna, S., Pathak, S., Wong, C., Holbrook, J., Martinon, F., Savic, S., Peckham, D., & McDermott, M. F. (2019). *ENaC-mediated sodium influx exacerbates NLRP3-dependent inflammation in cystic fibrosis*. <https://doi.org/10.7554/eLife.49248.001>
- Schmacke, N. A., O’Duill, F., Gaidt, M. M., Szymanska, I., Kamper, J. M., Schmid-Burgk, J. L., Mädler, S. C., Mackens-Kiani, T., Kozaki, T., Chauhan, D., Nagl, D., Stafford, C. A., Harz, H., Fröhlich, A. L., Pinci, F., Ginhoux, F., Beckmann, R., Mann, M., Leonhardt, H., & Hornung, V. (2022). IKK β primes inflammasome formation by recruiting NLRP3 to the trans-Golgi network. *Immunity*, *55*(12), 2271–2284.e7. <https://doi.org/10.1016/j.immuni.2022.10.021>
- Schmid-Burgk, J. L., Chauhan, D., Schmidt, T., Ebert, T. S., Reinhardt, J., Endl, E., & Hornung, V. (2016). A genome-wide CRISPR (clustered regularly interspaced short palindromic repeats) screen identifies NEK7 as an essential component of NLRP3 inflammasome activation. *Journal of Biological Chemistry*, *291*(1), 103–109. <https://doi.org/10.1074/jbc.C115.700492>
- Schroder, K., & Tschopp, J. (2010). The Inflammasomes. In *Cell* (Vol. 140, Issue 6, pp. 821–832). Elsevier B.V. <https://doi.org/10.1016/j.cell.2010.01.040>
- Shao-bin Wang. (2021). DDX17 is an essential mediator of sterile NLRC4 inflammasome activation by retrotransposon RNAs. *Sci Immunol*, *6*(66), 4493. <https://doi.org/10.6019/PXD016019>
- Sharif, H., Hollingsworth, L. R., Griswold, A. R., Hsiao, J. C., Wang, Q., Bachovchin, D. A., & Wu, H. (2021). Dipeptidyl peptidase 9 sets a threshold for CARD8 inflammasome formation by sequestering its active C-terminal fragment. *Immunity*, *54*(7), 1392–1404.e10. <https://doi.org/10.1016/j.immuni.2021.04.024>
- Shi, H., Wang, Y., Li, X., Zhan, X., Tang, M., Fina, M., Su, L., Pratt, D., Hui Bu, C., Hildebrand, S., Lyon, S., Scott, L., Quan, J., Sun, Q., Russell, J., Arnett, S., Jurek, P., Chen, D., Kravchenko, V. v., ... Beutler, B. (2016). NLRP3 activation and mitosis are mutually exclusive events coordinated by NEK7, a new inflammasome component. *Nature Immunology*, *17*(3), 250–258. <https://doi.org/10.1038/ni.3333>
- Shi, J., Zhao, Y., Wang, K., Shi, X., Wang, Y., Huang, H., Zhuang, Y., Cai, T., Wang, F., & Shao, F. (2015). Cleavage of GSDMD by inflammatory caspases determines pyroptotic cell death. *Nature*, *526*(7575), 660–665. <https://doi.org/10.1038/nature15514>
- Shi, J., Zhao, Y., Wang, Y., Gao, W., Ding, J., Li, P., Hu, L., & Shao, F. (2014). Inflammatory caspases are innate immune receptors for intracellular LPS. *Nature*, *514*(7521), 187–192. <https://doi.org/10.1038/nature13683>
- Shim, D. W., & Lee, K. H. (2018). Posttranslational regulation of the NLR family pyrin domain-containing 3 inflammasome. In *Frontiers in Immunology* (Vol. 9, Issue MAY). Frontiers Media S.A. <https://doi.org/10.3389/fimmu.2018.01054>
- Squires, R. C., Muehlbauer, S. M., & Brojatsch, J. (2007). Proteasomes control caspase-1 activation in anthrax lethal toxin-mediated cell killing. *Journal of Biological Chemistry*, *282*(47), 34260–34267. <https://doi.org/10.1074/jbc.M705687200>

- Stefan Bauernfried, & Veit Hornung. (2021). DPP9 restrains NLRP1 activation. In *Nature Structural and Molecular Biology* (Vol. 28, Issue 4, pp. 331–333). Nature Research. <https://doi.org/10.1038/s41594-021-00581-x>
- Stimson, K. M., & Vertino, P. M. (2002). Methylation-mediated silencing of TMS1/ASC is accompanied by histone hypoacetylation and CpG island-localized changes in chromatin architecture. *Journal of Biological Chemistry*, 277(7), 4951–4958. <https://doi.org/10.1074/jbc.M109809200>
- Sun, L., Wu, J., Du, F., Chen, X., & Chen, Z. J. (2013). Cyclic GMP-AMP synthase is a cytosolic DNA sensor that activates the type I interferon pathway. *Science*, 339(6121), 786–791. <https://doi.org/10.1126/science.1232458>
- Sutterwala, F. S., & Flavell, R. A. (2009). NLRC4/IPAF: a CARD carrying member of the NLR family. In *Clinical Immunology* (Vol. 130, Issue 1, pp. 2–6). <https://doi.org/10.1016/j.clim.2008.08.011>
- Suzuki, S., Franchi, L., He, Y., Muñoz-Planillo, R., Mimuro, H., Suzuki, T., Sasakawa, C., & Núñez, G. (2014). Shigella Type III Secretion Protein MxiI Is Recognized by Naip2 to Induce Nlrc4 Inflammasome Activation Independently of Pkc δ . *PLoS Pathogens*, 10(2). <https://doi.org/10.1371/journal.ppat.1003926>
- Swanson, K. V., Deng, M., & Ting, J. P. Y. (2019). The NLRP3 inflammasome: molecular activation and regulation to therapeutics. In *Nature Reviews Immunology* (Vol. 19, Issue 8, pp. 477–489). Nature Publishing Group. <https://doi.org/10.1038/s41577-019-0165-0>
- Taabazuig, C. Y., Griswold, A. R., & Bachovchin, D. A. (2020). The NLRP1 and CARD8 inflammasomes. In *Immunological Reviews* (Vol. 297, Issue 1, pp. 13–25). Blackwell Publishing Ltd. <https://doi.org/10.1111/imr.12884>
- Tang, A., Sharma, A., Jen, R., Hirschfeld, A. F., Chilvers, M. A., Lavoie, P. M., & Turvey, S. E. (2012). Inflammasome-mediated IL-1 β production in humans with cystic fibrosis. *PLoS ONE*, 7(5). <https://doi.org/10.1371/journal.pone.0037689>
- Tang, D., Kang, R., Berghe, T. vanden, Vandenabeele, P., & Kroemer, G. (2019). The molecular machinery of regulated cell death. In *Cell Research* (Vol. 29, Issue 5, pp. 347–364). Nature Publishing Group. <https://doi.org/10.1038/s41422-019-0164-5>
- Tapia-Abellán, A., Angosto-Bazarra, D., Alarcón-Vila, C., Baños, M. C., Hafner-Bratkovič, I., Oliva, B., & Pelegrín, P. (2021). Sensing low intracellular potassium by NLRP3 results in a stable open structure that promotes inflammasome activation. In *Sci. Adv* (Vol. 7). <https://doi.org/https://doi.org/10.1126/sciadv.abf4468>
- Tasaki, T., Sriram, S. M., Park, K. S., & Kwon, Y. T. (2012). The N-End rule pathway. *Annual Review of Biochemistry*, 81, 261–289. <https://doi.org/10.1146/annurev-biochem-051710-093308>
- Tattoli, I., Carneiro, L. A., Jéhanno, M., Magalhaes, J. G., Shu, Y., Philpott, D. J., Arnoult, D., & Girardin, S. E. (2008). NLRX1 is a mitochondrial NOD-like receptor that amplifies NF- κ B and JNK pathways by inducing reactive oxygen species production. *EMBO Reports*, 9(3), 293–300. <https://doi.org/10.1038/sj.embor.7401161>
- Tenthorey, J. L., Chavez, R. A., Thompson, T. W., Deets, K. A., Vance, R. E., & Rauch, I. (2020). Nlrc4 inflammasome activation is nlrp3- And phosphorylation-independent during infection and does not protect from melanoma. *Journal of Experimental Medicine*, 217(7). <https://doi.org/10.1084/jem.20191736>

- Ting, J. P. Y., Lovering, R. C., Alnemri, E. S., Bertin, J., Boss, J. M., Davis, B. K., Flavell, R. A., Girardin, S. E., Godzik, A., Harton, J. A., Hoffman, H. M., Hugot, J. P., Inohara, N., MacKenzie, A., Maltais, L. J., Nunez, G., Ogura, Y., Otten, L. A., Philpott, D., ... Ward, P. A. (2008). The NLR Gene Family: A Standard Nomenclature. In *Immunity* (Vol. 28, Issue 3, pp. 285–287). <https://doi.org/10.1016/j.immuni.2008.02.005>
- Tsu, B. V., Beierschmitt, C., Ryan, A. P., Agarwal, R., Mitchell, P. S., & Daugherty, M. D. (2021). Diverse viral proteases activate the nlrp1 inflammasome. *ELife*, 10, 1–76. <https://doi.org/10.7554/eLife.60609>
- Tuladhar, S., & Kanneganti, T. D. (2020). NLRP12 in innate immunity and inflammation. In *Molecular Aspects of Medicine* (Vol. 76). Elsevier Ltd. <https://doi.org/10.1016/j.mam.2020.100887>
- Valeria, M. R. R., Ramirez, J., Naseer, N., Palacio, N. M., Siddarthan, I. J., Yan, B. M., Boyer, M. A., Pensinger, D. A., Sauer, J. D., & Shin, S. (2017). Broad detection of bacterial type III secretion system and flagellin proteins by the human NAIP/NLRC4 inflammasome. *Proceedings of the National Academy of Sciences of the United States of America*, 114(50), 13242–13247. <https://doi.org/10.1073/pnas.1710433114>
- Van Laer, L., Huizing, E. H., Verstreken, M., Van Zuijlen, D., Wauters, J. G., Bossuyt, P. J., Van De Heyning, P., Mcguirt, W. T., Smith, R. J. H., Willems, P. J., Legan, P. K., Richardson, G. P., & Camp, G. Van. (1998). *Nonsyndromic hearing impairment is associated with a mutation in DFNA5*. <https://doi.org/10.1038/2503>
- Van Ness, B. G., Howard, J. B., & Bo&y, J. W. (1980). ADP-Ribosylation of Elongation Factor 2 by Diphtheria Toxin. In *THE JOURNAL OF BIOLOGICAL CHEMISTRY* (Vol. 255, Issue 22).
- Varshavsky, A. (2011). The N-end rule pathway and regulation by proteolysis. In *Protein Science* (Vol. 20, Issue 8, pp. 1298–1345). <https://doi.org/10.1002/pro.666>
- Venkatakrishnan, A., Stecenko, A. A., King, G., Blackwell, T. R., Brigham, K. L., Christman, J. W., & Blackwell, T. S. (2000). Exaggerated Activation of Nuclear Factor- κ B and Altered I κ B-Processing in Cystic Fibrosis Bronchial Epithelial Cells. In *Am. J. Respir. Cell Mol. Biol* (Vol. 23). www.atsjournals.org
- Vind, A. C., Snieckute, G., Blasius, M., Tiedje, C., Krogh, N., Bekker-Jensen, D. B., Andersen, K. L., Nordgaard, C., Tollenaere, M. A. X., Lund, A. H., Olsen, J. V., Nielsen, H., & Bekker-Jensen, S. (2020). ZAK α Recognizes Stalled Ribosomes through Partially Redundant Sensor Domains. *Molecular Cell*, 78(4), 700–713. <https://doi.org/10.1016/j.molcel.2020.03.021>
- Voet, S., Srinivasan, S., Lamkanfi, M., & Loo, G. (2019). Inflammasomes in neuroinflammatory and neurodegenerative diseases. *EMBO Molecular Medicine*, 11(6). <https://doi.org/10.15252/emmm.201810248>
- Volker-Touw, C. M. L., de Koning, H. D., Giltay, J. C., de Kovel, C. G. F., van Kempen, T. S., Oberndorff, K. M. E. J., Boes, M. L., van Steensel, M. A. M., van Well, G. T. J., Blokx, W. A. M., Schalkwijk, J., Simon, A., Frenkel, J., & van Gijn, M. E. (2017). Erythematous nodes, urticarial rash and arthralgias in a large pedigree with NLRC4-related autoinflammatory disease, expansion of the phenotype. In *British Journal of Dermatology* (Vol. 176, Issue 1, pp. 244–248). Blackwell Publishing Ltd. <https://doi.org/10.1111/bjd.14757>

- Wang, L., Wen, W., Deng, M., Li, Y., Sun, G., Zhao, X., Tang, X., & Mao, H. (2021). A Novel Mutation in the NBD Domain of NLRC4 Causes Mild Autoinflammation With Recurrent Urticaria. *Frontiers in Immunology*, 12. <https://doi.org/10.3389/fimmu.2021.674808>
- Wang, Q., Gao, H., Clark, K. M., Mugisha, C. S., Davis, K., Tang, J. P., Harlan, G. H., DeSelm, C. J., Presti, R. M., Kutluay, S. B., & Shan, L. (2021). CARD8 is an inflammasome sensor for HIV-1 protease activity. *Science*, 371(6535). <https://doi.org/10.1126/science.abe1707>
- Wang, Q., Hsiao, J. C., Yardeny, N., Huang, H.-C., O'Mara, C. M., Orth-He, E. L., Ball, D. P., Zhang, Z., & Bachovchin, D. A. (2023). The NLRP1 and CARD8 inflammasomes detect reductive stress. *Cell Reports*, 111966. <https://doi.org/10.1016/j.celrep.2022.111966>
- Wang, Y., Gao, W., Shi, X., Ding, J., Liu, W., He, H., Wang, K., & Shao, F. (2017). Chemotherapy drugs induce pyroptosis through caspase-3 cleavage of a gasdermin. *Nature*, 547(7661), 99–103. <https://doi.org/10.1038/nature22393>
- Wein, T., & Sorek, R. (2022). Bacterial origins of human cell-autonomous innate immune mechanisms. In *Nature Reviews Immunology* (Vol. 22, Issue 10, pp. 629–638). Nature Research. <https://doi.org/10.1038/s41577-022-00705-4>
- Weiss, E. S., Girard-Guyonvarc', C., Holzinger, D., De Jesus, A. A., Tariq, Z., Picarsic, J., Schiffrin, E. J., Foell, D., Grom, A. A., Ammann, S., Ehl, S., Hoshino, T., Goldbach-Mansky, R., Gabay, C., & Canna, S. W. (2018). *Interleukin-18 diagnostically distinguishes and pathogenically promotes human and murine macrophage activation syndrome*. <https://doi.org/10.1182/blood-2017-12-820852>
- Wen, H., Ting, J. P. Y., & O'Neill, L. A. J. (2012). A role for the NLRP3 inflammasome in metabolic diseases - Did Warburg miss inflammation? In *Nature Immunology* (Vol. 13, Issue 4, pp. 352–357). <https://doi.org/10.1038/ni.2228>
- Wen, J., Xuan, B., Liu, Y., Wang, L., He, L., Meng, X., Zhou, T., & Wang, Y. (2021). Updating the NLRC4 Inflammasome: from Bacterial Infections to Autoimmunity and Cancer. In *Frontiers in Immunology* (Vol. 12). Frontiers Media S.A. <https://doi.org/10.3389/fimmu.2021.702527>
- Whiteley, A. T., Eaglesham, J. B., de Oliveira Mann, C. C., Morehouse, B. R., Lowey, B., Nieminen, E. A., Danilchanka, O., King, D. S., Lee, A. S. Y., Mekalanos, J. J., & Kranzusch, P. J. (2019). Bacterial cGAS-like enzymes synthesize diverse nucleotide signals. *Nature*, 567(7747), 194–199. <https://doi.org/10.1038/s41586-019-0953-5>
- Wu, C. C. C., Peterson, A., Zinshteyn, B., Regot, S., & Green, R. (2020a). Ribosome Collisions Trigger General Stress Responses to Regulate Cell Fate. *Cell*, 182(2), 404-416.e14. <https://doi.org/10.1016/j.cell.2020.06.006>
- Wu, J., Sun, L., Chen, X., Du, F., Shi, H., Chen, C., & Chen, Z. J. (2013). Cyclic GMP-AMP is an endogenous second messenger in innate immune signaling by cytosolic DNA. *Science*, 339(6121), 826–830. <https://doi.org/10.1126/science.1229963>
- Xia, S., Zhang, Z., Magupalli, V. G., Pablo, J. L., Dong, Y., Vora, S. M., Wang, L., Fu, T. M., Jacobson, M. P., Greka, A., Lieberman, J., Ruan, J., & Wu, H. (2021). Gasdermin D pore structure reveals preferential release of mature interleukin-1. *Nature*, 593(7860), 607–611. <https://doi.org/10.1038/s41586-021-03478-3>
- Xiao, J., Wang, C., Yao, J. C., Alippe, Y., Xu, C., Kress, D., Civitelli, R., Abu-Amer, Y., Kanneganti, T. D., Link, D. C., & Mbalaviele, G. (2018). Gasdermin D mediates the pathogenesis of neonatal-onset

- multisystem inflammatory disease in mice. *PLoS Biology*, 16(11).
<https://doi.org/10.1371/journal.pbio.3000047>
- Xu, H., Yang, J., Gao, W., Li, L., Li, P., Zhang, L., Gong, Y. N., Peng, X., Xi, J. J., Chen, S., Wang, F., & Shao, F. (2014). Innate immune sensing of bacterial modifications of Rho GTPases by the Pyrin inflammasome. *Nature*, 513(7517), 237–241. <https://doi.org/10.1038/nature13449>
- Xu, J., & Núñez, G. (2022). The NLRP3 inflammasome: activation and regulation. In *Trends in Biochemical Sciences*. Elsevier Ltd. <https://doi.org/10.1016/j.tibs.2022.10.002>
- Yang, J., Zhao, Y., & Shao, F. (2015). Non-canonical activation of inflammatory caspases by cytosolic LPS in innate immunity. In *Current Opinion in Immunology* (Vol. 32, pp. 78–83). Elsevier Ltd. <https://doi.org/10.1016/j.coi.2015.01.007>
- Yang, J., Zhao, Y., Shi, J., & Shao, F. (2013). Human NAIP and mouse NAIP1 recognize bacterial type III secretion needle protein for inflammasome activation. *Proceedings of the National Academy of Sciences of the United States of America*, 110(35), 14408–14413. <https://doi.org/10.1073/pnas.1306376110>
- Yi Han, Haidong Zhang, Sucheng Mu, Wei Wei, Chaoyuan Jin, & Guorong Gu. (n.d.). *Lactate dehydrogenase, an independent risk factor of severe COVID-19 patients: a retrospective and observational study*. <https://doi.org/10.18632/aging.103372>
- Zaher, A., ElSaygh, J., ElSori, D., ElSaygh, H., & Sanni, A. (2021). A Review of Trikafta: Triple Cystic Fibrosis Transmembrane Conductance Regulator (CFTR) Modulator Therapy. *Cureus*. <https://doi.org/10.7759/cureus.16144>
- Zhang, Z., Zhang, Y., Xia, S., Kong, Q., Li, S., Liu, X., Junqueira, C., Meza-Sosa, K. F., Mok, T. M. Y., Ansara, J., Sengupta, S., Yao, Y., Wu, H., & Lieberman, J. (2020). Gasdermin E suppresses tumour growth by activating anti-tumour immunity. *Nature*, 579(7799), 415–420. <https://doi.org/10.1038/s41586-020-2071-9>
- Zhao, Y., Yang, J., Shi, J., Gong, Y. N., Lu, Q., Xu, H., Liu, L., & Shao, F. (2011). The NLRC4 inflammasome receptors for bacterial flagellin and type III secretion apparatus. *Nature*, 477(7366), 596–602. <https://doi.org/10.1038/nature10510>
- Zhong, F. L., Mamaï, O., Sborgi, L., Boussofara, L., Hopkins, R., Robinson, K., Szeverényi, I., Takeichi, T., Balaji, R., Lau, A., Tye, H., Roy, K., Bonnard, C., Ahl, P. J., Jones, L. A., Baker, P., Lacina, L., Otsuka, A., Fournie, P. R., ... Reversade, B. (2016). Germline NLRP1 Mutations Cause Skin Inflammatory and Cancer Susceptibility Syndromes via Inflammasome Activation. *Cell*, 167(1), 187–202.e17. <https://doi.org/10.1016/j.cell.2016.09.001>
- Zhong, F. L., Robinson, K., Teo, D. E. T., Tan, K. Y., Lim, C., Harapas, C. R., Yu, C. H., Xie, W. H., Sobota, R. M., Au, V. B., Hopkins, R., D’Osualdo, A., Reed, J. C., Connolly, J. E., Masters, S. L., & Reversade, B. (2018). Human DPP9 represses NLRP1 inflammasome and protects against autoinflammatory diseases via both peptidase activity and FIIND domain binding. *Journal of Biological Chemistry*, 293(49), 18864–18878. <https://doi.org/10.1074/jbc.RA118.004350>
- Zhou, B., Zhang, J. yuan, Liu, X. shuo, Chen, H. zi, Ai, Y. li, Cheng, K., Sun, R. yue, Zhou, D., Han, J., & Wu, Q. (2018). Tom20 senses iron-activated ROS signaling to promote melanoma cell pyroptosis. *Cell Research*, 28(12), 1171–1185. <https://doi.org/10.1038/s41422-018-0090-y>

- Zhou, J. Y., Sarkar, M. K., Okamura, K., Harris, J. E., Gudjonsson, J. E., & Fitzgerald, K. A. (2023). Activation of the NLRP1 inflammasome in human keratinocytes by the dsDNA mimetic poly(dA:dT). *Proceedings of the National Academy of Sciences of the United States of America*, *120*(5). <https://doi.org/10.1073/pnas.2213777120>
- Zhou, Q., Wang, H., Schwartz, D. M., Stoffels, M., Hwan Park, Y., Zhang, Y., Yang, D., Demirkaya, E., Takeuchi, M., Tsai, W. L., Lyons, J. J., Yu, X., Ouyang, C., Chen, C., Chin, D. T., Zaal, K., Chandrasekharappa, S. C., Hanson, E. P., Yu, Z., ... Aksentijevich, I. (2015). Loss-of-function mutations in TNFAIP3 leading to A20 haploinsufficiency cause an early-onset autoinflammatory disease. *Nature Genetics*, *48*(1), 67–73. <https://doi.org/10.1038/ng.3459>
- Zhou, Z., He, H., Wang, K., Shi, X., Wang, Y., Su, Y., Wang, Y., Li, D., Liu, W., Zhang, Y., Shen, L., Han, W., Shen, L., Ding, J., & Shao, F. (2020). Granzyme A from cytotoxic lymphocytes cleaves GSDMB to trigger pyroptosis in target cells. *Science*, *368*(6494). <https://doi.org/10.1126/science.aaz7548>
- Zhu, Q., & Kanneganti, T.-D. (2017). Cutting Edge: Distinct Regulatory Mechanisms Control Proinflammatory Cytokines IL-18 and IL-1 β . *The Journal of Immunology*, *198*(11), 4210–4215. <https://doi.org/10.4049/jimmunol.1700352>
- Zhu, X., & Zhu, J. (2020). CD4 T helper cell subsets and related human immunological disorders. In *International Journal of Molecular Sciences* (Vol. 21, Issue 21, pp. 1–26). MDPI AG. <https://doi.org/10.3390/ijms21218011>
- Zou, J., Zheng, Y., Huang, Y., Tang, D., Kang, R., & Chen, R. (2021). The Versatile Gasdermin Family: Their Function and Roles in Diseases. In *Frontiers in Immunology* (Vol. 12). Frontiers Media S.A. <https://doi.org/10.3389/fimmu.2021.751533>

VII. APPENDIX

1. Caspase-1 driven neutrophil pyroptosis and its role in host susceptibility to *Pseudomonas aeruginosa*

Contribution:

In this paper I participated in the purification, cell plating and infection of some experiments.

RESEARCH ARTICLE

Caspase-1-driven neutrophil pyroptosis and its role in host susceptibility to *Pseudomonas aeruginosa*

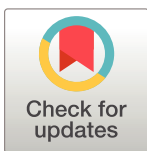
Karin Santoni¹, David Pericat¹, Leana Gorse¹, Julien Buyck², Miriam Pinilla¹, Laure Prouvensier², Salimata Bagayoko¹, Audrey Hessel¹, Stephen Adonai Leon-Icaza¹, Elisabeth Bellard¹, Serge Mazères¹, Emilie Doz-Deblauwe³, Nathalie Winter³, Christophe Paget⁴, Jean-Philippe Girard¹, Christine T. N. Pham⁵, Céline Cougoule¹, Renaud Poincloux¹, Mohamed Lamkanfi⁶, Emma Lefrançois¹, Etienne Meunier¹ ^{1‡‡*}, Rémi Planès^{1‡*}

1 Institute of Pharmacology and Structural Biology (IPBS), University of Toulouse, CNRS, Toulouse, France, **2** UFR Medicine and Pharmacy, INSERM U1070, University of Poitiers, Poitiers, France, **3** INRAE, Université de Tours, ISP, Nouzilly, France, **4** Institut national de la santé et de la recherche médicale, Centre d'Etude des Pathologies Respiratoires, UMR 1100, Tours, France, **5** Division of Rheumatology, Department of Internal Medicine, Washington University School of Medicine, Saint Louis, Missouri, United States of America, **6** Department of Internal Medicine and Pediatrics, Ghent University, Ghent, Belgium

‡ Current Address: Institute of Pharmacology and Structural Biology (IPBS), University of Toulouse, CNRS, Toulouse, France

‡ These authors equally supervised this work.

* etienne.meunier@ipbs.fr (EM); Remi.planes@ipbs.fr (RP)


 OPEN ACCESS

Citation: Santoni K, Pericat D, Gorse L, Buyck J, Pinilla M, Prouvensier L, et al. (2022) Caspase-1-driven neutrophil pyroptosis and its role in host susceptibility to *Pseudomonas aeruginosa*. PLoS Pathog 18(7): e1010305. <https://doi.org/10.1371/journal.ppat.1010305>

Editor: Vincent T. Lee, University of Maryland, UNITED STATES

Received: January 27, 2022

Accepted: June 1, 2022

Published: July 18, 2022

Peer Review History: PLOS recognizes the benefits of transparency in the peer review process; therefore, we enable the publication of all of the content of peer review and author responses alongside final, published articles. The editorial history of this article is available here: <https://doi.org/10.1371/journal.ppat.1010305>

Copyright: © 2022 Santoni et al. This is an open access article distributed under the terms of the [Creative Commons Attribution License](https://creativecommons.org/licenses/by/4.0/), which permits unrestricted use, distribution, and reproduction in any medium, provided the original author and source are credited.

Data Availability Statement: All relevant data are within the manuscript and its [Supporting information](#) files.

Abstract

Multiple regulated neutrophil cell death programs contribute to host defense against infections. However, despite expressing all necessary inflammasome components, neutrophils are thought to be generally defective in Caspase-1-dependent pyroptosis. By screening different bacterial species, we found that several *Pseudomonas aeruginosa* (*P. aeruginosa*) strains trigger Caspase-1-dependent pyroptosis in human and murine neutrophils. Notably, deletion of Exotoxins U or S in *P. aeruginosa* enhanced neutrophil death to Caspase-1-dependent pyroptosis, suggesting that these exotoxins interfere with this pathway. Mechanistically, *P. aeruginosa* Flagellin activates the NLRC4 inflammasome, which supports Caspase-1-driven interleukin (IL)-1 β secretion and Gasdermin D (GSDMD)-dependent neutrophil pyroptosis. Furthermore, *P. aeruginosa*-induced GSDMD activation triggers Calcium-dependent and Peptidyl Arginine Deaminase-4-driven histone citrullination and translocation of neutrophil DNA into the cell cytosol without inducing extracellular Neutrophil Extracellular Traps. Finally, we show that neutrophil Caspase-1 contributes to IL-1 β production and susceptibility to pyroptosis-inducing *P. aeruginosa* strains *in vivo*. Overall, we demonstrate that neutrophils are not universally resistant for Caspase-1-dependent pyroptosis.

Funding: This project was supported by the Fonds de Recherche en Santé Respiratoire - Fondation du Souffle (to EL), ATIP-Avenir program (to EM), FRM "Amorçage Jeunes Equipes" (AJE20151034460 to EM) and the ERC (StG INFLAME 804249 to EM), the NIH (AR073752 to CTNP), the European Society of Clinical Microbiology and Infectious Diseases (ESCMID, to RP), Invivogen-CIFRE PhD grant (to MP), Invivogen post-doctoral fellowship (to RP) and a PhD fellowship from the Minister of Research of Mali and Campus France agency (to SB). The funders had no role in study design, data collection and analysis, decision to publish, or preparation of the manuscript.

Competing interests: The authors have declared that no competing interests exist.

Author summary

Neutrophils play an essential role against infections. Although multiple neutrophil death programs contribute to host defense against infections, neutrophils are thought to be defective in Caspase-1-dependent pyroptosis. We screened several microbial species for the capacity to overcome neutrophil resistance to Caspase-1-driven pyroptosis, and show that the bacterium *Pseudomonas aeruginosa* specifically engages the NLR4 inflammasome to promote Caspase-1-dependent Gasdermin D activation and subsequent neutrophil pyroptosis. Furthermore, NLR4 inflammasome-driven pyroptosis leads to histone citrullination, nuclear DNA decondensation and expansion into the host cell cytosol. However, Neutrophil Extracellular Trap (NET) are not formed because DNA is kept in the intracellular space despite plasma membrane permeabilization and extracellular release of soluble and insoluble alarmins. Finally, *in vivo* *P. aeruginosa* infections highlight that Caspase-1-driven neutrophil pyroptosis is detrimental to the host upon *P. aeruginosa* infection. Altogether, our results demonstrate Caspase-1-dependent pyroptosis in neutrophils as a process that contributes to host susceptibility to *P. aeruginosa* infection.

Introduction

Over the last 30 years, non-apoptotic forms of cell death have emerged as crucial processes driving inflammation, host defense against infections but also (auto) inflammatory pathologies [1]. NETosis is an antimicrobial and pro-inflammatory form of cell death in neutrophils that promotes the formation of extracellular web-like structures called Neutrophil Extracellular Traps (NETs) [2]. Although the importance of NETosis in host immunity to infections has been well established [2–5], NETosis dysregulation also associates to autoimmunity, host tissue damage, aberrant coagulation and thrombus formation, which all contribute to inflammatory pathologies such as sepsis and autoimmune lupus [6–13].

NETosis consists of sequential steps that start with nuclear envelope disintegration, DNA decondensation, cytosolic expansion of nuclear DNA and its subsequent expulsion through the plasma membrane [14]. Completion of DNA decondensation and expulsion requires various cellular effectors. Among them, neutrophil serine proteases (Neutrophil elastase, Cathepsin G, Proteinase 3) or Caspase-11 may cleave histones, which relaxes DNA tension [3, 13, 15–17]. In addition, granulocyte-enriched Protein arginine deaminase 4 (PAD4) citrullinates histone-bound DNA to neutralize arginine positive charges and facilitate nuclear DNA relaxation and decondensation [4, 18, 19]. In a third step, decondensed DNA physically binds neutrophil cytoplasmic granule factors such as Neutrophil Elastase (NE), Cathepsin G (CathG), Proteinase 3 (Pr3) and Myeloperoxidase (MPO) proteins [3, 15, 18]. Finally, sub-cortical actin network disassembly promotes efficient DNA extrusion through the permeabilized plasma membrane [18, 20].

Depending on the initial trigger, various signaling pathways such as calcium fluxes [17, 18], necroptosis-associated MLKL phosphorylation [21], ROS-induced Neutrophil protease release [15] or endotoxin-activated Caspase-11 [3, 5, 22] have been shown to induce NETosis. ROS- and Caspase-11-dependent NETosis have been shown to share the requirement for cleavage of the pyroptosis executioner Gasdermin D (GSDMD) by neutrophil serine proteases and Caspase-11, respectively [3, 16]. Active GSDMD forms pores on PIP2-enriched domains of the plasma and nuclear membranes of neutrophils, which ensures both IL-1 β secretion [23–26] and osmotic imbalance-induced DNA decondensation and expulsion [3, 16]. However, the link between ROS and Gasdermin-D-dependent NETosis requires more investigations as a

recent study could show that a described GSDMD inhibitor, the LDC559, is actually a ROS inhibitor, but not a GSDMD inhibitor [27].

Intriguingly, despite inducing GSDMD cleavage, neutrophils were reported to resist induction of Caspase-1-dependent pyroptosis upon NLRC4 inflammasome activation by *Salmonella* Typhimurium and *Burkholderia thailandensis*, or upon Nigericin/ATP-mediated NLRP3 inflammasome activation [3, 5, 28, 29]. However, recent studies indirectly challenged canonical pyroptosis impairment in neutrophils by showing that sterile activators, but also the SARS-CoV-2 virus, could also contribute to canonical NLRP3 inflammasome-dependent neutrophil death and subsequent NETosis [30, 31]. However, whether bacterial species exist that can induce neutrophil pyroptosis by canonical inflammasomes has remained an open question.

Lung infections by the bacterium *Pseudomonas aeruginosa* (*P. aeruginosa*) can promote acute or chronic, life-threatening infections in immunocompromised and hospitalized patients [32]. *P. aeruginosa* strains express a Type-3 Secretion System (T3SS) that allows injecting a specific set of virulence factors into host target cells, including macrophages and neutrophils [33]. T3SS-expressing *Pseudomonas aeruginosa* strains classically segregate into two mutually exclusive clades. Those expressing the bi-cistronic ADP-ribosylating and GTPase Activating Protein (GAP) virulence factor ExoS, and those expressing the lytic phospholipase of the patatin-like family, ExoU [33]. Common to most of *P. aeruginosa* strains is the expression of two other toxins, ExoY and ExoT, whose functions in bacterial infection still remain unclear. All Exo toxins are injected by the T3SS into host target cells upon infections. Finally *P. aeruginosa* strains also use their T3SS to inject Flagellin but also some of the T3SS components (needle) into host target cells, which promotes activation of the NAIP-NLRC4 inflammasome and subsequent Caspase-1-driven and GSDMD-dependent pyroptosis of macrophages [34–40]. Although numerous studies underlined that neutrophils are targeted by *Pseudomonas aeruginosa* virulence factors, which could promote NETosis [12, 41–43], the critical bacterial effector molecules and their host cell targets remain extensively debated. Intriguingly, defective expression of the enzyme NADPH oxidase (Nox2) sensitizes murine neutrophils to Caspase-1-driven neutrophil death upon infection with *Pseudomonas aeruginosa* [44], which suggests that under certain conditions neutrophils might be prone to undergo Caspase-1-dependent pyroptosis. Whether caspase-1-mediated pyroptosis also occurs in WT neutrophils, and what its putative molecular and immune significance might be remains unknown.

Here, we screened several bacterial species for their ability to bypass neutrophil resistance to canonical inflammasome-induced pyroptosis induction and found that the bacterial pathogen *Pseudomonas aeruginosa* triggers Caspase-1-dependent pyroptosis in human and murine neutrophils. Notably, deletion of Exotoxins U or S in *P. aeruginosa* entirely rewires neutrophil death towards Caspase-1-driven pyroptosis, suggesting that these bacterial Exotoxins somehow suppress caspase-1-mediated neutrophil pyroptosis. Mechanistically, *P. aeruginosa*-induced pyroptosis requires the expression of a functional Type-3 Secretion System (T3SS) and Flagellin, but not the T3SS-derived toxins ExoS, ExoT, ExoY or ExoU. Consequently, *P. aeruginosa* selectively activates the neutrophil NLRC4 inflammasome, which ensures Caspase-1-driven Gasdermin D (GSDMD) cleavage and the induction of neutrophil pyroptosis. Furthermore, we show that GSDMD activation promotes Calcium-dependent Peptidyl Arginine Deaminase 4 (PAD4) activation. PAD4 goes on to citrullinates histones, which leads to DNA decondensation and translocation of decondensed neutrophil DNA in the host cell cytosol without it being expelled from the cells into the extracellular environment. Finally, we show by intravital microscopy that neutrophil pyroptosis occurs in lungs of *P. aeruginosa*-infected MRP8-GFP mice, and that neutrophil-targeted deletion of caspase-1 (in MRP8-CreCas1^{flox} mice) reduces both IL-1 β production and susceptibility to *P. aeruginosa* infection *in vivo*.

Overall, our results highlight that Caspase-1-dependent pyroptosis is a functional process in neutrophils that contributes to host susceptibility to *P. aeruginosa* infection *in vivo*.

Results

***Pseudomonas aeruginosa* strains variously trigger Caspase-1-dependent and -independent neutrophil lysis**

To determine whether neutrophils may undergo pyroptosis upon bacterial infection, we infected WT and *Caspase-1*^{-/-} (*Casp1*^{-/-}) mouse Bone Marrow Neutrophils (BMNs) with various bacterial strains that are known to activate different inflammasomes in macrophages, such as *Salmonella* Typhimurium (*S. Typhimurium*, strain SL1344), *Shigella flexnerii* (*S. flexnerii*, strain M90T), *Legionella pneumophila* (*L. pneumophila*, strain Philadelphia-1), *Burkholderia thailandensis* (*B. thailandensis*, strain E264), *Pseudomonas aeruginosa* (*P. aeruginosa*, strain PAO1), *Listeria monocytogenes* (*L. monocytogenes*, strain EGD), *Burkholderia cenocepaciae* (*B. cenocepaciae*, strain LMG 16656), *Francisella tularensis* spp *novicida* (*F. novicida*, strain U112), *Escherichia coli* (*E. Coli*, strain K12), *Staphylococcus aureus* (*S. aureus*, strain USA-300) and *Vibrio cholera* (*V. cholera*, strain El tor) (Fig 1A). In addition to tracking neutrophil lysis (LDH release), we measured IL-1 β release as a hallmark of inflammasome activation. Given that neutrophils are short-lived cells that undergo spontaneous apoptosis over time, which can result in secondary necrosis and LDH release *in vitro*, we first determined a suitable time-frame in which neutrophils resist spontaneous lysis. Having determined that culture media of WT and *Casp1*^{-/-} neutrophils lacked spontaneous LDH release during the first 4–5 hours (S1A Fig), we next performed infections within the first 3–4 hours in order to avoid confounding effects of spontaneous LDH release. With the notable exception of *Staphylococcus aureus*, we observed that all bacteria triggered Caspase-1-dependent IL-1 β release in our experimental set-ups (Fig 1A), thus confirming Caspase-1 activation in neutrophils upon infection with various bacterial pathogens. In addition, despite most of the tested bacteria inducing significant neutrophil lysis, only LDH release by *Pseudomonas aeruginosa* (PAO1 strain) was partially dependent on Caspase-1 (further referred to as pyroptosis) (Fig 1A). Furthermore, we confirmed that infection of human blood neutrophils with two different *Pseudomonas aeruginosa* strains (PAO1 and CHA) also triggered a Caspase-1-dependent, yet Caspase-4/5, -3/7 and -8-independent, IL-1 β release and neutrophil lysis (Fig 1B). These results demonstrate that various bacteria can trigger neutrophil lysis in a Caspase-1-independent manner, and that *Pseudomonas aeruginosa* PAO1 strain specifically promotes neutrophil lysis through a mechanism that is partially Caspase-1-dependent.

P. aeruginosa T3SS-mediated injection of Flagellin and toxins (ExoS, U, T, Y) play a major role in its virulence. To determine the role of these virulence factors in *P. aeruginosa*-induced neutrophil pyroptosis, we infected murine BMNs with WT *P. aeruginosa* PAO1 or mutant strains that are deficient in expression of individual toxins (PAO1 ^{Δ ExoS}, PAO1 ^{Δ ExoT}, PAO1 ^{Δ ExoY}); deficient for the expression of Flagellin (PAO1 ^{Δ FliC}); or for the T3SS (PAO1 ^{Δ ExsA}) (Figs 1C and S1B). We parallelly measured the ability of WT and *Casp1*^{-/-} neutrophils infected with these strains to undergo cell lysis (LDH release), to promote IL1 β release, and to exhibit plasma membrane permeabilization (SYTOX Green incorporation) (Figs 1C and S1B). Our results show that *P. aeruginosa* strains lacking expression of T3SS or Flagellin were unable to promote robust Caspase-1-dependent neutrophil lysis, IL-1 β release and plasma membrane permeabilization, suggesting that T3SS and Flagellin are major effectors of Caspase-1-driven neutrophil death (Figs S1B and 1C). Flagellin deficiency modifies the physical recognition and phagocytosis of *P. aeruginosa* by macrophages and neutrophils [45, 46] (S1C Fig), which could indirectly alter the amount of Flagellin injected into host target cells. To ensure similar

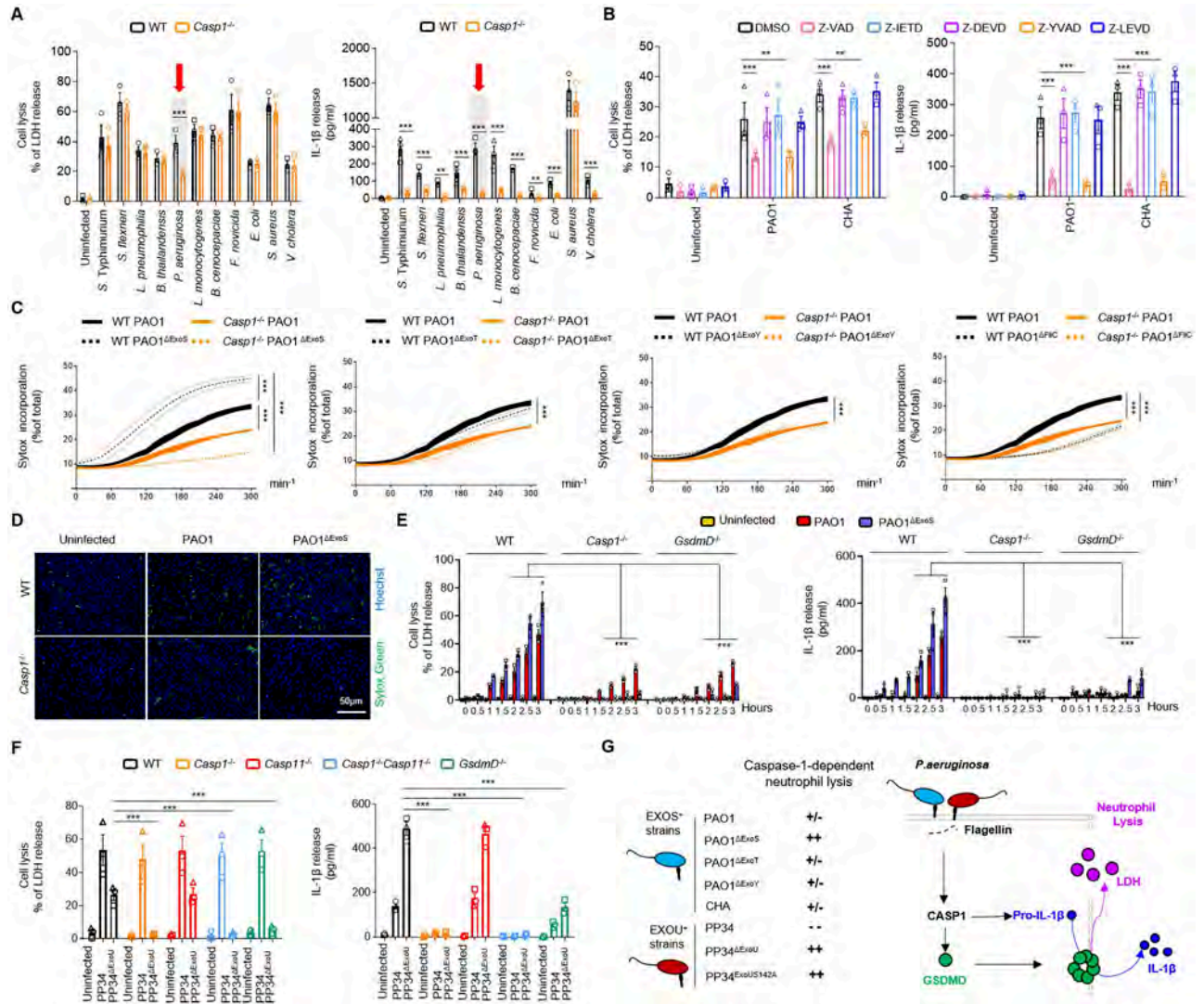


Fig 1. Various *Pseudomonas aeruginosa* strains trigger Caspase-1-dependent and -independent neutrophil lysis. **A.** Measure of cell lysis (release of LDH) and IL-1 β release in WT or *Casp1*^{-/-} murine Bone Marrow Neutrophils (BMNs) infected for 3 hours with various bacteria at a multiplicity of infection (MOI) of 10. ***p* < 0.01 ****p* < 0.001, Two-Way Anova with multiple comparisons. Values are expressed as mean \pm SEM. Graphs show combined values from three independent experiments. **B.** Measure of cell lysis (release of LDH) and IL-1 β release in human blood neutrophils infected for 3 hours with *Pseudomonas aeruginosa* strains PAO1 or CHA (MOI 5) in presence/absence of various Caspase inhibitors, Z-VAD (pan Caspase, 20 μ M), Z-YVAD (Casp1 inhibitor, 40 μ M), Z-DEVD (Casp3 inhibitor, 40 μ M), Z-IETD (Casp8 inhibitor, 40 μ M) or Z-LEVD (Casp4/5 inhibitor, 40 μ M). ***p* < 0.01 ****p* < 0.001, Two-Way Anova with multiple comparisons. Values are expressed as mean \pm SEM. Graphs show values from three independent experiments with one different donor each time. **C, D.** Measure of plasma membrane permeabilization and associated fluorescent microscopy images over time using SYTOX Green incorporation in WT or *Casp1*^{-/-} BMNs infected with *Pseudomonas aeruginosa* PAO1 or various isogenic mutants lacking Flagellin (FliC, PAO1 ^{Δ FliC}) or T3SS-derived toxins ExoS, ExoY, ExoT (PAO1 ^{Δ ExoS}, PAO1 ^{Δ ExoY}, PAO1 ^{Δ ExoT}). ****p* < 0.001, Two-Way Anova with multiple comparisons. Values are expressed as mean \pm SEM. Graphs show combined values from three independent experiments. **E.** Measure of cell lysis (release of LDH) and IL-1 β release in WT, *Casp1*^{-/-} and *GsdmD*^{-/-} murine Bone Marrow Neutrophils (BMNs) infected for the indicated times with PAO1 or its isogenic mutant PAO1 ^{Δ ExoS} at an MOI of 10. ****p* < 0.001, Two-Way Anova with multiple comparisons. Values are expressed as mean \pm SEM. Graphs show combined values from three independent experiments. **F.** Measure of cell lysis (release of LDH) and IL-1 β release in WT, *Casp1*^{-/-}, *Casp11*^{-/-}, *Casp1*^{-/-}*Casp11*^{-/-} and *GsdmD*^{-/-} murine Bone Marrow Neutrophils (BMNs) infected for 3 hours with *Pseudomonas aeruginosa* PP34 strain or its isogenic mutant PP34 ^{Δ ExoU} at a multiplicity of infection (MOI) of 2. ****p* < 0.001, Two-Way Anova with multiple comparisons. Values are expressed as mean \pm SEM. Graphs show combined values from three independent experiments. **G.** Overview of the importance of Caspase-1 at driving neutrophil pyroptosis in response to various *Pseudomonas aeruginosa* strains.

<https://doi.org/10.1371/journal.ppat.1010305.g001>

phagocytosis/recognition of *Pseudomonas aeruginosa* strains by neutrophils, we genetically invalidated the expression of Flagellin motors (namely MotABCD) in a WT PAO1 and Flagellin-deficient (PAO1^{ΔFliC}) genetic background. Both PAO1^{ΔMotABCD} and PAO1^{ΔMotABCD/ΔFliC} showed similar neutrophil uptake after 45 minutes of infection (S1C Fig), which allowed evaluating the direct importance of Flagellin in *P. aeruginosa*-driven Caspase-1-dependent neutrophil pyroptosis. Kinetic analysis of neutrophil lysis (LDH release) and IL-1β production in WT and *Casp1*^{-/-} neutrophils showed that PAO1^{ΔMotABCD}, but not PAO1^{ΔMotABCD/ΔFliC}, induced Caspase-1-dependent neutrophil lysis and IL-1β release over time (S1D Fig), suggesting that Flagellin plays a major role in *P. aeruginosa*-induced neutrophil pyroptosis.

To the contrary, deletion of Exo-Y or Exo-T in *P. aeruginosa* PAO1 did not significantly influence neutrophil lysis, IL-1β release or plasma membrane permeabilization (Fig 1C and 1D, and S1B). However, infection of neutrophils with *P. aeruginosa* PAO1 deficient for ExoS triggered significantly increased lysis, membrane permeabilization and IL-1β release (Fig 1C and 1D, and S1B). In addition, PAO1^{ΔExoS}-induced neutrophil lysis was strongly reduced in *Caspase-1*-deficient neutrophils, suggesting that ExoS expression suppresses Caspase-1-dependent neutrophil death (Fig 1C and 1D, and S1B).

Caspase-1 cleavage of the pyroptosis executioner Gasdermin D (GSDMD) is the central effector mechanism of canonical inflammasome-induced pyroptosis in macrophages. Kinetic measurements confirmed that both *Casp1*^{-/-} and *GsdmD*^{-/-} neutrophils exhibited reduced LDH and IL-1β release upon *P. aeruginosa* infection (Fig 1E). Consistent with our earlier observations (Fig 1C and 1D, and S1B), neutrophil lysis and IL-1β release by the PAO1^{ΔExoS} mutant (and to a lower extent also PAO1-induced responses) were strongly dependent on CASP1 and GSDMD expression (Fig 1E).

P. aeruginosa strains PAO1 and CHA belong to the 70% of the *P. aeruginosa* strains that express the Exotoxin S (ExoS). As 30% of *P. aeruginosa* strains do not express the Exotoxin S (ExoS) but instead are characterized as expressing the extremely lytic phospholipase toxin ExoU, we expanded our analysis to neutrophils infected with a strain expressing a catalytically inactive mutant of ExoU (PP34^{ExoUS142A}). In addition, we examined the response of neutrophils to a *P. aeruginosa* strain that naturally expresses ExoU (PP34 strain) or a mutant thereof that is genetically deficient for ExoU (PP34^{ΔExoU}). These experiments showed that the *P. aeruginosa* PP34 strain induces neutrophil lysis, yet in a Caspase-1- and Gasdermin D-independent manner (Figs 1F and S1E). However, both human and murine neutrophils infected with PP34^{ΔExoU} or PP34^{ExoUS142A} showed robust Caspase-1-dependent neutrophil lysis, plasma membrane permeabilization and IL-1β release (Figs 1E, S1E and S1F). These results suggest that Caspase-1 and GSDMD-dependent pyroptosis is masked or suppressed by ExoU activity in the *P. aeruginosa* PP34 strain.

Altogether, our results show the unexpected ability of Caspase-1 to promote GSDMD-dependent neutrophil pyroptosis upon *Pseudomonas aeruginosa* infection (Fig 1G).

NLRC4 drives *P. aeruginosa*-induced neutrophil pyroptosis

Next, we investigated the upstream molecular pathways by which *P. aeruginosa* promoted Caspase-1-dependent neutrophil pyroptosis. To address this specific question, we used the most potent pyroptotic strains of *P. aeruginosa*, namely PAO1^{ΔExoS}, PP34^{ΔExoU} or PP34^{ExoUS142A} (further referred to as “pyroptotic strains” for clarity) (Fig 1G). We infected WT murine neutrophils or neutrophils from mice lacking expression of various inflammasome sensors, namely *Casp1*^{-/-}, *Casp11*^{-/-}, *Casp1*^{-/-} *Casp11*^{-/-}, *Nlrp3*^{-/-}, *AIM2*^{-/-}, *Nlrc4*^{-/-} and *ASC*^{-/-} (S2A Fig). Among the different tested neutrophil genotypes, significant resistance to pyroptotic cell lysis (LDH release) was only observed in *Casp1*^{-/-}, *Casp1*^{-/-} *Casp11*^{-/-}, *Nlrc4*^{-/-} and *ASC*^{-/-} BMNs

upon infection with *P. aeruginosa* pyroptotic strains PAO1^{ΔExoS} and PP34^{ΔExoU} (S2A Fig). Contrastingly, *Casp11*^{-/-}, *Nlrp3*^{-/-} and *AIM2*^{-/-} neutrophils exhibited similar lysis levels (LDH release) as observed in WT BMNs (S2A Fig). This suggests that NLRC4—but not NLRP3, Caspase-11 or AIM2—efficiently promotes neutrophil pyroptosis upon infection with *P. aeruginosa* pyroptotic strains (S2A Fig). The role of NLRC4 in *P. aeruginosa*-induced neutrophil cell death is confined to Caspase-1-dependent pyroptosis because infection of WT and *Nlrc4*^{-/-} BMNs with *P. aeruginosa* strains that trigger Caspase-1-independent neutrophil lysis (PP34) resulted in similar LDH release levels, akin to our earlier results in *Casp1*^{-/-} and *GsdmD*^{-/-} neutrophils (Figs 1F and 2A). In contrast, infection of WT and *Nlrc4*^{-/-} BMNs with *P. aeruginosa* strains of which neutrophil cell lysis is partially Caspase-1-dependent (PAO1 and CHA strains) also showed a partial involvement of NLRC4 in controlling neutrophil lysis (Fig 2A). Importantly, IL-1β release was entirely dependent on NLRC4 upon infection with any of these different *Pseudomonas aeruginosa* strains, whereas the pyroptotic strains PAO1^{ΔExoS}, CHA^{ΔExoS} and PP34^{ΔExoU} triggered neutrophil lysis and IL-1β release that was fully NLRC4-dependent (Fig 2A).

Further analysis of Caspase-1 (p20) and GSDMD (p30) processing in response to various *P. aeruginosa* strains showed that the pyroptotic strains PAO1^{ΔExoS}, PP34^{ExoUS142A} and PP34^{ΔExoU} as well as partially Caspase-1-dependent PAO1 strain triggered robust neutrophil Caspase-1 and GSDMD processing, a process that required NLRC4 expression (Fig 2B and 2C). As expected, a PAO1 mutant strain lacking the T3SS regulator ExsA (PAO1^{ΔExsA}) failed to induce robust Caspase-1 and GSDMD processing (Fig 2B). Finally, the PP34 strain, which promotes NLRC4- and Caspase-1-independent neutrophil lysis, also failed to trigger efficient cleavage of Caspase-1 and GSDMD, suggesting that PP34-induced neutrophil lysis is inflammasome-independent (Fig 2C). These results suggest that NLRC4 drives Caspase-1 and GSDMD cleavage in response to various *P. aeruginosa* strains that are capable of inducing neutrophil pyroptosis, namely PAO1, PAO1^{ΔExoS}, CHA, CHA^{ΔExoS}, PP34^{ΔExoU} and PP34^{ExoUS142A}, but not in response to the PP34 strain that induces inflammasome-independent neutrophil lysis.

Based on this information, we sought to determine whether *P. aeruginosa* infection also induced neutrophil NLRC4 inflammasome activation *in vivo*. To this end, we infected ASC-Citrine mice with low doses (1.10⁵ CFUs) of *P. aeruginosa* strains that specifically triggered NLRC4-dependent neutrophil pyroptosis, namely PP34^{ΔExoU}. As control, we included its isogenic mutant PP34^{ΔExoU/ΔFlhC} that is deficient in Flagellin expression and hence unable to trigger NLRC4-dependent neutrophil pyroptosis *in vitro* (Figs 2D and S2B). ImageStreamX analysis of neutrophils presenting an active ASC supramolecular speck (ASC speck⁺/LY6G⁺ neutrophils) showed that PP34^{ΔExoU} infection triggered inflammasome activation in neutrophils, and that the amount of ASC speck⁺ neutrophils was reduced when mice were infected with Flagellin-deficient PP34^{ΔExoU/ΔFlhC} mutant bacteria (Figs 2D and S2B). Altogether, these results show that the NLRC4/CASP1/GSDMD axis is fully functional to promote neutrophil pyroptosis in response to several *P. aeruginosa* strains, namely PAO1, PAO1^{ΔExoS}, CHA, CHA^{ΔExoS}, PP34^{ΔExoU} or PP34^{ExoUS142A} (Fig 2E).

***P. aeruginosa*-induced inflammasome activation induces neutrophil DNA decondensation**

As multiple cell death pathways such as Caspase-11-induced pyroptosis, MLKL-driven necroptosis, Mitogen- and Calcium-induced NETosis, have been linked to a direct or secondary induction of neutrophil DNA decondensation and release, a hallmark of NETosis, we next sought to determine whether *P. aeruginosa*-induced neutrophil inflammasome activation

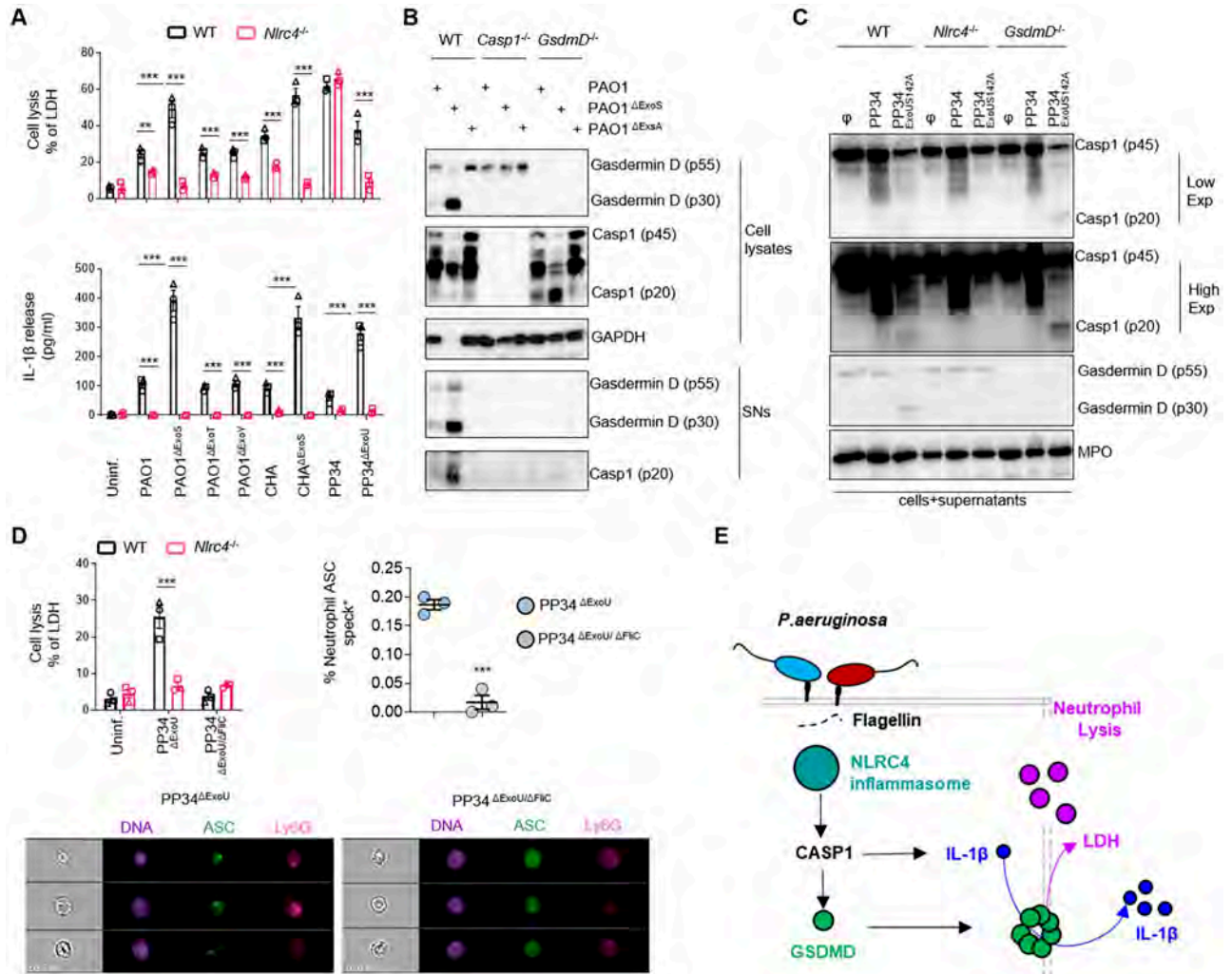


Fig 2. *P. aeruginosa* infection engages a canonical NLR4-Caspase-1-Gasdermin D-dependent pyroptosis axis in neutrophils. **A.** Measure of cell lysis (release of LDH) and IL-1 β release in WT or *Nlr4*^{-/-} murine Bone Marrow Neutrophils (BMNs) infected for 3 hours with *Pseudomonas aeruginosa* PAO1, CHA and PP34 strains and their isogenic mutants lacking T3SS-derived toxins ExoS, ExoY, ExoT or ExoU) at a multiplicity of infection (MOI) of 10 (PAO1 and CHA strains) and 2 (PP34 strains). ***p* ≤ 0.01 ****p* ≤ 0.001, Two-Way Anova with multiple comparisons. Values are expressed as mean ± SEM. Graphs show combined values from three independent experiments. **B.** Immunoblotting of GAPDH, pro-forms of Caspase-1 (p45) and Gasdermin-D (p55), processed Caspase-1 (p20) and Gasdermin D (p30), in WT, *Casp1*^{-/-} and *GsdmD*^{-/-} in cell lysates and cell supernatants (SNs) of BMNs infected for 3 hours with PAO1 or its isogenic mutants lacking T3SS expression (PAO1^{ΔExoS}) or ExoS (PAO1^{ΔExoS}) at a multiplicity of infection (MOI) of 10. Immunoblots show lysates and supernatants from one experiment performed three times. **C.** Immunoblotting of Myeloperoxidase (MPO), pro-forms of Caspase-1 (p45) and Gasdermin-D (p55), processed Caspase-1 (p20) and Gasdermin D (p30), in WT, *Nlr4*^{-/-} and *GsdmD*^{-/-} BMNs infected for 3 hours with *P. aeruginosa* strain PP34 or its isogenic mutant lacking ExoU activity (PP34^{ExoU142A}) at a multiplicity of infection (MOI) of 2. Immunoblots show combined lysates and supernatants from one experiment performed three times. **D.** Measure of cell lysis (release of LDH) in WT and *Nlr4*^{-/-} BMNs infected for 3 hours with *P. aeruginosa* mutant strains PP34^{ΔExoU} or PP34^{ΔExoU/ΔFliC} at a multiplicity of infection (MOI) of 2 and Imagestream experiments and quantifications of *in vivo* formation of ASC specks in bronchoalveolar (BALs) neutrophils from ASC-Citrine mice intranasally infected with 1.10⁵ PP34^{ΔExoU} or PP34^{ΔExoU/ΔFliC} for 6 hours. The gating strategy used to evaluate inflammasome activation in neutrophils was performed as follow: (i) a gate was set on cells in focus [Cells in Focus] and (ii) a sub-gate was created on single cells [Single Cells]. Then we gated first on (iii) LY6G+ Neutrophils [LY6G+] and second on (iv) ASC-citrine+ and Hoechst+ cells [Hoechst+/ASC-Citrine+] within LY6G+ population. (v) To distinguish cells with active (ASC-speck) versus inactive inflammasome (Diffuse ASC), we plotted the Intensity with the area of ASC-citrine. This strategy allows to distinguish cells with active inflammasome that were visualized and quantified. For Imagestream experiments ****p* ≤ 0.001, T-test with Bonferroni correction. Values are expressed as mean ± SEM. Graphs show one experiment representative of two independent experiments. For neutrophil *in vitro* experiments, ****p* ≤ 0.001, Two-Way Anova with multiple comparisons. Values are expressed as mean ± SEM. Graphs show combined values from three independent experiments. **E.** Overview of the importance of the NLR4 inflammasome at driving neutrophil pyroptosis in response to various *Pseudomonas aeruginosa* strains.

<https://doi.org/10.1371/journal.ppat.1010305.g002>

could also lead to DNA decondensation and expulsion. We infected WT, *Casp1*^{-/-} or *GsdmD*^{-/-} murine BMNs with the pyroptotic *P. aeruginosa* strains PAO1, PAO1^{ΔExoS}, PP34^{ExoUS142A}, or with the PP34 strain that triggers Caspase-1-independent neutrophil lysis (Figs 1 and 2). We specifically monitored the presence of DNA Neutrophil Extracellular Traps (NETs) using Scanning Electron Microscopy (SEM) (Fig 3A). PP34, and to a lower extent PAO1, induced NETs in WT, *Casp1*^{-/-} and *GsdmD*^{-/-} neutrophils (Fig 3A). However, we observed that the fully pyroptotic strains PAO1^{ΔExoS} and PP34^{ExoUS142A} failed to induce NETs (Fig 3A), which suggests that Caspase-1-induced neutrophil pyroptosis does not promote NETosis.

Rather, immunofluorescence experiments of WT, *Casp1*^{-/-} and *GsdmD*^{-/-} neutrophils infected with the fully pyroptotic *P. aeruginosa* strain PP34^{ExoUS142A} showed efficient DNA decondensation as well as exit from the nuclear envelope (Lamin-B1 staining) but little or no extracellular DNA release from BMNs exhibiting an active inflammasome complex (referred as ASC specks, ASC⁺), a process also observed in primary human blood neutrophils (Fig 3A and 3B, and S3A). Further experiments using time lapse fluorescent microscopy on ASC-Citrine neutrophils infected with the pyroptotic strain PP34^{ExoUS142A} or the NETosis-inducing strain PP34 showed that both bacterial strains triggered efficient neutrophil DNA decondensation (Fig 3C and S1 and S2 Movies). However, pyroptotic neutrophils uniquely failed to complete DNA release out from the plasma membrane (stained with WGA) (Fig 3C). These observations were also confirmed using 3D reconstruction of confocal fluorescent images (S3 and S4 Movies). Specifically, analyzing DNA decondensation induced by the pyroptotic strain PP34^{ExoUS142A} or the NETotic strain PP34 in ASC-Citrine neutrophils, we observed that in ASC specks⁺ cells, DNA efficiently decondensed and filled the entire intracellular space, but did not cross the plasma membrane (stained with WGA) (Fig 3C and S3 and S4 Movies). Given that NETosis features histone-bound DNA complexes outside from neutrophils, we reasoned that during pyroptosis, neutrophils might keep histone-bound DNA trapped intracellularly. Consistently, immunoblotting of histones in various neutrophil fractions (soluble, insoluble and supernatant) showed that PP34-induced NETosis efficiently promoted histone release in the extracellular medium (S3B Fig). However, the pyroptotic PP34^{ExoUS142A} strain failed to induce extracellular histone release, although it efficiently promoted the release of intracellular soluble and insoluble components such as GAPDH, the nuclear membrane structural component Lamin B1, the nuclear alarmin HMGB1 or NLRC4 in the extracellular environment (S3B Fig). Importantly, this process required NLRC4 expression (S3B Fig). This suggests that NLRC4-dependent neutrophil pyroptosis specifically promotes DNA decondensation and release from the nuclear membrane while retaining histone-bound DNA intracellularly despite soluble and insoluble factors being released in the extracellular environment (S3C Fig).

Inflammasome-induced neutrophil DNA decondensation is driven by Calcium-activated PAD4 downstream of GSDMD

Next, we wondered about the mechanisms by which inflammasome signaling promotes DNA decondensation and cytosolic redistribution. Two mechanisms that promote DNA decondensation in neutrophils have been reported. First, Neutrophil Serine proteases Neutrophil Elastase (NE), Cathepsin G (CatG) and Proteinase 3 (Pr3) can cleave Histones, which will favor DNA decondensation [15]. Second, upon Calcium release, the enzyme PAD4 promotes Histone Citrullination and subsequent DNA decondensation in neutrophils [4, 6, 7, 47].

We first explored if Caspase-1-induced neutrophil DNA delobulation and release required Neutrophil Serine proteases. We examined the extent of DNA decondensation in WT neutrophils and neutrophils lacking the three proteases NE, CatG and Pr3 (*NE*^{-/-}*CatG*^{-/-}*Pr3*^{-/-}) upon

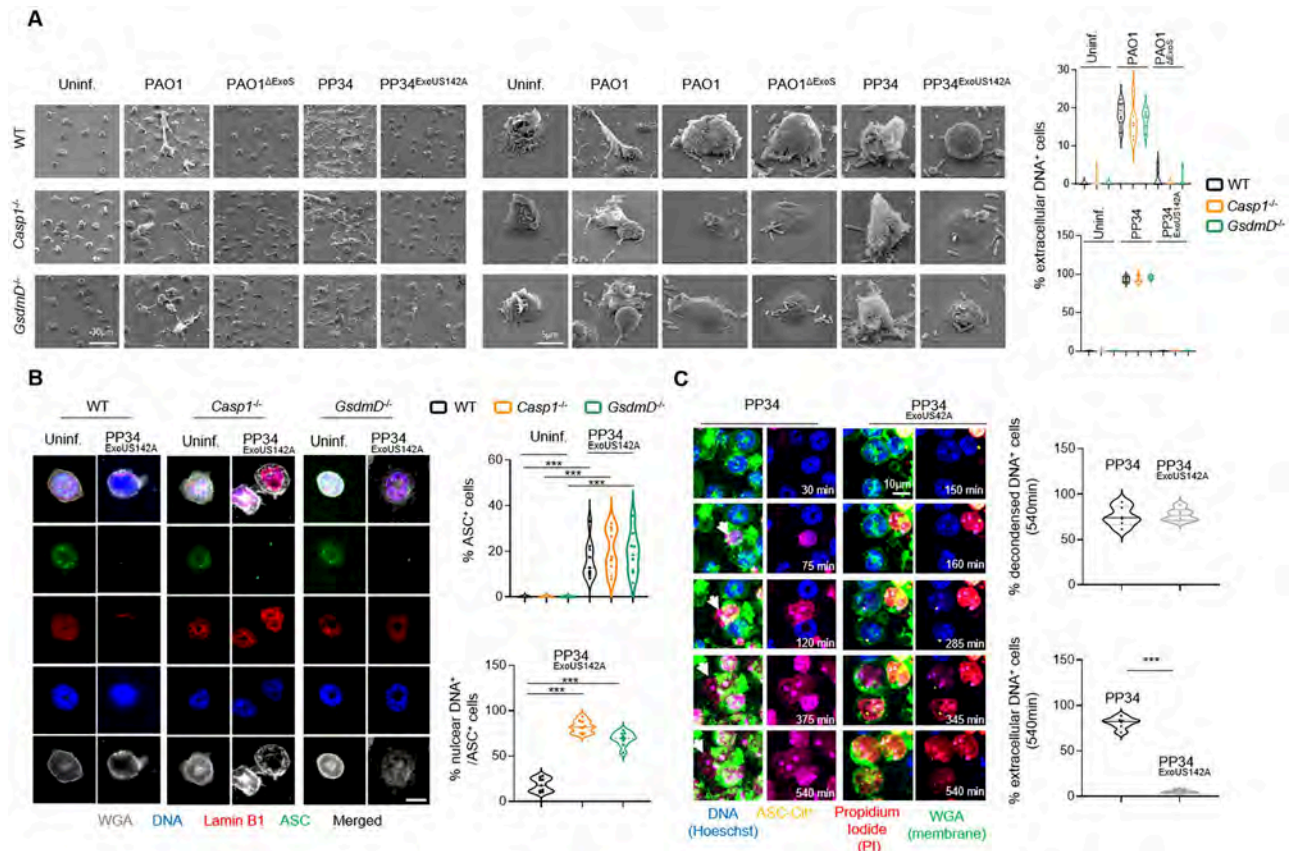


Fig 3. NLR4 inflammasome signaling in neutrophils promotes both pyroptosis and DNA decondensation but not DNA expulsion. **A.** Scanning electron microscopy (SEM) observations and quantifications of pyroptosis in WT, *Casp1*^{-/-} and *GsdmD*^{-/-} BMNs 3 hours after infection with *P. aeruginosa* strains PAO1, PAO1^{ΔExoS}, PP34 and PP34^{ExoUS142A} at an MOI of 10 (PAO1 strains) and 2 (PP34 strains). Images are representative of one experiment performed 3 times. Scale bars are directly indicated in the figure. For quantifications, the percentage of cells exhibiting extracellular DNA was determined by quantifying the ratios of cells positives for extracellular DNA over the total of cells. 6–10 fields from *n* = 3 independent experiments were analyzed. Values are expressed as mean ± SEM. ****p* ≤ 0.001, Two-Way Anova with multiple comparisons. **B.** Confocal microscopy observations and quantifications of WT, *Casp1*^{-/-} and *GsdmD*^{-/-} BMNs infected for 3 hours with the pyroptotic strain PP34^{ExoUS142A} (MOI 2) and harboring ASC complexes, decondensed DNA and nuclear membrane (LaminB1). Nucleus (blue) was stained with Hoechst; LaminB1 is in red (anti LaminB1); ASC is in Green (anti-ASC); plasma membrane is in grey (WGA staining). Scale bar 10μm. Images are representative of one experiment performed three times. For quantifications, the percentage of cells with ASC complexes and nuclear DNA was determined by quantifying the ratios of cells positives for ASC speckles and nuclear DNA. 6–10 fields from *n* = 3 independent experiments were analyzed. Values are expressed as mean ± SEM. ****p* ≤ 0.001, Two-Way Anova with multiple comparisons. **C.** Representative time lapse fluorescence microscopy images and quantifications of ASC-Citrine murine BMNs infected with the NETotic strain PP34 or the pyroptotic strain PP34^{ExoUS142A} (MOI 2) for 9 hours (540 minutes). Nucleus (blue) was stained with Hoechst; ASC is in yellow (ASC-Citrine); plasma membrane is in green (WGA staining); plasma membrane permeabilization is stained in red (cell impermeant DNA dye Propidium Iodide, PI). Images are representative of one movie out of three independent movies. For quantifications, the percentage of cells harboring decondensed DNA and/or extracellular decondensed DNA was determined by quantifying the ratios of cells with decondensed DNA (area surface) or cells with decondensed DNA crossing WGA staining (DNA area surface outside from plasma membrane) over the total amount of cells. At least 6 fields containing each 20–30 cells were quantified. Scale bar 10μm. ****p* ≤ 0.001, T-test with Bonferroni correction.

<https://doi.org/10.1371/journal.ppat.1010305.g003>

infection with the fully pyroptotic strain PP34^{ExoUS142A} (Fig 4A). We observed that WT and *NE*^{-/-}*CatG*^{-/-}*Pr3*^{-/-} neutrophils exhibited similar DNA decondensation levels (Fig 4A), but also that *NE*^{-/-}*CatG*^{-/-}*Pr3*^{-/-} murine neutrophils underwent a similar degree of pyroptosis and released similar amounts of IL-1β compared to their WT counterparts (Fig 4B). This suggested that neutrophil Serine proteases do not play a major role in inflammasome-induced neutrophil DNA delobulation and decondensation.

Next, we analyzed the importance of histone citrullination as a potential effector mechanism of inflammasome-driven DNA decondensation in neutrophils. Microscopy analysis of

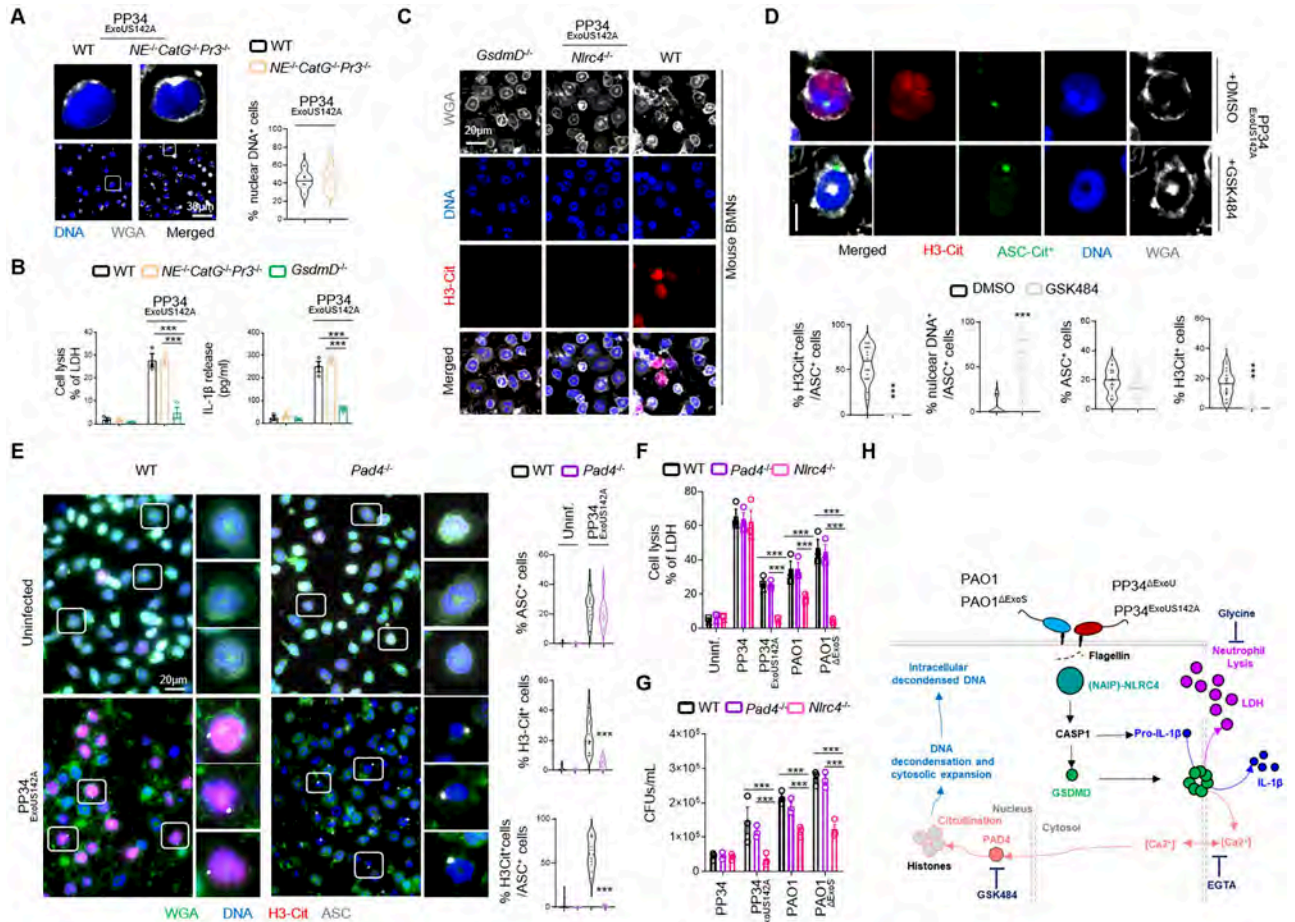


Fig 4. Canonical inflammasome activation-induced DNA decondensation requires PAD4-dependent Histone Citrullination and occurs independently of cell shrinkage. **A.** Confocal microscopy observations and quantifications of WT and *NE⁻¹CatG⁻¹Pr3⁻¹* BMNs infected for 3 hours with *P. aeruginosa* pyroptotic strain PP34^{ExoUS142A} (MOI 2) and harboring decondensed DNA and plasma membrane (WGA). Nucleus (blue) was stained with Hoechst; plasma membrane is in grey (WGA staining). For quantifications, the percentage of cells with nuclear DNA was determined by quantifying the ratios of cells positives for decondensed DNA on nuclear DNA. 6 fields from n = 3 independent experiments were analyzed. Scale bar 30µm. ***p ≤ 0.001, T-test with Bonferroni correction. **B.** Measure of cell lysis (release of LDH) and IL-1β release in WT, *NE⁻¹CatG⁻¹Pr3⁻¹* and *GsdmD⁻¹* murine Bone Marrow Neutrophils (BMNs) infected for 3 hours with *Pseudomonas aeruginosa* pyroptotic strain PP34^{ExoUS142A} (MOI 2). ***p ≤ 0.001, Two-Way Anova with multiple comparisons. Values are expressed as mean ± SEM. Graphs show combined values from three independent experiments. **C.** Confocal microscopy observations of WT, *Nlrc4⁻¹* and *GsdmD⁻¹* BMNs infected for 3 hours with *P. aeruginosa* pyroptotic strain PP34^{ExoUS142A} (MOI 2) and harboring Citrullinated Histone 3 (H3-Cit), decondensed DNA (Hoechst) and plasma membrane (WGA). Nucleus (blue) was stained with Hoechst; Citrullinated Histone-3 is in red (anti H3-Cit); plasma membrane is in grey (WGA staining). Scale bar 20µm. Images are representative of one experiment performed three times with at least 150 neutrophils observed/ experiment. **D.** Confocal microscopy observations and quantifications of cells harboring ASC complexes, H3Citrullination and nuclear/decondensed DNA in WT-ASC-Citrine BMNs infected for 3 hours with PP34^{ExoUS142A} in presence/absence of the PAD4 inhibitor GSK484 (10µM). Nucleus (blue) was stained with Hoechst; Histone-3 Citrullination is in red (Anti-H3Cit staining); plasma membrane is in grey (WGA staining). Scale bar 10µm. For quantifications, the percentage of cells with ASC complexes, nuclear DNA or positives for H3Cit (H3-Cit⁺) was determined by quantifying the ratios of cells positives for ASC speckles, nuclear DNA or H3Cit. At least 10 fields from n = 3 independent experiments were analyzed. Values are expressed as mean ± SEM. ***p ≤ 0.001, T-test with Bonferroni correction. **E.** Confocal microscopy observations and quantifications of WT and *Pad4⁻¹* BMNs infected for 3 hours with *P. aeruginosa* pyroptotic strain PAO1^{ΔExoS} (MOI 10) and harboring ASC complexes, Citrullinated Histone 3 (H3-Cit), decondensed DNA and plasma membrane (WGA). Nucleus (blue) was stained with Hoechst; Histone-3 Citrullination is in red (Anti-H3Cit staining); plasma membrane is in green (WGA staining), ASC is in grey (Anti-ASC). Scale bar 10µm. For quantifications, the percentage of cells with ASC complexes, nuclear DNA or positives for H3Cit (H3-Cit⁺) was determined by quantifying the ratios of cells positives for ASC speckles, nuclear DNA or H3Cit. At least 10 fields from n = 3 independent experiments were analyzed. Values are expressed as mean ± SEM. ***p ≤ 0.001, Two-Way Anova with multiple comparisons. **F.** Measure of cell lysis (release of LDH) and bacterial killing in WT, *Pad4⁻¹* and *Nlrc4⁻¹* murine Bone Marrow Neutrophils (BMNs) infected for 3 hours with *Pseudomonas aeruginosa* strains PP34 (MOI 2), PP34^{ExoUS142A} (MOI 2), PAO1 (MOI 10) or PAO1^{ΔExoS} (MOI 10). ***p ≤ 0.001, Two-Way Anova with multiple comparisons. Values are expressed as mean ± SEM. LDH graph shows combined values from three independent experiments and CFU graph is from one experiment representative of three independent experiments. **G.** Overview of the different steps induced in neutrophils during NLRC4 inflammasome activation by various *Pseudomonas aeruginosa* strains.

<https://doi.org/10.1371/journal.ppat.1010305.g004>

histone citrullination in WT, *Nlr4*^{-/-} and *GsdmD*^{-/-} showed that the fully pyroptotic strain PP34^{ExoUS142A} induced robust histone3-citrullination in an NLRC4- and GSDMD-dependent manner (Fig 4C). Similar experiments performed in human blood neutrophils highlighted that both pyroptotic strains PP34^{ExoUS142A} and PAO1^{ΔExoS} also promoted histone citrullination, a process that was inhibited by the use of the Caspase-1 inhibitor Z-YVAD (S4A Fig). In order to further validate these observations, we performed immunoblotting against citrullinated histones in WT, *Nlr4*^{-/-} and *GsdmD*^{-/-} neutrophils infected with the pyroptotic *P. aeruginosa* strains PAO1, PAO1^{ΔExoS}, PP34^{ΔExoU} or with the NETotic strain PP34. As control, we used Ionomycin, a known inducer of histone citrullination-driven NETosis. We observed that Ionomycin triggered NLRC4-independent histone citrullination in neutrophils (S4B Fig). To the contrary, pyroptotic strains of *P. aeruginosa* PAO1^{ΔExoS}, PP34^{ΔExoU} and to a lower extent PAO1 all triggered NLRC4- and GSDMD-dependent histone citrullination (S4B Fig). We noticed that in *Nlr4*^{-/-} and *GsdmD*^{-/-} neutrophils, citrullination was not fully abrogated, suggesting that minor alternative pathways might also promote histone citrullination upon infection with *P. aeruginosa* pyroptotic strains (S4B Fig).

As PAD4 is an enzyme that promotes histone citrullination and subsequent DNA decondensation in various contexts, we next tested the importance of PAD4 in inflammasome-driving DNA decondensation in neutrophils. Infection of ASC-Citrine BMNs with the pyroptotic strain PP34^{ExoUS142A} revealed that DNA decondensation required PAD4 as pharmacological inhibition (GSK484) of PAD4 abrogated both histone citrullination as well as nuclear DNA release (Fig 4D). In addition, measure of ASC specks (ASC⁺) in ASC-Citrine BMNs highlighted that PAD4 inhibition did not inhibit inflammasome assembly upon PP34^{ExoUS142A} infection (Fig 4D). Similarly, infection of WT or *Pad4*^{-/-} neutrophils with the pyroptotic strain PP34^{ExoUS142A} showed a strong defect in histone citrullination and DNA decondensation in *Pad4*^{-/-} neutrophils (Fig 4E). As observed previously, the induction of ASC specks was not modified in *Pad4*^{-/-} neutrophils, suggesting that PAD4 drives histone citrullination and DNA decondensation but not inflammasome assembly in response to PP34^{ExoUS142A} (Fig 4E). Further infections of WT, *Pad4*^{-/-} and *Nlr4*^{-/-} neutrophils with pyroptotic strains PP34^{ExoUS142A} and PAO1^{ΔExoS} also showed that WT and *Pad4*^{-/-} neutrophils underwent a similar degree of NLRC4-dependent pyroptosis, hence excluding that PAD4 might directly modulate assembly of the NLRC4 inflammasome upon *P. aeruginosa* infection (Fig 4F).

PAD4 activation has been described to require Calcium [47]. As GSDMD pores can also promote Calcium signaling, we wondered about the importance of Calcium at regulating inflammasome-driven PAD4-dependent histone citrullination in neutrophils. We infected WT and *GsdmD*^{-/-} neutrophils with the pyroptotic strains PP34^{ExoUS142A} and PAO1^{ΔExoS} in presence/absence of the extracellular Calcium chelator EGTA and measured neutrophil lysis, IL-1β release as well as histone citrullination and DNA decondensation (S4C and S4D Fig). Microscopy observations showed that infection of neutrophils with the pyroptotic strain PP34^{ExoUS142A} efficiently induced histone citrullination and DNA decondensation in WT neutrophils, but not in *GsdmD*^{-/-} neutrophils (S4C Fig). This was associated with a strong defect in *GsdmD*^{-/-} neutrophils to undergo pyroptosis and to release IL-1β (S4D Fig). Importantly, extracellular Calcium chelation with EGTA strongly impaired both histone citrullination and DNA decondensation upon PP34^{ExoUS142A} infection, suggesting a strong role for extracellular Calcium in driving PAD4 activation upon inflammasome activation in neutrophils (S4C and S4D Fig). Strikingly, neutrophil pyroptosis and IL-1β release were not modified by the use of EGTA upon infection with PP34^{ExoUS142A} or PAO1^{ΔExoS} pyroptotic strains, suggesting that Calcium fluxes are important players of histone citrullination and DNA decondensation downstream of inflammasome activation in neutrophils (S4C and S4D Fig).

As inflammasome signaling in neutrophils triggers Calcium and PAD4-dependent histone citrullination and DNA decondensation, we next aimed to determine if neutrophil shrinkage, the final step of cell lysis, could regulate Calcium- and PAD4-driven DNA decondensation. To this end, we made use of the osmoprotectant Glycine [48], which is able to protect cell integrity and to inhibit LDH release without affecting inflammasome-driven IL-1 β release (S4E and S4F Fig). Infection of WT and *GsdmD*^{-/-} neutrophils with PP34^{ExoUS142A} showed that Glycine did not modify neutrophil histone citrullination and DNA decondensation upon PP34^{ExoUS142A} infection, although it efficiently protected cells from LDH release without affecting IL-1 β release (S4E and S4F Fig). Again, *GsdmD*^{-/-} neutrophils showed strong resistance to DNA decondensation upon PP34^{ExoUS142A} infection (S4E and S4F Fig). This suggests that Calcium/PAD4-induced efficient DNA decondensation occurs in a Gasdermin-D-dependent manner, but is uncoupled from complete neutrophil lysis upon inflammasome activation.

Finally, to determine if *P. aeruginosa*-induced neutrophil pyroptosis and PAD4-dependent DNA decondensation play a microbicidal function, we infected WT, *Pad4*^{-/-} and *Nlrc4*^{-/-} BMNs with various *Pseudomonas* strains and evaluated their cell-autonomous immune capacities. *Nlrc4*^{-/-} BMNs had improved ability to restrict PAO1, PP34^{ExoUS142A} and PAO1 ^{Δ ExoS} infection than WT and *Pad4*^{-/-} neutrophils (Fig 4G), suggesting that neutrophil pyroptosis more than PAD4-driven DNA decondensation promotes neutrophil failure to restrict PAO1, PP34^{ExoUS142A} and PAO1 ^{Δ ExoS}. Altogether, our results describe a novel pathway wherein activation of the neutrophil NLRC4 inflammasome triggers the generation of Calcium/PAD4-dependent intracellular, but not extracellular, DNA structures in a GSDMD-dependent, yet cell shrinkage-independent, manner (Fig 4H).

Neutrophil Caspase-1 contributes *in vivo* to IL-1 β production and to mouse susceptibility to *Pseudomonas aeruginosa* lung infection

Our results showed that various *P. aeruginosa* strains trigger a Caspase-1-dependent neutrophil pyroptosis *in vitro* (Figs 1–4). Based on these findings, we next sought to understand the specific role of neutrophil Caspase-1 in *P. aeruginosa* infected animals. First, to determine if neutrophils undergo Caspase-1-dependent DNA decondensation without induction of extracellular NET formation *in vivo*, we infected MRP8-GFP⁺ (granulocytes, including neutrophils express GFP) mice and monitored for the granulocyte death features using intravital microscopy (Fig 5A). Although necrotic granulocytes exhibited NETotic features (e.g. extracellular DNA) upon exposure to the NETotic strain PP34, infection with the pyroptotic strain PP34^{ExoUS142A} led to the appearance of swelled-round necrotic granulocytes that exhibited intracellular decondensed DNA, similarly to what we observed *in vitro* (Fig 5A and S5 Movie). This suggests that upon lung infection, Caspase-1-induced neutrophil pyroptosis is well occurring and displays morphological and immunological characteristics that are distinct to NETs.

Next, we sought to determine the importance of neutrophil Caspase-1 in response to *Pseudomonas aeruginosa* infection. Thus, we intranasally infected mice lacking CASP1 expression in the granulocytic compartment (MRP8^{Cre+} *Casp1*^{fllox}) and their respective controls (MRP8^{Cre-} *Casp1*^{fllox}) with *ExoS*- or *ExoU*-expressing *P. aeruginosa* (respectively PAO1 and PP34) or with their isogenic mutants PAO1 ^{Δ ExoS} and PP34^{ExoUS142A}, both of which mostly triggered a Caspase-1-dependent neutrophil pyroptosis *in vitro*. We observed that, upon lung infections with PP34, MRP8^{Cre+} *Casp1*^{fllox} mice did not show any differences in bacterial elimination or IL1 β production, thus confirming previous work that *ExoU*-expressing *Pseudomonas aeruginosa* strains promote successful infection independently of the inflammasome pathways (Fig 5B–5D) [49, 50]. To the contrary, MRP8^{Cre+} *Casp1*^{fllox} mice infected with PAO1, showed a

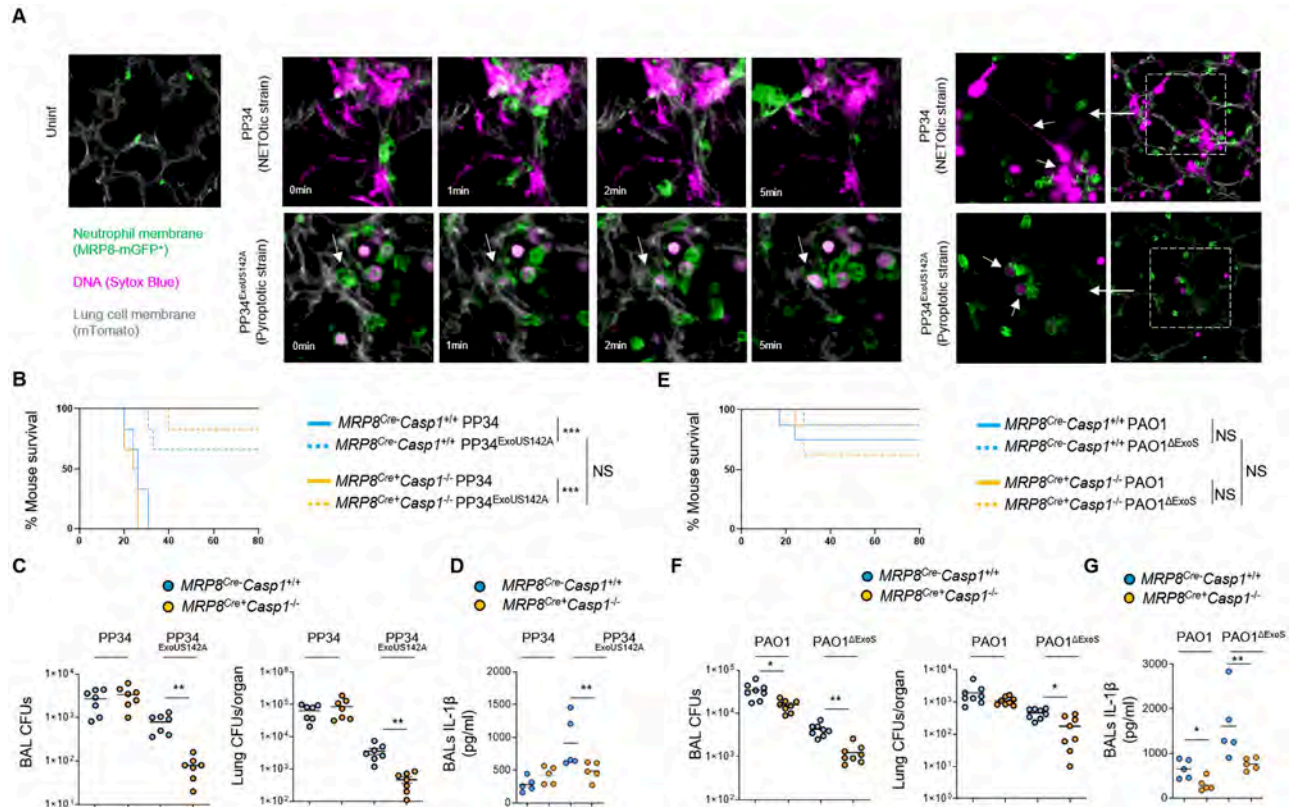


Fig 5. Neutrophil Caspase-1 contributes to IL-1 β production and to *Pseudomonas aeruginosa* spread in mice. **A.** Intravital microscopy visualization of granulocyte death in MRP8-GFP⁺ mice infected with 2.5.10⁵ CFUs of PP34 (NETosis-inducing strain) or PP34^{ExoUS142A} (pyroptotic strain) in presence of SYTOX Blue for 10 hours. Granulocyte death was observed in infected lungs by the appearance of SYTOX blue fluorescence. Pseudo colors represent vessels (gray, mTG); Granulocytes (Green, MRP8-GFP⁺); Dead cells (Purple, SYTOX blue). Scale bar: 20 μ m. Data show one experiment representative of 5 independent mice. **B.** Survival of MRP8^{Cre-} Casp1^{fllox} and MRP8^{Cre+} Casp1^{fllox} mice intranasally infected with 5.10⁵ CFUs of PP34 (NETotic strain) or PP34^{ExoUS142A} (pyroptotic strain) for 24 hours (n = 6 animals per condition). Graphs represent one experiment (6 mice/group) out of three independent *in vivo* experiments. Log-rank Cox-Mantel test was used for survival comparisons. ***p \leq 0.001. NS; Not significant. **C.** Bronchoalveolar (BAL) and lung bacterial loads (colony forming units, CFUs) in MRP8^{Cre-} Casp1^{fllox} and MRP8^{Cre+} Casp1^{fllox} mice intranasally infected with 2.5.10⁵ CFUs of PP34 (NETotic strain) or PP34^{ExoUS142A} (pyroptotic strain) for 24 hours. Graphs represent one experiment (7 mice/group) out of three independent *in vivo* experiments; **p \leq 0.01, Mann-Whitney analysis test. **D.** Determination of IL-1 β levels in Bronchoalveolar Fluids (BALFs) MRP8^{Cre-} Casp1^{fllox} and MRP8^{Cre+} Casp1^{fllox} mice at 10 hours after intranasal infection with 5 10⁵ CFUs (5 mice/group) of PP34 (NETotic strain) or PP34^{ExoUS142A} (pyroptotic strain). Graphs represent one experiment (5 mice/group) out of three independent *in vivo* experiments; **p \leq 0.01, Mann-Whitney analysis test. **E.** Survival of MRP8^{Cre-} Casp1^{fllox} and MRP8^{Cre+} Casp1^{fllox} mice intranasally infected with 1.10⁷ CFUs of PAO1 (NETotic and pyroptotic strain) or PAO1 ^{Δ ExoS} (pyroptotic strain) for 24 hours (n = 6 animals per condition). Graphs represent one experiment (6 mice/group) out of three independent *in vivo* experiments. Log-rank Cox-Mantel test was used for survival comparisons. NS; Not significant. **F.** Bronchoalveolar (BAL) and lung bacterial loads (colony forming units, CFUs) in MRP8^{Cre-} Casp1^{fllox} and MRP8^{Cre+} Casp1^{fllox} mice intranasally infected with 5.10⁶ CFUs of PAO1 (NETotic and pyroptotic strain) or PAO1 ^{Δ ExoS} (pyroptotic strain) for 24 hours. Graphs represent one experiment (7 mice/group) out of three independent *in vivo* experiments; *p \leq 0.05, **p \leq 0.01, Mann-Whitney analysis test. **G.** Determination of IL-1 β levels in Bronchoalveolar Fluids (BALFs) MRP8^{Cre-} Casp1^{fllox} and MRP8^{Cre+} Casp1^{fllox} mice at 8 hours after intranasal infection with 5. 10⁶ CFUs (5 mice/group) of PAO1 (NETotic and pyroptotic strain) or PAO1 ^{Δ ExoS} (pyroptotic strain). Graphs represent one experiment (5 mice/group) out of three independent *in vivo* experiments; **p \leq 0.01, Mann-Whitney analysis test.

<https://doi.org/10.1371/journal.ppat.1010305.g005>

slight but significant improved bacterial elimination in Bronchoalveolar Fluids (BALF) and lungs, a phenotype that was further amplified upon infection with PAO1 ^{Δ ExoS} and PP34^{ExoUS142A} pyroptotic strains (Fig 5B–5G). Furthermore, IL-1 β levels in BALFs were decreased in MRP8^{Cre+} Casp1^{fllox} mice infected with PAO1, PAO1 ^{Δ ExoS} and PP34^{ExoUS142A}. Although we cannot exclude that lower bacterial loads in MRP8^{Cre+} Casp1^{fllox} mice could influence the levels of IL-1 β measured in BALFs, those results suggest that neutrophil Caspase-1 is also a contributor of IL-1 β production upon PAO1, PAO1 ^{Δ ExoS} and PP34^{ExoUS142A} infections

(Fig 5D and 5G). Altogether, our results highlight that neutrophil Caspase-1 contributes to both IL-1 β release and mouse susceptibility to several *P. aeruginosa* strains.

Discussion

Our study initially aimed at determining if neutrophil resistance to undergo Caspase-1-dependent pyroptosis can be overcome upon bacterial infection. Screening various inflammasome-activating bacteria [5, 28, 29], we found that *P. aeruginosa* successfully triggers murine and human neutrophil pyroptosis through the engagement of the fully competent canonical NLRC4 inflammasome, a process that requires T3SS-dependent injection of bacterial Flagellin. Although those results show a clear ability of neutrophils to undergo Caspase-1-dependent pyroptosis upon *P. aeruginosa* infection, our investigations performed with mice specifically lacking Caspase-1 in the granulocyte compartment do suggest a minor contribution of Caspase-1 upon *P. aeruginosa* infection. Related to this, previous studies showed a robust contribution of NLRC4 at promoting *P. aeruginosa* spread in various organs, which suggests that macrophages or other NLRC4-expressing cells are stronger contributors of mouse susceptibility to *P. aeruginosa* [51, 52]. Related to this, NLRC4-driven both IL-1 β and IL-18 release upon *P. aeruginosa* infection has been linked to an altered IL-17 production and a defect of mice to efficiently control *P. aeruginosa* [51, 52]. Here, we speculate that the contribution of neutrophils at releasing IL-1 β might also help the deviated immune response of the host to *P. aeruginosa*, hence leading to a better survival of this bacterium in host tissues. Another guess relies on the preferred extracellular tropism of *P. aeruginosa*. Hence, one could speculate that T3SS-injected Flagellin directly through the neutrophil plasma membrane might trigger an inefficient pyroptosis and favors *P. aeruginosa* escape from microbial trapping and/or killing [53].

Although neutrophils show intrinsic resistance to NLRC4-dependent pyroptosis (e.g. ESCRT machinery, Caspase-1 expression levels, Ragulator pathway) [3, 54–56], the unique ability of *P. aeruginosa* strains and isogenic mutants (PAO1, CHA, PAO1 Δ ExoS, PP34 Δ ExoU) to trigger neutrophil pyroptosis suggests that several neutrophil factors could restrict the ability of other bacteria to promote NLRC4-dependent pyroptosis. Seminal study from Zychlinsky and colleagues found that neutrophil serine proteases could degrade the Type-3 Secretion System and flagellin virulence factors of *Shigella flexneri* [57], hence limiting their ability to hijack the neutrophil autonomous immunity and restraining *Shigella*-induced neutrophil necrosis. The lack of differences of pyroptosis induction between WT and *NE* $^{-/-}$ *CatG* $^{-/-}$ *Pr3* $^{-/-}$ neutrophils upon *P. aeruginosa* suggests that, at least in murine neutrophils, those components do not regulate *P. aeruginosa*-driven NLRC4-dependent neutrophil pyroptosis. Similarly, upon *P. aeruginosa* infection, mouse neutrophils deficient for the NADPH oxidase enzyme Nox2 undergo increased Caspase-1-dependent pyroptosis [44]. Supporting this, Warnatsch et al., could link the extracellular Oxygen Reactive Species (ROS) localization in neutrophils exposed to *Candida albicans* to an exacerbated IL-1 β production and Caspase-1 activation whereas intracellular ROS had an inhibitory effect on IL1 β production and Caspase-1 activity in neutrophils [58]. Whether this could explain the capacity of the extracellularly-adapted *Pseudomonas aeruginosa* to specifically promote Caspase-1-dependent neutrophil pyroptosis but not intracellularly-adapted bacterial pathogens such as *Shigella* or *Salmonella* will require further investigations.

Related to this, studies showing that activation of the neutrophil NLRC4 inflammasome by *S. Typhimurium* or the opportunistic pathogen *B. thailandensis* did not promote canonical pyroptosis also showed that Caspase-11-detected LPS could trigger neutrophil pyroptosis in response to those bacteria. This suggests that, in absence of efficient canonical inflammasome-driven pyroptosis, Caspase-11 might compensate at triggering neutrophil pyroptosis upon

Gram-negative bacterial infections. Here, the lack of Caspase-11-dependent pyroptosis in neutrophils upon *P. aeruginosa* infection suggests that NLR4 inflammasome-induced neutrophil pyroptosis upon *P. aeruginosa* infection is well effective and sufficient.

Striking to us was the observation that expression of the key virulence factors ExoS or ExoU strongly influences neutrophils to go into NETosis whereas strains lacking ExoU or ExoS induced a complete rewiring of neutrophil death toward a Caspase-1-driven way. We hypothesize that the potent cytotoxic effect of these toxins towards various cell types, including neutrophils, may overcome inflammasome detection of *Pseudomonas aeruginosa* and triggers other neutrophil death programs [42, 43, 59–61]. Another non mutually exclusive guess is that these toxins directly interfere with the activation of the inflammasome pathway, thus removal of such toxins leads to an exacerbated inflammasome-response as previously reported for ExoU [40] and ExoS [62].

Although NLR4 activation leads to Caspase-1 dependent neutrophil pyroptosis, in a pathway similar to what was previously reported in macrophage [40, 52], neutrophil pyroptosis exhibits a unique feature characterized by nuclear membrane rupture, DNA decondensation and expansion within cell cytosol. One key enzyme responsible for this morphological characteristic of neutrophil pyroptosis is the Protein arginine deiminase 4 (PAD4), activated by Calcium fluxes. Indeed, similar to the process induced by various NETosis inducers, Caspase-1 also promoted Calcium- and PAD4-dependent Histone Citrullination, which stimulated DNA relaxation and release from the nucleus but, surprisingly, not its extracellular expulsion. Why upon Caspase-11 [3], MLKL [21], NADPH [17] or NE/CatG/Pr3 [15] stimulation but not upon Caspase-1 activation neutrophils generate two different types of DNA structures remains yet to be investigated. Recently, Thiam et al., [18] observed that pharmacological stabilization of F-actin allowed the development of this “incomplete/aborted NETosis” upon Ionomycin-exposure. Interestingly, neutrophil elastase has also been shown to degrade actin [63], hence ensuring complete NETosis process. This, suggests that efficient actin degradation and/or depolymerization may be an essential player of extracellular DNA release, which would imply that the final step of NETosis might actually be a cell-regulated process involving various controllers [14, 20]. Interestingly, Chen and colleagues recently found that upon infection with *Yersinia*, murine neutrophils induce a pyroptotic program that involves virulence-inhibited innate immune sensing, hence promoting RIPK1-induced Caspase 3-dependent Gasdermin E cleavage and activation and pyroptosis [64], a process that does not trigger NETosis. This further suggests that multiple Gasdermins can trigger neutrophil pyroptosis through multiple molecular pathways and promote different morphological outcomes of neutrophils.

Regarding the immunological purpose of Caspase-1-induced neutrophil pyroptosis, we hypothesize that the decondensation of DNA but its conservation into the intracellular space might be a physical mean for neutrophils to trap some intracellular DAMPs, hence avoiding their passive release and a too strong exacerbation of the inflammatory response. Supporting this, we observed that DNA-bound Histones mostly remain trapped intracellularly, but not HMGB1 alarmin, both initially located in the nucleus. In the light of the recent discovery from Kayagaki and colleagues on the role for Ninjurin-1 at promoting active cell shrinkage and HMGB1/nucleosome DAMP release downstream of GSDMD pores in macrophages, the use of Ninjurin-1 deficient mice are full of promises [65]. Another hypothesis is that canonical inflammasome-induced neutrophil pyroptosis keeps DNA intracellularly to generate “Intracellular Traps” according to the “Pyroptosis-induced Intracellular Traps” model in macrophages described by Miao and colleagues [53]. In such a speculative model, intracellular pathogens, in addition to intracellular toxic DAMPs (e.g. Histones, DNA) might remain intracellularly, hence limiting both microbial spread and pathological DAMP-dependent inflammation.

Altogether, our results unveil the ability of neutrophils to undergo Caspase-1-dependent pyroptosis upon *Pseudomonas aeruginosa* infection which is associated with IL-1 β and soluble alarmin release in the extracellular environment, while maintaining decondensed DNA/citrullinated histone complexes intracellularly, hence expanding the spectrum of neutrophil death mechanisms. Finally, we show that this mechanism contributes to host susceptibility to *P. aeruginosa* infection *in vivo*.

Methods

Ethics statement

License to use human samples is under legal agreement with the EFS; contract n° 21PLER2017-0035AV02 after “Haute Garonne ethical committee reviewing”, according to Decret N° 2007–1220 (articles L1243-4, R1243-61).

Mice experiments are under legal authorizations APAFIS#8521–2017041008135771 and APAFIS#12812–2018031218075551 after “IPBS and regional ethical committee evaluation”, according to the local, French and European ethic laws.

All reagents, concentrations of use and their references are listed in [S1 Table](#)

Mice

Nlr4^{-/-} [66], *Nlrp3*^{-/-} [67], *ASC*^{-/-}, *Casp1*^{-/-}, *Casp11*^{-/-} [68, 69], *Casp1*^{-/-}*Casp11*^{-/-} [68, 69], *GsdmD*^{-/-}, *Aim2*^{-/-}, *Pad4*^{-/-}, *MRP8*^{Cre+}*GFP*⁺, *MRP8*^{Cre+}*Casp1*^{fllox} were generated and described in previous studies. Mice were bred at the IPBS (Toulouse, France) and INRAE (Tours Nouzilly, France) animal facilities in agreement to the EU and French directives on animal welfare (Directive 2010/63/EU). Charles Rivers provided WT C57BL/6 mice.

MRP8^{Cre}*Casp1*^{fllox} mice genotyping

Casp1^{fllox/fllox} mice were kindly provided by Mo Lamkanfi and were crossed to *MRP8*^{Cre} mice to generate *MRP8*^{Cre}*Casp1*^{fllox}. *Caspase-1* genotyping was performed using Primer Fw: CGAGGGTTGGAGCTCAAGTTGACC and Primer Rv: CACTTTGACTTCTCTAAGGACAG. *Cre* genotyping was performed using Primers Fw: CGCCGTAATCAATCGATGAGTTGCTTC and Primers Rv: GATGCCGGTGAACGTGCAAAACAGGCTC.

Bacterial cultures

P. aeruginosa strains (PAO1, CHA, PP34) and their isogenic mutants were grown overnight in Luria Broth (LB) medium at 37°C with constant agitation.

Legionella pneumophila (*L. pneumophila*, strain Philadelphia-1) was cultivated at 37°C in Charcoal Yeast Extract Buffered Medium according to ATCC recommendations.

Francisella tularensis spp *novicida* (*F. novicida*, strain U112) was cultivated overnight at 37°C in BHI medium supplemented with 0.2% L-Cysteine.

Staphylococcus aureus (*S. aureus*, strain USA-300) was cultivated in BHI medium, overnight at 37°C.

Shigella flexnerii (*S. flexnerii*, strain M90T) was cultivated overnight at 37°C in Tryptic Soy Broth (TSB) according to ATCC recommendations.

Salmonella Typhimurium (*S. Typhimurium*, strain SL1344), *Burkholderia thailandensis* (*B. thailandensis*, strain E264), *Listeria monocytogenes* (*L. monocytogenes*, strain EGD), *Burkholderia cenocepaciae* (*B. cenocepaciae*, strain LMG 16656), *Escherichia coli* (*E. Coli*, strain K12), *Vibrio cholera* (*V. cholera*, strain El tor) were cultivated overnight at 37°C in LB medium.

Bacteria were sub-cultured the next day by diluting overnight culture 1:25 and grew until reaching an optical density (OD) O.D.600 of 0.6–0.8.

Bacterial strains and their mutants are listed in [S1 Table](#).

Bacterial KO generation and complementation

The knockout vector pEXG2 was constructed and used based on the protocol described by Rietsch et al. [70] with the following modifications. Briefly, 700-bp sequences of the flanking regions of the selected gene were amplified by PCR with Q5 high fidelity polymerase (New England Biolabs). Then, the flanking regions were gel purified and inserted into pEXG2 plasmid by Gibson assembly [71]. The assembled plasmid was directly transformed into competent SM10λpir using Mix&Go competent cells (Zymo Research Corporation) and plated on selective LB plates containing 50 µg/mL kanamycin and 15 µg/mL gentamicin. The resulting clones were sequenced, and mating was allowed for 4 h with PAO1 strain at 37°C. The mated strains were selected for single cross over on plates containing 15 µg/mL gentamicin and 20 µg/mL Irgasan (removal of E.coli SM10 strains). The next day, some clones were grown in LB for 4 hours and streaked on 5% sucrose LB plates overnight at 30°C. *P. aeruginosa* clones were then checked by PCR for mutations. All primers were designed with Snapgene software (GSL Biotech LLC).

Mice infections

Age and sex-matched animals (5–8 weeks old) per group were infected intranasally with 5.10^5 (lethal doses) or $2.5.10^5$ CFUs of PP34/PP34^{ExoUS142A}/PP34^{ΔExoU} or with 1.10^7 CFUs (lethal doses) or 5.10^6 CFUs of PAO1/PAO1^{ΔExoS} strains suspended in 25µL of PBS. Animals were sacrificed at indicated times after infection and bronchoalveolar fluids (BALFs) and lungs were recovered. When specified, bacterial loads (CFU plating), cytokine levels (ELISA) were evaluated. No randomization or blinding were done.

Intravital microscopy experiments

We relied on the previously published lung intravital microscopy method using an intercoastal thoracic window [72, 73], adapted at the IPBS CNRS-University of Toulouse TRI platform.

MRP8-mTmG mice (8–12 weeks old) were infected intratracheally with 5.10^5 CFUs of *P. aeruginosa* PP34 or PP34^{ExoUS142A} strains resuspended in 50µL of PBS and imaged 6 to 8 hours after infection. 50µL of 50µM solution of SYTOX blue (Life Technologies) was injected both intravenously (retroorbital) and intratracheally just before imaging to visualize extracellular DNA.

Next, mice were anesthetized with ketamine and xylazine and secured to a microscope stage. A small tracheal cannula was inserted, sutured and attached to a MiniVent mouse ventilator (Harvard Apparatus). Mice were ventilated with a tidal volume of 10 µl of compressed air (21% O₂) per gram of mouse weight, a respiratory rate of 130–140 breaths per minute, and a positive-end expiratory pressure of 2–3 cm H₂O. Isoflurane was continuously delivered to maintain anesthesia and 300 µl of 0.9% saline solution were i.p. administered in mice every hour for hydration. Mice were placed in the right lateral decubitus position and a small surgical incision was made to expose the rib cage. A second incision was then made into the intercostal space between ribs 4 and 5, through the parietal pleura, to expose the surface of the left lung lobe. A flanged thoracic window with an 8 mm coverslip was inserted between the ribs and secured to the stage using a set of optical posts and a 90° angle post clamp (Thor Labs). Suction was applied to gently immobilize the lung (Dexter Medical). Mice were placed in 30°C heated box during microscopy acquisition to maintain the body temperature and the 2-photon

microscope objective was lowered over the thoracic window. Intravital imaging was performed using a Zeiss 7MP upright multi-photon microscope equipped with a 20×/1.0 objective and a Ti-Sapphire femtosecond laser, Chameleon-Ultra II (Coherent Inc.) tuned to 920 nm. SYTOX Blue, GFP and Tomato emission signals were detected thanks to the respective bandpass filters: Blue (SP485), Green (500–550) and Red (565–610). Images were analyzed using Imaris software (Bitplane) and Zen (Zeiss).

Isolation of primary murine neutrophils

Murine Bone marrow cells were isolated from tibias and femurs, and neutrophils were purified by positive selection using Anti-Ly-6G MicroBead Kit (Miltenyi Biotech) according to manufacturer's instructions. This process routinely yielded >95% of neutrophil population as assessed by flow cytometry of Ly6G⁺/CD11b⁺ cells.

Isolation of primary human neutrophils

Whole blood was collected from healthy donors by the "Ecole française du sang" (EFS, Toulouse Purpan, France) in accordance with relevant guidelines. Written, informed consent was obtained from each donor. Neutrophils were then isolated by negative selection using MACSxpress Whole Blood Human Neutrophil Isolation Kit (Miltenyi Biotech) according to manufacturer's instructions. Following isolations cells were centrifuged 10 min at 300 g and red blood cells were eliminated using Red blood cells (RBC) Lysis Buffer (BioLegend). This procedure gives >95% of neutrophil population as assessed by flow cytometry of CD15⁺/CD16⁺ cells.

Cell plating and treatment of Neutrophils

Following isolation, Neutrophils were centrifugated for 10 min at 300 g and pellet was resuspended in serum free OPTI-MEM medium. Absolute cell number was determined with automated cell counter Olympus R1 with trypan blue cell death exclusion method (typically living cells represent >70% of cell solution) and cell density was adjusted at 10⁶ / mL by adding OPTI-MEM culture medium. Neutrophils were then plated in either 96 well plates, 24 well plates or 6 well plates with 100 μL (10⁵ cells), 500 μL (5.10⁵ cells) or 2 mL (2.10⁶ cells) respectively. When indicated cells were incubated with chemical inhibitors Z-VAD-fmk (20 μM), Y-VAD-fmk (20 μM, 40 μM), Z-DEVD-fmk (40 μM), Z-IETD-fmk (40 μM), Z-LEVD (40 μM), GSK484 (10 μM), as indicated in each experimental setting. Neutrophils were infected with various bacterial strains and multiplicity of infections (M.O.I.) as indicated.

Kinetic analysis of Neutrophil's permeability by SYTOX Green incorporation assay

Cells are plated at density of 1 x 10⁵ per well in Black/Clear 96-well Plates in OPTI-MEM culture medium supplemented with SYTOX-Green dye (100ng/mL) and infected/treated as mentioned in figure legend. Green fluorescence are measured in real-time using Clariostar plate reader equipped with a 37°C cell incubator. Maximal cell death was determined with whole cell lysates from unstimulated cells incubated with 1% Triton X-100.

ELISA and plasma membrane lysis tests

Cell death was measured by quantification of the lactate dehydrogenase (LDH) release into the cell supernatant using LDH Cytotoxicity Detection Kit (Takara). Briefly, 100 μL cell supernatant were incubated with 100 μL LDH substrate and incubated for 15 min. The enzymatic reaction was stopped by adding 50 μL of stop solution. Maximal cell death was determined with

whole cell lysates from unstimulated cells incubated with 1% Triton X-100. Human and mouse IL-1 β secretion was quantified by ELISA kits (Thermo Fisher Scientific) according to the manufacturer's instructions.

Preparation of neutrophil lysates and supernatant for immunoblot

At the end of the treatment 5 mM of diisopropylfluorophosphate (DFP) cell permeable serine protease inhibitor was added to cell culture medium. Cell Supernatant was collected and clarified from non-adherent cells by centrifugation for 10 min at 300 g. Cell pellet and adherent cells were lysed in 100 μ L of RIPA buffer (150 mM NaCl, 50 mM Tris-HCl, 1% Triton X-100, 0.5% Na-deoxycholate) supplemented with 5 mM diisopropylfluorophosphate (DFP) in addition to the protease inhibitor cocktail (Roche). Cell scrapper was used to ensure optimal recovery of cell lysate. Collected cell lysate was homogenized by pipetting up and down ten times and supplemented with laemli buffer (1X final) before boiling sample for 10 min at 95°C. Soluble proteins from cell supernatant fraction were precipitated as described previously [74]. Precipitated pellet was then resuspended in 100 μ L of RIPA buffer plus laemli supplemented with 5 mM diisopropylfluorophosphate (DFP) and protease inhibitor cocktail (Roche) and heat denaturated for 10 min at 95°C. Cell lysate and cell supernatant fraction were then analysed by immunoblot either individually or in pooled sample of lysate plus supernatant (equal vol/vol).

Treatment of Neutrophils for Immunofluorescences

5×10^5 Cells were plated on 1.5 glass coverslips in 24 well plate and infected/treated as described above. At the end of the assay, cell supernatant was removed and cells were fixed with a 4% PFA solution for 10 min at 37°C. PFA was then removed and cells were washed 3 times with HBSS. When desired, plasma membrane was stained with Wheat Germ Agglutinin, Alexa Fluor 633 Conjugate (ThermoFisher Scientific) at 1/100th dilution in HBSS, and incubated for 30 min under 100 rpm orbital shaking conditions. Then cells were washed with HBSS and processed for further staining. Permeabilization was performed by incubating cells for 10 min in PBS containing 0.1% Triton X-100. To block unspecific binding of the antibodies cells are incubated in PBS-T (PBS+ 0.1% Tween 20), containing 2% BSA, 22.52 mg/mL glycine in for 30 min. 3 washes with PBS-T was performed between each steps. Primary antibodies staining was performed overnight at 4°C in BSA 2%—Tween 0.1%—PBS (PBS-T) solution. Coverslips were washed three times with PBS-T and incubated with the appropriate fluor-coupled secondary antibodies for 1 hour at room temperature. DNA was counterstained with Hoechst. Cells were then washed three times with PBS and mounted on glass slides using Vectashield (Vectalabs). Coverslips were imaged using confocal Zeiss LSM 710 (INFINITY, Toulouse) or Olympus Spinning disk (Image core Facility, IPBS, Toulouse) using a 40x or a 63x oil objective. Unless specified, for each experiment, 5–10 fields (~50–250 cells) were manually counted using Image J software.

Scanning electron microscopy experiments

For scanning electron microscopy observations, cells were fixed with 2.5% glutaraldehyde in 0.2M cacodylate buffer (pH 7.4). Preparations were then washed three times for 5min in 0.2M cacodylate buffer (pH 7.4) and washed with distilled water. Samples were dehydrated through a graded series (25 to 100%) of ethanol, transferred in acetone and subjected to critical point drying with CO₂ in a Leica EM CPD300. Dried specimens were sputter-coated with 3 nm platinum with a Leica EM MED020 evaporator and were examined and photographed with a FEI Quanta FEG250.

ImageStreamX

Cells isolated from Bronchoalveolar (BAL) washes were pelleted by centrifugation (10 min at 300 g). Neutrophils were stained prior to fixation with anti-Ly6G (APC-Vio770, Miltenyi-Biotec Clone: REA526 | Dilution: 1:50) in MACS buffer (PBS-BSA 0,5%-EDTA 2mM) in presence of FC block (1/100) and Hoechst (1 μ M). Then, cells were fixed in 4% PFA. Data were acquired on ImageStreamXMKII (Amnis) device (CPTP Imaging and Cytometry core facility) and analyzed using IDEAS software v2.6 (Amnis). The gating strategy used to evaluate inflammasome activation in neutrophils was performed as follow: (i) a gate was set on cells in focus [Cells in Focus] and (ii) a sub-gate was created on single cells [Single Cells]. Then we gated first on (iii) LY6G+ Neutrophils [LY6G+] and second on (iv) ASC-citrine+ and Hoechst+ cells [Hoechst +/ASC-Citrine+] within LY6G+ population. (v) To distinguish cells with active (ASC-speck) versus inactive inflammasome (Diffuse ASC), we plotted the Intensity with the area of ASC-citrine. This strategy allow to distinguish cells with active inflammasome that were visualized and quantified (S2D Fig).

Statistical tests used

Statistical analysis was performed with Prism 8.0a (GraphPad Software, Inc). Otherwise specified, data are reported as mean with SEM. T-test with Bonferroni correction was chosen for comparison of two groups. Two-way Anova with multiple comparisons test was used for comparison of more than two groups. For *in vivo* mice experiments and comparisons we used Mann-Whitney tests and mouse survival analysis were performed using log-rank Cox-Mantel test. P values are shown in figures with the following meaning; NS non-significant and Significance is specified as * $p \leq 0.05$; ** $p \leq 0.01$, *** $p \leq 0.001$.

Supporting information

S1 Table. List and reference of Reagents and Tools available.

(DOCX)

S1 Movie. Time Lapse Fluorescence microscopy of ASC-Citrine murine BMNs infected with PP34 (NETotic strain, MOI 2) for 9 hours (540 minutes). Nucleus (blue) was stained with Hoechst; ASC is in yellow (ASC-Citrine); plasma membrane is in green (WGA staining); plasma membrane permeabilization is stained in red (cell impermeant DNA dye Propidium Iodide, PI).

(AVI)

S2 Movie. Time Lapse Fluorescence microscopy of ASC-Citrine murine BMNs infected with PP34^{S142} (Pyroptotic strain, MOI 2) for 9 hours (540 minutes). Nucleus (blue) was stained with Hoechst; ASC is in yellow (ASC-Citrine); plasma membrane is in green (WGA staining); plasma membrane permeabilization is stained in red (cell impermeant DNA dye Propidium Iodide, PI).

(AVI)

S3 Movie. 3D reconstruction and projection of ASC-Citrine murine BMNs infected with *P. aeruginosa* NETotic strain PP34 (MOI 2) for 3 hours. Nucleus (blue) was stained with Hoechst; ASC is in red (ASC-Citrine); plasma membrane is in green (WGA staining).

(MP4)

S4 Movie. 3D reconstruction and projection of ASC-Citrine murine BMNs infected with *P. aeruginosa* pyroptotic strain PP34^{ExoUS142} (MOI 2) for 3 hours. Nucleus (blue) was stained

with Hoechst; ASC is in red (ASC-Citrine); plasma membrane is in green (WGA staining). (MP4)

S5 Movie. Intravital microscopy visualization of granulocyte death in MRP8-GFP⁺ mice infected with $2.5 \cdot 10^5$ CFUs of PP34 (NETosis-inducing strains) or PP34^{ExoUS142A} (pyroptosis-inducing strain) in presence of SYTOX Blue for 10 hours. Granulocyte death was observed in infected lungs by the appearance of SYTOX blue fluorescence. Pseudo colors represent vessels (gray, mTG); Granulocytes (Green, MRP8-GFP+); Dead cells (Purple, SYTOX blue). Scale bar: 20 μ m. (MP4)

S1 Fig. Multiple *P. aeruginosa* strains trigger Caspase-1-dependent pyroptosis in neutrophils. **A.** Measure of basal cell lysis (release of LDH) in WT and *Casp1*^{-/-} murine Bone Marrow Neutrophils (BMNs) in culture for the indicated times. Values are expressed as mean \pm SEM. Graphs show combined values from three independent experiments. **B.** Measure of cell lysis (release of LDH) and IL-1 β release in WT or *Casp1*^{-/-} murine Bone Marrow Neutrophils (BMNs) infected for 3 hours with *Pseudomonas aeruginosa* PAO1 and its isogenic mutants lacking T3SS expression (PAO1 ^{Δ ExsA}), Flagellin (PAO1 ^{Δ FliC}) or T3SS-derived toxins ExoS, ExoY, ExoT (PAO1 ^{Δ ExoS}, PAO1 ^{Δ ExoY}, PAO1 ^{Δ ExoT}) at a multiplicity of infection (MOI) of 10. *** $p \leq 0.001$, Two-Way Anova with multiple comparisons. Values are expressed as mean \pm SEM. Graphs show combined values from three independent experiments. Values are expressed as mean \pm SEM. **C.** Measure of bacterial uptake (Colony-forming Units, CFUs) in WT or *Casp1*^{-/-} BMNs infected for 45 minutes with *Pseudomonas aeruginosa* PAO1 and its isogenic mutants lacking Flagellin (PAO1 ^{Δ FliC}), Flagellin motors MotABCD (PAO1 ^{Δ MotABCD}) or both Flagellin and Flagellin motors MotABCD (PAO1 ^{Δ FliC/ Δ MotABCD}) at a MOI of 10. Here, due to their lack of motility, bacteria were centrifuged for 5 min/1000 rpm to ensure neutrophil/bacterial contact. *** $p \leq 0.001$, Two-Way Anova with multiple comparisons. Values are expressed as mean \pm SEM. Graph show one experiment representative of three independent experiments. **D.** Measure of cell lysis (release of LDH) and IL-1 β release in WT and *Casp1*^{-/-} murine Bone Marrow Neutrophils (BMNs) infected for the indicated times with PAO1 ^{Δ MotABCD} or PAO1 ^{Δ FliC/ Δ MotABCD} at an MOI of 10. Here, due to their lack of motility, bacteria were centrifuged for 5 min/1000 rpm to ensure neutrophil/bacterial contact. *** $p \leq 0.001$, Two-Way Anova with multiple comparisons. Values are expressed as mean \pm SEM. Graphs show combined values from three independent experiments. **E.** Measure of the percentage of cells with plasma membrane permeabilization over time using SYTOX Green incorporation in murine WT and *Casp1*^{-/-} BMNs infected with *Pseudomonas aeruginosa* mutant invalidated for ExoU catalytic activity PP34^{ExoUS142A} at a multiplicity of infection (MOI) of 2. *** $p \leq 0.001$, Two-Way Anova with multiple comparisons. Values are expressed as mean \pm SEM. Graphs show combined values from three independent experiments. **F.** Measure of the percentage of cells with plasma membrane permeabilization over time using SYTOX Green incorporation in human blood neutrophils BMNs infected with *Pseudomonas aeruginosa* mutant invalidated for ExoU catalytic activity PP34^{ExoUS142A} at a multiplicity of infection (MOI) of 2 in presence/absence of various Caspase inhibitors, Z-YVAD (Casp1 inhibitor, 20 μ M), Z-DEVD (Casp3/7 inhibitor, 20 μ M), Z-IETD (Casp8 inhibitor, 20 μ M). *** $p \leq 0.001$, Two-Way Anova with multiple comparisons. Values are expressed as mean \pm SEM. Graphs show combined values from three independent experiments. (TIF)

S2 Fig. *P. aeruginosa* triggers NLRC4-dependent pyroptosis in neutrophils. **A.** Measure of cell lysis (release of LDH) in WT, *Casp1*^{-/-}, *Casp11*^{-/-}, *Casp11*^{-/-}, *Casp1*^{-/-} *Casp11*^{-/-}, *Nlrp3*^{-/-},

AIM2^{-/-}, *Nlr4^{-/-}* and *ASC^{-/-}* murine Bone Marrow Neutrophils (BMNs) infected for 3 hours with *Pseudomonas aeruginosa* pyroptotic strains PP34^{ExoUS142A} (MOI 2) and PAO1^{ΔExoS} (MOI 10). ****p* ≤ 0.001, Two-Way Anova with multiple comparisons. Values are expressed as mean ± SEM. Graphs show combined values from three independent experiments. **B.** Gating strategy used to evaluate inflammasome activation in neutrophils was performed as follow: (i) a gate was set on cells in focus [Cells in Focus] and (ii) a sub-gate was created on single cells [Single Cells]. Then we gated first on (iii) LY6G⁺ Neutrophils [LY6G⁺] and second on (iv) ASC-citrine⁺ and Hoechst⁺ cells [Hoechst⁺/ASC-Citrine⁺] within LY6G⁺ population. (v) To distinguish cells with active (ASC-speck) versus inactive inflammasome (Diffuse ASC), we plotted the Intensity with the area of ASC-citrine. This strategy allow to distinguish cells with active inflammasome that were visualized and quantified.

(TIF)

S3 Fig. NLRC4-dependent neutrophil pyroptosis associates to DNA decondensation. A.

Confocal microscopy observations and quantification of primary human blood neutrophils infected for 3 hours with *P. aeruginosa* pyroptotic strain PP34^{ExoUS142A} (MOI 2) and harboring ASC complexes, decondensed DNA and plasma membrane. Nucleus (blue) was stained with Hoechst; ASC is in Red (anti-ASC); Plasma membrane is in grey (WGA). Scale bar 10μm.

Images are representative of one experiment performed three times with at least 6–10 fields neutrophils observed/ quantified for ASC specks ratios. ****p* ≤ 0.001, T-test with Bonferroni correction. **B.** Immunoblotting observation of Histone 3, HMGB1, Lamin B1, GAPDH, Actin,

Gasdermin D (GSDMD) and NLRC4 in cellular soluble and insoluble fractions as well as in the supernatant from WT and *Nlr4^{-/-}* murine BMNs infected with *P. aeruginosa* NETotic strain PP34 or pyroptotic strain PP34^{ExoUS142A} (MOI 2) for 3 hours. Immunoblots show one experiment performed two times. **C.** Overview of the different steps induced in neutrophils during NLRC4 inflammasome activation by various *Pseudomonas aeruginosa* strains.

(TIF)

(TIF)

S4 Fig. Inflammasome signalling induce neutrophil DNA decondensation through Calcium-dependent, but cell lysis-independent, manner. A.

Confocal microscopy observations and quantifications of human blood neutrophils infected for 3 hours with PAO1^{ΔExoS} (MOI 10) or PP34^{ExoUS142A} (MOI 2) in presence/absence of Caspase-1 inhibitor Z-YVAD (20μM) and harboring Citrullinated Histone 3 (H3-Cit), decondensed DNA and nuclear membrane (LaminB1). Nucleus (blue) was stained with Hoechst; Citrullinated Histone-3 is in red (anti H3-Cit); plasma membrane is in grey (WGA staining). Scale bar 10μm. Images are representative of one experiment performed three times with at least 150 neutrophils observed/ experiment.

B. Immunoblotting of Citrullinated Histone 3 (H3Cit), total Histone 3 and preformed and cleaved Gasdermin-D (p55/p30) in WT, *Nlr4^{-/-}* and *GsdmD^{-/-}* BMNs treated with Ionomycin (10μM, 3 hours) or infected for 3 hours with PAO1, PAO1^{ΔExoS}, PAO1^{ExsA⁻ (MOI 10) or with PP34, PP34^{ΔExoU} (MOI 2). Immunoblots show combined lysates and supernatants from one experiment performed three times. **C.** Confocal microscopy observations and quantifications of WT and *GsdmD^{-/-}* BMNs infected for 3 hours with *P. aeruginosa* pyroptotic strain PAO1^{ExoUS142A} (MOI 2) in presence/absence of EGTA (10mM) and harboring Citrullinated Histone 3 (H3-Cit) and decondensed DNA. Nucleus (blue) was stained with Hoechst; Histone-3 Citrullination is in red (Anti-H3Cit staining). For quantifications, the percentage of cells positives for H3Cit (H3-Cit⁺) and decondensed DNA was determined by quantifying the ratios of cells positives for H3Cit and decondensed DNA over the total amount of cells. At least 6 fields from n = 3 independent experiments were analyzed. Values are expressed as mean ± SEM. ****p* ≤ 0.001, Two-Way Anova with multiple comparisons. **D.** Measure of cell lysis (release of LDH) and IL-1β release in WT or *GsdmD^{-/-}* BMNs infected for 3 hours with}

PP34^{ExoUS142A} (MOI2) or PAO1^{ΔExoS} (MOI 10) in presence/absence of EGTA (10mM). *** $p \leq 0.001$, Two-Way Anova with multiple comparisons. Values are expressed as mean \pm SEM. Graphs show combined values from three independent experiments. E. Confocal microscopy observations and quantifications of WT and *GsdmD*^{-/-} BMNs infected for 3 hours with *P. aeruginosa* pyroptotic strain PAO1^{ExoUS142A} (MOI 2) in presence/absence of Glycine (5mM) and harboring Citrullinated Histone 3 (H3-Cit) and decondensed DNA. Nucleus (blue) was stained with Hoechst; Histone-3 Citrullination is in red (Anti-H3Cit staining). For quantifications, the percentage of cells positives for H3Cit (H3-Cit⁺) and decondensed DNA was determined by quantifying the ratios of cells positives for H3Cit and decondensed DNA over the total amount of cells. At least 6 fields from $n = 3$ independent experiments were analyzed. Values are expressed as mean \pm SEM. *** $p \leq 0.001$, Two-Way Anova with multiple comparisons. F. Measure of cell lysis (release of LDH) and IL-1 β release in WT or *GsdmD*^{-/-} BMNs infected for 3 hours with PP34^{ExoUS142A} (MOI2) or PAO1^{ΔExoS} (MOI 10) in presence/absence of Glycine (5mM). *** $p \leq 0.001$, Two-Way Anova with multiple comparisons. Values are expressed as mean \pm SEM. Graphs show combined values from three independent experiments. (TIF)

Acknowledgments

Nlrc4^{-/-} mice were provided by Clare E. Bryant [66] and generated by Millenium Pharmaceutical, *GsdmD*^{-/-} mice [75] came from P. Broz (Univ of Lausanne, Switzerland), *Casp11*^{-/-} and *Casp1*^{-/-}/*Casp11*^{-/-} came from B. Py (ENS Lyon, France) and Junying Yuan (Harvard Med School, Boston, USA) [68, 69]. Virginie Petrilli (ENS Lyon, France) provided *Nlrp3*^{-/-} mice that were generated by Fabio Martinon [67]. Thomas Henry (CIRI, Lyon, France) provided *ASC*^{-/-} and *AIM2*^{-/-} mice upon agreement with Genentech (Roche, San Francisco, USA) and *ASC-Citrine* (#030744) and *Pad4*^{-/-} (#030315) mice came from Jaxson Laboratory (USA) and were generated by Douglas T Golenbock (University of Massachusetts Medical School, USA) and Kerri Mowen (The Scripps Research Institute, USA) respectively. *MRP8*^{Cre}/*Casp1*^{flox} mice are provided by Natalie Winter (INRAE Tours Nouzilly, France) and were generated by crossing *MRP8*^{Cre} (Jackson # 021614) mice with *Caspase1*^{flox} mice generated by Mohamed Lamkanfi (Univ. of Ghent, Belgium)[76]. *MRP8*^{CreGFP} and *mTmG* mice were obtained from Jackson laboratories and generated respectively by Emmanuelle Passegue (UCSF, USA) and Liqun Luo, (Stanford University, USA). *Pseudomonas aeruginosa* strains were a kind gift of Ina Attrée (CNRS, Grenoble, France). Authors also acknowledge the animal facility and Cytometry/microscopy platforms of the INFINITY, CBI and IPBS institutes and particularly Valerie Duplan-Eche for Imagestream acquisition and analysis.

Author Contributions

Conceptualization: David Pericat, Emma Lefrançois, Etienne Meunier, Rémi Planès.

Data curation: David Pericat, Renaud Poincloux, Etienne Meunier, Rémi Planès.

Formal analysis: David Pericat, Jean-Philippe Girard, Céline Cougoule, Renaud Poincloux, Etienne Meunier, Rémi Planès.

Funding acquisition: Christine T. N. Pham, Céline Cougoule, Emma Lefrançois, Etienne Meunier, Rémi Planès.

Investigation: Karin Santoni, David Pericat, Leana Gorse, Julien Buyck, Miriam Pinilla, Laure Prouvensier, Salimata Bagayoko, Audrey Hessel, Stephen Adonai Leon-Icaza, Elisabeth

Bellard, Serge Mazères, Emilie Doz-Deblauwe, Nathalie Winter, Jean-Philippe Girard, Renaud Poincloux, Emma Lefrançais, Etienne Meunier, Rémi Planès.

Methodology: Karin Santoni, David Pericat, Leana Gorse, Julien Buyck, Miriam Pinilla, Laure Prouvensier, Salimata Bagayoko, Audrey Hessel, Stephen Adonai Leon-Icaza, Elisabeth Bellard, Serge Mazères, Emilie Doz-Deblauwe, Christophe Paget, Jean-Philippe Girard, Renaud Poincloux, Emma Lefrançais, Etienne Meunier, Rémi Planès.

Project administration: Céline Cougoule, Mohamed Lamkanfi, Emma Lefrançais, Etienne Meunier, Rémi Planès.

Resources: Nathalie Winter, Christine T. N. Pham, Renaud Poincloux, Mohamed Lamkanfi, Emma Lefrançais, Etienne Meunier, Rémi Planès.

Supervision: Nathalie Winter, Christophe Paget, Renaud Poincloux, Emma Lefrançais, Etienne Meunier, Rémi Planès.

Validation: Karin Santoni, David Pericat, Leana Gorse, Julien Buyck, Christophe Paget, Renaud Poincloux, Mohamed Lamkanfi, Emma Lefrançais, Etienne Meunier, Rémi Planès.

Visualization: Leana Gorse, Julien Buyck, Renaud Poincloux, Emma Lefrançais, Rémi Planès.

Writing – original draft: Karin Santoni, Mohamed Lamkanfi, Emma Lefrançais, Etienne Meunier, Rémi Planès.

Writing – review & editing: Karin Santoni, Nathalie Winter, Christophe Paget, Christine T. N. Pham, Céline Cougoule, Renaud Poincloux, Mohamed Lamkanfi, Emma Lefrançais, Etienne Meunier, Rémi Planès.

References

1. Galluzzi L, Vitale I, Aaronson SA, Abrams JM, Adam D, Agostinis P, et al. Molecular mechanisms of cell death: Recommendations of the Nomenclature Committee on Cell Death 2018. *Cell Death and Differentiation*. Nature Publishing Group; 2018. pp. 486–541. <https://doi.org/10.1038/s41418-017-0012-4> PMID: [29362479](https://pubmed.ncbi.nlm.nih.gov/29362479/)
2. Brinkmann V, Reichard U, Goosmann C, Fauler B, Uhlemann Y, Weiss DS, et al. Neutrophil Extracellular Traps Kill Bacteria. *Science* (80-). 2004; 303: 1532–1535. <https://doi.org/10.1126/science.1092385> PMID: [15001782](https://pubmed.ncbi.nlm.nih.gov/15001782/)
3. Chen KW, Monteleone M, Boucher D, Sollberger G, Ramnath D, Condon ND, et al. Noncanonical inflammasome signaling elicits gasdermin D-dependent neutrophil extracellular traps. *Sci Immunol*. 2018; 3: 6676. <https://doi.org/10.1126/sciimmunol.aar6676> PMID: [30143554](https://pubmed.ncbi.nlm.nih.gov/30143554/)
4. Li P, Li M, Lindberg MR, Kennett MJ, Xiong N, Wang Y. PAD4 is essential for antibacterial innate immunity mediated by neutrophil extracellular traps. *J Exp Med*. 2010; 207: 1853–1862. <https://doi.org/10.1084/jem.20100239> PMID: [20733033](https://pubmed.ncbi.nlm.nih.gov/20733033/)
5. Kovacs SB, Oh C, Maltez VI, McGlaughon BD, Verma A, Miao EA, et al. Neutrophil Caspase-11 Is Essential to Defend against a Cytosol-Invasive Bacterium. *Cell Rep*. 2020; 32. <https://doi.org/10.1016/j.celrep.2020.107967> PMID: [32726630](https://pubmed.ncbi.nlm.nih.gov/32726630/)
6. Martinod K, Fuchs TA, Zitomersky NL, Wong SL, Demers M, Gallant M, et al. PAD4-deficiency does not affect bacteremia in polymicrobial sepsis and ameliorates endotoxemic shock. *Blood*. 2015; 125: 1948–1956. <https://doi.org/10.1182/blood-2014-07-587709> PMID: [25624317](https://pubmed.ncbi.nlm.nih.gov/25624317/)
7. Biron BM, Chung C-S, Chen Y, Wilson Z, Fallon EA, Reichner JS, et al. PAD4 Deficiency Leads to Decreased Organ Dysfunction and Improved Survival in a Dual Insult Model of Hemorrhagic Shock and Sepsis. *J Immunol*. 2018; 200: ji1700639. <https://doi.org/10.4049/jimmunol.1700639> PMID: [29374076](https://pubmed.ncbi.nlm.nih.gov/29374076/)
8. Kahlenberg JM, Carmona-Rivera C, Smith CK, Kaplan MJ. Neutrophil Extracellular Trap-Associated Protein Activation of the NLRP3 Inflammasome Is Enhanced in Lupus Macrophages. *J Immunol*. 2013; 190: 1217–1226. <https://doi.org/10.4049/jimmunol.1202388> PMID: [23267025](https://pubmed.ncbi.nlm.nih.gov/23267025/)
9. Fuchs TA, Brill A, Duerschmied D, Schatzberg D, Monestier M, Myers DD, et al. Extracellular DNA traps promote thrombosis. *Proc Natl Acad Sci U S A*. 2010; 107: 15880–15885. <https://doi.org/10.1073/pnas.1005743107> PMID: [20798043](https://pubmed.ncbi.nlm.nih.gov/20798043/)

10. Apel F, Andreeva L, Knackstedt LS, Streeck R, Frese CK, Goosmann C, et al. The cytosolic DNA sensor cGAS recognizes neutrophil extracellular traps. *Sci Signal*. 2021; 14. <https://doi.org/10.1126/scisignal.aax7942> PMID: 33688080
11. Kumar SVR, Kulkarni OP, Mulay SR, Darisipudi MN, Romoli S, Thomasova D, et al. Neutrophil extracellular trap-related extracellular histones cause vascular necrosis in severe GN. *J Am Soc Nephrol*. 2015; 26: 2399–2413. <https://doi.org/10.1681/ASN.2014070673> PMID: 25644111
12. Lefrançois E, Mallavia B, Zhuo H, Calfee CS, Looney MR. Maladaptive role of neutrophil extracellular traps in pathogen-induced lung injury. *JCI insight*. 2018;3. <https://doi.org/10.1172/jci.insight.98178> PMID: 29415887
13. Knackstedt SL, Georgiadou A, Apel F, Abu-Abed U, Moxon CA, Cunnington AJ, et al. Neutrophil extracellular traps drive inflammatory pathogenesis in malaria. *Sci Immunol*. 2019; 4: 336. <https://doi.org/10.1126/sciimmunol.aaw0336> PMID: 31628160
14. Thiam HR, Wong SL, Wagner DD, Waterman CM. Cellular Mechanisms of NETosis. *Annual Review of Cell and Developmental Biology*. Annual Reviews Inc.; 2020. pp. 191–218. <https://doi.org/10.1146/annurev-cellbio-020520-111016> PMID: 32663035
15. Papayannopoulos V, Metzler KD, Hakkim A, Zychlinsky A. Neutrophil elastase and myeloperoxidase regulate the formation of neutrophil extracellular traps. *J Cell Biol*. 2010; 191: 677–691. <https://doi.org/10.1083/jcb.201006052> PMID: 20974816
16. Sollberger G, Choidas A, Burn GL, Habenberger P, Di Lucrezia R, Kordes S, et al. Gasdermin D plays a vital role in the generation of neutrophil extracellular traps. *Sci Immunol*. 2018; 3. <https://doi.org/10.1126/sciimmunol.aar6689> PMID: 30143555
17. Kenny EF, Herzig A, Krüger R, Muth A, Mondal S, Thompson PR, et al. Diverse stimuli engage different neutrophil extracellular trap pathways. *Elife*. 2017; 6. <https://doi.org/10.7554/eLife.24437> PMID: 28574339
18. Thiama HR, Wong SL, Qiu R, Kittisopikul M, Vahabikashi A, Goldman AE, et al. NETosis proceeds by cytoskeleton and endomembrane disassembly and PAD4-mediated chromatin decondensation and nuclear envelope rupture. *Proc Natl Acad Sci U S A*. 2020; 117: 7326–7337. <https://doi.org/10.1073/pnas.1909546117> PMID: 32170015
19. Wang Y, Li M, Stadler S, Correll S, Li P, Wang D, et al. Histone hypercitullination mediates chromatin decondensation and neutrophil extracellular trap formation. *J Cell Biol*. 2009; 184: 205–213. <https://doi.org/10.1083/jcb.200806072> PMID: 19153223
20. Neubert E, Meyer D, Rocca F, Günay G, Kwaczala-Tessmann A, Grandke J, et al. Chromatin swelling drives neutrophil extracellular trap release. *Nat Commun*. 2018; 9: 1–13. <https://doi.org/10.1038/s41467-018-06263-5> PMID: 30218080
21. D’Cruz AA, Speir M, Bliss-Moreau M, Dietrich S, Wang S, Chen AA, et al. The pseudokinase MLKL activates PAD4-dependent NET formation in necroptotic neutrophils. *Sci Signal*. 2018; 11: 1716. <https://doi.org/10.1126/scisignal.aao1716> PMID: 30181240
22. Chen W, Zhao J, Mu D, Wang Z, Liu Q, Zhang Y, et al. Pyroptosis Mediates Neutrophil Extracellular Trap Formation during Bacterial Infection in Zebrafish. *J Immunol*. 2021; j12001335. <https://doi.org/10.4049/jimmunol.2001335> PMID: 33712519
23. Xia S, Zhang Z, Magupalli VG, Pablo JL, Dong Y, Vora SM, et al. Gasdermin D pore structure reveals preferential release of mature interleukin-1. *Nature*. 2021; 1–5. <https://doi.org/10.1038/s41586-021-03478-3> PMID: 33883744
24. Tsuchiya K, Hosojima S, Hara H, Kushiyama H, Mahib MR, Kinoshita T, et al. Gasdermin D mediates the maturation and release of IL-1 α downstream of inflammasomes. *Cell Rep*. 2021; 34: 108887. <https://doi.org/10.1016/j.celrep.2021.108887> PMID: 33761363
25. Evavold CL, Ruan J, Tan Y, Xia S, Wu H, Kagan JC. The Pore-Forming Protein Gasdermin D Regulates Interleukin-1 Secretion from Living Macrophages. *Immunity*. 2018; 48: 35–44.e6. <https://doi.org/10.1016/j.immuni.2017.11.013> PMID: 29195811
26. Heilig R, Dick MS, Sborgi L, Meunier E, Hiller S, Broz P. The Gasdermin-D pore acts as a conduit for IL-1 β secretion in mice. *Eur J Immunol*. 2018; 48: 584–592. <https://doi.org/10.1002/eji.201747404> PMID: 29274245
27. Amara N, Cooper MP, Voronkova MA, Webb BA, Lynch EM, Kollman JM, et al. Selective activation of PFKL suppresses the phagocytic oxidative burst. *Cell*. 2021; 184: 4480–4494.e15. <https://doi.org/10.1016/j.cell.2021.07.004> PMID: 34320407
28. Karmakar M, Minns M, Greenberg EN, Diaz-Aponte J, Pestonjamas K, Johnson JL, et al. N-GSDMD trafficking to neutrophil organelles facilitates IL-1 β release independently of plasma membrane pores and pyroptosis. *Nat Commun*. 2020; 11. <https://doi.org/10.1038/s41467-020-16043-9> PMID: 32371889

29. Chen KW, Groß CJ, Sotomayor FV, Stacey KJ, Tschopp J, Sweet MJ, et al. The Neutrophil NLR4 Inflammasome Selectively Promotes IL-1 β Maturation without Pyroptosis during Acute Salmonella Challenge. *Cell Rep*. 2014; 8: 570–582. <https://doi.org/10.1016/j.celrep.2014.06.028> PMID: [25043180](https://pubmed.ncbi.nlm.nih.gov/25043180/)
30. Münzer P, Negro R, Fukui S, di Meglio L, Aymonnier K, Chu L, et al. NLRP3 Inflammasome Assembly in Neutrophils Is Supported by PAD4 and Promotes NETosis Under Sterile Conditions. *Front Immunol*. 2021; 12: 1977. <https://doi.org/10.3389/fimmu.2021.683803> PMID: [34122445](https://pubmed.ncbi.nlm.nih.gov/34122445/)
31. Aymonnier K, Ng J, Fredenburgh LE, Zambrano-Vera K, Münzer P, Gutch S, et al. Inflammasome activation in neutrophils of patients with severe COVID-19. *Blood Adv*. 2022 [cited 26 Jan 2022]. <https://doi.org/10.1182/bloodadvances.2021005949> PMID: [34991159](https://pubmed.ncbi.nlm.nih.gov/34991159/)
32. Lin CK, Kazmierczak BI. Inflammation: A Double-Edged Sword in the Response to *Pseudomonas aeruginosa* Infection. *J Innate Immun*. 2017; 9: 250–261. <https://doi.org/10.1159/000455857> PMID: [28222444](https://pubmed.ncbi.nlm.nih.gov/28222444/)
33. Hauser AR. The Type III Secretion System of *Pseudomonas aeruginosa*: Infection by Injection. *Nat Rev Microbiol*. 2009; 7: 654. <https://doi.org/10.1038/nrmicro2199> PMID: [19680249](https://pubmed.ncbi.nlm.nih.gov/19680249/)
34. Zhao Y, Shi J, Shi X, Wang Y, Wang F, Shao F. Genetic functions of the NAIP family of inflammasome receptors for bacterial ligands in mice. *J Exp Med*. 2016; 213: 647–656. <https://doi.org/10.1084/jem.20160006> PMID: [27114610](https://pubmed.ncbi.nlm.nih.gov/27114610/)
35. Zhao Y, Yang J, Shi J, Gong YN, Lu Q, Xu H, et al. The NLR4 inflammasome receptors for bacterial flagellin and type III secretion apparatus. *Nature*. 2011; 477: 596–602. <https://doi.org/10.1038/nature10510> PMID: [21918512](https://pubmed.ncbi.nlm.nih.gov/21918512/)
36. Rauch I, Tenthorey JL, Nichols RD, Al Moussawi K, Kang JJ, Kang C, et al. NAIP proteins are required for cytosolic detection of specific bacterial ligands in vivo. *J Exp Med*. 2016; 213: 657–665. <https://doi.org/10.1084/jem.20151809> PMID: [27045008](https://pubmed.ncbi.nlm.nih.gov/27045008/)
37. Miao EA, Ernst RK, Dors M, Mao DP, Aderem A. *Pseudomonas aeruginosa* activates caspase 1 through Ipaf. *Proc Natl Acad Sci U S A*. 2008; 105: 2562–2567. <https://doi.org/10.1073/pnas.0712183105> PMID: [18256184](https://pubmed.ncbi.nlm.nih.gov/18256184/)
38. Franchi L, Stoolman J, Kanneganti TD, Verma A, Ramphal R, Núñez G. Critical role for Ipaf in *Pseudomonas aeruginosa*-induced caspase-1 activation. *Eur J Immunol*. 2007; 37: 3030–3039. <https://doi.org/10.1002/eji.200737532> PMID: [17935074](https://pubmed.ncbi.nlm.nih.gov/17935074/)
39. Hardy KS, Tessmer MH, Frank DW, Audia JP. Perspectives on the *Pseudomonas aeruginosa* Type III Secretion System Effector ExoU and Its Subversion of the Host Innate Immune Response to Infection. *Toxins (Basel)*. 2021; 13: 880. <https://doi.org/10.3390/toxins13120880> PMID: [34941717](https://pubmed.ncbi.nlm.nih.gov/34941717/)
40. Sutterwala FS, Mijares LA, Li L, Ogura Y, Kazmierczak BI, Flavell RA. Immune recognition of *Pseudomonas aeruginosa* mediated by the IPAF/NLR4 inflammasome. *J Exp Med*. 2007; 204: 3235–3245. <https://doi.org/10.1084/jem.20071239> PMID: [18070936](https://pubmed.ncbi.nlm.nih.gov/18070936/)
41. Rada B, Jendrysik MA, Pang L, Hayes CP, Yoo DG, Park JJ, et al. Pyocyanin-Enhanced Neutrophil Extracellular Trap Formation Requires the NADPH Oxidase. *PLoS One*. 2013; 8: e54205. <https://doi.org/10.1371/journal.pone.0054205> PMID: [23342104](https://pubmed.ncbi.nlm.nih.gov/23342104/)
42. Thanabalasuriar A, Scott BNV, Peiseler M, Willson ME, Zeng Z, Warrener P, et al. Neutrophil Extracellular Traps Confine *Pseudomonas aeruginosa* Ocular Biofilms and Restrict Brain Invasion. *Cell Host Microbe*. 2019; 25: 526–536.e4. <https://doi.org/10.1016/j.chom.2019.02.007> PMID: [30930127](https://pubmed.ncbi.nlm.nih.gov/30930127/)
43. Skopelja-Gardner S, Theprungsirikul J, Lewis KA, Hammond JH, Carlson KM, Hazlett HF, et al. Regulation of *Pseudomonas aeruginosa*-Mediated Neutrophil Extracellular Traps. *Front Immunol*. 2019; 10. <https://doi.org/10.3389/fimmu.2019.01670> PMID: [31379861](https://pubmed.ncbi.nlm.nih.gov/31379861/)
44. Ryu JC, Kim MJ, Kwon Y, Oh JH, Yoon SS, Shin SJ, et al. Neutrophil pyroptosis mediates pathology of *P. aeruginosa* lung infection in the absence of the NADPH oxidase NOX2. *Mucosal Immunol*. 2017; 10: 757–774. <https://doi.org/10.1038/mi.2016.73> PMID: [27554297](https://pubmed.ncbi.nlm.nih.gov/27554297/)
45. Balakrishnan A, Karki R, Berwin B, Yamamoto M, Kanneganti TD. Guanylate binding proteins facilitate caspase-11-dependent pyroptosis in response to type 3 secretion system-negative *Pseudomonas aeruginosa*. *Cell Death Discov*. 2018; 4: 1–12. <https://doi.org/10.1038/s41420-018-0068-z> PMID: [30062052](https://pubmed.ncbi.nlm.nih.gov/30062052/)
46. Patankar YR, Lovewell RR, Poynter ME, Jyot J, Kazmierczak BI, Berwin B. Flagellar Motility Is a Key Determinant of the Magnitude of the Inflammasome Response to *Pseudomonas aeruginosa*. *Infect Immun*. 2013; 81: 2043. <https://doi.org/10.1128/IAI.00054-13> PMID: [23529619](https://pubmed.ncbi.nlm.nih.gov/23529619/)
47. Arita K, Hashimoto H, Shimizu T, Nakashima K, Yamada M, Sato M. Structural basis for Ca²⁺-induced activation of human PAD4. *Nat Struct Mol Biol*. 2004; 11: 777–783. <https://doi.org/10.1038/nsmb799> PMID: [15247907](https://pubmed.ncbi.nlm.nih.gov/15247907/)

48. Loomis WP, den Hartigh AB, Cookson BT, Fink SL. Diverse small molecules prevent macrophage lysis during pyroptosis. *Cell Death Dis* 2019 104. 2019; 10: 1–10. <https://doi.org/10.1038/s41419-019-1559-4> PMID: [30975978](https://pubmed.ncbi.nlm.nih.gov/30975978/)
49. Al Moussawi K, Kazmierczak BI. Distinct Contributions of Interleukin-1 α (IL-1 α) and IL-1 β to Innate Immune Recognition of *Pseudomonas aeruginosa* in the Lung. *Infect Immun*. 2014; 82: 4204. <https://doi.org/10.1128/IAI.02218-14> PMID: [25069982](https://pubmed.ncbi.nlm.nih.gov/25069982/)
50. Bagayoko S, Leon-Icaza SA, Pinilla M, Hessel A, Santoni K, Péricat D, et al. Host phospholipid peroxidation fuels ExoU-dependent cell necrosis and supports *Pseudomonas aeruginosa*-driven pathology. *PLoS Pathog*. 2021;17. <https://doi.org/10.1371/journal.ppat.1009927> PMID: [34516571](https://pubmed.ncbi.nlm.nih.gov/34516571/)
51. Faure E, Mear J-B, Faure K, Normand S, Couturier-Maillard A, Grandjean T, et al. *Pseudomonas aeruginosa* Type-3 Secretion System Dampens Host Defense by Exploiting the NLRC4-coupled Inflammasome. *Am J Respir Crit Care Med*. 2014; 189: 799–811. <https://doi.org/10.1164/rccm.201307-1358OC> PMID: [24555512](https://pubmed.ncbi.nlm.nih.gov/24555512/)
52. Cohen TS, Prince AS. Activation of inflammasome signaling mediates pathology of acute *P. aeruginosa* pneumonia. *J Clin Invest*. 2013; 123: 1630–1637. <https://doi.org/10.1172/JCI66142> PMID: [23478406](https://pubmed.ncbi.nlm.nih.gov/23478406/)
53. Jorgensen I, Zhang Y, Krantz BA, Miao EA. Pyroptosis triggers pore-induced intracellular traps (PITs) that capture bacteria and lead to their clearance by efferocytosis. *J Exp Med*. 2016; 213: 2113–2128. <https://doi.org/10.1084/jem.20151613> PMID: [27573815](https://pubmed.ncbi.nlm.nih.gov/27573815/)
54. Evavold CL, Hafner-Bratkovič I, Kagan JC. Downstream of gasdermin D cleavage, a Ragulator-RagmTORC1 pathway promotes pore formation and pyroptosis. *bioRxiv*. bioRxiv; 2020. p. 2020.11.02.362517. <https://doi.org/10.1101/2020.11.02.362517>
55. Rühl S, Shkarina K, Demarco B, Heilig R, Santos JC, Broz P. ESCRT-dependent membrane repair negatively regulates pyroptosis downstream of GSDMD activation. *Science (80-)*. 2018; 362: 956–960. <https://doi.org/10.1126/science.aar7607> PMID: [30467171](https://pubmed.ncbi.nlm.nih.gov/30467171/)
56. Bjanec E, Sillas RG, Matsuda R, Demarco B, Fettelet T, Delaney AA, et al. The Card19 locus of murine chromosome 13 regulates terminal cell lysis downstream of caspase activation and Gasdermin-D cleavage Card19 locus regulates caspase-dependent cell lysis. *bioRxiv*. 2021; 2021.03.19.436207.
57. Weinrauch Y, Drujan D, Shapiro SD, Weiss J, Zychlinsky A. Neutrophil elastase targets virulence factors of enterobacteria. *Nature*. 2002; 417: 91–94. <https://doi.org/10.1038/417091a> PMID: [12018205](https://pubmed.ncbi.nlm.nih.gov/12018205/)
58. Warnatsch A, Tsourouktsoglou TD, Branzk N, Wang Q, Reincke S, Herbst S, et al. Reactive Oxygen Species Localization Programs Inflammation to Clear Microbes of Different Size. *Immunity*. 2017; 46: 421–432. <https://doi.org/10.1016/j.immuni.2017.02.013> PMID: [28314592](https://pubmed.ncbi.nlm.nih.gov/28314592/)
59. Kaminski A, Gupta KH, Goldufsky JW, Lee HW, Gupta V, Shafikhani SH. *Pseudomonas aeruginosa* ExoS Induces Intrinsic Apoptosis in Target Host Cells in a Manner That is Dependent on its GAP Domain Activity. *Sci Reports* 2018 81. 2018; 8: 1–15. <https://doi.org/10.1038/s41598-018-32491-2> PMID: [30232373](https://pubmed.ncbi.nlm.nih.gov/30232373/)
60. Vareechon C, Zmina SE, Karmakar M, Pearlman E, Rietsch A. *Pseudomonas aeruginosa* Effector ExoS Inhibits ROS Production in Human Neutrophils. *Cell Host Microbe*. 2017; 21: 611–618.e5. <https://doi.org/10.1016/j.chom.2017.04.001> PMID: [28494242](https://pubmed.ncbi.nlm.nih.gov/28494242/)
61. Bagayoko S, Leon Icaza S, Pinilla M, Hessel A, Bordignon P-J, Moreau F, et al. Phospholipid peroxidation fuels ExoU phospholipase-dependent cell necrosis 1 and supports *Pseudomonas aeruginosa*-driven pathology 2. *bioRxiv*. 2021; 2021.02.17.431580.
62. Galle M, Schotte P, Haegman M, Wullaert A, Yang HJ, Jin S, et al. The *Pseudomonas aeruginosa* Type III secretion system plays a dual role in the regulation of caspase-1 mediated IL-1 β maturation. *J Cell Mol Med*. 2008; 12: 1767–1776. <https://doi.org/10.1111/j.1582-4934.2007.00190.x> PMID: [18081695](https://pubmed.ncbi.nlm.nih.gov/18081695/)
63. Metzler KD, Goosmann C, Lubojemska A, Zychlinsky A, Papayannopoulos V. Myeloperoxidase-containing complex regulates neutrophil elastase release and actin dynamics during NETosis. *Cell Rep*. 2014; 8: 883–896. <https://doi.org/10.1016/j.celrep.2014.06.044> PMID: [25066128](https://pubmed.ncbi.nlm.nih.gov/25066128/)
64. Chen KW, Demarco B, Heilig R, Ramos SP, Grayczyk JP, Assenmacher C-A, et al. RIPK1 activates distinct gasdermins in macrophages and neutrophils upon pathogen blockade of innate immune signaling. *bioRxiv*. 2021; 2021.01.20.427379. <https://doi.org/10.1101/2021.01.20.427379>
65. Kayagaki N, Kornfeld OS, Lee BL, Stowe IB, O'Rourke K, Li Q, et al. NINJ1 mediates plasma membrane rupture during lytic cell death. *Nature*. 2021; 591: 131–136. <https://doi.org/10.1038/s41586-021-03218-7> PMID: [33472215](https://pubmed.ncbi.nlm.nih.gov/33472215/)
66. Man SM, Hopkins LJ, Nugent E, Cox S, Glück IM, Tourlomis P, et al. Inflammasome activation causes dual recruitment of NLRC4 and NLRP3 to the same macromolecular complex. *Proc Natl Acad Sci U S A*. 2014; 111: 7403–7408. <https://doi.org/10.1073/pnas.1402911111> PMID: [24803432](https://pubmed.ncbi.nlm.nih.gov/24803432/)

67. Martinon F, Pétrilli V, Mayor A, Tardivel A, Tschopp J. Gout-associated uric acid crystals activate the NALP3 inflammasome. *Nature*. 2006; 440: 237–241. <https://doi.org/10.1038/nature04516> PMID: [16407889](https://pubmed.ncbi.nlm.nih.gov/16407889/)
68. Li P, Allen H, Banerjee S, Franklin S, Herzog L, Johnston C, et al. Mice deficient in IL-1 β -converting enzyme are defective in production of mature IL-1 β and resistant to endotoxic shock. *Cell*. 1995; 80: 401–411. [https://doi.org/10.1016/0092-8674\(95\)90490-5](https://doi.org/10.1016/0092-8674(95)90490-5) PMID: [7859282](https://pubmed.ncbi.nlm.nih.gov/7859282/)
69. Wang S, Miura M, Jung YK, Zhu H, Li E, Yuan J. Murine caspase-11, an ICE-interacting protease, is essential for the activation of ICE. *Cell*. 1998; 92: 501–509. [https://doi.org/10.1016/s0092-8674\(00\)80943-5](https://doi.org/10.1016/s0092-8674(00)80943-5) PMID: [9491891](https://pubmed.ncbi.nlm.nih.gov/9491891/)
70. Rietsch A, Vallet-Gely I, Dove SL, Mekalanos JJ. ExsE, a secreted regulator of type III secretion genes in *Pseudomonas aeruginosa*. *Proc Natl Acad Sci U S A*. 2005; 102: 8006–8011. <https://doi.org/10.1073/pnas.0503005102> PMID: [15911752](https://pubmed.ncbi.nlm.nih.gov/15911752/)
71. Gibson DG, Young L, Chuang RY, Venter JC, Hutchison CA, Smith HO. Enzymatic assembly of DNA molecules up to several hundred kilobases. *Nat Methods* 2009 65. 2009; 6: 343–345. <https://doi.org/10.1038/nmeth.1318> PMID: [19363495](https://pubmed.ncbi.nlm.nih.gov/19363495/)
72. Headley MB, Bins A, Nip A, Roberts EW, Looney MR, Gerard A, et al. Visualization of immediate immune responses to pioneer metastatic cells in the lung. *Nature*. 2016; 531: 513–517. <https://doi.org/10.1038/nature16985> PMID: [26982733](https://pubmed.ncbi.nlm.nih.gov/26982733/)
73. Looney MR, Thornton EE, Sen D, Lamm WJ, Glenn RW, Krummel MF. Stabilized imaging of immune surveillance in the mouse lung. *Nat Methods*. 2011; 8: 91–96. <https://doi.org/10.1038/nmeth.1543> PMID: [21151136](https://pubmed.ncbi.nlm.nih.gov/21151136/)
74. Eren E, Planès R, Bagayoko S, Bordignon P, Chaoui K, Hessel A, et al. Irgm2 and Gate-16 cooperatively dampen Gram-negative bacteria-induced caspase-11 response. *EMBO Rep*. 2020; 21: e50829. <https://doi.org/10.15252/embr.202050829> PMID: [33124769](https://pubmed.ncbi.nlm.nih.gov/33124769/)
75. Demarco B, Grayczyk JP, Bjanec E, Le Roy D, Tonnus W, Assenmacher CA, et al. Caspase-8-dependent gasdermin D cleavage promotes antimicrobial defense but confers susceptibility to TNF-induced lethality. *Sci Adv*. 2020; 6: 3465–3483. <https://doi.org/10.1126/sciadv.abc3465> PMID: [33208362](https://pubmed.ncbi.nlm.nih.gov/33208362/)
76. Van Gorp H, Saavedra PHV, De Vasconcelos NM, Van Opdenbosch N, Vande Walle L, Matusiak M, et al. Familial Mediterranean fever mutations lift the obligatory requirement for microtubules in Pyrin inflammasome activation. *Proc Natl Acad Sci U S A*. 2016; 113: 14384–14389. <https://doi.org/10.1073/pnas.1613156113> PMID: [27911804](https://pubmed.ncbi.nlm.nih.gov/27911804/)

2. Host phospholipid peroxidation fuels ExoU-dependent cell necrosis and supports *Pseudomonas aeruginosa*-driven pathology

Contribution: In this paper I participated in the design, execution and analysis of some flow cytometry experiments.

RESEARCH ARTICLE

Host phospholipid peroxidation fuels ExoU-dependent cell necrosis and supports *Pseudomonas aeruginosa*-driven pathology

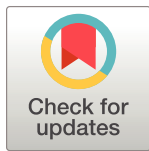
Salimata Bagayoko¹, Stephen Adonai Leon-Icaza¹, Miriam Pinilla¹, Audrey Hessel¹, Karin Santoni¹, David Péricat¹, Pierre-Jean Bordignon¹, Flavie Moreau^{1,2}, Elif Eren¹, Aurélien Boyancé¹, Emmanuelle Naser^{1,3}, Lise Lefèvre⁴, Céline Berrone^{1,2}, Nino Iakobachvili⁵, Arnaud Metais¹, Yoann Rombouts¹, Geanncarlo Lugo-Villarino¹, Agnès Coste⁴, Ina Attrée⁶, Dara W. Frank⁷, Hans Clevers⁸, Peter J. Peters⁵, Céline Cougoule¹, Rémi Planès^{1*}, Etienne Meunier^{1**}

1 Institute of Pharmacology and Structural Biology (IPBS), University of Toulouse, CNRS, Toulouse, France, **2** Level 3 Biosafety Animal Core facility, Anexplo platform, Institute of Pharmacology and Structural Biology (IPBS), University of Toulouse, CNRS, Toulouse, France, **3** Cytometry & Imaging Core facility, Institute of Pharmacology and Structural Biology (IPBS), University of Toulouse, CNRS, Toulouse, France, **4** RESTORE institute, University of Toulouse, CNRS, Toulouse, France, **5** Division of Nanoscopy, Maastricht Multimodal Molecular Imaging Institute, Maastricht University, Maastricht, The Netherlands, **6** Univ. Grenoble Alpes, CNRS, CEA, IBS, Bacterial Pathogenesis and Cellular Responses, Grenoble, France, **7** Department of Microbiology and Immunology, Medical College of Wisconsin, Milwaukee, Wisconsin, United States of America, **8** Oncode Institute, Hubrecht Institute, Royal Netherlands Academy of Arts and Sciences and University Medical Center, Utrecht, Netherlands

☞ These authors contributed equally to this work.

* Current Address: Institute of Pharmacology and Structural Biology (IPBS), CNRS, Toulouse; France

** remi.planes@ipbs.fr (RP); etienne.meunier@ipbs.fr (EM)



OPEN ACCESS

Citation: Bagayoko S, Leon-Icaza SA, Pinilla M, Hessel A, Santoni K, Péricat D, et al. (2021) Host phospholipid peroxidation fuels ExoU-dependent cell necrosis and supports *Pseudomonas aeruginosa*-driven pathology. *PLoS Pathog* 17(9): e1009927. <https://doi.org/10.1371/journal.ppat.1009927>

Editor: Gregory P. Priebe, Children's Hospital Boston, UNITED STATES

Received: February 19, 2021

Accepted: August 29, 2021

Published: September 13, 2021

Peer Review History: PLOS recognizes the benefits of transparency in the peer review process; therefore, we enable the publication of all of the content of peer review and author responses alongside final, published articles. The editorial history of this article is available here: <https://doi.org/10.1371/journal.ppat.1009927>

Copyright: © 2021 Bagayoko et al. This is an open access article distributed under the terms of the [Creative Commons Attribution License](https://creativecommons.org/licenses/by/4.0/), which permits unrestricted use, distribution, and reproduction in any medium, provided the original author and source are credited.

Data Availability Statement: All relevant data are within the manuscript and its [Supporting Information](#) files [S1](#) and [S2](#) Datas.

Abstract

Regulated cell necrosis supports immune and anti-infectious strategies of the body; however, dysregulation of these processes drives pathological organ damage. *Pseudomonas aeruginosa* expresses a phospholipase, ExoU that triggers pathological host cell necrosis through a poorly characterized pathway. Here, we investigated the molecular and cellular mechanisms of ExoU-mediated necrosis. We show that cellular peroxidised phospholipids enhance ExoU phospholipase activity, which drives necrosis of immune and non-immune cells. Conversely, both the endogenous lipid peroxidation regulator GPX4 and the pharmacological inhibition of lipid peroxidation delay ExoU-dependent cell necrosis and improve bacterial elimination *in vitro* and *in vivo*. Our findings also pertain to the ExoU-related phospholipase from the bacterial pathogen *Burkholderia thailandensis*, suggesting that exploitation of peroxidised phospholipids might be a conserved virulence mechanism among various microbial phospholipases. Overall, our results identify an original lipid peroxidation-based virulence mechanism as a strong contributor of microbial phospholipase-driven pathology.

Funding: This project was funded by grants from the National Research Agency (ANR, Endiabac), FRM “Amorçage Jeunes Equipes” (AJE20151034460), ERC StG (INFLAME 804249) and ATIP-Avenir program to EM, from National Research Agency (ANR, MacGlycoTB) to YR, from the European Society of Clinical Microbiology and Infectious Diseases (ESCMID, 2020) to RP, from the Van Gogh Programme to IPBS-M4i institutes, from Invivogen-CIFRE collaborative PhD fellowship to MP and from the FRM (FDT202106012794), Mali and Campus France cooperative agencies to SB. The funders had no role in study design, data collection and analysis, decision to publish, or preparation of the manuscript.

Competing interests: The authors have declared that no competing interests exist.

Author summary

Although a proper activation of various regulated cell necrosis confer a significant advantage against various infectious agents, their dysregulation drives host tissue damages that can end up with fatal sepsis. Specifically, 30% of the bacterial strains of *Pseudomonas aeruginosa* (*P. aeruginosa*) express the phospholipase A2-like toxin ExoU that is injected into host target cells through the Type-3 Secretion System. This toxin induces, through a yet unknown mechanism, a strong and fast necrotic cell death that supports fatal respiratory infections. Therefore, in this study, we sought to determine the cellular mechanisms by which ExoU triggers host cell necrosis. In this context, we found that ExoU exploits basal cellular phospholipid peroxidation to promote cell necrosis. Mechanistically, host cell lipid peroxidation stimulates ExoU phospholipase activity, which then triggers a pathological cell necrosis both *in vitro* and *in vivo*. Altogether, our results unveil that targeting host cell lipid peroxidation constitutes a virulence mechanism developed by microbial phospholipases, a process that contributes to *P. aeruginosa*-mediated pathology.

Introduction

Regulated cell necrosis (RCNs) drives physiological and immune processes, yet dysregulation of this process promotes pathological responses such as organ-failure and sepsis [1–4]. Mechanistically, oxygen-dependent cell death is an evolutionary conserved process that involves the production of reactive oxygen species (ROS), transition metals (e.g. iron) and peroxidised lipid accumulation [5–8]. In addition to cell necrosis, lipid peroxidation broadly involves cellular processes essential to mediate optimal efferocytosis of dead cells, cellular communication resulting from the formation of lipids derived from peroxidised phospholipids (e.g. isoprostanes, platelet activating factor) or the production of bioactive lipids (eicosanoids) from arachidonic acid [9,10]. In addition, the peroxidation of the mitochondrial phospholipid cardiolipin initiates apoptosis while the accumulation of peroxidised phosphatidyl ethanolamines (PE) promote the cellular necrosis, ferroptosis [11–17]. Specifically, the dysregulation of lipid peroxidation processes is associated with various human pathologies such as cancer chemoresistance, brain and ischemia injuries, neurological alterations, metabolic diseases as well as tuberculosis susceptibility [18–23]. In this context, the enzymes glutathione peroxidase 4 (GPX4) and ferroptosis-suppressor protein-1 (FSP1) that belongs to the CoQ antioxidant system, detoxify phospholipid hydroperoxide accumulation, hence allowing lipid peroxide amounts to be balanced in cells [5,11,12,14,24]. On the contrary, iron excess, lipoxygenase activity or cytochrome P450 oxidoreductase (CYPOR) all promote phospholipid peroxidation, which can end with ferroptosis induction in the absence of proper regulation [5,14–16,25,26].

In this regard, the bacterial pathogen *Pseudomonas aeruginosa* (*P. aeruginosa*) expresses ExoU, an A2 phospholipase from the patatin family, that triggers a necrosis-dependent pathology through a poorly understood pathway [27–36]. In presence of cellular co-factors such as ubiquitin [31] or the trafficking chaperone DNAJC5 [37], ExoU activity rapidly cleaves at the sn-2 position of host membrane phospholipids, liberating large amounts of arachidonic acid that are then metabolized into eicosanoids by cellular enzymes cyclooxygenases, cytochrome P450 or lipoxygenases [32,38–40]. Importantly, *in vivo*, ExoU expression by *P. aeruginosa* is associated with a robust production of oxidized lipids such the platelet activating factor (PAF) or isoprostanes [38,41]. In this context, we explored the possibility that *P. aeruginosa* ExoU mediates a necrosis-dependent host pathology involving lipid peroxidation.

Results

P. aeruginosa infection triggers ExoU-dependent alarmin and peroxidised lipid production in mice

P. aeruginosa ExoU is injected into cells by the Type-3 Secretion System (T3SS) [28,36], which triggers a fast and violent cellular necrosis. Therefore, we first monitored the profile of ExoU-dependent pathology in mice infected with the clinical isolate PP34 *exoU*⁺ or its isogenic mutant (*exoU*⁻). Similar to previous studies [27,29,42,43], intranasal instillation with either *exoU*⁺ or *exoU*⁻ strains highlighted a *P. aeruginosa*-induced acute pathology mainly due to ExoU, as mice infected with *exoU*⁻ bacteria showed improved survival to infection (Fig 1A). This observation was paralleled with lower bacterial loads of *P. aeruginosa* *exoU*⁻ than *exoU*⁺ in the bronchoalveolar lavage fluids (BALFs), the lungs, the blood and the spleen, suggesting that ExoU also promotes bacterial dissemination (Fig 1B). As *P. aeruginosa* triggers NLR4-, NLRP3- and Caspase-11-dependent inflammasome response [42,44,45–52,53], we infected inflammasome-deficient mice (*Casp1/Casp11*^{-/-}, *Nlrc4*^{-/-} and *GasderminD*^{-/-}) and observed that those mice were not protected against *P. aeruginosa* *exoU*⁺, hence suggesting that ExoU-promoted mouse pathology occurs independently from the inflammasome machineries (S1A and S1B Fig). A hallmark of host cell necrosis is the release of intracellular mediators such as alarmins that contribute to the initiation and the development of an inflammatory reaction, which occurs upon *P. aeruginosa* infection [42,54]. Therefore, we primarily focused our analysis on alarmin release. We observed a strong ExoU-dependent alarmin production in BALFs 6

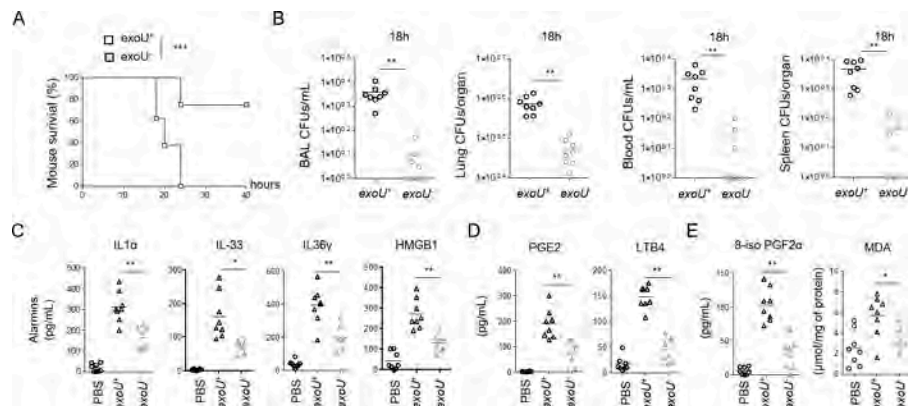


Fig 1. ExoU-dependent lung pathology in mice associates to an alarmin and peroxidized lipid signature. (A) Survival of WT mice intranasally infected ($n = 7$ animals per condition) with 5.10^5 CFUs of *P. aeruginosa* PP34 or its isogenic mutant PP34^{*exoU*⁻}. Graphs represent one experiment (8 mice/group) out of three independent *in vivo* experiments. Log-rank Cox-Mantel test was used for survival comparisons. *** $p \leq 0.001$. (B) Bronchoalveolar (BAL), lung, blood and spleen bacterial loads from WT mice ($n = 8$) 18 hours after intranasal infection with 5.10^5 CFUs of *P. aeruginosa* PP34 or its isogenic mutant PP34^{*exoU*⁻}. Graphs represent one experiment (8 mice/group) out of three independent *in vivo* experiments. ** $p \leq 0.01$, Mann-Whitney analysis test. (C) Alarmin levels in bronchoalveolar fluids (BALFs) from WT mice ($n = 8$) 6 hours after intranasal infection with 5.10^5 CFUs of *P. aeruginosa* PP34 or its isogenic mutant PP34^{*exoU*⁻}. Graphs represent one experiment (8 mice/group) out of three independent *in vivo* experiments; * $p \leq 0.05$; ** $p \leq 0.01$, Mann-Whitney analysis test. (D) Prostaglandin E2 (PGE2) and Leukotriene B4 (LTB4) levels in bronchoalveolar fluids (BALFs) from WT mice ($n = 8$) 6 hours after intranasal infection with 5.10^5 CFUs of *P. aeruginosa* PP34 or its isogenic mutant PP34^{*exoU*⁻}. Graphs represent one experiment (8 mice/group) out of three independent *in vivo* experiments; ** $p \leq 0.01$, Mann-Whitney analysis test. (E) Peroxidized lipid product (isoprostanes and MDA) levels in bronchoalveolar fluids (BALFs) from WT mice ($n = 8$) 6 hours after intranasal infection with 5.10^5 CFUs of *P. aeruginosa* PP34 or its isogenic mutant PP34^{*exoU*⁻}. Graphs represent one experiment (8 mice/group) out of three independent *in vivo* experiments; * $p \leq 0.05$; ** $p \leq 0.01$, Mann-Whitney analysis test. Data information: Data shown as means (Graphs B-E) and are representative of one experiment performed three times; * $p \leq 0.05$; ** $p \leq 0.01$, *** $p \leq 0.001$, Mann-Whitney analysis test (B-E) and log-rank Cox-Mantel test for survival comparisons (A).

<https://doi.org/10.1371/journal.ppat.1009927.g001>

h after infection, such as IL-1 family alarmins IL1 α , IL-33 or IL-36 γ [55] (Fig 1C). In addition, we also detected that *exoU*-expressing *P. aeruginosa* triggered a strong production of phospholipid- and arachidonic acid (aa)-derived mediators such as prostaglandin E2 and leukotriene B4, which correlates with the robust phospholipase activity of ExoU (Fig 1D) [38–40]. Importantly, BALFs of mice infected with *exoU*-expressing *P. aeruginosa* also exhibited a marked presence of oxidized lipid (by)-products such as isoprostanes (8-iso PGF2 α) or Malondialdehyde (MDA), which suggests that *exoU*-expressing *P. aeruginosa* also drives an exacerbated lipid oxidation response in mice (Fig 1E) [41,56].

Lipid peroxidation contributes to ExoU-induced cell necrosis and *P. aeruginosa* escape from phagocyte-mediated killing

The observation that *exoU*-expressing *P. aeruginosa* infection associates to a lipid peroxidation signature *in vivo*, encouraged us to determine the importance of lipid peroxidation on ExoU-induced cellular necrosis. As *P. aeruginosa* strains that do not express ExoU can promote an NLR4 inflammasome response in macrophages [50], we used mouse Bone-Marrow-Derived Macrophages (BMDMs) that lack *Nlr4* expression to specifically address the importance of lipid peroxidation on ExoU-dependent cell necrosis. We infected *Nlr4*^{-/-} primary murine BMDMs with *P. aeruginosa* strains expressing or not expressing ExoU. The pharmacological inhibition of various regulated necrosis pathways (e.g. pyroptosis, necroptosis, apoptosis, parthanatos) showed that only ferrostatin-1, a potent and well characterized inhibitor of phospholipid peroxidation [57], repressed ExoU-dependent cell necrosis (Figs 2A and 2B and S2A and S1–S6 Movies). Ferrostatin-1 action was specific to lipid peroxidation-dependent cell necrosis as it also inhibited Cumene hydroperoxide-induced ferroptosis (CuOOH, 400 μ M) but not Flagellin-/LPS-induced pyroptosis or TCPA-1/Z-VAD/TNF α -dependent necroptosis (Fig 2B). In addition, ExoU-induced IL-1 α and HMGB1 alarmin release in macrophages was reduced in presence of ferrostatin-1 whereas TNF α levels remained similar (Fig 2C), suggesting that lipid peroxidation contributes to alarmin release in response to ExoU. We noticed that ExoU-triggered ferrostatin-1-sensitive necrosis was not restricted to murine BMDMs as primary human macrophages, the human U937 monocytic cell line, human and murine neutrophils and eosinophils, the human bronchial epithelial (HBEs), A549 or HeLa epithelial cells were all sensitive to lipid peroxidation inhibition upon infection with *exoU*-expressing *P. aeruginosa* (S2A and S2B Fig). ExoU exhibits a calcium-independent phospholipase A2-like activity [33]. Hence, we transfected recombinant ExoU protein (rExoU) or its enzymatically inactive mutant ExoU^{S142A} [58] in WT BMDMs and monitored for cell necrosis. Only macrophages transfected with active ExoU underwent to cell death, a process that was inhibited by the use of ferrostatin-1 or the phospholipase inhibitor MAFP (S2C Fig). In line, we found that ferrostatin-1 itself did not alter bacterial growth or ExoU secretion (S2D and S2E Fig), suggesting that ferrostatin-1 does not directly alter bacterial physiology nor expression/secretion of ExoU. Upon phospholipase activation arachidonic acid release can be metabolized and oxidized by various cellular enzymes, including cyclooxygenases 1 and 2 (COX1, COX2), lipoxygenases (ALOX5 and ALOX12/15 in mice) or cytochrome p450 (CYPs) enzymes. Therefore, we transfected recombinant ExoU in WT, *Alox5*^{-/-} or *Alox12/15*^{-/-} BMDMs in presence or absence of various COX, CYP or different lipid peroxidation inhibitors (a-tocopherol, liprostatin-1, Resveratrol, ferrostatin-1). Although we observed that all lipid peroxidation inhibitors have a strong inhibitory impact on cell death, cyclooxygenase, cytochrome P450 or lipoxygenase targeting did not interfere with ExoU-dependent cell necrosis, hence suggesting that those enzymes do not regulate lipid-peroxidation-dependent cell necrosis upon ExoU exposure (Fig 2D). Importantly, we also observed that ferrostatin-1 delayed ExoU-induced cell necrosis,

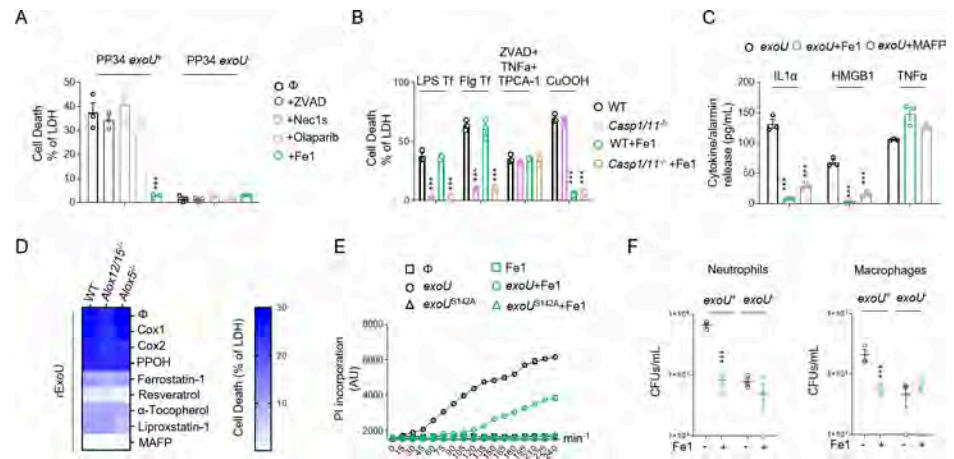


Fig 2. Lipid peroxidation inhibition delays ExoU-induced cell necrosis. Otherwise specified, cells were infected with an MOI of 0.5 of *P. aeruginosa* PP34, PP34^{exoU} or PP34^{exoUS142A} for various times. ****p* ≤ 0.001, t-test with Bonferroni correction. (A) Measure of LDH release in *Nlr4*^{-/-} BMDMs infected with PP34 or PP34^{exoU} in presence of Z-VAD (40μM), olaparab (10μM), Necrostatin-1s (Ne1s, 40μM) or Ferrostatin-1 (Fe1, 10μM) for 2 hours. ****p* ≤ 0.001, t-test with Bonferroni correction. (B) Measure of LDH release in WT or *Casp1*^{-/-}/*Casp11*^{-/-} BMDMs transfected (Lipofectamin 2000) with 1μg of LPS or Flagellin (Flg) to induce pyroptosis, treated with Z-VAD (40μM)/TNFα (500UI/mL)/TPCA-1 (5 μM) to induce necroptosis or with Cumene hydroperoxide (CuOOH, 400μM) to induce ferroptosis in presence or absence of Ferrostatin-1 (Fe1, 10μM) for 6 hours. ****p* ≤ 0.001, t-test with Bonferroni correction. (C) Measure of alarmin/cytokine release in *Nlr4*^{-/-} BMDMs infected with PP34 or PP34^{exoU} in presence of Z-VAD (40μM), olaparab (10μM), Necrostatin-1s (Ne1s, 40μM) or Ferrostatin-1 (Fe1, 10μM) for 2 hours. ****p* ≤ 0.001, t-test with Bonferroni correction. (D) Heat map representing measure of LDH release in WT, *ALOX5*^{-/-} and *ALOX12/15* BMDMs transfected with recombinant ExoU in presence/absence of Cox1 inhibitor (Ketorolac Tromethamine, 10μM), Cox2 inhibitor (NS 398, 25μM), Cyp450 epoxygenase activity inhibitor (PPOH, 10μM), phospholipase inhibitor MAFP (50μM) or lipid peroxidation inhibitors Ferrostatin-1 (Fe1, 20μM), Resveratrol (5μM), Liproxstatin-1 (30μM), a-Tocopherol (20μM) for 2 hours. The heat map shows the mean of three combined independent experiments, each performed in triplicate. (E) Time course measure of plasma membrane permeabilization using propidium iodide incorporation in *Nlr4*^{-/-} BMDMs infected with PP34 or PP34^{exoUS142A} in presence/absence of Ferrostatin-1 (Fe1, 20μM). ****p* ≤ 0.001, t-test with Bonferroni correction. (F) Microbicidal activity of macrophages (5h) and neutrophils (3h) after infection with *P. aeruginosa* *exoU*⁺ and *exoU*⁻ (MOI 0.5) in presence/absence of ferrostatin-1 (10μM). ****p* ≤ 0.001, t-test with Bonferroni correction. Data information: Data are represented as means +/- SEM (graphs A-F) from *n* = 3 independent pooled experiments; ****p* ≤ 0.001 for the indicated comparisons using t-test with Bonferroni correction.

<https://doi.org/10.1371/journal.ppat.1009927.g002>

suggesting either that the phospholipase activity of ExoU promotes lipid peroxidation-independent cell death or that the inhibitory effect of ferrostatin-1 is unstable over time (Fig 2E). Regarding this, the replenishment of *P. aeruginosa*-infected cells with fresh ferrostatin-1 each hour strongly improved cell viability, suggesting that the instability of Fe1 might also account in the delayed ExoU-induced cell necrosis we observed (S2F Fig). Finally, we evaluated if the inhibition of lipid peroxidation would modulate macrophage and neutrophil microbicidal response upon *exoU*-expressing *P. aeruginosa* infection. We observed that ferrostatin-1 strongly improved both macrophage and neutrophil microbicidal activities to a level close to those observed in response to *exoU*-deficient *P. aeruginosa* (Fig 2F), hence suggesting that *P. aeruginosa* ExoU relies on lipid peroxidation-dependent cell necrosis to escape from phagocyte attack. Together, our results suggest that host cell lipid peroxidation is important for ExoU-induced host cell necrosis and release of alarmins.

Lipid peroxidation fuels ExoU phospholipase activity

Lipid-peroxidation requires reactive oxygen species (ROS), such as H₂O₂, that can oxidize various phospholipids [5]. Therefore, we evaluated the ability of ExoU to induce ROS-dependent lipid peroxidation in macrophages. Although we observed that, 30 minutes after transfection,

ExoU but not its catalytically inactivated mutant ExoU^{S142A}, triggered an acute ROS production in BMDMs, we surprisingly failed to detect a robust lipid peroxidation accumulation as measured by the C11 Bodipy probe (Figs 3A and S3A and S3B). As control, the well-known lipid peroxidation inducer Cumene hydroperoxide (CuOOH) promoted cellular lipid peroxidation (Fig 3A) [59]. In contrast, we observed that basal lipid peroxidation in cells was reduced upon ExoU transfection or PP34 infection, a process that was further strengthened in presence of ferrostatin-1 (Figs 3A and S3B).

These results suggest that, instead of promoting pathological lipid peroxidation, ExoU might actually use cellular lipid peroxidation to promote cell necrosis. To this regard, various host phospholipase A2 enzymes have been described to specifically cleave and remove peroxidised phospholipids from membranes [60–62]. To address this hypothesis, we performed a redox phospholipidomic approach to determine if ExoU could interfere with the endogenous levels of peroxidised phospholipids (Figs 3B and S3C). We used a 45 min time-point to perform our experiments, as a point where plasma membrane permeabilization (propidium uptake monitoring) is not observed. This design excludes the possibility that a decrease in peroxidised phospholipids is due to cell necrosis induced by ExoU (S3D Fig). We observed that ExoU-treated macrophages had a decrease in peroxidised phospholipids as measured by the reduction in hydroperoxyl (-OOH)- and hydroxyl (-OH)-phosphoinositols (PIs)/- phosphoserines (PSs) and—phosphocholines (PCs) with arachidonic acid (C20:4/C22:4) acid side chains (Figs 3B and S3C).

In cells, peroxidised phospholipids are detoxified by various factors, one of the most important being the ferroptosis regulator glutathione peroxidase 4 (GPX4) [5]. Consequently, the use of pro oxidant molecules or *Gpx4* genetic inactivation both induce a strong accumulation of various peroxidised phospholipids in cell membranes [5]. Therefore, we hypothesized that prestimulation of macrophages with non-cytotoxic doses of the lipid peroxidation and ferroptosis inducer Cumene hydroperoxide (20 μ M, 1h) might sensitize cells to ExoU-induced cell necrosis. We transfected recombinant (r)ExoU in WT BMDMs in presence or absence of non-toxic doses of the pro-oxidant Cumene hydroperoxide (CuOOH, 20 μ M, 1h) [59]. Although CuOOH promoted lipid peroxidation but not BMDM cell death, rExoU transfection specifically induced an increased cell necrosis in CuOOH-primed BMDMs, a process that was inhibited by the use of ferrostatin-1 (Fig 3C and 3D). In agreement with this result, we measured a strong decrease in lipid peroxidation in CuOOH-primed cells transfected with rExoU (Fig 3C and 3D), confirming that ExoU efficiently targeted lipid peroxides induced by CuOOH. In addition, microscopy observations of CuOOH-primed cells highlighted a decrease of peroxidized lipids at the plasma membrane upon infection by ExoU-expressing strain of *P. aeruginosa* (PP34), suggesting that ExoU mostly target plasma membrane peroxidized phospholipids to promote cell necrosis (Fig 3E). The enzyme cytochrome p450 oxidoreductase (CYPOR) has recently been found to be an important provider of peroxidized phospholipids upon ferroptosis induction; we hypothesized that ExoU function might be regulated by CYPOR-regulated phospholipid peroxidation. We acquired *Cypor*-deficient HeLa cells but also generated *Cypor*^{-/-} immortalized (i)BMDMs using CRISPR (S3E Fig) and evaluated the importance of CYPOR on ExoU-driven cell necrosis. PP34 infection of WT and *Cypor*^{-/-} immortalized BMDMs triggered similar cell deaths, suggesting that in resting cells, CYPOR does not promote the basal lipid peroxidation involved in ExoU-dependent cell necrosis (Fig 3G and 3H). However, in CuOOH-primed macrophages, where phospholipid peroxidation is induced, we observed that CYPOR was a major contributor of phospholipid peroxidation (S3F Fig). This was associated to enhanced ability of PP34 to trigger cell necrosis in CuOOH-primed WT but not in *Cypor*^{-/-} iBMDMs and HeLa cells (Fig 3G and 3H), which suggests that CYPOR-induced lipid peroxidation heightens ExoU-dependent toxicity. However, in resting cells,

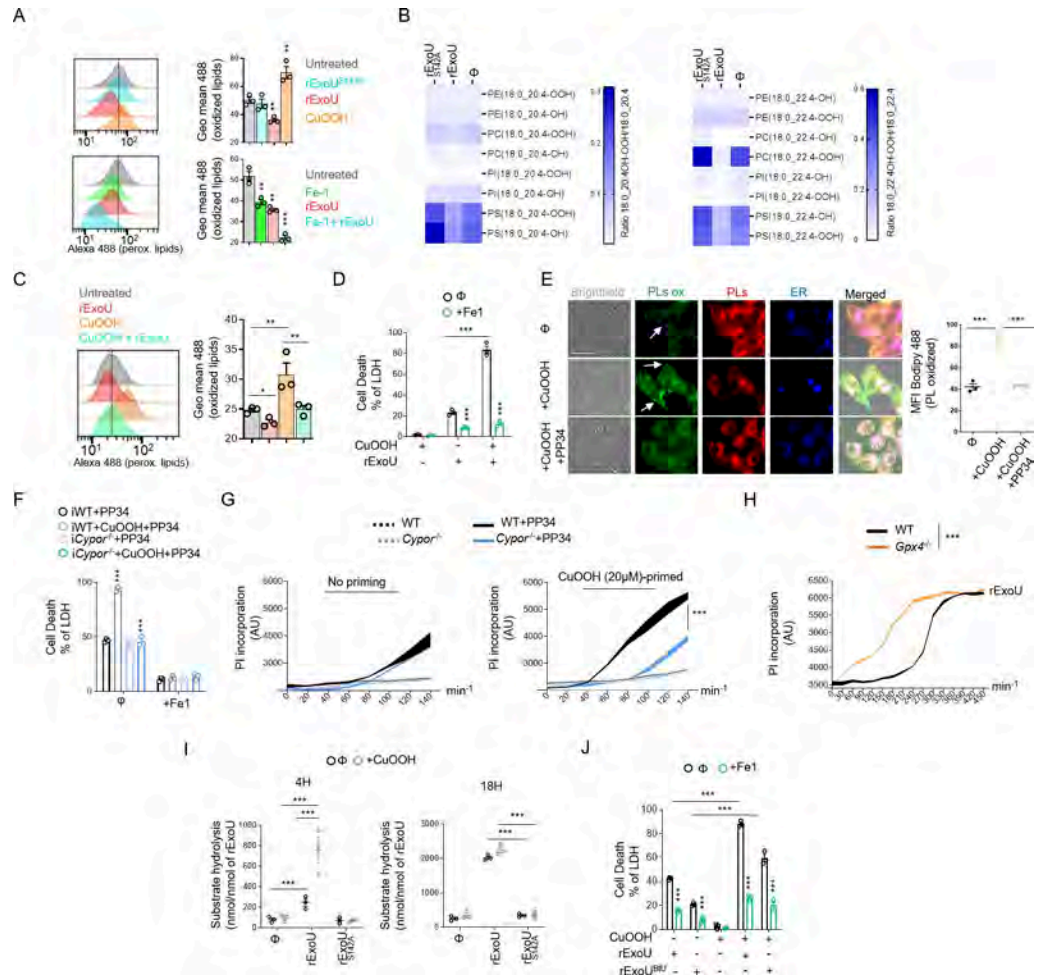


Fig 3. ExoU-induced cell death involves ROS-induced lipid peroxidation but proceeds in a ferroptosis independent manner. (A) Cytometry detection and quantification of (phospho)lipid peroxidation using the probe C11-bodipy in WT BMDMs treated with CuOOH (20µM) or transfected with rExoU (500ng) or its catalytically dead mutant rExoU^{S142A} (500ng) for 1 hour in presence or absence of Ferrostatin-1 (20µM). Sample were acquired using FACSCalibur (BD). The graphs shows the mean±SEM of one experiment performed in triplicate out of three independent experiments. **P≤0.001, ***P≤0.001 for the indicated comparisons using t-test with Bonferroni correction. (B) (Redox) lipidomic analysis of phospholipid peroxidation in BMDMs transfected with recombinant ExoU or its catalytically dead mutant ExoU^{S142A} for 45 minutes. Each value is standardized to the corresponding phospholipid content shown in (S3B Fig). The heat map shows the mean of one experiment performed in triplicate. (C) Cytometry detection and quantification of (phospho)lipid peroxidation using the probe C11-bodipy in WT BMDMs pre-treated or not for 1 hour with CuOOH (20µM) in presence or absence of Ferrostatin-1 (20µM) and then transfected with rExoU (500ng) for 1 hour. Sample were acquired using FACSCalibur (BD). The graphs shows the mean±SEM of one experiment performed in triplicate out of three independent experiments. *P≤0.05, **P≤0.001, for the indicated comparisons using t-test with Bonferroni correction. (D) Measure of LDH release in WT BMDMs pre-treated or not for 1 hour with CuOOH (20µM) in presence or absence of Ferrostatin-1 (20µM) and then transfected with rExoU (500ng) for 3 hours. ***p≤0.001, T-test with Bonferroni correction. (E) Representative microscopy images (phospho)lipid peroxidation and quantifications using the probe C11-bodipy in CuOOH-primed (20µM) HELA cells infected with PP34 (MOI5) for 2 hours. Images show two independent experiments, each performed three times at 2 hours post infection. Scale bar 20µm; Green, oxidized bodipy (oxidized phospholipids, PLs ox); Red, bodipy (phospholipids, PLs); Blue (Endoplasmic Reticulum, ER tracker probe, 1µM). Arrows show enriched peroxidised phospholipids in the plasma membrane area. Quantifications show the Mean Fluorescence Intensity (MFI) quantification of Peroxidized lipids from one experiment performed three times (50–60 cells counted). ***P<0.001 by T-test. (F) Measure of LDH release in immortalized (i) WT or *Cypor*^{-/-} BMDMs primed or not with CuOOH (20µM, 1hour) in presence or absence of ferrostatin-1 (20µM) and infected for 2 hours with PP34. ***p≤0.001, T-test with Bonferroni correction. (G) Time course measure of plasma membrane permeabilization using propidium iodide incorporation in WT and *Cypor*^{-/-} HELA cells primed or not with CuOOH (20µM, 1hour) and infected with PP34 (MOI5) for 2 hours. ***p≤0.001, T-test with Bonferroni correction. (H) Time course measure of plasma membrane permeabilization using propidium iodide incorporation in immortalised WT and *Gpx4*^{-/-} BMDMs transfected with rExoU (500ng) for 7 hours. ***p≤0.001, T-test with Bonferroni correction. (I) ExoU phospholipase

activity determination in WT BMDM lysates pre-treated or not with CuOOH (20 μ M, 1hour). 100 pmols of ExoU were used and phospholipase hydrolysis rate (nmoles of substrate hydrolysed/nmole of ExoU) was measured after 4 h and 16 hours. *** $p \leq 0.001$, T-test with Bonferroni correction. (J) Measure of LDH release in WT BMDMs primed or not with CuOOH (20 μ M, 1hour) in presence or absence of ferrostatin-1 (20 μ M) and transfected for 3 hours with 5 μ g of rExoU^{BtU} or 500ng rExoU. *** $p \leq 0.001$, T-test with Bonferroni correction. Data information: Data are plotted as means \pm SEM (D, F-J) from $n = 3$ independent pooled experiments; *** $P \leq 0.001$ for the indicated comparisons using t-test with Bonferroni correction.

<https://doi.org/10.1371/journal.ppat.1009927.g003>

basal lipid peroxidation appears to be regulated by other processes/enzymes. Finally, using Crispr-Cas9, we generated *Gpx4*^{-/-} immortalized BMDMs (S3G Fig). As previously observed by others in other cell lines [16,24], *Gpx4*^{-/-} immortalized BMDMs exhibited increased basal levels of peroxidised lipids (S3H Fig). Therefore, rExoU transfection triggered faster cell death of *Gpx4*^{-/-} macrophages than their WT counterpart, suggesting that lipid peroxidation of cells enhances ExoU-dependent toxicity (Figs 3H and S3G and S3H).

Upon phospholipid peroxidation, arachidonic acid-containing phospholipids form isoprostanes that are potent intra- and extra-cellular inflammatory mediators [9,10]. Once formed, these isoprostanes are released from phospholipids by the action of phospholipases [9,10]. Therefore, we reasoned that if ExoU targets peroxidised phospholipids, this would promote ExoU phospholipase-dependent release of endogenous pre-formed isoprostanes. Accordingly, the release of the 8-PGF2 α isoprostanone was specifically induced by ExoU in WT macrophages, a process that was further amplified by the co treatment of cells with non-toxic concentrations of Cumene hydroperoxide (CuOOH 20 μ M, 1 h) and ExoU (S3I Fig). Of importance, ferrostatin-1 strongly inhibited ExoU- and ExoU/CuOOH-induced 8-PGF2 α release (S3I Fig). In addition, we also detected that in CuOOH-primed macrophages, the amount of arachidonic acid-derived eicosanoids leukotriene B4 and prostaglandin E2, which are an indirect indication of the phospholipase activity of ExoU, were also strongly increased after the exposure to ExoU, hence suggesting that ExoU-targeted peroxidised phospholipids might increase its phospholipase activity toward all phospholipids (peroxidized or not) (S3J Fig). Consequently, we measured the phospholipase activity of ExoU in cell lysates where we chemically induced non-lethal lipid peroxidation with Cumene hydroperoxide (CuOOH, 20 μ M) for 1 h or not. We observed that in CuOOH-primed cell lysates, ExoU exhibited a stronger activity than in unprimed samples after 4 h of incubation (Fig 3I). Importantly, after 18 h incubation, we observed the same accumulation of hydrolysed substrate in CuOOH-primed and unprimed samples, which suggests that lipid peroxidation exacerbates the early activation of ExoU (Fig 3I). As control, ExoU^{S142A}- treated cell lysates did not show a significant phospholipase activity induction, suggesting that we mostly measured the PLA2 activity from ExoU, but not from cellular phospholipases (Fig 3I). Finally, we aimed at challenging our findings by determining if other toxic phospholipases also had a similar activation pattern to ExoU. Hence, we transfected macrophages with the closely related patatin-like phospholipase A2 from *Burkholderia thailandensis* (ExoU^{BtU}) [31]. We observed that recombinant ExoU^{BtU} transfection induced BMDMs necrosis, a process that was exacerbated by CuOOH priming and inhibited by the use of ferrostatin-1, suggesting that ExoU^{BtU} also follows a pattern involving host cell lipid peroxidation (Fig 3J). Altogether, our results suggest a surprising mechanism by which ExoU exploits cellular lipid peroxidation to trigger necrosis, a process that can be extended to the action of *B. thailandensis* ExoU^{BtU}-related phospholipase.

Ferrostatin-1 improves mouse resistance to infection by *exoU*-expressing *P. aeruginosa*

ExoU-induced necrosis promotes host lung pathology, which leads to a sepsis like response as well as respiratory failure syndrome. Therefore, we hypothesized that ferrostatin-1 use could

protect mice against *exoU*-expressing *P. aeruginosa*. Intranasal infection of mice using *P. aeruginosa* *exoU*⁺ showed that mice intraperitoneally pre-treated with ferrostatin-1 (6 h before infection, 6mg.k⁻¹) had diminished bacterial loads in BALFs, lungs and spleen. Ferrostatin-1 pre-treatment did not significantly modify bacterial loads of *exoU*-deficient bacteria, suggesting that ferrostatin-1 mainly modulates ExoU-dependent processes in mice (Fig 4A). Similarly, ferrostatin-1 also attenuated ExoU-dependent alarmin release (e.g. IL-36γ, IL33, IL1α) and the level of oxidized lipids (isoprostanes, MDA) in the BALs (Fig 4B and 4C). Additionally, evaluation of the cellular contents in BALFs showed that ferrostatin-1 significantly protected a pool of alveolar macrophage upon *P. aeruginosa* challenge simultaneously decreasing the number of recruited neutrophils, eosinophils and monocytes (Figs 4D and S4A). Although a pathological function of recruited immune cells such as neutrophils is probable, we hypothesize that ferrostatin-1-inhibited resident alveolar macrophage death in response to *exoU*-expressing *P. aeruginosa* might confer an improved immune protection characterized by lower immune cell recruitment and lower tissue damages. Regarding this, lung histological observations showed that the inflammatory status of mice infected with non-lethal doses of ExoU-expressing *P. aeruginosa* (1.10⁵ CFUs) was improved in presence of ferrostatin-1 (Fig 4E). Next, we addressed survival upon ExoU-expressing *P. aeruginosa* challenge. We observed that ferrostatin-1-treated mice (4–6 h before infection, 6mg.k⁻¹) had an improved survival rate than those treated with PBS after 40 h after infection (Fig 4F). We validated that ferrostatin-1 specifically protected mice against ExoU-induced pathology as ferrostatin-1-treated mice did not show enhanced protection (survival) against ExoU-deficient *P. aeruginosa* (Fig 4F).

Finally, we aimed to evaluate if *P. aeruginosa* ExoU would trigger pathological lipid peroxidation-dependent cell necrosis in human bronchial organoids. Organoids were derived from normal lung tissue adjacent to tumors obtained from patients undergoing lung resection due to non-small cell lung carcinoma (NSCLC). Live cell imaging of organoids microinjected with *P. aeruginosa* showed that ExoU triggered complete organoid collapse (Fig 4G and S7–S12 Movies). Importantly, ferrostatin-1 strongly attenuated *P. aeruginosa*-dependent organoid damages (Fig 4G and S7–S12 Movies). Altogether, our results identified that *P. aeruginosa* ExoU phospholipase benefits from lipid peroxidation to trigger pathology both in mice and in human bronchial organoids.

Discussion

As a preferential extracellular pathogen, *P. aeruginosa* uses its Type 3-Secretion System (T3SS) to inject virulence factors (Exo S, T, Y and U), allowing bacterial escape from phagocytic uptake and killing. Although *exoS*-expressing *P. aeruginosa* strains associate to the development of chronic infections, *exoU*-expressing *P. aeruginosa* triggers acute deadly infections that associate with a strong oxidative imbalance. In this study, we describe that endogenous basal lipid peroxidation contributes to ExoU-dependent cellular toxicity and mouse pathology. Though we do not exclude that *in vivo*, lipid peroxidation might play various pathological roles that go beyond the sole regulation of cell necrosis, such processes appear to be linked to ExoU expression. In this context, previous studies showed that ExoU promotes production of the platelet-activating factor or the 8-PGF2α isoprostane, two oxidized lipids [41]. In addition, ExoU directly promotes a strong release of arachidonic acid from phospholipids. Enzymes such as cytochrome P450/COXs/LOXs can enzymatically produce oxygenated arachidonic products such as prostaglandin E2/leukotriene B4 involved in pathological signalling pathways upon *P. aeruginosa* infection [38,40,63]. However, results from others and ours mostly suggest that, taken individually, those enzymes only play a negligible role in ExoU-induced cell necrosis [38,40,63]. Regarding the central cell types involved in ExoU-induced pathology, previous studies identified macrophages and

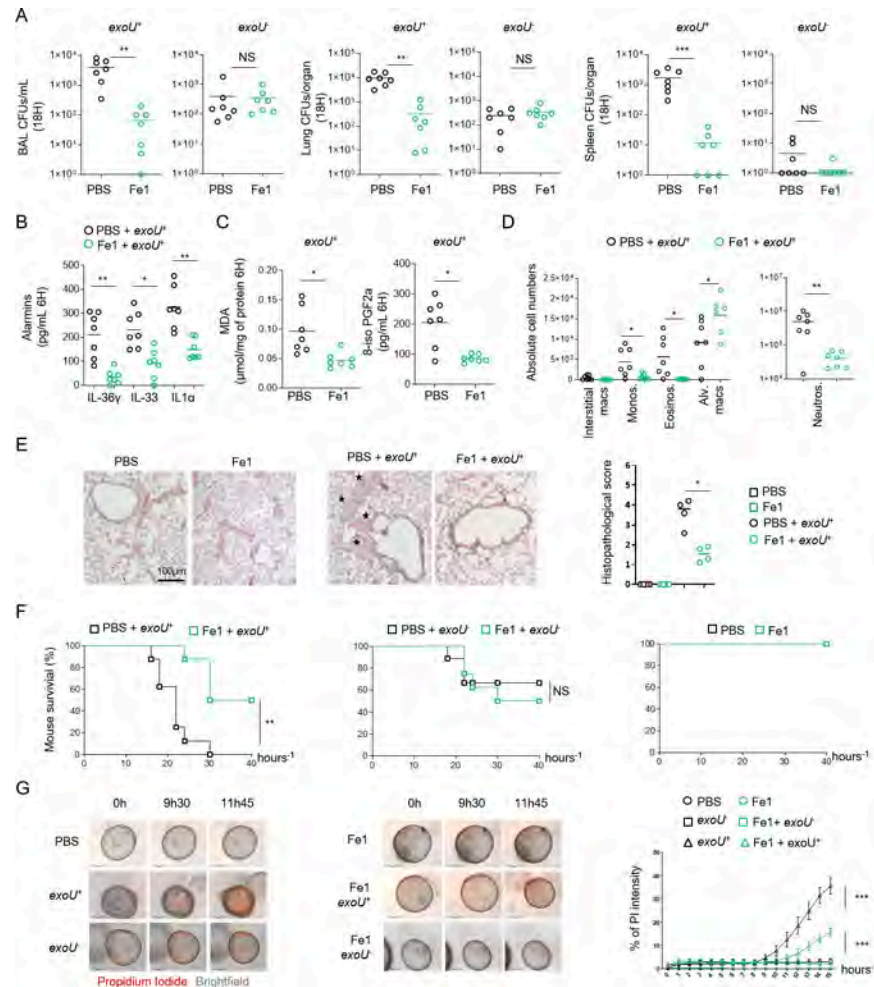


Fig 4. Ferrostatin-1 protects mice against ExoU-induced lung pathology. (A) Bronchoalveolar (BAL), lung and spleen bacterial loads from WT mice (n = 7/group) 18 hours after intranasal infection with 5.10⁵ CFUs of *P. aeruginosa* PP34 or its isogenic mutant PP34^{exoU-}. When specified, mice were intraperitoneally pretreated with ferrostatin-1 (6mg.k⁻¹ or PBS) 4 hours before intranasal infection. Graphs represent one experiment (7 mice/group) out of three independent *in vivo* experiments. **p ≤ 0.01, Mann-Whitney analysis test. NS: Not significant. (B, C) Alarmin and lipid peroxide products levels in bronchoalveolar fluids (BALFs) from WT mice (n = 7 mice/group) 6 hours after intranasal infection with 5.10⁵ CFUs of *P. aeruginosa* PP34 or its isogenic mutant PP34^{exoU-}. When specified, mice were intraperitoneally pretreated with ferrostatin-1 (6mg.k⁻¹ or PBS) 4 hours before intranasal infection. Graphs represent one experiment (7 mice/group) out of three independent *in vivo* experiments; *p ≤ 0.05; **p ≤ 0.01, Mann-Whitney analysis test. (D) Immune cell (CD45+) populations in bronchoalveolar fluids (BALFs) from WT mice (n = 7 mice/group) 6 hours after intranasal infection with 5.10⁵ CFUs of *P. aeruginosa* PP34 or its isogenic mutant PP34^{exoU-}. When specified, mice were intraperitoneally treated with ferrostatin-1 (6mg.k⁻¹ or PBS) 4–6 hours before intranasal infection. Graphs represent one experiment (7 mice/group) out of three independent *in vivo* experiments; *p ≤ 0.05; **p ≤ 0.01, Mann-Whitney analysis test. (E) Histological observation and scoring of bronchial and lung cellular infiltrations upon *exoU*-expressing *P. aeruginosa* intranasal infection. When specified, mice were intraperitoneally pretreated with ferrostatin-1 (6mg.k⁻¹ or PBS) 4–6 hours before intranasal infection. Stars show the cellular infiltrates. *p ≤ 0.05; Mann-Whitney analysis test. (F) Mice survival (n = 7 mice/group) 40 hours after intranasal infection with 5.10⁵ CFUs of *P. aeruginosa* PP34 or its isogenic mutant PP34^{exoU-}. Mice were intraperitoneally pretreated with ferrostatin-1 (6mg.k⁻¹ or PBS) 4 hours before intranasal infection. Graphs represent one experiment (7 mice/group) out of three independent *in vivo* experiments; **p ≤ 0.01, Log-rank Cox-Mantel test was used for survival comparisons. (G, H) Time-lapse microscopy and the associated quantifications of the measure of plasma membrane permeabilization using propidium iodide incorporation in human primary bronchial organoids infected (microinjection) with *P. aeruginosa* expressing *exoU*⁺ or its isogenic mutant (*exoU*⁻) in presence or absence of ferrostatin-1 (40μM) for 15 hours. Data are plotted as means± SEM. ***p ≤ 0.001, T-test with Bonferroni correction. Data information: Data shown as means (Graphs A-E) and are representative of one experiment performed three times; *p ≤ 0.05; **p ≤ 0.01, Mann-Whitney analysis test (A-E) and log-rank Cox-Mantel test for survival comparisons (F).

<https://doi.org/10.1371/journal.ppat.1009927.g004>

neutrophils as central targets of ExoU injection by *P. aeruginosa*. Therefore, future studies will be of importance to determine if the respective contribution of each cell type in pathology induced by ExoU-exploited lipid peroxidation. Regarding this, our *in vivo* observations that targeting lipid peroxidation confers some protection of mice against ExoU-dependent pathology is to put in the light of a decrease in some eicosanoid production such as LTB4 and PGE2, two important modulators of ExoU-driven pathology [38,40,63]. Therefore, the use of *Alox5^{-/-}* or *Cox^{-/-}* mice, unable to generate LTB4 or various prostaglandins respectively, will also help to determine the respective importance of eicosanoid burst or cell necrosis upon lipid peroxidation-driven ExoU activity.

Although controlled phospholipid peroxidation is of importance for the cells to perform various processes such as efferocytosis through the engagement of peroxidised-PS, mitochondria-dependent apoptosis through cardiolipin peroxidation, signal transduction through peroxidised PC-derived lipids, unrestricted accumulation of peroxidised PEs drives ferroptosis [9,10,64]. A question in both basal lipid peroxidation and ferroptosis-induced lipid peroxidation lies on the compartment phospholipid peroxidation occurs. Peroxisomes are key at providing ether-phospholipids that will be peroxidised upon ferroptosis induction, the Endoplasmic reticulum is also a central regulator of phospholipid turn over and plasma membrane constitutes the probable location of lipid peroxidation-driven cell lysis upon ferroptosis induction [16,65,66]. Our observations also suggest that although lipid peroxidation can occur in various cellular compartments, ExoU-induced cell necrosis mostly arises from plasma membrane cleaved peroxidized phospholipids. Yet, this does not exclude at all that phospholipid peroxidation could occur in other intracellular organelles, including the endoplasmic reticulum.

Ferroptosis is thought to be a constitutively activated form of cell death that is kept under control through the activity of endogenous regulators of lipid peroxidation such as GPX4, FSP1-mediated coQ10 production, α -tocopherol (vitamin E). In addition, the host cellular calcium (Ca^{2+})-independent PLA2 γ , the peroxiredoxin Prdx6 PLA2 or the PLA2G6 (Ca^{2+} -independent PLA2 β) can cleave and remove preferentially peroxidised phospholipids, hence contributing to phospholipid peroxide detoxification [61,62,67–71]. It is important to notice that both the iPLA2beta and iPLA2g belong to the patatin-like phospholipase family, as ExoU, which suggests that this family of phospholipases might have some conserved affinities to peroxidized phospholipids [72]. The activity of those phospholipases is tightly regulated by various cellular systems (e.g. ROS levels, calcium fluxes, phospholipid composition) that ensure an optimal but not dysregulated phospholipid cleavage [71]. To this regard, our findings that cellular phospholipid peroxidation is a strong enhancer of ExoU-induced pathological necrosis appears in first view counter intuitive. In this context, we envision that, as a virulence factor, ExoU activity does not follow host regulation and uses host peroxidized phospholipids to boost its patatin-like A2 phospholipase activity allowing to aberrantly target and cleave host (peroxidised) phospholipids. Consequently, the use of lipid peroxidation inhibitors such as resveratrol, lipoxstatin-1 or ferrostatin-1 attenuates the potency and the speed of ExoU-induced cell necrosis. This offers a key time window for macrophage and neutrophil-mediated bacterial uptake and killing. Although, the identification of cellular enzymatic systems that promote basal lipid peroxidation remains to be explored and characterized, lipid peroxidation accumulation upon *Gpx4* removal or oxidant stress enhances ExoU-induced cellular necrosis. It is intriguing that endogenous peroxidised phospholipids favour ExoU-induced cell necrosis, suggesting that ExoU-expressing strains of *P. aeruginosa* take advantage of the host ferroptosis pathways to maximally damage host tissues. Hence, oxidant-activated cytochrome P450 oxidoreductase CYPOR, a crucial regulator of ferroptosis, strongly enhanced ExoU-dependent cell necrosis, which suggests a important link between ferroptosis-regulated pathways and ExoU activity. Should other regulators of ferroptosis such as ACSL and LPCAT acyl transferases on ExoU-dependent toxicity warrants further investigations [15].

Phospholipases are also present in venoms or various microbial pathogens (e.g. *M. tuberculosis*, *L. monocytogenes*, *S. pyogenes*) and can also promote fast cell necrosis [73–75]. Conversely, we extended our findings to the ExoU closely related ExoU^{BtU} phospholipase from *B. thailandensis*. Remarkably, snake, scorpion or spider venoms are a complex mixture of various components, including the L-amino acid oxidase, able to generate H₂O₂-driven lipid peroxidation, and secreted phospholipases able to cleave phospholipids [73]. In this context, it is tempting to speculate that venoms have all components necessary to mediate cell damage in a complex single-injection mixture. L-amino acid oxidase-induced lipid peroxidation might work with venom PLA2 to optimize phospholipid cleavage and subsequent cell necrosis. Related to this, Sevanian and colleagues made pioneer observations that the PLA2 activity from the snake *Crotalus adamanteus* is exacerbated in contact of liposomes constituted of peroxidised phospholipids, a process that is thought to be due to the better accessibility of the sn2-peroxidized fatty acid to phospholipase [70]. Whether ExoU and its relatives follow a similar pathway of activation will be studied in future studies.

In a broader point of view, it is interesting to note that phospholipases can promote allergic shock associated with a strong release of the allergic alarmin interleukin-33 [76], a signature we also observed in mice infected with ExoU-expressing *P. aeruginosa*. Should lipid peroxidation be involved in IL33-driven allergy or asthma in response to phospholipases or other allergens (e.g. proteases) [77] will require additional study.

Understanding the mechanisms of regulated cell necrosis and their physio-pathological consequences is currently driving intensive research and debates. While the importance of lipid peroxidation in antigen presentation, anti-cancer treatments or in exacerbating neurodegenerative diseases becomes more and more clear, its function in infectious diseases remains less studied. Regarding this, Dar et al., recently described that, upon chronic infection, secreted *P. aeruginosa* lipoxygenase (loxA) could sensitize cells to lipid peroxidation-induced ferroptosis [22]. In addition, Kain and colleagues recently linked regulation of host lipid peroxidation and ferroptosis to restriction of liver-stage malaria, which suggests that host peroxidised phospholipids might play yet unsuspected functions in immunity or susceptibility to various pathogens [78]. Thus, our findings that the bacterial patatin-like phospholipase A2 ExoU contributes to pathology by exploiting target cell lipid peroxidation adds an additional piece of significance for the role of lipid peroxidation in infectious diseases but also offers novel insights to target host lipid peroxidation pathways in the frame of infectious diseases ([S1 Graphical Abstract](#)).

Material and method

Ethics statements

The use of human cells was performed under the agreement of the Research Ethical Committee, Haute-Garonne, France. Buffy coats came anonymously by the EFS (établissement français du sang, Toulouse, France). For each donor, a written informed consent was obtained according to the EFS contract agreement n° 21PLER2017-0035AV02, according, to “Decret N° 2007–1220 (articles L1243-4, R1243-61)”.

Animal experiments were approved by local (CE01 committee) and national ethic committees (License APAFIS#8521–2017041008135771, Minister of Research, France) and performed according to local guidelines (French ethical laws) and the European Union animal protection directive (Directive 2010/63/EU).

Mice

Nlr4^{-/-}, *Casp1*^{-/-}*Casp11*^{-/-}, *GsdmD*^{-/-}, *ALOX12/15*^{-/-} and *ALOX5*^{-/-} mice were generated and described in previous studies [79–82]. Mice were bred at the IPBS (Toulouse, France) animal

facilities in agreement to the EU and French directives on animal welfare (Directive 2010/63/EU). Charles Rivers provided WT C57BL/6 mice.

Animal infection models

6–10 mice/group were intranasally infected with 5.10^5 Colony Forming Units (CFUs) of *P. aeruginosa* PP34 strain (*ExoU*⁺) or its isogenic mutant (*ExoU*⁻) and animal survival was followed over 40–50 hours after infection. When specified, mice were intraperitoneally treated with 100 μ L of PBS or ferrostatin-1 (6mg.k⁻¹) 4–6 hours before intranasal infections with bacterial strains.

Regarding bacterial loads assays, 6–10 mice/group were intranasally infected with 2.10^5 bacteria for 24 hours, and Bronchoalveolar (BALs), lung spleen and blood bacterial numbers were evaluated using CFU plating. BAL fluids (BALFs) were also used to address cytokine, alarmin and lipid levels using ELISA, EIA and colorimetric kits. There were no randomization or blinding performed.

Histological experiments and scoring

Mice were intraperitoneally treated with 100 μ L of PBS or ferrostatin-1 (6mg.k⁻¹) 4–6 hours before intranasal infections with sub-lethal doses (2.10^5 CFUs) of *exoU*-expressing *P. aeruginosa*. 6 hours later, lung tissues were fixed for 48 h in 10% buffered formalin, washed 3 times in ethanol 70% and embedded in paraffin. 5 μ m sections were stained with hematoxylin and eosin (HE). Histopathological scoring from 0 to 3 were attributed based on the severity of peri-bronchial, perivascular, and interstitial cell infiltration, resulting in a maximum score of 9.

Bacterial cultures

P. aeruginosa (PP34, PA103, CHA, PAO1, PA14) bacteria and their isogenic mutants were grown overnight in Luria Broth (LB) medium at 37°C with aeration and constant agitation in the presence or absence of EGTA (10mM) to ensure T3SS expression. Bacteria were sub-cultured the next day by dilution overnight culture 1/50 and grew until reaching an optical density (OD) O.D600 of 0.6–1. Bacterial strains and their mutants are listed in [Table 1](#).

Bone Marrow-derived Macrophage (BMDMs), Eosinophil (BMDEs) or Neutrophil (BMDNs) isolation and culture

Murine Bone Marrow-Derived Macrophages (BMDMs) from bone marrow progenitors were differentiated in DMEM (Invitrogen) supplemented with 10% v/v FCS (Thermo Fisher Scientific), 10% v/v MCSF (L929 cell supernatant), 10 mM HEPES (Invitrogen), and nonessential amino acids (Invitrogen) for 7 days as previously described [85].

Murine Bone Marrow-Derived Eosinophils were differentiated *in-vitro* from bone marrow as previously described [86]. cells were resuspended and cultured at 10^6 /mL in RPMI glutamax medium with HEPES containing 20% FBS, 100 IU/ml penicillin and 10 μ g/ml streptomycin, 1 mM sodium pyruvate (Life Technologies), and 50 μ M 2-ME (Sigma-Aldrich) supplemented with 100 ng/ml stem cell factor (SCF; PeproTech) and 100 ng/ml FLT3 ligand (FLT3-L; PeproTech) from days 0 to 4. On day 4, the medium containing SCF and FLT3-L was replaced with medium containing 10 ng/ml recombinant mouse (rm) IL-5 (R&D Systems) only. Medium was replaced every 4 days and the concentration of the cells was adjusted each time to 10^6 /ml. After 10 to 14 days of culture, cells were recovered by gentle pipetting and used as Eosinophils in our experiments. Over 95% of cells had the standard phenotype of Eosinophils: CD11b⁺ Siglec F⁺ after FACS analysis.

Table 1. Resource of reagents used in this study. Information and reagents are available upon request to Etienne.meunier@ipbs.fr.

REAGENT or RESOURCE	SOURCE	IDENTIFIER
Antibodies		
GPX4, 1/1000	abcam	ab125066
ExoU, 1/1000	Ina Attree/CNRS, France.	[37]
CYPOR 1/1000	abcam	ab180597
Gapdh 1/10000	Gentex	GTX100118
Goat anti-Rabbit HRP (1/10000)	Advansta	R-05072-500
Bacterial and Virus Strains		
PAO1	J. Buyck/Univ of Poitiers/France	N.A.
PP34	Ina Attree/CNRS, France.	[37]
PP34 $exoU$	Ina Attree/CNRS, France.	[37]
PP34 $exoU^{\delta 142A}$	Ina Attree/CNRS, France.	[37]
CHA	Ina Attree/CNRS, France.	[37]
CHAdST	Ina Attree/CNRS, France.	[37]
CHAdST $exoU^+$	Ina Attree/CNRS, France.	[37]
PA103	J. Buyck/Univ of Poitiers/France	N.A.
PA103 $exoU$	J. Buyck/Univ of Poitiers/France	N.A.
PA14	J. Buyck/Univ of Poitiers/France	N.A.
PA14 $exoU$	J. Buyck/Univ of Poitiers/France	N.A.
Biological Samples		
Human lung biopsy	Hospital of Toulouse	CHU 19 244 C CNRS 205782
Human blood	EFS	21PLER2017-0035AV02
Chemicals, Peptides, and Recombinant Proteins		
Recombinant ExoU	This study	[31]
Recombinant ExoUS142A	This study	[31]
FCS	Fisher Scientific	16010-159
mMCSF	L929 cell supernatant	NA
HEPES	Fisher Scientific	SH30237.01
Non-essential amino acids	Invitrogen	
ECL Clarity Max Substrate	BioRad	1705060
ECL Clarity Max Substrate	BioRad	1705062
Western Blot Strip Buffer	Diagomics	R-03722-D50
Tris base	euromedex	200923-A
SDS ultra-pure (4x)	Euromedex	1012
Acrylamide / Bisacrylamide 37.5/1 30%	Euromedex	EU0088-B
Temed	Sigma	T9281-25ML
Ammonium persulfate	Sigma	248614-100g
Page Ruler 10–180 kDa	Fisher Scientific	15744052
Triton X-100	Euromedex	2000
DMEM	Fisher Scientific	41965-039
LB	Fisher Scientific	BP1426-2
LB Agar	INVITROGEN	22700025
Roche protease inhibitor cocktail	Sigma	000000011697498001
BSA	SIGMA	A9647-100G
Propidium iodide	Invitrogen	P3566
Beads Neutrophils human	Miltenyi biotec	130-104-434
Beads Neutrophils murine	Miltenyi biotec	130-120-337
Kit de coloration bleue et fixable des cellules mortes LIVE/DEAD pour excitation UV	ThermoFisher Scientifique	L34961

(Continued)

Table 1. (Continued)

REAGENT or RESOURCE	SOURCE	IDENTIFIER
APC/Cyanine7 anti-mouse CD45 Antibody	BioLegend	103116
PE/Dazzle 594 anti-human CD64 Antibody	BioLegend	305032
FITC anti-mouse MERTK (Mer) Antibody	BioLegend	151504
CD170 (Siglec F) Monoclonal Antibody (1RNM44N), Super Bright 780,	eBioscience	78-1702-82
Ly-6G Monoclonal Antibody (1A8-Ly6g), APC	eBioscience	17-9668-82
Brilliant Violet 650 anti-mouse/human CD11b Antibody	BioLegend	101259
Brilliant Violet 421 anti-mouse Ly-6C Antibody	BioLegend	128032
PE/Cyanine7 anti-mouse CD11c Antibody	BioLegend	117318
Eosinophil differentiation cocktail (IL-5)	R&D Systems	405-ML-005
Eosinophil differentiation cocktail (SCF)	Biolegend	579706
Eosinophil differentiation cocktail (Flt-3)	Biolegend	550706
Puromycin	ThermoFisher Scientifique	A1113803
G418 (Geneticin)	invivoGen	ant-gn-1
Blasticidin	nvivoGen	ant-bl-1
Cumene hydroperoxide	Sigma-Aldrich	247502-5G
RSL3	Sigma-Aldrich	SML2234
Ferrostatin-1	Sigma-Aldrich	SML0583
Lipoxstatin-1	Sigma-Aldrich	SML1414
DFO	Sigma-Aldrich	D9533
a-tocopherol	Sigma-Aldrich	258024
MAFP	Sigma-Aldrich	M2689
PPOH	CaymanChem	75770
Cox1 inhibitor	Ab142904 (Abcam)	Ab142904
Cox2 inhibitor	NS 398 (Abcam)	Ab120295
cPLA2 assay kit	Cayman Chemical	765021
CD14+ beads	Miltenyi biotec	130-050-201
RPMI	Fisher Scientific	72400-021
OPTIMEM	Fisher Scientific	31985-04
Z-VAD	Invivogen	tlrl-vad
TPCA-1	Tocris	2559
mTNFa	abcam	ab259411
Olaparib	CaymanChem	10621
Necrostatin-1s	Sigma-Aldrich	N9037 10MG
hMCSF	Miltenyi biotec	170-076-171
Fisher BioReagents Lymphocyte Separation Medium-LSM	Fisher Scientific	BP2663500
ExoU	This study	N.A.
ExoUS142A	This study	N.A.
Human bronchial organoid culture reagents		
Advanced DMEM/F12	Invitrogen	12634028
Gibco L-Glutamine (200 mM)	Fisher	11500626
Hepes 1 M	Fisher	11560496
Penicillin/Streptomycin	Fisher	11548876
Primocin	Invivogen	ant-pm-1
Basic Media	In house	NA
Rspo1	In house	NA
Noggin	In house	NA
B27	Gibco/Invitrogen	17504044

(Continued)

Table 1. (Continued)

REAGENT or RESOURCE	SOURCE	IDENTIFIER
N-Acetylcysteine	Sigma	A9165-5g
Nicotinamide	Sigma	N0636
Y-27632	Cayman	10005583
A83-01	Tocris	2939
SB 202190	Sigma	S7067
FGF-7	Peprotech	100-19
FGF-10	Peprotech	100-26
Critical Commercial Assays		
mIL-1alpha ELISA kit	Fisher Scientific	88-5019-88
mIL-36g ELISA kit	Ray Biotech	ELM-IL36G
LDH Cytotoxicity Detection Kit	Takara	MK401
mTNFalpha ELISA kit	Fisher Scientific	88-7324-22
mIL-33 ELISA kit	Fisher Scientific	88-7333-88
mHMGB1 ELISA kit	Clinisciences	LS-F4040-1
TBAR MDA colorimetric kit	Cayman	10009055
PGE2 EIA Kit	Cayman	514010
LTB4 EIA kit	Cayman	520111
8-PGF2 EIA kit	Cayman	516351
H2DCFDA ROS detecting probe	Invitrogen	D399
C11 bodipy phospholipid peroxide detection probe	Invitrogen	D3861
ER-Tracker Blue-White DPX, for live-cell imaging	Invitrogen	E12353
Experimental Models: Cell Lines		
WT Mouse Bone marrow derived macrophages	This study	
Alox5 ^{-/-} Mouse Bone marrow derived macrophages	This study	
Alox12/15 ^{-/-} Mouse Bone marrow derived macrophages	This study	
Nlrc4 ^{-/-} Mouse Bone marrow derived macrophages	This study	
Casp1 ^{-/-} /Casp11 ^{-/-} Mouse Bone marrow derived macrophages	This study	
GsdmD ^{-/-} Mouse Bone marrow derived macrophages	This study	
WT Mouse bone marrow derived eosinophils	This study	
WT Mouse bone marrow derived neutrophils	This study	
Human blood monocyte derived macrophages	This study	
Human blood neutrophils	This study	
Immortalized WT murine bone marrow derived macrophages	This study	
Immortalized Gpx4 ^{-/-} murine bone marrow derived macrophages	This study	
Human Bronchial epithelial cells	This study	
Human Alveolar epithelial A549 cell line	This study	
Human intestinal epithelial HELA cell line	This study	
Experimental Models: Organisms/Strains		
WT C57Bl6J mice	C. Rivers	
WT C57Bl6N mice	C. Rivers	
Alox5 ^{-/-} C57Bl6 mice	A.Coste	[79]
Alox12/15 ^{-/-} C57Bl6 mice	A.Coste	[79]
Nlrc4 ^{-/-} C57Bl6 mice	C.Bryant	[80]
Casp1 ^{-/-} /Casp11 ^{-/-} C57Bl6 mice	B.Py/ Junying Yuan	[81]
GsdmD ^{-/-} C57Bl6 mice	P.Broz	[82]
Human Bronchial organoids	This study	[83,84]
Oligonucleotides		

(Continued)

Table 1. (Continued)

REAGENT or RESOURCE	SOURCE	IDENTIFIER
Guide Crispr mGpx4- Exon1 Forward	Sigma-Aldrich	GGACGCTGCAGACAGCGCGG
Guide Crispr mCypor- Exon1 Forward	Sigma-Aldrich	
Recombinant DNA		
Plasmid: ExoU	[31]	[31]
Plasmid: ExoUS142A	[31]	[31]
Plasmid: ExoU ^{BtU}	[31]	[31]
LentiGuide-Puro	Feng Zhang lab	Addgene #52963
Lenti-multi-Guide	From Qin Yan	Addgene #85401
pMD.2G	Didier Trono lab	Addgene #12259
p8.91	Didier Trono lab	N.A.
LentiCas9-Blast	Feng Zhang lab	Addgene #52962
Software and Algorithms		
Graph Pad Prism 8.0		
Image J		
Snapgene	GSL Biotech LLC, Chicago, U.S.A	
FlowJo	FlowJo LLC	
Benchling Software		
Other		

<https://doi.org/10.1371/journal.ppat.1009927.t001>

Murine Bone Marrow-derived Neutrophils were isolated and purified from fresh bone marrows using Anti-Ly-6G micro bead kit (Miltenyi Biotec). Analysis of cell purity by FACS show that over 95% of cells had the standard phenotype of Neutrophils Ly6G+/Ly6C+.

2.5×10^5 BMDMs or 1.1×10^6 BMDEs/BMDNs were seeded in 24 well-plates and infected or exposed to various treatments. Regarding ferroptosis experiments, BMDMs were infected with various bacterial strains of *P. aeruginosa* expressing or not *exoU* at an MOI 0.1–1 for various times. When specified, recombinant microbial phospholipases (10ng–1 μ g) were transfected in BMDMs using Fugene (3 μ l per 1 μ g of transfected protein) for 2–4 hours. Compound-induced ferroptosis was achieved using RSL-3 (10 μ M, 8H) or Cumene hydroperoxide (CuOOH, 500 μ M, 3H).

When required, BMDMs were pretreated for 2 hours with pharmacological inhibitors necrostatin-1s (40 μ M), Z-VAD (40 μ M), olaparib (10 μ M), ferrostatin-1 (1–40 μ M), MAFP (50 μ M), liproxstatin (30 μ M), α -tocopherol (20 μ M).

For all stimulations, cell culture medium was replaced by serum-free and antibiotic-free Opti-MEM medium and triggers were added to the cells for various times.

Cell line culture

Immortalized murine bone-marrow derived macrophages have been described previously [85]. U937 cells were cultured in RPMI glutamax medium containing 10% FBS, 100 IU/ml penicillin and 10 μ g/ml streptomycin, 1 mM sodium pyruvate (Life Technologies), and 50 μ M 2-ME (Sigma-Aldrich). Medium was renewed every 3 days and the concentration of the cells was adjusted each time to 5×10^5 /ml. A549, HeLa and HBE cells were cultured in DMEM glutamax medium with HEPES containing 10% FBS, 100 IU/ml penicillin and 10 μ g/ml streptomycin, 1 mM sodium pyruvate (Life Technologies). When the cells reach approximately 90% confluency, cells are detached with Trypsin 0.05% (Gibco), cell suspension is diluted 1/10 in fresh medium, and placed back in the incubator for culture.

Purification and generation of human blood neutrophils and monocyte-derived Macrophages

Monocytes were isolated from Peripheral Blood Mononuclear Cells (PBMCs) from the buffy coat of healthy donors obtained from the EFS Toulouse Purpan (France) as described previously [87]. Briefly, PBMCs were isolated by centrifugation using standard Ficoll-Paque density (GE Healthcare) [85]. The blood was diluted 1:1 in phosphate-buffered saline (PBS) pre-warmed to 37°C and carefully layered over the Ficoll-Paque gradient. The tubes were centrifuged for 25 min at 2000 rpm, at 20°C. The cell interface layer was harvested carefully, and the cells were washed twice in PBS (for 10 min at 1200 rpm followed by 10 min at 800 rpm) and re-suspended in RPMI-1640 supplemented with 10% of foetal calf serum (FCS), 1% penicillin (100 IU/mL) and streptomycin (100 µg/ml). Monocytes were separated from lymphocytes by positive selection using CD14+ isolation kit (Myltenyi biotec). To allow differentiation into monocyte-derived macrophages, cells were cultured in RPMI medium (GIBCO) supplemented with 10% FCS (Invitrogen), 100 IU/ml penicillin, 100µg/ml streptomycin, 10 ng/ml M-CSF for 7 days.

Human blood neutrophils were isolated from whole blood of healthy donors obtained from the EFS Toulouse Purpan (France). Neutrophils were enriched using MACSxpress Whole Blood Neutrophil Isolation Kit whole blood neutrophil isolation kit (Myltenyi biotec) according to manufacturer instructions. Red blood cells (RBC) were removed by 10 min incubation in RBC Lysis Buffer (BioLegend).

Genetic invalidation of *Gpx4* and *Cypor* genes in immortalized BMDMs

Targeted genes were knocked-out using the crispr/cas9 system in immortalized BMDMs. Single guide RNAs (sgRNA) specifically targeting *Gpx4* exon1 (for 5' GGACGCTGCAGA-CAGCGCGG 3' *Cypor* exon2 (for 5' AGTGTCTCTATTCAGCACAA 3' were designed using Benchling tool (Benchling.com), and oligonucleotides were synthesized by Sigma-Aldrich. Crispr guide RNA oligonucleotides were hybridized and subsequently cloned into the vector Lenti-gRNA-Puromycin using BsmBI restriction enzyme (Addgene 52963, Feng Zhang lab). Generated constructs were then transfected in lipofectamine 2000 into HEK293T for 48 hours together with the lentiviral packaging vector p8.91 (Didier Trono lab, EPFL, Switzerland) and the envelop coding VSVg plasmid (pMD.2G, Addgene 12259, Didier Trono lab). Viral supernatants were harvested, filtered on 0.45 µm filter and used to infect cells expressing Cas9 (1,000,000 cells/well in 6-well plates. Efficient infection viral particles was ensured by centrifuging cells for 2 h at 2900 rpm at 32°C in presence of 8µg/ml polybrene. 48 h later, medium was replaced and Puromycin selection (10µg/mL) was applied to select positive clones for two weeks. Puromycin-resistant cells were sorted at the single cell level by FACS (Aria cell sorter). Individual clones were subjected to western blotting to confirm the absence of targeted proteins.

Human bronchial organoid production and maintenance

Airway organoids were derived from lung biopsies as described [83,84]. Briefly, Human lung tissue was provided by the CHU of Toulouse under the CNRS approved protocols CHU 19 244 C and CNRS 205782. All patients participating in this study consented to scientific use of their material. Biopsies (1 mm³) of normal lung tissue adjacent to the tumor obtained from patients who underwent lung resection due to Non-small cell lung carcinoma (NSCLC) were minced and digested with 2 mg ml⁻¹ collagenase (Sigma) on an orbital shaker at 37°C for 1h. The digested tissue suspension was sheared using flamed glass Pasteur pipettes and strained

over a 100- μm cell strainer (Falcon). The resultant single cell suspensions were embedded in 10 mg ml⁻¹ of Cultrex growth factor reduced BME type 2 (R & D Systems) and 40 μl drops were seeded on Nunclon Delta surface 24-well plates (Thermo Scientific). Following polymerization, 500 μl of Advanced DMEM/F12 (Invitrogen) supplemented with 1x L-Glutamine (Fisher Scientific), 10mM Hepes (Fisher Scientific), 100 U ml⁻¹ / 100 μg ml⁻¹ Penicillin / Streptomycin (Fisher Scientific), 50 μg ml⁻¹ Primocin (InvivoGen), 10% Noggin (homemade), 10% Rspo1 (homemade), 1x B27 (Gibco), 1.25mM N-Acetylcysteine (Sigma-Aldrich), 10mM Nicotinamide (Sigma-Aldrich), 5 μM Y-27632 (Cayman Chemical), 500nM A83-01 (Tocris Bioscience), 1 μM SB 202190 (Sigma-Aldrich), 25 ng ml⁻¹ FGF-7 (PeproTech), 100 ng ml⁻¹ FGF-10 (PeproTech) was added to each well and plates transferred to humidified incubator at 37°C with 5% CO₂. The organoids were passaged every 4 weeks.

Organoid infections

Before infection, 35 μl drops of Matrigel (Fisher Scientific) containing organoids were seeded on Nunclon Delta surface 35x10mm Dish (Thermo Scientific) and 2ml of Advanced DMEM/F12 supplemented with 1x L-Glutamine and 10mM Hepes was added to each plate. Depending on the indicated conditions, organoids were pretreated or no with 40 μM Ferrostatin-1 for 1hr before infection. Ferrostatin-1 was maintained throughout the experiment. PP34 *exoU* or *exoU*^{S142A} were grown as previously described until reach OD600 = 1. Bacterial density was adjusted to OD600 = 0.0005, and phenol red added at 0.005% to visualize successful microinjection (2). Injected organoids were individually collected and re-seeded into fresh matrix for subsequent analysis. For time-lapse imaging, injected and stimulated organoids were stained with 50 μg ml⁻¹ Propidium Iodide (Thermo Scientific). Images were acquired every 15 minutes for the duration of experiments under an EVOS M7000 (Thermo Scientific) Imaging System (10x, at 37°C with 5% CO₂). Data was analyzed using Fiji/ImageJ.

Cell necrosis, alarmin/cytokine and lipid release assays

LDH Cytotoxicity Detection Kit (Takara) was used to determine the percentage of cell lysis. Normalization of spontaneous lysis was calculated as follows: (LDH infected-LDH uninfected)/(LDH total lysis-LDH uninfected)*100.

Murine IL-1 α , IL-33, IL-36 α , IL-36 γ , HMGB1, TNF α , cytokine levels in cell supernatants or in BALFs were measured by ELISA listed in resource [Table 1](#).

Oxidized lipids isoprostanes, eicosanoids PGE2 and LTB4 were detected in cellular supernatants or BALFs using EIA kits listed in resource [Table 1](#).

Plasma membrane permeabilization assays

Cells are plated at density of 1 x 10⁵ per well in 96-well Plates or at 2x10⁵/well in 24-well plates (Corning 356640) in complete culture medium. The following day, medium is replaced by Opti-MEM supplemented with Propidium iodide (100 ng/ml) or SYTOX green (100ng/mL). Pharmacological inhibitors are added 1h before infection. Red (Propidium Iodide) or green (SYTOX) fluorescence are measured in real-time using Clariostar plate reader or an EVOS7000 microscope, both equipped with a 37°C cell incubator.

Malondialdehyde (MDA) assays

Malondialdehyde production was addressed using the MDA lipid peroxidation kit according to the manufacturer's instructions (Abcam, ab118970). Cells were lysed using 500 μl of lysis buffer supplemented with butylated hydroxytoluene. Cell lysates were centrifuged for 10 min

at 13,000 g (RCF) and the supernatants were used for MDA assay. TBA solution was added to each replicate, and samples were then incubated at 95°C for 1 hour. 100µL of each sample was then processed for fluorometric assay at Ex/Em = 532/553 nm. BAL levels of MDA were normalized to the total protein concentration.

Recombinant protein production

Plasmids coding for *exoU*^{BtU}, *exoU* or *exoU*^{S142A} were a kind gift from Dara W. Frank's lab. All recombinant proteins were expressed in BL21(DE3) pLysS strain in LB medium, according to Anderson DM et al. [31]. Proteins fused with an N-terminus hexahistidine-tag were purified as previously described with slight modifications. Briefly, after cell harvest, bacteria were lysed by sonication under ice and recombinant proteins were purified by nickel metal affinity chromatography (Takara). After sample concentration, Superose 6 was exchanged for a Superdex 200 size exclusion column (GE Healthcare) as a final purification step. Samples were either used fresh or kept at -80°C for long-term storage. ExoU and ExoUS142A activities were validated on cellular lysates (Fig 3I) based on the advices and experience of our collaborator [37].

Cytometry quantification of immune cells in mice BAL fluids (BALFs)

C57BL/6 mice received an injection of Ferrostatine (6mg/kg) or PBS as control intraperitoneally. 4-6h after, mice were infected by intranasal instillation of 50 µL of PBS containing or not 5x10⁶ bacteria (PP34) in presence or absence of Ferrostatin-1 (6mg /kg). 18h after infection, BALFs were collected and quality/quantity of immune cells content was assayed by flow cytometry. Briefly, cells were pelleted (1000 rpm, 5 minutes), Red blood cells (RBC) were removed by 10 min incubation in RBC Lysis Buffer (BioLegend), monocytes, macrophages, neutrophils, and eosinophils were subsequently stained with a cocktail of fluorochrome-conjugated antibodies detailed in the "Material and Method" section. Cells were then fixed in 4% PFA before fluorescence associated cell sorting (FACS) analysis using a LSRII instrument. AccuCheck Counting Beads (ThermoFisher) were used to determine absolute cell number. Data analysis and processing were performed using FlowJO software.

Lipid peroxidation or ROS production

To measure lipid peroxidation or ROS production, cells were first washed with PBS 1X, and then incubated with either C11-BODIPY(581/591) (ThermoFisher) at 2 µM, or H2DCFDA (ThermoFisher) at 10 µM in Opti-MEM medium for 30 min at 37°C. After three washes with PBS 1X cells are resuspended in Opti-MEM medium and infected/treated in presence or absence of pharmacological inhibitors. After 1-3h of infection, cells are washed with PBS, detached in MACS buffer (PBS-BSA 0.5%-EDTA 2mM) and samples were acquired within one hour using a flow cytometer (BD FORTESSA LSR II or a FACS Calibur). Data were analysed with FlowJO software (version 10). When specified, adherent cells loaded with Bodipy probes where infected at indicated MOIs of *P. aeruginosa* and lipid peroxidation is observed using an EVOS7000 microscope. For live imaging, the GFP brightness threshold was kept equal for all the independent experiments. Mean fluorescence intensity (MFI) was analyzed using Fiji/ImageJ.

Immunoblotting

Cell lysate generation has been described previously [85]. Briefly, proteins were loaded in 12% SDS-PAGE gels and then transferred on PVDF membranes. After saturation for 1 hour in Tris-buffered saline (TBS) supplemented with 0.05% Tween 20 containing 5% non-fat milk (pH8), membranes were exposed with antibodies at 4°C overnight (Table 1). Next day,

membranes were washed 3 times in TBS 0.1% Tween 20 and incubated with the corresponding secondary antibodies conjugated to horseradish peroxidase (HRP) (Table 1) for 1h at room temperature. Immunoblottings were revealed using a chemiluminescent substrate ECL substrate (Biorad) and images were acquired on a ChemiDoc Imaging System (Biorad). All antibodies and their working concentrations are listed in Table 1.

(Redox) lipidomic

1 million bone-marrow-derived macrophages were seeded into 6-well plates. Next day, BMDMs were transfected with recombinant ExoU or ExoU^{S142A} proteins (500ng/well) for one hour. Then, supernatant was removed, cells were washed two times in PBS. Finally, 500μL of a cold solution of 50% PBS/50% Methanol was added to cells and samples were transferred to -80°C for storage and subsequent analyses.

After thawing, lipids were extracted using a methyl-tert-butyl ether (MTBE)-based liquid-liquid extraction method. Cell suspensions (500 μL in PBS/methanol 1:1, v/v) were thawed on ice before adding 100 μL methanol MeOH containing 50 ng each of the internal standards PC (15:0/18:1-d7), PE(15:0/18:1-d7), PG(15:0/18:1-d7), PI(15:0/18:1-d7) and PS(15:0/18:1-d7) (EquisPLASH, Avanti Polar Lipids). Samples were then transferred into 8-mL screw-cap tubes, and then 1.125 methanol and 5 mL MTBE were added. After vigorous mixing, samples were incubated at room temperature on a tabletop shaker for 45 min. For phase separation, 1.25 mL water was added, and samples were vortexed and centrifuged for 15 min at 2000 x g. The upper organic phase of each sample was carefully removed using a Pasteur pipette, transferred into an empty glass round-bottom tube, and dried under vacuum in a SpeedVac concentrator. The dried lipid extracts were resuspended in 200 μL HPLC mobile phase A/mobile phase B 3:1 (v/v) for targeted lipidomic analysis of oxidized phospholipids. For LC-MS/MS, using a Sciex ExionLC Integrated System, 20 μL of each lipid extract was injected using Column Kinetex 2.6 μm HILIC 100 Å 100x2.1 mm, Phenomenex and a Flow Rate of 200 μL/min. Then, the analyte-specific m/z transition profile was determined and the area under the peak (ion intensity vs. elution time) was calculated using MultiQuant, Sciex software.

Data calculation was performed by doing ratio between the values of “area ratio analyte/internal standard” of each oxidized phospholipid and its non-oxidized phospholipid. The fold induction in oxidized phospholipid was then calculated by doing a ratio between each oxidized ratio and the non-stimulated condition. Accordingly, the unstimulated condition oxidized ratios were 1 or 0 when no peroxidation was detected in any condition.

Phospholipase activity measurement

Evaluation of ExoU phospholipase activity was performed using the Cayman Chemical cPLA2 kit and performed as previously described with minor modifications [37]. Briefly, 10 μL of a 1mg/mL (160pmols) solution of recombinant ExoU or ExoU^{S142} proteins were mixed in 96-well plates with 10μL of lysed cell samples and 10μL of Assay Buffer. Then, samples were incubated for 1 hour at room temperature with 250μL of substrate solution (1.5 mM arachidonyl thiophosphatidylcholine) and then for additional 4 or 16 hours in dark. Reaction was stopped using 25mM solution of DTNB according to manufacturer instructions and absorbance was detected at 405nm using a Clariostar plate reader. Phospholipase activity of ExoU or ExoU^{S142} was calculated as the hydrolysis rate accordingly to the manufacturer instructions.

Statistical analysis

Statistical data analysis was performed using Prism 8.0a (GraphPad Software, Inc.). We used t-test with Bonferroni correction for comparison of two groups. Data are reported as mean with

SEM. Regarding animal experiments, we used Mann-Whitney tests and mouse survival analysis were done using log-rank Cox-Mantel test. P values in figures have the following meaning; NS non-significant and Significance is specified as * $p \leq 0.05$; ** $p \leq 0.01$, *** $p \leq 0.001$.

Supporting information

S1 Data. Original immunoblotting membranes.

(TIF)

S2 Data. Numerical values obtained in the current study.

(XLSX)

S1 Fig. ExoU-dependent lung pathology in mice occurs in an inflammasome-independent manner. (A) Survival of WT, *Casp1^{-/-}/Casp11^{-/-}*, *Nlrc4^{-/-}* and *GsdmD^{-/-}* mice intranasally infected (n = 6 animals per condition) with 5.10^5 CFUs of *P. aeruginosa* PP34. Graphs represent one experiment (6 mice/group) out of three independent *in vivo* experiments. NS: Not significant using Log-rank Cox-Mantel test for survival comparisons. (B) Bronchoalveolar (BAL) and lung bacterial loads from WT, *Casp1^{-/-}/Casp11^{-/-}*, *Nlrc4^{-/-}* and *GsdmD^{-/-}* mice (n = 6) 18 hours after intranasal infection with 5.10^5 CFUs of *P. aeruginosa* PP34. Graphs represent one experiment (6 mice/group) out of three independent *in vivo* experiments. NS: Not significant using Mann-Whitney analysis test.

(TIF)

S2 Fig. Lipid peroxidation contributes to ExoU-induced necrosis in various cell types. (A, B) Measure of LDH release in various human and murine cell types infected with various *P. aeruginosa* strains expressing or not *exoU* in presence of Ferrostatin-1 (Fe1, 10 μ M) for 2 hours. (C) LDH release in BMDMs transfected with recombinant ExoU (100ng) or its catalytically inactive mutant ExoU^{S142A}, in presence of MAFP (50 μ M) or Ferrostatin-1 (Fe1, 10 μ M) for 3 hours. *** $p \leq 0.001$, T-test with Bonferroni correction. (D) Immunoblotting of ExoU secretion by *P. aeruginosa* in presence of ferrostatin-1 (20 μ M). Star (*) show non-specific bands. (E) Measure of bacterial growth (O.D 600) in presence or absence of ferrostatin-1 (10, 20 μ M) for 14 hours. (F) Measure of LDH release in *Nlrc4^{-/-}* BMDMs infected with PP34 (MOI5) in presence of Ferrostatin-1 (Fe1, 10 μ M) for 3 hours. Each hour, fresh Ferrostatin-1 (10 μ M) was added to cells (+) or not (ϕ). “pi” refers to post-infection.

(TIF)

S3 Fig. Lipid peroxidation fuels ExoU-dependent necrosis. (A) ROS production in WT BMDMs transfected with ExoU or its catalytically dead mutant ExoU^{S142A} for 45 minutes using H2DCFDA (1 μ M) probe. (B) Cytometry detection and quantification of (phospho)lipid peroxidation using the probe C11-bodipy in WT BMDMs infected with PP34^{ExoU+} or PP34^{ExoU-} (MOI 5) for 1 hour. Sample were acquired using FACSCalibur (BD). The graph shows the mean \pm SEM of one experiment performed in triplicate out of three independent experiments. * $P \leq 0.05$, for the indicated comparisons using t-test with Bonferroni correction. (C) Lipidomic analysis of the relative amount of each phospholipid upon rExoU transfection analysed in Fig 3B. (D) Representative microscopy images and time course experiment of propidium iodide uptake in WT BMDMs transfected with rExoU or its catalytically inactive mutant ExoU^{S142A} (500ng) in presence or not of ferrostatin-1 (Fe1, 10 μ M). Images show two independent experiments, each performed three times at 45 minutes or 3 hours post transfection. (E) Immunoblotting of Crispr Cas9-mediated *Cypor* gene deletion in immortalized (i)BMDMs or of *Cypor*-deficient HELA cells. The *Cypor*#2 (red) was selected for further analysis. GFP means that cells were transduced with sgRNA targeting *Gfp* and used as control. (F) Cytometry detection and

quantification of (phospho)lipid peroxidation using the probe C11-bodipy in WT or *Cypor*^{-/-} immortalized (i)BMDMs pre-treated or not for 1 hour with CuOOH (20μM) in presence or absence of Ferrostatin-1 (20μM) and then infected with PP34^{ExoU+} or PP34^{ExoU-} (MOI 5) for 1 hour. Sample were acquired using FACSCalibur (BD). The graphs shows the mean±/-SEM of one experiment performed in triplicate out of three independent experiments. *P ≤ 0.05, **P ≤ 0.001, for the indicated comparisons using t-test with Bonferroni correction. (G) Immunoblotting of Crispr Cas9-mediated *Gpx4* gene deletion in immortalized BMDMs. The Gpx4#1 (red) was selected for further analysis. CD8 and GFP means that cells were transduced with sgRNA targeting *Gfp* or *Cd8* genes and used as controls. (H) Cytometry detection and quantification of phospholipid peroxidation using the probe C11-bodipy in immortalized WT or *Gpx4*^{-/-} BMDMs using a fortessa cytometer. (I) Measure of 8-iso PGF2α isprostane in cell supernatant in WT BMDMs pre-treated or not for 1 hour with CuOOH (20μM) in presence or absence of Ferrostatin-1 (20μM) and then transfected with rExoU (500ng) for 3 hours. ***p ≤ 0.001, T-test with Bonferroni correction. (J) PGE2 and LTB4 eicosanoid release in WT BMDMs pre-treated or not for 1 hour with CuOOH (20μM) and then transfected with 100ng of ExoU or its catalytically dead mutant ExoU^{S142A} for 3 hours. (TIF)

S4 Fig. Ferrostatin-1 protects mice against ExoU-induced lung pathology. (A) Gating strategy to analyse Immune cell populations in bronchoalveolar fluids (BALFs). Immune cells were identified as CD45+ cells. Among CD45+ cells, different subset of immune cells including Interstitial/Alveolar Macrophages, Eosinophils and Neutrophils are identified based on specific cell surface marker expression. (TIF)

S1 Graphical Abstract. Host lipid peroxidation fuels ExoU-induced cell necrosis-dependent pathology. In resting cells or in cells with induced lipid peroxidation (e.g. ferroptosis pathway), ExoU (purple) becomes hyper-activated by host cell peroxidised phospholipids, which drives an exacerbated cell necrosis, alarmin and lipid release and contributes to the subsequent pathology. Consequently, targeting lipid peroxidation (ferrostatin-1) inhibits ExoU-dependent cell necrosis and attenuates the host deleterious consequences. EM and SB used Biorender.com to create this figure. (TIF)

S1 Movie. Live cell imaging of uninfected immortalized murine *Nlrc4*^{-/-} BMDMs cell death using SYTOX green. 1 “time point” corresponds to 150s. (AVI)

S2 Movie. Live cell imaging of uninfected immortalized murine *Nlrc4*^{-/-} BMDMs cell death in presence of 20μM of ferrostatin-1 using SYTOX green. 1 “time point” corresponds to 150s. (AVI)

S3 Movie. Live cell imaging of immortalized murine *Nlrc4*^{-/-} BMDMs cell death infected with *exoU*-expressing *P. aeruginosa* (MOI1) using SYTOX green. 1 “time point” corresponds to 150s. (AVI)

S4 Movie. Live cell imaging of immortalized murine *Nlrc4*^{-/-} BMDMs cell death infected with *exoU*-expressing *P. aeruginosa* (MOI1) in presence of ferrostatin-1 (20μM) using SYTOX green. 1 “time point” corresponds to 150s. (AVI)

S5 Movie. Live cell imaging of immortalized murine *Nlrc4*^{-/-} BMDMs cell death infected with *exoU*-deficient *P. aeruginosa* (MOI1) using SYTOX green. 1 “time point” corresponds to 150s.

(AVI)

S6 Movie. Live cell imaging of immortalized murine *Nlrc4*^{-/-} BMDMs cell death infected with *exoU*-deficient *P. aeruginosa* (MOI1) in presence of ferrostatin-1 (20μM) using SYTOX green. 1 “time point” corresponds to 150s.

(AVI)

S7 Movie. Live cell imaging of uninfected human bronchial organoids using Propidium Iodide up to 12 hours.

(AVI)

S8 Movie. Live cell imaging of uninfected human bronchial organoids in presence of ferrostatin-1 (40μM) using Propidium Iodide up to 12 hours.

(AVI)

S9 Movie. Live cell imaging of human bronchial organoids microinjected with *exoU*-expressing *P. aeruginosa* using Propidium Iodide up to 12 hours.

(AVI)

S10 Movie. Live cell imaging of human bronchial organoids microinjected with *exoU*-expressing *P. aeruginosa* in presence of ferrostatin-1 (40μM) using Propidium Iodide up to 12 hours.

(AVI)

S11 Movie. Live cell imaging of human bronchial organoids microinjected with *exoU*-deficient *P. aeruginosa* using Propidium Iodide up to 12 hours.

(AVI)

S12 Movie. Live cell imaging of human bronchial organoids microinjected with *exoU*-deficient *P. aeruginosa* in presence of ferrostatin-1 (40μM) using Propidium Iodide up to 12 hours.

(AVI)

Acknowledgments

Alox5^{-/-} and *Alox12/15*^{-/-} mice came from Jaxson Laboratory. *Nlrc4*^{-/-} mice were provided by Clare E. Bryant and generated by Millenium, *GsdmD*^{-/-} mice came from P. Broz (Univ of Lausanne), and *Casp1*^{-/-}/*Casp11*^{-/-} came from B. Py (ENS Lyon, France) and were generated by Junying Yuan (Harvard Med School, Boston, USA). Phospholipid redox lipidomic experiments were performed by Cayman Chemical Company (Ann Arbor, USA). Authors also acknowledge the animal facility and Cytometry/microscopy platforms of the IPBS institute. The graphical abstract was generated using Biorender.com.

Author Contributions

Conceptualization: Rémi Planès, Etienne Meunier.

Data curation: Salimata Bagayoko, Rémi Planès, Etienne Meunier.

Formal analysis: Salimata Bagayoko, Céline Cougoule, Rémi Planès, Etienne Meunier.

Funding acquisition: Yoann Rombouts, Céline Cougoule, Rémi Planès, Etienne Meunier.

Investigation: Stephen Adonai Leon-Icaza, Miriam Pinilla, Audrey Hessel, Karin Santoni, David Péricat, Pierre-Jean Bordignon, Flavie Moreau, Elif Eren, Aurélien Boyancé, Céline Berrone, Yoann Rombouts, Céline Cougoule.

Methodology: Emmanuelle Naser, Nino Iakobachvili, Arnaud Metais.

Project administration: Salimata Bagayoko, Rémi Planès, Etienne Meunier.

Resources: Lise Lefèvre, Geanncarlo Lugo-Villarino, Agnès Coste, Ina Attrée, Dara W. Frank, Hans Clevers, Peter J. Peters.

Supervision: Rémi Planès, Etienne Meunier.

Validation: Salimata Bagayoko, Rémi Planès, Etienne Meunier.

Visualization: Salimata Bagayoko, Céline Cougoule, Rémi Planès, Etienne Meunier.

Writing – original draft: Salimata Bagayoko, Rémi Planès, Etienne Meunier.

Writing – review & editing: Salimata Bagayoko, Rémi Planès, Etienne Meunier.

References

1. Galluzzi L, Vitale I, Aaronson SA, Abrams JM, Adam D, Agostinis P, et al. Molecular mechanisms of cell death: Recommendations of the Nomenclature Committee on Cell Death 2018. *Cell Death and Differentiation*. Nature Publishing Group; 2018. pp. 486–541. <https://doi.org/10.1038/s41418-017-0012-4> PMID: [29362479](https://pubmed.ncbi.nlm.nih.gov/29362479/)
2. Tang L, Lu C, Zheng G, Burgering BMT. Emerging insights on the role of gasdermins in infection and inflammatory diseases. *Clinical and Translational Immunology*. John Wiley and Sons Inc; 2020. <https://doi.org/10.1002/cti2.1186> PMID: [33033617](https://pubmed.ncbi.nlm.nih.gov/33033617/)
3. Bedoui S, Herold MJ, Strasser A. Emerging connectivity of programmed cell death pathways and its physiological implications. *Nature Reviews Molecular Cell Biology*. Nature Research; 2020. pp. 678–695. <https://doi.org/10.1038/s41580-020-0270-8> PMID: [32873928](https://pubmed.ncbi.nlm.nih.gov/32873928/)
4. Place DE, Lee SJ, Kanneganti TD. PANoptosis in microbial infection. *Current Opinion in Microbiology*. Elsevier Ltd; 2021. pp. 42–49. <https://doi.org/10.1016/j.mib.2020.07.012> PMID: [32829024](https://pubmed.ncbi.nlm.nih.gov/32829024/)
5. Dixon SJ, Lemberg KM, Lamprecht MR, Skouta R, Zaitsev EM, Gleason CE, et al. Ferroptosis: An iron-dependent form of nonapoptotic cell death. *Cell*. 2012; 149: 1060–1072. <https://doi.org/10.1016/j.cell.2012.03.042> PMID: [22632970](https://pubmed.ncbi.nlm.nih.gov/22632970/)
6. Conrad M, Kagan VE, Bayir H, Pagnussat GC, Head B, Traber MG, et al. Regulation of lipid peroxidation and ferroptosis in diverse species. *Genes and Development*. Cold Spring Harbor Laboratory Press; 2018. pp. 602–619. <https://doi.org/10.1101/gad.314674.118> PMID: [29802123](https://pubmed.ncbi.nlm.nih.gov/29802123/)
7. Jenkins NL, James SA, Salim A, Sumardy F, Speed TP, Conrad M, et al. Changes in ferrous iron and glutathione promote ferroptosis and frailty in aging *Caenorhabditis elegans*. *Elife*. 2020; 9: 1–28. <https://doi.org/10.7554/eLife.56580> PMID: [32690135](https://pubmed.ncbi.nlm.nih.gov/32690135/)
8. Bogacz M, Krauth-Siegel RL. Tryparedoxin peroxidase-deficiency commits trypanosomes to ferroptosis-type cell death. *Elife*. 2018;7. <https://doi.org/10.7554/eLife.37503> PMID: [30047863](https://pubmed.ncbi.nlm.nih.gov/30047863/)
9. Bochkov VN, Oskolkova O V., Birukov KG, Levonen AL, Binder CJ, Stöckl J. Generation and biological activities of oxidized phospholipids. *Antioxidants and Redox Signaling*. Mary Ann Liebert, Inc.; 2010. pp. 1009–1059. <https://doi.org/10.1089/ars.2009.2597> PMID: [19686040](https://pubmed.ncbi.nlm.nih.gov/19686040/)
10. Tyurina YY, Tyurin VA, Anthonymuthu T, Amoscato AA, Sparvero LJ, Nesterova AM, et al. “Redox lipomics technology: Looking for a needle in a haystack.” *Chemistry and Physics of Lipids*. Elsevier Ireland Ltd; 2019. pp. 93–107. <https://doi.org/10.1016/j.chemphyslip.2019.03.012> PMID: [30928338](https://pubmed.ncbi.nlm.nih.gov/30928338/)
11. Bersuker K, Hendricks JM, Li Z, Magtanong L, Ford B, Tang PH, et al. The CoQ oxidoreductase FSP1 acts parallel to GPX4 to inhibit ferroptosis. *Nature*. 2019; 575: 688–692. <https://doi.org/10.1038/s41586-019-1705-2> PMID: [31634900](https://pubmed.ncbi.nlm.nih.gov/31634900/)
12. Doll S, Freitas FP, Shah R, Aldrovandi M, da Silva MC, Ingold I, et al. FSP1 is a glutathione-independent ferroptosis suppressor. *Nature*. 2019; 575: 693–698. <https://doi.org/10.1038/s41586-019-1707-0> PMID: [31634899](https://pubmed.ncbi.nlm.nih.gov/31634899/)

13. Conrad M, Pratt DA. The chemical basis of ferroptosis. *Nat Chem Biol*. 2019; 15: 1137–1147. <https://doi.org/10.1038/s41589-019-0408-1> PMID: 31740834
14. Yang WS, Kim KJ, Gaschler MM, Patel M, Shchepinov MS, Stockwell BR. Peroxidation of polyunsaturated fatty acids by lipoxygenases drives ferroptosis. *Proc Natl Acad Sci U S A*. 2016; 113: E4966–E4975. <https://doi.org/10.1073/pnas.1603244113> PMID: 27506793
15. Doll S, Proneth B, Tyurina YY, Panzilius E, Kobayashi S, Ingold I, et al. ACSL4 dictates ferroptosis sensitivity by shaping cellular lipid composition. *Nat Chem Biol*. 2017; 13: 91–98. <https://doi.org/10.1038/nchembio.2239> PMID: 27842070
16. Kagan VE, Mao G, Qu F, Angeli JPF, Doll S, Croix CS, et al. Oxidized arachidonic and adrenic PEs navigate cells to ferroptosis. *Nat Chem Biol*. 2017; 13: 81–90. <https://doi.org/10.1038/nchembio.2238> PMID: 27842066
17. Wiernicki B, Dubois H, Tyurina YY, Hassannia B, Bayir H, Kagan VE, et al. Excessive phospholipid peroxidation distinguishes ferroptosis from other cell death modes including pyroptosis. *Cell Death Dis*. 2020; 11: 922. <https://doi.org/10.1038/s41419-020-03118-0> PMID: 33110056
18. Stockwell BR, Jiang X, Gu W. Emerging Mechanisms and Disease Relevance of Ferroptosis. 2020 [cited 13 Nov 2020]. <https://doi.org/10.1016/j.tcb.2020.02.009> PMID: 32413317
19. Amaral EP, Costa DL, Namasivayam S, Riteau N, Kamenyeva O, Mittereder L, et al. A major role for ferroptosis in *Mycobacterium tuberculosis*-induced cell death and tissue necrosis. *J Exp Med*. 2019; 216: 556–570. <https://doi.org/10.1084/jem.20181776> PMID: 30787033
20. Li N, Wang W, Zhou H, Wu Q, Duan M, Liu C, et al. Ferritinophagy-mediated ferroptosis is involved in sepsis-induced cardiac injury. *Free Radic Biol Med*. 2020; 160: 303–318. <https://doi.org/10.1016/j.freeradbiomed.2020.08.009> PMID: 32846217
21. Zhu H, Santo A, Jia Z, Li Y. GPx4 in Bacterial Infection and Polymicrobial Sepsis: Involvement of Ferroptosis and Pyroptosis. *React Oxyg Species*. 2019; 7: 154. <https://doi.org/10.20455/ros.2019.835> PMID: 31106276
22. Dar HH, Tyurina YY, Mikulska-Ruminska K, Shrivastava I, Ting HC, Tyurin VA, et al. *Pseudomonas aeruginosa* utilizes host polyunsaturated phosphatidylethanolamines to trigger theft-ferroptosis in bronchial epithelium. *J Clin Invest*. 2018; 128: 4639–4653. <https://doi.org/10.1172/JCI99490> PMID: 30198910
23. Meunier E, Neyrolles O. Die another way: Ferroptosis drives tuberculosis pathology. *J Exp Med*. 2019; 216: 471–473. <https://doi.org/10.1084/jem.20190038> PMID: 30787032
24. Friedmann Angeli JP, Schneider M, Proneth B, Tyurina YY, Tyurin VA, Hammond VJ, et al. Inactivation of the ferroptosis regulator Gpx4 triggers acute renal failure in mice. *Nat Cell Biol*. 2014; 16: 1180–1191. <https://doi.org/10.1038/ncb3064> PMID: 25402683
25. Yan1 B, Ai1 Y, Zhang1 Z, Sun1 Q, Ma1 Y, Zhang1 Z, et al. Oxidoreductases generate hydrogen peroxide that drives iron-dependent lipid peroxidation during ferroptosis 2 The inhibition of antioxidant systems of glutathione peroxidase 4 (GPX4) or ferroptosis suppressor protein 1 (FSP1) causes iron-dependent peroxid. *bioRxiv*. 2020; 2020.08.01.231993. <https://doi.org/10.1101/2020.08.01.231993>
26. Zou Y, Li H, Graham ET, Deik AA, Eaton JK, Wang W, et al. Cytochrome P450 oxidoreductase contributes to phospholipid peroxidation in ferroptosis. *Nat Chem Biol*. 2020; 16: 302–309. <https://doi.org/10.1038/s41589-020-0472-6> PMID: 32080622
27. Howell HA, Logan LK, Hauser AR. Type III secretion of ExoU is critical during early *Pseudomonas aeruginosa* Pneumonia. *MBio*. 2013;4. <https://doi.org/10.1128/mBio.00032-13> PMID: 23481600
28. Gendrin C, Contreras-Martel C, Bouillot S, Elsen S, Lemaire D, Skoufias DA, et al. Structural Basis of Cytotoxicity Mediated by the Type III Secretion Toxin ExoU from *Pseudomonas aeruginosa*. Saper MA, editor. *PLoS Pathog*. 2012; 8: e1002637. <https://doi.org/10.1371/journal.ppat.1002637> PMID: 22496657
29. Phillips RM, Six DA, Dennis EA, Ghosh P. In Vivo Phospholipase Activity of the *Pseudomonas aeruginosa* Cytotoxin ExoU and Protection of Mammalian Cells with Phospholipase A2 Inhibitors. *J Biol Chem*. 2003; 278: 41326–41332. <https://doi.org/10.1074/jbc.M302472200> PMID: 12915403
30. Sato H, Frank DW. ExoU is a potent intracellular phospholipase. *Molecular Microbiology*. *Mol Microbiol*; 2004. pp. 1279–1290. <https://doi.org/10.1111/j.1365-2958.2004.04194.x> PMID: 15387809
31. Anderson DM, Sato H, Dirck AT, Feix JB, Frank DW. Ubiquitin activates patatin-like phospholipases from multiple bacterial species. *J Bacteriol*. 2015; 197: 529–541. <https://doi.org/10.1128/JB.02402-14> PMID: 25404699
32. Wilson SK, Knoll LJ. Patatin-like phospholipases in microbial infections with emerging roles in fatty acid metabolism and immune regulation by Apicomplexa. *Molecular Microbiology*. Blackwell Publishing Ltd; 2018. pp. 34–46. <https://doi.org/10.1111/mmi.13871> PMID: 29090840
33. Dessen A. Phospholipase A2 enzymes: Structural diversity in lipid messenger metabolism. *Structure*. *Current Biology Ltd*; 2000. pp. R15–R22. [https://doi.org/10.1016/s0969-2126\(00\)00097-6](https://doi.org/10.1016/s0969-2126(00)00097-6) PMID: 10673441

34. Sitkiewicz I, Nagiec MJ, Sumbly P, Butler SD, Cywes-Bentley C, Musser JM. Emergence of a bacterial clone with enhanced virulence by acquisition of a phage encoding a secreted phospholipase A2. *Proc Natl Acad Sci U S A*. 2006; 103: 16009–16014. <https://doi.org/10.1073/pnas.0607669103> PMID: [17043230](https://pubmed.ncbi.nlm.nih.gov/17043230/)
35. Diaz MH, Hauser AR. *Pseudomonas aeruginosa* cytotoxin ExoU is injected into phagocytic cells during acute pneumonia. *Infect Immun*. 2010; 78: 1447–1456. <https://doi.org/10.1128/IAI.01134-09> PMID: [20100855](https://pubmed.ncbi.nlm.nih.gov/20100855/)
36. Rabin SDP, Hauser AR. *Pseudomonas aeruginosa* ExoU, a toxin transported by the type III secretion system, kills *Saccharomyces cerevisiae*. *Infect Immun*. 2003; 71: 4144–4150. <https://doi.org/10.1128/IAI.71.7.4144-4150.2003> PMID: [12819106](https://pubmed.ncbi.nlm.nih.gov/12819106/)
37. Deruelle V, Bouillot S, Job V, Taillebourg E, Fauvarque M-O, Attrée I, et al. The bacterial toxin ExoU requires a host trafficking chaperone for transportation and to induce necrosis. *bioRxiv*. 2020; 2020.11.04.367706. <https://doi.org/10.1101/2020.11.04.367706>
38. Machado GB, de Oliveira A V., Saliba AM, de Lima CDM, Suassuna JHR, Plotkowski MC. *Pseudomonas aeruginosa* toxin ExoU induces a PAF-dependent impairment of alveolar fibrin turnover secondary to enhanced activation of coagulation and increased expression of plasminogen activator inhibitor-1 in the course of mice pneumosepsis. *Respir Res*. 2011; 12: 104. <https://doi.org/10.1186/1465-9921-12-104> PMID: [21819560](https://pubmed.ncbi.nlm.nih.gov/21819560/)
39. Pazos MA, Lanter BB, Yonker LM, Eaton AD, Pirzai W, Gronert K, et al. *Pseudomonas aeruginosa* ExoU augments neutrophil transepithelial migration. *PLoS Pathog*. 2017;13. <https://doi.org/10.1371/journal.ppat.1006548> PMID: [28771621](https://pubmed.ncbi.nlm.nih.gov/28771621/)
40. Saliba AM, Nascimento DO, Silva MCA, Assis MC, Gayer CRM, Raymond B, et al. Eicosanoid-mediated proinflammatory activity of *pseudomonas aeruginosa* ExoU. *Cell Microbiol*. 2005; 7: 1811–1822. <https://doi.org/10.1111/j.1462-5822.2005.00635.x> PMID: [16309466](https://pubmed.ncbi.nlm.nih.gov/16309466/)
41. da Cunha LG, Ferreira MF, de Moraes JA, Reis PA, Castro-Faria-Neto HC, Barja-Fidalgo C, et al. ExoU-induced redox imbalance and oxidative stress in airway epithelial cells during *Pseudomonas aeruginosa* pneumosepsis. *Med Microbiol Immunol*. 2015; 204: 673–680. <https://doi.org/10.1007/s00430-015-0418-x> PMID: [25904542](https://pubmed.ncbi.nlm.nih.gov/25904542/)
42. Al Moussawi K, Kazmierczak BI. Distinct contributions of interleukin-1 α (IL-1 α) and IL-1 β to innate immune recognition of *Pseudomonas aeruginosa* in the lung. *Infect Immun*. 2014; 82: 4204–4211. <https://doi.org/10.1128/IAI.02218-14> PMID: [25069982](https://pubmed.ncbi.nlm.nih.gov/25069982/)
43. Shaver CM, Hauser AR. Relative contributions of *Pseudomonas aeruginosa* ExoU, ExoS, and ExoT to virulence in the lung. *Infect Immun*. 2004; 72: 6969–6977. <https://doi.org/10.1128/IAI.72.12.6969-6977.2004> PMID: [15557619](https://pubmed.ncbi.nlm.nih.gov/15557619/)
44. Miao EA, Ernst RK, Dors M, Mao DP, Aderem A. *Pseudomonas aeruginosa* activates caspase 1 through Ipaf. *Proc Natl Acad Sci U S A*. 2008; 105: 2562–2567. <https://doi.org/10.1073/pnas.0712183105> PMID: [18256184](https://pubmed.ncbi.nlm.nih.gov/18256184/)
45. Eren E, Planès R, Buyck J, Bordignon P-J, Colom A, Cunrath O, et al. Type-3 Secretion System–induced pyroptosis protects *Pseudomonas* against cell-autonomous immunity. *bioRxiv*. 2019; 650333. <https://doi.org/10.1101/650333>
46. Santos JC, Dick MS, Lagrange B, Degrandi D, Pfeffer K, Yamamoto M, et al. LPS targets host guanylate-binding proteins to the bacterial outer membrane for non-canonical inflammasome activation. *EMBO J*. 2018;37. <https://doi.org/10.15252/embj.201798089> PMID: [29459437](https://pubmed.ncbi.nlm.nih.gov/29459437/)
47. Bitto NJ, Baker PJ, Dowling JK, Wray-McCann G, De Paoli A, Tran LS, et al. Membrane vesicles from *Pseudomonas aeruginosa* activate the noncanonical inflammasome through caspase-5 in human monocytes. *Immunol Cell Biol*. 2018; 96: 1120–1130. <https://doi.org/10.1111/imcb.12190> PMID: [30003588](https://pubmed.ncbi.nlm.nih.gov/30003588/)
48. Franchi L, Stoolman J, Kanneganti TD, Verma A, Ramphal R, Núñez G. Critical role for Ipaf in *Pseudomonas aeruginosa*-induced caspase-1 activation. *Eur J Immunol*. 2007; 37: 3030–3039. <https://doi.org/10.1002/eji.200737532> PMID: [17935074](https://pubmed.ncbi.nlm.nih.gov/17935074/)
49. Balakrishnan A, Karki R, Berwin B, Yamamoto M, Kanneganti T-D. Guanylate binding proteins facilitate caspase-11-dependent pyroptosis in response to type 3 secretion system-negative *Pseudomonas aeruginosa*. *Cell Death Discov*. 2018; 4: 66. <https://doi.org/10.1038/s41420-018-0068-z> PMID: [30062052](https://pubmed.ncbi.nlm.nih.gov/30062052/)
50. Sutterwala FS, Mijares LA, Li L, Ogura Y, Kazmierczak BI, Flavell RA. Immune recognition of *Pseudomonas aeruginosa* mediated by the IPAF/NLRC4 inflammasome. *J Exp Med*. 2007; 204: 3235–3245. <https://doi.org/10.1084/jem.20071239> PMID: [18070936](https://pubmed.ncbi.nlm.nih.gov/18070936/)
51. Cohen TS, Prince AS. Activation of inflammasome signaling mediates pathology of acute *P. aeruginosa* pneumonia. *J Clin Invest*. 2013; 123: 1630–1637. <https://doi.org/10.1172/JCI66142> PMID: [23478406](https://pubmed.ncbi.nlm.nih.gov/23478406/)
52. Faure E, Mear JB, Faure K, Normand S, Couturier-Maillard A, Grandjean T, et al. *Pseudomonas aeruginosa* type-3 secretion system dampens host defense by exploiting the NLRC4-coupled inflammasome. *Am J Respir Crit Care Med*. 2014; 189: 799–811. <https://doi.org/10.1164/rccm.201307-1358OC> PMID: [24555512](https://pubmed.ncbi.nlm.nih.gov/24555512/)





53. Iannitti RG, Napolioni V, Oikonomou V, De Luca A, Galosi C, Pariano M, et al. IL-1 receptor antagonist ameliorates inflammasome-dependent inflammation in murine and human cystic fibrosis. *Nat Commun*. 2016; 7: 1–16. <https://doi.org/10.1038/ncomms10791> PMID: 26972847
54. Aoyagi T, Newstead MW, Zeng X, Nanjo Y, Peters-Golden M, Kaku M, et al. Interleukin-36γ and IL-36 receptor signaling mediate impaired host immunity and lung injury in cytotoxic *Pseudomonas aeruginosa* pulmonary infection: Role of prostaglandin E2. *PLoS Pathog*. 2017;13. <https://doi.org/10.1371/journal.ppat.1006737> PMID: 29166668
55. Yang D, Han Z, Oppenheim JJ. Alarmins and immunity. *Immunological Reviews*. Blackwell Publishing Ltd; 2017. pp. 41–56. <https://doi.org/10.1111/imr.12577> PMID: 29027222
56. Saliba AM, De Assis MC, Nishi R, Raymond B, Marques EDA, Lopes UG, et al. Implications of oxidative stress in the cytotoxicity of *Pseudomonas aeruginosa* ExoU. *Microbes Infect*. 2006; 8: 450–459. <https://doi.org/10.1016/j.micinf.2005.07.011> PMID: 16293434
57. Skouta R, Dixon SJ, Wang J, Dunn DE, Orman M, Shimada K, et al. Ferrostatis inhibit oxidative lipid damage and cell death in diverse disease models. *J Am Chem Soc*. 2014; 136: 4551–4556. <https://doi.org/10.1021/ja411006a> PMID: 24592866
58. Tamura M, Ajayi T, Allmond LR, Moriyama K, Wiener-Kronish JP, Sawa T. Lysophospholipase A activity of *Pseudomonas aeruginosa* type III secretory toxin ExoU. *Biochem Biophys Res Commun*. 2004; 316: 323–331. <https://doi.org/10.1016/j.bbrc.2004.02.050> PMID: 15020221
59. Lovatt M, Adnan K, Kocaba V, Dirisamer M, Peh GSL, Mehta JS. Peroxiredoxin-1 regulates lipid peroxidation in corneal endothelial cells. *Redox Biol*. 2020; 30: 101417. <https://doi.org/10.1016/j.redox.2019.101417> PMID: 31901729
60. Beatty A, Singh T, Tyurina YY, Nicolas E, Maslar K, Zhou Y, et al. Conjugated linolenic fatty acids trigger ferroptosis in triple-negative breast cancer. [cited 11 Jan 2021]. <https://doi.org/10.1101/556084>
61. Lu B, Chen X, Hong Y, Cai Z, Zhu H, He Q, Jun, Yang B, et al. Identification of PRDX6 as a regulator of ferroptosis. *Acta Pharmacol Sin*. 2019; 40: 1334–1342. <https://doi.org/10.1038/s41401-019-0233-9> PMID: 31036877
62. Beharier O, Tyurin VA, Goff JP, Guerrero-Santoro J, Kajiwarra K, Chu T, et al. PLA2G6 guards placental trophoblasts against ferroptotic injury. *Proc Natl Acad Sci U S A*. 2020; 117: 27319–27328. <https://doi.org/10.1073/pnas.2009201117> PMID: 33087576
63. Sadikot RT, Zeng H, Azim AC, Joo M, Dey SK, Beyer RM, et al. Bacterial clearance of *Pseudomonas aeruginosa* is enhanced by the inhibition of COX-2. *Eur J Immunol*. 2007; 37: 1001–1009. <https://doi.org/10.1002/eji.200636636> PMID: 17330822
64. Tyurin VA, Balasubramanian K, Winnica D, Tyurina YY, Vikulina AS, He RR, et al. Oxidatively modified phosphatidylserines on the surface of apoptotic cells are essential phagocytic “eat-me” signals: Cleavage and inhibition of phagocytosis by Lp-PLA2. *Cell Death Differ*. 2014; 21: 825–835. <https://doi.org/10.1038/cdd.2014.1> PMID: 24464221
65. Magtanong L, Ko PJ, To M, Cao JY, Forcina GC, Tarangelo A, et al. Exogenous Monounsaturated Fatty Acids Promote a Ferroptosis-Resistant Cell State. *Cell Chem Biol*. 2019; 26: 420–432.e9. <https://doi.org/10.1016/j.chembiol.2018.11.016> PMID: 30686757
66. Zou Y, Henry WS, Ricq EL, Graham ET, Phadnis V V., Maretich P, et al. Plasticity of ether lipids promotes ferroptosis susceptibility and evasion. *Nature*. 2020; 585: 603–608. <https://doi.org/10.1038/s41586-020-2732-8> PMID: 32939090
67. Kinsey GR, Blum JL, Covington MD, Cummings BS, McHowat J, Schnellmann RG. Decreased iPLA2γ expression induces lipid peroxidation and cell death and sensitizes cells to oxidant-induced apoptosis. *J Lipid Res*. 2008; 49: 1477–1487. <https://doi.org/10.1194/jlr.M800030-JLR200> PMID: 18398221
68. Miyamoto S, Dupas C, Murota K, Terao J. Phospholipid hydroperoxides are detoxified by phospholipase A2 and GSH peroxidase in rat gastric mucosa. *Lipids*. 2003; 38: 641–649. <https://doi.org/10.1007/s11745-003-1109-6> PMID: 12934674
69. van Kuijk FJGM, Sevastian A, Handelman GJ, Dratz EA. A new role for phospholipase A2: protection of membranes from lipid peroxidation damage. *Trends Biochem Sci*. 1987; 12: 31–34. [https://doi.org/10.1016/0968-0004\(87\)90014-4](https://doi.org/10.1016/0968-0004(87)90014-4)
70. Sevastian A, Wratten M, Lou, McLeod LL, Kim E. Lipid peroxidation and phospholipase A2 activity in liposomes composed of unsaturated phospholipids: a structural basis for enzyme activation. *Biochim Biophys Acta (BBA)/Lipids Lipid Metab*. 1988; 961: 316–327. [https://doi.org/10.1016/0005-2760\(88\)90079-3](https://doi.org/10.1016/0005-2760(88)90079-3) PMID: 3401498
71. Yedgar S, Cohen Y, Shoseyov D. Control of phospholipase A2 activities for the treatment of inflammatory conditions. *Biochimica et Biophysica Acta—Molecular and Cell Biology of Lipids*. Elsevier; 2006. pp. 1373–1382. <https://doi.org/10.1016/j.bbalip.2006.08.003> PMID: 16978919

72. Kienesberger PC, Oberer M, Lass A, Zechner R. Mammalian patatin domain containing proteins: A family with diverse lipolytic activities involved in multiple biological functions. *Journal of Lipid Research*. American Society for Biochemistry and Molecular Biology; 2009. p. S63. <https://doi.org/10.1194/jlr.R800082-JLR200> PMID: [19029121](https://pubmed.ncbi.nlm.nih.gov/19029121/)
73. Hiu JJ, Yap MKK. Cytotoxicity of snake venom enzymatic toxins: Phospholipase A2 and L-amino acid oxidase. *Biochemical Society Transactions*. Portland Press Ltd; 2020. pp. 719–731. <https://doi.org/10.1042/BST20200110> PMID: [32267491](https://pubmed.ncbi.nlm.nih.gov/32267491/)
74. Flores-Díaz M, Monturiol-Gross L, Naylor C, Alape-Girón A, Flieger A. Bacterial Sphingomyelinases and Phospholipases as Virulence Factors. *Microbiol Mol Biol Rev*. 2016; 80: 597–628. <https://doi.org/10.1128/MMBR.00082-15> PMID: [27307578](https://pubmed.ncbi.nlm.nih.gov/27307578/)
75. Sitkiewicz I, Stockbauer KE, Musser JM. Secreted bacterial phospholipase A2 enzymes: better living through phospholipolysis. *Trends Microbiol*. 2007; 15: 63–69. <https://doi.org/10.1016/j.tim.2006.12.003> PMID: [17194592](https://pubmed.ncbi.nlm.nih.gov/17194592/)
76. Palm NW, Rosenstein RK, Yu S, Schenten DD, Florsheim E, Medzhitov R. Bee venom phospholipase A2 induces a primary type 2 response that is dependent on the receptor ST2 and confers protective immunity. *Immunity*. 2013; 39: 976–985. <https://doi.org/10.1016/j.immuni.2013.10.006> PMID: [24210353](https://pubmed.ncbi.nlm.nih.gov/24210353/)
77. Cayrol C, Duval A, Schmitt P, Roga S, Camus M, Stella A, et al. Environmental allergens induce allergic inflammation through proteolytic maturation of IL-33. *Nat Immunol*. 2018; 19: 375–385. <https://doi.org/10.1038/s41590-018-0067-5> PMID: [29556000](https://pubmed.ncbi.nlm.nih.gov/29556000/)
78. Kain HS, Glennon EKK, Vijayan K, Arang N, Douglass AN, Fortin CL, et al. Liver stage malaria infection is controlled by host regulators of lipid peroxidation. *Cell Death Differ*. 2020; 27: 44–54. <https://doi.org/10.1038/s41418-019-0338-1> PMID: [31065106](https://pubmed.ncbi.nlm.nih.gov/31065106/)
79. Lefèvre L, Authier H, Stein S, Majorel C, Couderc B, Dardenne C, et al. LRH-1 mediates anti-inflammatory and antifungal phenotype of IL-13-activated macrophages through the PPAR γ ligand synthesis. *Nat Commun*. 2015; 6: 1–13. <https://doi.org/10.1038/ncomms7801> PMID: [25873311](https://pubmed.ncbi.nlm.nih.gov/25873311/)
80. Man SM, Hopkins LJ, Nugent E, Cox S, Glöck IM, Tourlomousis P, et al. Inflammasome activation causes dual recruitment of NLRC4 and NLRP3 to the same macromolecular complex. *Proc Natl Acad Sci U S A*. 2014; 111: 7403–7408. <https://doi.org/10.1073/pnas.1402911111> PMID: [24803432](https://pubmed.ncbi.nlm.nih.gov/24803432/)
81. Li P, Allen H, Banerjee S, Franklin S, Herzog L, Johnston C, et al. Mice deficient in IL-1 β -converting enzyme are defective in production of mature IL-1 β and resistant to endotoxic shock. *Cell*. 1995; 80: 401–411. [https://doi.org/10.1016/0092-8674\(95\)90490-5](https://doi.org/10.1016/0092-8674(95)90490-5) PMID: [7859282](https://pubmed.ncbi.nlm.nih.gov/7859282/)
82. Demarco B, Grayczyk JP, Bjanec E, Roy D Le, Tonnus W, Assenmacher CA, et al. Caspase-8-dependent gasdermin D cleavage promotes antimicrobial defense but confers susceptibility to TNF-induced lethality. *Sci Adv*. 2020; 6: 3465–3483. <https://doi.org/10.1126/sciadv.abc3465> PMID: [33208362](https://pubmed.ncbi.nlm.nih.gov/33208362/)
83. Bartfeld S, Clevers H. Organoids as model for infectious diseases: Culture of human and murine stomach organoids and microinjection of helicobacter pylori. *J Vis Exp*. 2015;2015. <https://doi.org/10.3791/53359> PMID: [26650279](https://pubmed.ncbi.nlm.nih.gov/26650279/)
84. Sachs N, Papaspyropoulos A, Zomer-van Ommen DD, Heo I, Böttinger L, Klay D, et al. Long-term expanding human airway organoids for disease modeling. *EMBO J*. 2019;38. <https://doi.org/10.15252/embj.2018100300> PMID: [30643021](https://pubmed.ncbi.nlm.nih.gov/30643021/)
85. Eren E, Planès R, Bagayoko S, Bordignon P, Chaoui K, Hessel A, et al. Irgm2 and Gate-16 cooperatively dampen Gram-negative bacteria-induced caspase-11 response. *EMBO Rep*. 2020; 21. <https://doi.org/10.15252/embr.202050829> PMID: [33124769](https://pubmed.ncbi.nlm.nih.gov/33124769/)
86. Dyer KD, Moser JM, Czapiga M, Siegel SJ, Percopo CM, Rosenberg HF. Functionally Competent Eosinophils Differentiated Ex Vivo in High Purity from Normal Mouse Bone Marrow. *J Immunol*. 2008; 181: 4004–4009. <https://doi.org/10.4049/jimmunol.181.6.4004> PMID: [18768855](https://pubmed.ncbi.nlm.nih.gov/18768855/)
87. Troegeler A, Lastrucci C, Duval C, Tanne A, Cougoule C, Maridonneau-Parini I, et al. An efficient siRNA-mediated gene silencing in primary human monocytes, dendritic cells and macrophages. *Immunol Cell Biol*. 2014; 92: 699–708. <https://doi.org/10.1038/icb.2014.39> PMID: [24890643](https://pubmed.ncbi.nlm.nih.gov/24890643/)

3. Irgm2 and Gate-16 cooperatively dampen Gram-negative bacteria-induced caspase-11 response

Contribution: In this paper I participated in the help of the realization of the western blot during the revisions of the paper.

Irgm2 and Gate-16 cooperatively dampen Gram-negative bacteria-induced caspase-11 response

Elif Eren^{1,†} , Rémi Planès^{1,†}, Salimata Bagayoko¹ , Pierre-Jean Bordignon¹, Karima Chaoui^{1,2}, Audrey Hessel¹, Karin Santoni¹, Miriam Pinilla¹, Brice Lagrange³, Odile Burlet-Schiltz^{1,2}, Jonathan C Howard⁴, Thomas Henry³ , Masahiro Yamamoto^{5,6} & Etienne Meunier^{1,†,*} 

Abstract

Inflammatory caspase-11 (rodent) and caspases-4/5 (humans) detect the Gram-negative bacterial component LPS within the host cell cytosol, promoting activation of the non-canonical inflammasome. Although non-canonical inflammasome-induced pyroptosis and IL-1-related cytokine release are crucial to mount an efficient immune response against various bacteria, their unrestrained activation drives sepsis. This suggests that cellular components tightly control the threshold level of the non-canonical inflammasome in order to ensure efficient but non-deleterious inflammatory responses. Here, we show that the IFN-inducible protein Irgm2 and the ATG8 family member Gate-16 cooperatively counteract Gram-negative bacteria-induced non-canonical inflammasome activation, both in cultured macrophages and *in vivo*. Specifically, the Irgm2/Gate-16 axis dampens caspase-11 targeting to intracellular bacteria, which lowers caspase-11-mediated pyroptosis and cytokine release. Deficiency in *Irgm2* or *Gate16* induces both guanylate binding protein (GBP)-dependent and GBP-independent routes for caspase-11 targeting to intracellular bacteria. Our findings identify molecular effectors that fine-tune bacteria-activated non-canonical inflammasome responses and shed light on the understanding of the immune pathways they control.

Keywords Caspase-11; Gate-16; infections/Interferons; Irgm2; non-canonical inflammasome

Subject Categories Autophagy & Cell Death; Immunology; Microbiology, Virology & Host Pathogen Interaction

DOI 10.15252/embr.202050829 | Received 7 May 2020 | Revised 11 September 2020 | Accepted 25 September 2020 | Published online 30 October 2020

EMBO Reports (2020) 21: e50829

See also: R Finethy *et al* and A Linder & V Hornung (November 2020)

Introduction

Inflammasomes are cytosolic innate immune complexes that initiate inflammatory responses upon sensing of microbe- and damage-associated molecular patterns (MAMPs and DAMPs, respectively) (Hayward *et al*, 2018). Specifically, the rodent caspase-11 (and its human orthologs caspase-4 and caspase-5) detects the presence of the Gram-negative bacterial cell wall component lipopolysaccharide (LPS) within the host cell cytosol (Kayagaki *et al*, 2011, 2013; Broz *et al*, 2012; Aachoui *et al*, 2013; Hagar *et al*, 2013; Yang *et al*, 2015). LPS interaction with the caspase activation and recruitment domain (CARD) of caspase-11 promotes its oligomerization and activation, which triggers the activation of the non-canonical inflammasome (Yang *et al*, 2015). Upon activation (Lee *et al*, 2018), caspase-11 cleaves and activates the pyroptosis executioner gasdermin-D (gsdmD) into the p30 active fragment (Kayagaki *et al*, 2015; Shi *et al*, 2015). Cleaved gsdmD then forms a pore into phosphatidylinositol-4,5-bisphosphate (PIP2)-enriched domains at the plasma membrane, which triggers pyroptosis, a pro-inflammatory form of cell death (Shi *et al*, 2015; Aglietti *et al*, 2016; Liu *et al*, 2016; Sborgi *et al*, 2016). In parallel, gsdmD pore-induced ionic perturbations also trigger activation of the canonical NLRP3 inflammasome, which results in the caspase-1-dependent maturation of the pro-inflammatory cytokines interleukins (IL)-1 β and IL-18 (Kayagaki *et al*, 2011; Rühl & Broz,

- Institute of Pharmacology and Structural Biology (IPBS), CNRS, UMR5089, University of Toulouse, Toulouse, France
 - Mass Spectrometry Core Facility, Institute of Pharmacology and Structural Biology (IPBS), CNRS, UMR5089, University of Toulouse, Toulouse, France
 - CIRI, Centre International de Recherche en Infectiologie, Inserm, U1111, CNRS, UMR5308, École Normale Supérieure de Lyon, Université Claude Bernard Lyon 1, Univ Lyon, Lyon, France
 - Fundação Calouste Gulbenkian, Instituto Gulbenkian de Ciência, Oeiras, Portugal
 - Department of Immunoparasitology, Research Institute for Microbial Diseases, Osaka University, Osaka, Japan
 - Laboratory of Immunoparasitology, WPI Immunology Frontier Research Center, Osaka University, Osaka, Japan
- *Corresponding author. Tel: +33 0 561175832; E-mail: etienne.meunier@ipbs.fr
[†]These authors contributed equally to this work
[‡]Present Address: Institute of Pharmacology and Structural Biology (IPBS), CNRS, Toulouse, France

2015; Schmid-Burgk *et al.*, 2015). Although caspase-11 confers host protection against intracellular Gram-negative bacteria (Aachoui *et al.*, 2013; Cerqueira *et al.*, 2018; Chen *et al.*, 2018), its unrestrained activation provokes irreversible organ failure, blood clotting and sepsis (Kayagaki *et al.*, 2011, 2013, 2015; Napier *et al.*, 2016; Cheng *et al.*, 2017; Deng *et al.*, 2018; Rathinam *et al.*, 2019; Yang *et al.*, 2019). This suggests that host regulators might fine-tune the non-canonical inflammasome in order to optimize caspase-11-dependent response. To date, only few of them were described including SERPINB1-inhibited caspase-11/-4/-1 activation in resting cells or ESCRT-mediated plasma membrane repair (Rühl *et al.*, 2018; Choi *et al.*, 2019).

Crucial at regulating the activation the non-canonical inflammasome pathway are the IFN-inducible GTPases, the so-called guanylate binding proteins (GBPs) and the immunity-related GTPase (Irg) Irgb10 (Meunier *et al.*, 2014, 2015; Pilla *et al.*, 2014; Finethy *et al.*, 2015; Man *et al.*, 2015, 2016; Wallet *et al.*, 2017; Zwack *et al.*, 2017; Cerqueira *et al.*, 2018; Costa Franco *et al.*, 2018; Lagrange *et al.*, 2018; Liu *et al.*, 2018). Specifically, GBPs (1, 2, 3, 4 and 5) are recruited on LPS-enriched structures such as cytosolic Gram-negative bacteria and their derived products outer membrane vesicles (OMVs) (Meunier *et al.*, 2014; Man *et al.*, 2015; Finethy *et al.*, 2017; Lagrange *et al.*, 2018; Santos *et al.*, 2018; Fisch *et al.*, 2019). As such, these GBPs then engage caspase-11 that will bind the LPS moiety lipid A, hence promoting the non-canonical inflammasome pathway (Fisch *et al.*, 2019). Beyond their role at triggering GBP expression, IFNs induce more than 2,000 antimicrobial genes (Green *et al.*, 2018). Among them, many IFN-inducible regulatory genes also counter-balance overactivation of the cells (Green *et al.*, 2018). For instance, SOCS1 and USP18 are ISGs that balance the level of the host cell response (Basters *et al.*, 2018; Liau *et al.*, 2018). In this context, we hypothesized that IFNs, in addition to their ability to promote GBP expression, might also induce negative regulators of the non-canonical inflammasome. In this regard, Irgm proteins belong to the IFN-inducible immunity-related GTPase (Irg) family proteins (Kim *et al.*, 2012, 2019; Pilla-Moffett *et al.*, 2016). Human being possess one IRGM protein, with various spliced variants, that is not IFN-inducible but that requires IFN signalling to be functional (Kim *et al.*, 2019). By contrast, mice display three different Irgms, namely Irgm1, Irgm2 and Irgm3 (Kim *et al.*, 2012). All Irgms lack the ability to hydrolyse the GTP due to a mutation in their catalytic domain (GMS), whereas other Irgs are GTPase active (GKS) (Coers, 2013). Previous studies underscored an inhibitory role of Irgm1 and Irgm3 on the recruitment and/or activation of the GBPs and Irg-GKS on microbial membranes although independent processes can also occur (Haldar *et al.*, 2013, 2015; Feeley *et al.*, 2017). In addition, recent studies identified Irgm1 and its human homologous IRGM, as being critical for the NLRP3 canonical inflammasome regulation by modulating the autophagy pathway, suggesting a close link between Irgm proteins and inflammasomes (Pei *et al.*, 2017; Mehto *et al.*, 2019a, b). In this context, we hypothesized that Irgm proteins might be IFN-inducible regulators of the non-canonical inflammasome activation threshold.

Here, we report that IFN-inducible Irgm2 and the non-canonical autophagy effector Gate-16 indirectly fine-tune non-canonical inflammasome activation by intracellular bacteria, which protects against endotoxemia.

Results and Discussion

IFN-inducible protein Irgm2 restrains Caspase-11-dependent responses to Gram-negative bacteria

IFN-inducible Irgms control Irg and GBP microbicidal activity against intracellular pathogens (Pilla-Moffett *et al.*, 2016). In this context, we sought to determine whether Irgms might also modulate the non-canonical inflammasome response. Using an RNA interference approach (siRNA), we silenced the three murine Irgms in primary murine bone marrow-derived macrophages (BMDMs) and measured their ability to undergo caspase-11-dependent cell death and IL-1 β maturation upon *Salmonella* Typhimurium challenge. To ensure that the inflammasome response in macrophages is caspase-11-dependent, we used an isogenic mutant of *Salmonella* (*orgA*⁻) lacking expression of SP1-encoded T3SS secretion system (Broz *et al.*, 2012). As previously published, *Casp11* and *Gbp2* silencing reduced macrophage death (LDH release) and IL-1 β release after 16 h of infection (Figs 1A and EV1A; Meunier *et al.*, 2014). Importantly, *Irgm2*-silenced BMDMs had higher levels of cell death and IL-1 β release than the wild-type (WT) macrophages (Figs 1A and EV1A). Such process was specific to Irgm2 given that *Irgm1*- and *Irgm3*-targeted siRNAs did not induce significant variation in macrophage death and IL-1 β release upon *Salmonella* (*orgA*⁻) infection, despite the fact that their mRNA levels were efficiently reduced (Figs 1A and EV1A). To further validate that Irgm2 is a regulator of the non-canonical inflammasome response, we challenged WT, *Irgm2*^{-/-}, *Casp11*^{-/-} and *GBP*^{Chr3-/-} BMDMs with a panel of Gram-negative bacteria all known to activate the non-canonical inflammasome. Immunoblotting experiments in WT and *Irgm2*^{-/-} BMDMs showed that Irgm2 is IFN-inducible and that *Irgm2* deficiency does not lead to a defect in caspase-1, caspase-11, GBP2 or GBP5 expression, all involved in the non-canonical inflammasome pathway (Fig EV1B and C). Yet, when challenged with various Gram-negative bacteria, *Irgm2*^{-/-} macrophages showed an exacerbated cell death, IL-1 β release and gasdermin-D p30 (active) and processed caspase-1 p20 (inactive) fragments compared with their WT counterparts (Fig 1B and C). In addition, Irgm2-regulated cell pyroptosis upon Gram-negative bacterial challenge was independent of NLRP3 as the use of the NLRP3 inhibitor MCC950 or *Nlrp3*^{-/-} BMDMs did not drive any defect in cell death but significantly reduced NLRP3-dependent IL-1 β release (Fig EV1D). As expected, both *Casp11*^{-/-} and *GBP*^{Chr3-/-} BMDMs were protected against Gram-negative bacteria-induced non-canonical inflammasome response (Fig 1B). Importantly, CRISPR-deleted *Irgm2* gene expression in immortalized (i) *Casp11*^{-/-} BMDMs (referred as *Casp11*^{-/-}sg*Irgm2*) did not reinstate pyroptosis and IL-1 β release upon Gram-negative bacterial infections (*S. Typhimurium orgA*⁻ and *Escherichia coli*) or *E. coli*-derived OMVs exposure, thus confirming that Irgm2 negatively regulated caspase-11-dependent response (Figs 1D and EV1E). Next, we assessed whether Irgm2 directly or indirectly regulates the non-canonical inflammasome response. To this end, we electroporated LPS into the host cell cytosol of IFN γ -primed WT, *Irgm2*^{-/-} and *Casp11*^{-/-} BMDMs and evaluated their ability to undergo pyroptosis. Surprisingly, we observed that WT and *Irgm2*^{-/-} macrophages engaged cell death to the same extent 4 h after LPS electroporation whereas *Casp11*^{-/-} BMDMs were protected against LPS-induced cell death (Fig 1E). This suggests that

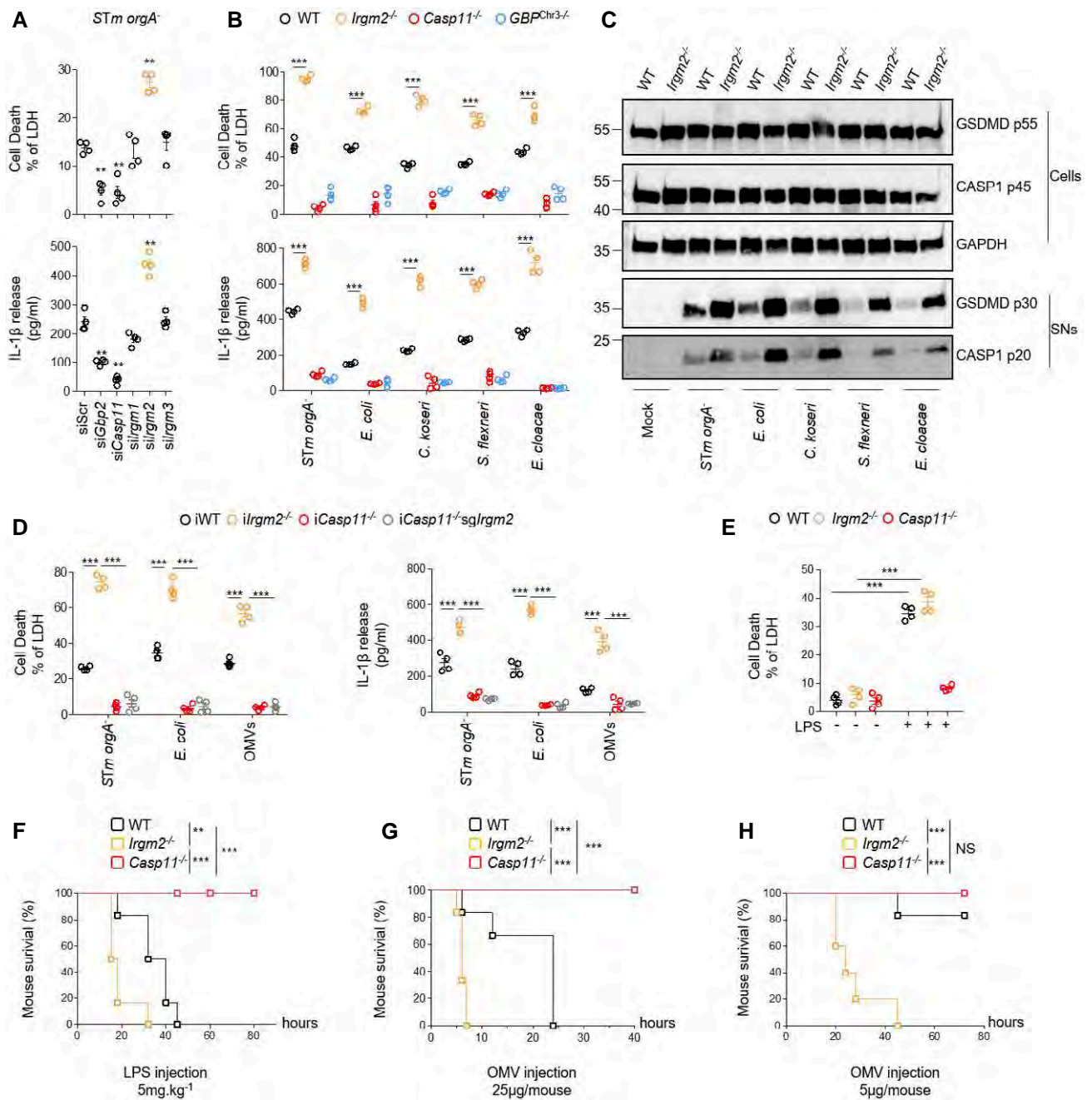


Figure 1. IFN-inducible protein *Irgm2* restrains caspase-11-dependent response to Gram-negative bacteria.

Unless otherwise specified, BMDMs were either infected with various Gram-negative bacterial strains (MOI25) or stimulated with outer membrane vesicles (OMVs) for 16 h.

- A** siRNA-treated BMDMs were infected for 16 h with *S. Typhimurium* (*orgA*⁻), and LDH and IL-1β release were measured.
- B** Cell death (LDH) and IL-1β release evaluation in WT, *Irgm2*^{-/-}, *GBP*^{Chr3-/-} and *Casp11*^{-/-} BMDMs infected for 16 h with different Gram-negative bacteria (MOI 25).
- C** Western blot examination of processed caspase-1 (p20) and gasdermin-D (p30) in supernatants and pro-caspase-1 (p45), pro-gasdermin-D (p55) and GAPDH in cell lysates of WT and *Irgm2*^{-/-} BMDMs infected for 16 h with different Gram-negative bacterial strains.
- D** IL-1β and cell death (% LDH) evaluation in immortalized WT, *Irgm2*^{-/-}, *Casp11*^{-/-} and *Casp11*^{-/-}*Irgm2*^{-/-} (referred as *sgIrgm2*) BMDMs after 16 h of *Escherichia coli*, *S. Typhimurium orgA*⁻ and OMV treatment.
- E** Cell death (% LDH) evaluation in IFNγ-primed WT, *Irgm2*^{-/-} and *Casp11*^{-/-} BMDMs 4 h after electroporation or not with 1 μg of *E. coli* LPS.
- F–H** Survival of WT, *Casp11*^{-/-} and *Irgm2*^{-/-} mice primed with 100 μg poly(I:C) for 6 h and injected (i.p.) with 5 mg/kg LPS or 5 and 25 μg of OMVs (*n* = 6 animals per condition).

Data information: Data shown as means ± SEM (graphs A, B, D and E) from *n* = 4 independent pooled experiments; ***P* ≤ 0.01, ****P* ≤ 0.001 for the indicated comparisons using *t*-test with Bonferroni correction. Image (C) is representative of one experiment performed three times. (F–H) are representative of three independent experiments; **P* ≤ 0.05; ***P* ≤ 0.01, ****P* ≤ 0.001, log-rank Cox–Mantel test for survival comparisons (F–H).

Source data are available online for this figure.

Irgm2-inhibited caspase-11 response occurs upstream from LPS sensing by caspase-11.

Based on these results, we next determined whether Irgm2 also inhibited canonical inflammasomes. We treated WT, *Irgm2*^{-/-}, *Casp11*^{-/-} and *Casp11*^{-/-}*Casp11*^{-/-} BMDMs with various inflammasome activators, including flagellin (NLRC4), poly-dAdT (AIM2), Nigericin (NLRP3) and TcdB (PYRIN), and measured their ability to commit pyroptosis and to release IL-1 β . Although all canonical inflammasome activators induced significant caspase-1-dependent response, cell death and IL-1 β release levels remained similar in both WT and *Irgm2*^{-/-} BMDMs (Fig EV1F). In addition, activation of the NLRC4 inflammasome by T3SS-expressing *Pseudomonas aeruginosa* and *S. Typhimurium* remained similar between WT and *Irgm2*^{-/-} BMDMs (Fig EV1G), suggesting that Irgm2 specifically regulates the non-canonical inflammasome response to Gram-negative bacteria.

As caspase-11 also drives mouse susceptibility to LPS-induced inflammatory-related damages, we also evaluated whether *Irgm2* deficiency might sensitize mice to sepsis. We used two LPS-dependent sepsis models, where WT, *Irgm2*^{-/-} and *Casp11*^{-/-} mice were intraperitoneally injected with poly(IC) to induce ISG expression (Kayagaki et al., 2013; Santos et al., 2018). Then, mice were injected either with pure LPS (5 mg/kg) or with OMVs (25 μ g/ml; Vanaja et al., 2016; Santos et al., 2018). Mouse survival showed that while *Casp11*^{-/-} mice had resistance to LPS- and OMV-induced sepsis, WT mice succumbed faster, hence validating our sepsis model (Fig 1F and G). Noticeably, *Irgm2*^{-/-} mice were even more susceptible than WT mice to both LPS- and OMV-induced sepsis (Fig 1F and G). Therefore, we used a sub-lethal model of OMV-induced sepsis by injecting 5 μ g of OMVs in mice. In such model, both WT and *Casp11*^{-/-} mice recovered from OMV injection whereas all *Irgm2*^{-/-} mice did succumb (Fig 1H). Moreover, cytokine assays showed that *Irgm2*^{-/-} mice had an exacerbated release of all pro-inflammatory and inflammasome-related cytokines tested upon OMV challenge, a phenotype that was reduced in *Casp11*^{-/-} mice, hence confirming that Irgm2 expression is crucial to temperate the activation level of the non-canonical inflammasome (Fig EV1H). Altogether, our data suggest that Irgm2 indirectly inhibits caspase-11-dependent endotoxemia, which protects against sepsis.

Irgm2 regulates GBP-independent caspase-11 targeting to Gram-negative bacteria

IFN-inducible GBPs are important regulators of the non-canonical inflammasome response. Specifically, GBP-1 and GBP-2 regulate human caspase-4/-5 activation while GBP-2 and GBP-5 control mouse caspase 11. Therefore, we hypothesized that Irgm2 might control caspase-11 response through the modulation of the GBPs. To this end, we silenced *Irgm2* in WT and *GBP*^{Chr3-/-} BMDMs (lacking 5 GBPs, 1-3, 5 and 7) and evaluated the caspase-11 response upon OMV stimulation (Fig EV2A). While OMV-induced both cell death and IL-1 β release was strongly reduced in *GBP*^{Chr3-/-}, *Irgm2*-silenced *GBP*^{Chr3-/-} BMDMs partially recovered a caspase-11-dependent response, suggesting that Irgm2-inhibited caspase-11 response could occur independently of GBPs (Fig 2A). Other and we previously showed that GBPs also controlled canonical AIM2 inflammasome activation upon *Francisella tularensis* spp *novicida* infection. In this context, we evaluated the importance of Irgm2 at controlling AIM2 inflammasome response upon *F. novicida* infection. Surprisingly, IL-1 β and cell

death levels were not different between WT and *Irgm2*^{-/-}, although they were strongly reduced in *Casp11*^{-/-}*Casp11*^{-/-} and *GBP*^{Chr3-/-} BMDMs (Figs 2B and EV2B). In addition, we observed that *Irgm2*-silenced *GBP*^{Chr3-/-} BMDMs did not recover an inflammasome response upon *F. novicida* infection. Then, we generated *iGBP*^{Chr3-/-}*Irgm2*^{-/-} (referred hereafter as *iGBP*^{Chr3-/-}*sgIrgm2*) by crisper Cas9 and evaluated their response upon *S. Tm* (*orgA*⁻) challenge. *iIrgm2*^{-/-} BMDMs showed time-dependent increased cell death compared with iWT cells (Fig EV2C and D). While cell death in *iGBP*^{Chr3-/-} BMDMs was strongly impaired, it was partially reversed in *iGBP*^{Chr3-/-}*sgIrgm2*, alluding that *Irgm2* deficiency was sufficient to specifically promote caspase-11-dependent response in the absence of GBPs (Fig EV2C and D). GBP enrichment on microbial ligand is of importance for efficient caspase-11 and human caspase-4 recruitment (Thurston et al., 2016; Fisch et al., 2019). However, monitoring for GBP loading on mCherry-expressing *S. Typhimurium* did not show a significant change in the percentage of bacteria targeted by GBP2 (10–15%) in WT and *Irgm2*^{-/-} BMDMs (Fig 2C), which suggests that Irgm2-inhibited non-canonical inflammasome response does not involve GBP2 recruitment modulation.

As caspase-11 activation needs binding to LPS, we hypothesized that Irgm2 expression regulates caspase-11 recruitment to bacterial LPS. In order to monitor this, we generated WT, *Irgm2*^{-/-}, *GBP*^{Chr3-/-} and *GBP*^{Chr3-/-}*Irgm2*^{-/-} iBMDMs that expressed a catalytically inactive mutant of caspase-11 coupled to GFP (Thurston et al., 2016) and primed them with IFN γ to induce ISG expression. The recruitment of CASP11-C254G-GFP on *S. Typhimurium* (*orgA*⁻) occurred after 4 h of infection in *Irgm2*^{-/-} iBMDMs, whereas the percentage of caspase-11-targeted bacteria in iWT *GBP*^{Chr3-/-} and *GBP*^{Chr3-/-}*Irgm2*^{-/-} iBMDMs remained low or null (Fig EV2E). After 8 h of infection, however, the levels of CASP11-C254G-GFP-associated bacteria increased in iWT (10%), albeit the percentage of CASP11-C254G-GFP⁺ bacteria remained below those observed in *Irgm2*^{-/-} cells (15–16%) (Fig 2D). Strikingly, we noticed that CASP11-C254G-GFP targeting to *Salmonella* was partially restored in *GBP*^{Chr3-/-}*Irgm2*^{-/-} iBMDM after 8 h of infection, although it was strongly impaired in *GBP*^{Chr3-/-} cells (Fig 2D). Altogether, our results point out that *Irgm2* deficiency accelerates caspase-11 recruitment on bacterial membranes. Although we cannot entirely exclude that Irgm2 might also regulate GBP-dependent caspase-11 recruitment to bacterial membranes, our result show that an *Irgm2* deficiency opens a *GBP*^{Chr3} alternative road for caspase-11 response.

Irgm2 cooperates with GATE16 to dampen Gram-negative bacteria-induced non-canonical inflammasome activation

As *Irgm2* deficiency can promote caspase-11 activation independently of *GBP*^{Chr3}, we next searched for additional regulators. We used a GFP-Trap coupled to mass spectrometry (MS) strategy using IFN γ -primed *iIrgm2*^{-/-} BMDMs complemented with a doxycycline-inducible *Irgm2*-GFP construct (Fig 3A). Although we detected some important described immune regulators (e.g., galectin-8), the three independent MS datasets (Fig EV3A) showed that one protein, namely gamma-aminobutyric acid (GABA)-A-receptor-associated protein (GabarapL2, referred as Gate-16), was reproducibly enriched in the top 10 hits of the *Irgm2*-GFP fraction (Figs 3A and EV3A). Therefore, we decided to investigate whether Gate-16 played a role in *Irgm2*-inhibited caspase-11 response. Co-immunoprecipitation

experiments confirmed that Gate-16 was present in the *Irgm2*-GFP fraction, hence validating our MS results (Fig 3B). Gabarap proteins (Gabarap, GabarapL1 and Gate-16) belong to the ATG8 superfamily proteins, all involved in autophagy/membrane remodelling regulation. While *Gabarap* deficiency leads to increased canonical NLRP3 inflammasome response in mice, there is no information regarding the putative function of Gate-16 at regulating the non-canonical inflammasome. In this context, we found that silencing of *Gate-16*,

but no other *gabaraps*, increased OMV-induced caspase-11-dependent cell death and IL-1 β release (Figs 3C, and EV3B and C). As a control, *Gate-16* silencing did not alter BMDM response to canonical NLRP3 inflammasome activators (Fig EV3D). Then, we sought to determine whether Gate-16-inhibited caspase-11 response was part of the *Irgm2* path. Consequently, we silenced *Gate-16* gene expression in WT, *GBP^{Chr3}*^{-/-}, *Casp11*^{-/-} and *Irgm2*^{-/-} BMDMs and evaluated the ability of OMVs to induce a caspase-11-dependent response. *Gate-16*

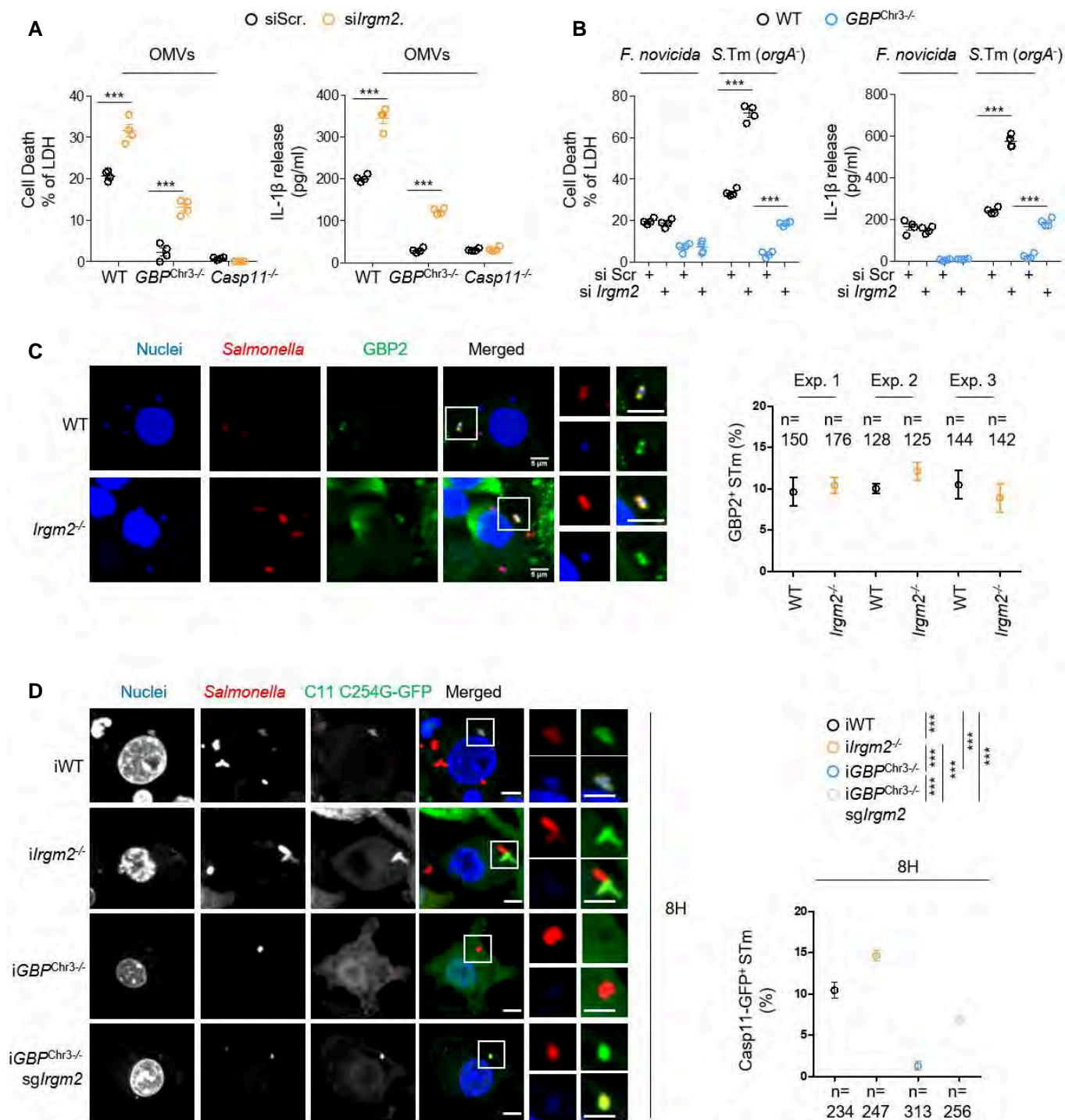


Figure 2.

Figure 2. Irgm2 regulates GBP-independent caspase-11 targeting to Gram-negative bacteria.

Unless otherwise specified, BMDMs were treated with $2.5 \mu\text{g}/2 \times 10^5$ cells of OMVs or infected with either *S. Typhimurium orgA⁻* (*S. Tm orgA⁻*) or *F. tularensis* spp *novicida* (*F. novicida*) with an MOI of 25 for various times.

- A Measure of LDH and IL-1 β release in WT, *GBP^{chr3-/-}* and *Casp11^{-/-}* BMDMs where *Irgm2* was knocked down 16 h after exposure to $2.5 \mu\text{g}/2 \times 10^5$ cells of OMVs. Si Scramble (siScr.) refers to RNAi pools with non-targeting sequences.
- B Cell death (LDH) and IL-1 β release evaluation in *Irgm2*-silenced WT and *GBP^{chr3-/-}* BMDMs infected for 16 h with either *S. Tm orgA⁻* or *F. novicida* (MOI 25). Si Scramble (siScr.) refers to RNAi pools with non-targeting sequences.
- C Florescence microscopy and associated quantifications of GBP-2 (green) recruitments to intracellular *S. Tm orgA⁻*-mCherry (MOI 10, red) in IFN γ -primed WT and *Irgm2^{-/-}* BMDMs. Nucleus was stained with Hoechst (blue). Confocal images shown are from one experiment and are representative of $n = 3$ independent experiments; scale bars 5 μm . For quantifications, the percentage of GBP-associated bacteria was quantified and "n=" refers to the number of intracellular bacteria counted in each experiment; quantifications from $n = 3$ independent experiments were then plotted and expressed as mean \pm SEM.
- D Confocal fluorescence microscopy images and associated quantifications of caspase-11-C254G-GFP (green) recruitment to *S. Tm*-mCherry (*orgA⁻*, red) in IFN γ -primed iWT, *iIrgm2^{-/-}*, *iGBP^{chr3-/-}* and *iGBP^{chr3-/-}/sgIrgm2* BMDMs after 8 h of infection. Nucleus (blue) was stained with Hoechst, scale bar 5 μm . For quantifications, the percentage of bacteria positive for caspase-11-C254G-GFP was determined by combining the bacterial counts from $n = 3$ independent experiments and expressed as mean \pm SEM. *** $P \leq 0.001$ for the indicated comparisons using t-test with Bonferroni correction.

Data information: Data shown as means \pm SEM (graphs A, B) from $n = 4$ independent pooled experiments; *** $P \leq 0.001$ for the indicated comparisons using t-test with Bonferroni correction. Images (C, D) are representative of one experiment performed three times.

silencing in WT BMDMs increased the non-canonical inflammasome response while *Casp11^{-/-}* macrophages remained unresponsive to OMV-induced cell death, IL-1 β release (Fig 3D). Interestingly, we observed that *GBP^{chr3-/-}* macrophages silenced for Gate-16 partially recovered their ability to respond to caspase-11 activators (Fig 3E). Finally, *Gate-16* knock down in *Irgm2^{-/-}* BMDMs did not exacerbate cell death and IL-1 β release nor gasdermin-D or caspase-1 cleavages (Fig 3D and E), suggesting that *Irgm2* and Gate-16 work together to restrain non-canonical inflammasome response. Since *Irgm2* deficiency leads to caspase-11 enrichment to bacterial membranes, we wondered about the role of Gate-16 in this process. We silenced *Gate-16* in iWT-expressing CASP11-C254G-GFP and checked for its recruitment on *S. Tm* membranes. Consequently, iWT BMDMs knocked down for *Gate-16* had a more pronounced accumulation of caspase-11 on *S. Tm* membranes than the controls after 4 and 8 h of infection (Fig 3F), which mirrored what we previously observed in *Irgm2^{-/-}* macrophages. By contrast, *Gate-16* silencing in *Irgm2^{-/-}* did not increase the percentage of bacteria targeted by CASP11-C254G-GFP after 4 h of infection (Fig EV3E). Recent work suggested that caspase-11 activation could restrict *Salmonella* proliferation in macrophages and epithelial cells (Meunier *et al*, 2014; Thurston *et al*, 2016). Therefore, we monitored bacterial load in WT and *Casp11^{-/-}* BMDMs in which we silenced *Irgm2* and *Gate-16*. Whereas *Gate-16* silencing led to slight increased colony forming unit (CFUs) 24 h after infection, *Irgm2* silencing did not modify intracellular bacterial loads, suggesting that Gate-16 also covers a caspase-11-independent cell autonomous immune process (Fig EV3F). Altogether, these results suggest that *Irgm2* and Gate-16 cooperate to restrict the non-canonical inflammasome response by restraining caspase-11 targeting to bacterial membranes.

Irgm2- and Gate16-inhibited *Salmonella*-induced non-canonical inflammasome responses do not involve canonical autophagy

As Gate-16 is involved in the canonical and non-canonical autophagy regulation, we wondered if the exacerbated non-canonical inflammasome response observed in the absence of Gate-16 and *Irgm2* relied on autophagy modulation. Therefore, we pharmacologically inhibited canonical autophagy (3-MA or Wortmannin) in WT and *Casp11^{-/-}* BMDMs targeted with siRNA against *Irgm2* or *Gate-16*. Autophagy inhibition in BMDMs triggered exacerbated

Salmonella (*orgA⁻*)-induced cell death and IL-1 β release, a process that required caspase-11 (Fig EV4A). However, although *Irgm2* and Gate16 knock down drove increased caspase-11-dependent response, autophagy inhibition also exacerbated the macrophage response to *Salmonella* infection (Fig EV4A). LC3b targeting to bacteria is also a hallmark of anti-bacterial autophagy (Masud *et al*, 2019; Wu & Li, 2019). Consequently, we infected WT BMDMs silenced for *Irgm2* or *Gate16* with *Salmonella* and analysed by fluorescence microscopy the recruitment of LC3b on bacterial compartments. We found that the percentage of LC3b⁺ bacteria in control siRNA-treated BMDMs was not significantly altered in BMDMs silenced for *Irgm2* or *Gate16*, although we noticed a trend for LC3b accumulation in si*Gate16*-treated cells (Fig EV4B). This suggests that *Gate16* and *Irgm2* deficiencies modulate the non-canonical inflammasome response independently of canonical autophagy. This is in agreement with the findings of Finethy *et al* (2020) that underlined a lack of canonical autophagy markers (e.g., LC3 lipidation) alteration in *Irgm2^{-/-}* BMDMs. Yet, BMDMs deficient for canonical autophagy regulators had an exacerbated non-canonical inflammasome response. Altogether, these results suggest that Gate-16/*Irgm2*-inhibited non-canonical inflammasome response does not involve canonical autophagy modulation.

GATE16 inhibits non-canonical inflammasome activation in human myeloid cells

Gate-16 is expressed in both humans and rodents, yet humans only express one IRGM, although mice have three (*Irgm1-3*). Therefore, we performed siRNA-based experiments in primary human monocyte-derived macrophages (hMDMs) to determine whether IRGM and GATE16 might also regulate the caspase-4/5 non-canonical inflammasome. Although the use of the caspase-4/5 inhibitor LEVD and of the NLRP3 inhibitor MCC950 showed that hMDMs responded to *Salmonella orgA⁻* infection by activating the non-canonical inflammasome, we failed to observe any regulatory role for IRGM at regulating such a process (Figs 4A and EV5A). However, *GATE16* silencing increased their ability to respond to *Salmonella* through the non-canonical inflammasome (Figs 4A and EV5A). When we used Nigericin to trigger the canonical NLRP3 inflammasome, hMDMs knocked down for *GATE16* did not show cell death and IL-1B alterations (Fig 4B). To the contrary, *IRGM*-silenced hMDMs had

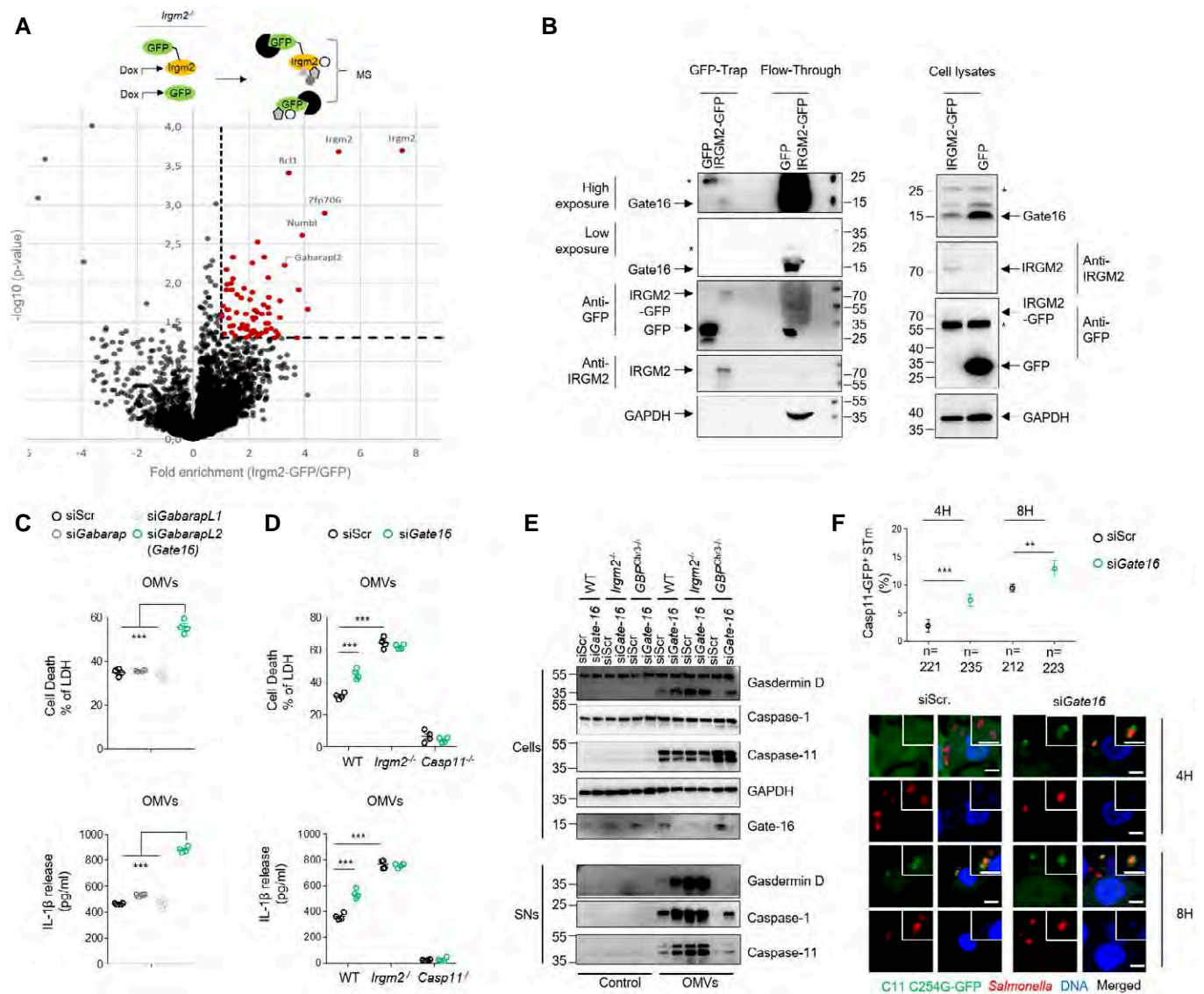


Figure 3. Irgm2 cooperates with GATE16 to dampen Gram-negative bacteria-induced non-canonical inflammasome activation.

- A** GFP-Trap coupled to mass spectrometry strategy used. The volcano plot represents three independent combined experiments. Threshold selection of enriched proteins (red dots) in *Irgm2*-GFP fraction was set at 2-fold enrichment (x -axis) and P -value < 0.05 (y -axis). Blacks and grey dots indicate proteins that did not reach a P -value < 0.05 using t -test with Bonferroni correction. Labeled proteins represent the top 6 enriched proteins in the *Irgm2* fraction.
- B** Green fluorescent protein (GFP)-Trap assay of the presence of Gate16 in *Irgm2*-GFP-enriched fraction from the lysates of IFN γ -primed *iirgm2*^{-/-} BMDMs complemented with lentiviral constructs coding for a fusion of *Irgm2* with GFP (*Irgm2*-GFP) or GFP alone. Arrows show the presence or not of Gate16, *Irgm2*-GFP and GAPDH in the *Irgm2*-GFP-enriched fractions, flow-through and total cell lysates. * means non-specific band.
- C** LDH and IL-1 β release from siRNA-treated WT BMDMs, and then exposed to $2.5 \mu\text{g}/2 \times 10^5$ cells of OMVs for 16 h.
- D** LDH and IL-1 β release from WT, *Irgm2*^{-/-} and *Casp11*^{-/-} BMDMs silenced for *Gate16* and treated for 16 h with $2.5 \mu\text{g}/2 \times 10^5$ cells of OMVs. Si Scramble (siScr) refers to RNAi pools with non-targeting sequences.
- E** Western blot examination of caspase-11 and processed caspase-1 (p20) and gasdermin-D (p30) in supernatants and pro-caspase-1 (p45), pro-gasdermin-D (p55), pro-caspase-11, Gate16 and GAPDH in cell lysates of *Gate16*-silenced WT, *Irgm2*^{-/-} and *GBP*^{chr3-/-} BMDMs exposed to $2.5 \mu\text{g}/2 \times 10^5$ cells of OMVs for 16 h. Si Scramble (siScr) refers to RNAi pools with non-targeting sequences.
- F** Representative confocal fluorescence microscopy images and associated quantifications of caspase-11-C254G-GFP (green) recruitment to *S. Tm*-mCherry (*orgA*⁻, red, MOI 10) in IFN γ -primed iWT BMDMs silenced for *Gate16* after 4 and 8 h of infection. Nucleus (blue) was stained with Hoechst, scale bar 5 μm . For quantifications, the percentage of bacteria positive for caspase-11-C254G-GFP was determined by combining the bacterial counts from $n = 3$ independent experiments and expressed as mean \pm SEM. ** $P \leq 0.01$, *** $P \leq 0.001$ for the indicated comparisons using t -test with Bonferroni correction. Si Scramble (siScr) refers to RNAi pools with non-targeting sequences.

Data information: Data shown as means \pm SEM (graphs C, D) from $n = 4$ independent pooled experiments; *** $P \leq 0.001$ for the indicated comparisons using t -test with Bonferroni correction. Image (B) is representative of one experiment performed two times, and (E) represents one experiment out of three. (A) represents one experiment out of three independent experiments.

Source data are available online for this figure.

higher IL-1B and cell death levels than their respective controls, which is reminiscent of previous studies that showed a regulatory role for IRGM on the canonical NLRP3 inflammasome (Fig 4B). Although the research of a protein with a similar function of rodent *Irgm2* in humans warrants further investigations, our results suggest that GATE16 function is conserved between both species. Next, we wondered if GATE16-inhibited non-canonical inflammasome response to *Salmonella* depended on human GBPs. GBP1, GBP2 and GBP5 have recently been described as being important for efficient CASP4 recruitment and activation on bacterial membranes. Hence, we used human monocytic cell line U937 genetically invalidated for GBP1, GBP2 and GBP5 (*GBP1/2/5^{-/-}*) (Fig EV5B). Infection of IFN γ -primed WT or *GBP1/2/5^{-/-}* U937 cells with *Salmonella* triggered both GBP-dependent cell death and IL-1B release (Fig 4C). Importantly, GATE16 silencing in *GBP1/2/5^{-/-}* cells reinsured significant cell death and IL-1B release, suggesting that the human non-canonical inflammasome response relies on GBP-dependent and GBP-independent mechanisms (Fig 4C). Finally, we aimed at determining if GATE16 is a direct regulator of the non-canonical inflammasome response in human cells. Therefore, we electroporated LPS in WT or *GBP1/2/5^{-/-}* U937 cells in the presence or absence of GATE16 siRNA (Fig 4D). Our results showed that electroporated LPS-induced cell death and IL1B release did not involve GATE16 (Fig 4D), suggesting that GATE16 acts upstream of the non-canonical inflammasome. Altogether, our results identified *Irgm2* and GATE16 that cooperatively restrict Gram-negative bacteria-induced non-canonical inflammasome activation in both mice and humans.

Tight regulation of the non-canonical inflammasome pathway is of major importance as its uncontrolled non-canonical inflammasome response drives endotoxic shock. Conversely, two recent studies have uncovered that the IRF2 transcription factor (and to a lower extent IRF1) transcriptionally controls murine gasdermin-D and human caspase-4 expression (Benaoudia *et al*, 2019; Kayagaki *et al*, 2019). In addition, SERPINB1 has also been found to directly interact and inhibit activation of the inflammatory caspase-1, caspase-4 and caspase-11 (Choi *et al*, 2019). Here, both Finethy *et al* (2020) and us report a critical role of *Irgm2* and Gate-16 at balancing the non-canonical inflammasome activity. The *Irgm2*/Gate-16 axis was required to inhibit caspase-11 recruitment to Gram-negative bacteria in the host cell cytosol, which provided controlled caspase-11 response and protection against sepsis. These findings open many yet unanswered questions such as at which step the *Irgm2*/Gate16 axis is regulating caspase-11 recruitment to bacterial products. Gate-16 has been found to control proper cytosolic localization of various GBPs (Park *et al*, 2016; Sasai *et al*, 2017), including GBP2, crucial at regulating caspase-11 recruitment on intracellular pathogen PAMPs. However, results from Finethy *et al* (2020) and ours indicate that *Gate16/Irgm2* removal in GBP-deficient macrophages (lacking GBPs 1, 2, 3, 5 and 7) partially restores a caspase-11-dependent response, suggesting that the Gate-16/*Irgm2* path might regulate caspase-11, at least to certain extent, independently of these GBPs. Recently, two publications described that hGBP4 participated with GBP1 and GBP3 to the recruitment of CASP4 to cytosolic Gram-negative bacterial membranes in human

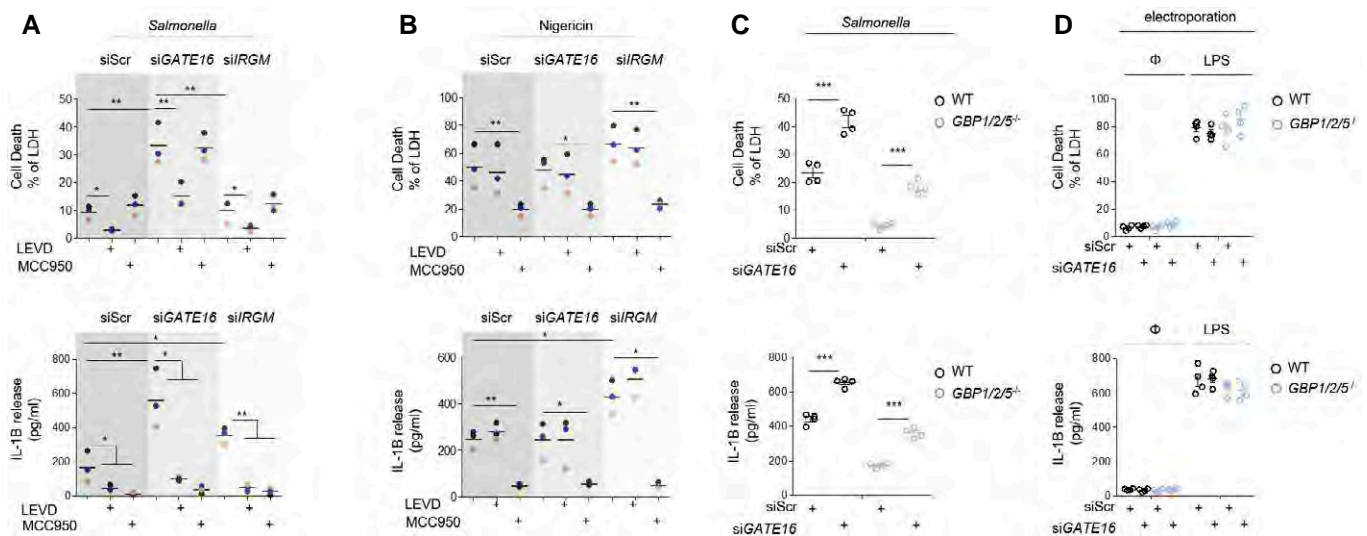


Figure 4. GATE16 inhibits non-canonical inflammasome activation in human myeloid cells.

- A LDH and IL-1B release from siRNA-treated primary human monocyte-derived macrophages (hMDMs) infected with *S. Typhimurium orgA⁻* (MOI25) for 16 h. When specified, the caspase-4/5 inhibitor Z-LEVD (25 μ M) or the NLRP3 inhibitor MCC950 (10 μ M) was added to the experiments.
- B LDH and IL-1B release from siRNA-treated primary human monocyte-derived macrophages (hMDMs), primed with IFN γ (10 UI/ml) and PAM3CSK4 (100 ng/ml) and then stimulated with Nigericin (20 μ M) for 4 h. When specified, the caspase-4/5 inhibitor Z-LEVD (25 μ M) or the NLRP3 inhibitor MCC950 (10 μ M) was added to the experiments.
- C, D LDH and IL-1B release from siRNA-treated WT or *GBP1/2/5^{-/-}* U937 monocytic cell line, primed with IFN γ (10 UI/ml) and PAM3CSK4 (100 ng/ml) and then infected with (C) with *S. Typhimurium orgA⁻* (MOI25) for 10 h or (D) electroporated with 1 μ g of *Escherichia coli* LPS for 4 h. Φ indicates that no LPS electroporation was performed. Data shown as means \pm SEM from $n = 4$ independent pooled experiments; *** $P \leq 0.001$ for the indicated comparisons using *t*-test with Bonferroni correction.

Data information: Data shown as means (graphs A, B) from $n = 3$ different donors; each donor is represented with a coloured circle; * $P \leq 0.05$, ** $P \leq 0.01$ for the indicated comparisons using one-way ANOVA with multiple Bonferroni correction.

epithelial cells (Santos *et al*, 2020; Wandel *et al*, 2020). Whether Irgm2/Gate-16-inhibited caspase-11 (or hCASP4) enrichment on bacterial membranes involves other GBPs (4 and 6) remains to be addressed. So far, due to the lack of information, a possible function of Irgm2 remains elusive, but Irgm1 and its human homologous IRGM have been described to participate in the autophagy/xenophagy processes (Maric-Biresev *et al*, 2016; Azzam *et al*, 2017). In addition, Gate-16 belongs to the ATG8-like proteins, including LC3 (abc), Gabarap and GabarapL1, all involved in various autophagy/membrane remodelling step regulation such as lysosome biogenesis, autophagosome formation and closure (Lee & Lee, 2016; Nguyen *et al*, 2016; Gu *et al*, 2019). To this regard, both Irgm1/IRGM (Finethy *et al*, 2020) and Gabarap proteins inhibit the activation of the Nlrp3 inflammasome (Pei *et al*, 2017; Mehto *et al*, 2019a,b). In addition, Irgm-1 and Irgm-3 deficiencies also rescue exacerbated inflammasome response from Irgm2-deficient macrophages (Finethy *et al*, 2020). Therefore, one can hypothesize that Gate-16 and Irgm2 deficiencies could lead to defective autophagy, which would promote cytosolic LPS accumulation and an exacerbated caspase-11 activation. However, results from Finethy *et al* (2020) and our own suggest that Gate-16 and Irgm2 regulate Gram-negative bacteria-induced non-canonical inflammasome response in an autophagy-independent manner. Should those effectors modulate the non-canonical autophagy pathway is an attractive hypothesis that deserves further investigations. Another possible explanation relies on the Golgi enrichment of both Irgm2 and Gate-16 (Sagiv, 2000; Zhao *et al*, 2010). Indeed, Gate-16 also regulates Snare-dependent vesicular trafficking, independently of its autophagy function (Sagiv, 2000). Various groups previously found that endocytosed and intracellular monomeric LPS could be targeted to the Golgi apparatus (Thieblemont & Wright, 1999; Latz *et al*, 2002). Caspase-4, caspase-5 and caspase-11 need accessible lipid A to oligomerize and auto activate, which can be extremely difficult in the presence of multimeric and hydrophobic LPS particles to the contrary of monomeric LPS that might present a more accessible lipid A. An attractive hypothesis is that GBP-mediated bacterial membrane damages allow LPS retrieval from aggregates in order to ensure proper lipid A exposure to caspase-11 (Santos *et al*, 2018, 2020; Kutsch *et al*, 2020; Wandel *et al*, 2020). Therefore, one could speculate that Golgi-regulated monomeric LPS trafficking might be impaired in the absence of either Irgm2 or Gate-16, which would allow direct caspase-11/lipid A interactions without the need for GBPs.

Our results showed that both murine and human Gate-16 regulate the non-canonical inflammasome response to LPS-containing particles. Yet, we failed to isolate IRGM as a human functional homologous of Irgm2. Given the strong role of Irgm2 at regulating the non-canonical inflammasome in mice, there is a possibility that another, yet unidentified, human protein holds a similar function of the one carried out by Irgm2. Therefore, this warrants future investigations to identify such Irgm2-like human protein. Humans and mice have different sensitivities to LPS. Indeed, LPS-induced sepsis in mice requires 1–25 mg/kg of LPS whereas humans have a 100–1,000,000 time lower sepsis threshold (2–4 ng/kg of LPS) (Fink, 2014). Another explanation could be that the evolutionary loss of Irgm2 in humans would leave human cells with only Gate-16, which would greatly lower the sensitivity of human cells to cytosolic LPS-activated non-canonical inflammasome.

In summary, our work identified two negative regulators of caspase-11 recruitment to bacterial membranes, namely Irgm2 and

Gate-16. Additional investigations will be necessary to understand how both effectors balance caspase-4, caspase-5 and caspase-11 sensitivity to Gram-negative bacteria, and what specific physiological and cellular processes Irgm2 and Gate-16 cover together.

Materials and Methods

Reagents, biological samples and their concentration of use are referenced in the Appendix Table S1.

Mice

Casp11^{-/-}, *Casp1^{-/-}Casp11^{-/-}*, *Nlrp3^{-/-}* and *GBP^{Chr3^{-/-}}* mice have been described in previous studies (Li *et al*, 1995; Wang *et al*, 1998; Martinon *et al*, 2006; Yamamoto *et al*, 2012). *Irgm2^{-/-}* mice were provided by the Jackson laboratory (USA). All mice were bred at the IPBS institute (Toulouse, France) animal facilities according to the EU and French directives on animal welfare (Directive 2010/63/EU). Charles Rivers provided WT C57BL/6J and C57BL/6N mice.

Animal sepsis models

8- to 12-week-old mice (sex-matched, 6–10 per group) were injected intraperitoneally with a solution of 100 μ l of poly(IC) LMW (InvivoGen, 100 μ g/animal) for 6 h. Then, mice were intraperitoneally injected with 5 mg/kg of LPS (InvivoGen, O111:B4) or 5 or 25 μ g/animal of outer membrane vesicles (*E. coli*, InvivoGen). Mouse survival was monitored over 80 h. For cytokine assays, poly(IC)-primed mice were injected with 25 μ g/animal of OMVs for 8 h and plasma cytokine amounts were addressed using ELISA kits (listed in the Appendix Table S1). There was no randomization or blinding performed.

Animal experiments were approved (Licence APAFIS#8521-2017041008135771, Minister of Research, France) and performed according to local guidelines (French ethical laws) and the European Union animal protection directive (Directive 2010/63/EU).

BMDM isolation and culture

Murine bone marrow-derived macrophage (BMDM) generation has previously been described. Briefly, bone marrow progenitors were differentiated in DMEM (Invitrogen) supplemented with 10% *v/v* FCS (Thermo Fisher Scientific), 10% *v/v* MCSF (L929 cell supernatant), 10 mM HEPES (Invitrogen) and nonessential amino acids (Invitrogen) for 7 days. For experiments, 1.25×10^6 , 2.5×10^5 or 5×10^4 BMDMs were seeded in 6-, 24- or 96-well plates, respectively, when described BMDMs were prestimulated overnight with either PAM3CSK4 (InvivoGen, 100 ng/ml) or IFN γ (PeProtech, 100 UI/ml). For non-canonical inflammasome stimulation, we used pure LPS (O111B4, InvivoGen, 1 μ g/ml), outer membrane vesicles (*E. coli*, InvivoGen, 0.5, 1 and 2.5 μ g/ 2×10^5 cells) or various Gram-negative bacterial strains were used including, *Shigella flexneri* (M90T, MOI25), *Salmonella* Typhimurium *orgA⁻* (SL1344, MOI25), *E. coli* (K12, MOI25), *Citrobacter koseri* (MOI25) and *Enterobacter cloacae* (MOI25). When required, Wortmannin (Wort, 10 μ M) and 3-methyladenine (3-MA, 1 mM) were added 2 h after infection in order to inhibit autophagy. When

specified, 1 μg of *E. coli* ultrapure LPS (O111:B4) was electroporated with Neon™ Transfection System (Thermo Fisher) according to manufacturer's protocol. Briefly, 5×10^5 cells were resuspended in Buffer R and 1 $\mu\text{g}/\text{ml}$ of LPS was electroporated in 10 μl tips using two pulses of 1,720 V and 10 width. Cells were then plated in 24-well plates.

For canonical inflammasome stimulations, overnight (ON) IFN γ -primed BMDMs were then prestimulated with PAM3CSK4 (InvivoGen, 100 ng/ml) for 4 h to induce pro-IL1 β expression. Then, Nigericin (NLRP3 activator, 40 μM , InvivoGen), dA:dT (AIM2 activator, 1 $\mu\text{g}/\text{ml}$, InvivoGen), TcdB toxin (PYRIN inducer, 0.05 $\mu\text{g}/\text{ml}$, List Biological Laboratories) or flagellin (NLRC4 trigger, 1 $\mu\text{g}/\text{ml}$, InvivoGen) was used to stimulate various canonical inflammasomes. Both flagellin and poly(dA:dT) were transfected into cells using FuGeneHD (Promega) transfection reagent in Opti-MEM culture medium. When specified, *P. aeruginosa* (PAO1) and *S. Tm* strains (SL1344) (MOI 5) were used to trigger NLRC4 inflammasome response.

For all stimulations, macrophage medium was replaced by serum-free and antibiotic-free Opti-MEM medium and inflammasome triggers were added to the macrophages for various times.

Specific to infections, plates were centrifuged for 1 min, 800 rpm to ensure homogenous infections. Then, extracellular bacteria were eliminated with gentamicin (100 $\mu\text{g}/\text{ml}$, Invitrogen).

Bacterial cultures

Bacteria were grown overnight in Luria Broth (LB) medium at 37°C with aeration and constant agitation in the presence or absence of antibiotics (specified in the Appendix Table S1), stationary phase (OD of 2–2.5) bacteria when then used for infections. Stimulation of the NLRC4 inflammasome by *S. Typhimurium* SL1344 and *P. aeruginosa* PAO1 bacteria required proper T3SS and flagellin expression; therefore, bacteria were sub-cultured the next day by dilution overnight culture 1/50 and grew until reaching an O.D600 of 0.6–1.

CFU evaluation

2.5×10^5 BMDMs were infected with stationary phase *Salmonella orgA*[−] (MOI10) for 1 h. Cells were treated with gentamicin (100 $\mu\text{g}/\text{ml}$) for 30 min to kill extracellular bacteria and then washed three times in PBS. Medium was replaced with BMDM medium supplemented with 20 $\mu\text{g}/\text{ml}$ of gentamicin to avoid extracellular bacterial replication. At the end of the experiment, cells were lysed in Triton 0.1% and intracellular bacterial loads were evaluated using CFU plating.

Gene knock down

Gene silencing was achieved using siRNA pools (Dharmacon, 25 nM/well listed in Appendix Table S1) as previously described (Meunier *et al.*, 2015; Santos *et al.*, 2018) or accell siRNA technology. siRNA smart pools from Dharmacon were transfected into cells using the DharmaFECT 4 transfection reagent (Dharmacon) for 48 h. Primary human macrophages were treated with 1 μM siRNA Accell (Dharmacon, smart pool) in the absence of transfection reagent for 72 h. Then, murine BMDMs and human macrophages were stimulated with 1 $\mu\text{g}/2 \times 10^5$ cells of OMVs or infected with *Salmonella Typhimurium* (*orgA*[−]) to trigger non-canonical inflammasome

response. For siRNA experiments, gene knock down efficiency was monitored by qRT-PCR or immunoblotting (WB) assays.

Quantitative real-time PCR

Cellular RNAs were extracted from 2.5×10^5 cells using RNeasy Mini Kit (Qiagen). mRNAs were reverse transcribed with the Verso cDNA Synthesis Kit (Thermo Scientific). Regarding qPCR experiments, 1 μM of primers (Appendix Table S1), SYBR™ Select Master Mix (Thermo Scientific) and 15 ng of cDNA were mixed in a 10 μl reaction in a QuantStudio 5 device (Applied Biosystems). Primers were generated using primer3 software.

Cytokine and pyroptosis measurement

Murine IL-1 α , IL-1 β , TNF- α , IL12, IL18, IFN γ , IL-6, and human IL-1B cytokine levels were measured by ELISA (listed in Appendix Table S1). LDH cytotoxicity detection kit (Takara) allowed to monitor for cell lysis. Normalization of spontaneous lysis was calculated as follows: (LDH infected – LDH uninfected)/(LDH total lysis – LDH uninfected) \times 100.

Immunoblotting

Preparation of cell lysates and supernatants has been described previously. Proteins were loaded and separated in 12% SDS-PAGE gels and then transferred on PVDF membranes. After 1 h of saturation in Tris-buffered saline (TBS) with 0.05% Tween 20 containing 5% non-fat milk (pH 8), membranes were incubated overnight with various antibodies (referenced in Appendix Table S1). The next day, membranes were washed three times in TBS 0.1% Tween 20 and incubated with appropriate secondary horseradish peroxidase (HRP)-conjugated antibody (dilution 1/5,000–10,000, listed in Appendix Table S1) for 1 h at room temperature. Then, after three washes, immunoblottings were revealed with a chemiluminescent substrate ECL substrate (Bio-Rad) and images were acquired using ChemiDoc Imaging System (Bio-Rad). All antibody references and working dilutions are presented in Appendix Table S1.

Microscopy

2.5×10^5 BMDMs on glass coverslips were infected with *S. Typhimurium* (MOI10) expressing an mCherry fluorescent protein. At the indicated times, cells were washed three times with PBS and fixed with 4% PFA for 10 min at 37°C. 0.1 M glycine was used to quench excess of PFA for 10 min at room temperature. Then, cells were permeabilized and incubated with primary antibodies O/N at 4°C in saponin 0.1%/BSA 3% solution. Cellular stainings were achieved using Hoescht (DNA labelling), GBP2 antibody (gift from J Howard). Coverslips were then washed with Saponin/BSA solution and further incubated with the appropriate secondary antibodies coupled to fluorochromes (1/1,000; Appendix Table S1). After three washes with PBS, cells were mounted on glass slides using VECTASHIELD (Vectalabs). Coverslips were imaged using confocal Zeiss LSM 710 (Image core Facility, IPBS, Toulouse or an Olympus/Andor CSU-X1 Spinning disk microscope using a 63 \times oil objective. Otherwise specified, 5–10 fields/experiment were manually counted using ImageJ software.

Transduction of iBMDMs

HEK 293-based retroviral packaging cell line (GP2-293) was plated in 10-cm Petri dish in DMEM + 10% FCS + 1% PS. When cell's confluency reached 60–80%, cells were placed in serum and antibiotic-free Opti-mem medium and transfected with VSV-G encoding vector (pMD.2G) along with CASP11-C254G-GFP or pRetro (-GFP or -Irgm2-GFP) vectors using PEI transfection reagent. 10 h after transfection, cell medium was replaced by DMEM + 10% FCS + 1% PS. At 48 h post-transfection, cell's supernatant containing retroviral particles were collected, filtered 0.45 μ m and used to transduce target cells. After 48 h, puromycin (5 μ g/ml) was used to select cells positively transduced with the transgene. When vectors contained GFP fusions, cells were sorted using fluorescence-activated cell sorting.

Immunoprecipitation and GFP-Trap

Irgm2^{-/-} immortalized macrophages were transduced with retroviral vectors carrying a doxycycline-inducible *Irgm2*-GFP, or GFP alone constructs, cloned into Retro-XTM Tet-On[®] 3G vector (Clontech Laboratories, Inc.). To ensure proper *Irgm2*-GFP expression, cells were incubated 16 h with doxycycline 1 μ g/ml in the presence of IFN γ . *Irgm2*-GFP and associated protein complexes were pull-down using GFP-Trap magnetic beads according to manufacturer's instructions (chromotek). Briefly, cells were lysed in CoIP lysis buffer (10 mM Tris/Cl pH 7.5; 150 mM NaCl; 0.5 mM EDTA; 0.5% NP-40, 0.09% Na-Azide) supplemented with a protease inhibitor cocktail (Roche). Cell lysates were then incubated with GFP-Trap-MA beads for 1 h at 4°C. After two washes with wash-buffer (10 mM Tris/Cl pH 7.5; 150 mM NaCl; 0.5 mM EDTA, 0.018% Na-Azide), GFP-Trap complexes were boiled for 10 min at 95°C in RIPA buffer + Laemmli before separation on SDS-PAGE and mass spectrometry or immunoblotting.

Mass spectrometry analysis

Immuno-purified protein samples were reduced with β -mercaptoethanol by heating at 95°C for 5 min, and cysteines were alkylated by addition of 90 mM iodoacetamide. Samples were loaded on a 1D SDS-PAGE gel, and proteins were isolated in a single gel band, which was excised and washed with several cycles of 50 mM ammonium bicarbonate-acetonitrile (1:1). Proteins were in-gel digested using 0.6 μ g of modified sequencing grade trypsin (Promega) in 50 mM ammonium bicarbonate overnight at 37°C. Resulting peptides were extracted from the gel by successive incubations in 50 mM ammonium bicarbonate and 10% formic acid-acetonitrile (1:1), then dried in a speed-vac and resuspended with 22 μ l of 5% acetonitrile, 0.05% trifluoroacetic acid (TFA) for MS analysis. Peptides were analysed by nanoLC-MS/MS using an UltiMate Nano/Cap System NCS-3500RS coupled to a Q-Exactive HFX mass spectrometer (Thermo Fisher Scientific, Bremen, Germany). Separation was performed on a C-18 column (75 μ m ID \times 50 cm, Reprosil C18) equilibrated in 95% solvent A (5% acetonitrile, 0.2% formic acid) and 5% solvent B (80% acetonitrile, 0.2% formic acid), using a gradient from 10 to 45% gradient of solvent B over 60 min at a flow rate of 350 nl/min. The mass spectrometer was operated in data-dependent acquisition mode with the Xcalibur software. Survey MS scans were acquired in the Orbitrap on the 350–1,400 *m/z* range, with the resolution set to 60,000, and the 12 most intense ions were

selected for fragmentation by higher-energy collisional dissociation (HCD) using a normalized collision energy of 28. MS/MS scans were collected at 15,000 resolution with an AGC target value of 1e5 and a maximum injection time of 22 ms. Dynamic exclusion was used within 30 s to prevent repetitive selection of the same peptide. Three replicate MS analyses were performed for each sample.

Bioinformatic processing of mass spectrometry data

Raw mass spectrometry files were searched using Mascot (Matrix Science) against the Mouse entries of the SwissProt-TrEmbl protein database. The enzyme specificity was “trypsin”, with a maximum of two misscleavages. Cysteine carbamidomethylation was set as a fixed modification, and N-terminal protein acetylation and methionine oxidation were specified as variable modifications. For the search, mass tolerance parameters were set at 5 ppm on the parent ion and 20 mmu on the fragment ions. Protein identification results were then validated with the Proline software by the target-decoy approach using a reverse database at a both a peptide and a protein FDR of 1%. To perform label-free relative quantification of proteins, the “abundance” metric retrieved by Proline was used, after global normalization of the MS signal across all MS runs. For each protein, a mean abundance value was computed from technical LC-MS replicate runs, and log₂-transformed. Missing protein abundance values were then replaced by a noise value estimated for each analysis as the 1% lowest percentile of the protein abundance values distribution. Bona fide *Irgm2* interactors were identified by comparing *Irgm2*-GFP immuno-purified samples and GFP control samples. For each protein, an enrichment ratio relative to the control and a Student *t*-test *P*-value was calculated from the protein abundance values derived from three independent biological replicate experiments. Relevant interactors were selected based on an enrichment ratio higher than 2 and a Student *t*-test *P*-value lower than 0.05.

Genetic invalidation of *Caspase-11* and *Irgm2* genes in immortalized BMDMs

Casp11 and *Irgm2* genes were knocked out using the crispr/cas9 system in onco J2-immortalized (i) bone marrow-derived macrophages (BMDMs) iWTs or *iIrgm2*^{-/-} macrophages. Single guide RNAs (sgRNA) specifically targeting caspase-11 exon 2 forward (5'CACCGCTTAAGGTGTTGGAACAGCT3') reverse (5'AAACAGCTGTTCCAACACCTTAAGC3'), *Irgm2* exon 2 forward (5'CACCGTTCCA TGTTGTCGAGCAACG3') reverse (5'AAACCGTTGCTCGACAACATG GAAC3') were designed using Benchling tool (Benchling.com), and oligonucleotides were synthesized by Sigma-Aldrich. Crispr guide RNA oligonucleotides were then hybridized and cloned in Lenti-grNA-Puromycin vector using BsmBI restriction enzyme (lenti-Guide-Puro, Addgene 52963, Feng Zhang Lab). HEK293T cells were transfected for 48 h with all constructs (Lipofectamine 2000) together with the lentiviral packaging vector p8.91 (Didier Trono Lab, EPFL, Switzerland) and the envelop coding VSV-G plasmid (pMD.2G, Addgene 12259, Didier Trono Lab). 48 h later, viral supernatants were harvested and subsequently filtered on 0.45- μ m filter. Recipient cells expressing Cas9 (1,000,000 cells/well in 6-well plates) were generated using lentiviral transduction with a Cas9-expressing lentiviral vector (lentiCas9-Blast, Addgene 52962, Feng Zhang Lab). Then, Cas9⁺ cells were infected with packaged viral

particles. To ensure efficient infection, viral particles were centrifuged for 2 h at 1,081 g at 32°C in presence of 8 µg/ml polybrene. 48 h later, medium was replaced and puromycin selection (10 µg/ml) was applied to select positive clones for 2 weeks. Puromycin-resistant cells were sorted at the single-cell level by FACS (Aria cell sorter). Individual clones were subjected to Western blotting to confirm the absence of targeted proteins.

Genetic invalidation of human GBPs in U937 cell line

To generate GBP1/2/5 knock-out cell line, deletion of genes was performed in a Cas9-expressing U937 clone obtained by transduction with the plasmid LentiCas9-Blast (from Feng Zhang; Addgene plasmid # 52962) followed by blasticidin selection and clonal isolation using the limit dilution method. A clone strongly expressing Cas9 was selected based on Western blot analysis using anti-Cas9 antibody (Millipore; # MAC133; 1:1,000 dilution). gRNAs targeting GBP1, GBP2 and GBP5 (Appendix Table S1) were cloned into the pKLV-U6gRNA(BbsI)-PGKpuro2ABFP vector (from Kosuke Yusa; Addgene plasmid # 50946). For each gene, two pairs of gRNAs were used. Lentiviral particles were produced in 293T cells using pMD2.G and psPAX2 (from Didier Trono, Addgene plasmids #12259 and #12260), and pKLV-U6gRNA(BbsI)-PGKpuro2ABFP. Cas9-expressing U937 cells were transduced by spinoculation. Gene deletion invalidation was verified by Western blotting analysis (Appendix Table S1).

Generation of human monocyte-derived macrophages

Peripheral blood mononuclear cells (PBMCs) were isolated from buffy coat of healthy donors obtained from the EFS Toulouse Purpan (France). Briefly, PBMCs were isolated by centrifugation using standard Ficoll-Paque density (GE Healthcare). The blood was diluted 1:1 in phosphate-buffered saline (PBS) pre-warmed to 37°C and carefully layered over the Ficoll-Paque gradient. The tubes were centrifuged for 25 min at 514 g, at 20°C. The cell interface layer was harvested carefully, and the cells were washed twice in PBS (for 10 min at 185 g followed by 10 min at 800 rpm) and resuspended in RPMI-1640 supplemented with 10% of foetal calf serum (FCS), 1% penicillin (100 IU/ml) and streptomycin (100 µg/ml). Monocytes were separated from lymphocytes by positive selection using CD14⁺ isolation kit (Miltenyi Biotec). To allow differentiation into monocyte-derived macrophages, cells were cultured in RPMI medium (GIBCO) supplemented with 10% FCS (Invitrogen), 100 IU/ml penicillin, 100 µg/ml streptomycin and 10 ng/ml MCSF for 7 days.

Ethics statements

The use of human cells was approved by the Research Ethical Committee, Haute-Garonne, France. Buffy coats were provided anonymously by the EFS (établissement français du sang, Toulouse, France). Written informed consent was obtained from each donor under EFS contract no 21PLER2017-0035AV02, according to “Decret No 2007-1220 (articles L1243-4, R1243-61)”.

Statistical analysis

Statistical data analysis was performed using Prism 5.0a (GraphPad Software, Inc.). *t*-Test with Bonferroni correction was used for

comparison of two groups. For multiple comparisons, one-way ANOVA with multiple Bonferroni correction test was used. Data are reported as mean with SEM. For animal experiments, Mann–Whitney tests were performed, and for mouse survival analysis, log-rank Cox–Mantel test was selected. *P*-values are given in figures, NS means non-significant. Significance is specified as **P* ≤ 0.05; ***P* ≤ 0.01, ****P* ≤ 0.001.

Data availability

The mass spectrometry proteomic data have been deposited to the ProteomeXchange Consortium via the PRIDE (Perez-Riverol *et al*, 2019) partner repository with the data set identifier PXD020457 (<http://proteomecentral.proteomexchange.org/cgi/GetDataset?ID=PX020457>).

Expanded View for this article is available online.

Acknowledgements

We would like to acknowledge Biotem company for generating anti-Irgm2 antibodies; Junying Yuan (Harvard Med School, Boston, USA) and B. Py (CIRI institute, Lyon, France) for sharing *Caspase1^{-/-}Caspase11^{-/-}* and *Caspase11^{-/-}* mice (Li *et al*, 1995; Wang *et al*, 1998); V. Petrilli and B. Py for providing the *Nlrp3^{-/-}* mice (Martinon *et al*, 2006). *Irgm2^{-/-}* mice came from the Jackson laboratory. The authors also acknowledge the animal facility, mass spectrometry and microscopy platforms of the IPBS institute. We specifically acknowledge Drs. A. Gonzalez de Peredo for mass spectrometry data processing, G. Lugo-Villarino, C. Cougoule and Y. Rombouts for fruitful discussions and suggestions as well as for reading and implementing the MS. This project was funded by grants from FRM “Amorçage Jeunes Equipes” (AJE20151034460), ERC StG (INFLAME 804249) and ATIP to EM and from the European Society of Clinical Microbiology and Infectious Diseases (ESCMID) to RP. MY (Masahiro Yamamoto) is supported by the Research ProGram on Emerging and Re-emerging Infectious Diseases (JP19fk0108047), Japanese Initiative for Progress of Research on Infectious Diseases for global Epidemic (JP19fm0208018) and Strategic International Collaborative Research ProGram (19jm0210067h) from Agency for Medical Research and Development (AMED), Grant-in-Aid for Scientific Research on Innovative Areas (Production, function and structure of neo-self; 19H04809), for Scientific Research (B) (18KK0226 and 18H02642) and for Scientific Research (A) (19H00970) from Ministry of Education, Culture, Sports, Science and Technology of Japan.

Author contributions

EE and EM designed the experiments with the help of RP. EE, RP and EM wrote the manuscript. EE and RP performed the experiments with the help of SB, P-JB, AH, KS and MP. KC and OB-S performed essential mass spectrometry run acquisitions and analysis. TH, BL, MY and JCH provided essential reagents to conduct the project.

Conflict of interest

The authors declare that they have no conflict of interest.

References

- Aachoui Y, Leaf IA, Hagar JA, Fontana MF, Campos CG, Zak DE, Tan MH, Cotter PA, Vance RE, Aderem A *et al* (2013) Caspase-11 protects against bacteria that escape the vacuole. *Science* 339: 975–978

- Aglietti RA, Estevez A, Gupta A, Ramirez MG, Liu PS, Kayagaki N, Ciferri C, Dixit VM, Dueber EC (2016) GsdmD p30 elicited by caspase-11 during pyroptosis forms pores in membranes. *Proc Natl Acad Sci USA* 113: 7858–7863
- Azzam KM, Madenspacher JH, Cain DW, Lai L, Gowdy KM, Rai P, Janardhan K, Clayton N, Cunningham W, Jensen H et al (2017) Irgm1 coordinately regulates autoimmunity and host defense at select mucosal surfaces. *JCI Insight* 2: e91914
- Basters A, Knobeloch KP, Fritz G (2018) USP18 – a multifunctional component in the interferon response. *Biosci Rep* 38: BSR20180250
- Benaoudia S, Martin A, Puig Gamez M, Gay G, Lagrange B, Cornut M, Krasnykov K, Claude J, Bourgeois CF, Hughes S et al (2019) A genome-wide screen identifies IRF2 as a key regulator of caspase-4 in human cells. *EMBO Rep* 20: e48235
- Broz P, Ruby T, Belhocine K, Bouley DM, Kayagaki N, Dixit VM, Monack DM (2012) Caspase-11 increases susceptibility to *Salmonella* infection in the absence of caspase-1. *Nature* 490: 288–291
- Carqueira DM, Gomes MTR, Silva ALN, Rungue M, Assis NRG, Guimarães ES, Morais SB, Broz P, Zamboni DS, Oliveira SC (2018) Guanylate-binding protein 5 licenses caspase-11 for Gasdermin-D mediated host resistance to *Brucella abortus* infection. *PLoS Pathog* 14: e1007519
- Chen KW, Monteleone M, Boucher D, Sollberger G, Ramnath D, Condon ND, von Pein JB, Broz P, Sweet MJ, Schroder K (2018) Noncanonical inflammasome signaling elicits gasdermin D-dependent neutrophil extracellular traps. *Sci Immunol* 3: eaar6676
- Cheng KT, Xiong S, Ye Z, Hong Z, Di A, Tsang KM, Gao X, An S, Mittal M, Vogel SM et al (2017) Caspase-11-mediated endothelial pyroptosis underlies endotoxemia-induced lung injury. *J Clin Invest* 127: 4124–4135
- Choi YJ, Kim S, Choi Y, Nielsen TB, Yan J, Lu A, Ruan J, Lee HR, Wu H, Spellberg B et al (2019) SERPINB1-mediated checkpoint of inflammatory caspase activation. *Nat Immunol* 20: 276–287
- Coers J (2013) Self and non-self discrimination of intracellular membranes by the innate immune system. *PLoS Pathog* 9: e1003538
- Costa Franco MM, Marim F, Guimarães ES, Assis NRG, Carqueira DM, Alves-Silva J, Harms J, Splitter G, Smith J, Kanneganti T-D et al (2018) *Brucella abortus* triggers a cGAS-independent STING pathway to induce host protection that involves guanylate-binding proteins and inflammasome activation. *J Immunol* 200: 607–622
- Deng M, Tang Y, Li W, Wang X, Zhang R, Zhang X, Zhao X, Liu J, Tang C, Liu Z et al (2018) The endotoxin delivery protein HMGB1 mediates caspase-11-dependent lethality in sepsis. *Immunity* 49: 740–753
- Feeley EM, Pilla-Moffett DM, Zwack EE, Piro AS, Finethy R, Kolb JP, Martinez J, Brodsky IE, Coers J (2017) Galectin-3 directs antimicrobial guanylate binding proteins to vacuoles furnished with bacterial secretion systems. *Proc Natl Acad Sci USA* 114: E1698–E1706
- Finethy R, Jorgensen I, Haldar AK, De Zoete MR, Strowig T, Flavell RA, Yamamoto M, Nagarajan UM, Miao EA, Coers J (2015) Guanylate binding proteins enable rapid activation of canonical and noncanonical inflammasomes in *Chlamydia*-infected macrophages. *Infect Immun* 83: 4740–4749
- Finethy R, Luoma S, Orench-Rivera N, Feeley EM, Haldar AK, Yamamoto M, Kanneganti T-D, Kuehn MJ, Coers J (2017) Inflammasome activation by bacterial outer membrane vesicles requires guanylate binding proteins. *MBio* 8: e01188-17
- Finethy R, Dockterman J, Kutsch M, Orench-Rivera N, Wallace G, Piro A, Luoma S, Haldar AK, Hwang S, Martinez J et al (2020) Dynamin-related Irgm proteins modulate LPS-induced caspase-11 activation and septic shock. *EMBO Rep* 21: e50830
- Fink MP (2014) Animal models of sepsis. *Virulence* 5: 143–153
- Fisch D, Bando H, Clough B, Hornung V, Yamamoto M, Shenoy AR, Frickel E (2019) Human GBP 1 is a microbe-specific gatekeeper of macrophage apoptosis and pyroptosis. *EMBO J* 38: e100926
- Green R, Ireton RC, Gale M (2018) Interferon-stimulated genes: new platforms and computational approaches. *Mamm Genome* 29: 593–602
- Gu Y, Princely Abudu Y, Kumar S, Bissa B, Choi SW, Jia J, Lazarou M, Eskelinen E, Johansen T, Deretic V (2019) Mammalian Atg8 proteins regulate lysosome and autolysosome biogenesis through SNAREs. *EMBO J* 38: e101994
- Hagar JA, Powell DA, Aachoui Y, Ernst RK, Miao EA (2013) Cytoplasmic LPS activates caspase-11: implications in TLR4-independent endotoxic shock. *Science* 341: 1250–1253
- Haldar AK, Saka HA, Piro AS, Da Dunn J, Henry SC, Taylor GA, Frickel EM, Valdivia RH, Coers J (2013) IRG and GBP host resistance factors target aberrant, “non-self” vacuoles characterized by the missing of “Self” IRGM proteins. *PLoS Pathog* 9: e1003414
- Haldar AK, Foltz C, Finethy R, Piro AS, Feeley EM, Pilla-Moffett DM, Komatsu M, Frickel EM, Coers J (2015) Ubiquitin systems mark pathogen-containing vacuoles as targets for host defense by guanylate binding proteins. *Proc Natl Acad Sci USA* 112: E5628–E5637
- Hayward JA, Mathur A, Ngo C, Man SM (2018) Cytosolic recognition of microbes and pathogens: inflammasomes in action. *Microbiol Mol Biol Rev* 82: e00015-18
- Kayagaki N, Warming S, Lamkanfi M, Walle LV, Louie S, Dong J, Newton K, Qu Y, Liu J, Heldens S et al (2011) Non-canonical inflammasome activation targets caspase-11. *Nature* 479: 117–121
- Kayagaki N, Wong MT, Stowe IB, Ramani SR, Gonzalez LC, Akashi-takamura S, Miyake K, Zhang J, Lee WP, Forsberg LS et al (2013) Independent of TLR4. *Science* 330: 1246–1249
- Kayagaki N, Stowe IB, Lee BL, O'Rourke K, Anderson K, Warming S, Cuellar T, Haley B, Roose-Girma M, Phung QT et al (2015) Caspase-11 cleaves gasdermin D for non-canonical inflammasome signalling. *Nature* 526: 666–671
- Kayagaki N, Lee BL, Stowe IB, Kornfeld OS, O'Rourke K, Mirrashidi KM, Haley B, Watanabe C, Roose-Girma M, Modrusan Z et al (2019) IRF2 transcriptionally induces GSDMD expression for pyroptosis. *Sci Signal* 12: eaax4917
- Kim BH, Shenoy AR, Kumar P, Bradfield CJ, MacMicking JD (2012) IFN-inducible GTPases in host cell defense. *Cell Host Microbe* 12: 432–444
- Kim S, Eun H, Jo E-K (2019) Roles of autophagy-related genes in the pathogenesis of inflammatory bowel disease. *Cells* 8: 77
- Kutsch M, Sistemich L, Lesser CF, Goldberg MB, Herrmann C, Coers J (2020) Direct binding of polymeric GBP1 to LPS disrupts bacterial cell envelope functions. *EMBO J* 39: e104926
- Lagrange B, Benaoudia S, Wallet P, Magnotti F, Provost A, Michal F, Martin A, Di Lorenzo F, Py BF, Molinaro A et al (2018) Human caspase-4 detects tetra-acylated LPS and cytosolic Francisella and functions differently from murine caspase-11. *Nat Commun* 9: 242
- Latz E, Visintin A, Lien E, Fitzgerald KA, Monks BG, Kurt-Jones EA, Golenbock DT, Espevik T (2002) Lipopolysaccharide rapidly traffics to and from the golgi apparatus with the toll-like receptor 4-MD-2-CD14 complex in a process that is distinct from the initiation of signal transduction. *J Biol Chem* 277: 47834–47843
- Lee YK, Lee JA (2016) Role of the mammalian ATG8/LC3 family in autophagy: differential and compensatory roles in the spatiotemporal regulation of autophagy. *BMB Rep* 49: 424–430
- Lee BL, Stowe IB, Gupta A, Kornfeld OS, Roose-Girma M, Anderson K, Warming S, Zhang J, Lee WP, Kayagaki N (2018) Caspase-11 auto-

- proteolysis is crucial for noncanonical inflammasome activation. *J Exp Med* 215: 2279–2288
- Li P, Allen H, Banerjee S, Franklin S, Herzog L, Johnston C, McDowell J, Paskind M, Rodman L, Salfeld J et al (1995) Mice deficient in IL-1 β -converting enzyme are defective in production of mature IL-1 β and resistant to endotoxic shock. *Cell* 80: 401–411
- Liau NP, Laktyushin A, Lucet IS, Murphy JM, Yao S, Whitlock E, Callaghan K, Nicola NA, Kershaw NJ, Babon JJ (2018) The molecular basis of JAK/STAT inhibition by SOCS1. *Nat Commun* 9: 1–14
- Liu X, Zhang Z, Ruan J, Pan Y, Magupalli VG, Wu H, Lieberman J (2016) Inflammasome-activated gasdermin D causes pyroptosis by forming membrane pores. *Nature* 535: 153–158
- Liu BC, Sarhan J, Panda A, Muendlein HI, Ilyukha V, Coers J, Yamamoto M, Isberg RR, Poltorak A (2018) Constitutive interferon maintains GBP expression required for release of bacterial components upstream of pyroptosis and anti-DNA responses. *Cell Rep* 24: 155–168
- Man SM, Karki R, Malireddi RKS, Neale G, Vogel P, Yamamoto M, Lamkanfi M, Kanneganti TD (2015) The transcription factor IRF1 and guanylate-binding proteins target activation of the AIM2 inflammasome by Francisella infection. *Nat Immunol* 16: 467–475
- Man SM, Karki R, Sasai M, Place DE, Kesavardhana S, Temirov J, Frase S, Zhu Q, Malireddi RKS, Kuriakose T et al (2016) IRGB10 liberates bacterial ligands for sensing by the AIM2 and Caspase-11-NLRP3 inflammasomes. *Cell* 167: 382–396
- Maric-Biresev J, Hunn JP, Krut O, Helms JB, Martens S, Howard JC (2016) Loss of the interferon- γ -inducible regulatory immunity-related GTPase (IRG), Irgm1, causes activation of effector IRG proteins on lysosomes, damaging lysosomal function and predicting the dramatic susceptibility of Irgm1-deficient mice to infection. *BMC Biol* 14: 33
- Martinon F, Pétrilli V, Mayor A, Tardivel A, Tschopp J (2006) Gout-associated uric acid crystals activate the NALP3 inflammasome. *Nature* 440: 237–241
- Masud S, Prajsnar TK, Torraca V, Lamers GEM, Benning M, Van Der Vaart M, Meijer AH (2019) Macrophages target Salmonella by LC3-associated phagocytosis in a systemic infection model. *Autophagy* 15: 796–812
- Mehto S, Chauhan S, Jena KK, Chauhan NR, Nath P, Sahu R, Dhar K, Das SK, Chauhan S (2019a) IRGM restrains NLRP3 inflammasome activation by mediating its SQSTM1/p62-dependent selective autophagy. *Autophagy* 15: 1645–1647
- Mehto S, Jena KK, Nath P, Chauhan S, Kolapalli SP, Das SK, Sahoo PK, Jain A, Taylor GA, Chauhan S (2019b) The Crohn's disease risk factor IRGM limits NLRP3 inflammasome activation by impeding its assembly and by mediating its selective autophagy. *Mol Cell* 73: 429–445
- Meunier E, Dick MS, Dreier RF, Schürmann N, Broz DK, Warming S, Roose-Girma M, Bumann D, Kayagaki N, Takeda K et al (2014) Caspase-11 activation requires lysis of pathogen-containing vacuoles by IFN-induced GTPases. *Nature* 509: 366–370
- Meunier E, Wallet P, Dreier RF, Costanzo S, Anton L, Rühl S, Dussurget S, Dick MS, Kistner A, Rigard M et al (2015) Guanylate-binding proteins promote activation of the AIM2 inflammasome during infection with Francisella novicida. *Nat Immunol* 16: 476–484
- Napier BA, Brubaker SW, Sweeney TE, Monette P, Rothmeier GH, Gertsvolf NA, Puschnik A, Carette JE, Khatri P, Monack DM (2016) Complement pathway amplifies caspase-11-dependent cell death and endotoxin-induced sepsis severity. *J Exp Med* 213: 2365–2382
- Nguyen TN, Padman BS, Usher J, Oorschot V, Ramm G, Lazarou M (2016) Atg8 family LC3/GAB ARAP proteins are crucial for autophagosomal-lysosome fusion but not autophagosome formation during PINK1/Parkin mitophagy and starvation. *J Cell Biol* 215: 857–874
- Park S, Choi J, Biering SB, Dominici E, Williams LE, Hwang S (2016) Targeting by Autophagy proteins (TAG): targeting of IFNG-inducible GTPases to membranes by the LC3 conjugation system of autophagy. *Autophagy* 12: 1153–1167
- Pei C, Wang C, Xu H (2017) Irgm1 suppresses NLRP3 inflammasome-mediated IL-1 β production. *J Immunol* 198 (1 Supplement): 201.25
- Pilla DM, Hagar JA, Haldar AK, Mason AK, Degrandi D, Pfeffer K, Ernst RK, Yamamoto M, Miao EA, Coers J (2014) Guanylate binding proteins promote caspase-11-dependent pyroptosis in response to cytoplasmic LPS. *Proc Natl Acad Sci USA* 111: 6046–6051
- Pilla-Moffett D, Barber MF, Taylor GA, Coers J (2016) Interferon-inducible GTPases in host resistance, inflammation and disease. *J Mol Biol* 428: 3495–3513
- Rathinam VAK, Zhao Y, Shao F (2019) Innate immunity to intracellular LPS. *Nat Immunol* 20: 527–533
- Rühl S, Broz P (2015) Caspase-11 activates a canonical NLRP3 inflammasome by promoting K⁺ efflux. *Eur J Immunol* 45: 2927–2936
- Rühl S, Shkarina K, Demarco B, Heilig R, Santos JC, Broz P (2018) ESCRT-dependent membrane repair negatively regulates pyroptosis downstream of GSDMD activation. *Science* 362: 956–960
- Sagiv Y (2000) GATE-16, a membrane transport modulator, interacts with NSF and the Golgi v-SNARE GOS-28. *EMBO J* 19: 1494–1504
- Santos JC, Dick MS, Lagrange B, Degrandi D, Pfeffer K, Yamamoto M, Meunier E, Pelczar P, Henry T, Broz P (2018) LPS targets host guanylate-binding proteins to the bacterial outer membrane for non-canonical inflammasome activation. *EMBO J* 37: e98089
- Santos JC, Boucher D, Schneider LK, Demarco B, Dilucca M, Shkarina K, Heilig R, Chen KW, Lim RYH, Broz P (2020) Human GBP1 binds LPS to initiate assembly of a caspase-4 activating platform on cytosolic bacteria. *Nat Commun* 11: 1–15
- Sasai M, Sakaguchi N, Ma JS, Nakamura S, Kawabata T, Bando H, Lee Y, Saitoh T, Akira S, Iwasaki A et al (2017) Essential role for GABARAP autophagy proteins in interferon-inducible GTPase-mediated host defense. *Nat Immunol* 18: 899–910
- Sborgi L, Rühl S, Mulvihill E, Pipercevic J, Heilig R, Stahlberg H, Farady CJ, Müller DJ, Broz P, Hiller S (2016) GSDMD membrane pore formation constitutes the mechanism of pyroptotic cell death. *EMBO J* 35: 1766–1778
- Schmid-Burgk JL, Gaidt MM, Schmidt T, Ebert TS, Bartok E, Hornung V (2015) Caspase-4 mediates non-canonical activation of the NLRP3 inflammasome in human myeloid cells. *Eur J Immunol* 45: 2911–2917
- Shi J, Zhao Y, Wang K, Shi X, Wang Y, Huang H, Zhuang Y, Cai T, Wang F, Shao F (2015) Cleavage of GSDMD by inflammatory caspases determines pyroptotic cell death. *Nature* 526: 660–665
- Perez-Riverol Y, Csordas A, Bai J, Bernal-Llinares M, Hewapathirana S, Kundu DJ, Inuganti A, Griss J, Mayer G, Eisenacher M et al (2019) The PRIDE database and related tools and resources in 2019: improving support for quantification data. *Nucleic Acids Res* 2019 47: D442–D450
- Thieblemont N, Wright SD (1999) Transport of bacterial lipopolysaccharide to the Golgi apparatus. *J Exp Med* 190: 523–534
- Thurston TLM, Matthews SA, Jennings E, Alex E, Shao F, Shenoy AR, Birrell MA, Holden DW (2016) Growth inhibition of cytosolic Salmonella by caspase-1 and caspase-11 precedes host cell death. *Nat Commun* 7: 1–15
- Vanaja SK, Russo AJ, Behl B, Banerjee I, Yankova M, Deshmukh SD, Rathinam VAK (2016) Bacterial outer membrane vesicles mediate cytosolic localization of LPS and Caspase-11 activation. *Cell* 165: 1106–1119
- Wallet P, Benaoudia S, Mosnier A, Lagrange B, Martin A, Lindgren H, Golovliov I, Michal F, Basso P, Djebali S et al (2017) IFN- γ extends the immune functions of Guanylate Binding Proteins to inflammasome-

- independent antibacterial activities during *Francisella novicida* infection. *PLoS Pathog* 13: e1006630
- Wandel MP, Kim BH, Park ES, Boyle KB, Nayak K, Lagrange B, Herod A, Henry T, Zilbauer M, Rohde J et al (2020) Guanylate-binding proteins convert cytosolic bacteria into caspase-4 signaling platforms. *Nat Immunol* 21: 880–891
- Wang S, Miura M, Jung YK, Zhu H, Li E, Yuan J (1998) Murine caspase-11, an ICE-interacting protease, is essential for the activation of ICE. *Cell* 92: 501–509
- Wu Y-W, Li F (2019) Bacterial interaction with host autophagy. *Virulence* 10: 352–362
- Yamamoto M, Okuyama M, Ma JS, Kimura T, Kamiyama N, Saiga H, Ohshima J, Sasai M, Kayama H, Okamoto T et al (2012) A cluster of interferon- γ -inducible p65 gtpases plays a critical role in host defense against *Toxoplasma gondii*. *Immunity* 37: 302–313
- Yang J, Zhao Y, Shao F (2015) Non-canonical activation of inflammatory caspases by cytosolic LPS in innate immunity. *Curr Opin Immunol* 32: 78–83
- Yang X, Cheng X, Tang Y, Qiu X, Wang Y, Kang H, Wu J, Wang Z, Liu Y, Chen F et al (2019) Bacterial endotoxin activates the coagulation cascade through gasdermin D-dependent phosphatidylserine exposure. *Immunity* 51: 983–996
- Zhao YO, Könen-Waisman S, Taylor GA, Martens S, Howard JC (2010) Localisation and mislocalisation of the interferon-inducible immunity-related GTPase, Irgm1 (LRG-47) in mouse cells. *PLoS ONE* 5: e8648
- Zwack EE, Feeley EM, Burton AR, Hu B, Yamamoto M, Kanneganti TD, Bliska JB, Coers J, Brodsky IE (2017) Guanylate binding proteins regulate inflammasome activation in response to hyperinjected *Yersinia* translocon components. *Infect Immun* 85: e00778-16